https://ntrs.nasa.gov/search.jsp?R=19740004409 2020-03-23T12:28:25+00:00Z

CONTRACT NUMBER: NAS 9-13004
DRL NUMBER: T-825
DRD NUMBER: MA-129TA
MDC E0696

CR-134136

HIGH TEMPERATURE ANTENNA DEVELOPMENT FOR SPACE SHUTTLE

FINAL REPORT
VOLUME I

30 JULY 1973

(NASA-CR-134136) HIGH TEMPERATURE ANTENNA DEVELOPMENT FOR SPACE SHUTTLE, VOLUME 1 Final Report (McDonnell-Douglas Astronautics Co.) 333 p HC $18.75

CSCL 22B G3/31

N74-12522

Unclas 23322

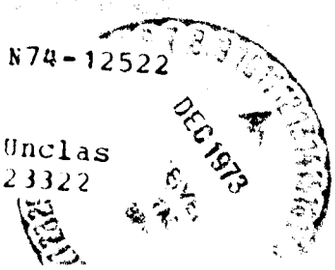

MCDONNELL DOUGLAS ASTRONAUTICS COMPANY - EAST

MCDONNELL DOUGLAS CORPORATION

CONTRACT NUMBER: NAS 9-13004
DRL NUMBER: T-825
DRD NUMBER: MA-129TA
MDC E0896

COPY NO. 3

HIGH TEMPERATURE ANTENNA DEVELOPMENT FOR SPACE SHUTTLE

FINAL REPORT
VOLUME I

30 JULY 1973

Prepared by E. A. Kuhlman
E.A. Kuhlman
Group Engineer, Electronics

Approved by A. L. Furfine
A.L. Furfine
Manager, Advanced Electronic Techniques

Approved by H. L. Motchan
H.L. Motchan
Director, Avionics Engineering

MCDONNELL DOUGLAS ASTRONAUTICS COMPANY • EAST
Saint Louis, Missouri 63166 (314) 232-0232

MCDONNELL DOUGLAS CORPORATION

ABSTRACT

Design concepts for high temperature flush mounted Space Shuttle Orbiter antenna systems are discussed. The design concepts include antenna systems for VHF, L-band, S-band, C-band and Ku-band frequencies. The S-band antenna system design was completed and test hardware fabricated. It was then subjected to electrical and thermal testing to establish design requirements and determine reuse capabilities. The thermal tests consisted of applying ten high temperature cycles simulating the Orbiter entry heating environment in an arc tunnel plasma facility and observing the temperature distributions. Radiation pattern and impedance measurements before and after high temperature exposure were used to evaluate the antenna systems performance.

The design approach is based on combining an RF window, which provides thermal protection, with a conventional antenna. The antenna window design is based on using the Orbiter thermal protection system insulation as the basic window material. Alternate window design concepts are considered.

Layout drawings, supported by thermal and strength analyses, are given for each of the antenna system designs. Maximum accessibility and minimum integration impact were stressed.

The results of the electrical and thermal testing of the S-band antenna system are given. The test data shows negligible change in electrical performance, and establishes the validity and reuse capability of the design approach.

PRECEDING PAGE BLANK NOT FILMED

THIS PAGE INTENTIONALLY LEFT BLANK

CONTENTS

LIST OF FIGURES xi

LIST OF TABLES. xvi

SUMMARY 1-1

CONCLUSIONS 2-1

RECOMMENDATIONS 3-1

INTRODUCTION. 4-1

DESIGN CONSIDERATIONS AND CONSTRAINTS 5-1
Antenna Requirements 5-1
Structural Requirements. 5-1
Thermal Requirements 5-4
Strength Requirements. 5-10

CONCEPT AND FEASIBILITY STUDIES 6-1
Electrical Studies 6-2
Antenna equipment survey. 6-2
Antenna window transmission loss. 6-8
Design tests. 6-13
Material Studies 6-20
Antenna window materials. 6-20
Attachment materials. 6-27
RF transparent structural panel. 6-27
Strain isolator sponge 6-27
Adhesive 6-27
Antenna cavity foams. 6-27
Materials interfaces. 6-28
Replacement and repair. 6-28
Thermal Studies. 6-29
Environmental factors 6-29
Thermal models. 6-30
Results 6-30
Structural Integration Studies 6-37
Antenna installation concepts 6-37
S-band antenna system installation 6-38
Ku-band antenna system installation. 6-43
VHF antenna system installation. 6-43
L-band antenna system installation 6-49
C-band horn antenna system installation. 6-53
C-band linear slot antenna system installation 6-53
Alternate antenna system integration concepts 6-53
Integration concepts 6-53
Alternate structural environments. 6-60
Alternate TPS configurations 6-63
Alternate antenna window concept 6-63

Strength Studies 6-67
S- and Ku-band antenna systems. 6-67
VHF antenna system. 6-67

S-BAND ANTENNA SYSTEM DESIGN. 7-1
Electrical Design 7-1
Electrical design tests. 7-3
Test configurations 7-3
Test techniques 7-4
Test results (preliminary). 7-5
Test results (antenna tuning) 7-20
Test results (antenna mounting effects) 7-28
Test results (antenna system mockup). 7-28
Transmission loss. 7-28
Structural Design 7-32
Breadboard unit design 7-32
Prototype unit design. 7-34
Test container assembly. 7-47
Cover assembly 7-47
Wedge mount assembly 7-47
Materials Evaluation. 7-54
S-band antenna 7-54
Thermocouple installation. 7-54
Strain isolator. 7-54
Bonding. 7-54
Thermal Analyses. 7-55
S-band antenna system thermal model. 7-56
Thermal response results 7-56
Strength Analyses 7-59
Quality Assurance 7-63
Reliability 7-64

TEST HARDWARE FABRICATION 8-1
Component Fabrication 8-1
S-band antenna 8-1
LI-1500 antenna window and guard tiles 8-1
Silicone sponge. 8-3
Fiberglass-phenolic honeycomb panel. 8-3
Panel support assembly 8-3
Antenna support. 8-3
Breadboard Unit Assembly. 8-3
Thermocouple installation. 8-5
Antenna window assembly. 8-5
Panel assembly 8-7
Final assembly 8-9
Prototype Unit Assembly 8-9
Test Fixture Fabrication. 8-13

ELECTRICAL TESTING. 9-1
Component Testing 9-1
Test configurations. 9-1
Test techniques. 9-1

Test results 9-1
Breadboard Unit Testing 9-5
Test configuration 9-7
Test techniques. 9-7
Test results 9-7
Prototype Unit Testing. 9-7
Test results 9-7
Thermal Test Support. 9-9
Test configuration 9-13
Test techniques. 9-13
Test results - breadboard unit 9-17
Test results - prototype unit. 9-21

THERMAL TESTING 10-1
Facility Description. 10-1
Test Installation 10-3
Test Environment. 10-5
Test environment control 10-7
Breadboard Unit Testing 10-9
Instrumentation. 10-9
Test results 10-9
Prototype Unit Tests. 10-24
Instrumentation. 10-24
Test results 10-28

EVALUATION. 11-1
Electrical Test Evaluation. 11-1
Component test 11-1
Breadboard tests 11-3
Prototype tests. 11-6
Thermal Test Data Evaluation. 11-10
Test heating time. 11-10
Thermal performance. 11-12
Thermal conductivity 11-12
Thermal conductivity verification 11-12
Channel flow nozzle heating. 11-14
Attachment hole heating. 11-15
Bondline thermal response. 11-15
Silicone resin exothermic reaction 11-15
Comparison of calculated and measured data 11-16
Physical Examination. 11-16
Visual inspection. 11-19
Surface coating 11-19
Antenna window. 11-19
Tile joints 11-23
Coating cracks 11-26
Water absorption 11-28
Surface emittance. 11-28

REFERENCES. 12-1

APPENDIX A Material Design Properties. A-1

APPENDIX B Equations for Calculating Power Transmission Loss Through Multiple Layers of Lossy Dielectric B-1

APPENDIX C Relationship of Circular and Linear Gain. C-1

APPENDIX D Bonding Lightweight Thermal Insulation. D-1

APPENDIX E Radiation Patterns for S-Band Antennas S/N 102 and 105. . . E-1

APPENDIX F Test Data for Prototype Unit No. 2. . . . . F-1

APPENDIX G Breadboard Unit Thermal Test Plan G-1

APPENDIX H Prototype Unit Thermal Test Plan. H-1

LIST OF PAGES

Title

iii thru xvi
1-1 thru 1-2
2-1 thru 2-2
3-1 thru 3-2
4-1 thru 4-2
5-1 thru 5-14
6-1 thru 6-70
7-1 thru 7-66
8-1 thru 8-14
9-1 thru 9-36
10-1 thru 10-40
11-1 thru 11-30
12-1 thru 12-2
A-1 thru A-2
B-1 thru B-4
C-1 thru C-2
D-1 thru D-4
E-1 thru E-2
F-1 thru F-4
G-1 thru G-12
H-1 thru H-11

LIST OF FIGURES

FIGURE

1	Orbiter Antenna Locations	5-2
2	Primary Structure/TPS Concepts	5-3
3	Ascent Trajectory	5-5
4	Ascent Temperature History	5-5
5	Ascent Local Static Pressure History	5-6
6	Entry Trajectory	5-7
7	Entry Temperature History	5-7
8	Maximum Entry Temperature Isotherms	5-8
9	Entry Total Heat Distribution	5-9
10	Entry Local Static Pressure History	5-10
11	Ascent Design Pressures	5-11
12	Entry Design Pressure History	5-12
13	Ultimate Longitudinal Fuselage Design Loads	5-13
14	Transmission Loss at VHF and UHF	6-10
15	Transmission Loss at S- and C-Band Frequencies	6-10
16	Transmission Loss at Ku-Band Frequencies	6-11
17	Transmission Loss for Thick Bondlines at Ku-Band Frequencies	6-12
18	Transmission Loss for Alternate HRSI Material	6-12
19	Antenna Coordinate System	6-13
20	Ku-Band Reference Patterns	6-14
21	Ku-Band Patterns with Antenna Window and TPS	6-16
22	Ku-Band Patterns with Extended TPS	6-17
23	Ku-Band Patterns with Auxiliary Ground Plane	6-18
24	Ku-Band Antenna System Impedance	6-19
25	One-Dimensional Antenna System Thermal Models	6-31
26	One-Dimensional TPS Thermal Model	6-31
27	LI-1500 HRSI Requirements	6-32
28	LI-900 HRSI Requirements	6-33
29	GE MOD 1A HRSI Requirements	6-34
30	Dynaquartz Insulation Requirements	6-35
31	Antennna Configurations	6-39
32	S-Band Antenna System Installation	6-41
33	Ku-Band Antenna Syste' Installation	6-45
34	VHF Antenna System Installation	6-47
35	L-Band Antenna System Installation	6-51
36	C-Band Horn Antenna System Installation	6-55
	C-Band Linear Slot Antenna System Installation	6-57
38	Alternate Antenna System Integration Concepts	6-60
39	Alternate S-Band Antenna System Installation	6-61
40	Installation Concepts for Alternate TPS Configurations	6-64
41	L-Band Antenna System Installation - Multiple-Layer Window	6-65
42	Honeycomb Panel Design Parameters	6-68
43	Finite Element Structural Model	6-69
44	Structural Load Redistribution	6-70
45	S-Band Antenna (Amecom #46325)	7-2
46	Design Test Configuration	7-3

47 Radiation Patterns Test Set-Up Block Diagram. 7-4
48 Radiation Pattern Recording and Control Console 7-4
49 Impedance Test Set-Up Block Diagram 7-5
50 Conversion from Peak Linear to Circular Gain. 7-6
51 Effects of Extending Aperture Above Ground Plane (2.2875 GHz) . 7-7
52 Effects of Extending Aperture Above Ground Plane (2.2 GHz). . . 7-13
53 Effects of Extending Aperture Above Ground Plane (2.1 GHz). . . 7-15
54 Effects of Extending Aperture Above Ground Plane (1.75 GHz) . . 7-18
55 Effects of Extending Aperture Above Ground Plane (3.45 GHz) . . 7-21
56 Impedance - Aperture Flush with Ground Plane. 7-23
57 Impedance - Aperture 1.91 cm (0.75 in.) Above Ground Plane. . . 7-24
58 Impedance - Aperture 3.81 cm (1.50 in.) Above Ground Plane. . . 7-25
59 Effects of Antenna Tuning 7-26
60 Antenna Tuning Test Configuration with AN-75 Border 7-27
61 Effects of AN-75 Border on Ground Plane Edge Diffraction. . . . 7-27
62 Effects of Antenna Support Cavity Depth on Axial Ratio. 7-29
63 Radiation Patterns - S-Band Antenna System Mockup (S/N 101) . . 7-30
64 Impedance - S-Band Antenna System Mockup (S/N 101). 7-31
65 Transmission Loss 7-31
66 S-Band Antenna System 7-32
67 S-Band Antenna. 7-33
68 Antenna Support 7-33
69 Antenna Window and Panel Assembly 7-35
70 LI-1500 Tile Configurations 7-39
71 FI-600 Filler Strips. 7-41
72 Strain Isolator Pads. 7-41
73 Panel Support Assembly. 7-44
74 S-Band Antenna System Test Assembly 7-45
75 S-Band Antenna System/Channel Nozzle Test Configuration 7-48
76 S-Band Antenna System/Wedge Mount Test Configuration. 7-49
77 Test Container Assembly 7-51
78 Water Cooled Cover Assembly 7-53
79 Typical TPS Pull-Test Specimen. 7-55
80 S-Band Antenna System Thermal Model 7-57
81 Maximum Temperatures for Entry Heating. 7-58
82 Temperature Histories for Entry Heating 7-58
83 Maximum Temperatures for Entry Heating/Test Pressures 7-59
84 Maximum Temperatures for Breadboard Unit. 7-60
85 Maximum Temperatures for Prototype Unit 7-61
86 HRSI Thickness Versus Recess Diameter 7-62
87 S-Band Antenna System Block Diagram 7-64
88 HRSI Tile X-Rays. 8-2
89 Typical HRSI Tile Dimensions. 8-4
90 Breadboard Unit Antenna Window Components 8-5
91 Breadboard Unit Antenna Window and Guard Tiles. 8-6
92 Breadboard Panel Assembly in Bonding Fixture. 8-8
93 Breadboard Unit Assembly. 8-10
94 Skin Penetration Seals. 8-11
95 Prototype Unit No. 1 Assembly 8-12
96 Radiation Patterns - Antenna S/N 101. 9-2
97 Effect of Mounting Configuration on Axial Ratio 9-4
98 Impedance - Antenna S/N 101 9-5

99 Impedance - Antenna S/N 102 9-6
100 Impedance - Antenna S/N 105 9-6
101 S-Band Antenna System Test Configuration. 9-8
102 Swept Frequency Impedance Measurement Test Set-Up 9-9
103 Breadboard Unit Radiation Patterns. 9-10
104 Breadboard Unit Impedance 9-13
105 Prototype Unit No. 1 Radiation Patterns 9-14
106 Prototype Unit No. 1 Impedance. 9-17
107 Radiation Pattern Test Configuration at NASA-JSC. 9-18
108 Breadboard Unit Radiation Patterns - Effects of High Temperature. 9-19
109 Breadboard Unit Impedance - Effects of High Temperatures. . . . 9-22
110 Breadboard Unit Radiation Patterns - Postthermal Test 9-23
111 Breadboard Unit Impedance - Postthermal Test. 9-26
112 Prototype Unit No. 1 Radiation Patterns - Effects of High Temperature Cycling. 9-27
113 Prototype Unit No. 1 Impedance - Effects of High Temperature Cycling. 9-31
114 Prototype Unit No. 1 Radiation Patterns - Postthermal Reuse Test. 9-32
115 Prototype Unit No. 1 Impedance - Postthermal Reuse Test 9-35
116 NASA-JSC 10 Megawatt ARMSEF ARC Tunnel. 10-2
117 Test Components 10-3
118 Test Installation - Side View Through Calibration Port. 10-4
119 Test Installation - End View. 10-4
120 Test Installation - Back View 10-5
121 Entry and Test Heating Conditions 10-6
122 Entry and Test Pressure Conditions. 10-6
123 Entry and Test Flow Parameters. 10-7
124 Breadboard Data Track 10-8
125 Prototype Data Track. 10-8
126 Breadboard Thermocouple Locations 10-10
127 Breadboard Plan View X-Ray. 10-11
128 Breadboard Side View X-Rays 10-12
129 Gap (Downstream End), Filler Strip and Skin (Test B-1). 10-13
130 Antenna Window Joint (Test B-1) 10-13
131 Breadboard Test Control Parameters. 10-15
132 Antenna Window Surface (Test B-2) 10-15
133 Indepth Survey - TPS HRSI (Test B-3). 10-16
134 Indepth Survey - Antenna Window HRSI (Test B-3) 10-16
135 Antenna Window and Backcap (Test B-3) 10-17
136 Antenna Window Surface (Test B-3) 10-17
137 Skin Structure and Antenna Backcap and Support (Test B-3) . . . 10-18
138 Skin Structure (Test B-3) 10-18
139 Antenna Window Joint (Test B-3) 10-19
140 Gap (Downstream End), Filler Strip and Skin (Test B-3). 10-19
141 Antenna Test Unit Surface - Axial (Test B-3). 10-20
142 Antenna Test Unit Surface - Transverse (Test B-3) 10-20
143 Antenna Backcap and Test Container Assembly (Test B-3). 10-21
144 Local Static Pressures - Calibration Plate (Test B-3) 10-21
145 Pitot Pressure - Nozzle Exit (Test B-3) 10-22

146 Heating Rate - Calibration Plate Water Cooled Calorimeter (Test B-3). 10-22
147 Heating Rates - Calibration Plate HRS 1 thru 6 (Test B-3) . . . 10-23
148 Heating Rates - Calibration Plate HRS 7 thru 12 (Test B-3). . . 10-23
149 Prototype Installation - Back View. 10-25
150 Prototype Thermocouple locations. 10-26
151 Prototype Plan View X-Ray 10-27
152 Calibration Plate Map 10-28
153 Filler Strip Top, Bottom, Skin - Upstream Position (Test P-1) . 10-29
154 Filler Strip Top, Bottom, Skin - Downstream Position (Test P-1) 10-29
155 Filler Strip Top, Bottom, Skin - Downstream Position (Test P-4) 10-31
156 Prototype Test Control Parameters 10-32
157 Antenna Test Unit Surface - Axial (Test P-10) 10-33
158 Forward Tile Surface, Bondline, Skin (Test P-10). 10-33
159 Aft Tile Surface, Bondline, Skin (Test P-10). 10-34
160 Filler Strip Top, Bottom, Skin - Downstream Position (Test P-10) 10-34
161 Filler Strip Top, Bottom, Skin - Upstream Position (Test P-10). 10-35
162 Skin Near Window Attachment Nuts (Test P-10). 10-35
163 Skin Structure (Test P-10). 10-36
164 Skin Structure and Antenna Backcap and Support (Test P-10). . . 10-36
165 Antenna Backcap and Test Container Assembly (Test P-10) 10-37
166 Heating Rate - Calibration Plate Water Cooled Calorimeter (Test P-10) 10-37
167 Heating Rates - Calibration Plate HRS 1 Thru 5 (Test P-10). . . 10-38
168 Heating Rates - Calibration Plate HRS 6 Thru 9 (Test P-10). . . 10-38
169 Heating Rates - Calibration Plate HRS 10 Thru 13 (Test P-10). . 10-39
170 Typical Effects of Thermocouple Lead Routing on Breadboard Unit Radiation Patterns. 11-5
171 Effect of High Temperature on Radiation Patterns - Prototype Unit. 11-7
172 Test and Entry Surface Temperatures 11-11
173 Test and Entry HRSI Bondline Temperatures 11-11
174 Maximum Measured Temperatures of S-Band Antenna System Test Models 11-13
175 Effect of Repeated Thermal Cycles on Bondline Temperature Rise. 11-13
176 LI-1500 Thermal Conductivity Verification 11-14
177 Double Peak Temperature Response - Prototype (Test P-1) 11-15
178 FI-600 Filler Strip Surface Temperature Behavior on First Test. 11-16
179 Correlation of HRSI Antenna Window Temperatures (Test B-2). . . 11-17
180 Peak Temperature Distribution of HRSI Over Honeycomb Panel (Test B-2). 11-17
181 Breadboard Temperature Correlation (Test B-2) 11-18
182 Prototype Temperature Correlation (Test P-10) 11-18
183 Breadboard Unit Surface 11-20
184 Prototype Unit Surface. 11-21
185 High Temperature Effect on Antenna Window - Breadboard Unit . . 11-22
186 Plasma Flow Effect on Attachment Hole 11-23
187 Gap Measurement Results for Breadboard Unit 11-24
188 High Temperature Effects on Filler Strip - Breadboard Unit. . . 11-25
189 Filler Strip Closeup - Guard Tile 11-26

190 Coating Crack Pattern on Breadboard Unit. 11-27
191 Coating Crack Pattern Sequence on Prototype Unit. 11-29
192 Radiation Patterns - Antenna S/N 102. . . . . E-1
193 Radiation Patterns - Antenna S/N 105. . . . . E-2
194 Radiation Patterns - Prototype Unit No. 2 . . . . . F-1
195 Impedance - Prototype Unit No. 2. . . . . F-4

LIST OF TABLES

I	Orbiter Antenna System Requirements	5-2
II	Maximum Ultimate Design Pressures	5-12
III	Ultimate Design Loads	5-14
IV	Antenna Performance Requirements	6-2
V	Candidate Antennas	6-4
VI	Antenna Window Configurations	6-9
VII	Antenna Window/Thermal Protection System Materials Properties	6-21
VIII	High Density Antenna Window Material Properties	6-23
IX	Auxiliary Antenna Window Materials	6-25
X	HRSI Electrical Properties	6-26
XI	Thermal Properties of Organic Materials	6-28
XII	One-Dimensional Thermal Insulation Sizing Results	6-36
XIII	VHF Antenna System Integration Concepts	6-59
XIV	S-Band Antenna System Electrical Performance Goals	7-2
XV	Design Test Circular Gains and Axial Ratios	7-17
XVI	Quantitative Reliability Evaluation	7-65
XVII	Breadboard Unit Axial Ratios - Effects of High Temperature	9-21
XVIII	Prototype Unit No. 1 Axial Ratios - Effects of High Temperature Cycling	9-31
XIX	Component Test Axial Ratios	11-2
XX	Component Test Circular Gains	11-2
XXI	Design Goal and Measured Antenna Parameters	11-2
XXII	Breadboard Unit Axial Ratios and Peak Linear Gains	11-3
XXIII	Design Goal and Measured Prototype Unit Performance Parameters	11-6
XXIV	Prototype Unit No. 1 Gain and Axial Ratio Comparisons	11-9
XXV	Average Peak Surface Temperatures	11-14
XXVI	LI-1500 Thermal Properties	A-1
XXVII	FI-600 Thermal Properties	A-1
XXVIII	RL-524 Type S-105 Thermal Properties	A-2
XXIX	Mechanical Properties	A-2

SUMMARY

Design concepts for high temperature flush mounted Space Shuttle Orbiter antenna systems are discussed. The design concepts include antenna systems for VHF communications, L-band TACAN and air traffic control, S-band communications, C-band radar altimeter, and C- and Ku-band microwave landing systems. The S-band antenna system design was completed and test hardware fabricated. This hardware was then subjected to electrical and thermal testing. A breadboard unit was fabricated for preliminary tests and the results used to complete the design of a prototype unit which was subjected to multiple electrical and thermal tests to determine the reuse capability of the antenna system design. In the thermal tests, heat was applied to the test unit surface in an arc tunnel plasma facility, which simulated the Orbiter thermal environment, and the temperature distributions measured. Radiation pattern and impedance measurements were used to evaluate the antenna systems performance.

The design approach was based on combining an RF window, which provides thermal protection, with a conventional antenna. The antenna window design was based on using the Orbiter thermal protection system insulation as the basic window material. Window design concepts were considered which can accommodate alternate thermal protection insulation materials or other high temperature dielectric materials.

Each of the antenna system designs were integrated into the Orbiter structure. Maximum accessibility and minimum impact on the surrounding structure and thermal protection system were stressed. The structural integration studies were supported by thermal and strength analyses. Layout drawings are given for each of the antenna systems.

The S-band antenna system design was supported by a detailed thermal and strength analyses as required. A detailed thermal model was prepared to predict temperatures throughout the antenna system for establishing design parameters and comparison with test results.

The results of the electrical and thermal tests are given to demonstrate the reuse capability of the S-band antenna system and validity of the design concept. The test data shows that the change in electrical performance was negligible. Measured temperatures are in excellent agreement with predicted temperatures when actual test conditions are used in the thermal calculation. The test model was also in excellent physical condition after completion of ten entry cycles.

THIS PAGE INTENTIONALLY LEFT BLANK

CONCLUSIONS

A number of conclusions can be reached from the results of tests and analyses performed during this study. They are:

(a) Practical antenna systems consisting of conventional antennas thermally protected by RF windows can be designed for Space Shuttle Orbiter application.

(b) The conventional antennas may well be off-the-shelf, low cost airplane hardware with or without modification.

(c) The configuration of these designs is flexible, and dependent to a considerable degree upon the maintenance accessibility desired.

(d) The antenna windows can be fabricated using standard HRSI tile sizes in most cases.

(e) The electrical and thermal test results verify the validity of the design approach and establish the credibility of thermal reuse.

(f) The high temperature entry environment has negligible effect on the electrical performance of the antenna system, either during or after high temperature exposure.

(g) The thermal prediction techniques used for this study provide an effective design tool to pre-evaluate production designs.

(h) The antenna window attachment holes used did not result in a significant increase in structural temperature.

(i) The LI-1500 material characterization appears to be accurate.

(j) The electrical characteristics of LI-900 are slightly better than LI-1500.

(k) The basic test results are applicable to LI-900 as well as LI-1500.

(l) The major hazard to the HRSI tiles appears to be handling because the waterproof coating is fragile.

(m) The LI-1500 tile fabrication techniques need development to control shrinkage during firing of the waterproof coating.

(n) The waterproof coating appears to become more brittle and may develop microcracks with continued high temperature cycling.

(o) The waterproofing silicone burns off the outer portion of the LI-1500 during the initial entry cycle and can continue to burn off additional silicone which is wicked up during succeeding cycles.

(p) The repair coating (emittance coating only) appears to be durable.

(q) The emittance coating on the FI-600 filler strip is fragile.

(r) The FI-600 Filler strip requires delicate handling to prevent damage or loss of material during installation.

RECOMMENDATIONS

The work during this study leads to the following recommendations to complete the development of the design approach:

(a) The S-band antenna system should be subjected to orbital cold soak followed by entry heating to establish total mission capability. This can be accomplished in a vacuum chamber using both radiating cooling and heating (graphite heater), and will provide the data comparing the arc tunnel plasma facility and the graphite radiant heater as test tools. Once correlated, the graphite heater is much less expensive to apply for further antenna thermal development work, and can accommodate larger area test specimens of particular significance at UHF.

(b) One or more of each of the aircraft off-the-shelf antenna candidates should be subjected to orbital cold soak followed by entry heating to maximum temperature predicted for the antenna (i.e. essentially Orbiter aluminum skin temperatures). This is necessary to determine if antenna hardware already developed and of low unit cost is capable of withstanding a cold space environment, or if practical modifications will enable these and similar units to survive the Shuttle space environment.

(c) One or more of the candidate aircraft antenna system designs should be fabricated and subjected to preliminary Orbiter launch environmental tests, specifically mechanical and acoustical vibration. Other than orbital cold soak and entry heating, these are considered the most hostile environments to be accommodated.

THIS PAGE INTENTIONALLY LEFT BLANK

INTRODUCTION

The purpose of this program was to develop an antenna design approach having generic application to the baseline flush mounted high temperature antenna systems for the Space Shuttle Orbiter. The objectives were to: (1) prepare preliminary design concepts for each unique Orbiter antenna system; (2) prepare a detailed design of an S-band antenna system, which employs materials and design features most common to all the Orbiter antenna systems, using Lockheed's LI-1500 insulation as the baseline thermal protection system; (3) fabricate one breadboard S-band antenna system for preliminary electrical and thermal tests and two prototype S-band antenna systems for electrical and thermal reuse tests; (4) perform electrical tests to establish performance levels and evaluate the effects of exposure to entry heating; (5) perform thermal tests which subject the antenna systems to predicted Orbiter entry temperatures to aid in the antenna system design and determine reuse capabilities; and (6) evaluate the test results relative to the objective goals. This study extends and builds upon the results obtained under NASA contract NAS 9-11273 performed for the Langley Research Center.

The design approach is based on the use of conventional antennas thermally protected by an RF transparent window. In some cases off-the-shelf antenna may be adequate, and in others minor design modifications may be required to obtain optimum performance. Although most of the antenna system designs are based on specific antenna hardware, minor dimensional changes can be made to easily accommodate an alternate unit. The thermal, strength and structural requirements were determined at chosen nominal antenna locations on the underside of the Orbiter. Throughout this report, the term "antenna system" means the combination of antenna, antenna window and the immediate structural items designed to integrate the antenna and window into the structure.

The requirements for the McDonnell Douglas Corporation (MDC) Orbiter (as proposed for the Space Shuttle prime contract competition) were used for this study. These requirements are not unique to the MDC Orbiter design; thus the results of this study may be applied directly to the Rockwell Orbiter design with only minor modification in certain design details. During this study the VHF antenna system design was redirected to reflect Rockwell's baseline VHF antenna requirement for a circularly polarized antenna 76.2 (30.0 in.) in diameter.

The antenna window design approach is based on using the same insulation as used in the Orbiter thermal protection system for the principal antenna window material. Lockheed's LI-1500 was specified as the baseline thermal protection insulation for this study. Alternate window design concepts were also considered which can accommodate other thermal protection insulation or high temperature dielectric materials.

After establishing the basic design concepts under the Task 1.1 Concept and Feasibility Studies, Task 1.2 S-band Antenna System Design was initiated making use of the design features most common to all the flush mounted Orbiter antennas. Electrical tests established the optimum performance configuration,

after which this configuration was integrated into the simulated Orbiter structure. The structural design efforts were supported by thermal and strength analyses to ensure the integrity of local thermal protection system and structural strength. The results of Task 1.2 provided the drawings for Task 2 Test Hardware Fabrication. Electrical and Thermal Testing then followed as Tasks 3 and 4, with the results assessed in the Task 5 Evaluation.

The test results demonstrate the validity and reuse capability of the basic design concept. Changes in electrical performance after high temperature exposure and cycling were negligible. Comparison of measured and predicted temperature show that thermal models can provide a means for accurately predicting temperatures throughout an antenna system. Physical examination shows the test model to be in excellent shape after completion of ten entry cycles.

Mr. E. A. Kuhlman, Study Manager, was responsible for overall technical direction of this study. Other members of the McDonnell Douglas Astronautics Company - East (MDAC-E) engineering staff who contributed to this study are J. C. Blome, Wm. K. Gamble, V. M. Gerler, B. M. Kavanaugh, J. B. Magyar, J. C. Reeder, J. M. Romberg, and R. F. Sorensen. Test hardware fabrication was supervised by E. F. Disser and B. J. Myers. Messrs. B. M. Kavanuagh and R. F. Sorensen conducted and evaluated the thermal and electrical tests at NASA-JSC.

Mr. J. S. Kelley of the Antenna System Section of the Telemetry and Communications Systems Division, Lyndon B. Johnson Space Center, Houston, Texas, was the NASA Technical Monitor for this study.

The units used for the physical quantities defined in this report are given in both the International System of Units (SI) and the U. S. customary units in the text. U. S. customary units are used in the drawings and in some of the graphs and tables.

This report is designated as Volume I in anticipation of additional work related to this contract which will be reported in a subsequent volume.

The task numbers used in the text correspond to the tasks given in the Program Plan, Report No. MDC E0663, dated 15 August 1973.

DESIGN CONSIDERATIONS AND CONSTRAINTS

This section defines the Space Shuttle Orbiter antenna requirements and the Orbiter structural, thermal, and strength considerations and constraints used in antenna designs developed during this study. They are based on the requirements determined during the MDAC-E Space Shuttle Phase 3 and proposal studies. Although some changes in the Orbiter equipment and configuration have occurred since the beginning of this study, the requirements used for this study are still representative and, therefore, the study results are applicable to current design activities.

Antenna Requirements

The Orbiter antenna system requirements are summarized in table I. Although these antenna types and/or location are subject to change as the Shuttle program progresses, there is sufficient variety to provide a range of design features having wide applicability. The antenna types were determined by radiation pattern and frequency requirements of the respective avionics system functions. The interpretation of how best to satisfy these requirements may also influence a particular selection. It may be noted that many of the Orbiter avionics systems are like those used on commercial and military airplanes rather than entry vehicles and are used when the Orbiter is in an aeroflight mode. Consequently, most of the high temperature antennas developed for entry vehicles are not directly applicable to the Orbiter avionics systems. Further, these antennas were designed for "one shot" operation and, therefore, will not, in general, meet the Space Shuttle requirements for reuse.

Figure 1 shows the locations for each of the Orbiter antennas. They were selected to obtain the best radiation patterns from the particular antenna type. These locations may not always be ideal, since other Orbiter equipment requirements as landing gear location, for example, may preempt the use of a more preferred location. The respective locations also provide the basis for determining the structural, thermal and strength requirements applicable to the antenna system installation designs.

Structural Requirements

The Orbiter structural configuration consists of an all aluminum, semimonocoque, stiffened skin structure covered with a reusable surface insulation (RSI) which serves as the thermal protection system (TPS). A rigid, low density insulation is used for a high temperature RSI (HRSI) and an elastomeric ablator is used for a low temperature RSI (LRSI). The LRSI is used in areas where the radiation equilibrium surface temperature is less than 616 K (650°F) and serves as an insulator rather than an ablator.

TABLE I

ORBITER ANTENNA SYSTEM REQUIREMENTS

ANTENNA	FREQUENCY RANGE		VSWR (MAXIMUM)	RF POWER (ESTIMATE)	PATTERN (COVERAGE)	GAIN	POLARIZATION	ANTENNA TYPE SELECTED	LOCATION	OPERATIONAL USE
	TRANSMIT (MHz)	RECEIVE (MHz)								
TACAN	1025–1087 1088–1150 (960–1220 TOTAL RANGE)	962–1024 1151–1213	2:1 TRANSMIT 5:1 RECEIVE	4 KW PK PULSE (WORST CASE)	OMNI-DIRECTIONAL IN PLANE OF AEROFLIGHT	OMNI TYPE	VERTICAL	ANNULAR SLOT	BOTTOM AND TOP CENTERLINE	PRE AND POST ENTRY
AIR TRAFFIC CONTROL TRANSPONDER	1090	1030	2:1 TRANSMIT 5:1 RECEIVE	4 KW PK PULSE (WORST CASE)	OMNI-DIRECTIONAL IN PLANE OF AEROFLIGHT	OMNI TYPE	VERTICAL	ANNULAR SLOT	BOTTOM AND TOP CENTERLINE	PRE AND POST ENTRY
RADAR ALTIMETER	4210–4390	4210–4390	1.3:1	10 WATT CW (WORST CASE)	PATTERN DIRECTED PERPENDICULAR TO PLANE OF AEROFLIGHT	11 dB	LINEAR	HORN	BOTTOM CENTERLINE	POST ENTRY
VHF COMMUNICATIONS	118–136 136–138 (BACKUP)	118–136 148–150 (BACKUP)	2:1 2:1	100 WATT CW (WORST CASE)	OMNI-DIRECTIONAL IN PLANE OF AEROFLIGHT	OMNI TYPE	VERTICAL	MODIFIED PARTIAL SLEEVE	BOTTOM AND TOP CENTERLINE, SIDES	PRE AND POST ENTRY
S BAND COMMUNICATIONS • USAF RENDEZVOUS • NASA RENDEZVOUS • USAF GROUND COMMUNICATIONS • NASA GROUND COMMUNICATIONS	1750–1850 2020–2120 2200–2300 2200–2300	2200–2300 2200–2300 1750–1850 2020–2120	1.5:1 TRANSMIT	20 WATT CW (WORST CASE)	3 ANTENNAS PROVIDE SPHERICAL COVERAGE	OMNI TYPE	RIGHT HAND CIRCULAR	CAVITY BACKED HELIX	BOTTOM AND TOP CENTERLINE, SIDES	PRE AND POST ENTRY
MICROWAVE LANDING SYSTEM (Ku BAND)	N/A	15400–15700	2.0:1 RECEIVE	RECEIVE ONLY	FORWARD DIRECTED	4 dB	VERTICAL	SURFACE WAVE SLOT	BOTTOM CENTERLINE	POST ENTRY
MICROWAVE LANDING SYSTEM (C BAND)	5000–5060	5068–5125 5130–5250		2 KW PK (WORST CASE)			VERTICAL	SLOT	BOTTOM CENTERLINE	POST ENTRY

NOTES 1 HIGH GAIN ANTENNA REQUIREMENTS NOT INCLUDED
2 VERTICAL AND HORIZONTAL POLARIZATION IS REFERENCED TO ORBITER AEROFLIGHT ATTITUDE

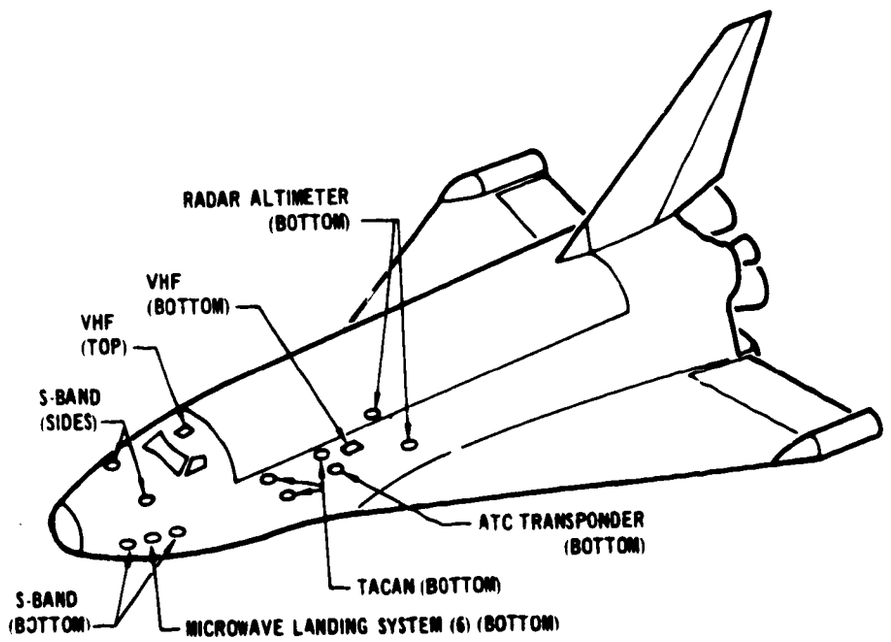

ORBITER ANTENNA LOCATIONS

FIGURE 1

A typical structural section through the bottom surface of the center fuselage where HRSI is used, is shown in figure 2(a). It consists of 0.51 mm (0.020 in.) thick aluminum skins riveted to fore and aft running stringers, attached between bulkheads. Stringer and bulkhead spacing are 10.16 cm (4.00 in.) and 50.80 cm (20.00 in.) respectively. The stringer thickness is nominally 0.813 mm (0.032 in.). A different structural approach considered for the forward fuselage section, which contains the pressurized cabin, is shown in figure 2(b). In this area an integrally stiffened aluminum pressure wall is submerged approximately 17.78 cm (7.00 in.) inside the aerodynamic moldline. Frame members and stiffened panels (e.g. honeycomb) are then used to support the TPS. Alternatively, honeycomb panels, appropriately attached to frames, may be considered in place of the skin-stringer arrangement.

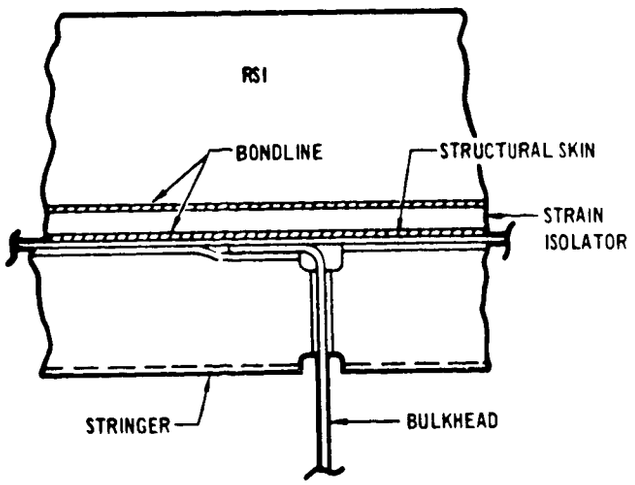

(a) CENTER FUSELAGE

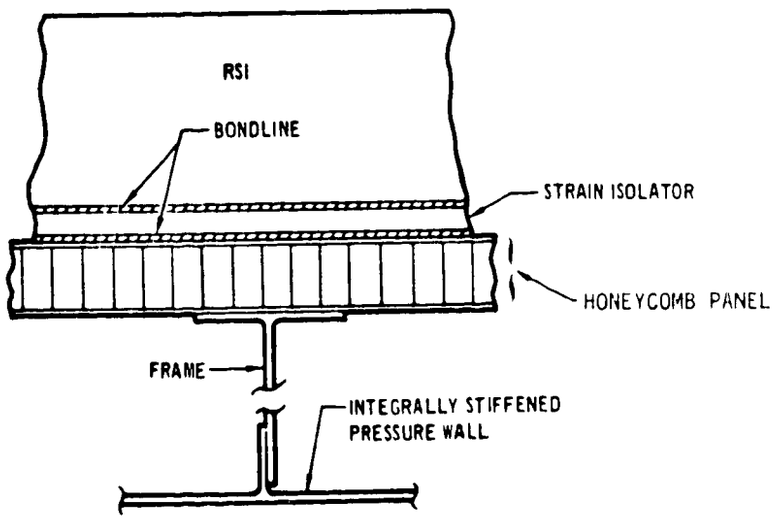

(b) STIFFENED HONEYCOMB STANDOFF PANEL (FORWARD FUSELAGE)

PRIMARY STRUCTURE/TPS CONCEPTS FIGURE 2

For all these approaches the HRSI, in the form of flat or contoured tiles, is bonded to the structural skin or to the support panel together with an intermediate silicone sponge. The thickness of the HRSI tiles vary as a function of the local heat input. In the lower fuselage, where antennas are located, the HRSI thickness is nominally 5.08 cm (2.00 in.). The HRSI tiles are covered with a thin inorganic oxide based coating to obtain a waterproof surface. The oxide pigment provides a high emittance surface in order to minimize surface temperature during entry heating.

The silicone sponge, 6.35 mm (0.250 in.) average thickness, is used as a mechanical strain isolator. This permits using buckling skins and protruding head rivets for the primary structure, thereby minimizing structural weight and fabrication costs. The silicone sponge and the HRSI tiles are bonded together and attached to the skin with RTV 560 adhesive. The adhesive layer between both the strain isolator and the HRSI tile, and the strain isolator and the skin is approximately 0.25 mm (0.010 in.) thick.

Although bonding was selected for attaching the HRSI tiles, other techniques have been considered. Mechanical fastener techniques for attaching either individual HRSI tiles or large panels of RSI tiles have been studied and tested by MDAC-E under contract to NASA-LaRC (NAS 9-12854) as an alternative TPS attachment technique.

Thermal Requirements

The thermal requirements for the Space Shuttle Orbiter antenna systems are influenced by the local TPS design and the local thermal environments. The thermal environments are principally surface temperature, heat input and pressure. The thermal conductivity of the HRSI material used in the TPS is a function of both the local pressure and temperature.

The local thermal environment is defined by the Orbiter missions, vehicle configuration and trajectories, and specific antenna locations. The most severe thermal environment results from Orbiter Mission 3, a single-orbit delivery or retrieval of an 18 000 kg (40 000 lb) payload. Characteristics of Mission 3 include a south polar launch, a 187 km (100 n. mi.) circular orbit and return to the Western Test Range.

The ascent trajectory for insertion into a 93 x 185 km (50 x 100 n. mi.) polar transfer orbit is shown in figure 3. At 185 km (100 n. mi.), the Orbit Maneuvering Subsystem (OMS) is used to circularize the orbit. The external surface temperature history for this ascent trajectory is shown in figure 4. Interference heating induced by the mated external tank is included. The local static surface pressure (at the edge of the boundary layer) for the ascent trajectory is shown in figure 5.

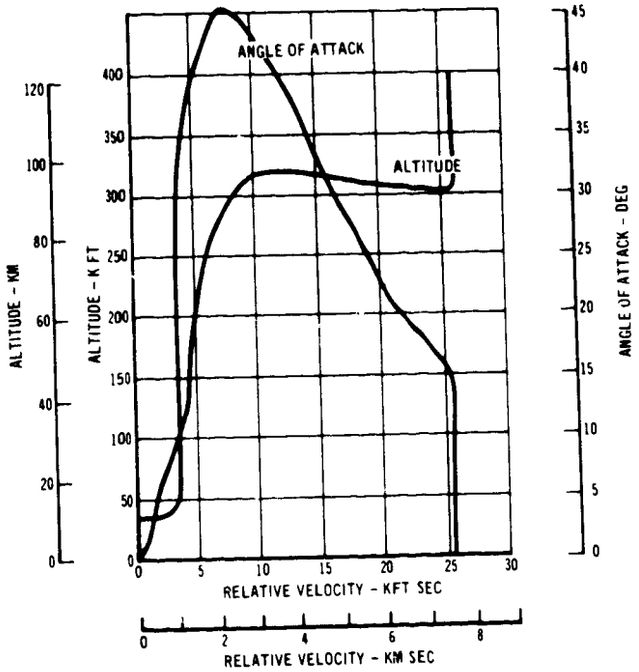

ASCENT TRAJECTORY

FIGURE 3

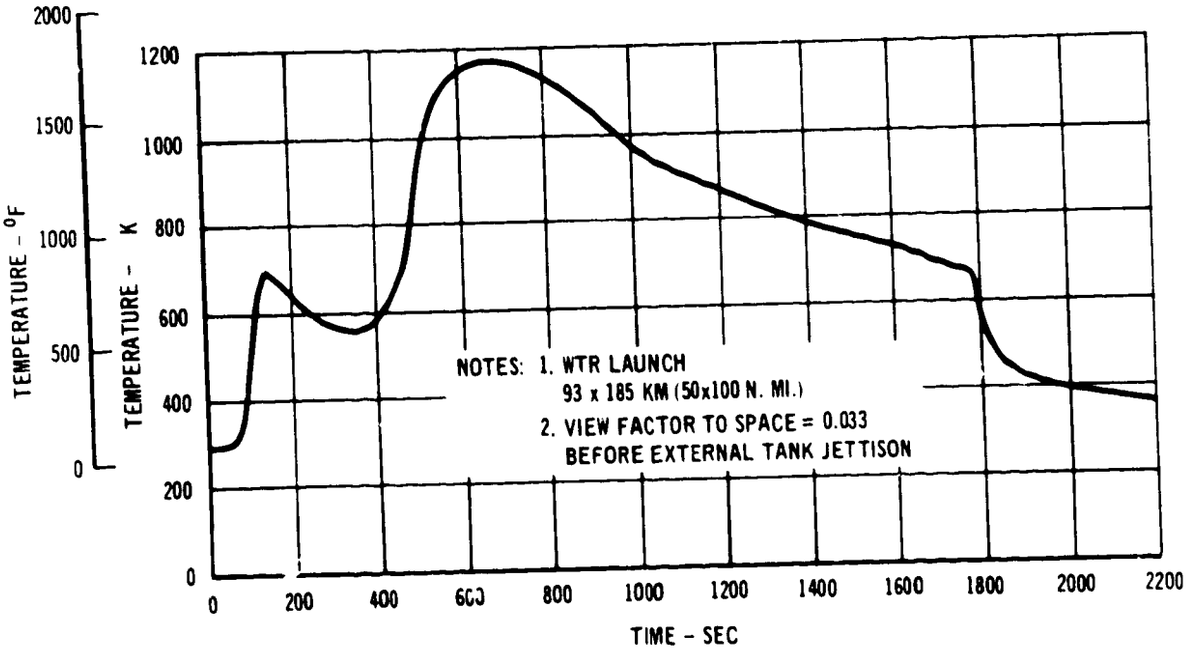

ASCENT TEMPERATURE HISTORY

FIGURE 4

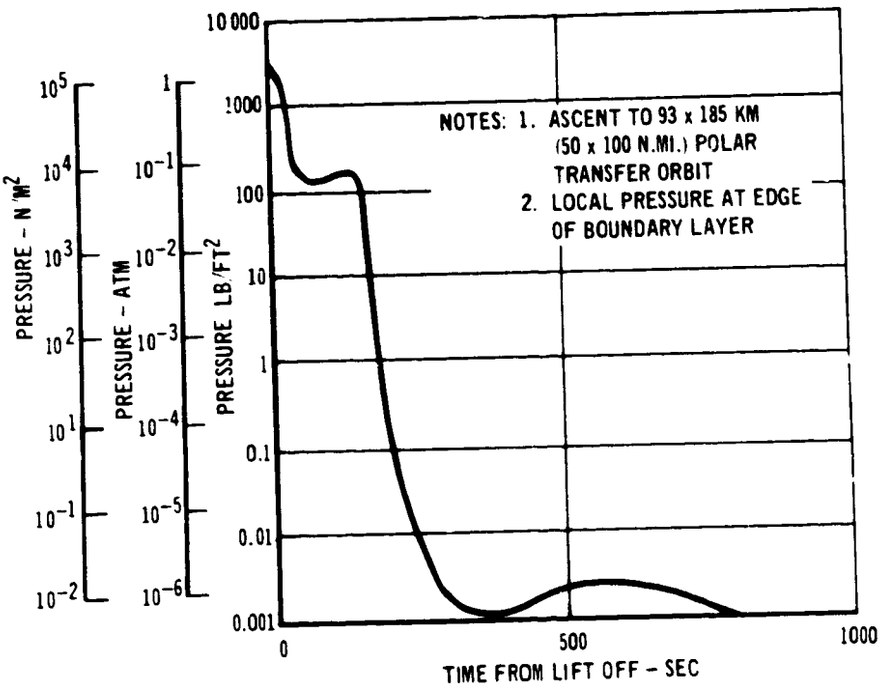

ASCENT LOCAL STATIC PRESSURE HISTORY

FIGURE 5

The entry trajectory is shown in figure 6. It causes more severe temperatures (figure 7) and total heat loads than the ascent trajectory. Trajectory shaping was used to minimize HRSI TPS thickness. This entry trajectory provides maximum cross range of 2037 km (1100 n. mi.) and maximum downrange maneuvering margin of 370 km (200 n. mi.). Downrange maneuvering is used to compensate for deorbit, atmosphere, guidance and navigation, and wind dispersions. A final approach and landing trajectory was added to the entry trajectory shown in figure 6. Maximum entry temperature isotherms are shown in figure 8. The entry total heat distribution is shown in figure 9. The local thermal environment for the rear L-band antenna was selected, since it has the most severe thermal environment of the antenna locations on the fuselage bottom. The rear L-band antenna is located off centerline within the 2.16×10^8 J/m^2 (19 000 Btu/ft^2) region on the fuselage bottom. An external surface temperature history for this location was used for all the antenna system designs. The local static surface pressures (at edge of local boundary layer) during entry are shown in figure 10.

Orbital environments employed were 0.37 albedo (reflectivity), a solar constant of 1395 W/m^2 (444 $Btu/hr\text{-}ft^2$) and an effective earth temperature of 252 K (-6°F). Surface free convection and sky radiation to 300 K (80°F) were used for the landed environment.

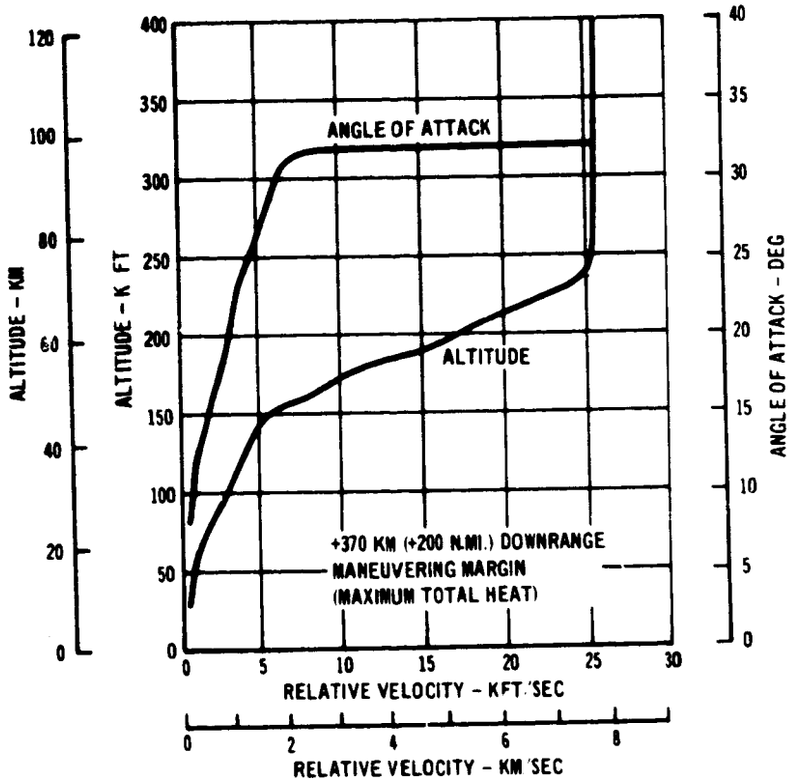

ENTRY TRAJECTORY

FIGURE 6

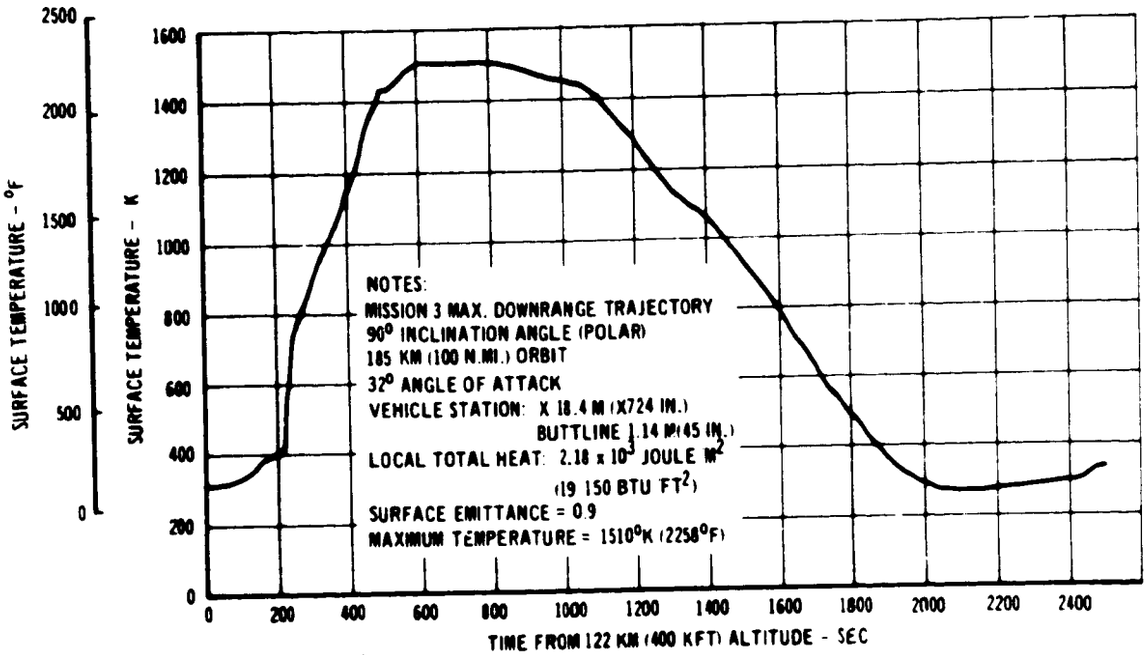

ENTRY TEMPERATURE HISTORY

FIGURE 7

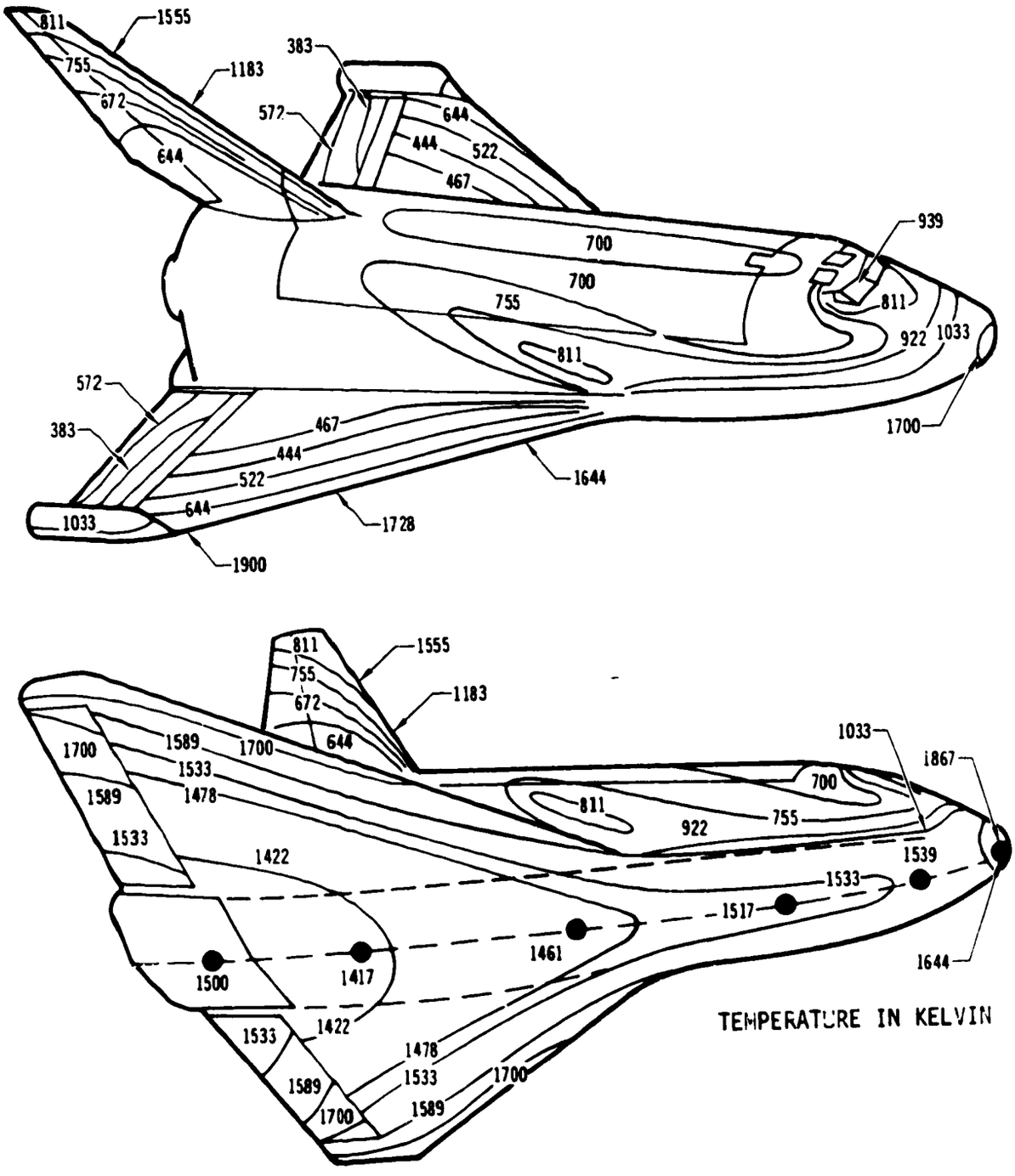

TEMPERATURE IN KELVIN

MAXIMUM ENTRY TEMPERATURE ISOTHERMS

FIGURE 8

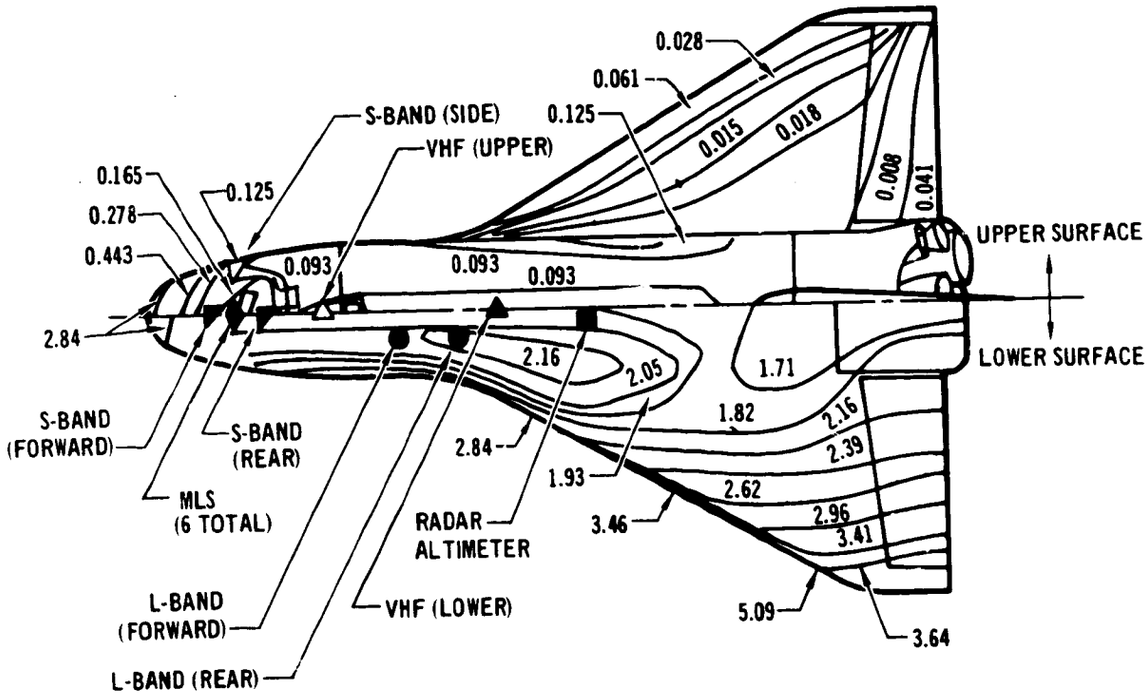

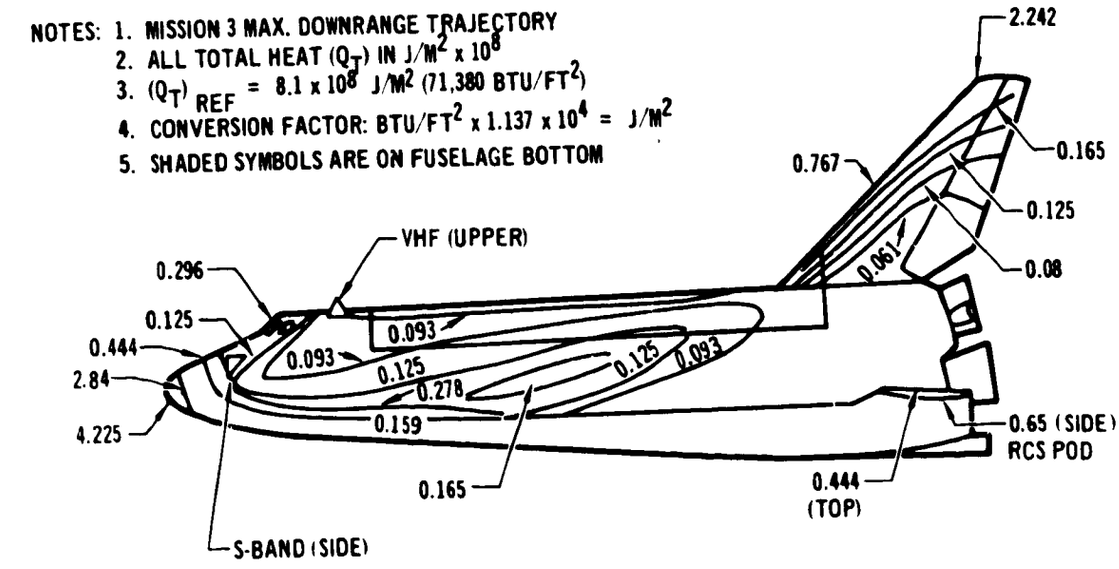

ENTRY TOTAL HEAT DISTRIBUTION

FIGURE 9

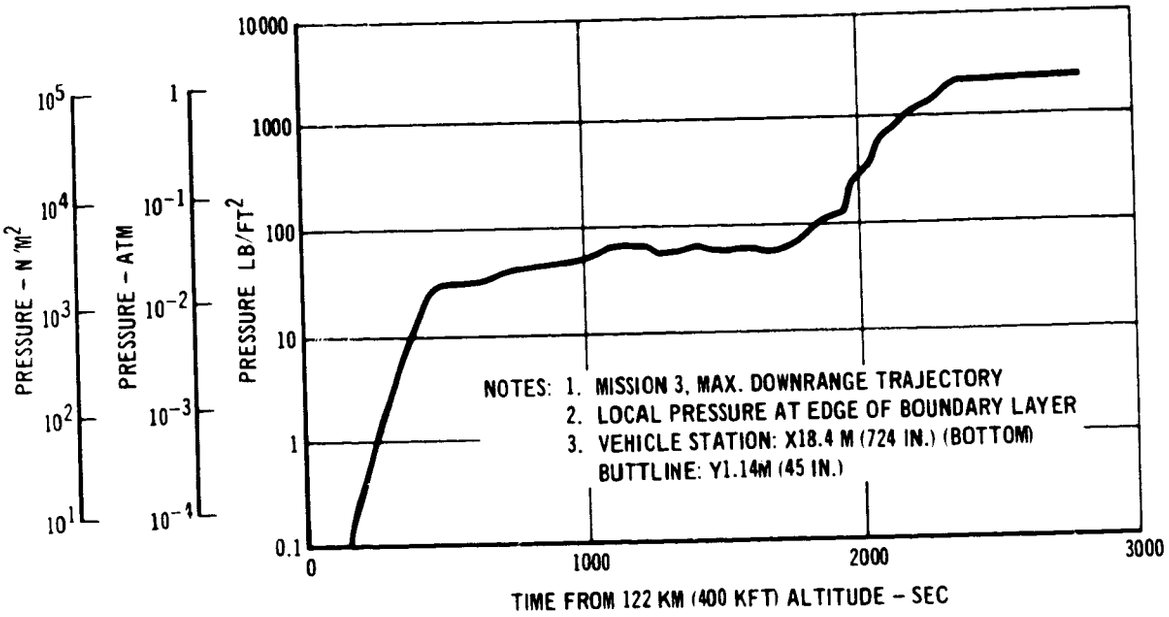

ENTRY LOCAL STATIC PRESSURE HISTORY FIGURE 10

Strength Requirements

The loads developed during the launch and entry phases of the Orbiter mission are of primary interest in determining the strength design criteria and requirements for the antenna system designs. The sources of these loads are differential pressures, fuselage bending and thermal gradients. It is important to use realistic design loads for this study because the thermal heat sink is a function of the structural material gages established using these design loads.

A minimum factor of safety of 1.4 was applied to the sum of the expected loads. This product is related to the combined mechanical and thermally induced loads to determine ultimate loads according to the expression given as follows:

$$K_1 L_e + K_2 L_t \geq 1.40\ (\Sigma_L)$$

where

K_1 = 1.4 for boost conditions when the term is additive to the algebraic sum, Σ_L

K_1 = 1.5 for entry, atmospheric cruise, and landing when the term is additive to the algebraic sum, Σ_L

K_2 = 1.5 when the term is additive to the algebraic sum, Σ_L

L_e = mechanical externally applied loads

L_t = thermally induced loads

Σ_L = algebraic sum of loads

Design pressures for ascent and entry are shown in figures 11 and 12. The maximum ultimate pressures were used for design to ensure that the antennas will be structurally adequate for installation at any fuselage location and are summarized in table II. The entry pressure was assumed to act at maximum thermal gradient and/or structural temperature.

Ultimate tensile and compressive design loads for fuselage structure resulting from Solid Rocket Motor (SRM) burn out and landing are shown in figure 13 for various locations on the Shuttle. The ultimate loads chosen for antenna system installation design are given in table III. These are representative of loads on the bottom surface of the Shuttle in the region of antenna locations and occur at low temperature ($\leq$ 450 K (350°F)).

Pressure loads, Post SRM Burn Out and Main Gear Landing loads are conditions which do not peak simultaneously, occurring respectively during ascent and landing. Material properties were either taken from MIL-Handbook-5B or are shown in Appendix A.

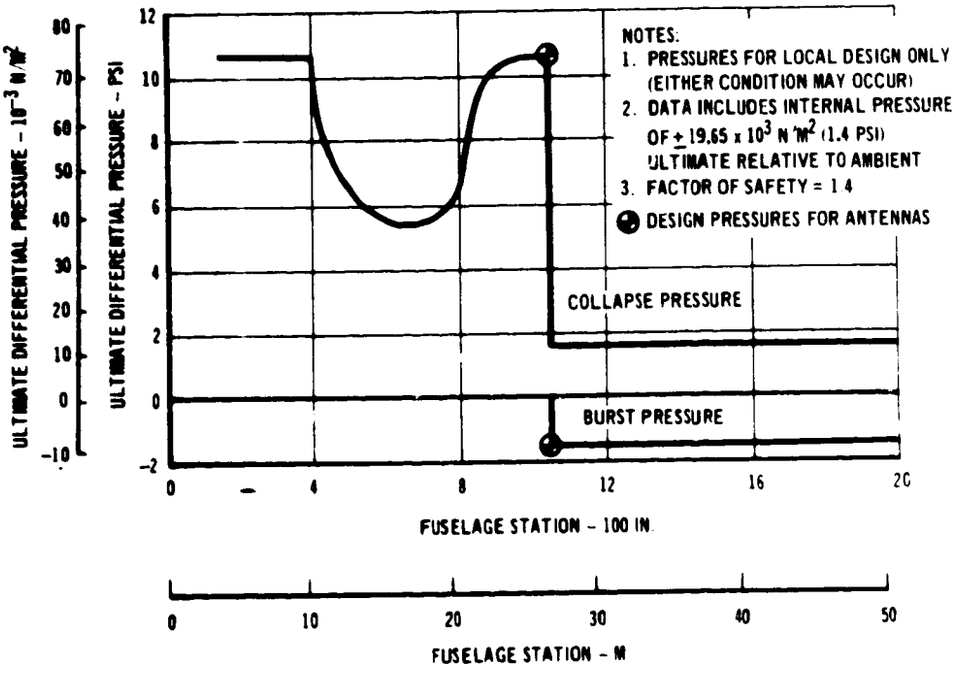

ASCENT DESIGN PRESSURES

FIGURE 11

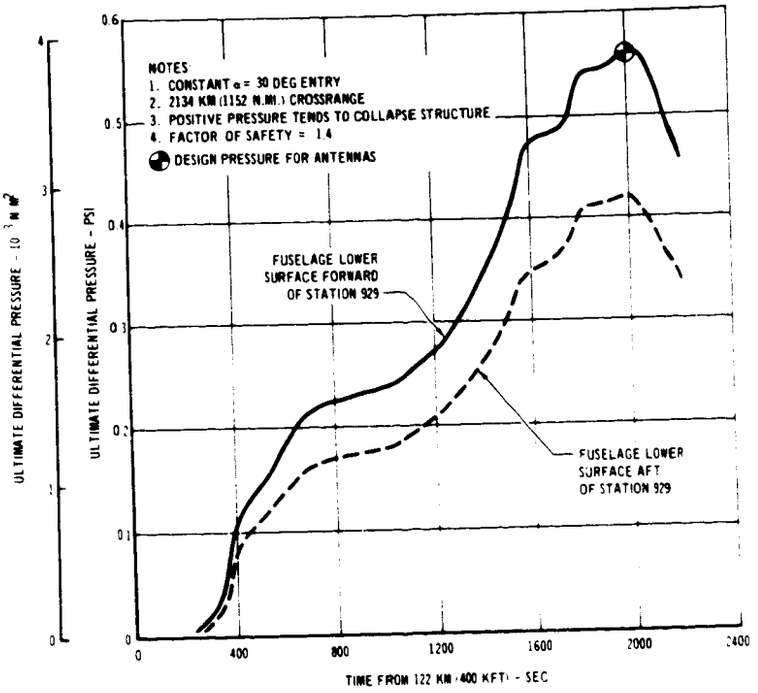

ENTRY DESIGN PRESSURE HISTORY

FIGURE 12

TABLE II

MAXIMUM ULTIMATE DESIGN PRESSURES

MISSION PHASE	PRESSURE N/M^2(PSI)	TYPE	FACTOR OF SAFETY
ASCENT	73 085 (10.6)	COLLAPSE	1.4
ASCENT	9653 (1.40)	BURST	1.4
ENTRY	4137 (0.60)	COLLAPSE	1.5

TW – MAX αq (TAILWIND)
SW – MAX β q (SIDEWIND)
MAX N_X – MAX AXIAL LOAD FACTOR
PSB – POST SRM BURNOUT
MGL – MAIN GEAR LANDING

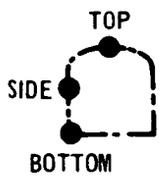

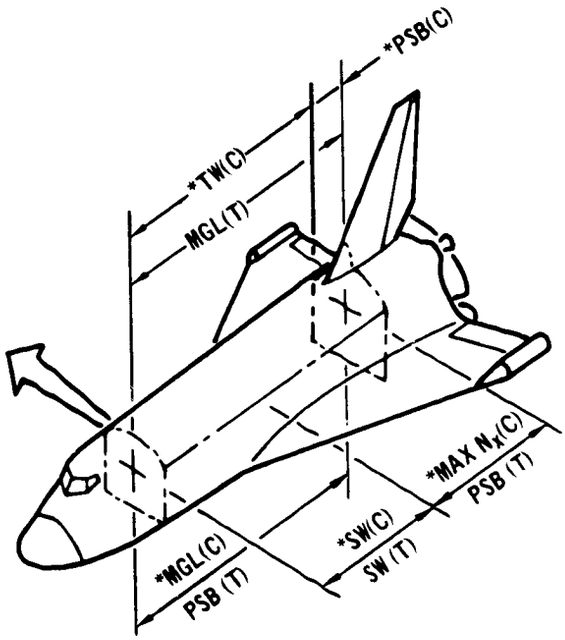

*CRITICAL DESIGN CONDITION
(T) = TENSION
(C) = COMPRESSION

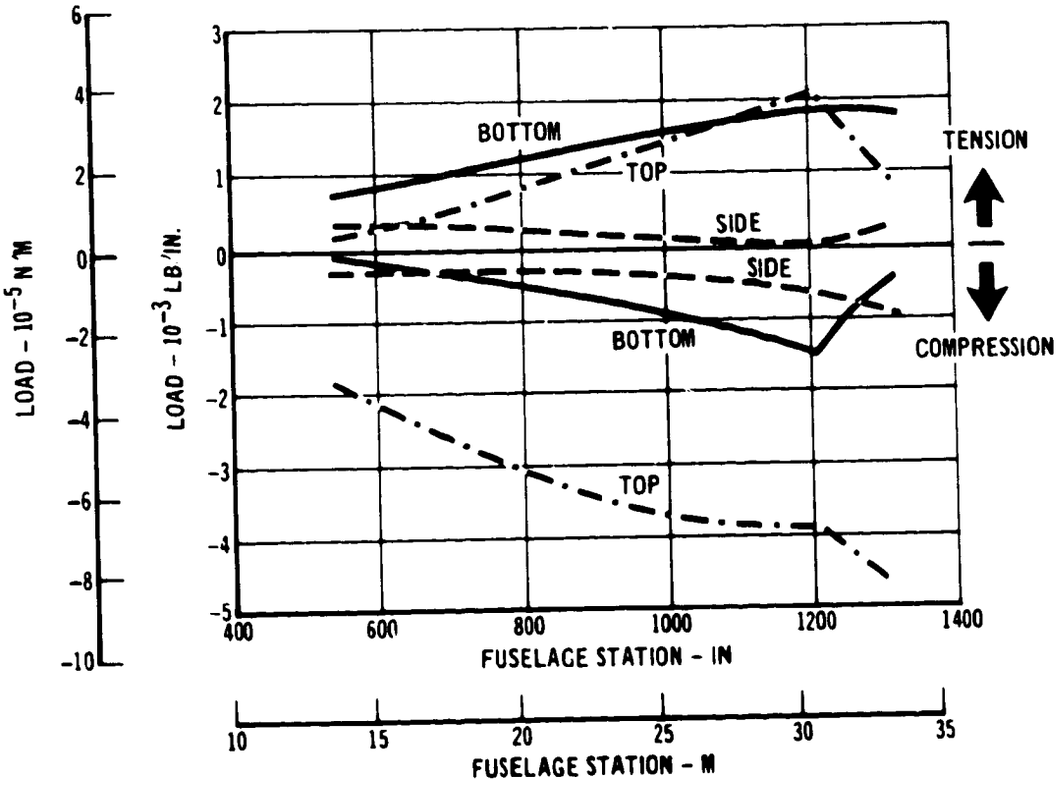

ULTIMATE LONGITUDINAL FUSELAGE DESIGN LOADS

FIGURE 13

TABLE III

ULTIMATE DESIGN LOADS

MISSION PHASE	LOADS N/M (LB./IN.)	TYPE	FACTOR OF SAFETY
POST SRM BURN OUT	175 000 (1000)	TENSION	1.4
MAIN GEAR LANDING	43 700 (400)	COMPRESSION	1.4

CONCEPT AND FEASIBILITY STUDIES

The objective of the Concept and Feasibility Studies (Task 1.1) was to study and prepare preliminary design concepts for each Space Shuttle Orbiter high temperature antenna installation. The designs are based on the requirements given in the section on DESIGN CONSIDERATIONS AND CONSTRAINTS. Alternate installation concepts and thermal protection systems materials were considered and assessed.

The design approach used was that of a window covering a low temperature conventional antenna, where the window provides both thermal protection for the antenna and a means for transmitting RF energy through the thermal protection system. The designs developed for the L-band annular slot, C-band horn, and C-band linear slot antennas under NASA contract, NAS1-11273, were based on this approach and provided the basis for the detailed designs developed in this study. Since this study did not uncover any new data which indicated that design or design approach revisions were desirable, primary effort was directed toward the S-band, Ku-band, and VHF antenna installation concepts.

The alternate approaches developed are primarily variations in assembly and mounting, while the electrical and thermal configurations are essentially unchanged. The use of alternate high temperature reusable surface insulation (HRSI) materials for the antenna window and/or the Orbiter thermal protection system (TPS) was also considered. The use of HRSI, identical or similar to that used for the Orbiter TPS, for the antenna window material provides the simplest and most direct approach. Alternate approaches for providing a window over an antenna result in increased complexity and weight. An example is the multiple-layer window design apporach (ref. 1) developed during the NASA-LaRC high temperature antenna study (NAS1-11273).

Several factors cause the increase in complexity and weight:

(a) The materials other than HRSI considered for antenna windows (e.g., boron nitride, slip cast fused silica) are considerably more dense (approximately eight times greater) and have higher thermal conductivities. Therefore, thicker windows would be required or a second low density insulation material used with the high density material to maintain both acceptable window thickness and weight.

(b) The high density window materials and the low density insulation material cannot be readily bonded with RTV 560 or other adhesives. Therefore, a refractory metal retaining fixture (increased complexity) would be required to hold the window in place over the antenna.

(c) The metal retaining fixture provides a heat short from the TPS surface to the Orbiter structure. Therefore, a heat sink (increased weight) or other means would be required to maintain the proper heat transfer characteristics in the area around the antenna.

Electrical Studies

The electrical studies part of the concept and feasibility task included: (1) a survey of antenna suppliers to determine the status of candidate, conventional off-the-shelf antennas with regard to electrical characteristics and operating temperature capabilities to 422 K (300°F); (2) plane wave transmission loss as a function of frequency and window configuration; (3) a comparison of the plane wave transmission characteristic of alternate window materials; (4) limited electrical design tests for the Ku-band antenna; and (5) consideration of surface wave effects.

Antenna equipment survey. - Electrical and mechanical information on existing antennas, that best meet the requirements given in table IV, was requested from twelve antenna suppliers. The information requested included:

(a) electrical properties

(b) form factor

(c) thermal properties

(d) materials list

(e) structural capabilities

(f) venting method

(g) RF power

(h) altitude capabilities.

TABLE IV

ANTENNA PERFORMANCE REQUIREMENTS

FUNCTION	FREQUENCY	VSWR(Z_o=50Ω)	POLARIZATION	PATTERN	GAIN	BEAMWIDTH	POWER
S-BAND COMMUNICATION	1.75 - 2.3 GHz	≤ 1.5:1	RIGHT CIRCULAR		0 dB ABOVE ISOTROPIC	120°	20 WATTS CW, MAX
VHF COMMUNICATION	118 - 154 MHz	≤ 2.0:1	LINEAR	LIKE QUARTER WAVE STUB	>0 dB ABOVE ISOTROPIC OVER 90% OF VOLUME ABOVE GROUND PLANE		50 WATTS CW
TACAN/ATC	960 - 1220 MHz	≤ 2.0:1	LINEAR	LIKE QUARTER WAVE STUB	>3 dB DOWN FROM QUARTER-WAVE STUB IN HORIZONTAL PLANE		4 K WATTS PEAK AT 10^{-3} DUTY CYCLE
RADAR ALTIMETER	4.21 - 4.39 GHz	1.3:1	LINEAR		11 dB MINIMUM	40 ±5°	10 WATTS AVERAGE
MICROWAVE LANDING SYSTEM (C BAND)	5.0 - 5.25 GHz	<2.0:1	LINEAR				2 K WATTS PEAK
MICROWAVE LANDING SYSTEM (KU BAND)	15.4 - 15.7 GHz	<2.0:1	LINEAR				

The applicable information received is summarized in table V. In some cases it represents the suppliers' best estimates based on extrapolated test data and therefore, does not necessarily represent actual test results. However, this information provides a good review of the existing antenna equipment which can be considered applicable to the Space Shuttle Orbiter antenna system.

The survey indicates that the basic fabrication techniques used for most existing antennas is adequate. In some cases higher temperature (422-450 K (300-350°F)) foams, adhesives and/or aperture covers must replace those currently in use. The 7.31×10^4 N/m^2 (10.6 psi) differential pressure requirement does not appear to be a problem since most of the antennas were designed for a differential pressure of 1.03×10^5 N/m^2 (15 psi) or greater. The existing waterproofed antennas, that are completely foam-filled in place (or bonded in place) with closed cell foam that adheres to the antenna structural wall, include L-band C-band TACAN, radar altimeter, and C-band slot antennas.

During normal aircraft operation and short duration aircraft flights up to 80 000 ft altitude this fabrication approach has proven satisfactory for prevention of water absorption and corona. However, operations with long durations at near vacuum conditions have not been determined. MDAC-E Skylab tests have shown that closed cell foam of very low density 32.0 kg/m^3 (2 lb/ft^3) and low strength value may burst when transitioning from a standard atmosphere to a vacuum environment. However, the density of many of the foams found in the existing antennas was typically 96.1 kg/m^3 (6 lb/ft^3) or greater and therefore bursting cells should not be a problem. The effects of breathing moist air after entry, following long exposures to vacuum environments, low pressures due to slow leakdown or out gassing after insertion in orbit, and slow repressurization after entry on the power handling capacity need to be determined. Antenna power breakdown or corona discharge, that could make the antenna temporarily inoperative, could occur at low (critical) pressures.

The antenna connector thermal capabilities appear adequate for teflon loaded connectors provided that a good grade of virgin teflon is used and that the design is such that thermal expansion of the teflon does not break antenna seals under elevated temperatures (422-450 K (300-350°F)).

The existing antennas typically have been qualified for low temperatures of 219 to 208 K (-65 to -85°F). Therefore, the mechanical integrity of aircraft antennas must be determined at orbital cold temperatures lower than 208 K (-85°F).

The S-band archimedes spiral antennas, of the survey, provide a larger bandwidth capability than the S-band cavity backed helix antennas. The larger bandwidth could cover USAF and Russian S-band frequencies in addition to the NASA S-band frequencies. However, the beamwidth of the archimedes spirals are smaller and, therefore, more antennas may be required for adequate Orbiter antenna pattern coverage. Amecom, Division of Litton, has investigated a larger diameter S-band cavity spiral antenna to cover the USAF and NASA frequencies. This antenna was estimated at 7.87 cm (3.10 in.) in diameter as opposed

TABLE V

CANDIDATE ANTENNAS

[illegible]	[illegible]	[illegible]	MAXIMUM [illegible] TEMPERATURE	MATERIALS	MODIFICATIONS FOR 600°F CAPABILITY	VENTING	WEIGHT (OUNCES)	ELECTRICAL CHARACTERISTICS	REMARKS
[illegible] COMMUNICATIONS	[illegible] ANTENNA, [illegible]	[illegible]	[illegible]	SINTERED QUARTZ CORNING P/N 7941, COATED WITH PLATINUM BASED MATERIAL, INVAR BACKCAP, TEFLON LOADED CONNECTOR	NONE	SEALED	4)	2.1-2.3 GHz, 120° BEAMWIDTH, -4DB A.R. OVER +60°, 79% EFFICIENCY 1.5:1 VSWR, RHC POL. GAIN +5DB	APOLLO UNIT WITH IMPROVED AXIAL RATIO. *MUST VERIFY TEMPERATURE CAPABILITY OF CONNECTOR
C-BAND COMMUNICATIONS	[illegible] (CAVITY BACKED [illegible])	[illegible]	1500-2000°F AFTERFIRE, 250-450°F CONNECTOR	SINTERED QUARTZ, CORNING 7941, COATED WITH PLATINUM BASED MATERIAL, TEFLON LOADED CONNECTOR	NONE** (ANTENNA MUST HOWEVER BE SCALED DOWN FROM C-BAND TO S-BAND)	SEALED	5) (EST.)	C-BAND, 100° BEAMWIDTH MIN., -4DB A.R. OVER +60°, 85% EFFICIENCY, 1.5:1 VSWR OVER 300 MHz BANDWIDTH, RHC POL., GAIN +5DB	MUST BE SCALED TO S-BAND FROM C-BAND **MUST VERIFY TEMPERATURE CAPABILITY OF CONNECTOR
S-BAND COMMUNICATIONS	[illegible] (CAVITY BACKED ARCHIMEDES SPIRAL)	FREQUENCY ENGINEERING LABORATORIES	TESTED SATISFACTORILY TO 800°F FOR 10 MINUTES, 270°F FOR 1 HOUR	SPIRAL ON FIBERGLASS CARD. CARD BONDED TO POLYURETHANE FOAM WITH HYSOL EPON EPOXY, POLYURETHANE FOAM BONDED TO CASE WITH EPON EPOXY	USE HIGHER TEMPERATURE GLASS FOAM. USE HIGHER TEMPERATURE ADHESIVES IF REQUIRED.	NOT HERMETICALLY SEALED, MOISTURE SEALED, COMPLETELY FOAM FILLED WITH CLOSED CELL FOAM	3.8	1.75 TO 3.0 GHz***, 85° BEAMWIDTH @ 0DB, 2.5DB A.R. OVER +42.5°, 75% EFFICIENCY, 1.8:1 VSWR RHC POL., 20 WATT CW POWER	***COMMERCIAL BROADBAND UNIT MUST BE MODIFIED TO HANDLE THIS FREQUENCY BAND. LABORATORY TESTS HAVE BEEN PERFORMED SATISFACTORILY OVER THIS FREQUENCY BAND.
S-BAND COMMUNICATIONS	[illegible] (CAVITY BACKED ARCHIMEDES SPIRAL)	SANDERS ASSOCIATES	300°F	SPIRAL ON NEMA G11 EPOXY FIBERGLASS. CAVITY AIR FILLED.	NONE	NOT SEALED	4	2.6 TO 5.2 GHz, 70° BEAMWIDTH (3DB), 1.5DB A.R. ON BORESIGHT, 2:1 VSWR MAX, RHC OR LHC POL., 15 WATTS CW POWER	MUST BE SCALED TO COVER LOWER S-BAND FREQUENCIES
VHF COMMUNICATIONS	[illegible] OF DC-10 DESIGN (MODIFIED FAR-TIAC ANTENNA)	MCDONNELL DOUGLAS	DESIGN AS REQUIRED, 300-500°F	ALUMINUM HOUSING WITH FOAM FILLER OR OTHER STRUCTURAL SUPPORT, HIGH TEMPERATURE G11 OR EQUIVALENT FIBERGLASS RADOME	NONE (SIZE 29" X 40" X 6" DEEP)	AS REQUIRED	400 (EST.)	118-154 MHz, PATTERN LIKE QUARTER WAVE STUB ON GROUND PLANE, 2.0:1 VSWR MAX, VERTICAL POL. 50 OHM	MODIFIED VERSION OF THE DC-10 VHF SATCOM ANTENNA DESIGNED FOR OPERATION WITH AN FAA VHF COMMUNICATIONS SATELLITE.
VHF COMMUNICATIONS	[illegible] (DOUBLE [illegible])	ARMY ASSOCIATES	DESIGN AS REQUIRED, 300-500°F	ALUMINUM HOUSING WITH FOAM FILLER OR OTHER STRUCTURAL SUPPORT, HIGH TEMPERATURE G11 OR EQUIVALENT FIBERGLASS RADOME	NONE (SIZE 12" DIA X 3" DEEP)	AS REQUIRED	48 (NOT INCLUDING FOAM FILLER OR LOAD CARRYING CAPABILITY)	118-136 MHz, NO PATTERN DATA AVAILABLE, 1.8:1 VSWR, VERTICAL POL., 50 OHM, GAIN -12DB	ANTENNA GAIN IS -12DB DUE TO SMALL SIZE OF ANTENNA, PROTOTYPE ONLY PRODUCED

TABLE V (CONTINUED)

CANDIDATE ANTENNAS

FUNCTION	CANDIDATE ANTENNA	MANUFACTURER	MAXIMUM REUSE TEMPERATURE	MATERIALS	MODIFICATIONS FOR 300 F CAPABILITY	VENTING	WEIGHT (OUNCES)	ELECTRICAL CHARACTERISTICS	REMARKS
L-BAND TACAN	P/N OM N17 (ANNULAR SLOT)	DORNE AND MARGOLIN	250 F	ALUMINUM HOUSING; NOPCO CO. FOAM NO. A206, 6#/CU FT FILLER; FIBERGLASS WINDOW	USE HIGHER TEMPERATURE FOAM AND FIBERGLASS WINDOW. USE HIGHER TEMPERATURE ADHESIVES	SEALED, CAVITY COMPLETELY FILLED WITH CLOSED CELL FOAM	21	960-1220 MHz, 50 OHM, 1.5:1 VSWR, VERTICAL POL.	WHOLE ANTENNA CURED AT 250°F, WITHSTANDS 25 PSID PRESSURE
L-BAND TACAN	P/N OMR 29-2 (ANNULAR SLOT)	DORNE AND MARGOLIN	275-300 F	ALUMINUM HOUSING; NOPCO CO. FOAM NO. A206, 6#/CU FT FILLER, FIBERGLASS WINDOW	USE HIGHER TEMPERATURE FOAM	SEALED, CAVITY COMPLETELY FILLED WITH CLOSED CELL FOAM	32	700-1,375 MHz, 50 OHM, 3.0:1 VSWR MAX, VERTICAL POL., WITHIN 2DB OF 1/4 STUB ON HORIZON	WHOLE ANTENNA CURED AT 250°F, USES HIGHER TEMPERATURE ADHESIVES THAN OM N17 ANTENNA
L-BAND TACAN	P/N AT 740 (ANNULAR SLOT)	TRANSCO PRODUCTS	400 F	ALUMINUM HOUSING; CPR INTERNATIONAL CO. FOAM NO. CPR 747-3 FILLER	NONE	WATER-PROOF NOT HERMETICALLY SEALED, COMPLETELY FOAM FILLED	12	960-1,220 MHz, 50 OHM, 1.6:1 VSWR 990 TO 1200 MHZ, VERTICAL POL. 5KW PEAK POWER	80,000 FT ALTITUDE DESIGNED FOR 15 PSID PRESSURE, HAS RF TEST PROBE
L-BAND TACAN	P/N 16001700 (ANNULAR SLOT)	TRANSCO PRODUCTS	480 F	ALUMINUM HOUSING; EMERSON AND CUMING ECOSPHERES FT120 FOAM FILLER, FIBERGLASS WINDOW	NONE	WATER-PROOF, NOT HERMETICALLY SEALED, COMPLETELY FOAM FILLED	21	960-1,220 MHz, 50 OHM, 1.8:1 VSWR, 1.6:1 VSWR, 1000 TO 1100 MHZ, VERTICAL POL., 4 KW PEAK POWER AT .004 DUTY CYCLE (16 WATT AVG POWER)	70,000 FT ALTITUDE WILL BE TESTED TO: 4.5 PSIA CRUSHING & 2.25 BURST PRESSURE, AND 200 LB IN. SHEAR FLOW @ 475°, USED ON F-15, ONE HALF DB BELOW GAIN OF A QUARTER WAVE STUB ANTENNA.
C-BAND RADAR ALTIMETER	P/N OM FN3 (HORN)	DORNE AND MARGOLIN	280 F	ALUMINUM CAST HOUSING; NOPCO CO. FOAM NO. A206 6#/CU FT. FILLER; FIBERGLASS WINDOW	USE HIGHER TEMPERATURE FOAM AND FIBERGLASS WINDOW; USE HIGHER TEMPERATURE ADHESIVES	SEALED CAVITY, COMPLETELY FILLED WITH CLOSED CELL FOAM	20	4,210-4,390 MHz, BEAMWIDTH 50° ROLL PLANE-40° PITCH PLANE, 1.3:1 VSWR, LINEAR POL., 50 OHM, 100 WATT CW POWER	WHOLE ANTENNA CURED AT 250°F
C-BAND RADAR ALTIMETER	P/N AN APN-201 (HORN)	RANTEC FOR HOFFMAN NAVCOM SYSTEMS	300 F CONTINUOUS 350 F (QUALIFIED FOR 2 HOURS)	ALUMINUM ALLOY HOUSING; DIAMOND SHAMROCK CO. OPEN CELL FOAM NO. BX 251 FILLER; G10 GLASS EPOXY RADOME SURFACE	NONE	SEALED CAVITY, COMPLETELY FILLED WITH FOAM, WATERPROOF, NOT PRESSURE SEALED	10	4,200-4,300 MHz, BEAMWIDTH 56° POLL PLANE, 43° PITCH PLANE, 1.35:1 VSWR, LINEAR POL., 50 OHM, 11 DB GAIN	VIBRATION-.036" D.A OR 10G 5 TO 500 Hz WHICHEVER IS LESS. VIBRATION-2G PK TO 500 Hz DWELLING AT RESONANCE POINTS, USED ON S-3A AIRCRAFT

TABLE V (CONCLUDED)

CANDIDATE ANTENNAS

FUNCTION	CANDIDATE ANTENNA	MANUFACTURER	MAXIMUM REUSE TEMPERATURE	MATERIALS	MODIFICATIONS FOR 300 F CAPABILITY	VENTING	WEIGHT (OUNCES)	ELECTRICAL CHARACTERISTICS	REMARKS
C-BAND RADAR ALTIMETER	P/N 01-34-04551 (HORN)	TRANSCO PRODUCTS	250 F	ALUMINUM HOUSING, UP JOHN CO. URETHANE CPR 17-3 OR -4 FOAM FILLER	HIGHER TEMPERATURE FOAM - EMERSON & CUMING FPH, GOOD FOR 300°-350 F	WATER-PROOF SEAL, NOT PRESSURE SEALED, COMPLETELY FOAM FILLED	11	4,250-4,350 MHz, BEAM-WIDTH 45° x 45°. 1.30:1, VSWR MAX, LINEAR POL., 50 OHM, 11DB GAIN	
C-BAND RADAR ALTIMETER	P/N 01-34-04550 (HORN)	TRANSCO PRODUCTS	250 F	ALUMINUM HOUSING, UP JOHN CO. URETHANE CPR 17-3 OR -4 FOAM FILLER	HIGHER TEMPERATURE FOAM - EMERSON & CUMING FPH, GOOD FOR 300-350°F	WATER-PROOF SEAL, NOT PRESSURE SEALED, COMPLETELY FOAM FILLED	16	4,250-4,350 MHz, BEAM-WIDTH 35° x 35°, VSWR 1.30:1 MAX, LINEAR POL. 50 OHM, 13DB GAIN, 1 KW PEAK POWER	75,000 FT ALTITUDE
C-BAND RADAR ALTIMETER	P/N M45295 (HORN)	AMECOM DIV. OF LITTON	160°F FOR 48 HR. (QUALIFICATION LEVEL), 266 F RADOME, 392 F LEFKOWELD TYPE 109	CAST ALUMINUM HOUSING: DOW CHEMICAL HD-1 STYROFOAM FILLER: SILVER PLATED BRASS CONNECTOR AND PROBE: FIBERGLASS RADOME SEALED TO FLANGE WITH LEFKOWELD TYPE 109 ADHESIVE	UNKNOWN	WATER-PROOF SEAL, NOT PRESSURE SEALED	11	4,200-4,400 MHz, BEAM-WIDTH 48° x 46°, VSWR 1.1:1 AT CENTER FREQUENCY, LINEAR POL., 50 OHM, 13DB GAIN	QUALIFIED TO: 50,000 FT ALTITUDE ACCELERATION-7G PEAK, SHOCK-20G @ 11 MSEC. PERIOD, VIBRATION-10G PEAK 74 TO 1,000 Hz. STYROFOAM LAID IN HOUSING
C-BAND MICROWAVE LANDING SYSTEM	P/N 1700[illegible] (SLOT)	TRANSCO PRODUCTS	400 F	ALUMINUM HOUSING, REYNOLDS TAYLOR CO., G7 SILICONE GLASS FILLER	NONE	FILLER IS BONDED TO HOUSING, MOISTURE SEALED	4.5	5.4 to 5.9 GHz, SLOT PATTERN, 1.5:1 VSWR, LINEAR POL., 50 OHM	
C-BAND MICROWAVE LANDING SYSTEM	P/N CA-32 (SLOT)	SANDERS ASSOCIATES	300 F	ALUMINUM OR BRASS HOUSING	NONE	OPEN CAVITY	3	3-6 GHz, SLOT PATTERN, 140° X 35°, 3:1 VSWR MAX LINEAR POL.	CAN FOAM FILL CAVITY?
Ku-BAND MICROWAVE LANDING SYSTEM	P/N 9024100 (SURFACE WAVE SLOT)	TRANSCO PRODUCTS	300 F	ALUMINUM HOUSING AND TEFLON FILLER. HOLLOW IN WAVE-GUIDE AREA AT FEED POINT.	NONE	MOISTURE SEALED, NOT PRESSURE SEALED	5	15.4 to 15.7 GHz, +10° TO -20° ELEVATION BEAM-WIDTH, +35° AZIMUTH BEAMWIDTH, 1.5:1 VSWR MAX, VERTICAL POLARIZATION	USED FOR C-SCAN LANDING SYSTEM ANTENNA, WAVE-GUIDE TYPE
Ku-BAND MICROWAVE LANDING SYSTEM	P/N CA-100A (SURFACE WAVE SLOT)	SANDERS ASSOCIATES	270 F	ALUMINUM HOUSING, GENERAL ELECTRIC LEXAN FILLER, G11 EPOXY FIBERGLASS RADOME	POLYPHENYLENE (PPL) OXIDE FOAM CAN BE USED TO INCREASE TEMPERATURE CAPABILITY TO 380°F, WAVE GUIDE TYPE AND HIGHER TEMPERATURE G11 COVER MATERIAL	MOISTURE SEALED, NOT PRESSURE SEALED. HOLLOW IN WAVE GUIDE AREA AT FEED POINT	6 TO 8	15.4 TO 15.7 GHz, 30° ELEVATION BEAMWIDTH, AND 70° AZIMUTH BEAM-WIDTH @ 4DB ABOVE ISOTROPIC OR GREATER	LEXAN FILLER BONDED IN PLACE: USED FOR C-SCAN LANDING SYSTEM ANTENNA

NOTES: P/N - PART NUMBER; RHC - RIGHT HAND CIRCULAR; LHC - LEFT HAND CIRCULAR; EST - ESTIMATE; A.R. - AXIAL RATIO; POL - POLARIZATION; MAX - MAXIMUM; MIN - MINIMUM

to the 6.48 cm (2.55 in.) diameter for the improved Apollo S-band antenna used in this development contract. The larger bandwidth antenna would use the same basic design as the Apollo, and improved Apollo S-band antennas and, therefore, would not result in any large new development effort. The apertures of the Amecom and Watkins Johnson S-band antennas can be reused multiple times when exposed to temperatures of 1255 K (1800°F) or less and therefore, may not have to be covered with HRSI in the cooler areas of the Orbiter. However, the effects of placing the S-band aperture above the metal ground plane and flush with the HRSI on radiation patterns (see section on S-BAND ANTENNA SYSTEM DESIGN) and antenna backside temperatures must be considered.

Both the VHF antennas surveyed require significant development effort to meet Orbiter VHF antenna requirements. The small size of the Sanders Associates antenna results in very low gain (-12 dB) compared to a normal 3 dB gain for this type of antenna.

The L-band TACAN antenna surveyed revealed several with electrical and high temperature capabilities necessary to meet the Orbiter requirements. The antenna cavities for these antennas are waterproofed but not hermetically sealed. However, the adequacy of the venting, waterproofing and cold soak capability have not been determined.

The C-band microwave landing system antennas surveyed provide a slot pattern and, therefore, must be mounted very near the forward end of the Orbiter to obtain an accepted radiation pattern. The Transco antenna is moisture sealed and the temperature capabilities meet Orbiter requirements.

The microwave landing system Ku-band antennas surveyed are surface wave antennas. With the aperture mounted flush with the bottom of the Orbiter the pattern will be pointed predominately forward toward the landing site. These antennas are filled with a dielectric foam in the aperture area but not in the connector area. The basic electrical characteristics are consistent with the Orbiter requirements but the patterns may be affected by the TPS as discussed later in this subsection. These antennas are not hermetically sealed and may breath moist air after entry which could cause corrosion. This antenna is used for receive only (as specified in the FAA/Defense Department universal landing system) and, therefore, critical pressures due to leakage is not a problem.

No information was obtained on microstrip antenna designs during the antenna survey which specifically meets the Orbiter frequency and pattern requirements. However, since these antennas (refs. 2 and 3) offer low profile, low weight, low cost, simplicity of design, low impact on design for installation, and have been used in space application they should be considered for applications where a new design is required to meet expanded requirements or limited mounting space. One of the principal disadvantages is a narrow bandwidth. Therefore, more than one element may be required to cover a particular frequency band. The effect of HRSI over a microstrip antenna is not known, but should not cause a major problem due to the low dielectric constant of the HRSI materials.

Photoetch printed circuit board technology is used to manufacture the microstrip antennas. The microstrip antennas as manufactured by Ball Brothers Research Corporation consists of a teflon fiberglass board that has a solid copper backside for the ground plane and copper circuitry on the frontside. The frontside circuitry includes the antenna radiation element, power dividers, phasing networks and matching networks. The excess copper is photoetched away to form the radiating and circuit elements. The antenna thickness (except for the connector) typically varies from 0.81 to 3.18 mm (0.032 to 0.125 in.). Electrical design and feasibility test cost for a specific antenna design is relatively low due to the type of construction.

Ball Brothers Research Corporation and the Navy (Pt. Mugu) have extensive experience in microstrip antenna designs and NASA-LaRC is currently investigating several microstrip antenna configurations. Microstrip designs have been successfully used in numerous space, missile and airplane applications.

The antenna survey indicated that exploratory simulation is necessary to further evaluate the capability of the candidate aircraft antenna elements. It should be determined if the existing candidate antennas can meet Orbiter cold soak, vacuum soak, and thermal-pressure histories during launch and entry. The results of the survey indicate that 422 K (300°F) is not a significant problem. However, orbital cold and vacuum soak performance is unknown. The required modifications to meet Orbiter electrical design requirement when covered with an antenna window should also be determined. The following should be evaluated before, during and after multiple environmental simulations:

(a) Reusability performance of antenna materials - investigate for bond fractures, cracks, shrinkage and distortion of antenna materials.

(b) Electrical performance - impedance, radiation patterns before and after tests.

(c) Power breakdown - determine if corona occurs during or following vacuum soak due to out gassing or insufficient venting.

Antenna window transmission loss. - The plane wave transmission characteristics of the antenna window design configuration considered in this study were analyzed to obtain an estimate of expected losses, assuming normal incidence. Each identifiable layer of material was considered as a section of transmission line with the characteristic impedance dependent on the dielectric constant, loss tangent and angle of incidence to the layer. The transmission line length corresponds to the layer thickness. The results using this analysis are only an indication of the expected transmission loss, since the antenna windows discussed in this report are normally in the near field of the antenna.

The expressions for calculating transmission loss are given in Appendix B. These expressions were programmed on a Hewlett-Packard 9100A calculator with a 1901A Extended Memory. The program can currently accommodate up to twenty (20) layers of dielectric material. The program was validated by comparing the

results for a single layer of dielectric with the results obtained using formulas given in Jasik (ref. 4). The results were in excellent agreement for loss tangent magnitudes less than 0.2. For loss tangents greater than 0.2 the results from the formulas given in Jasik are less exact because the squared terms of loss tangent are ignored. However, the programmed expressions used for the transmission loss calculations discussed below are exact, within the limits of the theory, for large values of loss tangent since the squared loss tangent terms are not ignored.

The details of the basic antenna window configurations which were analyzed are given in table VI. Although these configurations are considered to be a single layer window, there are eight (8) identifiable material layers. The additional materials consist of LI-1500 waterproof coating, sponge rubber strain isolator, fiberglass-phenolic honeycomb core and facesheets, and RTV 560 bonding adhesive.

TABLE VI

ANTENNA WINDOW CONFIGURATIONS

CONFIGURATION	LAYER	MATERIAL	THICKNESS (IN.)	DIELECTRIC CONSTANT	LOSS TANGENT
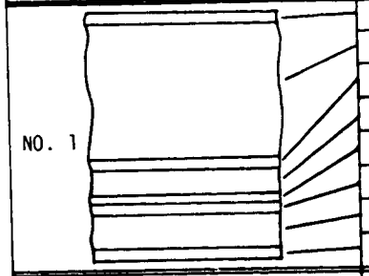 NO. 1	1	COATING	0.010	4.0	0.1000
	2	LI-1500	2.000	1.2	0.0016
	3	RTV-560	0.010	4.0	0.0050
	4	SPONGE	0.080	1.3	0.0080
	5	RTV-560	0.010	4.0	0.0050
	6	FACE SHEET	0.012	5.0	0.0200
	7	CORE	0.146	1.1	0.0010
	8	FACE SHEET	0.012	5.0	0.0200
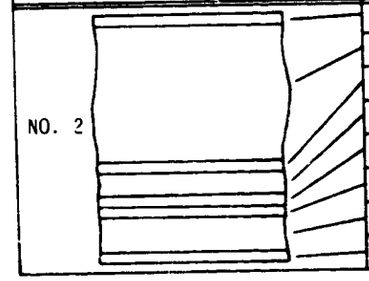 NO. 2	1	COATING	0.010	4.0	0.1000
	2	LI-1500	2.350	1.2	0.0016
	3	RTV-560	0.010	4.0	0.0050
	4	SPONGE	0.080	1.3	0.0080
	5	RTV-560	0.010	4.0	0.0050
	6	FACE SHEET	0.012	5.0	0.0200
	7	CORE	0.276	1.1	0.0010
	8	FACE SHEET	0.012	5.0	0.0200

The transmission loss for the respective configurations are shown in figures 14, 15, and 16. For reference, transmission loss is also shown for a panel of LI-1500 only, 5.08 cm (2.0 in.) thick. The transmission loss for a similar panel of LI-900 will be slightly lower, since LI-900 has both a lower dielectric constant and loss tangent. The transmission loss over frequency bands encompassing all the potential Orbiter frequencies are shown in figures 14, 15 and 16. The maximum transmission loss (figure 16) is less than 0.7 dB at the Ku-band frequencies compared to 0.16 dB for just the LI-1500 panel.

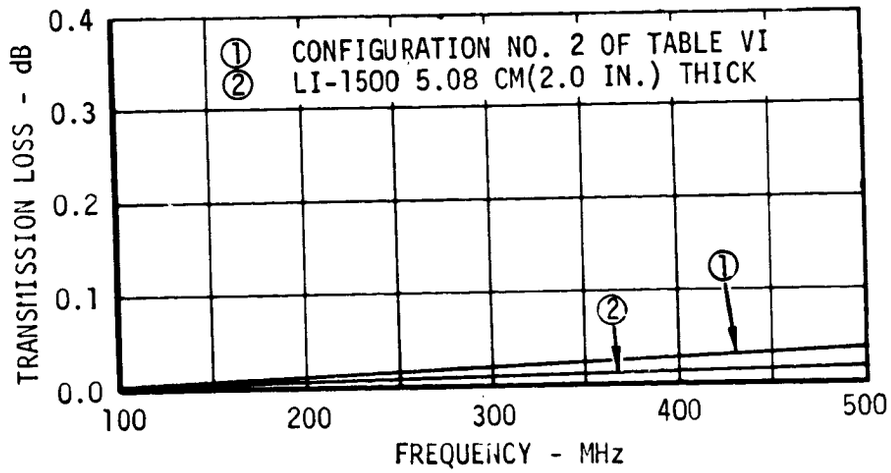

TRANSMISSION LOSS AT VHF AND UHF

FIGURE 14

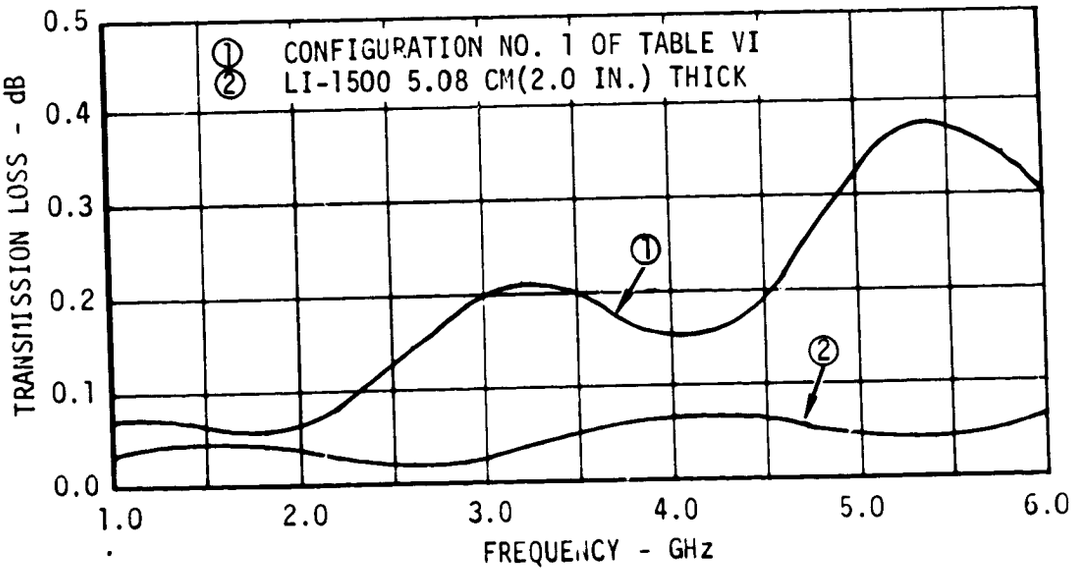

TRANSMISSION LOSS AT S- AND C-BAND FREQUENCIES

FIGURE 15

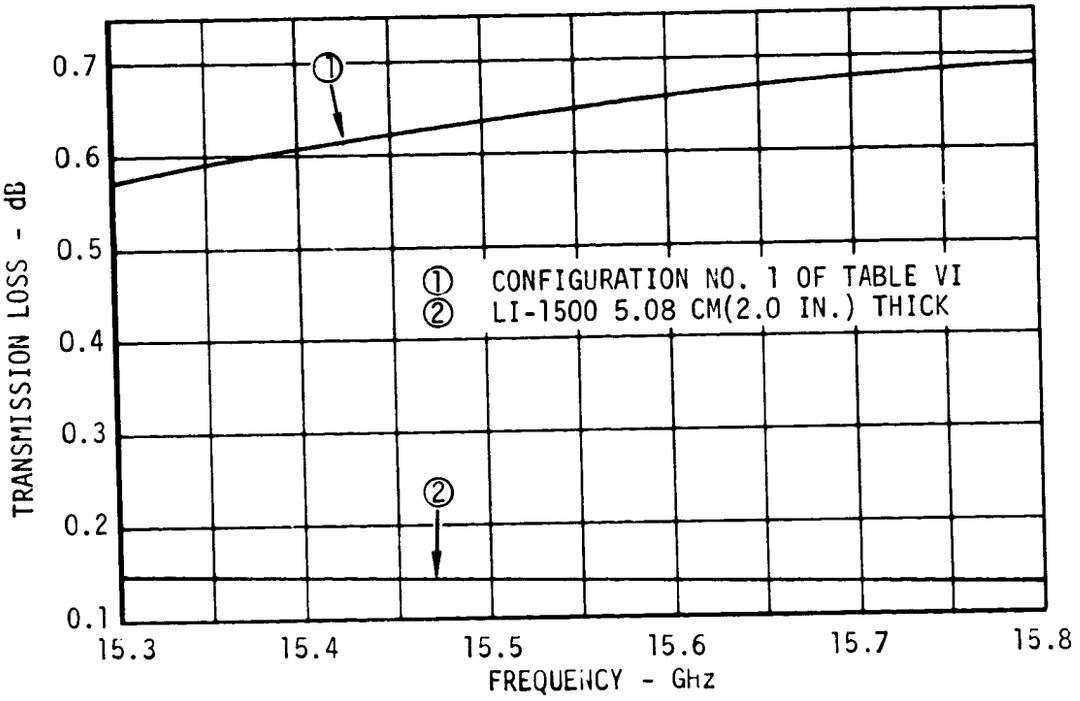

TRANSMISSION LOSS AT Ku-BAND FREQUENCIES

FIGURE 16

Above 200 MHz the material layers other than LI-1500 have the greatest influence on the transmission loss. At frequencies corresponding to Orbiter requirements below 7.0 GHz (figures 14 and 15) the maximum transmission loss is less than 0.4 dB. Calculations were also made to determine the change in transmission loss due to an increase in the bond layer thickness; perhaps the most difficult fabrication process to accurately control. The RTV 560 adhesive thickness was increased from 0.254 mm (0.010 in.) to 0.508 mm (0.020 in.). The results at Ku-band, where the effects are greatest, are shown in figure 17. The increased bond thickness increased the transmission loss about 0.15 dB. The results at lower frequencies show an insignificant increase in transmission loss for a 0.254 mm (0.10 in.) increase in adhesive thickness.

The results of transmission loss calculations for the VHF antenna window, Configuration No. 2, table VI, (figure 14) show that the transmission loss is insignificant at these frequencies. In this window configuration both the LI-1500 and the fiberglass-phenolic honeycomb thickness are increased. The transmission loss was calculated for both VHF and UHF frequencies.

Calculations were made to show the effect of using an alternate window material. For the case where GE's Mod 1A REI was substituted for LI-1500. The primary difference in the two materials is an increase in Mod 1A loss tangent from 0.0016 to 0.006. The results (figure 18) show an increase in transmission loss of less than 0.1 dB.

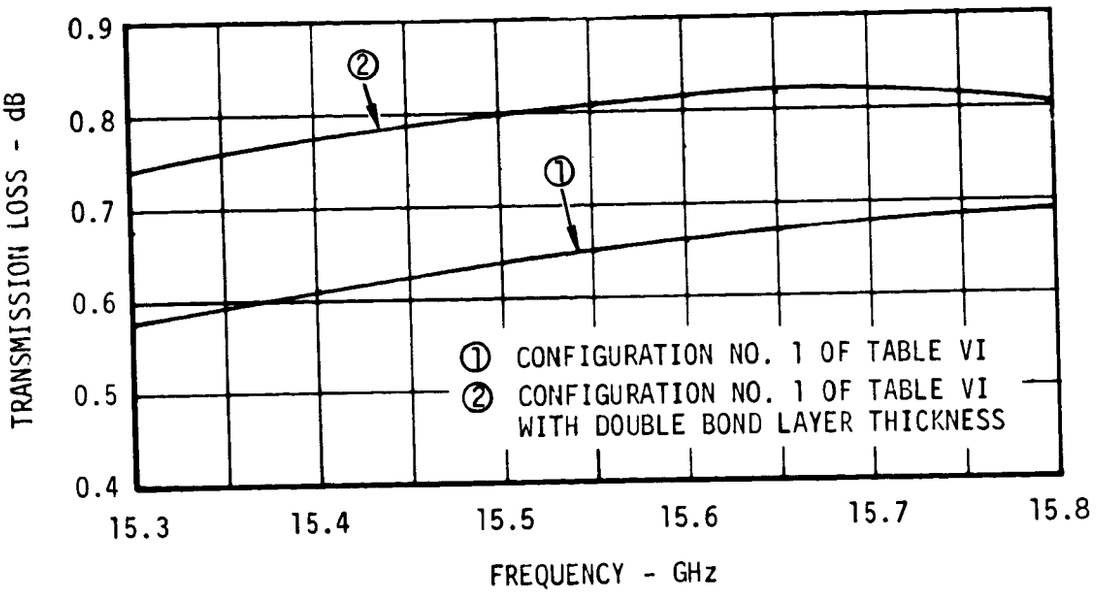

TRANSMISSION LOSS FOR THICK BONDLINES AT Ku-BAND FREQUENCIES

FIGURE 17

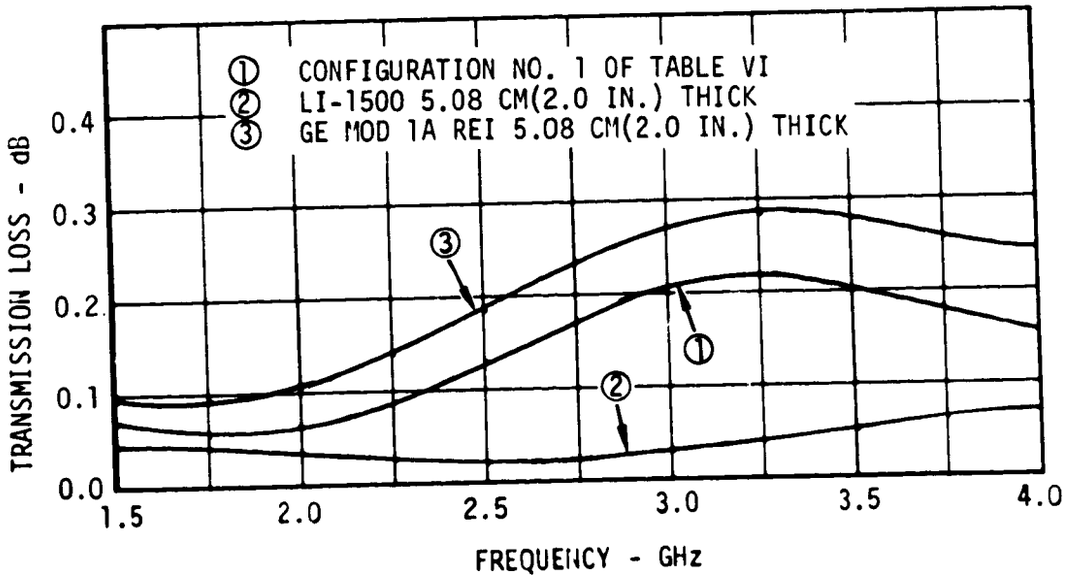

TRANSMISSION LOSS FOR ALTERNATE HRSI MATERIAL

FIGURE 18

The results of transmission loss calculations for other window configurations are given in reference 1. These results also show that a single-layer antenna window using LI-1500 have low transmission losses at L-band and C-band frequencies. Results for a multiple-layer antenna window (ref. 1) show that the transmission loss is significantly higher unless the outer layer of dense high temperature dielectric can be optimized (i.e., made equal to 0.5 wavelengths).

Design tests. - The antenna system design developed during the concept and feasibility studies is supported by the results of electrical tests, except for the VHF antenna system design. Test results of the L-band and C-band antenna system designs are reported in reference 1. Test results of the S-band antenna system are reported in the section on S-BAND ANTENNA SYSTEM DESIGN. Electrical design test results for the Ku-band antenna system design are described in this section.

Radiation pattern and impedance measurements were made using standard measurement techniques. The radiation patterns were recorded on standard 40 dB polar graph paper. The coordinate system used for pattern identification is shown in figure 19. A standard gain horn was used to establish the isotropic gain level shown on each pattern.

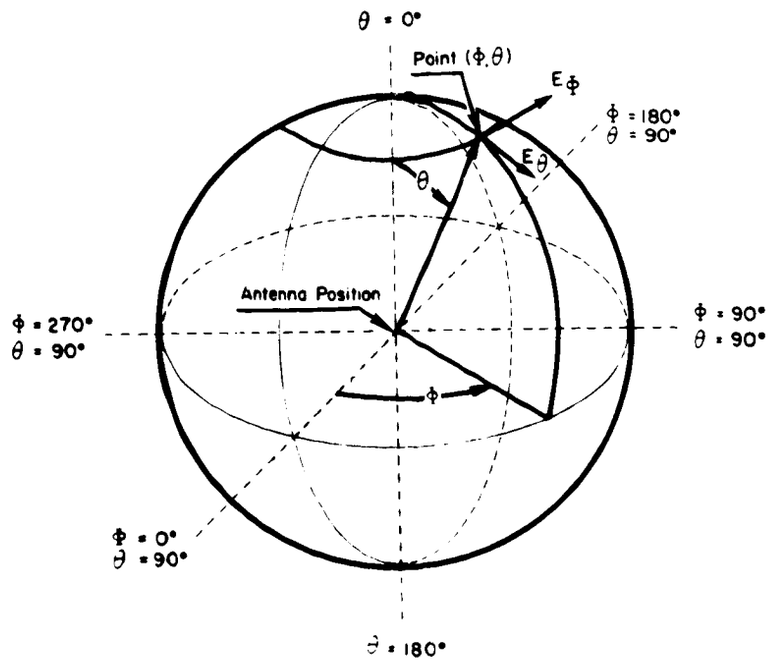

ANTENNA COORDINATE SYSTEM

FIGURE 19

Test results: The radiation patterns for the Ku-band antenna flush mounted in the center of a 1.83 m (6.00 ft) diameter ground plane (reference configuration) are shown in figure 20. These patterns are typical of a surface wave antenna and are used for comparison with the patterns of other configurations. The cross polarization magnitude is typically greater than 25 dB below

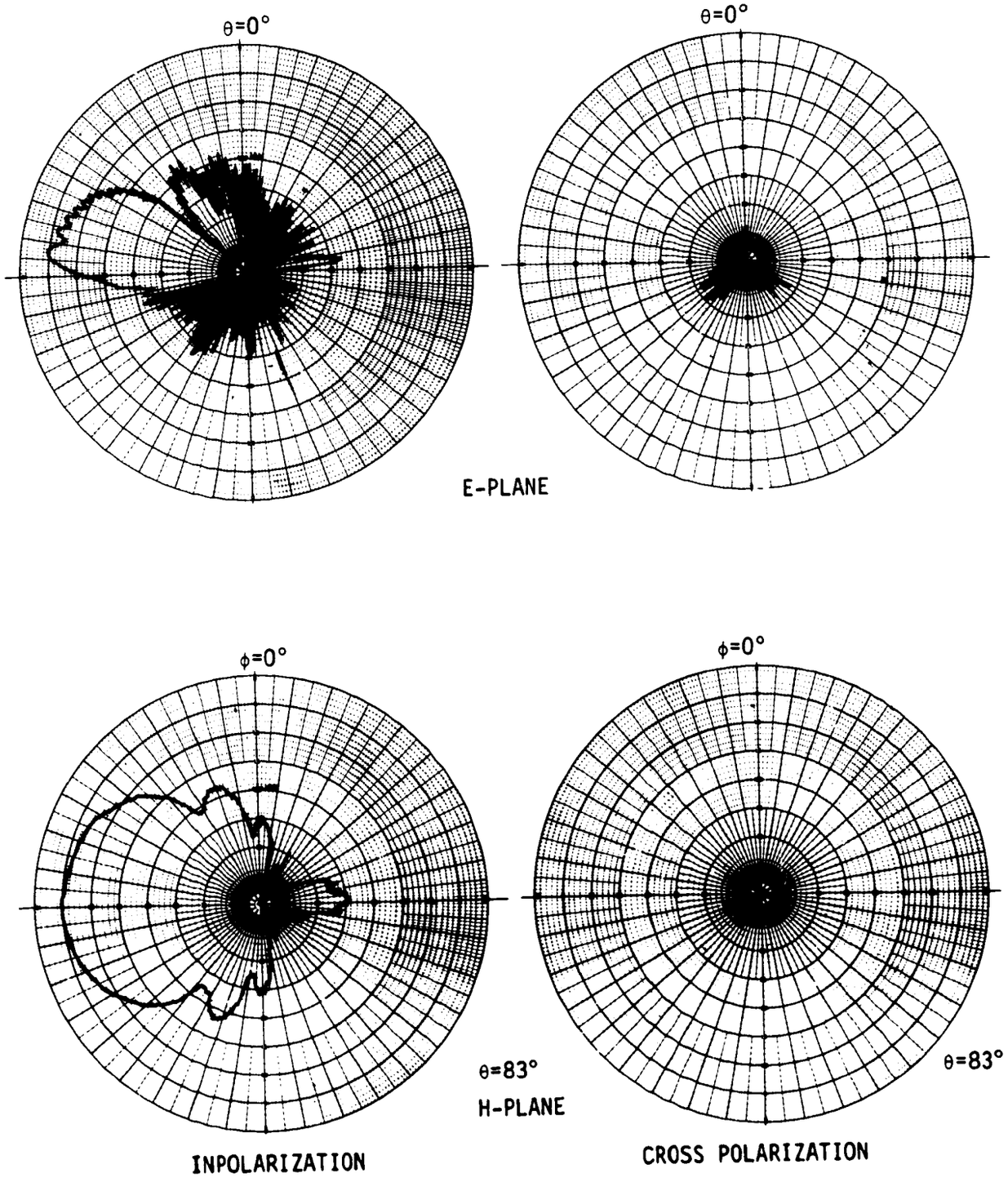

Ku-BAND REFERENCE PATTERNS

FIGURE 20

the peak gain. Very little difference in pattern level and shape was noted over the antenna frequency range. These patterns in general meet or exceed the requirements for a Ku-band microwave landing system.

The effects of an antenna window and surrounding TPS on the radiation patterns are shown in figure 21. In this configuration the TPS covers a 76.2 cm (30.0 in.) square area around the antenna window. The antenna window is 15.88 cm (6.25 in.) square and composed of the following layers: (1) simulated HRSI 5.08 cm (2.00 in.) thick; (2) silicone sponge (RL-524 Type S105) 2.03 mm (0.080 in.) thick; and (3) fiberglass-phenolic honeycomb 4.32 mm (0.17 in.) thick. The HRSI in both the TPS and antenna window was simulated with Emerson & Cuming Inc. ECCOFOAM PS ($\varepsilon_r = 1.2$).

The patterns show significant degradation and an overall decrease in gain of 5 to 10 dB. The main lobe of the E-plane pattern breaks up into a number of minor lobes at about $\theta = 60°$. The H-plane pattern at $\theta = 83°$ also breaks up into several minor lobes. Cross polarization levels increased in both the E- and H-planes. The most significant increase was measured in H-plane pattern at $\phi = 40°$ and $\phi = 140°$. These patterns show evidence of surface wave excitation in the TPS.

To further assess the effects of surface wave excitation, a 30.48 x 76.20 cm (12.00 x 30.00 in.) section was added to the previous configuration in the $\phi = 90°$ direction. The radiation patterns (figure 22) show an increase in the pattern degradation. The main lobe in the E-plane pattern is broken up more and the largest lobe appears to be centered at $\theta = 90°$. The increase in radiation at $\theta = 90°$ can be attributed to surface wave excitation, since the simulated TPS extended beyond the ground plane edge.

The transmission loss through the antenna window and TPS were calculated as a function of incidence angle. The results showed the maximum variation in transmission loss was less than 0.75 dB from $\theta = 0$ to $\theta = 68°$. Therefore, the lobing below $\theta = 70°$ cannot be attributed to transmission loss variations.

Subsequent testing showed the silicone sponge caused the most degradation. Pattern improvement was obtained with the fiberglass honeycomb/sponge panel directly over the antenna aperture removed. This testing led to a configuration in which the fiberglass honeycomb/sponge panel was removed from directly over the antenna and the remaining fiberglass honeycomb/sponge panel and sponge in the direction of the main lobe were covered with a metallic ground plane as shown in view E-E of figure 33 in the subsection on Structural Integration Studies of this section. The radiation patterns (figure 23) show considerable improvement. The distortion obtained in previous patterns (figure 22) is significantly reduced in both the E- and H-plane patterns. The ground plane over the sponge pad, which has a higher dielectric constant than the simulated HRSI, tends to reduce the surface wave excitation and, therefore, the pattern distortion. By optimizing the ground plane over the sponge strain isolation pad in the local area around the antenna it appears that an acceptable pattern can be obtained.

The results of impedance measurements (figure 24) show the Ku-band antenna impedance is well behaved for all configurations. The VSWR is less than 1.15:1 for all configurations as shown on expanded scale Smith charts.

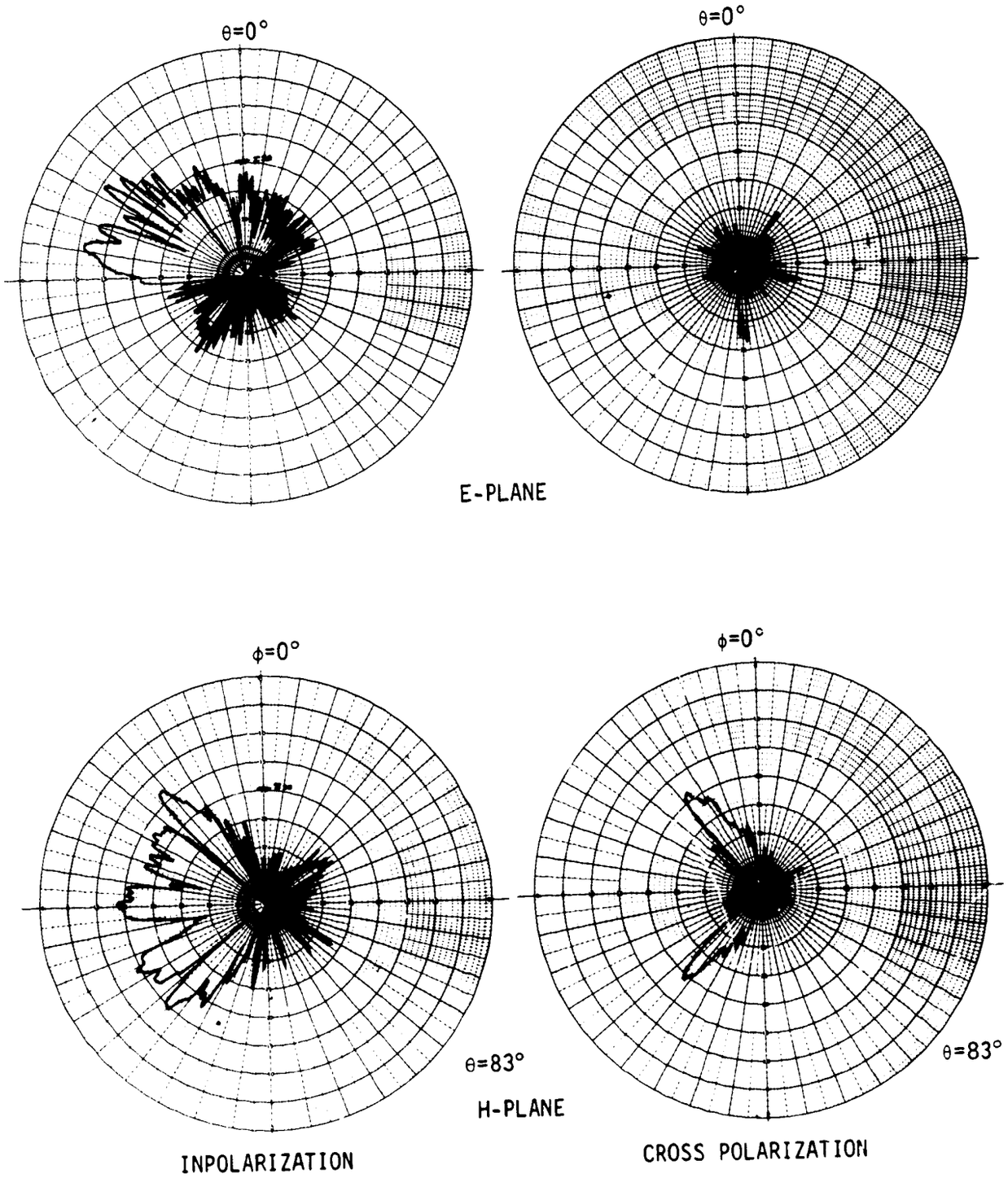

Ku-BAND PATTERNS WITH ANTENNA WINDOW AND TPS

FIGURE 21

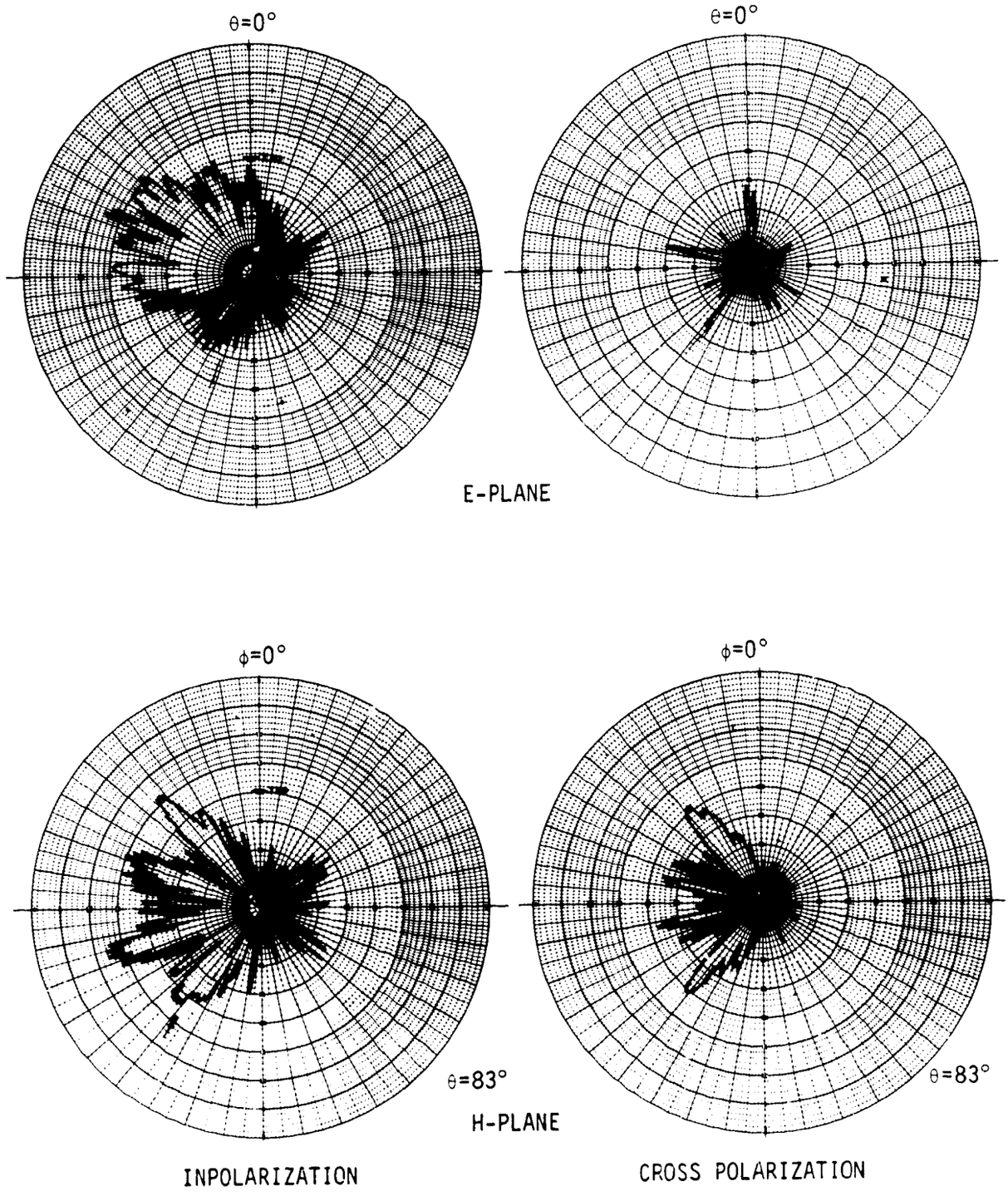

Ku-BAND PATTERNS WITH EXTENDED TPS

FIGURE 22

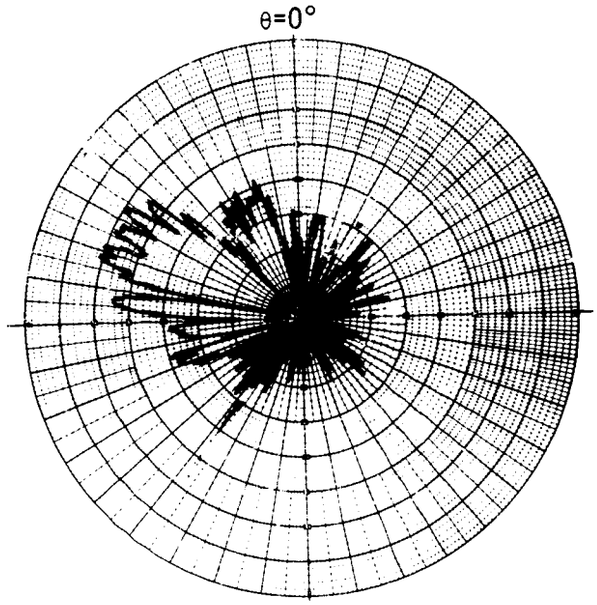

E-PLANE

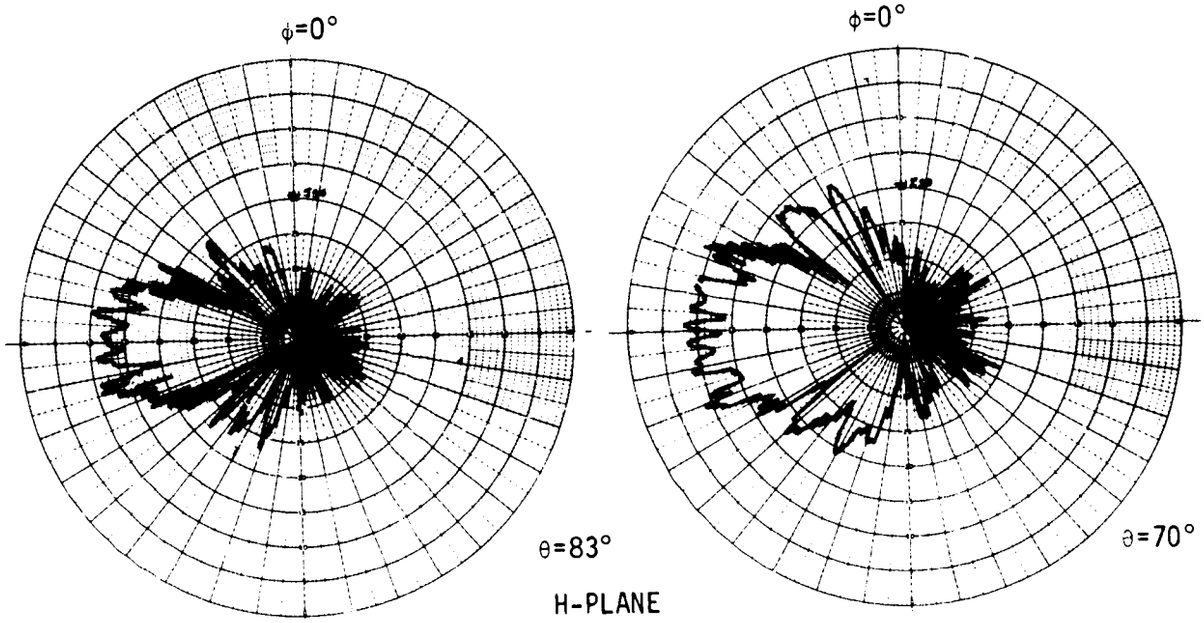

H-PLANE

INPOLARIZATION

Ku-BAND PATTERNS WITH AUXILIARY GROUND PLANE

FIGURE 23

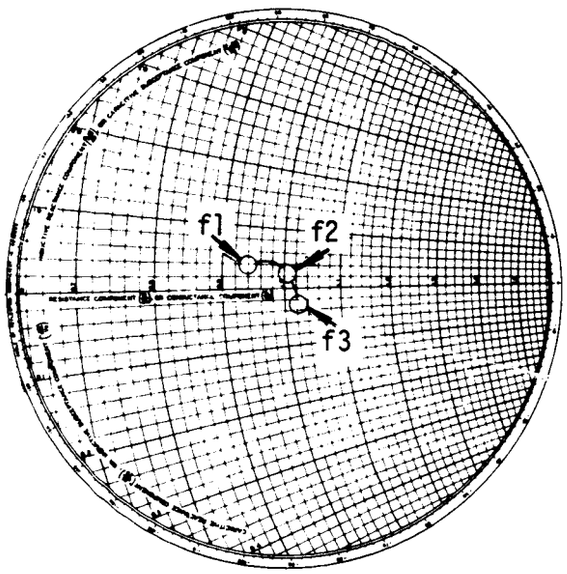

REFERENCE CONFIGURATION

Z_o = 50 OHMS
f1 = 15.0 GHz
f2 = 15.55 GHz
f3 = 15.7 GHz

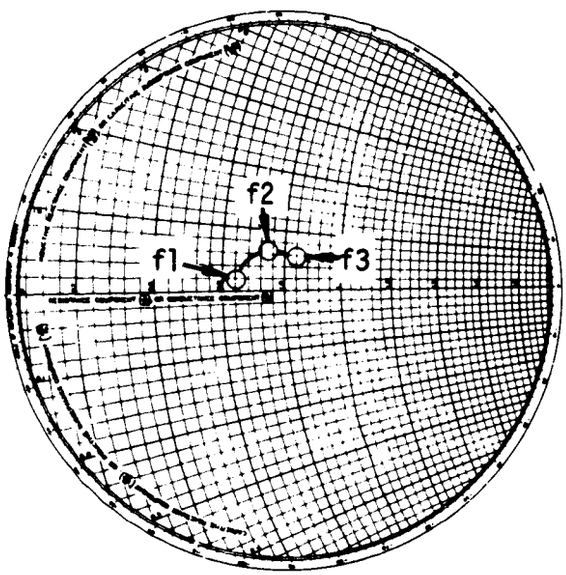

ANTENNA WINDOW AND TPS

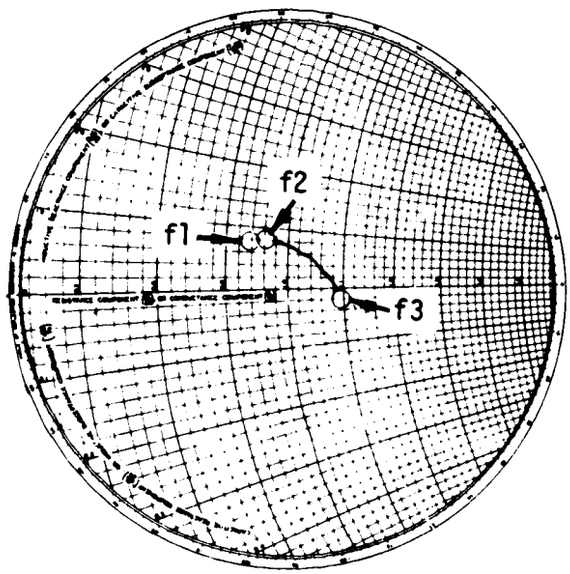

TPS AND AUXILIARY GROUND PLANE

Ku-BAND ANTENNA SYSTEM IMPEDANCE

FIGURE 24

Materials Studies

Material studies were conducted to identify applicable materials, and determine the compatibility of candidate materials in support of the respective antenna system design concepts. The materials study conducted under NASA contract, NAS 1-11273 (ref. 1) served as a starting point for this study. That information was reviewed and updated where new or better information could be obtained. However, the revisions did not result in any changes in trade study results or conclusions.

The results of the trade study (ref. 1) indicated that LI-1500 is the best antenna window material. LI-1500 was also a candidate HRSI material for the Orbiter TPS. For an alternate window concept (discussed in the subsection on Structural Integration Studies of this section, using a combination of high and low density materials, the trade study identified hot pressed boron nitride (BN) Union Carbide grade HD-0092, and Johns-Manville Dynaquartz (160 kg/m^3 (10 lb/ft^3) density). The results of tests (ref. 5) performed by the Georgia Institute of Technology essentially agree with MDAC-E's trade study. The properties of low and high density antenna window materials candidates are given in tables VII and VIII. The properties of auxiliary materials used in antenna windows and TPS design employing HRSI as the basic materials are given in table IX.

Antenna window materials. - The low density HRSI materials considered for both the Orbiter TPS and antenna windows were Lockheed's LI-1500, GE's MOD IA REI, and MDAC-E's MOD IIIA HCF. The properties of these materials are given in table VII. Lockheed's LI-1500 was specified as the baseline TPS HRSI material for this study.

LI-1500 is a rigidized silica fiber matrix with an inorganic binder. It is normally cut into 15.24 x 15.24 cm (6.00 x 6.00 in.) tiles for TPS assembly. The tile thickness is a function of the local thermal environment, but is nominally no greater than 5.08 cm (2.00 in.). The tiles require a waterproof coating on five sides because of the hygroscopic nature of the silica fibers. This coating, Lockheed's LI-0042, is basically silica with silicon carbide added to provide a high emittance surface which minimizes surface temperatures during entry heating. The tile is then impregnated with hydrolized silicone to complete the waterproofing. The silicone burns off of the outer portion of the tile during entry. That remaining in the inner portion of the tile wicks to the outside and will continue to do so with each entry cycle until the silicone is expended. The principal design properties used for LI-1500 are given in Appendix A.

The GE and MDAC-E HRSI materials employ mullite fibers instead of silica fibers as the base constituent. Similar waterproof coatings, which are compatible with the base material, are also required.

TABLE VII

ANTENNA WINDOW/THERMAL PROTECTION SYSTEM MATERIALS PROPERTIES

MATERIAL	DENSITY KG/M^3	DIELECTRIC CONSTANT AND LOSS TANGENT				YOUNG'S MODULUS N/M^2 (PSI)	TENSILE STRENGTH N/M^2 (PSI)	COMPRESSIVE STRENGTH N/M^2 (PSI)	MODULUS OF RUPTURE N/M^2 (PSI)
		DIELECTRIC CONSTANT	LOSS TANGENT	TEMPERATURE K (°F)	FREQUENCY (MHz)				
MULLITE-RSI (MDC MOD IIIA HCF)	240 ±15	1.20 1.28	0.002 0.062	ROOM 1473 (2192)	10 000 10 000	5.1 x 10^8 (7.4 x 10^4) ‖ TEN (8) 3.9 x 10^8 (5.6 x 10^4) ‖ COMP 9.7 x 10^7 (1.4 x 10^4) ⊥ TEN 8.3 x 10^7 (1.2 x 10^4) ⊥ COMP	6.8 x 10^5 (98) ‖ (8) 2.3 x 10^5 (33) ⊥ (STF = 0.14%)	1.01 x 10^6 (146) ‖ (8) 3.72 x 10^5 (54) ⊥	
MULLITE-RSI (MDC MOD V HCF)	240 ±48	1.31 1.42	0.003 0.085	ROOM 1473 (2192)	9050 9050	7.1 x 10^8 (10.3 x 10^4) ‖ TEN 3.7 x 10^8 (2.6 x 10^4) ⊥ TEN	1.70 x 10^6 (247) ‖ 7.31 x 10^5 (106) ⊥	ND	
MULLITE-RSI (G.E. MOD 1A REI)	185	1.19 1.21	0.0002 0.0066	ROOM 1473 (2192)	10 000 10 000	3.0 x 10^8 (4.4 x 10^4) ‖ TEN (8) 3.7 x 10^8 (5.4 x 10^4) ‖ COMP	4.0 x 10^5 (58) ‖ (8) 1.7 x 10^5 (25) ⊥	7.79 x 10^5 (113) ‖ (8) 2.55 x 10^5 (37) ⊥	
SILICA-RSI (LOCKHEED LI-1500)	252	1.23 1.25	0.00024 0.0011	ROOM 1473 (2192)	10 000 10 000	6.9 x 10^8 (10 x 10^4) ‖ TEN (8) 7.6 x 10^7 (11.1 x 10^4) ‖ COMP 6.9 x 10^7 (1 x 10^4) ⊥ TEN 6.2 x 10^7 (0.9 x 10^4) ⊥ COMP	7.9 x 10^5 (115) ‖ (8) 1.2 x 10^5 (18) ⊥ (STF = 0.12%)	1.86 x 10^6 (270) ‖ (8) 3.24 x 10^5 (47) ⊥	
SILICA-RSI (LOCKHEED) LI-900)	144 ±15	1.13 1.15	0.0012 0.0008	ROOM 1473 (2192)	10 000 10 000	1.65 x 10^8 (2.4 x 10^4) ‖ TEN 2.18 x 10^8 (3.16 x 10^4) ‖ COMP 4.1 x 10^7 (0.6 x 10^4) ⊥ TEN 4.1 x 10^7 (0.6 x 10^4) ⊥ COMP	1.19 x 10^5 (29) ‖ 0.53 x 10^5 (8) ⊥ (9)	1.72 x 10^5 (25) ‖ 1.72 x 10^5 (25) ⊥	
FI-600 (LOCKHEED)	96.5	1.06 (EST) 1.06 (EST)	0.0001 (EST) 0.0002 (EST)	ROOM 1473 (2192)	10 000 10 000	NA	NA	NA	
DYNAQUARTZ (JOHNS-MANVILLE)	160	1.11 1.12 1.13	0.0006 0.003 0.007	ROOM 873 (1112) 1473 (2192)	10 000 10 000 10 000	3.4 x 10^5 (50) (EST)	6.2 x 10^5 (90)	3.45 x 10^5 (50) (EST) WITH DEFLECTION	
MICROQUARTZ (JOHNS-MANVILLE)	56	1.06 (UC)	0.0027 (UC)	ROOM	13 400	NA	NA	NA	
SLA-561 (MARTIN)	VIRGIN 232	1.30	0.0083	ROOM	10 000	1.896 x 10^7 (2750)	2.27 x 10^6 (329) AT 133 K (-200°F) 1.86 x 10^5 (27) AT 366 K (+200°F)	ND	
	CHAR 128								
SLA-220 (MARTIN)	VIRGIN 250	1.31	0.005	ROOM	10 000	2.027 x 10^7 (2940)	5.46 x 10^5 (79.2)	7.58 x 10^5 (110)	
	CHAR 188								
SILICA FOAM (GLASROCK OR CARBORUNDUM)	830	1.50	0.0008	394 (250)	8500	4.8 x 10^9 (0.7 x 10^6) (EST)	ND	6.89 x 10^6 (1000)	
	510	1.40	0.0006	394 (250)	8500	2.1 x 10^9 (0.3 x 10^6) (EST)	ND	3.45 x 10^6 (500)	

NOTES:
1. ND = NO DATA; EST = ESTIMATED; NA = NOT APPLICABLE; UC = UNCOMPRESSED; STF = STRAIN TO FAILURE.
2. ALL PROPERTIES AT ROOM TEMPERATURE UNLESS OTHERWISE NOTED.
3. MELTING TEMPERATURE DOES NOT IMPLY MAXIMUM USE TEMPERATURE. THE MAXIMUM USE TEMPERATURE WILL BE LESS AND IS AFFECTED BY SEVERAL FACTORS SUCH AS PURITY, PROCESSING AND CONFIGURATION OF THE MATERIAL.
4. TEN = TENSION.
5. COMP = COMPRESSION.
6. ‖ = PARALLEL (NOTED STRESS APPLIED PARALLEL TO THE LONG AXES OF THE FIBERS).
7. ⊥ = PERPENDICULAR (NOTED STRESS APPLIED PERPENDICULAR TO THE LONG AXES OF THE FIBERS).
8. "EVALUATION OF NONMETALLIC THERMAL PROTECTION MATERIALS FOR THE MANNED SPACE SHUTTLE," VOLUME V, BATTELLE, MEMORIAL INST, 1 JUNE 1972.
9. LMSC - D336595, VOLUME I.

PAGE 6-22 INTENTIONALLY LEFT BLANK.

...GTS	MODULUS OF RUPTURE N/M² (PSI)	COEFFICIENT OF THERMAL EXPANSION M/M/K (IN/IN/°F)	THERMAL CONDUCTIVITY W/M/K (BTU-IN/FT²-HR-°F)	SPECIFIC HEAT J/KG K (BTU/LB-°F)	EMITTANCE (NORMAL)	(3) MELTING TEMPERATURE K (°F)	REMARKS
... (8)	6.89×10^5 (100) (EST)	5.4×10^{-6} (3.0×10^{-6})	0.384 (2.66) AT 1366 K (2000°F)	1.05×10^3 (0.25) AT 1422 K (2100°F)	>0.8	1866 (2900)	PRODUCTION MATERIAL
	ND	5.4×10^{-6} (3.0×10^{-6}) (EST)	0.303 (2.1) (EST) AT 1366 K (2000°F)	9.63×10^2 (0.23) EST	ND	1866 (2900)	IN PILOT PLANT PRODUCTION
... (8)	4.14×10^5 (60) (EST)	5.2×10^{-6} (2.9×10^{-6})	0.101 (0.7) AT 533 K (500°F) 0.387 (2.7) AT 1366 K (2000°F)	6.82×10^2 (0.163) AT 225 K (0°F) 1.34×10^3 (0.32) AT 922 K (1200°F)	0.65 TO 0.75	ND	
... (8)	7.93×10^5 (115)	0.54×10^{-6} (0.3×10^{-6})	0.225 (1.56) AT 1366 K (2000°F)	1.34×10^3 (0.32) AT 1366 K (2000°F)	0.85 0.95 AT 1366 K (2000°F)	1978 (3100)	PRODUCTION MATERIAL
... (9)	8.2×10^5 (119)	0.54×10^{-6} (0.3×10^{-6})	0.128 (0.4) AT 311 K (100°F) 0.228 (1.6) AT 1366 K (2000°F)	1.56×10^3 (0.35) AT 1366 K (2000°F)	0.85 0.95 AT 1366 K (2000°F)	1978 (3100)	PRODUCTION MATERIAL
	NA	0.54×10^{-6} (0.3×10^{-6}) (EST)	0.120 (0.83) AT 811 K (1000°F)	1.34×10^3 (0.32) AT 1366 K (2000°F)	0.8 (EST)	1978 (3100)	A RESILENT FORM OF LI-1500
(EST)	ND	0.54×10^{-6} (0.3×10^{-6}) (EST)	0.095 (0.68) AT 811 K (1000°F)	1.13×10^3 (0.27) AT 811 K (1000°F)	0.84	1978 (3100)	SEMIRIGID 99% SiO_2 SHRINKAGE <1% AT 1783 K (2750°F) FOR 24 HOURS DEFLECTION 8% AT 1.39×10^5 N/M² (20 PSI)
	NA	NA	0.098 (0.68) AT 811 K (1000°F)	1.13×10^3 (0.27) (EST) AT 811 K (1000°F)	0.8	1978 (3100)	FLEXIBLE FELT MATERIAL 98.5% SiO_2 SHRINKAGE 4% AT 1089 K (1500°F)
	ND	29.5×10^{-6} (16.4×10^{-6})	0.063 (0.44) AT 444 K (340°F)	1.26×10^3 (0.30)	0.7	NA	A SILICONE BASED ABLATION MATERIAL.
				1.55×10^3 (0.37)	0.9		
	ND	21.3×10^{-6} (11.7×10^{-6})	0.079 (0.55) (EST)	1.51×10^3 (0.36) (EST)	0.85	NA	A SILICONE BASED ABLATION MATERIAL.
				9.63×10^3 (0.23)	0.84		
...9)	3.59×10^6 (520)	0.72×10^{-6} (0.4×10^{-6})	0.259 (1.8) AT 811 K (1000°F)	9.63×10^3 (0.27) AT 811 K (1000°F)	>0.78 AT 311 K (1000°F)	1978 (3100)	COMMERCIALLY AVAILABLE PURITY 99.6% SiO_2 (MINIMUM) POROSITY 75%, OPEN CELL
...)	8.27×10^5 (120)	0.72×10^{-6} (0.4×10^{-6})	0.187 (1.3) AT 811 K (1000°F)	9.63×10^3 (0.27) AT 811 K (1000°F)	>0.78 AT 811 K (1000°F)	1978 (3100)	COMMERCIALLY AVAILABLE PURITY 99.6% SiO_2 (MINIMUM) POROSITY 60%, OPEN CELL

FOLDOUT FRAME

2

TABLE VIII

HIGH DENSITY ANTENNA WINDOW MATERIAL PROPERTIES

MATERIAL	PURITY %	DENSITY (KG M3)	DIELECTRIC CONSTANT AND LOSS TANGENT				YOUNG'S MODULUS N/M2 (PSI)	TENSILE STRENGTH N/M2 (PSI)	COMPRESSIVE STRENGTH N/M2 (PSI)	MODULUS OF RUP N/M2 (PSI)
			DIELECTRIC CONSTANT	LOSS TANGENT	TEMPERATURE K (°F)	FREQUENCY (MHz)				
ALUMINA (Al2O3) AD-99 (COORS)	99	3830	9.5 10.5	0.0002 0.0006	ROOM 1073 (1472)	10 000 10 000	3.45 x 10^11 (50 x 10^6) 3.38 x 10^11 (49 x 10^6) AT 810 K (1000°F)	2.41 x 10^8 (35 x 10^3) 1.52 x 10^8 (22 x 10^3) AT 1366 K (2000°F)	2.07 x 10^9 (300 x 1	[illegible]
BERYLLIA (BeO) BD-98 (COORS)	98	2850	6.6 7.6	0.0006 0.0008	ROOM 1073 (1472)	10 000 10 000	3.10 x 10^11 (45 x 10^6)	1.17 x 10^8 (17 x 10^3) 8.27 x 10^5 (1.2 x 10^2) AT 1644 K (2500°F)	1.55 x 10^9 (225 x 1	[illegible]
MAGNESIA (MgO)	90–99.5	3420	9.5 10.8	0.0001 0.0001	ROOM 1283 (1850)	9375 9375	2.07 x 10^11 (30 x 10^6) 1.72 x 10^11 (25 x 10^6) AT 810 K (1000°F)	8.27 x 10^7 (12 x 10^3) TO 1089 K (1500°F) 3.45 x 10^7 (5 x 10^3) AT 1644 K (2500°F)	1.39 x 10^9 (200 x 1	[illegible]
PYROCERAM (GLASS CERAMIC)	NA	2600	5.5 5.5	0.00033 0.004	ROOM 973 (1292)	8500 8500	1.24 x 10^11 (7 x 10^5)	ND	2.07 x 10^9 (300 x 1 (EST)	[illegible]
SLIP CAST FUSED SILICA	98.5–99.5	1980	3.38 3.54	0.0006 0.003	ROOM 1473 (2192)	10 000 10 000	4.83 x 10^10 (10 x 10^6)	1.39 x 10^7 (2 x 10^3)	1.39 x 10^8 (20 x 10^3	[illegible]
CLEAR VITREOUS SILICA	99.5	2200	3.82 4.00	0.0002 0.0003	ROOM 1673 (2552)	6100 6100	6.89 x 10^10 (10 x 10^6)	ND	1.03 x 10^9 (150 x 1	[illegible]
ISOTROPIC PYROLYTIC BORON NITRIDE (PBN)	99.5	1220	3.01 3.01	0.0015 0.0006	ROOM 1473 (2192)	10 000 10 000	1.21 x 10^10 (1.75 x 10^6	7.58 x 10^7 (11 x 10^3)	2.28 x 10^8 (33 x 10^3	[illegible]
ANISOTROPIC PYROLYTIC BORON NITRIDE BORALLOY	99.5	2200	5.12 5.24 3.4	0.00015 0.00039 0.0001	ROOM 1673 2552 BOTH ⊥ TO PD ROOM ⊥ TO PD	4000 4000 4000	2.07 x 10^10 (3 x 10^6 ⊥ TO PD)	4.14 x 10^7 (6 x 10^3) (⊥ TO PD)	4.96 x 10^7 (72 x 10^	[illegible]
BORON NITRIDE HBN-98 UNION CARBIDE	98.5	1990	4.08 4.24 4.04 4.20	0.00026 0.0046 0.003 0.0005	ROOM 1143 2678 ROOM 1473 2192	440 450 10 000 10 000	4.83 x 10^10 (7 x 10^6) (⊥ TO PD)	ND	4.14 x 10^7 (6 x 10^3) ⊥ TO PD 5.17 x 10^7 (7.5 x 10^ ⊥ TO PD	[illegible]
SILICON NITRIDE REACTION SINTERED	98.0	2200 TO 2400	5.5 5.6	0.0002 0.0065	ROOM 1255 1800	8000 8000	1.39 x 10^11 (20 x 10^6)	1.17 x 10^8 (17 x 10^3)	4.14 x 10^8 (60 x 10^3	[illegible]
FUSED SILICA (COMPOSITE	99.5	1650 TO 1710	2.9 2.9	0.01 MAX 0.008	ROOM 1272 1830	8520 8520	1.72 x 10^11 (2.5 x 10^6 ⊥ AND ⊥ TO RADIALS	ND	1.45 x 10^7 (2.1 x 10^	[illegible]

NOTE:
- ND = NO DATA
- [illegible] PROPERTIES ARE AT MEMBRANE TEMPERATURE (SEE THERMAL NOTE).
- [illegible] MAXIMUM TEMPERATURE IS THE MAXIMUM TEMPERATURE WHICH CAN BE ENDURED AFFECTED BY SEVERAL FACTORS (SHAPE OF [illegible] AND LOADING OF THE MATERIAL).
- EST = ESTIMATE
- NA = NOT APPLICABLE
- ⊥ = PERPENDICULAR TO REFERENCE AXIS
- PD = PRESSING DIRECTION

PRECEDING PAGE BLANK NOT FILMED

PAGE 6-24 INTENTIONALLY LEFT BLANK.

FOLDOUT FRAME

	MODULUS OF RUPTURE N/M^2 (PSI)	COEFFICIENT OF THERMAL EXPANSION M/M/ K (IN./IN./^{o}F)	THERMAL CONDUCTIVITY W/M K (BTU–IN./FT^2-HR-^{o}F)	SPECIFIC HEAT J/KG K (BTU/LB-^{o}F)	EMITTANCE (NORMAL)	MELTING TEMPERATURE K (^{o}F) (3)
	3.59×10^8 (52×10^3) 1.72×10^8 (25×10^3) AT 1366 K (2000^{o}F)	6.0×10^{-6} (3.3×10^{-6})	29.3 (203) 6.3 (44) AT 1073 K (1472^{o}F)	8.79×10^2 (0.21) AT 373 K (212^{o}F)	0.79 0.5 AT 1366 K (2000^{o}F)	2311 (3700)
	1.86×10^8 (27×10^3) 8.96×10^7 (13×10^3) AT 1366 K (2000^{o}F)	5.8×10^{-6} (3.2×10^{-6})	205.0 (1422) 25.1 (174) AT 1073 K (1472^o)	1.30×10^3 (0.31) AT 373 K (212^{o}F) 1.26×10^3 (0.30) AT 373 K (212^{o}F)	0.60 0.33 AT 1144 K (1600^{o}F)	2839 (4650)
	1.39×10^8 (20×10^3) 6.90×10^7 (10×10^3) AT 1644 K (2500^{o}F)	14.0×10^{-6} (7.8×10^{-6})	43.3 (300)	1.17×10^3 (0.28) AT 373 K (212^{o}F)	ND	3072 (5070)
3)	2.41×10^8 (35×10^3) 6.89×10^7 (10×10^3) AT 1283 K (1850^{o}F)	5.8×10^{-6} (3.2×10^{-6})	3.3 (23)	9.76×10^2 (.233)	0.85	1670 (2600 EST)
	2.76×10^7 (4×10^3)	0.5×10^{-6} (0.3×10^{-6})	0.58 (4)	9.21×10^2 (0.22)	0.84	1978 (3100)
3)	4.83×10^7 (7×10^3) 6.89×10^7 (10×10^3) AT 1311 K (1900^{o}F)	0.5×10^{-6} (0.3×10^{-6})	6.9 (48)	7.12×10^2 (0.17)	0.84	1978 (3100 EST)
	9.65×10^7 (14×10^3) 1.17×10^8 (17×10^3) AT 1978 K (3100^{o}F)	7.2×10^{-6} (4×10^{-6})	18.7 (130) AT 573 K (572^{o}F)	1.21×10^3 (0.29)	0.80	3255 (5400) (SUBLIMES IN INERT ATMOSPHERE)
E)	1.03×10^8 (15×10^3)	3.2×10^{-6} (1.8×10^{-6}) AT 373–1273 K (212–1832^{o}F) ($\perp$ TO PD) 8×10^{-6} (4.5×10^{-6}) II TO PD	1.66 (11.5) II TO PD AT 373 K (212^{o}F) 62.9 (435) $\perp$ TO PD AT 373 K (212^{o}F)	1.00×10^3 (0.24)	0.80	3255 (5400) (SUBLIMES IN INERT ATMOSPHERE)
3)	4.14×10^7 (6×10^3) 5.52×10^7 (8×10^3) AT 1473 K (2192^{o}F)	1×10^{-6} (0.56×10^{-6})	1.83 (127) 13.8 (96) AT 810 K (1000^{o}F) 9.4 (65) AT 1366 K (2000^{o}F) ALL II TO PD	1.33×10^2 (0.193)	0.93	3255 (5400) (SUBLIMES IN INERT ATMOSPHERE)
3)	1.72×10^8 (25×10^3) 1.39×10^8 (20×10^3) AT 1572 K (2372^{o}F)	3.6×10^{-6} (2×10^{-6})	10.1 (70) AT 1172 K (1650^{o}F)	1.05×10^3 (0.25)	0.75–0.80 (EST)	2172 (3450) DISSOCIATES)
3)	2.76×10^8 (4×10^3)	ND	1.44 (10 EST)	8.37×10^2 (.20) (EST)	0.80 (EST)	1978 (3100)

FOLDOUT FRAME 7

TABLE IX

AUXILIARY ANTENNA WINDOW MATERIALS

MATERIAL	DENSITY KG M^3	DIELECTRIC CONSTANT	LOSS TANGENT	TENSILE STRENGTH N M^2 (PSI)	COEFFICIENT OF THERMAL EXPANSION M/M K (IN. IN./°F)	THERMAL CONDUCTIVITY W M K (BTU IN. FT^2-HR-°F)	SPECIFIC HEAT WS KG K (BTU LB^{-1}°F)	LOW TEMPERATURE STIFFENING POINT K (°F)	DEGRADATION TEMPERATURE K (°F)	REMARKS
PD-200	456	ND	ND	1.21×10^6 (175) AT 339 K (150°F) 1.39×10^5 (15.8) AT 422 K (300°F) 6.27×10^4 (9.8) AT 616 K (650°F)	36.2×10^{-6} 20.1×10^{-6}	1.4	9.63×10^2 (.23) AT 144 K (-200°F) 1.4×10^3 (.34) AT K (300°F)	164 (-165) EST	533 (500)	GENERAL ELECTRIC'S STRAIN ISOLATOR
[illegible] HAYNES "MANHATTAN"	46[illegible]	3.69 AT 323 K (122°F) 3.51 AT 429 K (313°F)	0.013 AT 323 K (122°F) 0.003 AT 3.4 K (313°F)	5.31×10^5 [illegible]	2.9×10^{-6} 12.7×10^{-6}	0.208 1.44	1.34×10^3 [illegible]	164 (-165)	533 (500)	MDC'S BASELINE STRAIN ISOLATOR A LOW STIFFENING POINT SILICONE
[illegible] "MANHATTAN"	[illegible]	[illegible] AT [illegible] K (-459°F) 3.29 AT 422 K (300°F)	[illegible] AT [illegible] K (-459°F) 0.0048 AT 422 K (300°F)	2.1×10^5 [illegible]	[illegible] 164 K (-275°F) [illegible] 311 K (100°F) [illegible] 422 K (300°F)	[illegible] 111 K (-265°F) 0.5[illegible] 3.4 K (124°F) [illegible] [illegible] K (-265°F)	[illegible] 144 K (-200°F) [illegible] 700 (800°F) [illegible] (-265°F)	111 (-265)	811 (900)	LOCKHEED'S BASELINE STRAIN ISOLATOR
RTV-560 GENERAL ELECTRIC	1420	4.8 AT 60 Hz 4.2 AT 10^5 Hz	0.006 AT 60 HZ 0.061 AT 10^5 Hz	4.90×10^6 (711)	265×10^{-6} 314×10^{-6}	0.13	1.34×10^3 (.32)	164 (-165)	533 (500)	A FLEXIBLE IRON OXIDE FILLED SILICONE ADHESIVE
HONEYCOMB FIBERGLASS - PHENOLIC	[illegible]	[illegible] EST	0.01 EST	NA	ND	[illegible]	[illegible]	NA	533 (500)	1/4 INCH HEXAGONAL CELLS
FACE SHEETS FIBERGLASS - PHENOLIC	[illegible]	[illegible] EST	[illegible] EST	[illegible] IN PLANE	[illegible] IN PLANE	0.13	[illegible]	NA	533 (500)	USED ON GEMINI HEAT SHIELD
HT-435 STRUCTURAL ADHESIVE	[illegible] EST	[illegible] EST	0.02 EST	NA	ND	[illegible] EST	[illegible]	NA	478 (400)	HT424 FILM WITHOUT ALUMINUM FILLER FOR ELECTRICAL TRANSPARENCY

NOTES

1. ND - NO DATA
2. ALL PROPERTIES AT ROOM TEMPERATURE UNLESS OTHERWISE NOTED
3. EST - ESTIMATED
4. NA - NOT APPLICABLE

PRECEDING PAGE BLANK NOT FILMED

During this study Lockheed's LI-900, which has lower density than LI-1500, was selected for the Orbiter baseline TPS HRSI. The thermal conductivity is higher and the strength lower. However, the use of LI-900 results in a significant weight saving for the TPS. Although LI-1500 was considered as the baseline HRSI material for the design concepts considered in this study, it could be replaced with LI-900 without antenna system degradation because of the similarity in electrical properties. The dielectric constant and loss tangent of these and the GE and MDAC-E HRSI materials are given in table X. This data was obtained from NASA-LaRC measurements (ref. 6). The dielectric constant of all the HRSI materials are comparable. However, the loss tangent of both LI-1500 and LI-900 is considerably lower at elevated temperatures than that of the other two HRSI candidates. Therefore, LI-1500 and LI-900 can be expected to give the best RF transmission characteristics.

TABLE X

HRSI ELECTRICAL PROPERTIES

TEMPERATURE K(°F)	LSMC SILICA LI-1500		LSMC SILICA LI-900		GE MULLITE MOD 1A		MDAC MULLITE MOD IIIA	
	ε_r	tan δ	ε_r	tan δ	ε_r	tan δ	ε_r	tan δ
298(77)	1.23	0.00025	1.14	0.0012	1.19	0.0002	1.28	0.003
473(392)	1.23	0.00025	1.14	0.0012	1.19	0.0003	1.29	0.004
673(752)	1.23	0.00025	1.15	0.0010	1.19	0.0007	1.30	0.008
873(1112)	1.24	0.00025	1.15	0.0005	1.20	0.0015	1.32	0.015
1073(1472)	1.24	0.00035	1.15	0.0004	1.20	0.0028	1.34	0.028
1273(1832)	1.24	0.00060	1.15	0.0006	1.20	0.0045	1.37	0.049
1473(2192)	1.25	0.00115	1.16	0.0008	1.21	0.0066	1.40	0.076

NOTE: DATA FROM REFERENCE 6

The LI-1500 tile joint design has a recess around the inner edge of the tile next to the bonded surface to permit inclusion of an FI-600 filler strip. FI-600 is a resilient silica fiber mat insulation, which prevents a direct view through the tile gaps to the structure. FI-600 is 96.1 kg/m^3 (6 lb/ft^3) in density and is impregnated with hydrolized silicone for waterproofing. The thermal properties of FI-600 are given in Appendix A. The dielectric constant and loss tangent are somewhat lower than those of LI-1500 due to the lower density. The estimated values are given in table VII.

Attachment materials. - In order to attach the HRSI materials to the Orbiter structure, additional materials are required. They include an RF transparent structural panel, a strain isolation sponge, and an adhesive. The properties of the materials considered for these functions are given in table IX.

RF transparent structural panel: The basic structural member which provides the means for fastening the antenna window to the Orbiter is a fiberglass-phenolic honeycomb sandwich. The face sheets and core are composed of a fiberglass cloth impregnated with a heat resistant phenolic resin. The facesheets consist of three layers of fiberglass cloth laminated with their warp direction oriented at 0, 30, and 60 degrees to provide uniform strength properties in all directions. The honeycomb core is a 56.1 kg/m^3 (3.5 lb/ft^3), 6.35 mm (0.25 in.) hexagonal cell, manufactured by the Hexcel Company. The facesheets are bonded to the core with HT-435 (American Cyanamid Co.) which is specially formulated for RF transmission. Structural adhesives for applications such as this are usually formulated with an aluminum powder for high temperature strength; however, no aluminum is used in HT-435.

Both the facesheet thickness and the core density can be varied to obtain a minimum weight panel as a function of panel stiffness requirements as discussed in the subsection on Strength Studies in this section. Core sizes are nominally 4.76 - 6.35 mm (0.188 - 0.250 in.). For thin facesheets, larger core sizes could result in buckling between cell walls.

Strain isolator sponge: LI-1500 and the other candidate HRSI materials are rigid and have relatively low strengths. Therefore, they must be isolated from thermally and mechanically induced strains of the structure to which they are attached. Two candidate silicone rubber sponges, RL-524 type S-105 and RL-1973, both manufactured by Raybestos Manhattan, were evaluated. RL-524 was selected primarily because of its low temperature stiffening point. Vendor data indicated that RL-524 remained more flexible than RL-1973 at 117 K (-200°F) due to the methyl-phenol ratio in the silicone rubber formulation. The properties of both RL-524 and RL-1973 are given in table IX.

Adhesive: RTV-560, a General Electric silicone elastomeric adhesive, is used to bond the HRSI to the strain isolator sponge, and the strain isolator sponge to the fiberglass-phenolic window panel or the aluminum Orbiter structural skin. The RTV-560 silicone withstands both low and high temperatures (158 to 561 K (-175 to 550°F)). Without loading, the low temperature can be extended to 117 K (-250°F). A menthyl-phenyl silicone polymer provides the low temperature flexibility and an iron oxide provides the high temperature stability. The properties of RTV-560 are given in table IX.

Antenna cavity foams. - Many of the commercial antennas listed in the Antenna Survey subsection of this section use a rigid foam inside the antenna. A list of the properties of some of these foams are shown in table XI. All of these rigid foams withstand 394 K (250°F) but the lower density (320 - 640 kg/m^3 (2 - 4 lb/ft^3)) closed cell urethane foam can rupture during vacuum exposure. Urethane foams denser than 96.1 kg/m^3 (6 lb/ft^3) are rigid enough to withstand vacuum conditions. If the rigid urethane foams are heated above 422 K (300°F)

TABLE XI

THERMAL PROPERTIES OF ORGANIC MATERIALS

MATERIAL	DENSITY KG/M^3 (LB/FT^3)	THERMAL CONDUCTIVITY W/M°K(BTU-IN./FT^2-HR-°F)	SPECIFIC HEAT WS/KG-K(BTU/LB-F) AT 15 K(-432°F)	MAXIMUM ③ TEMPERATURE K(°F)
CPR747-30 (UPJOHN CO.) ①	481(30)	0.075(0.52)	1800(0.43)	422(300)
CPR747-30 (UPJOHN CO.) ①	96(6)	0.038(0.26)	1800(0.43)	394(250)
CPR-17-3 (UPJOHN CO.) ①	48(3)	0.035(0.24)	1717(0.41)	394(250)
CPR-17-4 (UPJOHN CO.) ①	64(4)	0.036(0.25)	1758(0.42)	394(250)
NOPCOFOAM A-206 ① (DIAMOND SHAMROCK CHEMICAL CO.)	96(6)	0.040(0.28)	1800(0.43)	394(250)
NOPCOFOAM H-402 ① (DIAMOND SHAMROCK CHEMICAL CO.)	32(2)	0.019(0.13)	1675(0.40)	422(300)
ECCOSPHERE FT-102 (EMERSON AND ② CUMING)	160(10)	0.058(0.40)	963(0.23)	522(480)
TEFLON TFE	2196(137)	0.245(1.70)	1047(0.25)	533(500)
TEFLON FEP	2196(137)	0.245(1.70)	1172(0.28)	505(450)

NOTES: ① RIGID URETHANE
② GLASS SPHERES - 10 TO 250 MICRON DIAMETER
③ MINIMUM TEMPERATURE IS LESS THAN 116 K (-250 F) FOR ALL MATERIALS

they start to soften slightly on the hot face. By special compounding, this high temperature limitation can be increased. Urethane foams have been used for cryogenic insulation to low temperatures of 20.4 K (-432°F). Therefore, the use of the urethane foams to 117 K (-250°F) should not cause a problem. The FT-102 eccosphere should be capable of stable performance at temperatures of 117 to 450 K (-250 to 350°F) and in a vacuum.

Material interfaces. - There do not appear to be any adverse reactions possible between the basic materials used in the antenna system design concepts considered in this study. In some cases it may be necessary to use a series of metallic plating steps in order to prevent galvanic action due to an adverse metal couple. An alodine coating, which is conductive, can be applied to aluminum mounting flanges to prevent corrosion due to oxidation.

Replacement and repair. - The antenna system design concepts considered in this study permit the antenna window to be removed easily for either replacement of the window or access to the antenna. Minor chips in the LI-1500 coating can be repaired with Lockheed's LI-0010 coating. LI-0010 is not waterproof, but provides the proper surface emittance. It is unlikely that a single tile in a large window could be replaced since the honeycomb panel which supports the tiles over the antenna may not withstand the cleaning process required to remove the old adhesive and sponge pad. In general the antenna window tiles are no more susceptible to damage during Orbiter assembly or Orbiter mission than the surrounding TPS tiles.

Minor separations or unbonded areas around the HRSI tile edges can be repaired by injecting catalyzed (RTV-560) into those areas. Major unbonded areas should be refurbished using established techniques.

Damaged honeycomb structure can be evaluated by X-ray and ultrasonic nondestructive examination evaluation (NDE) methods. X-ray NDE would be used to determine the core integrity, and ultrasonic NDE would be used to determine the presence of unbonded areas between the facesheets and honeycomb core. Either of these conditions would require the replacement of the antenna window.

Thermal Studies

Thermal sizing analyses were conducted to determine thickness requirements when using silica HRSI's, mullite HRSI or ablative material as the antenna window and surrounding TPS materials. Detailed thermal analysis was conducted for only the S-band antenna system as discussed in the section on S-BAND ANTENNA SYSTEM DESIGN.

Environmental factors. - The required thermal protection for the Shuttle depends on the antenna system concept and a number of other factors. These factors include: (1) the initial and maximum allowable temperature; (2) the local pressure environment of the insulation; (3) the mass or heat capacitance of the antenna system concept; (4) the heat transfer boundary condition on the inboard side of the antenna system; (5) the emittance, absorptance and view factor of the antenna window surface material to space; and (6) the critical temperature for the particular antenna system concept. The thermal sizing analyses utilized the following environmental factors:

(a) The maximum preentry initial temperature design value was 311 K (100°F).

(b) The maximum allowable antenna/primary structure temperature was 422 K (300°F) requirement for this contract.

(c) The local static surface pressure was used to determine insulation thermal conductivity.

(d) The aluminum primary structure equivalent thickness was 1.525 mm (0.06 in.).

(e) The backface boundary condition included heat transfer from primary structure or antenna backcap to internal thermal control insulation backed by an aluminum cabin wall equivalent thickness of 1.0 mm (0.04 in.).

(f) The surface emittance variation due to temperature was included.

(g) The entry aerothermodynamic heat transfer coefficients and recovery temperatures where used as surface heating boundary conditions.

(h) The external surface radiation sink temperatures were 0 K (-460°F) during entry and 300 K (80°F) after 15.3 km (50 kft).

The critical thermal environment occurs during entry. However, launch interference heating between the Orbiter and its external tank combined with a once-around mission may increase initial entry temperatures and, therefore, the required antenna window thicknesses. This problem is not peculiar to antenna system design but is common to the adjacent TPS design as well. This problem would be considered as a candidate design detail modification upon integration into the Orbiter.

Thermal models. - One-dimensional thermal analyses and MDC's General Heat Transfer Program (HEATRAN Code) were used to determine the thickness requirements of the antenna window and surrounding TPS materials. The computer program is a "block type" thermal analyzer in which physical properties, geometry and linkage relationships are input to the program which then calculates lumped thermal capacitance and conductance terms. Backward finite difference techniques were then used to obtain transient solutions.

Two one-dimensional antenna system thermal models and one one-dimensional TPS model were used. The two antenna system thermal models shown in figure 25 include the S-band and VHF antennas behind the antenna windows. Of the antennas under study, these represent the largest and smallest thermal capacitances and, therefore, their use bounds the analysis results. Both thermal models were divided into 35 nodes and included inboard radiation to thermal control insulation. These thermal models were also modified for the multiple-layer antenna window concept. The thermal model for the adjacent TPS (figure 26) was also divided into 35 nodes to obtain a consistent level of detail.

Results. - One-dimensional thermal sizing results were obtained for LMSC LI-1500, LMSC LI-900, GE MOD 1A and multiple-layer window thermal insulation materials. Plots of maximum interface temperature versus the primary insulation material thicknesses are shown in figures 27 through 30. From these results the insulation thickness can be determined for specific interface requirements. The results for three specific temperature constraints are presented in table V in terms of thickness and unit weight.

The VHF antenna window thicknesses were sized to maintain the temperature of the spiral radiating element below 422 K (300°F). The spiral is located on the outer surface of a fiberglass honeycomb structural panel at the top of the antenna cavity. The results (table XII) show that the antenna window thicknesses can be 17 to 25% more than the adjacent TPS thickness if the same thermal protection material is used for both. Larger differences in thickness can occur with dissimilar materials.

The S-band antenna window thicknesses were sized to limit the RTV adhesive bondline between the HRSI and strain isolator pad to 533 K (500°F). The critical temperature was determined by plotting the maximum temperatures for the bondline, the antenna aperture and the Kevar antenna backcap as a function

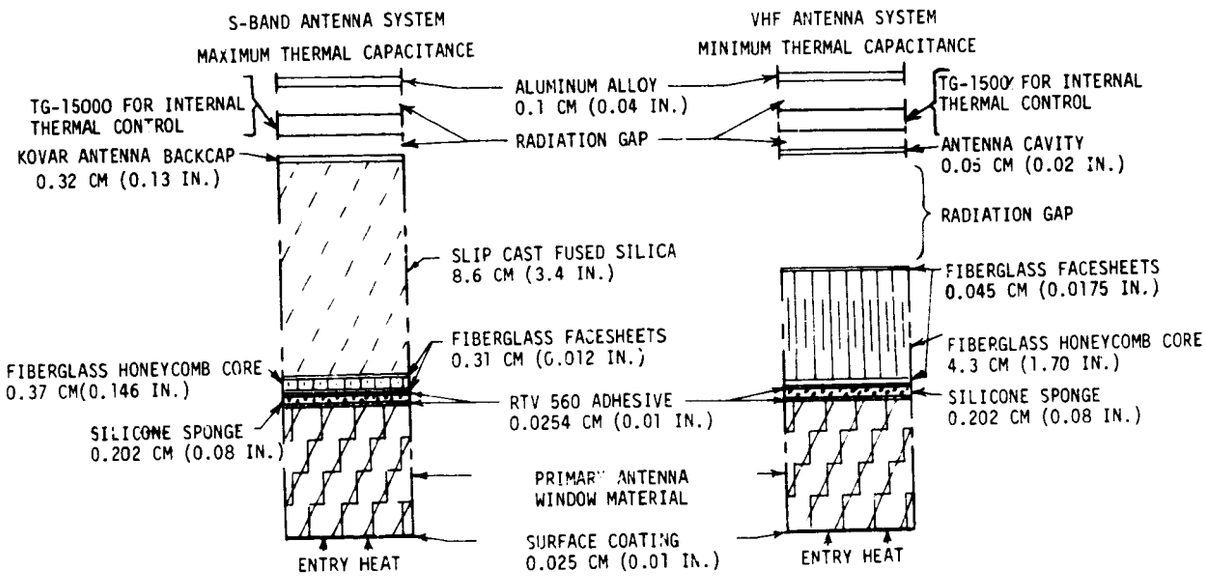

ONE-DIMENSIONAL ANTENNA SYSTEM THERMAL MODELS

FIGURE 25

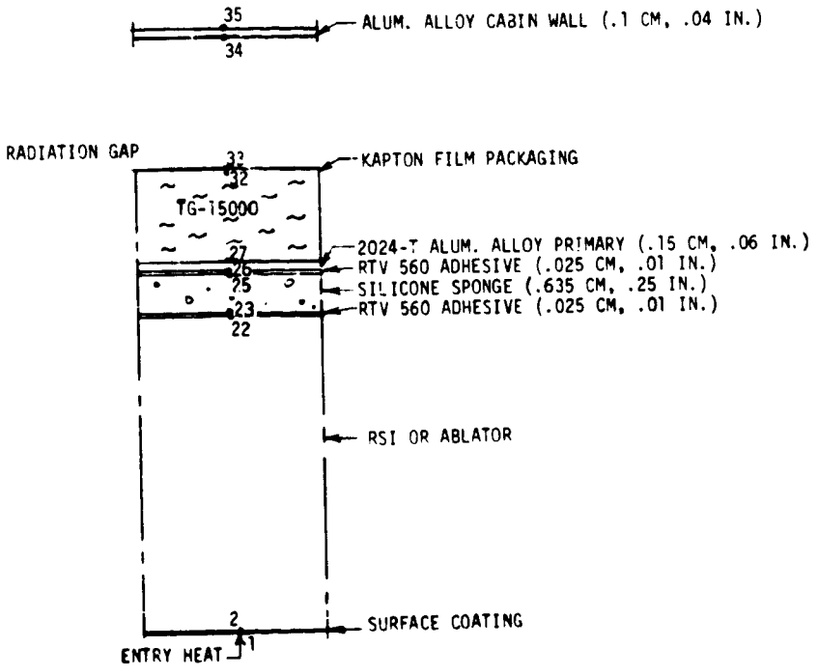

ONE-DIMENSIONAL TPS THERMAL MODEL

FIGURE 26

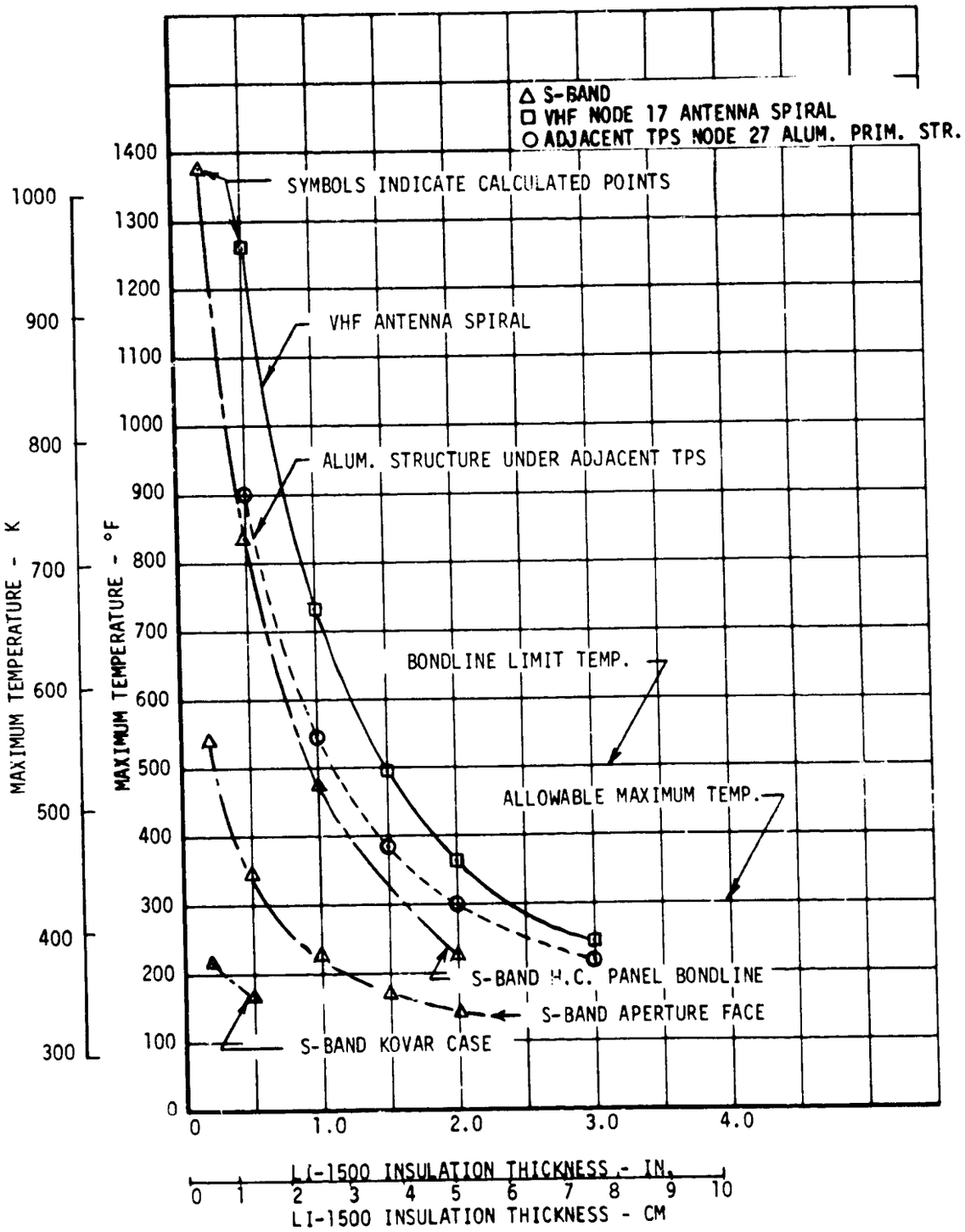

LI-1500 HRSI REQUIREMENTS

FIGURE 27

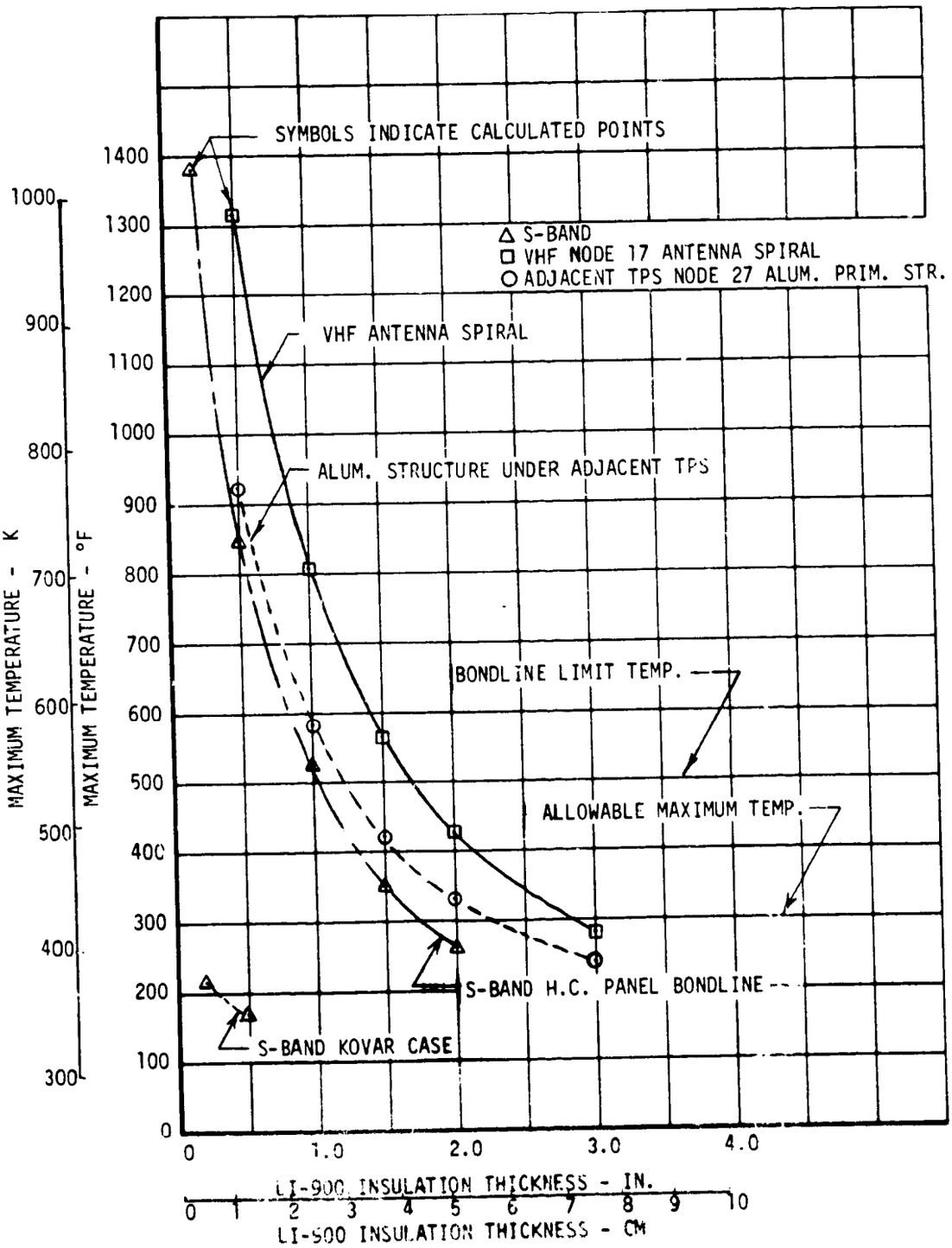

LI-900 HRSI REQUIREMENTS

FIGURE 28

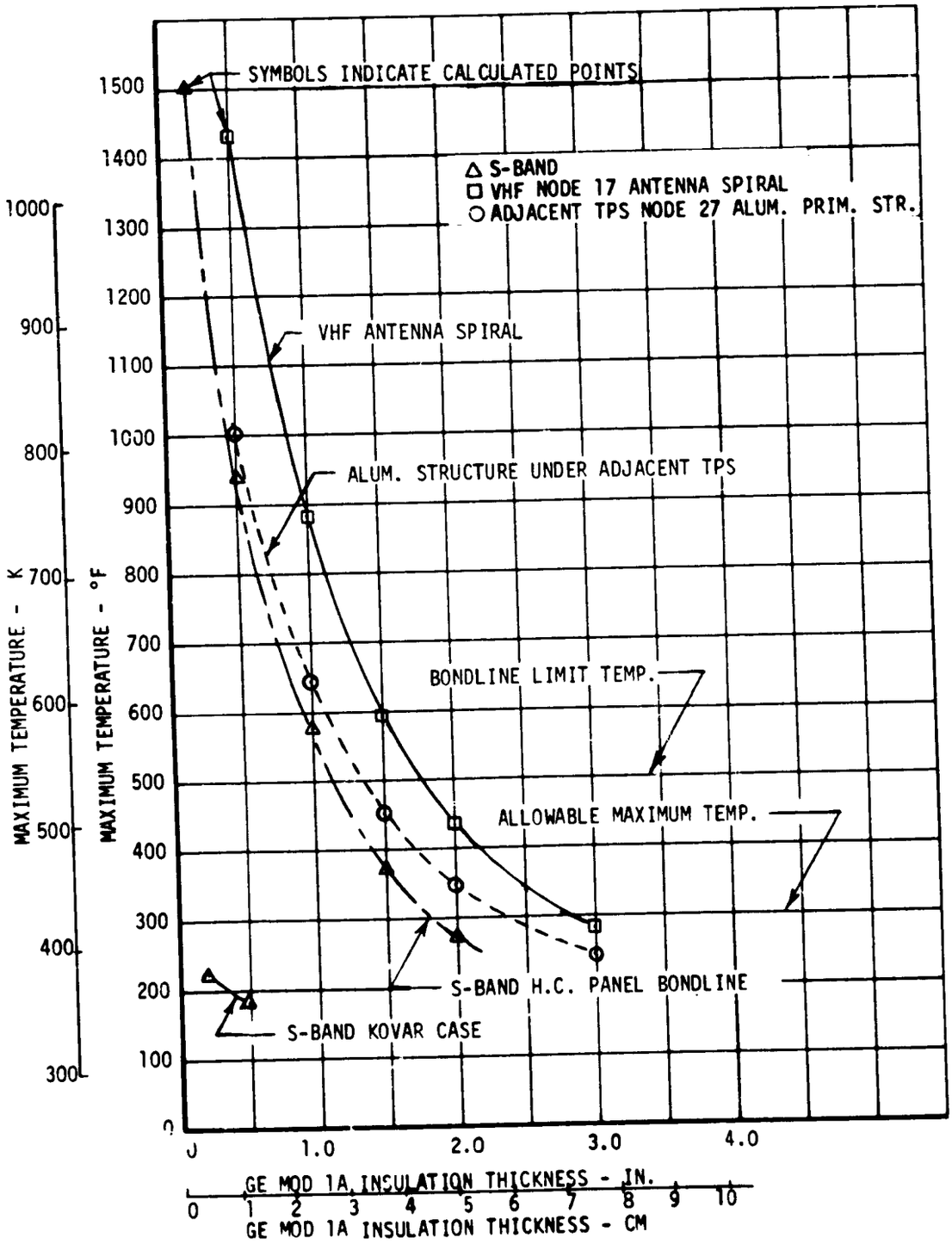

GE MOD 1A HRSI REQUIREMENTS

FIGURE 29

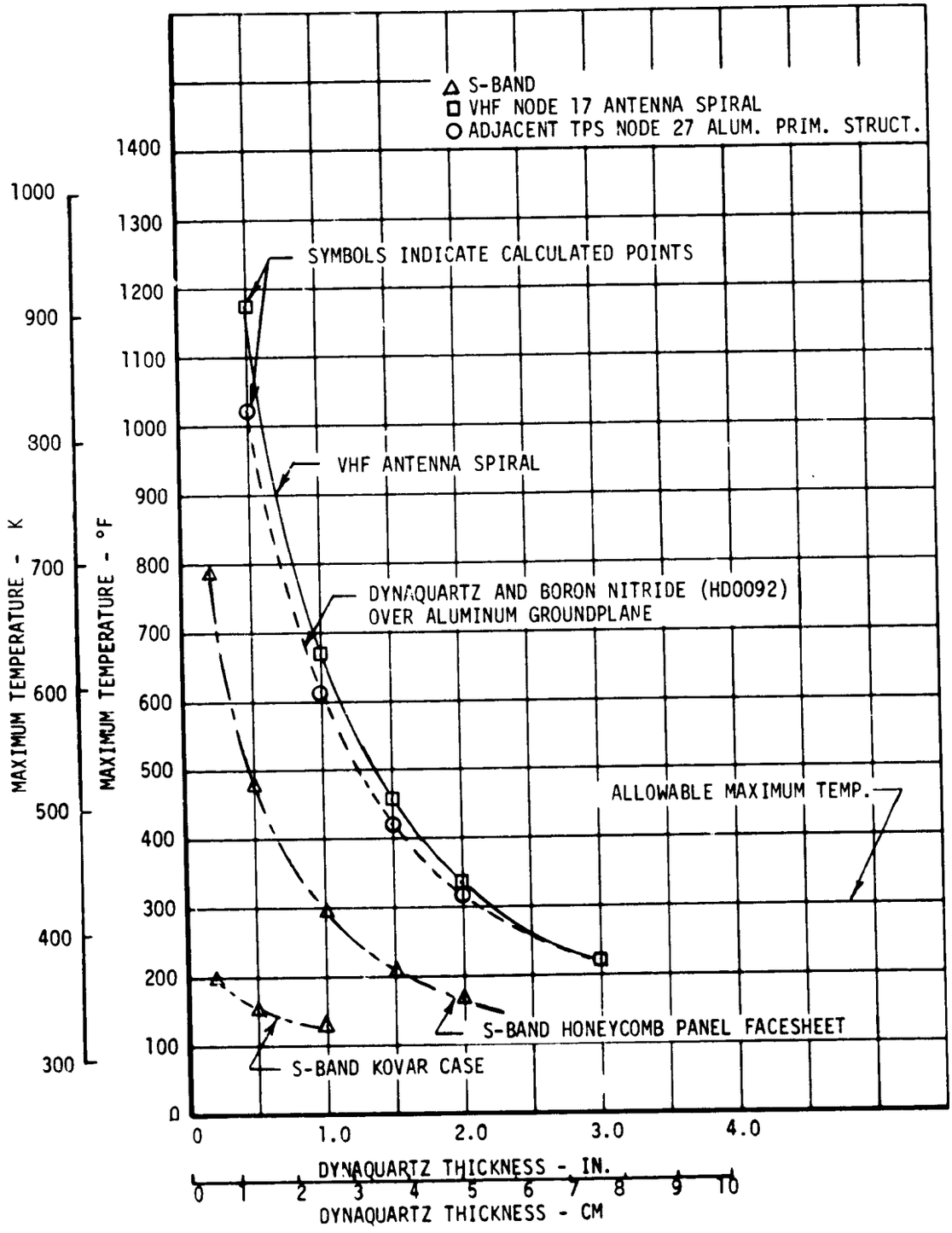

DYNAQUARTZ INSULATION REQUIREMENTS

FIGUR · 30

TABLE XII

ONE-DIMENSIONAL THERMAL INSULATION SIZING RESULTS

THERMAL MODEL	CRITICAL TEMPERATURE AND LOCATION	THERMAL PROTECTION MATERIAL							
		LI-1500 HRSI		LI-900 HRSI ①		GE MOD 1A HRSI		DYNAQUARTZ BORON NITRIDE	
		THICKNESS CM(IN.)	WEIGHT/AREA KG/M^2(PSF)	THICKNESS CM(IN.)	WEIGHT/AREA KG/M^2(PSF)	THICKNESS CM(IN.)	WEIGHT/AREA KG/M^2(PSF)	THICKNESS CM(IN.)	WEIGHT/AREA ② KG/M^2(PSF)
VHF ANTENNA (MINIMUM THERMAL MASS)	422 K(300°F) (ANTENNA SPIRAL)	5.97(2.35)	4.35(2.94)	7.29(2.85)	10.45(2.14)	7.11(2.80)	13.67(2.80)	6.65(2.62)	29.44(6.03)
S-BAND ANTENNA (MAXIMUM THERMAL MASS)	533 K(500°F) (WINDOW ADHESIVE)	2.36(0.93)	5.66(1.16)	2.62(1.03)	3.76(0.77)	2.87(1.13)	5.52(1.13)	1.57(0.62) ③	21.33(4.37)
ADJACENT TPS	422 K(300°F) (ALUMINUM SKIN STRUCTURE)	5.08(2.00)	12.21(2.50)	5.84(2.30)	1.45(1.73)	6.02(2.37)	11.57(2.37)	5.08(2.00) ④	12.21(2.50)

NOTES: ①BASED ON DENSITY CHANGE ONLY.
②INCLUDES BORON NITRIDE SURFACE LAYER.
③BASED ON 900°F TEMPERATURE LIMIT OF KOVAR BACKCAP.
④LI-1500 TPS

of LI-1500 insulation thickness as shown in figure 27. By definition the maximum allowable temperatures for the S-band antenna aperture face is 422 K (300°F). However, slip-cast fused silica in the S-band antenna can withstand temperatures of 1255 K (1800°F) or greater. The maximum allowable temperature for the Kovar antenna backcap is 422 K (300°F). An LI-1500 insulation thickness of 5.08 mm (0.2 in.) is more than sufficient to protect the Kovar antenna case; 1.52 cm (0.60 in.) is needed to limit the S-band antenna aperture to 422 K (300°F). However, a 2.36 cm (0.93 in.) thickness is required to limit the LI-1500 bondline to 533 K (500°F). Thus, the bondline is the critical element in the S-band antenna window design. The results (table XII) also show that the window thickness required for the S-band antenna system is significantly less than that of the adjacent TPS. For LI-1500 thermal protection material the required S-band window thickness is 2.36 cm (0.93 in.) compared to 5.08 cm (2.0 in.) for the adjacent TPS. This is due to the greater thermal mass of the S-band antenna.

Once the critical element for the S-band antenna system design was found using LI-1500, plots were not made to find critical elements for other thermal protection materials, except for the multiple-layer antenna window concept. The thermal model was modified to include the 1.07 cm (0.42 in.) HD-0092 boron nitride surface layer and eliminate the strain isolator pad. The critical element was found to be the Kovar antenna backcap (figure 30). From a weight per unit area basis, the multiple-layer antenna window is much heavier than single-layer antenna window using HRSI thermal protection materials.

Structural Integration Studies

Structural integration is one of the important considerations in achieving a satisfactory high temperature antenna system design for the Orbiter. Not only must the antenna system provide the required radiation pattern and impedance characteristics, but it must do so in a structural environment which includes TPS in addition to the load carrying members. It is also necessary to preserve the TPS so that heat transfer through the antenna area is equal to or less than that in the surrounding structure. Particular attention was directed toward the installation attachment and removal factors to provide maximum accessibility for installation and maintenance. At the expense of accessibility the designs could be modified. The alternate approaches which were considered are, in general, applicable to all the designs but result in reduced accessibility.

Antenna installation concepts. - Six antenna system concepts were selected as candidates for integration into the Space Shuttle Orbiter. The antenna system concepts are based on the following antenna types:

(a) S-band cavity backed helix

(b) Ku-band surface wave slot

(c) VHF cavity backed spiral

(d) L-band annular slot

(e) C-band horn

(f) C-band linear slot

The L-band and C-band antenna system concepts were initially developed by MDAC-E under NASA-LaRC contract NAS 1-11273 (ref. 1) and are essentially unchanged, since changes were not indicated by the results of analyses performed during this study. The basic description of these concepts are repeated in this report. The S-band, Ku-band and VHF antenna system concepts were developed during this study. Layout drawings were prepared for each concept to show the principal design features.

The respective designs are based on the structural requirements given in the section on DESIGN CONSIDERATIONS AND CONSTRAINTS and reflect the results of the electrical, thermal and strength studies. Although the structural designs are based on these requirements, the design can easily be adapted to other bulkhead and stringer spacings. Stringer spacing (nominally 10.16 cm (4.00 in.)) in the region of the antenna systems was allowed to vary locally depending on the size of the antenna and antenna window. Structural members were added as necessary to carry the structural loads around the antenna system installation.

The TPS thickness used for the antenna system design is 5.766 cm (2.270 in.); 5.08 cm (2.00 in.) for the HRSI tile thickness, 6.35 mm (0.250 in.) for the strain isolation pad thickness, and 0.51 mm (0.020 in.) for the RTV-560 bonding thickness. The antenna window thickness used for the antenna system designs, except for the VHF antenna system, is also 5.766 cm (2.270 in.); 5.08 cm (2.00 in.) for the HRSI thickness, 2.03 mm (0.080 in.) for the strain isolator pad thickness, 4.3 mm (0.170 in.) for the fiberglass-phenolic honeycomb subpanel, and 0.51 mm (0.020 in.) for the RTV-560 bonding thickness. For the VHF antenna system both the HRSI and the honeycomb thickness are increased. RTV-560 is used to bond the strain isolation pad to both the HRSI and the fiberglass-phenolic honeycomb subpanel. High density laminated phenolic inserts are provided where the fasteners attach the honeycomb panel to the primary structure. The thermal expansion of these inserts and the panel match.

The antenna window assembly is attached to primary structure with four or more Allen head cap screws. Access to these fasteners, which are captive in the window assembly, is obtained through holes in the HRSI. Measured data from MDAC-E's Contract NAS 9-12854, Development and Design Application of Rigidized Reusable Surface Insulation Thermal Protection System, has shown no increase in local bondline temperature for dead-end holes with diameters of 0.475 cm (0.1875 in.). Also, plasma arc tunnel testing of Gemini ablative heat shield indicated no significant charring for heat shield holes of 0.635 cm (0.25 in.) diameter. Therefore, 0.554 cm (0.218 in.) holes through the HRSI are considered acceptable. Experience gained through the above contract also indicated the HRSI tiles are less prone to damage and simpler to install using an Allen head shaped tool instead of a screw driver. The shape of the screw head keeps the tool end from slipping and damaging the fragile HRSI material.

Two of the antenna system concepts also have a super-alloy foil window enclosure for radiation pattern control. This enclosure does not extend to the outer surface of the HRSI, but stops at a level where the temperature maximum is approximately 700 K (800°F).

The basic geometric data associated with the various antenna configurations considered are shown in figure 31. There is a large size variation between the VHF antenna and the other antennas.

S-band antenna system installation: The S-band antenna system installation is shown in figure 32. The antenna window assembly is similar to the C-band slot antenna configuration except that no window edge enclosure is used. Modification to the primary structure and TPS of the Orbiter is minimal. The cylindrical antenna is attached to an aluminum support housing, which in turn is attached to the support bracket. This attachment arrangement allows the antenna to be removed from either the outside or inside of the Orbiter. The antenna support housing requires an increase in longitudinal stringer spacing to 12.00 cm (4.72 in.). Two transverse stringers are required to provide structural continuity around the skin cutout. The size and shape of the LI-1500 antenna window is identical to the adjacent HRSI tiles.

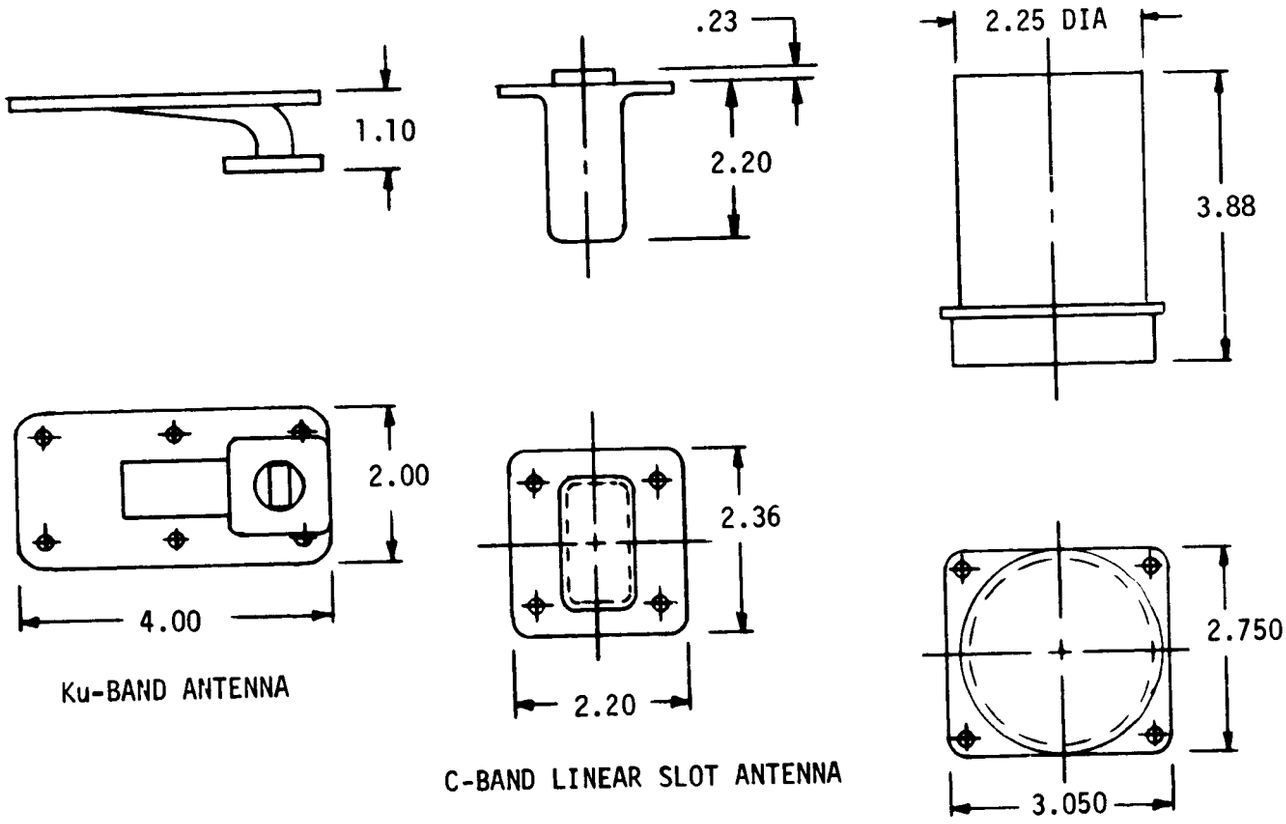

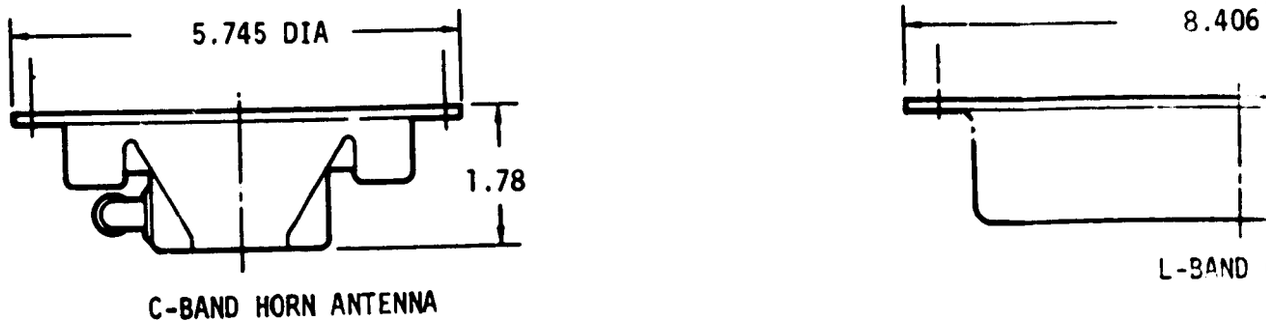

ANTENNA CONFIGURATIONS

FIGURE 31

PAGE 6-40 INTENTIONALLY LEFT BLANK.

FOLDOUT FRAME

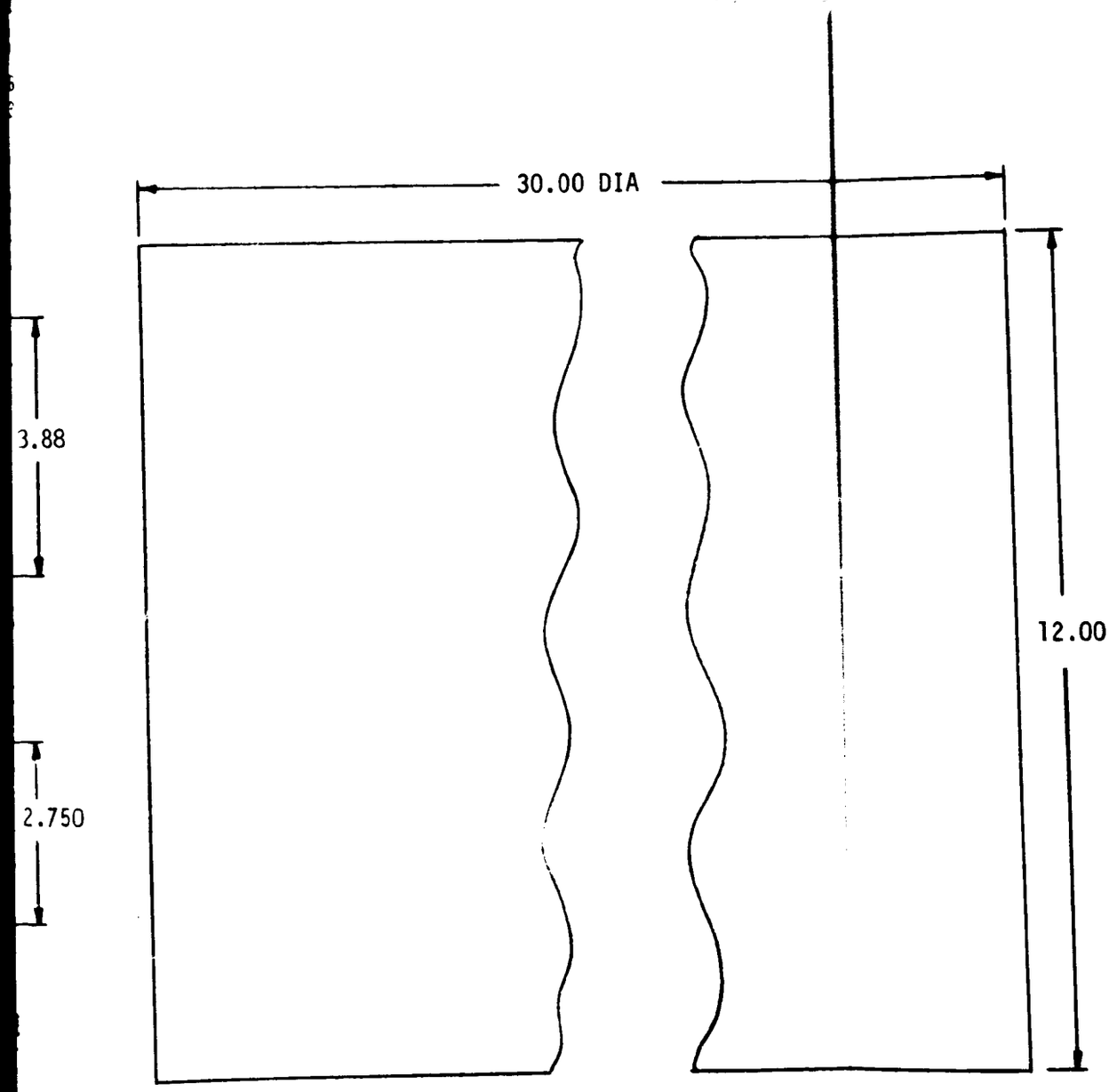

VHF ANTENNA

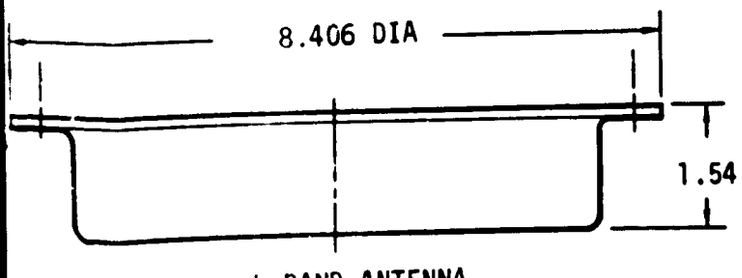

L-BAND ANTENNA

DIMENSIONS GIVEN IN INCHES.

NK.

FOLDOUT FRAM

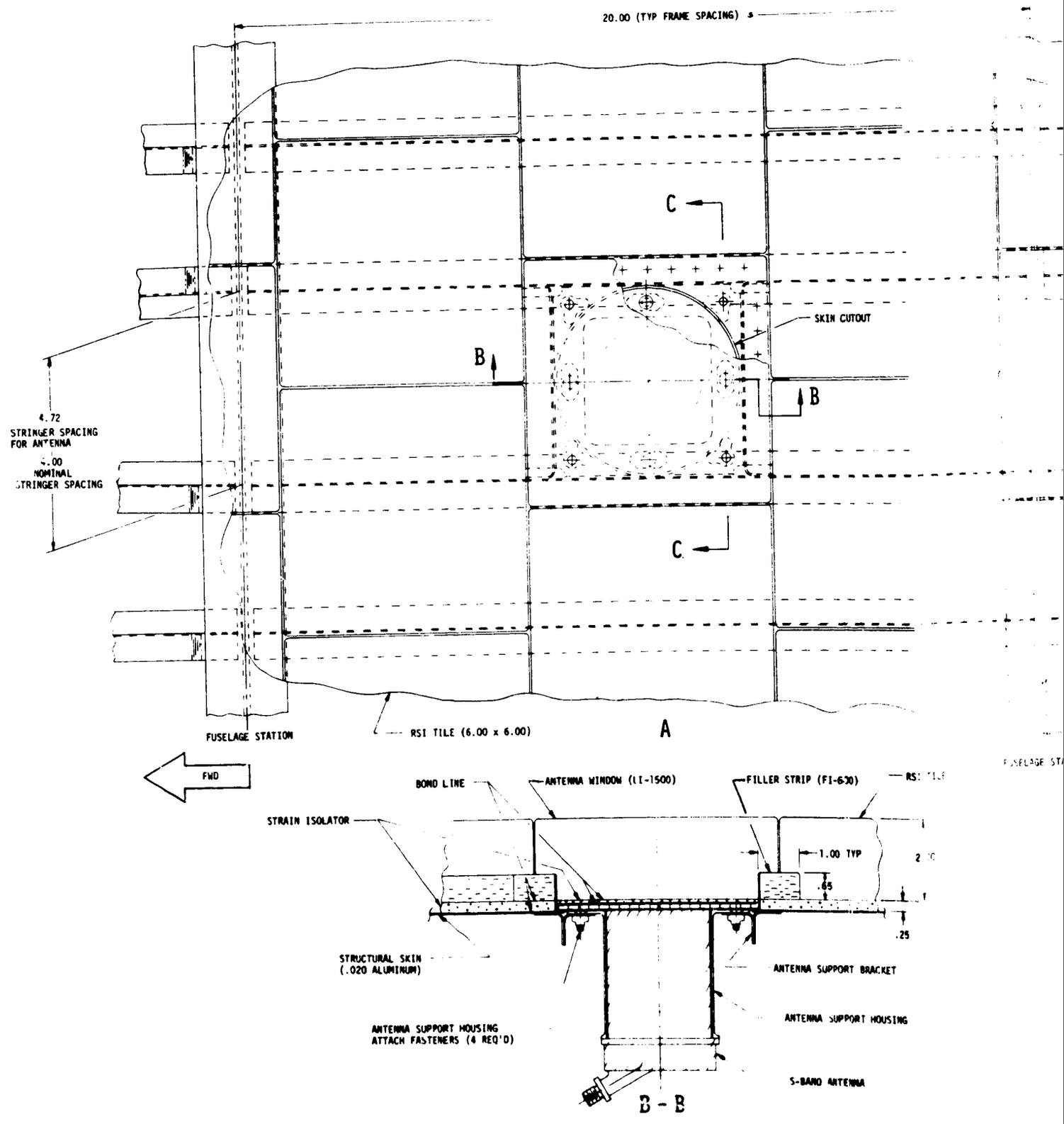

S-BAND ANTENNA SYSTEM INSTALLATION

FIGURE 32

PRECEDING PAGE BLANK NOT FILMED

PAGE 6-42 INTENTIONALLY LEFT BLANK.

FOLDOUT FRAME

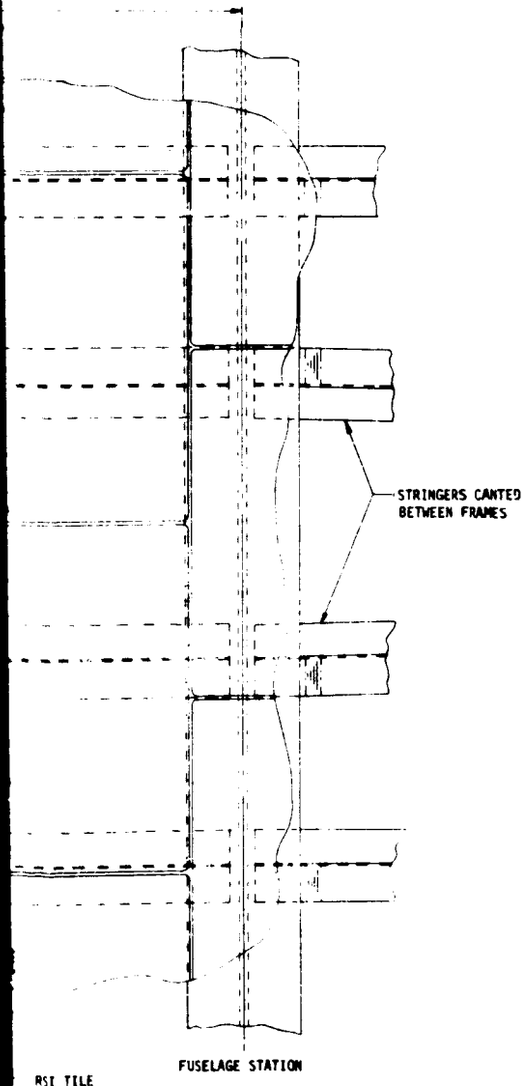

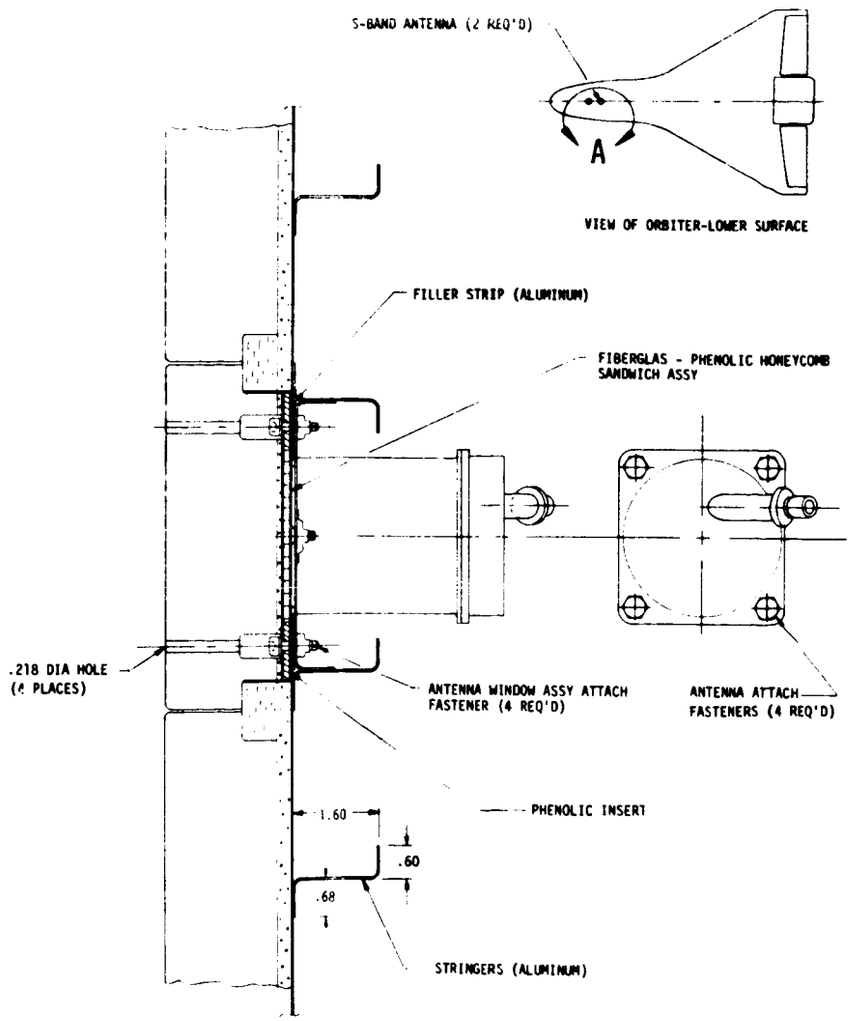

C - C

2.00

ALL DIMENSIONS GIVEN IN INCHES.

FOLDOUT FRAME

1

It may be noted that the antenna window size is slightly smaller (3.05 cm (1.20 in.)) on the side than that shown for the test model discussed in the section on S-BAND ANTENNA SYSTEM DESIGN. This design was completed after fabrication of the test articles had started and could not be changed without serious schedule impact.

Ku-band antenna system installation: The Ku-band antenna system installation is shown in figure 33. Modification to the primary structure and TPS is minimal. The size of the antenna is such that it can be positioned between the 10.6 cm (4.00 in.) spaced longitudinal stringers. The antenna is attached to a mounting plate, which is also used to strengthen the structural skin around the cutout. A cutout is provided in the mounting plate allowing the waveguide attach flange to be passed through and mated with the waveguide. If access from the interior of the Orbiter is not available, an access door, adjacent to the antenna, must be provided for making the waveguide flange interface connection. An alternate approach would be to modify the antenna attach flange. By rearranging the attach hole pattern and machining access holes in the attach flange and the mounting plate, the waveguide attach fasteners could be installed from outside the Orbiter.

The antenna window assembly consists of a LI-1500 tile (having the same dimensions as the adjacent RSI tiles), a silicone sponge pad and a fiberglass honeycomb subpanel. It is mechanically attached to the mounting plate with four Allen head cap screw fasteners. In order to minimize and control the pattern degradation due to surface wave excitation, as discussed in the subsection on Electrical Studies of this section, a wire screen covering the strain isolator in the immediate area around the antenna and extending some distance forward is required. Figure 33 shows a #20 mesh stainless steel screen imbedded in the adhesive between the HRSI tile and the silicone sponge strain isolator. The screen adjacent to the antenna has a triangular shape which flares to a width of 15.24 cm (6.00 in.) in the primary direction of the radiation pattern. The screen extends 30.50 cm (12.00 in.) forward of the base of the triangular shaped screen. These dimensions correspond to a configuration which was tested.

VHF antenna system installation: The VHF antenna system installation is shown in figure 34. The VHF antenna is much larger than the other antennas considered in this study. However, the design approach used is generally the same as used for the other designs. Since there is no off-the-shelf flush mounted antenna for the VHF frequency range, a cavity backed spiral antenna with a 76.2 cm (30.0 in.) aperture diameter and a 30.48 cm (12.00 in.) cavity depth was designed. Unlike the other antenna system installations, the VHF installation included the design of the basic antenna structure.

The VHF antenna window assembly is 86.36 cm (34.00 in.) wide and 104.14 cm (41.00 in.) long. The basic window construction is similar to that used for the smaller antennas described previously. A total of 33 LI-1500 tiles are used to cover the window area; 27 are the same size as the basic TPS tiles and 6 are half size. Alternatively, 30 tiles, 24 regular size and 6 oversize, could be used. Due to the low thermal capacity of the antenna, the LI-1500 tiles for the antenna window were increased from 5.08 cm (2.00 in.) to 5.98 cm (2.35 in.) as discussed in the subsection on Thermal Studies of this section.

PAGE 6-44 INTENTIONALLY LEFT BLANK.

PRECEDING PAGE BLANK NOT FILMED

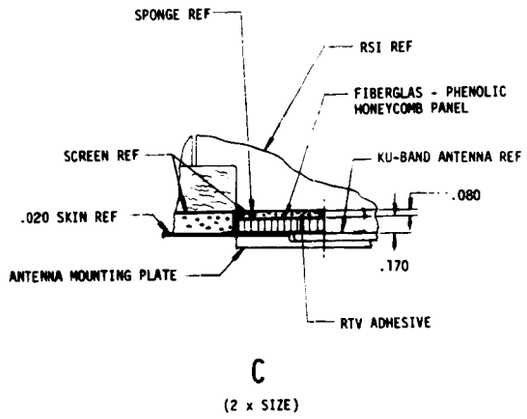

C
(2 x SIZE)

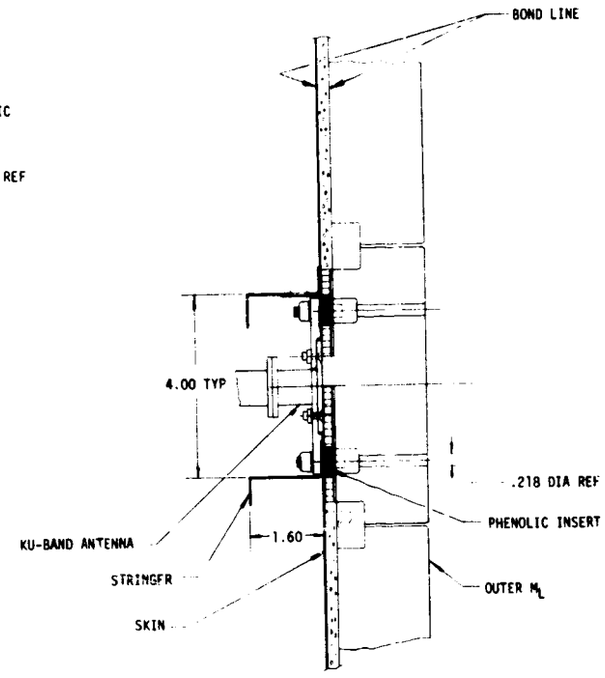

D - D

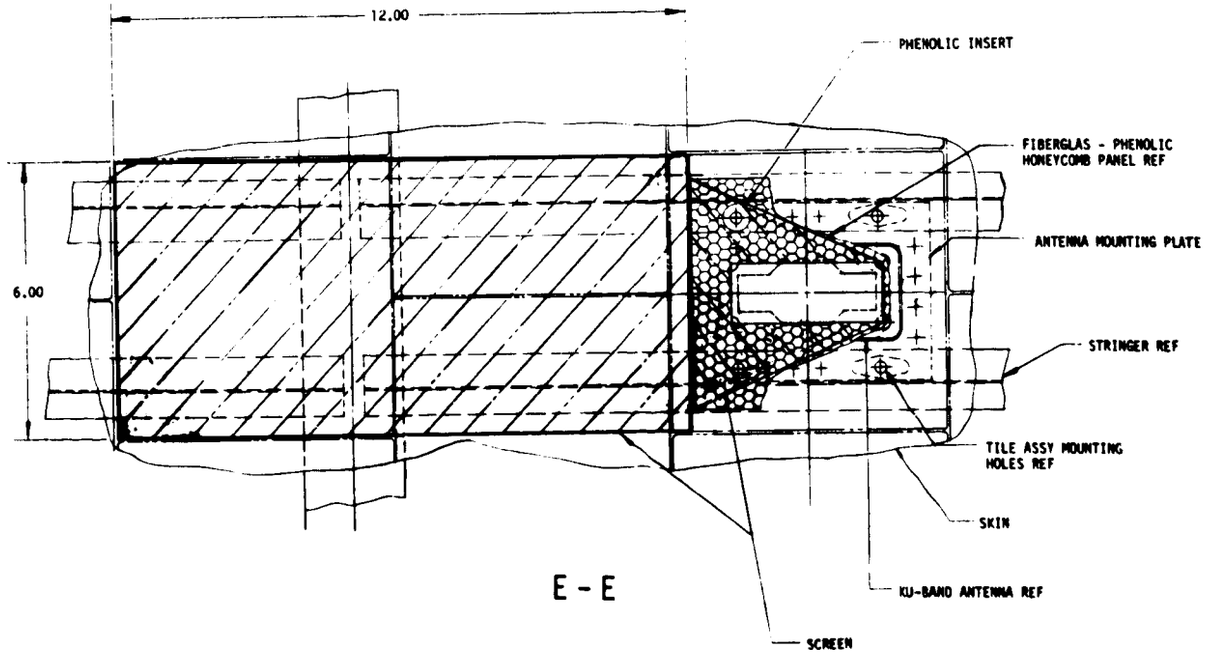

E - E

Ku-BAND ANTENNA SYSTEM INSTALLATION

FIGURE 33

PRECEDING PAGE BLANK NOT FILMED

PAGE 6-46 INTENTIONALLY LEFT BLANK.

FOLDOUT FRAME

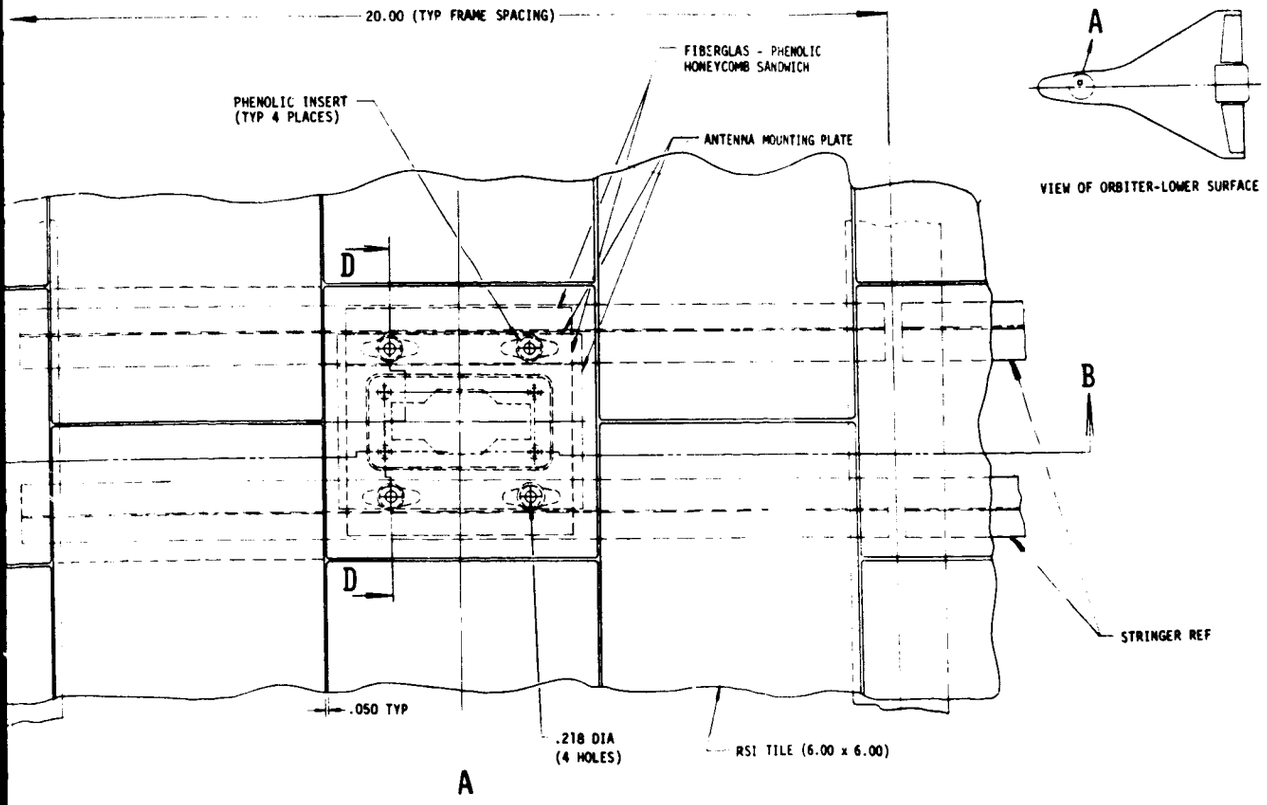

VIEW OF ORBITER-LOWER SURFACE

A

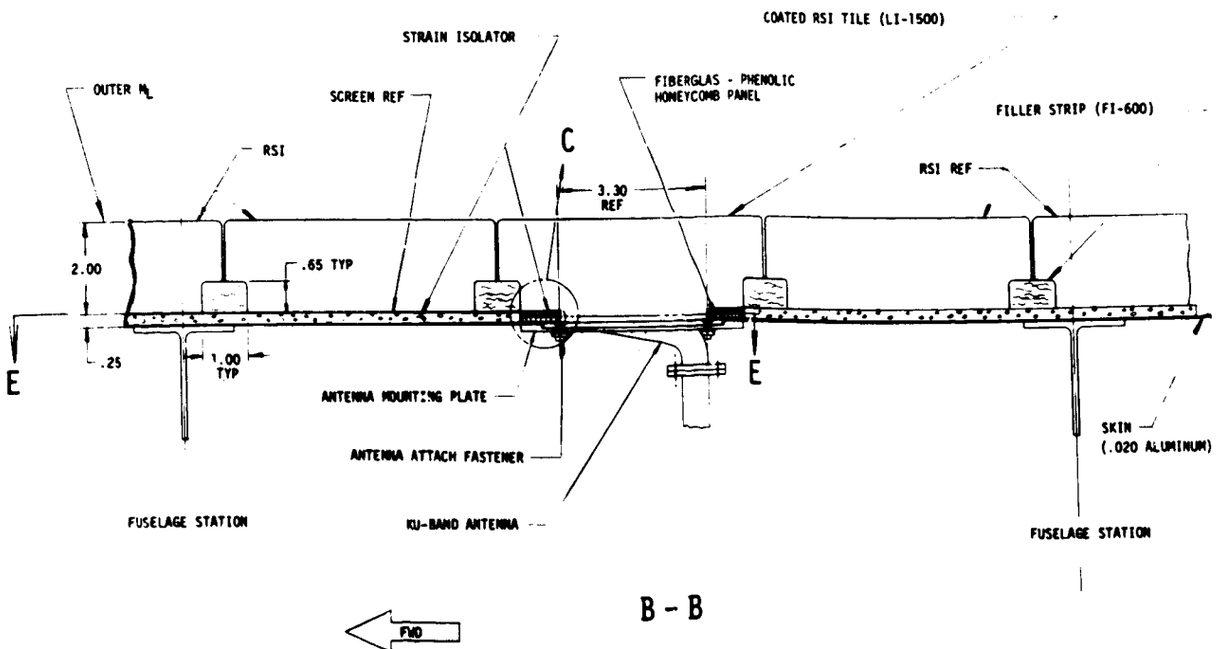

B - B

FWD

DIMENSIONS GIVEN IN INCHES.

FOLDOUT FRAME

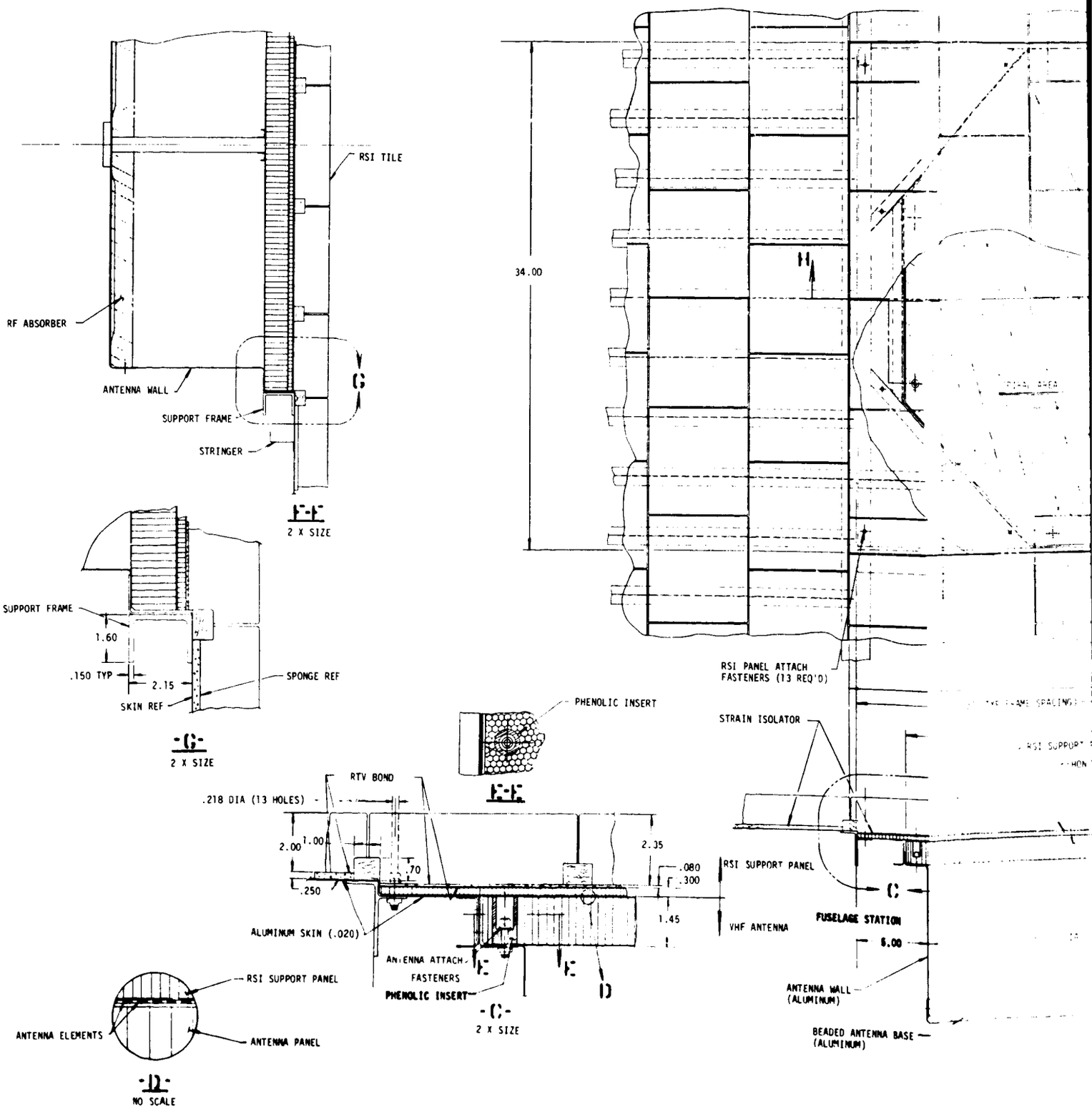

VHF ANTENNA SYSTEM INSTALLATION

FIGURE 34

PRECEDING PAGE BLANK NOT FILMED

PAGE 6-48 INTENTIONALLY LEFT BLANK.

FOLDOUT FRAME

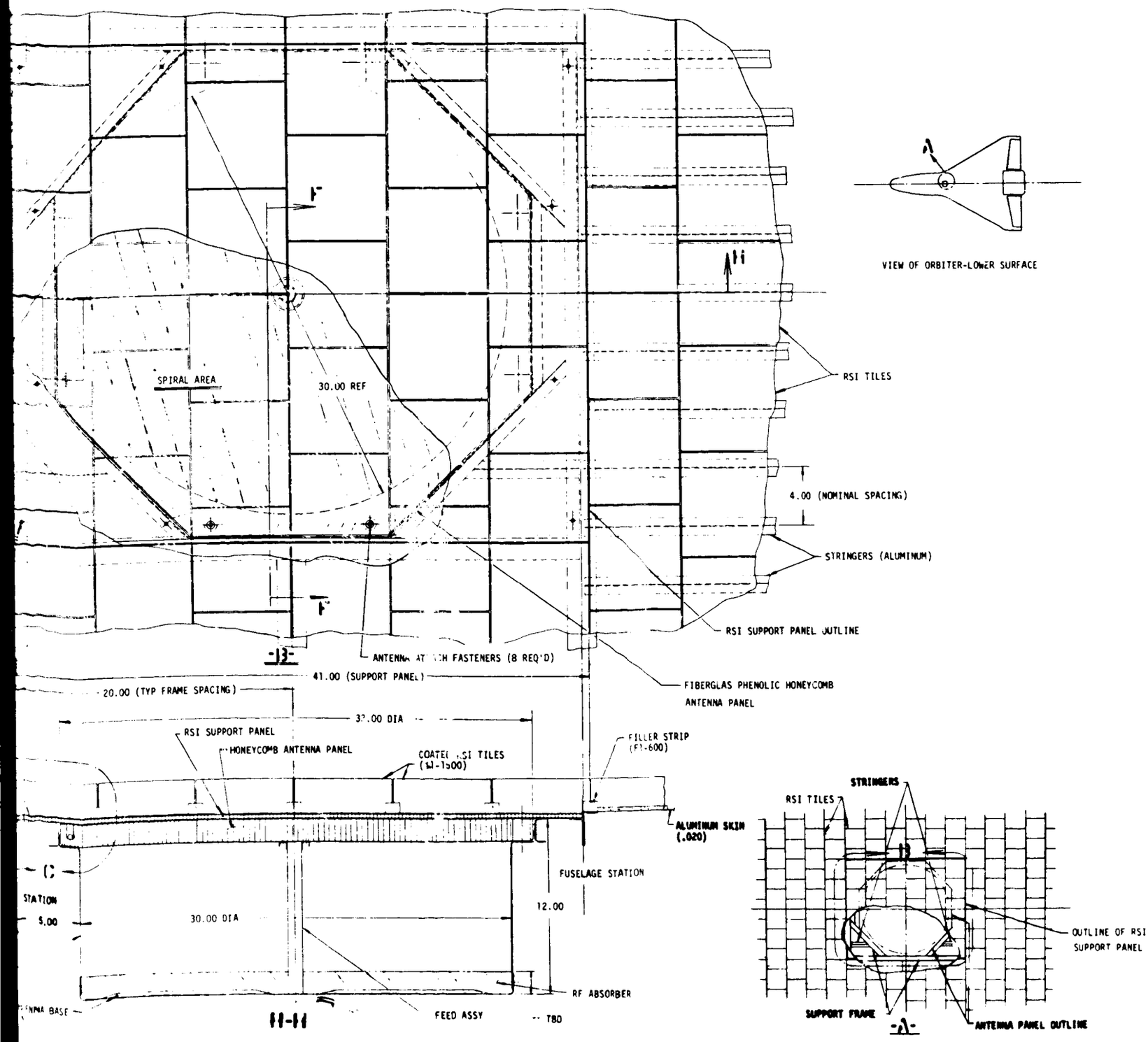

DIMENSIONS GIVEN IN INCHES

FOLDOUT FRAME 2

The size of the fiberglass-phenolic honeycomb support panel was increased from 4.32 mm (0.170 in.) to 7.5 mm (0.30 in.) to accommodate handling loads. The increase in the LI-1500 thickness and the honeycomb thickness results in a total window thickness of 6.98 cm (2.75 in.). Thirteen fasteners, one of which is located in the center of the antenna window, are used to attach window assembly to the primary structure and antenna.

The VHF antenna assembly consists of a cavity, dielectric cover, radiating element (spiral), feed assembly, and RF absorber. The cavity is 76.7 cm (30.0 in.) in diameter, 30.48 cm (12.00 in.) deep and made of 0.051 cm (0.02 in.) thick aluminum. Both the sides and bottom of the cavity are beaded to add stiffness. The top 3.68 cm (1.45 in.) of the cavity is increased in diameter to accommodate the dielectric cover. The flange created by the increased cavity diameter also provides the primary means for mounting the antenna. The dielectric cover is a basic element of the antenna design. It consists of a 3.68 cm (1.45 in.) thick double-faced fiberglass-phenolic honeycomb panel which provides the support for the spiral radiating element and carries the major portion of the external compression loads. The panel is octagonal in shape and is attached to the upper flange of the cavity. The antenna assembly is attached to the primary structure with eight fasteners.

The spiral radiating element is attached to the outer surface of the thick honeycomb panel. A dielectric tube containing the feed assembly is attached to both the honeycomb panel and the cavity bottom. An RF absorber on the bottom of the cavity (figure 34) is included to compensate for the shallow cavity depth ($< \lambda/4$) at the low VHF frequency.

Due to the large size of the VHF antenna, integration into the Orbiter structure is considerably more difficult than for the smaller antennas. Seven longitudinal stringers and one circumferential bulkhead were interrupted. The large depth of the antenna cavity may also affect other subsystem arrangements. A support frame was designed (see subsystem on Strength Studies) to compensate for the large cut-out in primary structure. The support frame consists of two heavy longitudinal channels, four diagonal members and two transverse members. The frame design provides structural continuity and redistributes the pressure loads to the primary structure.

L-band antenna system installation: The L-band antenna system installation is shown in figure 35. The airframe structure in this area consists of 0.081 cm (0.032 in.) thick aluminum sheet metal stringers running fore and aft. The size of the antenna required interrupting one stringer and canting the outer stringers, locally, by 2.24 cm (0.88 in.). A frame consisting of two transverse stringers and a sheet metal ring are added to provide structural continuity in the area of the interrupted stringer. A machined aluminum ring attached to the sheet metal ring, provides a sill for attaching the antenna from the outside of the vehicle. The antenna window assembly, consisting of four HRSI (LI-1500) tiles bonded to a strain isolator covered honeycomb subpanel, is attached with eight Allen head cap screw fasteners.

PRECEDING PAGE BLANK NOT FILMED

PAGE 6-50 INTENTIONALLY LEFT BLANK.

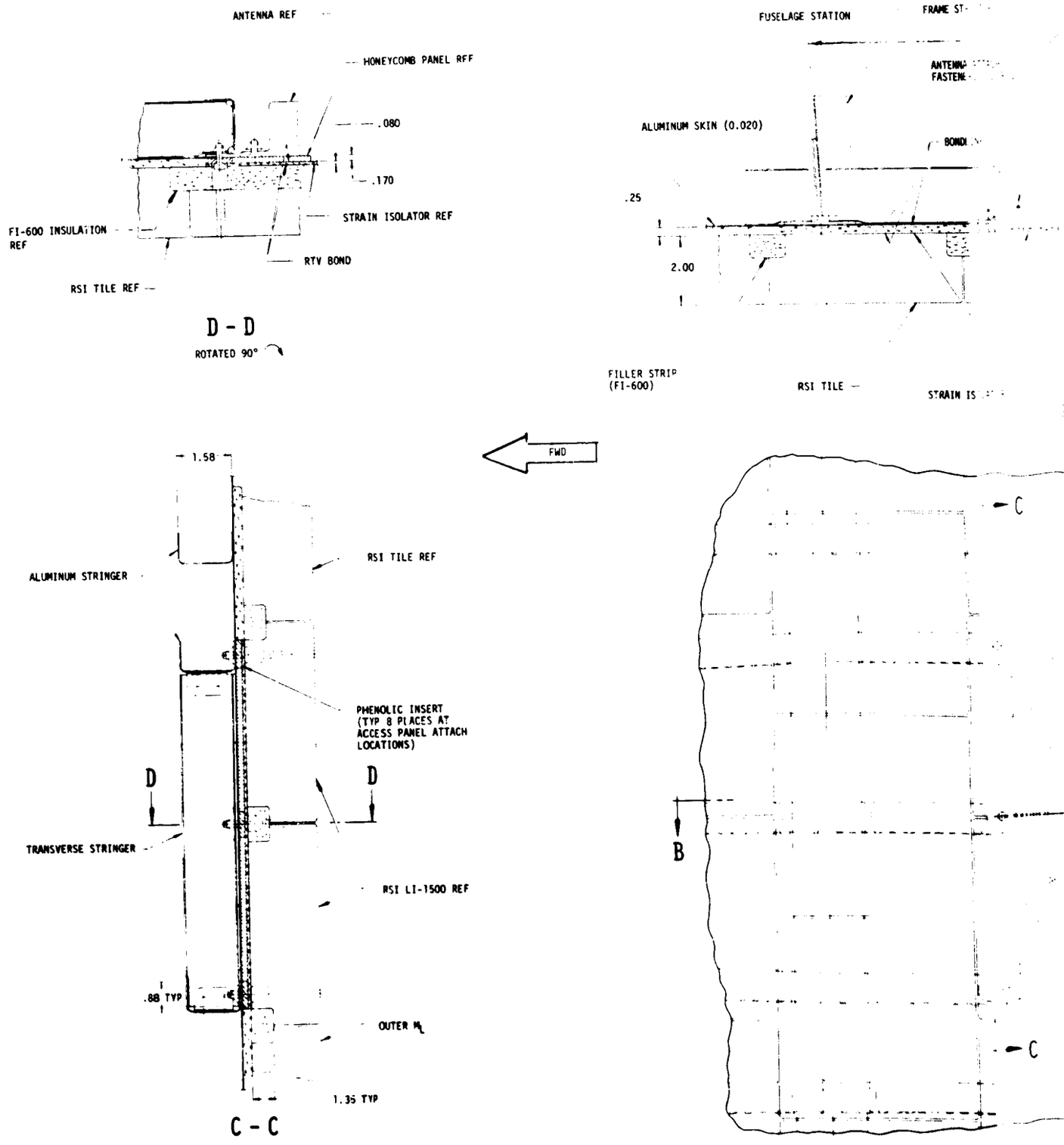

L-BAND ANTENNA SYSTEM INSTALLATION

FIGURE 35

PRECEDING PAGE BLANK NOT FILMED

6-51 PAGE 6-52 INTENTIONALLY LEFT BLANK.

FOLDOUT FRAME

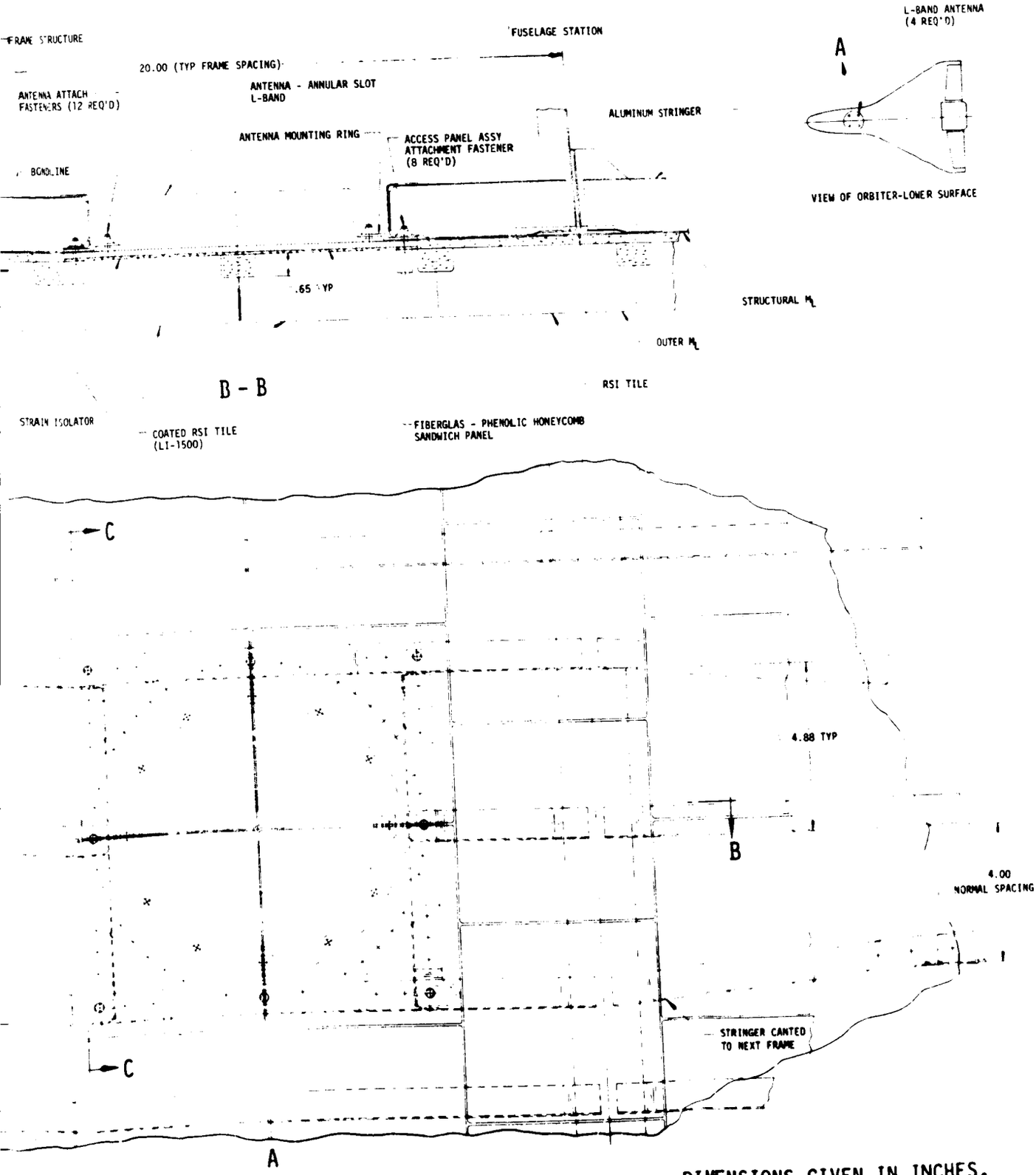

DIMENSIONS GIVEN IN INCHES.

NK.

FOLDOUT FRAME

C-band horn antenna system installation: The C-band horn antenna system installation (figure 36) is similar to the L-band antenna system installation with the LI-1500 antenna window. However, instead of interrupting one of the stringers the smaller size antenna permits canting two adjacent stringers, allowing the antenna to fit between them. The stringer spacing is increased from 10.16 cm (4.00 in.) to 15.49 cm (6.10 in.) in the area of the antenna. Two transverse stringers are added to form a box frame that cradles the antenna mounting ring. The antenna is attached to the mounting ring with twelve flush fasteners. The mounting ring, in turn, is attached with six flush fasteners.

The antenna window assembly consists of a circular LI-1500 tile, a strain isolator, fiberglass honeycomb subpanel, antenna window edge enclosure, fibrous insulation filler strips and an aluminum mounting ring. The aluminum mounting ring, which is bonded to the tabs on the subpanel, retains the donut shaped filler strip and the antenna window edge enclosure. This assembly is attached to the support structure with six Allen head recessed cap screws. The four HRSI tiles around the window require special corner cut-outs as shown in figure 36.

C-band linear slot antenna system installation: The C-band linear slot antenna system installation is shown in figure 37. Modification to the primary Orbiter structure for this antenna installation is very minimal. The size of this antenna permits installing it between adjacent stringers without changing the nominal 10.16 cm (4.00 in.) spacing. An aluminum mounting ring is riveted to the structural skin as shown in figure 37. This mounting ring is used for supporting both the antenna and the antenna window assembly. A circular groove is machined in the LI-1500 antenna window to allow the window edge enclosure to penetrate into the tile. A spacer is required to eliminate the wide area gap and to retain the shape of the thin enclosure member. This spacer, however, could be eliminated if vibration testing shows that a very narrow gap with square corners is not detrimental to the tile. The antenna window assembly is attached with four fasteners. Note that the size and shape of the LI-1500 tile used for the antenna window is identical to the adjacent HRSI tiles.

Alternate antenna system integration concepts. - Alternate antenna system integration concepts were considered with respect to method, structural environment, and TPS configuration.

Integration concepts: Three design concepts for integrating antenna systems into the Orbiter structure were considered in this study. In each, TPS materials are used for the antenna window. They include component, modular, and integral concepts. The component concept was applied to each of the antenna system designs discussed above under "Antenna installation concepts." Table XIII shows a comparison of each of the concepts as applied to the VHF antenna. The electrical configuration is essentially the same for all three concepts.

In the component concept, the antenna assembly and the antenna window are fabricated and installed as individual units. In order to keep the antenna aperture (spiral plane) as close to the ground plane (primary skin) as possible, the honeycomb panel which supports the antenna window HRSI tiles is

PRECEDING PAGE BLANK NOT FILMED

PAGE 6-54 INTENTIONALLY LEFT BLANK.

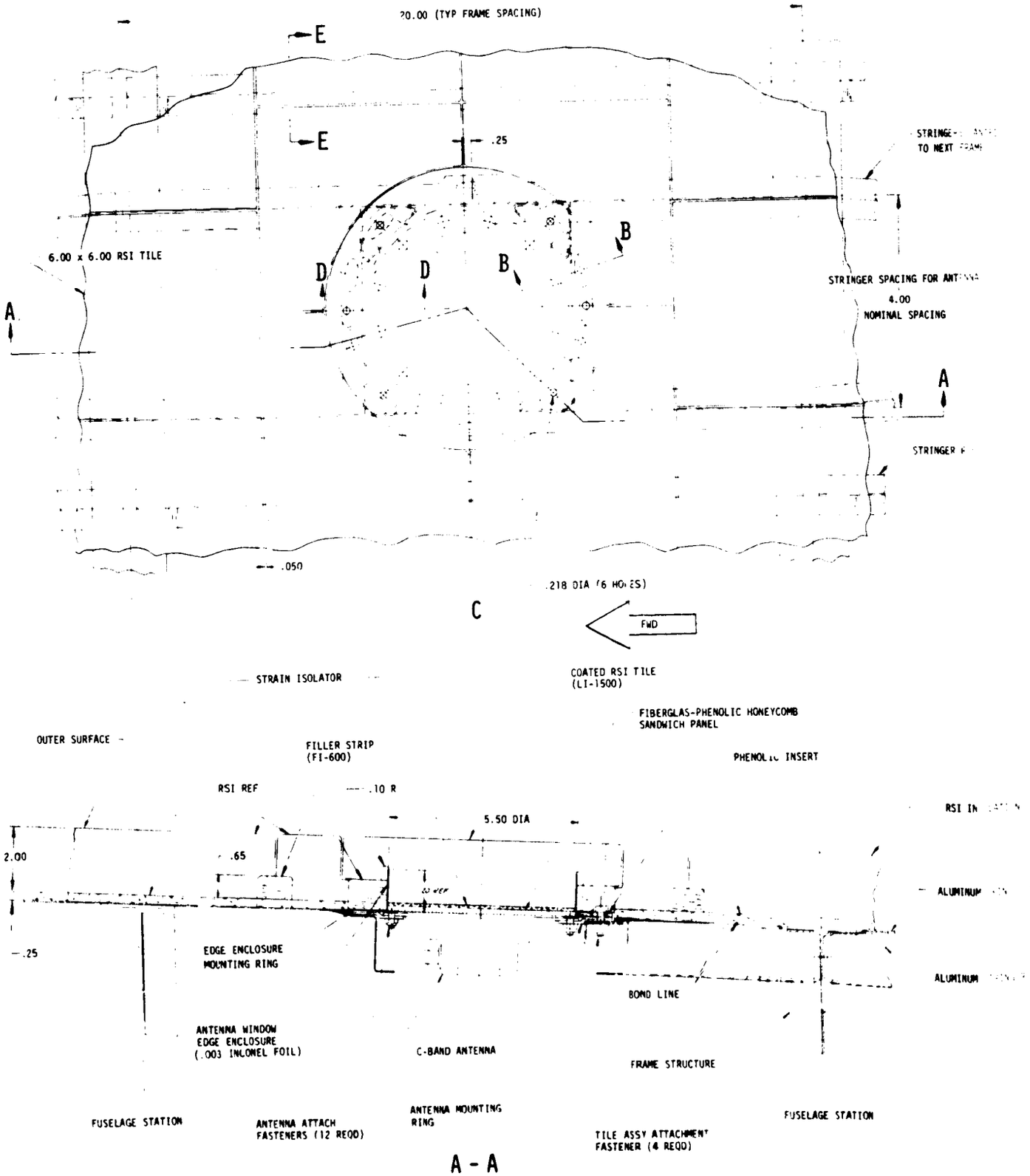

A - A

C-BAND HORN ANTENNA SYSTEM INSTALLATION **FIGURE 36**

PRECEDING PAGE BLANK NOT FILMED

PAGE 6-56 INTENTIONALLY LEFT BLANK.

FOLDOUT FRAME

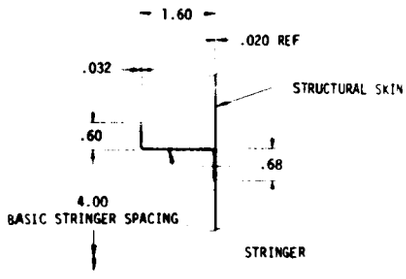

E - E

(TPS OMITTED FOR CLARITY)

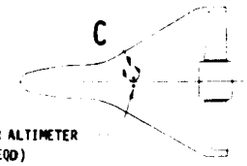

VIEW OF ORBITER-LOWER SURFACE

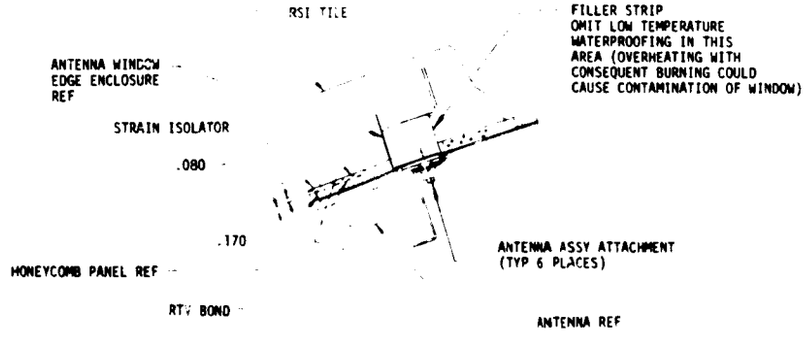

B - B

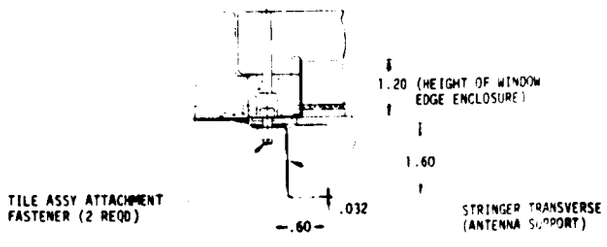

D - D

DIMENSIONS GIVEN IN INCHES.

FOLDOUT FRAME

2

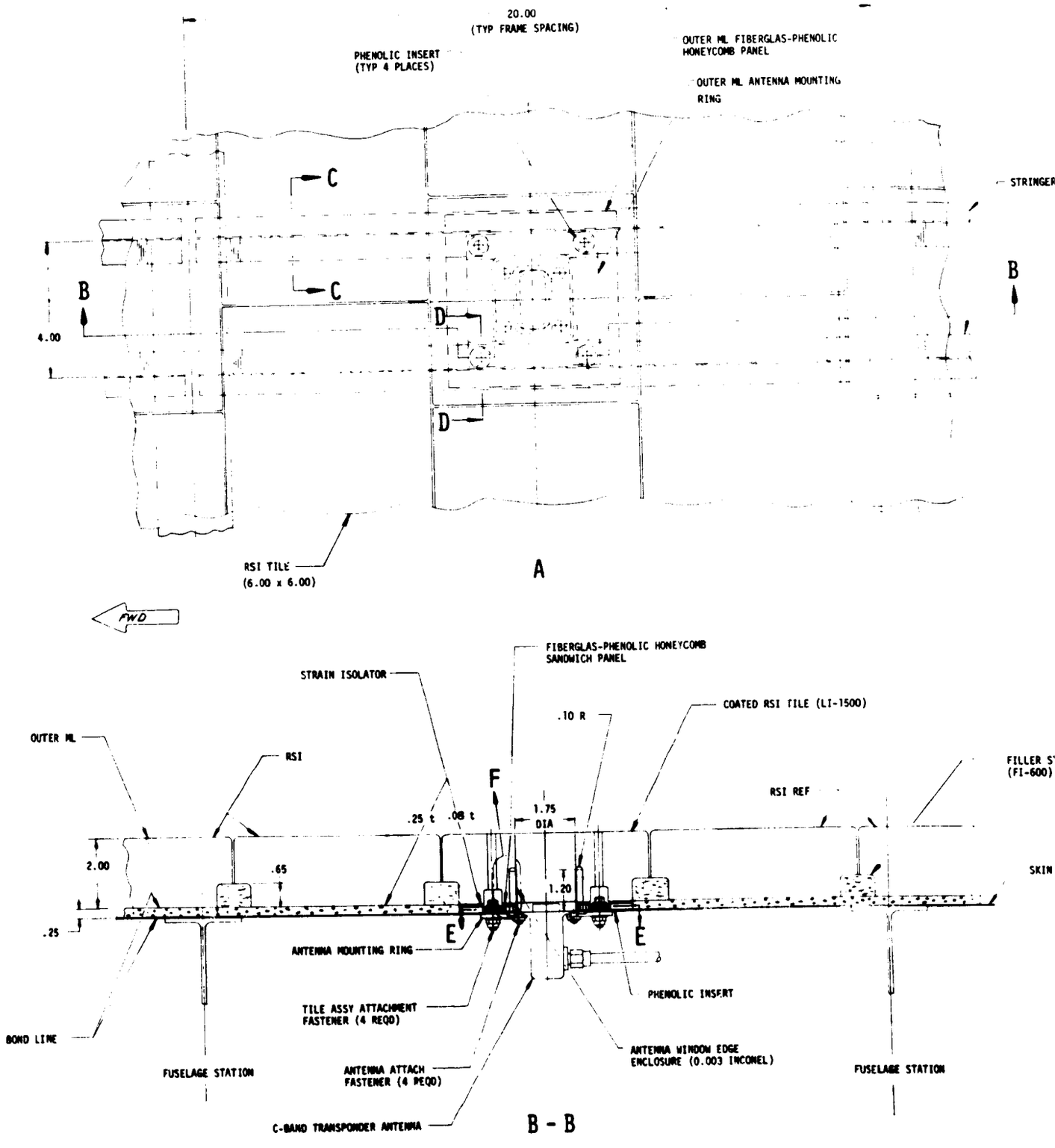

C-BAND LINEAR SLOT ANTENNA SYSTEM INSTALLATION

FIGURE 37

PAGE 6-58 INTENTIONALLY LEFT BLANK.

PRECEDING PAGE BLANK NOT FILMED

FOLDOUT FRAME

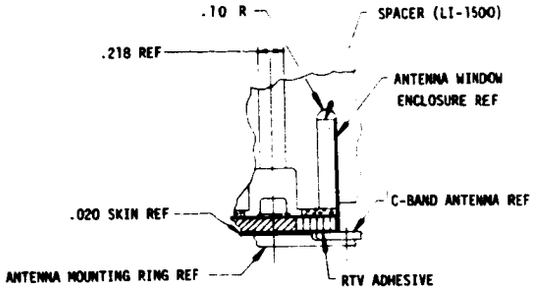

F

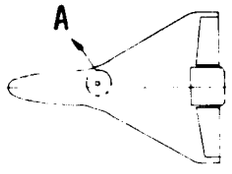

VIEW OF ORBITER-LOWER SURFACE

STRINGER REF

B

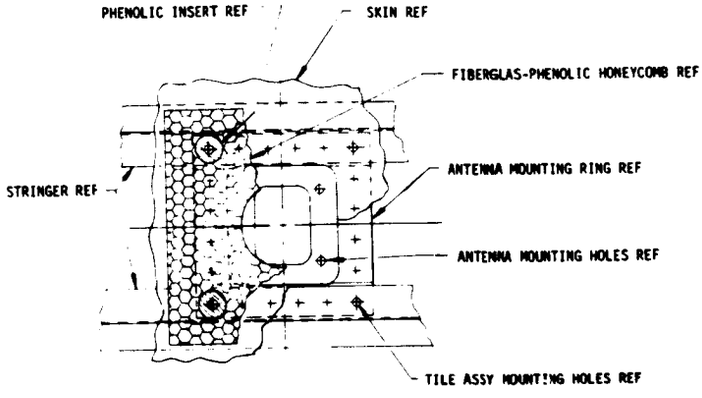

E - E

(ANTENNA AND WINDOW EDGE ENCLOSURE RING OMITTED FOR CLARITY)

FILLER STRIP (FI-600)

SKIN (0.020 ALUMINUM)

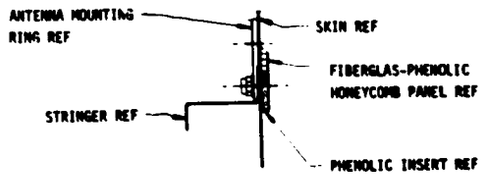

D - D

(TPS OMITTED FOR CLARITY)

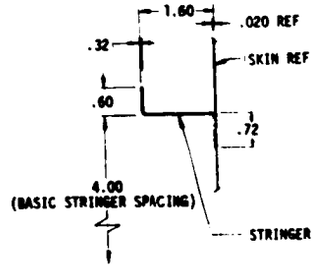

C - C

(TPS OMITTED FOR CLARITY)

DIMENSIONS GIVEN IN INCHES.

FOLDOUT FRAME

2

TABLE XIII

VHF ANTENNA SYSTEM INTEGRATION CONCEPTS

DESIGN CONCEPT / CRITERIA	INTEGRAL 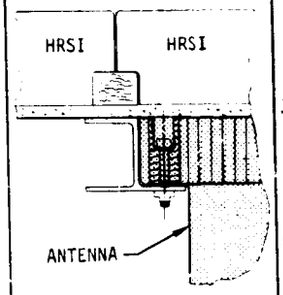	MODULAR 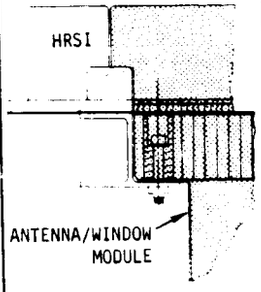	COMPONENT 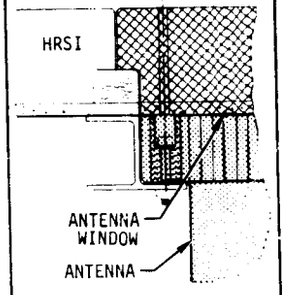
ANTENNA REPLACEMENT	DIFFICULT AND TIME CONSUMING	ENTIRE MODULE CAN BE READILY REPLACED	EITHER UNIT CAN BE READILY REPLACED
RELATIVE WEIGHT	LIGHTER	LIGHTER	HEAVIER
HRSI VS ANTENNA WINDOW INTERFACE	ESSENTIALLY NO COORDINATION REQUIRED	IN DEPTH COORDINATION REQUIRED FOR CONTROLLING GAP WIDTH	IN DEPTH COORDINATION REQUIRED FOR CONTROLLING GAP WIDTH
TOOLING	MINIMAL	GAP WIDTH CONTROL REQUIRES TIGHT TOOLING	GAP WIDTH CONTROL REQUIRES VERY TIGHT TOOLING

sized to carry handling loads only. The vertical loads are carried by the antenna support panel (dielectric antenna cover). The component approach allows the antenna window assembly to be removed without removing the antenna. In addition, this approach allows the antenna to be removed, refurbished or replaced without destroying the antenna window materials. In-plane loads are carried around the antenna by a support frame and skin-stringer shear panels which are compatible with the primary structure. Cross-plane (pressure) loads are carried by the honeycomb support panel (dielectric antenna cover).

In the modular concept the TPS (antenna window) is bonded directly to the dielectric antenna cover (antenna support panel). This combination forms a module which can be fastened to the primary Orbiter structure. In-plane and cross-plane loads are treated in the same manner as described for the component concept.

In the integral concept the antenna is mounted in the structure with the outer surface of the dielectric cover (antenna support panel) flush with the structural skin surface. The antenna is covered with the TPS as though it were ordinary skin structure. This approach eliminates the requirement for a special window, but makes replacement or maintenance of the antenna virtually impossible without destroying the TPS over it, and possibly the antenna as

PRECEDING PAGE BLANK-NOT FILMED

well. Refurbishment of the TPS over the antenna will also likely damage the antenna and require replacement. In the case of the VHF antenna, the TPS must be thicker in the area around the antenna because of the low thermal mass (see subsection on Thermal Studies in this section). In-plane and cross-plane loads are treated in the same manner as described for the component concept.

Although the three integration concepts shown in table XIII are for a VHF antenna system, with few exceptions they could be applied to antenna systems at other frequencies. Figure 38 shows an example of the component and modular concepts applied to a small antenna (e.g., C-band horn).

Alternate structural environments: Installation of an antenna into a stiffened honeycomb standoff panel (figure 2(b)) was also investigated. Figure 39 shows an S-band antenna system installation. The antenna support housing is mounted directly to a machined aluminum ring. The ring is set into a cut-out in the honeycomb panel and bonded to the facesheets. The antenna window is attached to the ring by four fasteners captived by standard inserts molded in place. The structural ring carries the in-plane loads around the antenna.

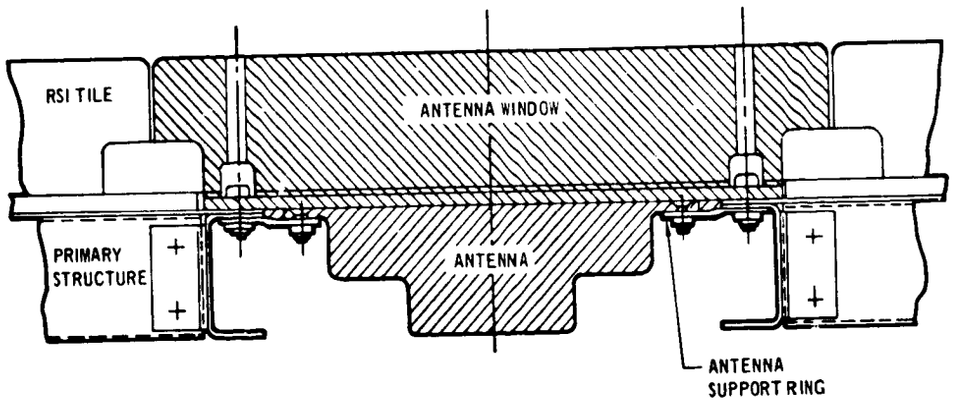

(a) COMPONENT

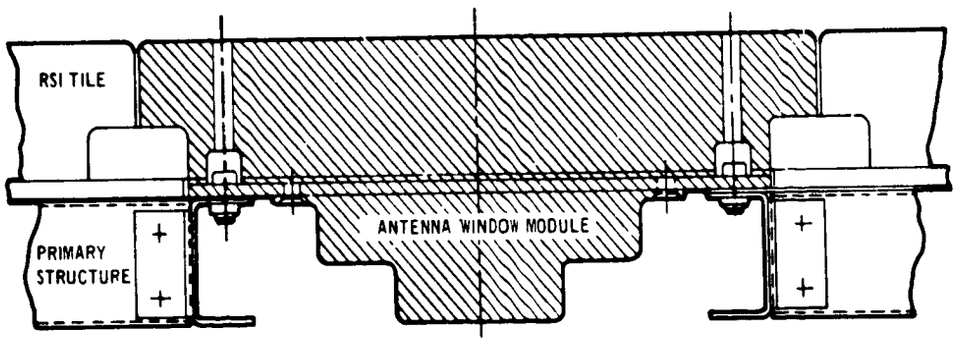

(b) MODULAR

FIGURE 38

ALTERNATE ANTENNA SYSTEM INTEGRATION CONCEPTS

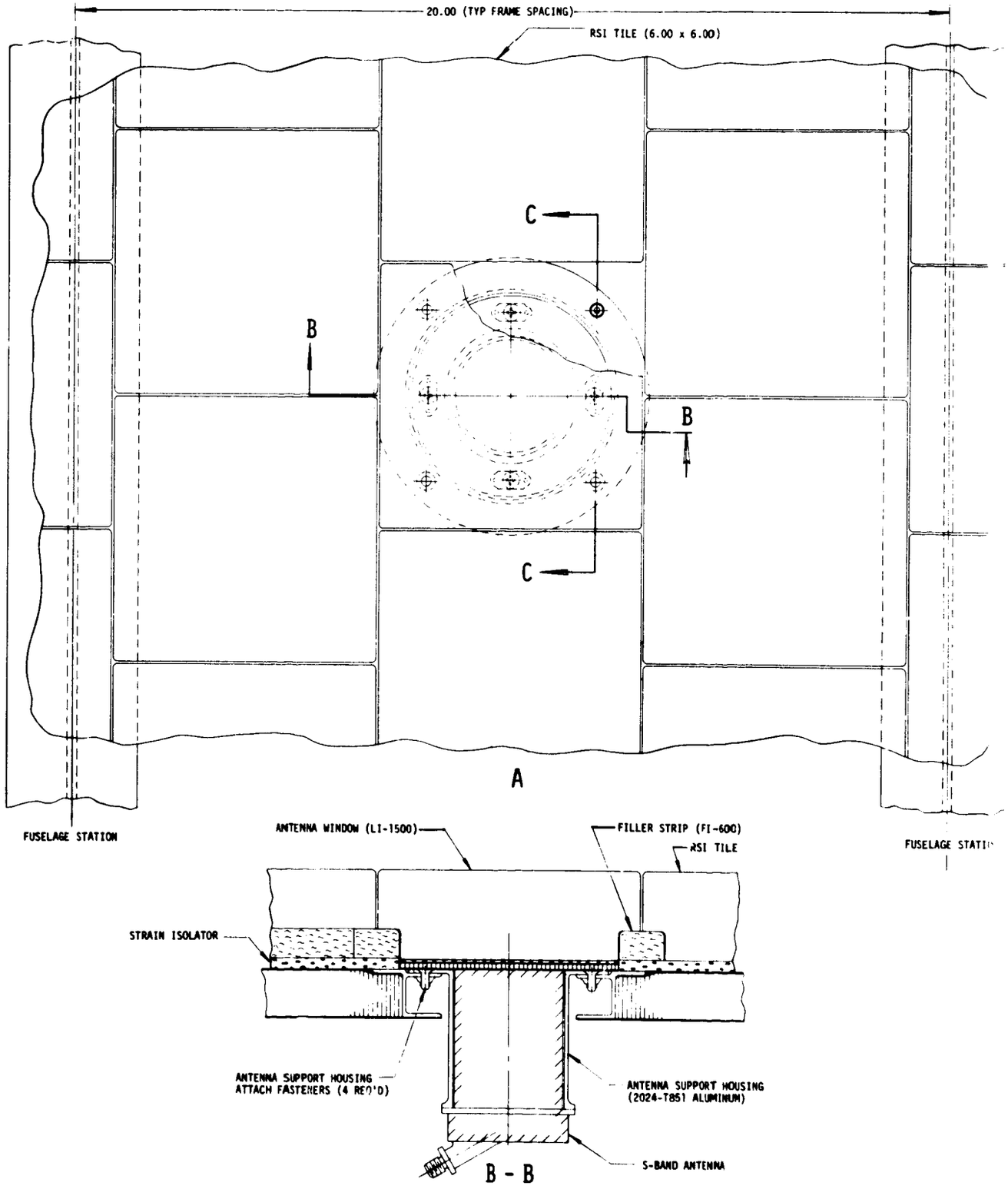

BOND LINE

ALTERNATE S-BAND ANTENNA SYSTEM INSTALLATION

FIGURE 39

PAGE 6-62 INTENTIONALLY LEFT BLANK.

FOLDOUT FRAME

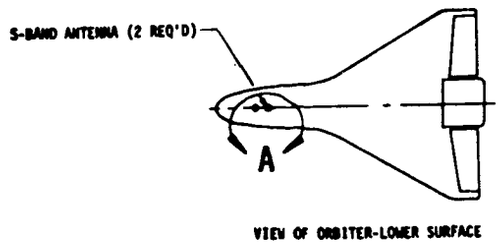

VIEW OF ORBITER-LOWER SURFACE

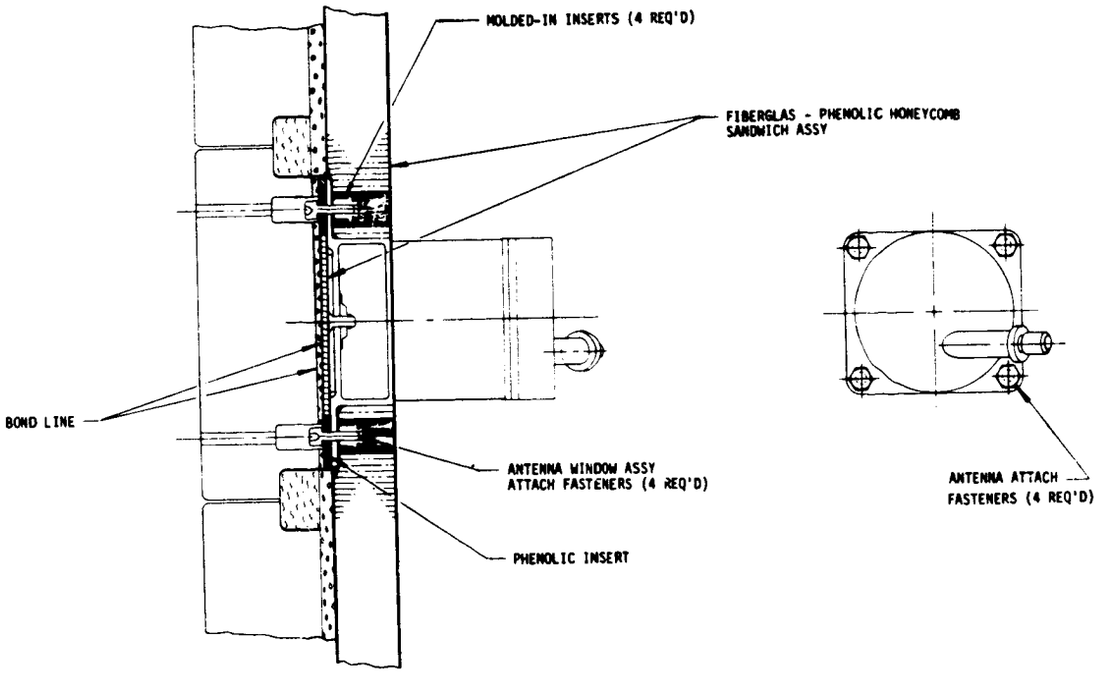

C - C

DIMENSIONS GIVEN IN INCHES.

FOLDOUT FRAME 4

For larger antennas, the same general configuration can be used. However, a deeper ring may be required to obtain the proper ring stiffness.

Alternate TPS configurations: The impact of alternate TPS configurations (figure 40) was considered using the S-band antenna system as a model. Three conditions were considered: (1) the required antenna window thickness is less than or equal to the surrounding TPS thickness; (2) the required antenna window thickness is greater than the TPS thickness because the thermal mass of the antenna is low; and (3) the required antenna window thickness is greater than the TPS thickness because the thickness of the strain isolation pad is less than the window honeycomb panel and strain isolation pad.

The first condition (figure 40a), where the required antenna window thickness is less than the surrounding TPS, the window thickness would be increased to equal that of the adjacent TPS. The condition for equal thickness does not require any compensating changes.

The second condition (figure 40b) can be handled by widening the stringer spacing adjacent to the antenna mounting bracket by approximately 1.02 cm (0.40 in.). This allows the antenna window assembly to fit between the stringers. The antenna mounting bracket is moved inboard to maintain a smooth TPS surface over the installation area.

The third condition (figure 40c) reduces to the same design requirements as the second condition. Therefore, this design requirement can be met using the same changes used for the thicker antenna window design.

Although these alternate designs featured only the S-band antenna system, the same basic approach can be adopted for the other antenna configurations. If the step formed by the depression affects the antenna radiation pattern, the window could be made larger and the step made more remote from the antenna aperture. The maximum step size can be determined by analyzing the one dimensional thermal insulation sizing results given in table XII. Assuming the TPS strain isolation pad is reduced to 1.52 mm (0.060 in.) and the antenna has a low thermal mass, the maximum step size is 1.88 cm (0.74 in.) for LI-900 HRSI. Where the thermal mass of the antenna is not low and the required HRSI thickness is the same for both antenna window and TPS, the step size would be 4.8 mm (0.190 in.) for a 1.52 mm (0.060 in.) thick strain isolation pad.

Alternate antenna window concept: An alternate antenna window design based on an L-band annular slot antenna (figure 41) consists of two layers of high temperature dielectric material. The outer layer is boron nitride (HD-0092) and the inner layer is Dynaquartz. The two layers are positioned over the antenna with a coated columbium window edge enclosure. The depth of the edge enclosure and the Dynaquartz are designed to place the Dynaquartz under a slight compression to prevent damage due to acoustical vibration. The edge enclosure is attached with eight bolts and thermally isolated with load bearing insulation. The boron nitride outer layer is held in place by a coated columbium retainer with twelve columbium fasteners. A thick aluminum ring is required to provide a heat sink to dissipate the heat conducted through the window edge enclosure. A sheet metal ring, supported by four brackets and attached to the heat sink is used to support the antenna behind the window.

The structural modification consists of installing five off-set aluminum stringers, 0.81 mm (0.032 in.) thick, beneath the antenna. The depth of the adjacent interrupted stringers are increased locally to provide continuity with the off-set stringers. The mounting structure (excluding the window material) for this installation design is approximately sixteen times heavier than that of LI-1500 window design for the L-band antenna system installations discussed previously in this subsection.

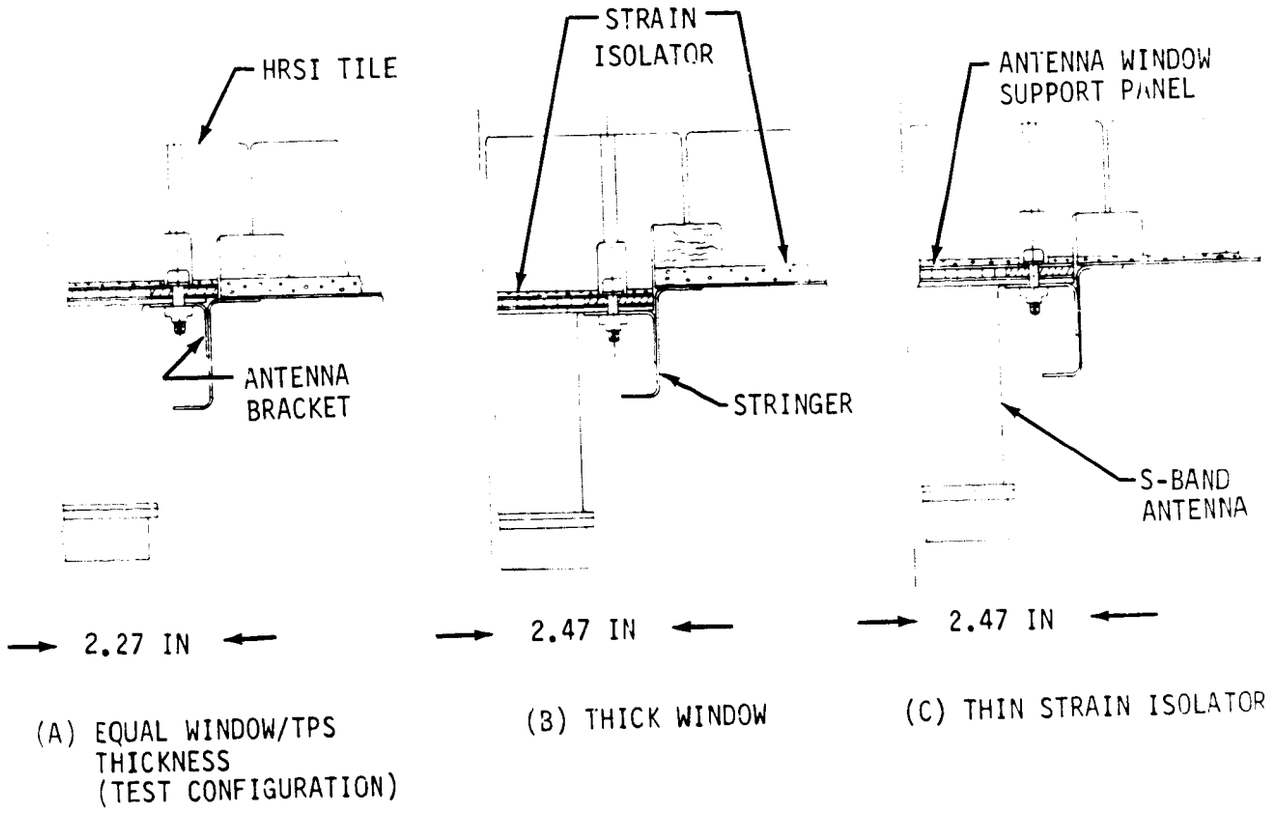

INSTALLATION CONCEPTS FOR ALTERNATE TPS CONFIGURATIONS

FIGURE 40

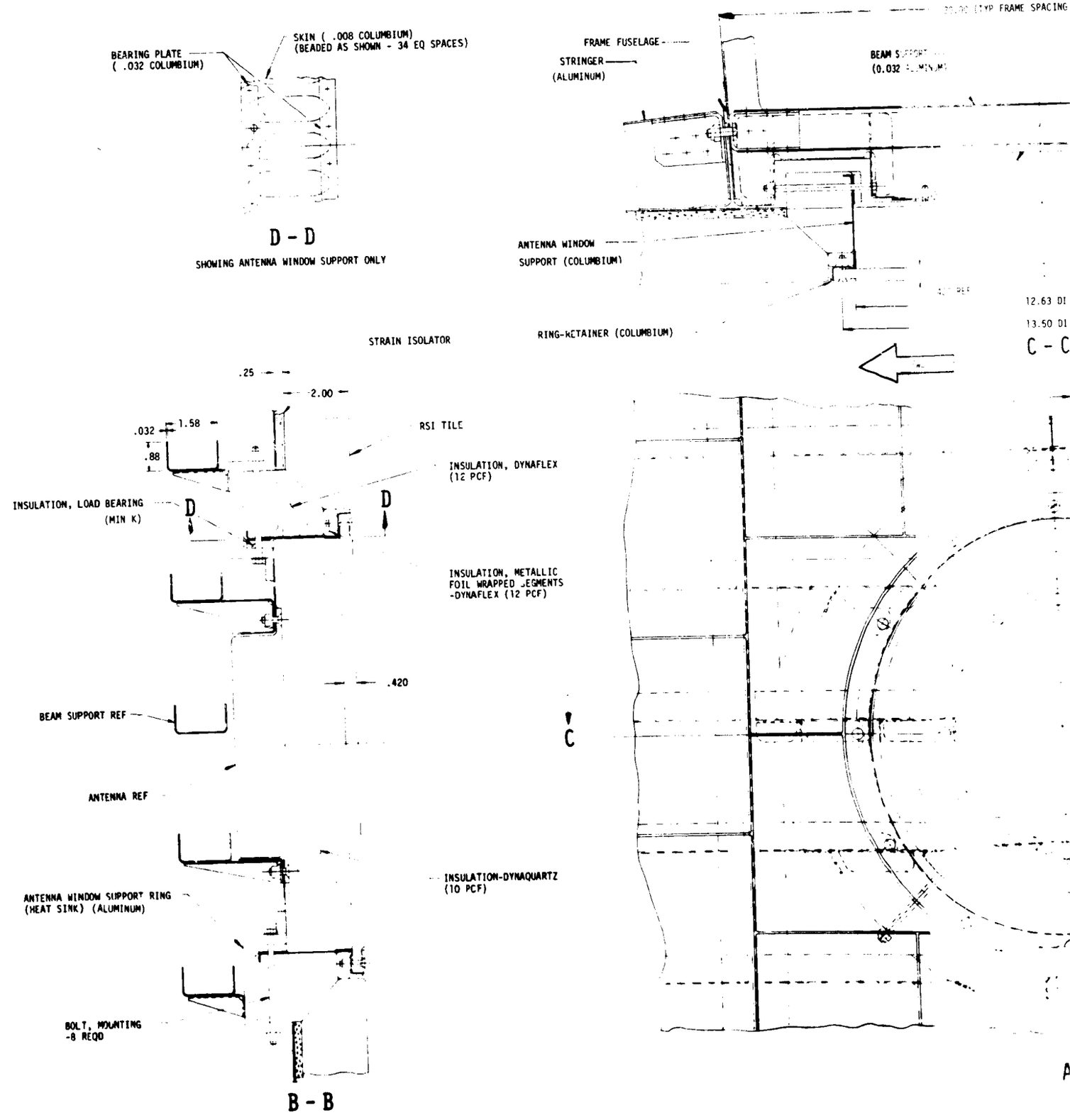

L-BAND ANTENNA SYSTEM INSTALLATION - MULTIPLE-LAYER WINDOW

FOLDOUT FRAME

FIGURE 41

PAGE 6-66 INTENTIONALLY LEFT BLANK.

C7

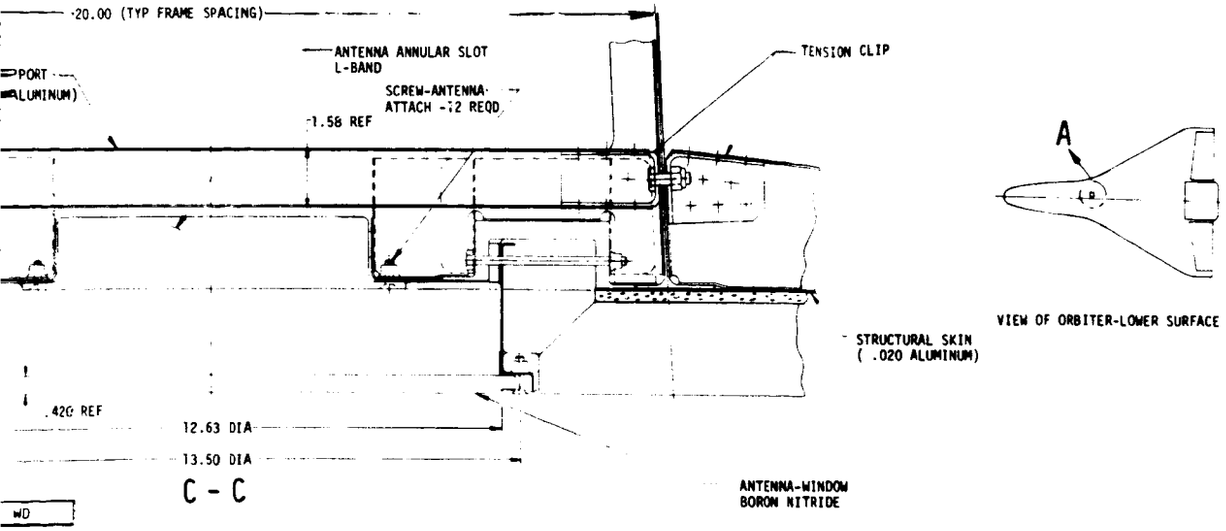

VIEW OF ORBITER-LOWER SURFACE

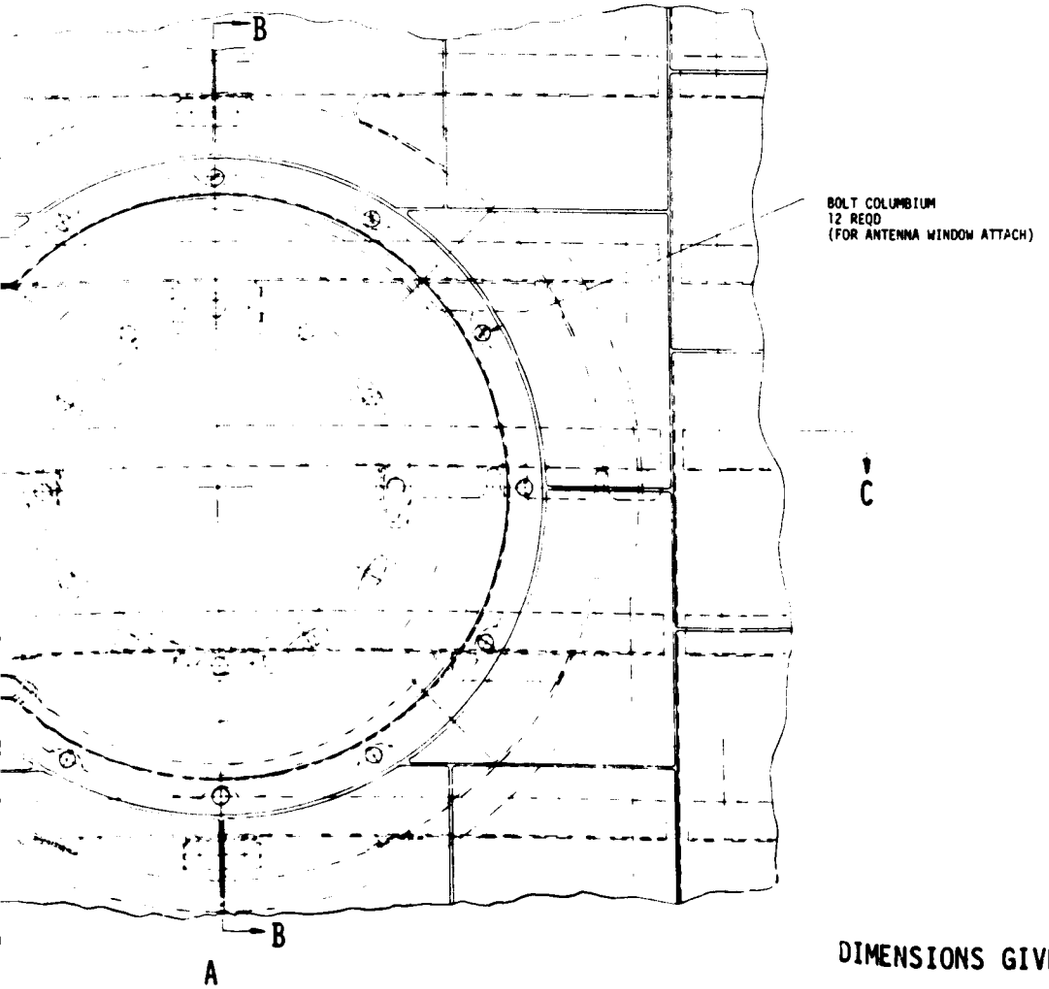

DIMENSIONS GIVEN IN INCHES.

FOLDOUT FRAME

Strength Studies

Strength analyses were performed to support the antenna system installation designs in the preceding subsection on Structural Integration Studies. The respective installations were designed to withstand the loads given in the section on DESIGN CONSIDERATIONS AND CONSTRAINTS under Strength Requirements. In some instances the design analysis was detailed, as in the case of the VHF antenna system, and in others, little analysis was necessary since the Orbiter structure was not significantly perturbed. In the latter case, only the pressure loads are of significant concern. Standard strength analysis methods were used to analyze and size components for the respective antenna designs. Material properties were taken from MIL-HDBK-5B, or Appendix A.

Except for the VHF antenna system, the structural integration concept for each antenna system considered is basically the same. The stringers are stabilized locally by a transverse member which also frames the skin cut-out. The box formed by this frame provides support for the antenna and the antenna window. The frame also carries the pressure loads transmitted through the window to the primary structure. The skin, which acts as shear panels, carries the fuselage loads around the skin cut-out.

The results of a thermal-stress analysis, performed for the C-band horn antenna system design (figure 36) during the NASA-LaRC study (ref. 1), show the maximum stress due to thermal gradients is well within the allowable for each of the components used in the antenna window design. These results are also applicable to all the antenna window designs considered in this study, because the sizes of those antenna windows or the HRSI tile sizes used in the large VHF antenna windows are comparable to the size of the C-band horn antenna window.

S- and Ku-band antenna systems. - The analysis for the S- and Ku-band antenna systems (figures 32 and 33) was limited since the stringer spacing was increased very little for these antenna system installations. In both cases there was no stringer size increase required.

VHF antenna system. - The VHF antenna system (figure 34) presented a significant structural problem. Seven longitudinal stringers and one circumferential bulkhead were interrupted to accommodate the 76.2 cm (30.0 in.) diameter antenna. The two areas of primary concern were how to carry the pressure loads through and the fuselage loads around the structural opening.

The pressure loads were accommodated by including a structural fiberglass-phenolic honeycomb panel similar to that used for the antenna window. A study was performed to optimize the dimensions in order to keep the deflection within that required by the LI-1500 tile joint gap spacing considerations. The results of this study showed that a design deflection of 8.1 mm (0.32 in.), over a 76.2 cm (30.0 in.) span, provide for an edge clearance of approximately 0.51 mm (0.020 in.) for 5.08 cm (2.00 in.) thick HRSI tiles with a nominal spacing of 1.27 mm (0.050 in.). The parameters, facesheet thickness, core height, and weight per square foot of panel area as a function of deflection are shown in

figure 42. Deflection of a minimum weight panel is 2.41 cm (0.95 in.). For deflections less than 2.41 cm (0.95 in.), a combination of facesheet thickness and core height was determined which defines a minimum weight configuration. The facesheet and core stresses are below their respective allowable stresses. For deflections greater than 2.41 cm (0.95 in.), the facesheet stress is constrained by the allowable stress (2.07×10^8 N/m^2 (30 000 psi)). In this region figure 42 shows a combination of facesheet thickness and core height, which yields minimum weight and satisfies the allowable facesheet stress limitation for a given deflection.

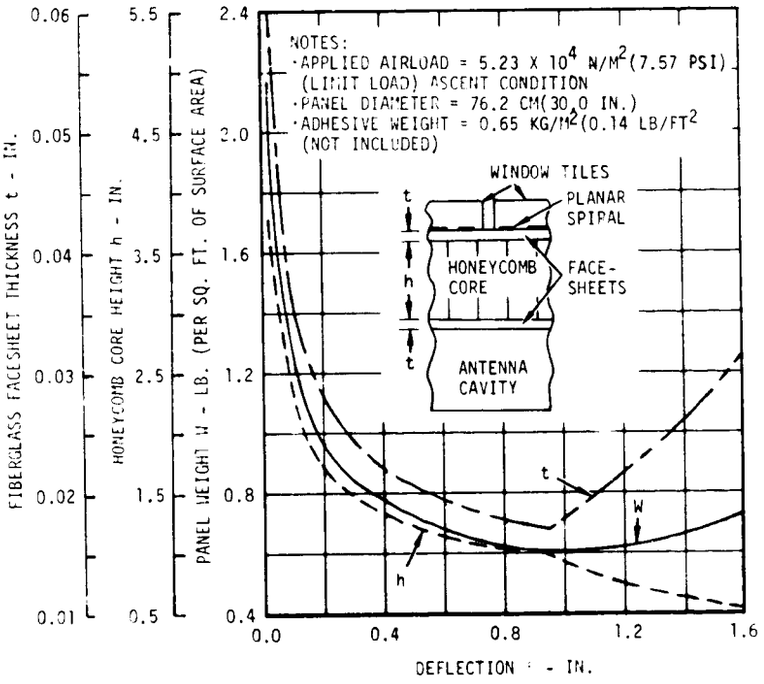

HONEYCOMB PANEL DESIGN PARAMETERS

FIGURE 42

Using a maximum allowable deflection of 8.1 mm (0.32 in.), figure 42 shows an optimum structural panel configuration is:

(a) facesheet thickness = 0.61 mm (0.024 in.),

(b) core height = 3.56 cm (1.40 in.), and

(c) weight = 4.10 kg/m^2 (0.84 lb/ft^2).

The channels and angles supporting the antenna installation were sized using the ascent pressure loads, the most critical condition. The support frame was designed to provide an octagonal cut-out in order to support the antenna in at least eight places.

For the VHF antenna installation seven Orbiter fuselage stringers were disrupted. The ultimate load in each stringer away from the cut-out is 725.7 kg (1600 lbs) compression or 1814.4 kg (4000 lbs) tension. In the region of the cut-out, loads in the discontinuous stringers are redistributed by the shear panels (fuselage skin) to the continuous stringers on both sides of the antenna. To determine internal loads distribution, a finite element model of the structure was constructed using a computer interactive graphics terminal. Axial bars and shear panels were used to represent the structure as shown in figure 43. Due to symmetry, only the structure on one side of the antenna centerline was modeled. Internal loads were obtained using the MDC finite element computer program, CASD. This computer program has the capability of resizing members to obtain a minimum weight configuration. The process is iterative because a change in relative member sizes changes the loads distribution. Three resizing iterations were performed for the condition where 725.7 kg (1600 lb) compressive load is applied at the extremities of the stringers. Stringer loads are redistributed around the antenna installation as shown in figure 44. Loads in the remaining stringers on either side of the antenna are significantly higher than the 725.7 kg (1600 lb) applied stringer load because they carry the loads applied to the discontinuous stringers.

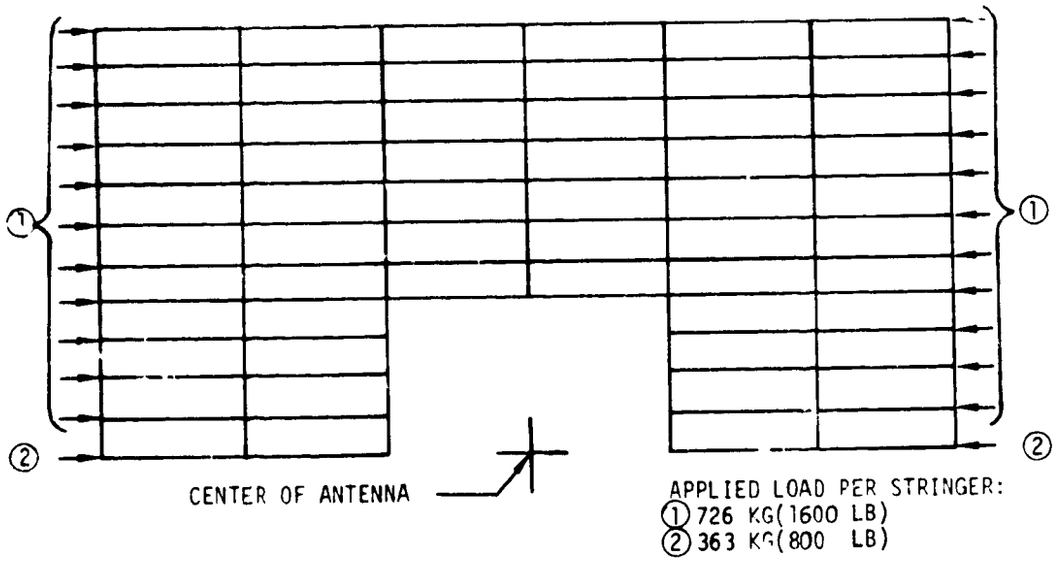

FINITE ELEMENT STRUCTURAL MODEL

FIGURE 43

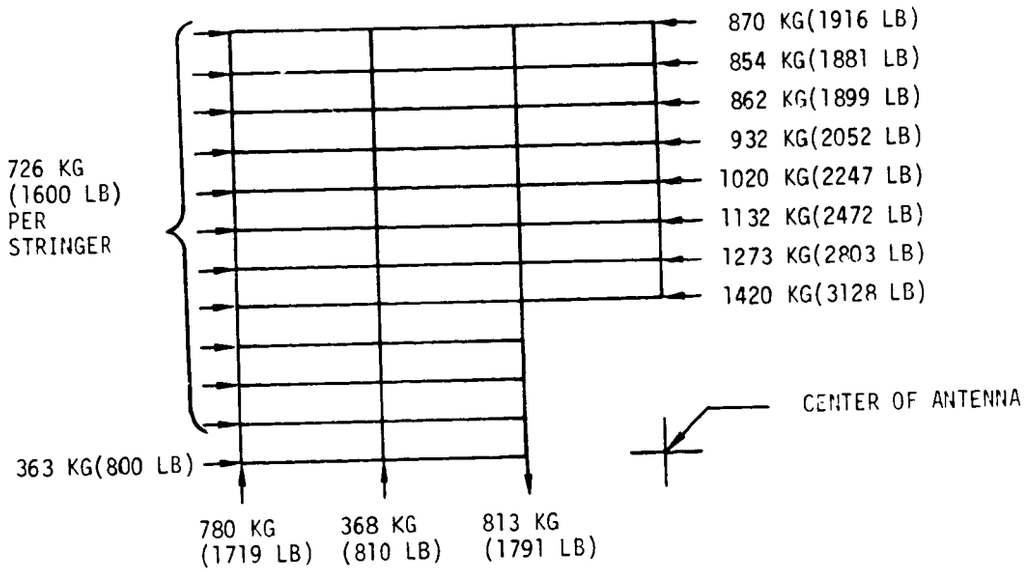

STRUCTURAL LOAD REDISTRIBUTION

FIGURE 44

Shear panels 5.10 mm (0.020 in.) thick have the capability to withstand the shear loads developed in redistributing the stringer loads. Therefore, an increase in skin thickness is not required.

The 1814.4 kg (4000 lb) tension stringer load condition is not critical because the allowable tension stress is much higher than the allowable compression stress. Load distributions would be proportionally the same for both 725.7 kg (1600 lb) and 1814.4 kg (4000 lb) stringer load conditions.

Structural weight penalties for the antenna installation are 2.73 kg (6.03 lb) for the fiberglass honeycomb structural panel and typically 4.54 kg (10.00 lb) for the cut-out in the fuselage ring. Weight penalty for cutting the fuselage ring would vary appreciably depending on the ring location and its specific configuration and function. The change in net stringer weight caused by removing stringers at the antenna cut-out and beefing up others to carry more load is negligible in this case, primarily because the net total load is the same.

S-BAND ANTENNA SYSTEM DESIGN

The objective of the S-band Antenna System Design (Task 1.2) was to design a prototype antenna system compatible with the Orbiter TPS, which could be subjected to simulated entry temperature to determine the effect of ten entry cycles on the durability and performance of the antenna system. Insofar as possible, the results of the Concept and Feasibility task were used in the design effort to obtain an antenna system which had as many features common to the other antenna design concepts as possible without compromising the S-band antenna system performance. This approach provides thermal and electrical test results which potentially have the broadest applicability to the other antenna systems. Electrical design tests, radiation pattern and impedance measurements were used to establish the physical configuration. These tests were accompanied by detailed structural integration, material, thermal and strength design analyses and studies.

Electrical Design

The design approach for the S-band antenna system was based on results discussed in the section on CONCEPT AND FEASIBILITY STUDIES. This approach consists of covering the S-band antenna aperture with a window of HRSI bonded to a thin panel of fiberglass honeycomb. A thin layer of sponge rubber is used between the HRSI and fiberglass honeycomb as a strain isolator. The fiberglass honeycomb panel provides the means for holding the antenna window in place.

The electrical performance goals for the S-band antenna system are given in table XIV. These goals provide the design standard for comparison with design test results and prototype system performance.

An improved Apollo S-band antenna, a cavity backed helix, was selected for the radiating element. To provide a more structurally sound attachment, the backcap was modified to include a mounting flange. This antenna is mounted with a friction fit graphite ring. The modified S-band antenna is shown in figure 45. The Apollo S-band antenna was selected because: (1) it meets the basic electrical performance goals for this study; (2) it will adequately represent a reusable antenna of any temperature (1255 K (1800°F) or less); (3) it can potentially be used in its present configuration in other low temperature areas on the Orbiter; (4) it has been qualified for space flight; and (5) it has the potential for the lowest development costs.

The initial design concept considered the possibility for penetrating the HRSI to a depth where the antenna aperture could reach a temperature of 1225 K (1800°F). This approach provided the possibility for obtaining the best configuration for radiation patterns and minimizing the window losses.

TABLE XIV

S-BAND ANTENNA SYSTEM ELECTRICAL PERFORMANCE GOALS

PARAMETER	VALUE
OPERATING FREQUENCY BAND	2.1 - 2.3 GHz
DESIGN FREQUENCY*	2.2875 GHz
GAIN-BEAMWIDTH	$\geq$ 0 dB OVER 120° BEAMWIDTH
AXIAL RATIO	$\leq$ 4 dB OVER BEAMWIDTH
VSWR	$\leq$ 1.5:1
EFFICIENCY	$\geq$79% ($\geq$ - 1 dB)
POLARIZATION	RIGHT CIRCULAR

*HELIX LENGTH ADJUSTED FOR LOWEST AXIAL RATIO AT THIS FREQUENCY

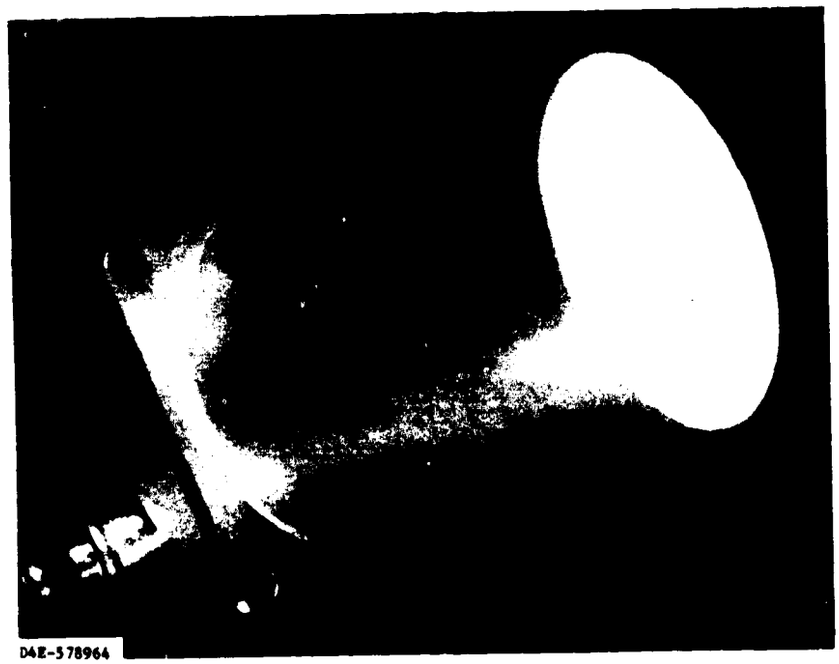

S-BAND ANTENNA (AMECOM M46325)

FIGURE 45

Radiation pattern and impedance measurements were also taken in the U.S. Air Force and Russian frequency bands, 1.75-1.85 GHz and 3.4-3.5 GHz, respectively, to evaluate the S-band antenna performance at these frequencies. These frequencies are above and below the NASA design frequency range (2.1-2.3 GHz) of the antenna.

Electrical design tests. - Radiation pattern and impedance measurements were used to establish the best configuration for optimum electrical performance within the constraints determined by the results of accompanying structural integration, materials, thermal, and strength analyses.

Test configurations: The radiation pattern and impedance measurements were made with the antenna installation located in the center of a 76.2 cm (30.0 in.) square ground plane. Figure 46 shows a sketch of the antenna system installation and surrounding TPS, with the antenna aperture shown flush with the ground plane. The dashed lines indicate the maximum depth, 4.43 cm (1.75 in.), to which the antenna was permitted to penetrate the antenna window above the ground plane. An improved Apollo S-band antenna without a modified backcap, but electrically equivalent to the antenna purchased for this study, was used for these tests. The antenna connector was fixed in the $\theta = 90°$ direction (figure 19) in order to maintain configuration uniformity between patterns. In later tests, the ground plane size was increased to 86.4 cm (34.0 in.) on a side to permit more direct comparison of test results with those of the S-band antenna manufacture. A strip of Emerson & Cuming AN75 absorber 5.1 cm (2.0 in.) wide was placed at the ground plane edges to minimize the ground plane edge effects. The antenna window and TPS were simulated using Emerson & Cuming Inc. ECCOFOAM PS ($\varepsilon_r = 1.2$) for the LI-1500 HRSI and RL-524 type S-105 elastomer for the strain isolator. A simulated HRSI thickness of 5.1 cm (2.0 in.) was used for all the test configurations.

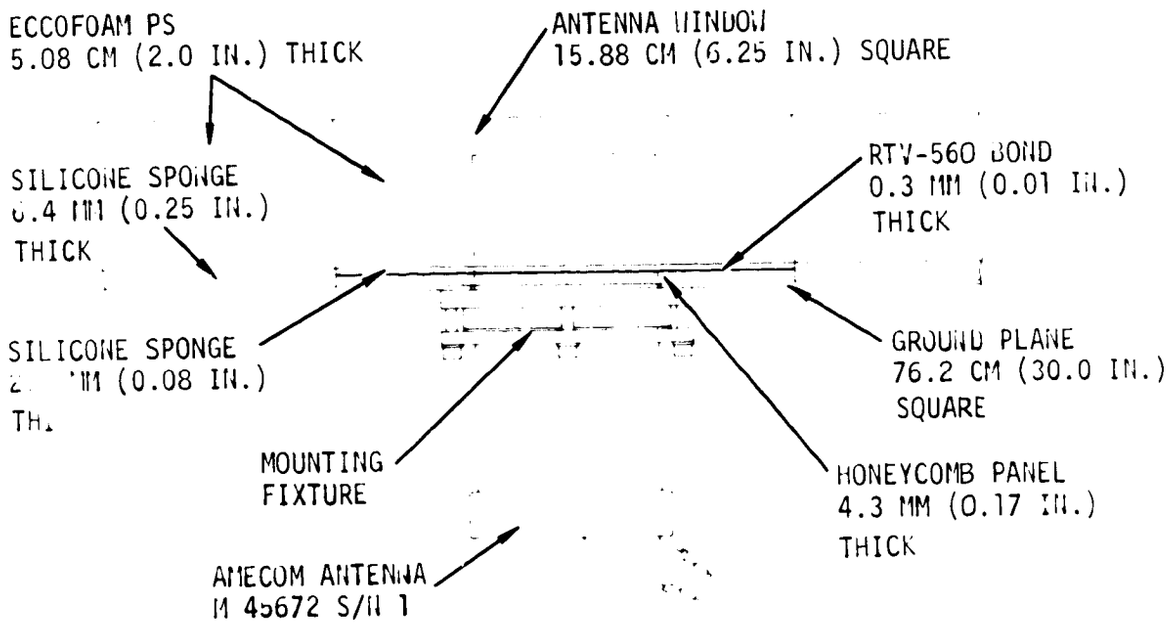

DESIGN TEST CONFIGURATION

FIGURE 46

Test techniques: Standard radiation pattern and impedance measurement techniques were used to obtain the data given in this report. Figure 47 shows a block diagram of a typical test setup used for measuring the radiation patterns. The patterns were measured in an anechoic chamber with transmission distances of approximately 13.7 m (45 ft). Figure 48 shows a photo of the recording and control console. Impedance measurements were taken with a Hewlett Packard Model 8410A Network Analyzer System. Figure 49 shows a block diagram of a typical test setup for swept frequency impedance measurements.

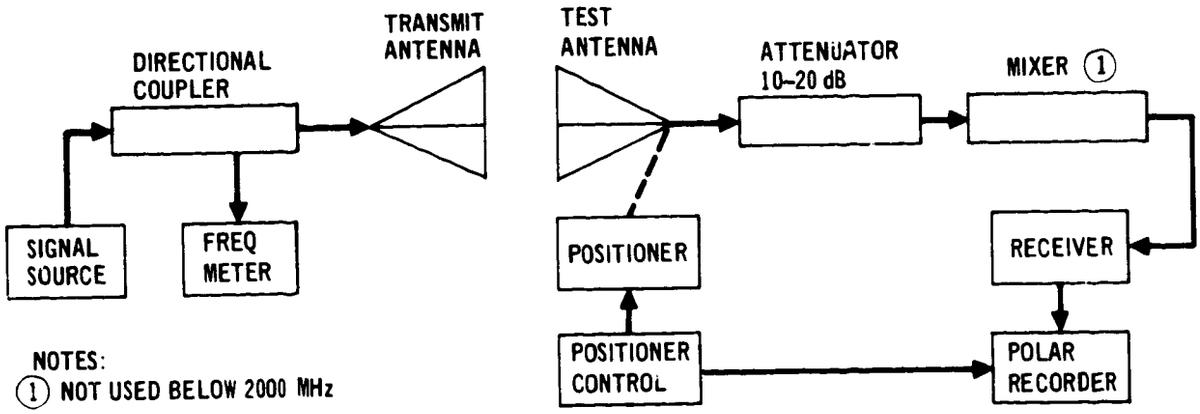

RADIATION PATTERNS TEST SET-UP BLOCK DIAGRAM FIGURE 47

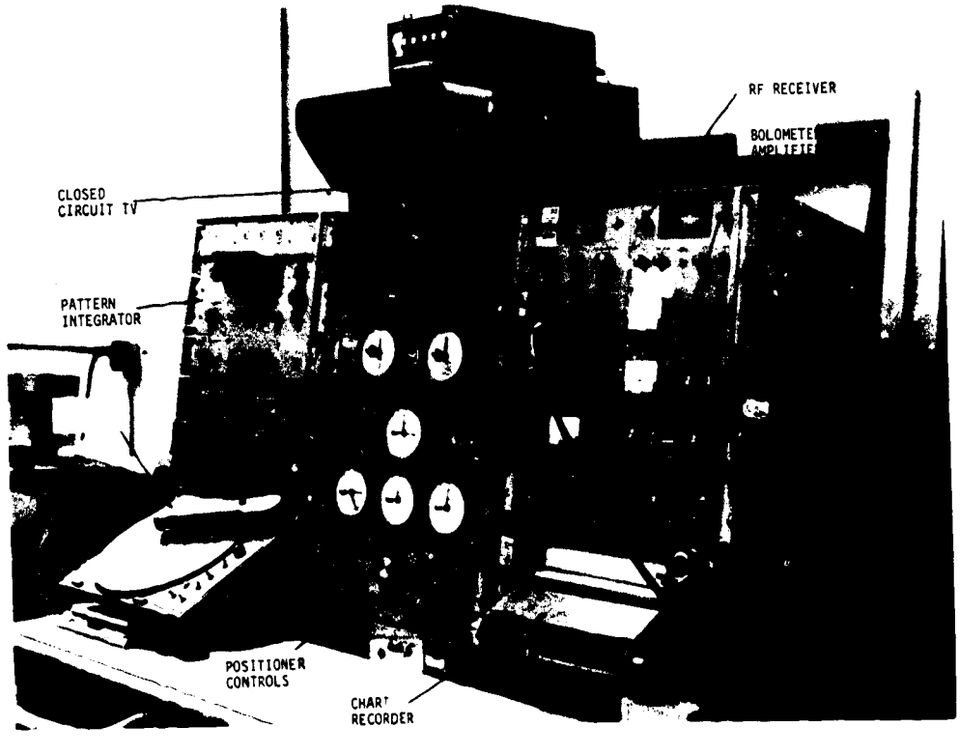

RADIATION PATTERN RECORDING AND CONTROL CONSOLE FIGURE 48

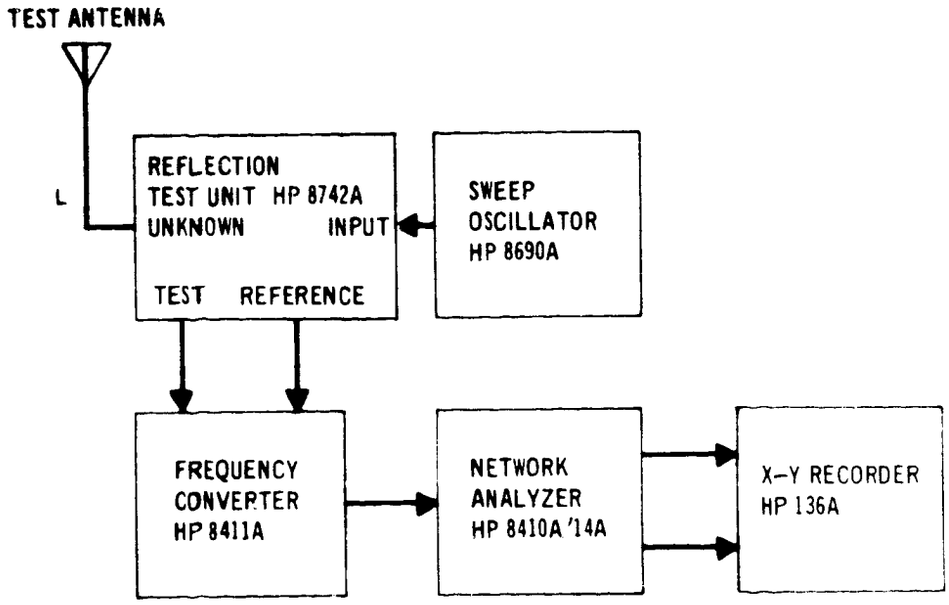

IMPEDANCE TEST SET-UP BLOCK DIAGRAM FIGURE 49

Rotating linear polarization was used to provide a continuous axial ratio measurement. The linear field was obtained using a Scientific Atlanta SGH-1.7 horn. The radiation patterns are recorded on a standard 40 dB polar graph paper. The linear isotropic gain level was measured using a standard gain horn reference and recorded on each pattern. The coordinate system used for the radiation patterns is shown in figure 19. Unless otherwise identified, all radiation patterns presented for the S-band antenna system are oriented with $\theta = 0°$ toward the top of the page. For convenience, the principal plane patterns, which are in orthogonal planes, are referred to as X-plane ($\phi = 0°$ on pattern left) and Y-plane ($\phi = 90°$ on pattern right).

The circular gain may be derived from the rotating linear patterns by adding the conversion gain factor (figure 50), which is a function of the voltage axial ratio, to the peak linear gain. Both axial ratio and peak linear are taken at a particular angle. The derivation of this function is discussed in Appendix C.

Test results (preliminary): The results of the radiation pattern measurements show a definite change in pattern shape and axial ratio as the S-band antenna aperture is positioned at different heights above the ground plane. Radiation patterns measured over the design frequency range (2.1 to 2.3 GHz) are shown in figures 51 through 53. The patterns generally show some scalloping which can be attributed to ground plane edge effects. The addition of the TPS appears to increase the scalloping. This increase can be attributed to increased edge radiation due to surface wave excitation. Similar effects were found in the test results reported in reference 1. Patterns were measured for each aperture height above the ground plane at 2.1, 2.2 and

2.2875 GHz both with and without the antenna window and surrounding TPS. The configuration without the antenna window and TPS is considered a reference configuration. The upper test frequency of 2.2875 GHz, rather than 2.3 GHz, was selected by MDAC-E because the S-band antenna is optimized for lowest axial ratio at this frequency. The improved Apollo S-band antenna was optimized for the Apollo CSM Unified S-band communications transmit frequency (2.2875 GHz) by Amecom under NASA Contract NAS 9-8334. Therefore, the axial ratio at the lower frequencies may be greater than the axial ratio values given in the performance goals for the antenna.

The results of pattern measurements at 2.2875 GHz are shown in figure 51 for all aperture heights tested. Both X- and Y-plane patterns are shown. The best overall pattern characteristics were obtained for the aperture flush with the ground plane. For this configuration the gain and axial ratio are more uniform over the desired beamwidth ($\theta = \pm 60°$). Positioning the aperture above the ground plane tended to increase the axial ratio over the entire beamwidth and particularly at angles above $\theta = 50°$. At aperture heights of 3.81 cm (1.50 in.) and 4.45 cm (1.75 in.) the gain and axial ratio improved at angles below $\theta = 50°$. The antenna system gain at $\theta = 0°$ decreased at the 1.91 (.75 in.) aperture level but increased at the 3.81 cm (1.50 in.) level. In general the addition of the antenna window and TPS appeared to increase the gain at $\theta = 0°$.

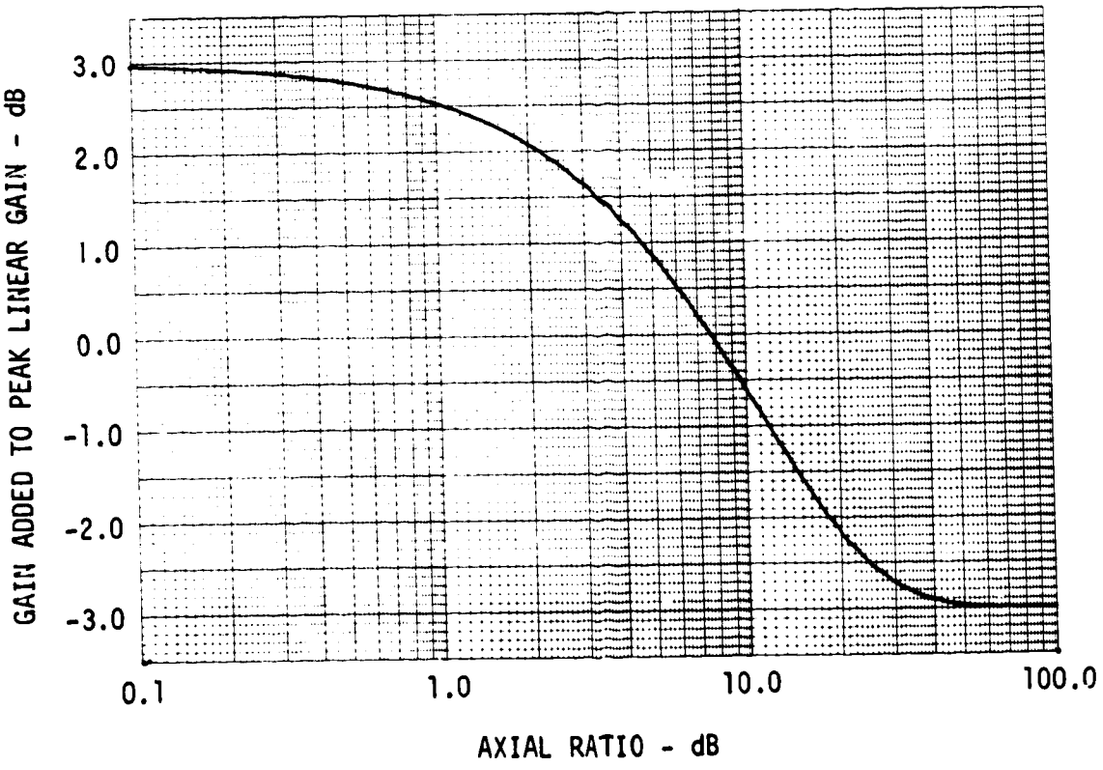

CONVERSION FROM PEAK LINEAR TO CIRCULAR GAIN

FIGURE 50

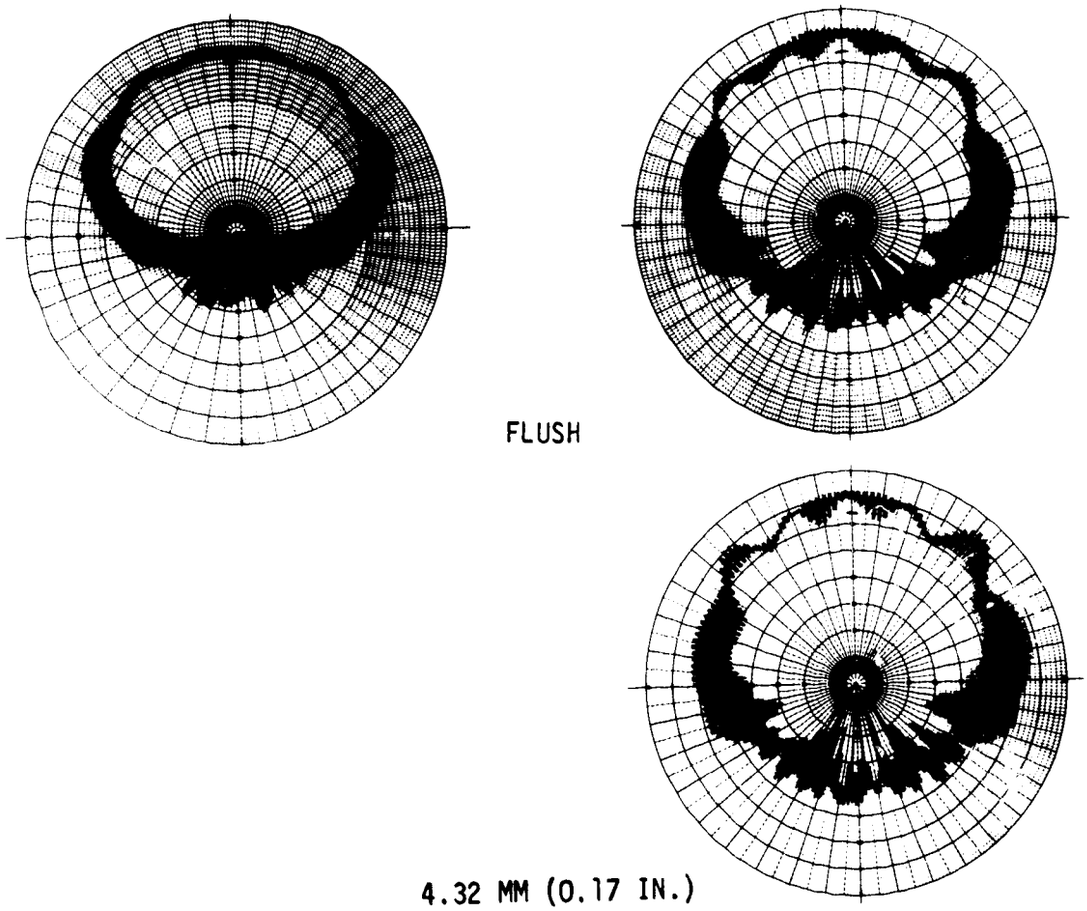

EFFECTS OF EXTENDING APERTURE ABOVE GROUND PLANE (2.2875 GHz)

FIGURE 51

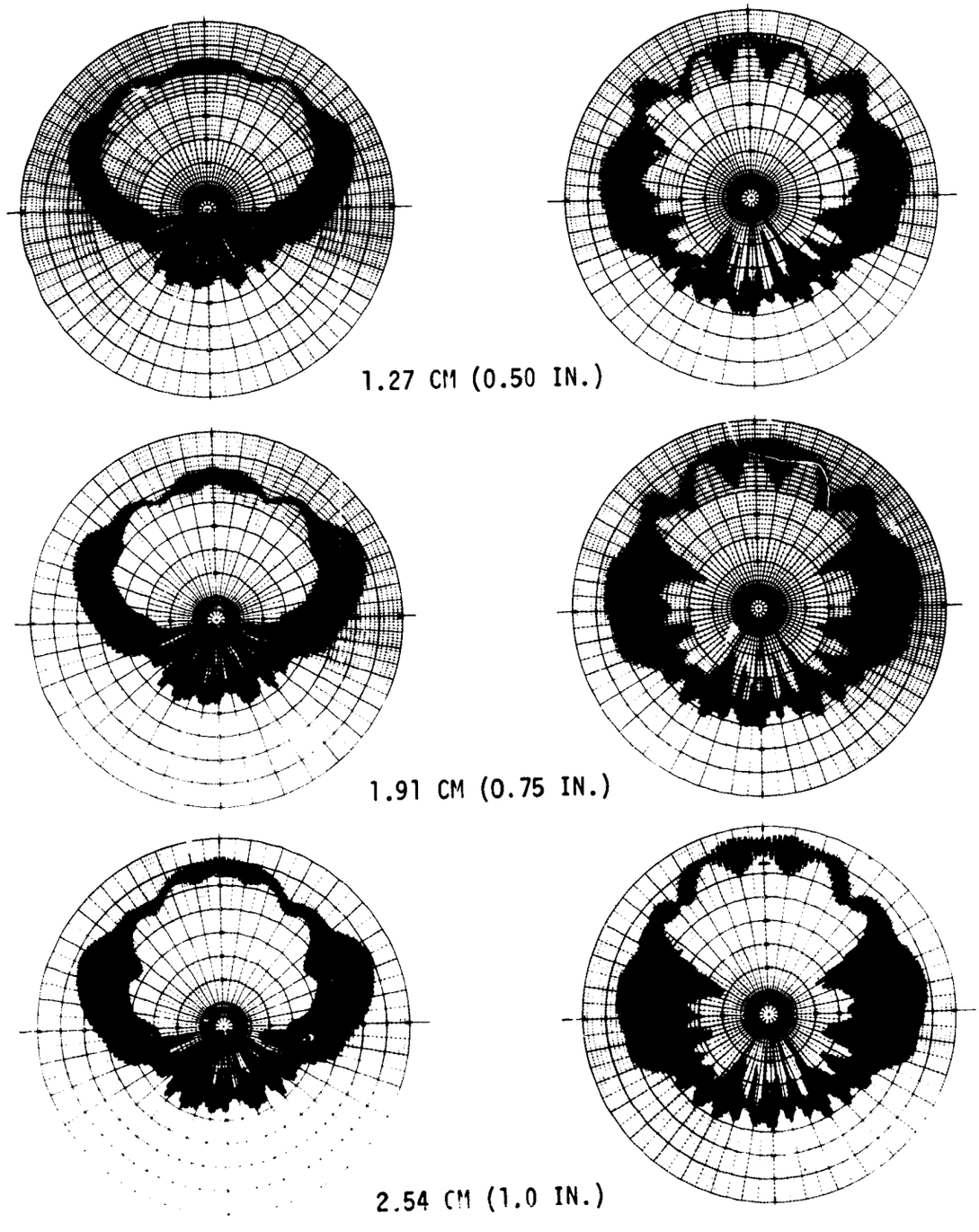

EFFECTS OF EXTENDING APERTURE ABOVE GROUND PLANE (2.2875 GHz)

FIGURE 51 (Continued)

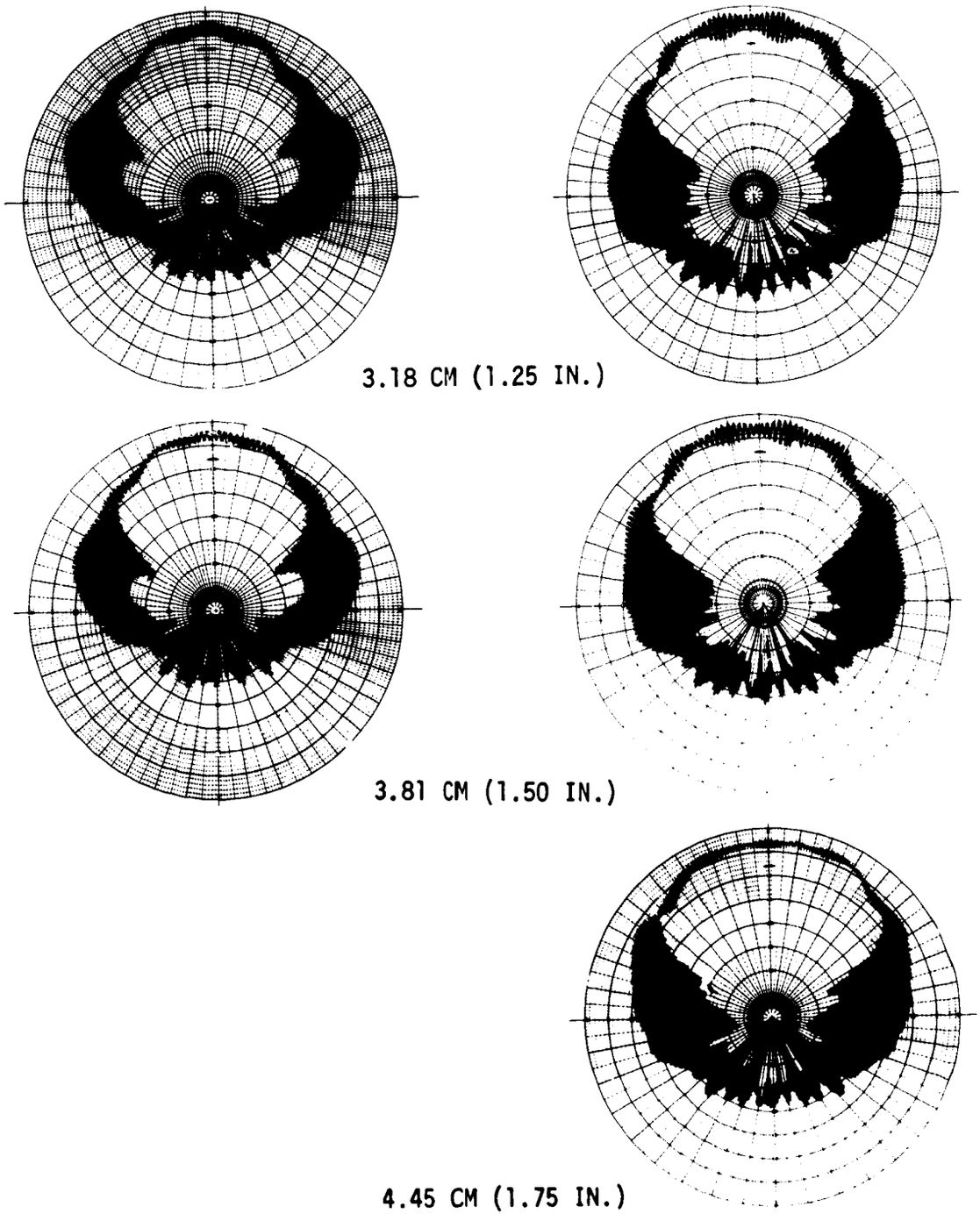

EFFECTS OF EXTENDING APERTURE ABOVE GROUND PLANE (2.2875 GHz)

FIGURE 51 (Continued)

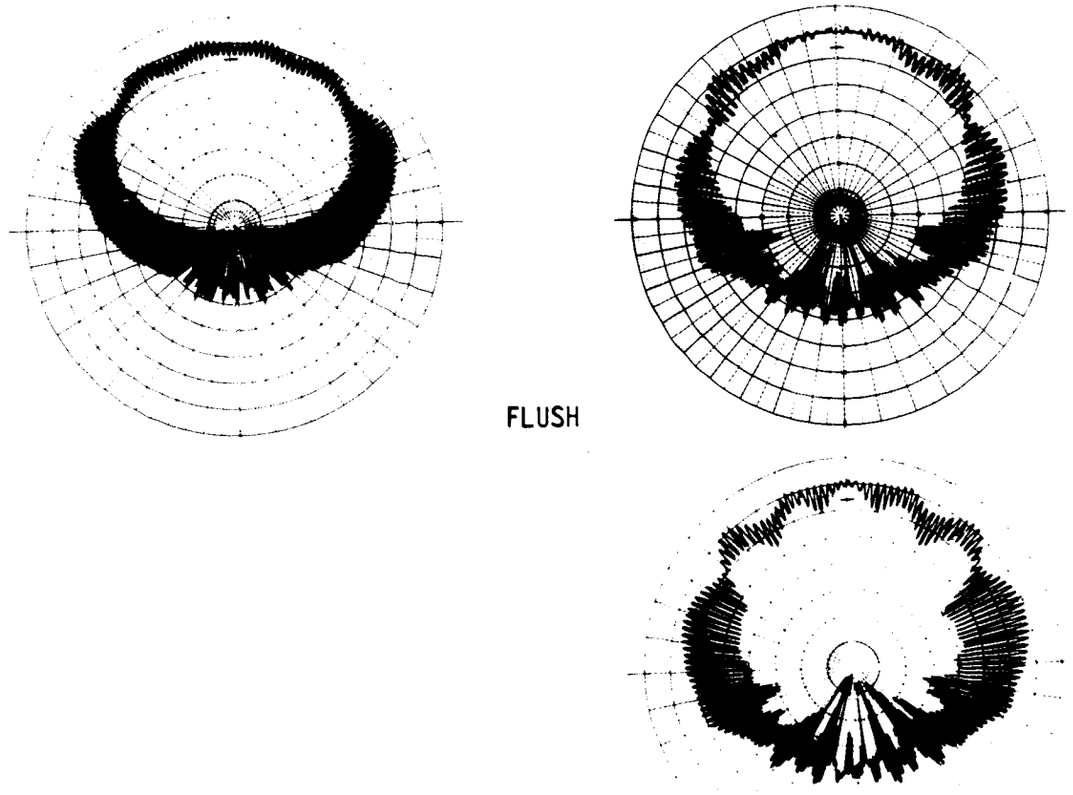

EFFECTS OF EXTENDING APERTURE ABOVE GROUND PLANE (2.2875 GHz)

FIGURE 51 (Continued)

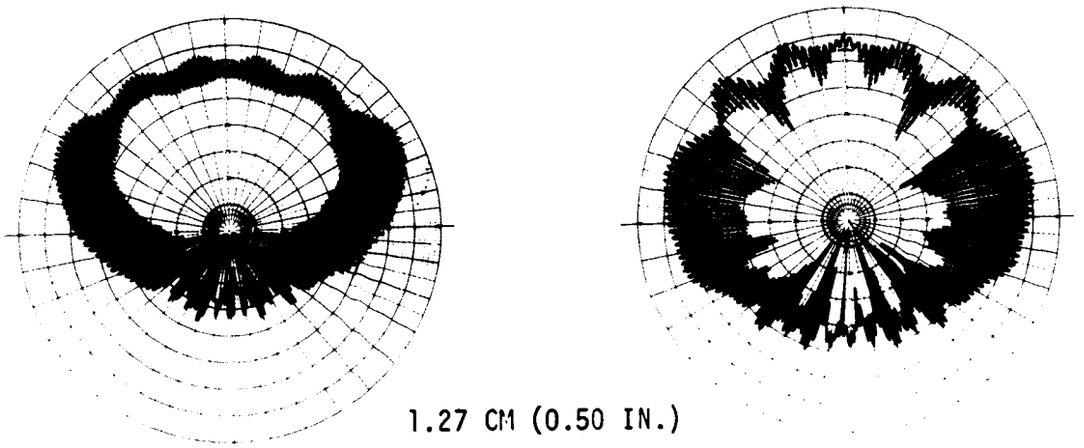

1.27 CM (0.50 IN.)

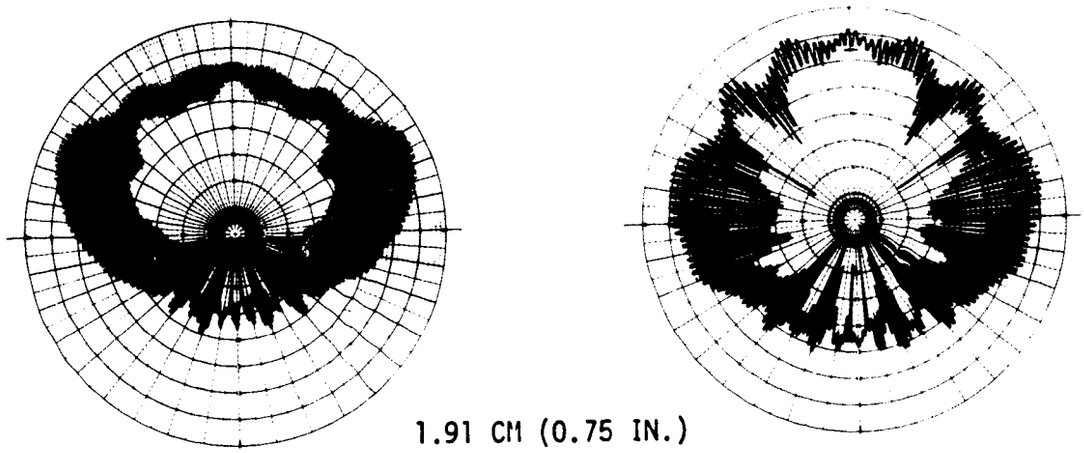

1.91 CM (0.75 IN.)

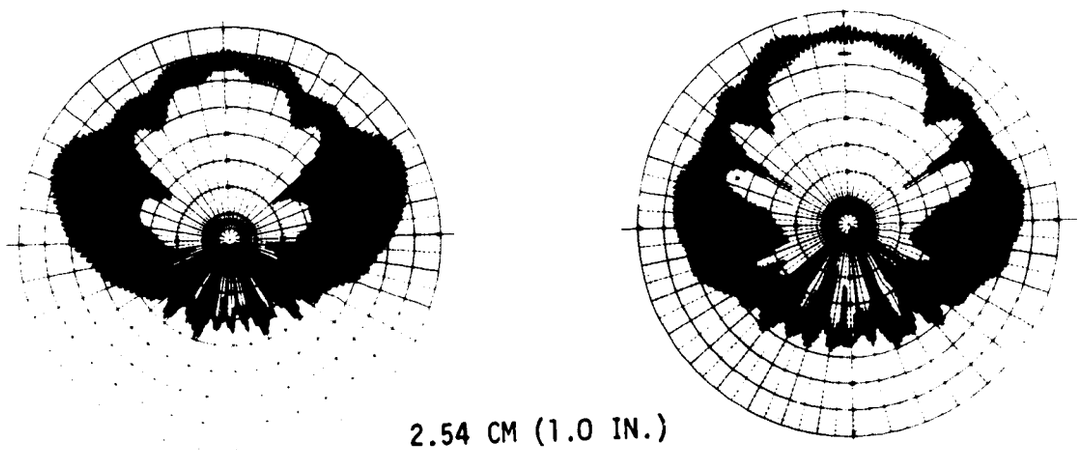

2.54 CM (1.0 IN.)

REFERENCE X-PLANE ANTENNA WINDOW AND TPS

EFFECTS OF EXTENDING APERTURE ABOVE GROUND PLANE (2.2875 GHz)

FIGURE 51 (Continued)

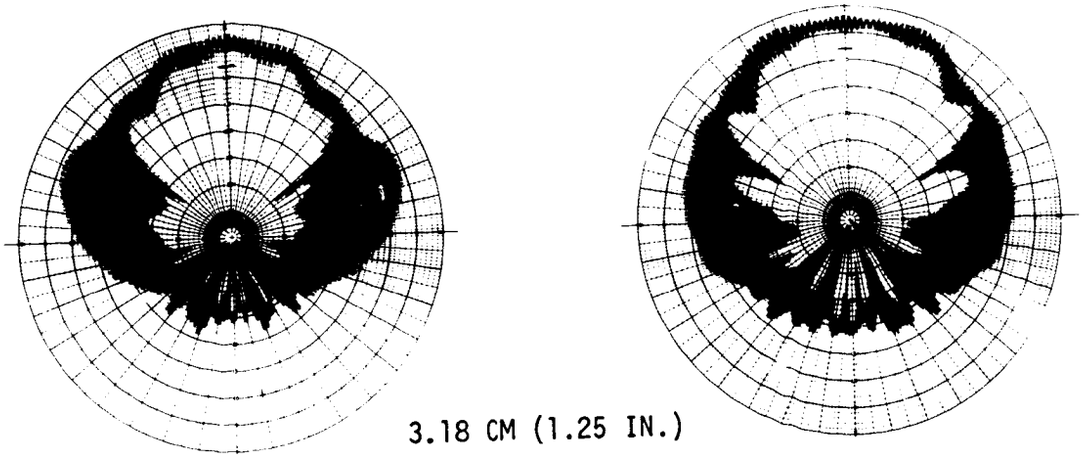

3.18 CM (1.25 IN.)

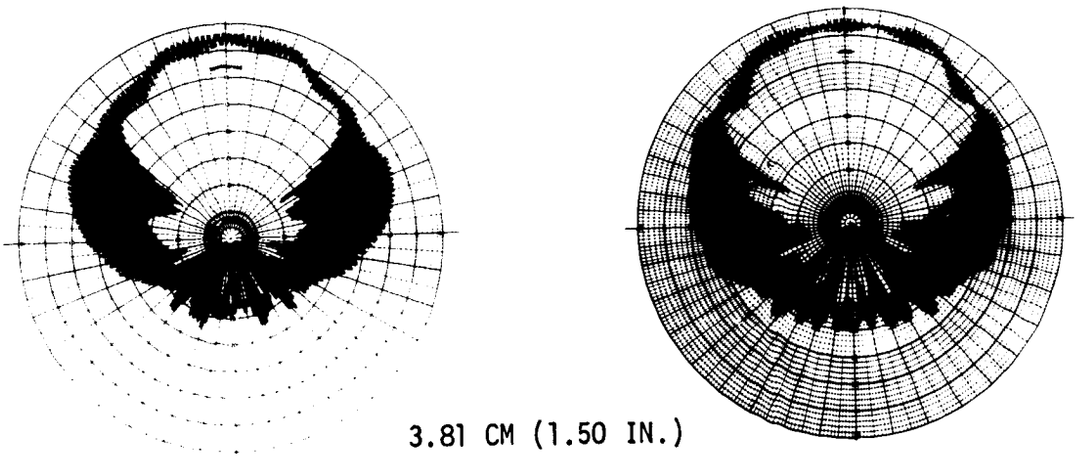

3.81 CM (1.50 IN.)

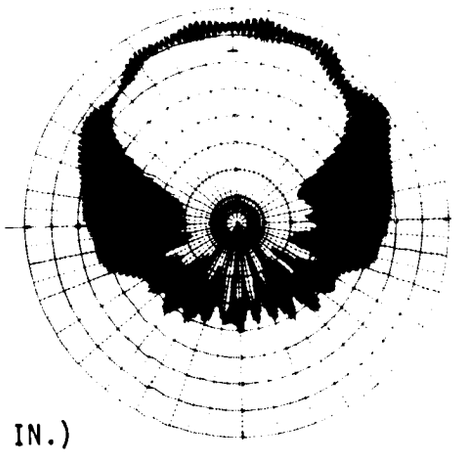

4.45 CM (1.75 IN.)

REFERENCE X-PLANE ANTENNA WINDOW AND TPS

EFFECTS OF EXTENDING APERTURE ABOVE GROUND PLANE (2.2875 GHz)

FIGURE 51 (Continued)

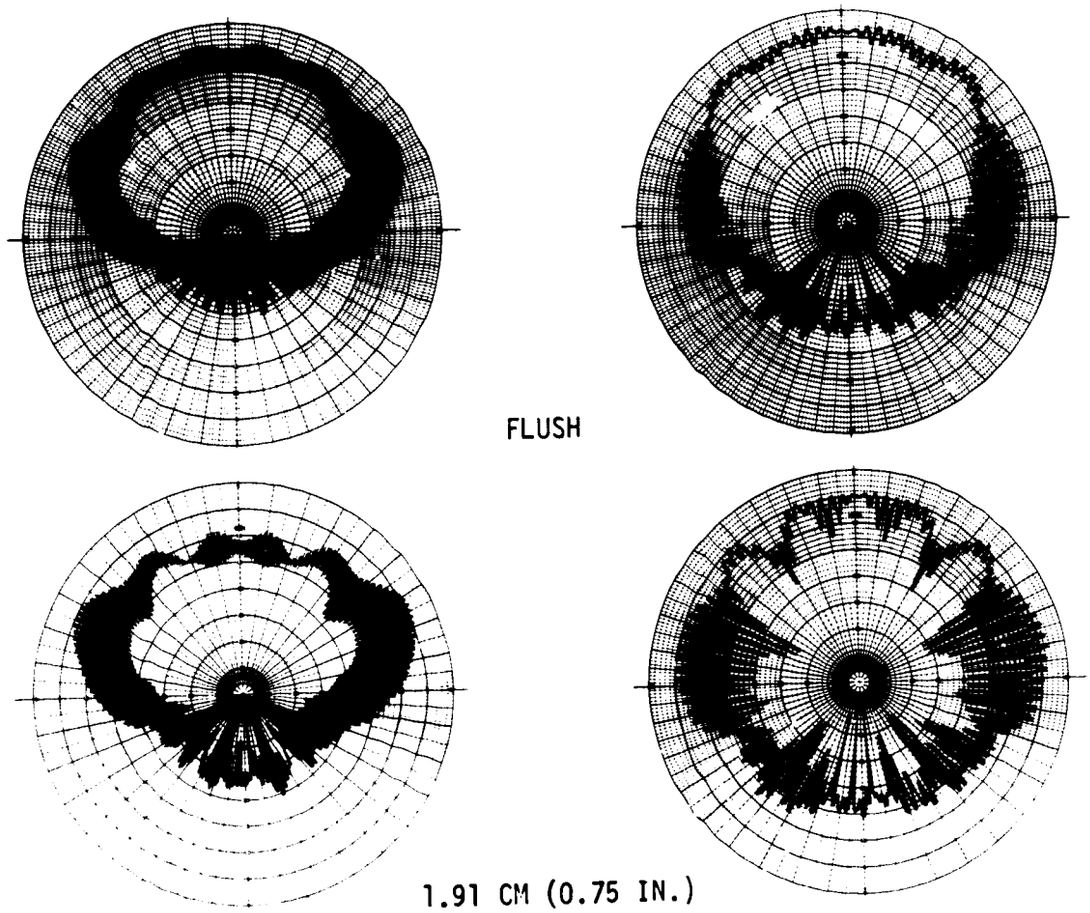

EFFECTS OF EXTENDING APERTURE ABOVE GROUND PLANE (2.2 GHz)

FIGURE 52

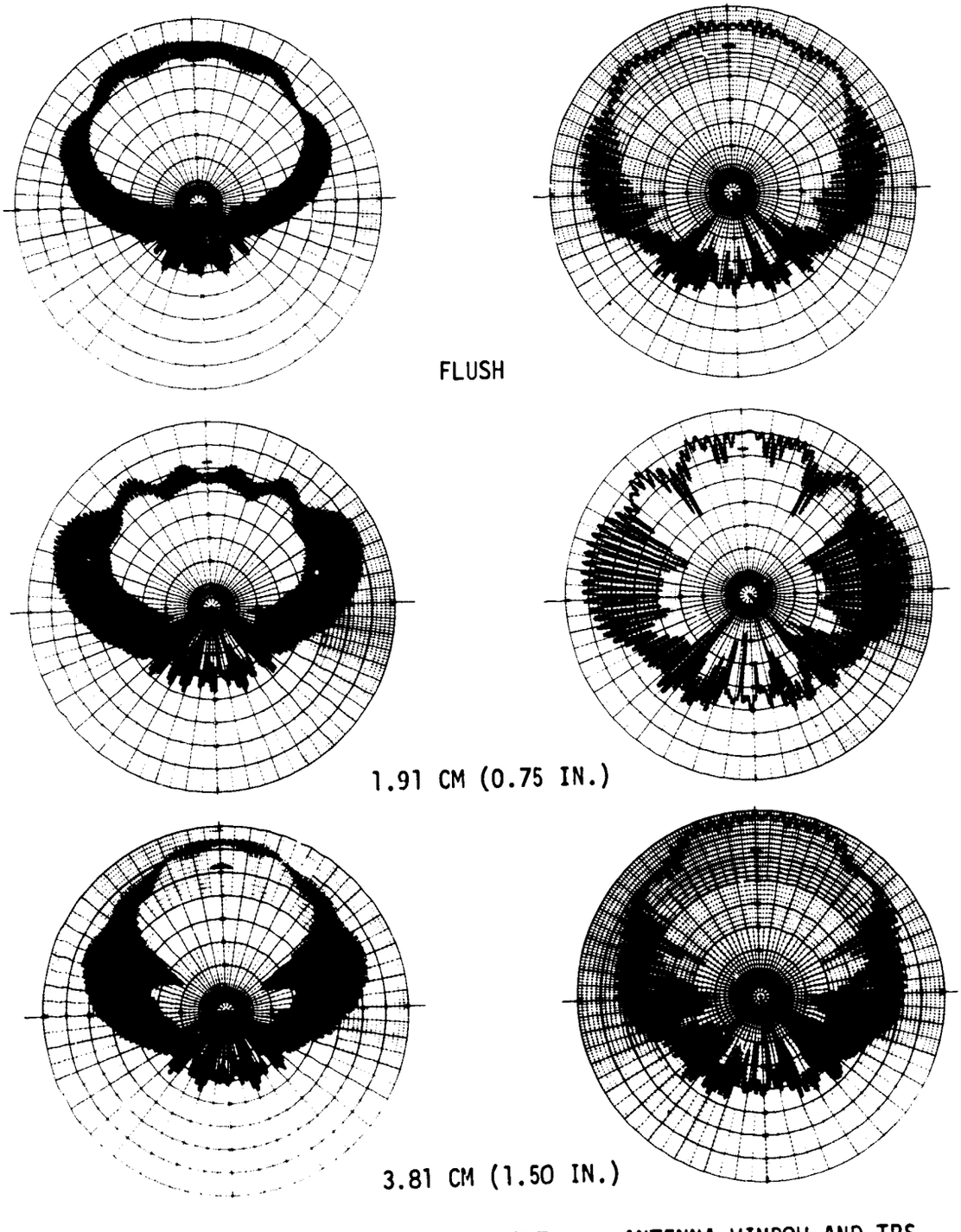

EFFECTS OF EXTENDING APERTURE ABOVE GROUND PLANE (2.2 GHz)

FIGURE 52 (Continued)

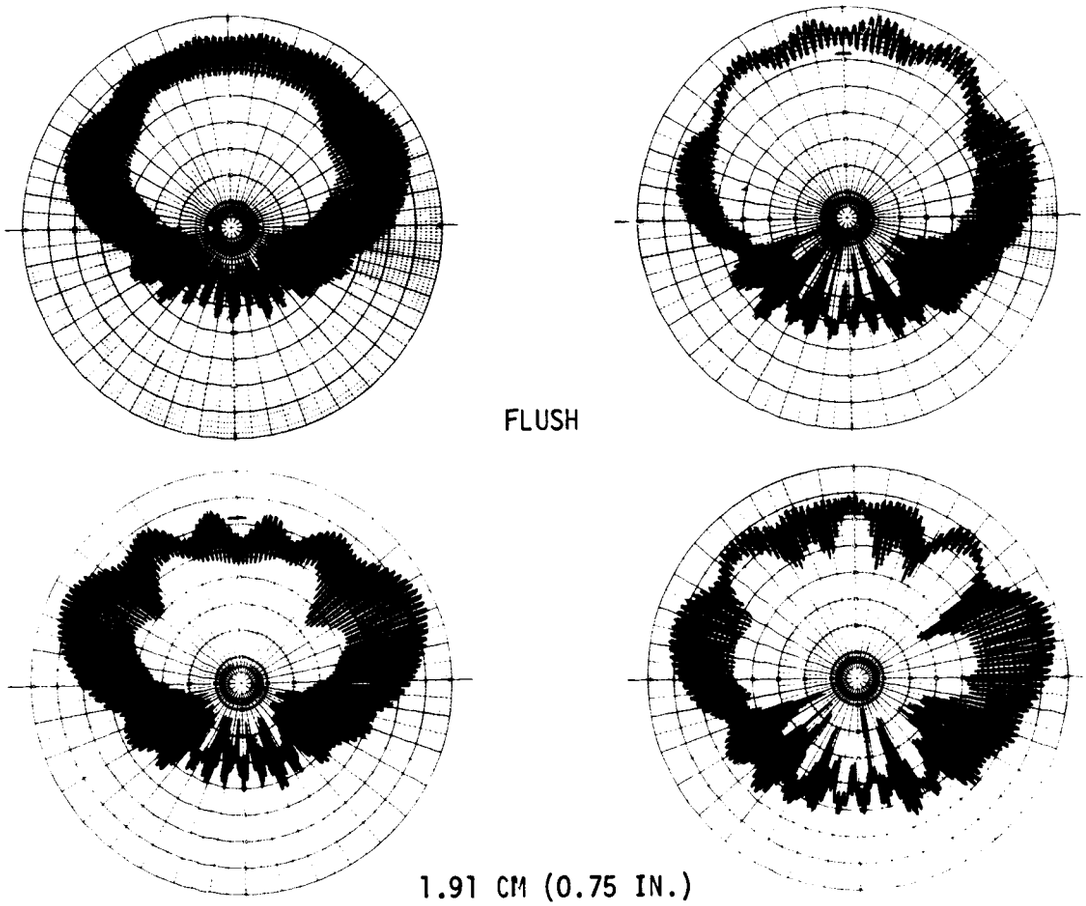

EFFECTS OF EXTENDING APERTURE ABOVE GROUND PLANE (2.1 GHz)

FIGURE 53

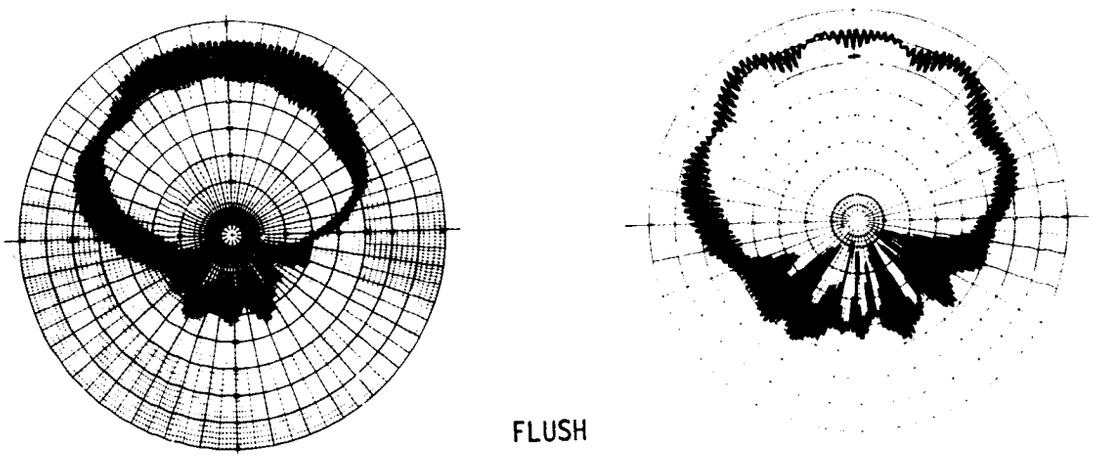

FLUSH

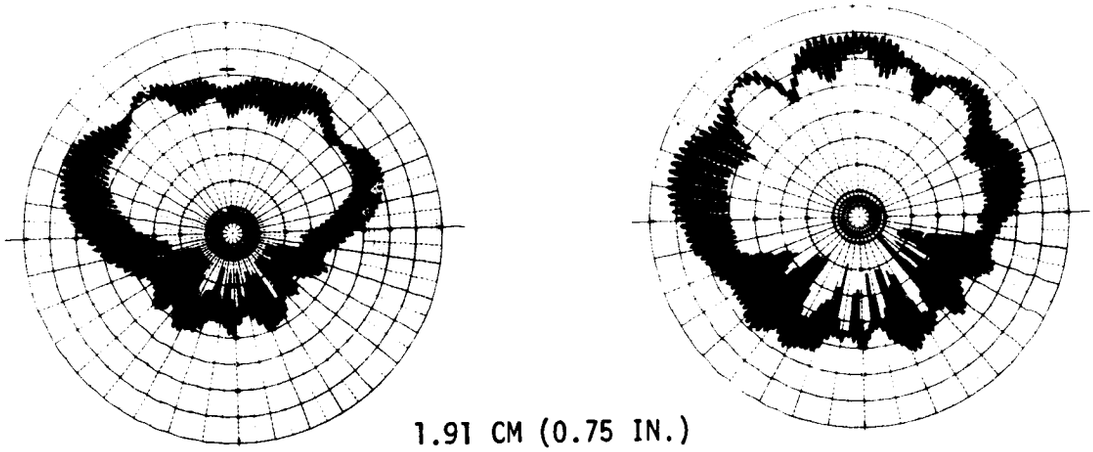

1.91 CM (0.75 IN.)

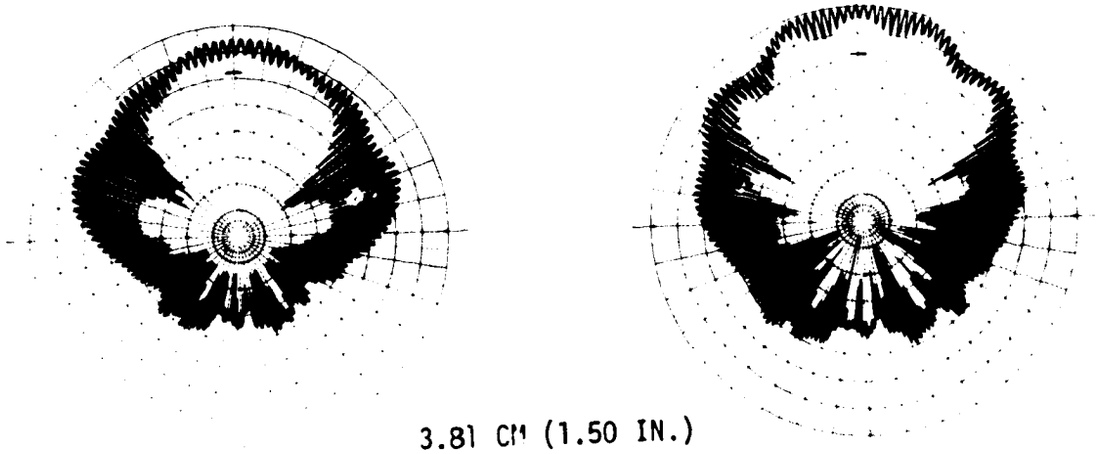

3.81 CM (1.50 IN.)

REFERENCE X-PLANE ANTENNA WINDOW AND TPS

EFFECTS OF EXTENDING APERTURE ABOVE GROUND PLANE (2.1 GHz)

FIGURE 53 (Continued)

The results of pattern measurements at 2.1 and 2.2 GHz are shown in figures 52 and 53 for antenna aperture heights of flush, 1.91 cm (.75 in.) and 3.81 cm (1.50 in.), respectively. The results are essentially the same as observed at 2.2875 GHz.

To facilitate a more direct comparison of the pattern described above, the circular gain was calculated at $\theta = 0°$ and $\theta = \pm 60°$ for each configuration tested, except for the antenna aperture heights of 4.32 mm (0.17 in.) and 4.45 cm (1.75 in.). The patterns for these aperture heights are nearly identical to the patterns for aperture heights of 6.35 mm (0.25 in.) and 3.81 cm (1.50 in.), respectively, as shown by figure 51. The results of the circular gain calculation and the measured axial ratios are shown in table XV. An

TABLE XV

DESIGN TEST CIRCULAR GAINS AND AXIAL RATIOS

FREQ (GHz)	ANTENNA APERTURE HEIGHT CM(IN.)	REFERENCE CONFIGURATION										ANTENNA WINDOW AND TPS									
		CIRCULAR GAIN (dB)					AXIAL RATIO (dB)					CIRCULAR GAIN (dB)					AXIAL RATIO (dB)				
		θ=0	θ=60		θ=-60		θ=0	θ=60		θ=-60		θ=0	θ=60		θ=-60		θ=0	θ=60		θ=-60	
			X	Y	X	Y		X	Y	X	Y		X	Y	X	Y		X	Y	X	Y
2.1	0.00(0.00)	5.1	-0.5	5.7	2.5	2.8	7.3	4.2	14.3	4.8	12.5	6.6	2.1	4.3	4.2	2.8	3.7	3.8	9.2	1.2	4.3
	0.64(0.25)	4.3	-0.8	4.7	3.0	3.1	6.6	3.1	14.3	5.3	12.3	5.1	1.1	3.9	4.1	2.8	5.1	5.7	12.0	2.0	7.0
	1.27(0.50)	1.8	-0.6	4.8	3.3	4.9	5.9	3.6	15.3	7.0	13.3	3.5	0.4	2.7	3.7	3.0	4.5	4.0	13.2	4.6	7.8
	1.91(0.75)	-2.5	0.0	4.6	3.7	4.4	5.5	4.0	16.7	8.1	15.0	4.9	-0.2	0.7	2.3	1.8	3.8	7.7	18.9	11.4	10.6
	2.54(1.00)	1.0	0.7	3.3	3.5	3.9	4.7	7.5	20.5	10.8	17.9	10.2	-1.3	-0.6	0.3	-0.2	1.8	16.5	10.0	18.5	15.7
	3.18(1.25)	5.9	-0.2	1.5	1.3	2.3	3.2	13.0	23.8	16.2	20.5	10.6	-0.1	-0.6	1.0	0.3	2.0	19.2	13.2	15.4	13.0
	3.81(1.50)	7.8	-1.4	-0.3	0.1	0.9	3.0	21.4	21.5	21.7	17.2	10.9	1.8	0.1	1.4	0.3	2.4	14.1	16.0	19.4	12.3
2.2	0.00(0.00)	4.8	2.1	4.0	2.3	2.7	4.0	4.5	9.4	5.8	9.4	7.5	3.5	3.7	3.5	3.1	1.9	4.8	5.6	4.8	5.3
	0.64(0.25)	3.5	2.8	3.7	3.6	2.6	3.5	7.3	8.8	6.5	7.0	6.6	2.9	3.5	3.3	2.4	2.5	5.1	8.4	4.6	7.1
	1.27(0.50)	1.0	3.1	3.6	4.1	2.8	2.8	9.0	9.4	9.8	8.4	5.7	2.3	2.8	3.4	1.7	1.6	7.2	10.0	7.8	10.1
	1.91(0.75)	-0.4	3.6	3.2	4.5	3.1	2.4	11.0	11.4	11.2	9.2	6.6	0.4	0.5	2.0	0.3	0.2	16.0	17.0	18.0	16.0
	2.54(1.00)	4.0	2.6	2.1	3.7	1.8	1.5	15.1	15.0	13.3	14.0	9.0	-0.5	0.2	1.2	0.2	1.4	15.0	18.0	13.0	16.4
	3.18(1.25)	6.9	0.4	-0.4	0.9	0.5	0.6	21.8	19.0	19.0	17.6	10.0	0.8	0.6	0.5	0.4	1.5	14.0	16.3	15.5	16.4
	3.81(1.50)	8.2	-1.2	-0.9	-0.5	-0.7	1.0	23.0	23.1	20.4	20.4	10.4	1.5	1.2	1.0	0.4	1.3	15.7	16.0	18.0	17.4
2.2875	0.00(0.00)	5.1	2.7	2.3	2.2	1.4	2.2	9.0	6.0	8.8	5.8	6.5	1.2	-0.4	1.9	0.0	1.6	4.7	5.8	3.7	6.3
	0.64(0.25)	3.9	2.9	2.4	2.6	1.2	2.0	10.2	6.4	9.6	5.5	6.1	0.0	0.0	0.1	-0.7	0.6	10.8	7.0	1.0	6.0
	1.27(0.50)	1.4	3.4	2.6	3.5	1.3	2.6	12.8	7.4	11.8	6.6	4.7	-1.8	-1.0	-1.4	-1.9	2.0	12.2	9.9	17.8	10.5
	1.91(0.75)	1.6	3.1	2.2	3.6	1.0	3.0	16.5	9.6	15.0	9.1	5.5	-0.6	-2.2	-1.5	-2.7	3.2	8.2	18.0	11.9	17.0
	2.54(1.00)	5.2	1.4	1.1	1.9	0.8	3.1	21.4	13.2	19.0	12.3	7.0	-0.7	-2.0	-1.2	-2.5	3.4	10.5	18.2	11.9	19.6
	3.18(1.25)	7.5	-0.2	0.0	-0.2	-0.4	2.8	16.1	15.4	19.8	15.2	7.7	-0.6	-1.4	-0.8	-1.4	3.0	18.3	19.8	1.6	16.4
	3.81(1.50)	8.3	-1.9	-1.4	-1.6	-1.6	2.0	17.0	16.6	20.0	16.4	7.7	0.2	-0.8	-0.4	-0.1	2.5	13.5	19.3	17.0	13.6

evaluation of these results confirms the conclusion reached from the visual comparison, that the antenna aperture flush with the ground plane gives the best overall pattern coverage.

Radiation patterns were measured at 1.75 GHz to determine the antenna system performance in the U.S. Air Force frequency band of 1.75 to 1.85 GHz. The results (figure 54) indicate acceptable pattern shape but very poor axial ratios and reduced gain. Axial ratios vary from 12 to 8 dB over angles up to $\theta = \pm 60°$ for the antenna aperture flush with the ground plane, but improve 3 to 4 dB with the antenna window and TPS. Over the desired beamwidth, the circular gain is marginal at $\theta = \pm 32°$ and is -1 dB at $\theta = \pm 60°$ wichout the antenna

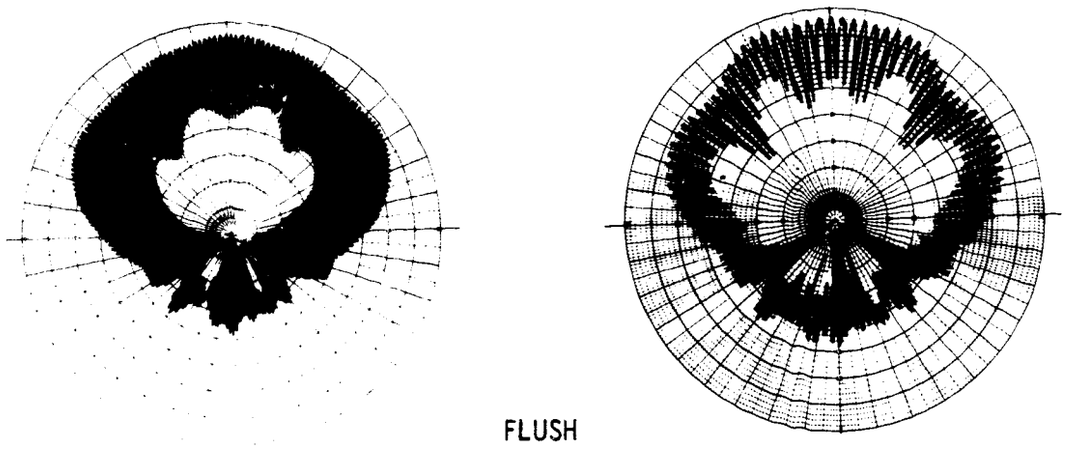

FLUSH

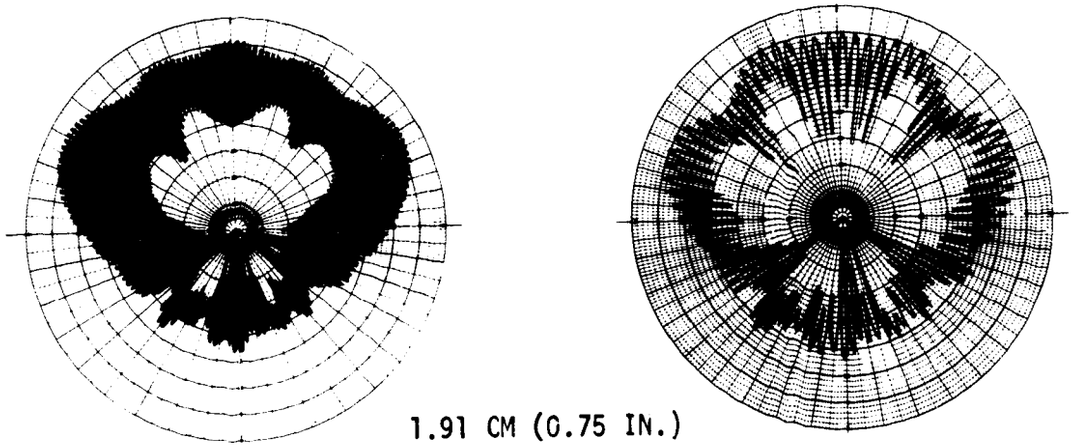

1.91 CM (0.75 IN.)

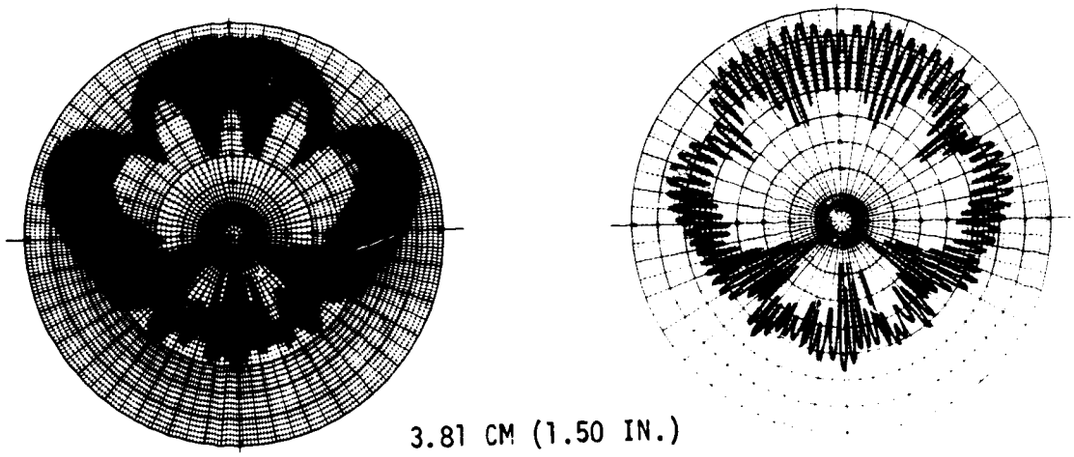

3.81 CM (1.50 IN.)

REFERENCE Y-PLANE ANTENNA WINDOW AND TPS

EFFECTS OF EXTENDING APERTURE ABOVE GROUND PLANE (1.75 GHz)

FIGURE 54

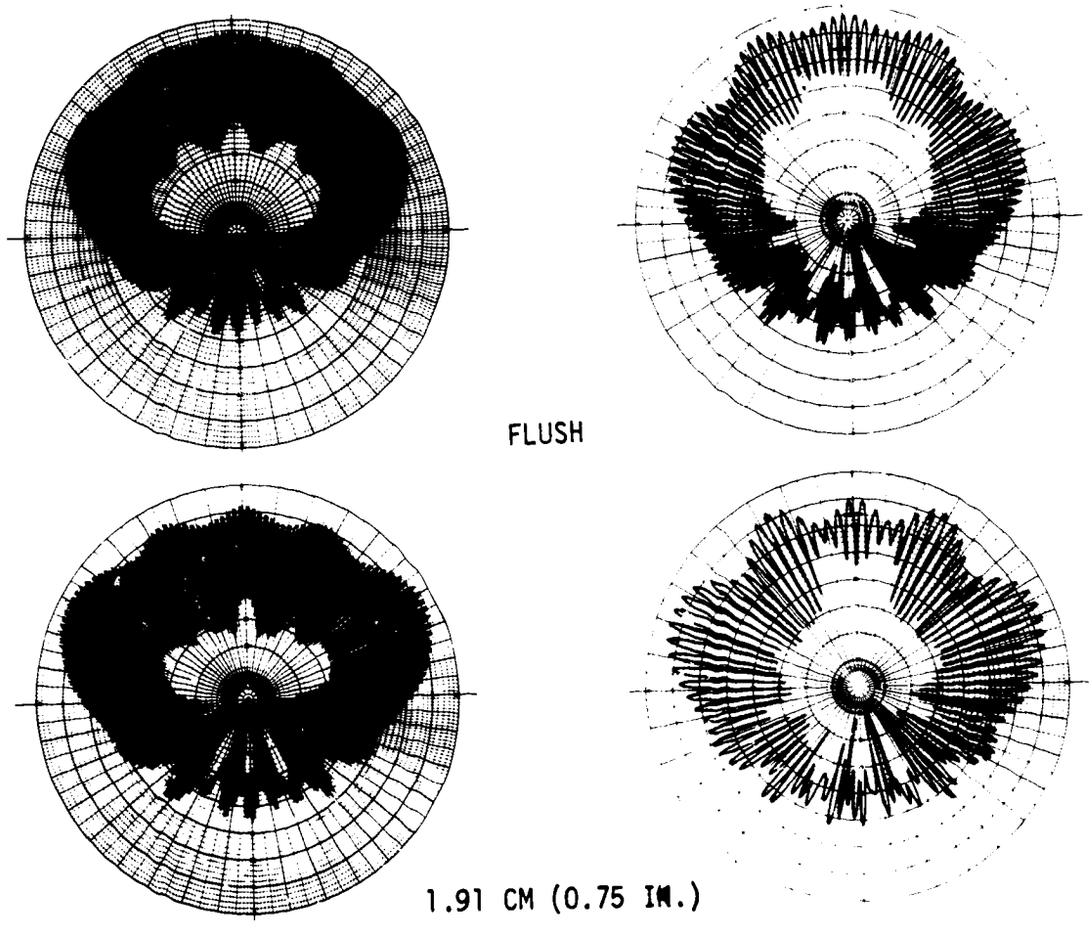

EFFECTS OF EXTENDING APERTURE ABOVE GROUND PLANE (1.75 GHz)

FIGURE 54 (Continued)

window and TPS. With the antenna window and TPS the gain drops from about 5 dB at $\theta = 0°$ to about -1.7 dB at $\theta = \pm 44°$ and increases to about 2.5 dB at $\theta = \pm 60°$. Except for the two 10° segments centered at $\theta = \pm 44°$ the circular gain is above 0 dB over the desired beamwidth ($\theta = \pm 60°$).

Radiation patterns were also measured at 3.45 GHz to determine the antenna system performance in the Russian frequency band of 3.4 to 3.5 GHz. The results (figure 55) show both pattern shape and axial ratios are poor. This is not unexpected since the antennas were designed for operation from 2.1 to 2.3 GHz. Figure 55 shows that a deep null exists in the X-plane patterns. This null does not appear in the Y-plane although there is a reduction of gain at or near $\theta = 0°$. This results in flat and square looking Y-plane patterns. The patterns are also unsymmetrical and the gain is less than 0 dB over 50% of the beamwidth.

The results of impedance measurements (figures 56 through 58) show that the antenna window and TPS have only minor effects on the input impedance of the S-band antenna. The impedance was measured within three separate frequency bands, 1.77 to 1.85 GHz, 2.02 to 2.3 GHz, and 3.4 to 3.5 GHz. The impedance over these three frequency bands is shown in figures 56, 57 and 58 for the antenna aperture height of flush, 1.91 cm (.75 in.) and 3.81 cm (1.50 in.), respectively, with and without the antenna window and TPS. With the antenna window and TPS in place, the impedance over each frequency band tends to group closer together.

The VSWR over the design frequency range (2.1 to 2.3 GHz) is less than 1.5:1 for all conditions. The VSWR's for other frequencies and for all configurations are: (1) less than 4.5:1 for the 1.7 to 1.85 GHz frequency band; (2) less than 2.2:1 for the 3.4 to 3.5 GHz frequency band; and (3) less than 3.4:1 for the 2.02 to 2.1 GHz band. Due to equipment limitations, 1.77 GHz was used as the lower end of the U.S. Air Force frequency band instead of 1.75 GHz.

Test results (antenna tuning): Radiation measurements were conducted at Amecom's facility during the final assembly of the antennas. These tests were made to determine if the antenna window and TPS affected the axial ratio, and if the axial ratio could be improved by tuning the antenna with the antenna window over the antenna. The antenna window and TPS were the same as used in the electrical design tests, and the tests were witnessed by an MDAC-E representative. Two antennas were tested, one with a 4-5/16 turn helix and the other with a 4-1/2 turn helix. The test configuration differed from MDAC-E's in three respects: (1) the ground plane size was increased by 5.1 cm (2.0 in.) on a side; (2) the antenna was mounted to the ground plane with 4 long bolts; and (3) the antenna was surrounded with RF absorber behind the ground plane. The antenna aperture was mounted flush with the ground plane surface. The results of the pattern measurements (figure 59) show the 4-1/2 turn helix has slightly lower axial ratios both with and without the antenna window and TPS. In both cases the antenna window tends to reduce the axial ratio only slightly. Therefore, it does not appear that significant improvement can be made in the axial ratio by tuning the antennas with the antenna window and TPS present.

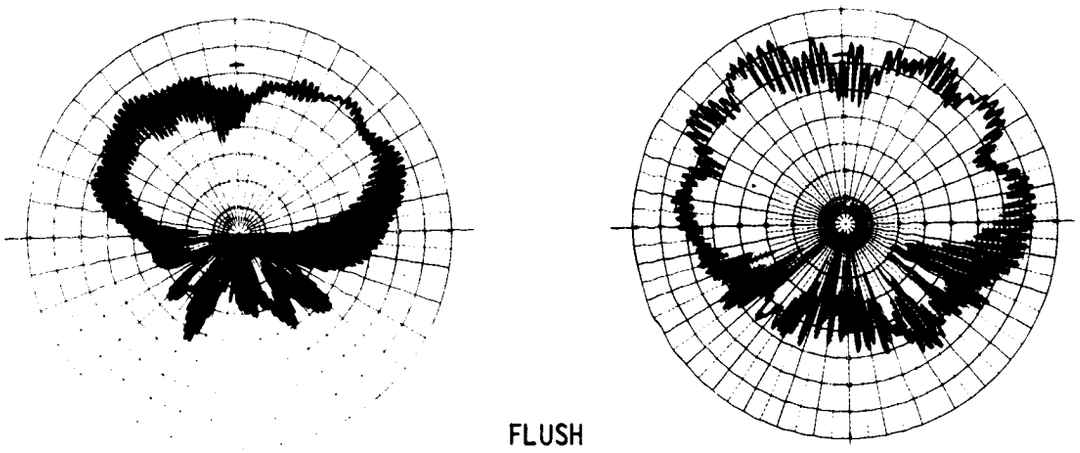

FLUSH

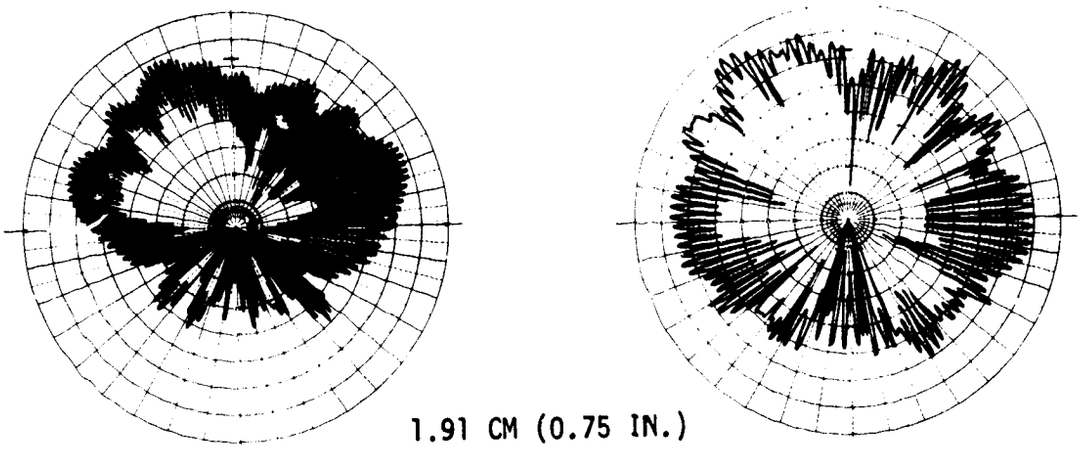

1.91 CM (0.75 IN.)

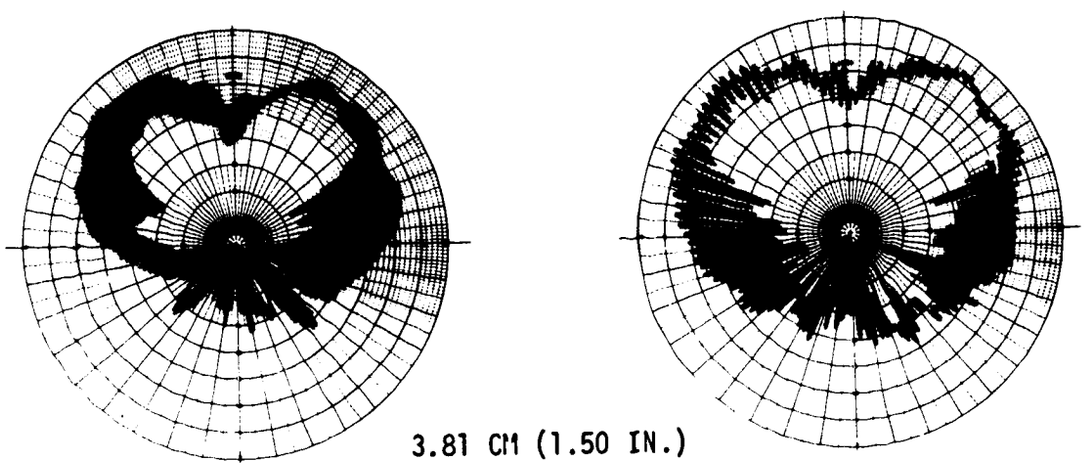

3.81 CM (1.50 IN.)

REFERENCE Y-PLANE ANTENNA WINDOW AND TPS

EFFECTS OF EXTENDING APERTURE ABOVE GROUND PLANE (2.45 GHz)

FIGURE 55

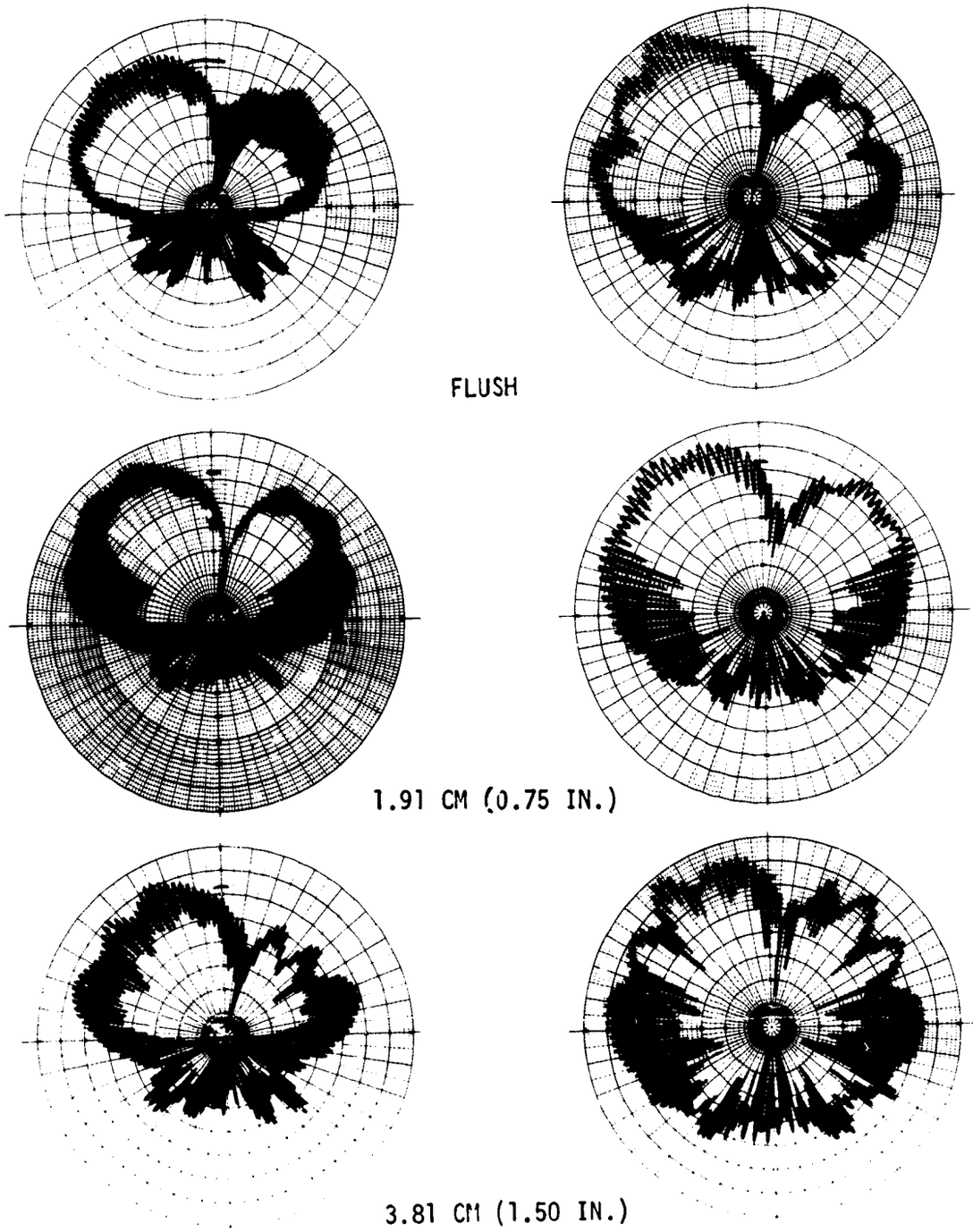

EFFECTS OF EXTENDING APERTURE ABOVE GROUND PLANE (3.45 GHz)

FIGURE 55 (Continued)

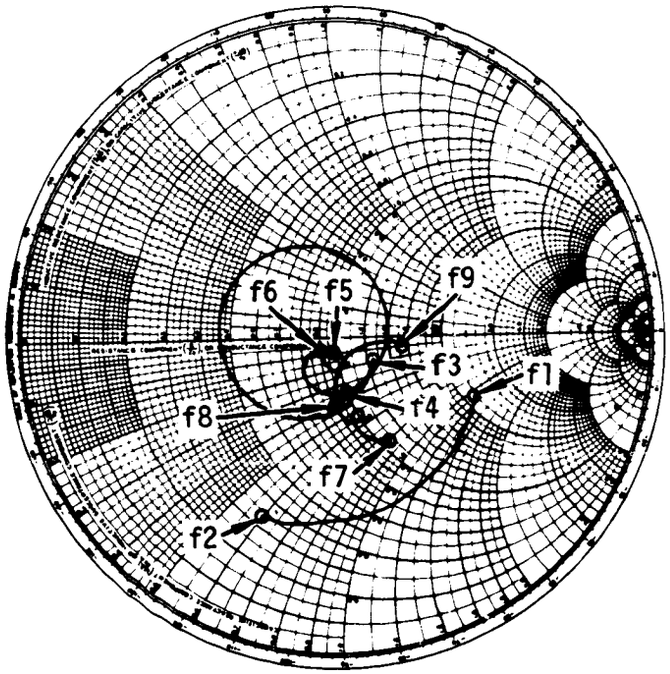

REFERENCE

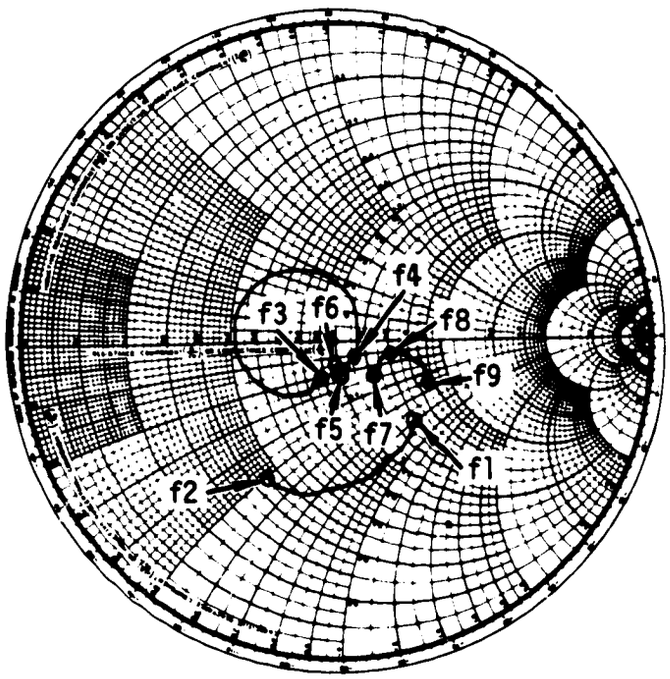

ANTENNA WINDOW AND TPS

Z_o = 50 OHMS
f1 = 1.77 GHz
f2 = 1.85 GHz
f3 = 2.02 GHz
f4 = 2.1 GHz
f5 = 2.2 GHz
f6 = 2.3 GHz
f7 = 3.4 GHz
f8 = 3.45 GHz
f9 = 3.5 GHz

IMPEDANCE - APERTURE FLUSH WITH GROUND PLANE

FIGURE 56

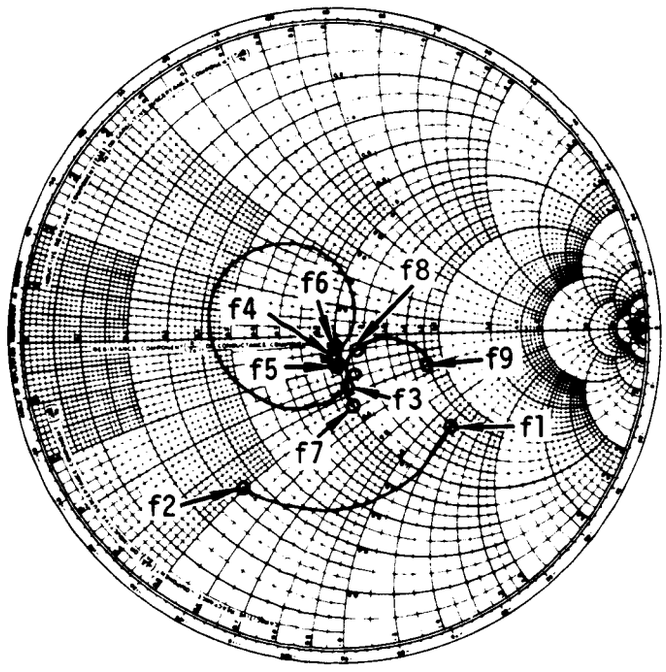

REFERENCE

Z_o = 50 OHMS
f1 = 1.77 GHz
f2 = 1.85 GHz
f3 = 2.02 GHz
f4 = 2.1 GHz
f5 = 2.2 GHz
f6 = 2.3 GHz
f7 = 3.4 GHz
f8 = 3.45 GHz
f9 = 3.5 GHz

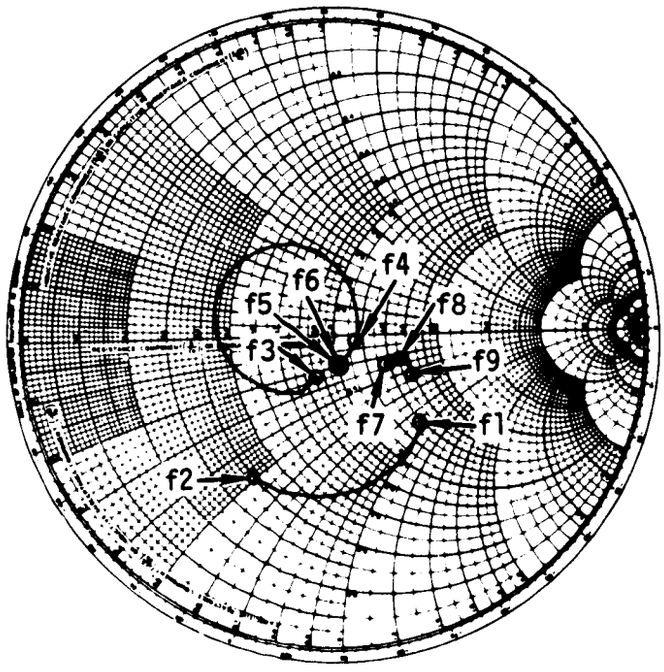

ANTENNA WINDOW AND TPS

IMPEDANCE - APERTURE 1.91 CM (0.75 IN.) ABOVE GROUND PLANE

FIGURE 57

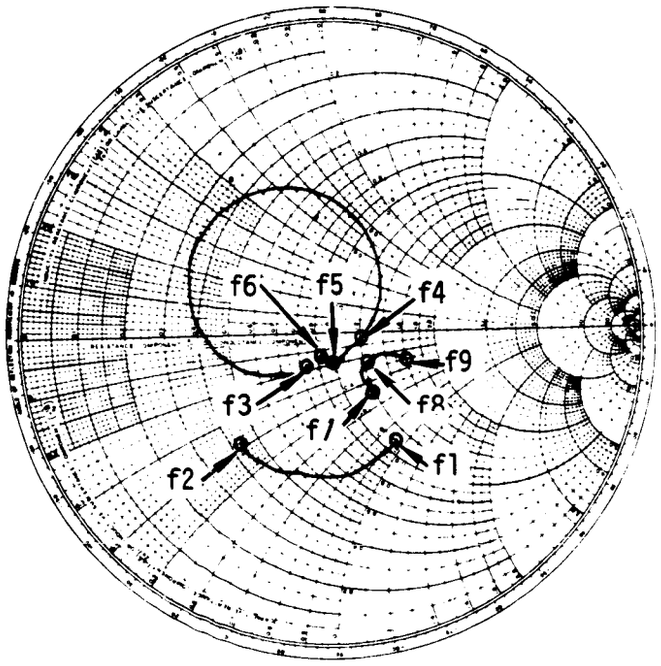

REFERENCE

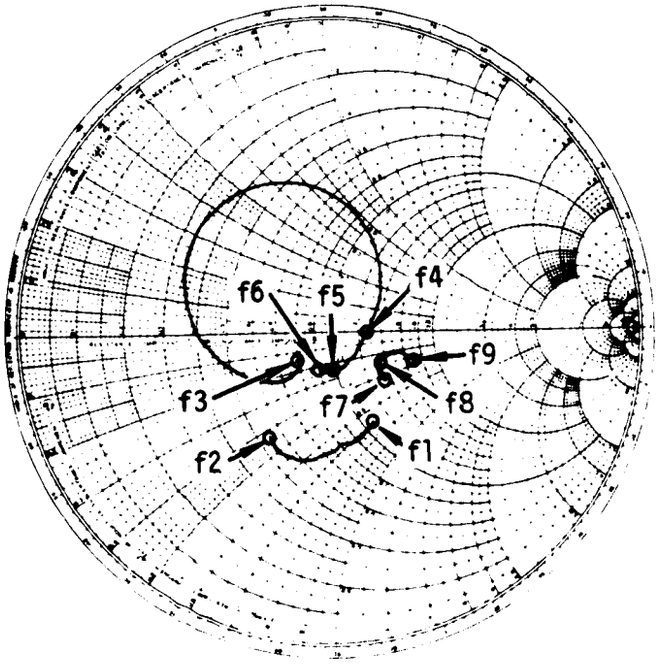

ANTENNA WINDOW AND TPS

Z_o = 50 OHMS
f1 = 1.77 GHz
f2 = 1.85 GHz
f3 = 2.02 GHz
f4 = 2.1 GHz
f5 = 2.2 GHz
f6 = 2.3 GHz
f7 = 3.4 GHz
f8 = 3.45 GHz
f9 = 3.5 GHz

IMPEDANCE - APERTURE 3.81 CM (1.50 IN.) ABOVE GROUND PLANE

FIGURE 58

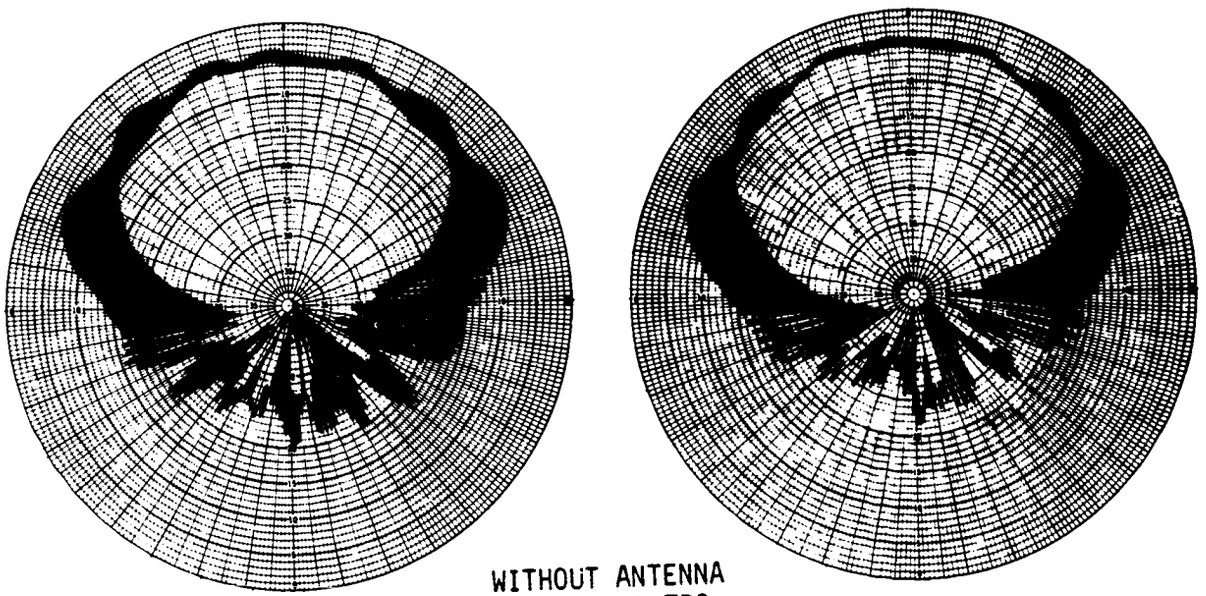

WITHOUT ANTENNA
WINDOW AND TPS

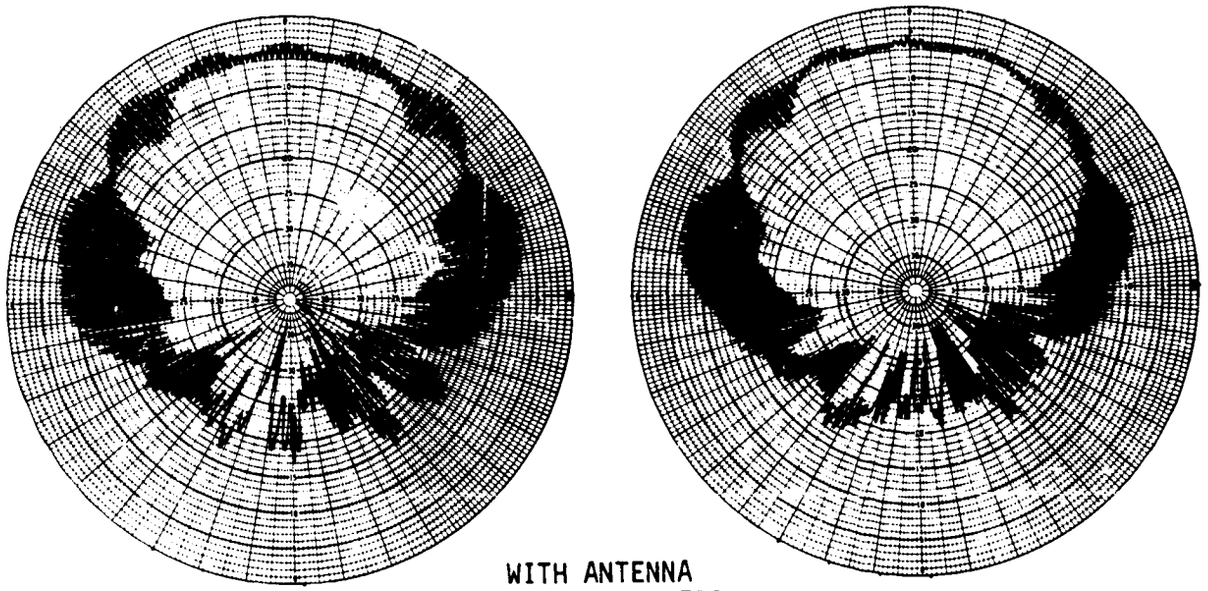

WITH ANTENNA
WINDOW AND TPS

4-5/16 TURN

4-1/2 TURN

EFFECTS OF ANTENNA TUNING

FIGURE 59

The patterns show some scalloping accompanied by increased axial ratio which can be attributed to edge effects. To reduce these effects, a 5.1 cm (2.0 in.) wide border of AN-75 absorber was added to the edges of the ground plane as shown in figure 60. The tape which was used to hold the simulated TPS and absorber in place over the ground plane is clearly visible. The effect of the absorber is shown in figure 61. The axial ratio is significantly reduced at the beam edges ($\theta = \pm 60°$). However, the axial ratio tended to increase slightly at other angles, indicating the edge effects were not completely eliminated.

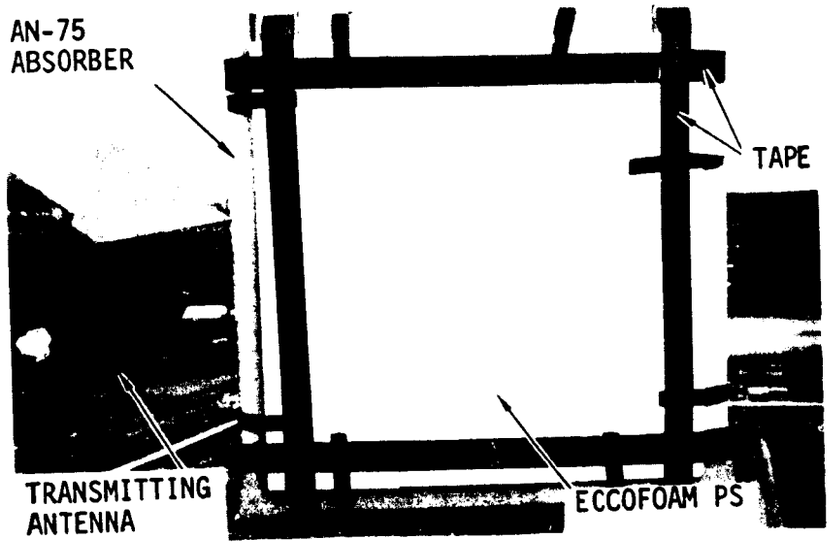

ANTENNA TUNING TEST CONFIGURATION WITH AN-75 BORDER FIGURE 60

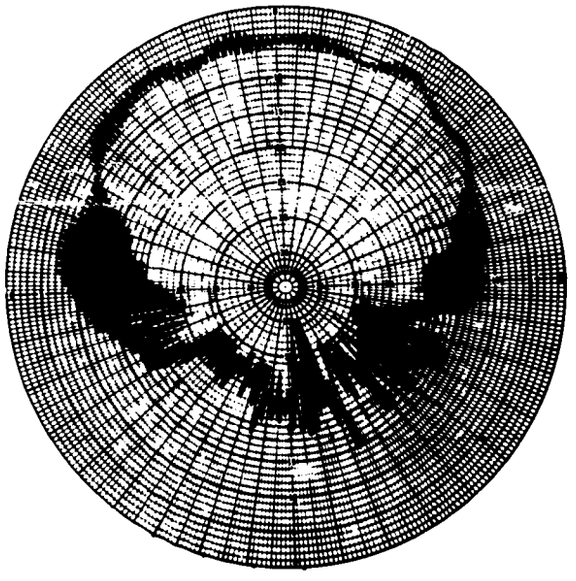

EFFECTS OF AN-75 BORDER ON GROUND PLANE EDGE DIFFRACTION FIGURE 61

Test results (antenna mounting effects): Radiation pattern measurements were made to assess the effects of a cylindrical cavity 1.27 mm (0.05 in.) wide around the antenna aperture and 7.9 cm (3.1 in.) deep. The cavity is between the antenna support housing which holds the antenna in position behind the antenna window and the antenna, as shown by figure 32. A prototype antenna (S/N 101) was used for these tests. The cavity depths tested were: (1) zero cavity depth (i.e., antenna aperture terminated in ground plane); (2) 3.3 cm (1.3 in.) (one quarter wavelength at 2.2875 GHz); (3) 5.1 cm (2.0 in.); and (4) 7.9 cm (3.1 in.) (maximum cavity depth). The test results (figure 62) show that the cavity depth does not have a significant effect on any of the pattern shapes or axial ratio. The worst axial ratios occurred for a cavity depth of 3.3 cm (1.3 in.) where the axial ratio at the beam edges ($\theta = \pm 60°$) is 0.5 to 2 dB higher than for the other test configurations. The results for the zero and maximum cavity depths are essentially the same. Therefore, design changes in the antenna support housing are not required for improved radiation patterns or axial ratio.

Test results (antenna system mockup): Radiation patterns were measured with a prototype antenna (S/N 101) mounted in a mockup of the S-band antenna system. That is, the antenna was mounted to the ground plane with a cylindrical antenna support housing instead of the graphite ring holder used for the preliminary electrical design tests. The patterns (figure 63) are similar to those given in the preliminary test results (figures 51, 52 and 53).

Comparison of the impedance measurements (figure 64) with those of the S-band antenna (figure 98) (discussed in the section on ELECTRICAL TESTING under Component Testing) shows that the addition of the antenna window over the antenna reduces the VSWR. The VSWR of the S-band antenna system mockup is 1.3:1 or less compared to 1.5:1 or less for the S-band antenna alone.

Transmission loss. - The plane wave transmission characteristics of the S-band antenna window were calculated using the expressions given in Appendix B. The window configuration is identified by Configuration No. 1 in table VI. The results for this window configuration (figure 65) show the maximum transmission loss is about 0.22 dB at 3.25 GHz, which is near the Russian frequency band. The transmission loss in the NASA frequency band, 2.1 to 2.3 GHz, is only about 0.15 dB. The transmission loss of a 5.08 cm (2.00 in.) thick layer of LI-1500 is also shown for reference. Calculations were made to determine the effect of doubling the two RTV-560 bond layer thicknesses, probably the most difficult dimension to control. The results (figure 65) show an increase in transmission loss of less than 0.1 dB. Therefore, a small increase in bondline thickness is not expected to increase the transmission loss significantly.

The results of these calculations indicate that the antenna window configuration used in the S-band antenna system design has very low transmission loss.

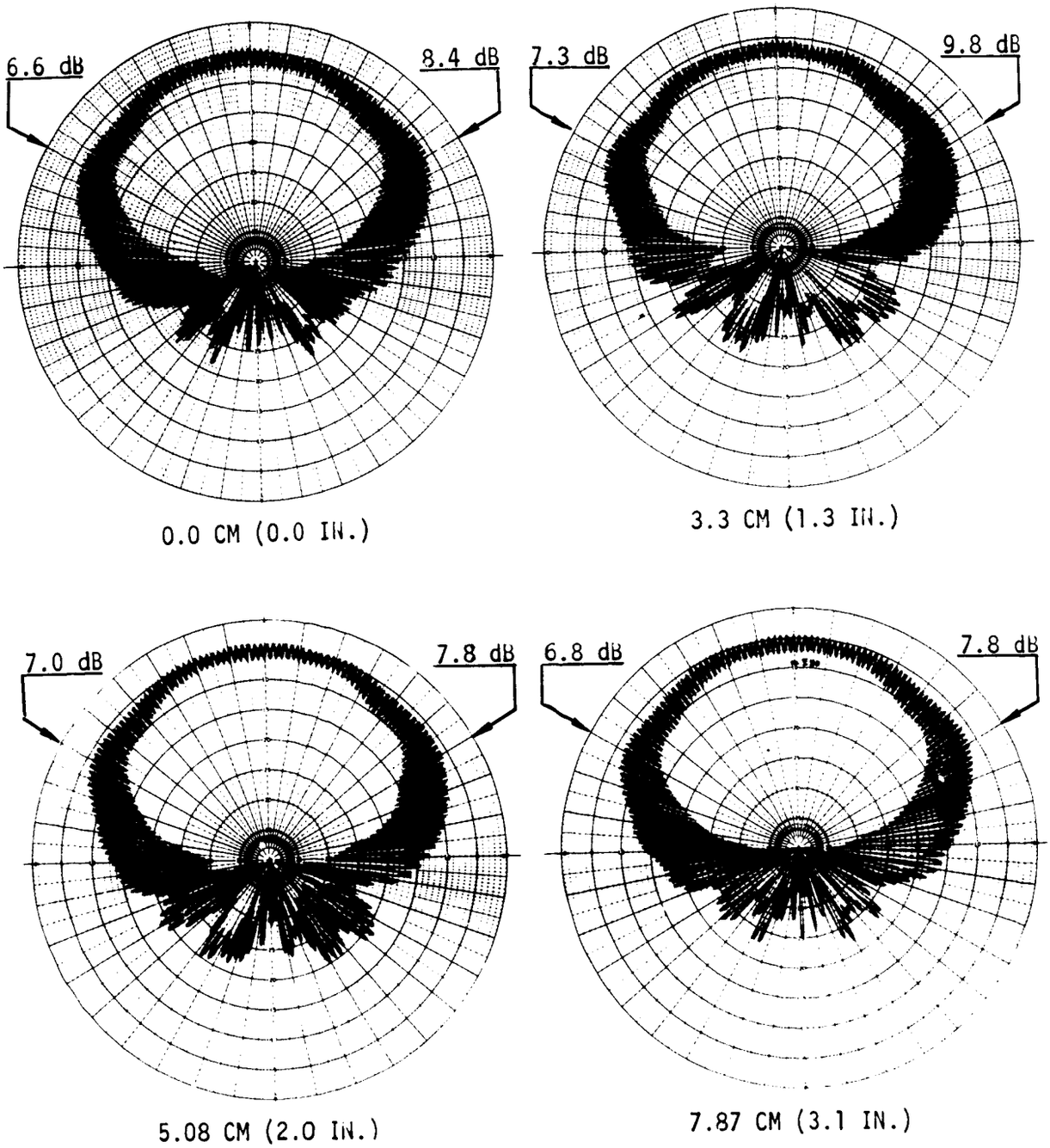

EFFECTS OF ANTENNA SUPPORT CAVITY DEPTH ON AXIAL RATIO

FIGURE 62

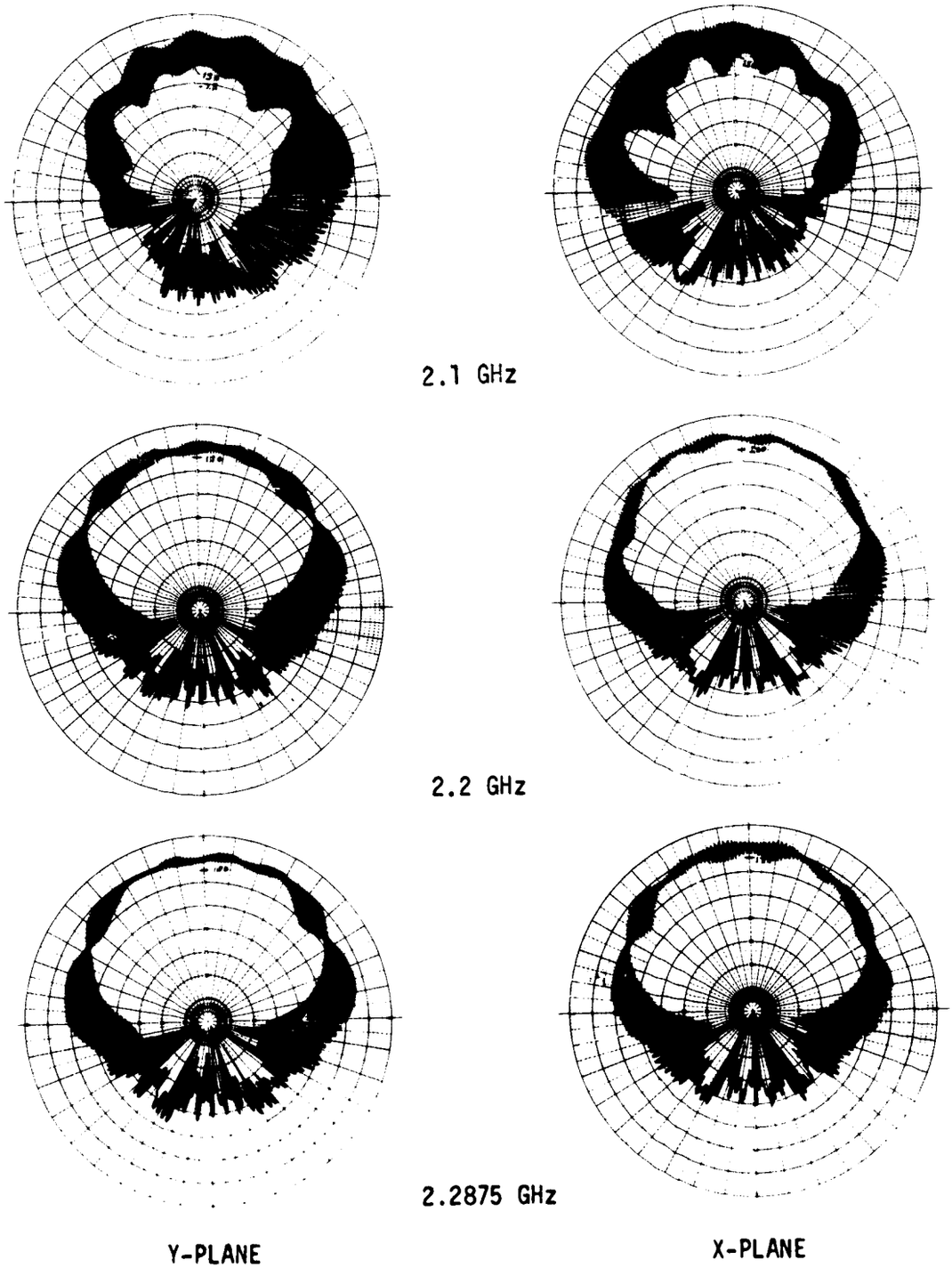

RADIATION PATTERNS - S-BAND ANTENNA SYSTEM MOCKUP (S/N 101)

FIGURE 63

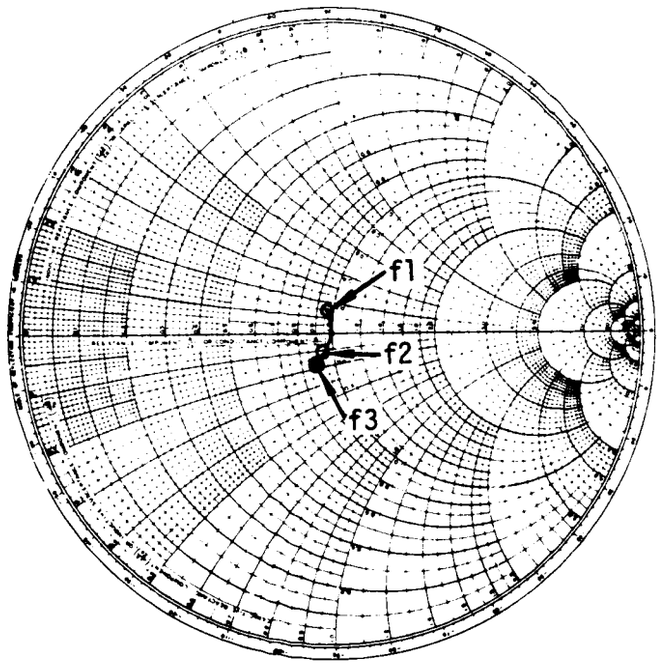

Z_0 = 50 OHMS
f1 - 2.1 GHz
f2 = 2.13 GHz
f3 = 2.3 GHz

IMPEDANCE - S-BAND ANTENNA SYSTEM MOCKUP (S/N 101)

FIGURE 64

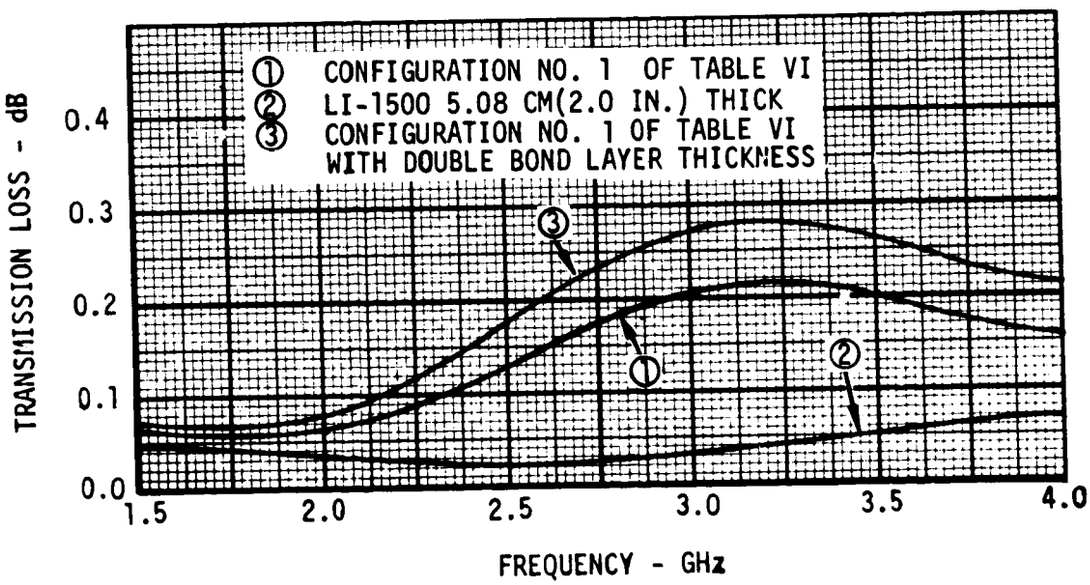

TRANSMISSION LOSS

FIGURE 65

Structural Design

The S-band antenna system structural design is based on the results of the Electrical Design, Material Evaluation, Thermal Analyses, and Strengtn Analyses tasks. The basic design (figure 66) is based on the component integration concept. It was adapted to the area requirements of a thermal test fixture which supports the antenna system in either channel nozzle or wedge mount fixtures designed for the NASA-JSC 10 megawatt ARMSEF facility. A breadboard unit was first designed for preliminary electrical and thermal testing, as described in the sections on ELECTRICAL TESTING and THERMAL TESTING, to verify the design approach and analyses. The results of the breadboard unit tests were used to complete the design of the prototype unit. Since no design changes were necessary as a result of the breadboard tests, the breadboard and prototype units are essentially identical, except for the number and location of the thermocouples.

Breadboard unit design. - A sketch of the breadboard S-band antenna system is shown in figure 66. It includes the S-band antenna, antenna support, antenna window assembly, panel assembly, and surrounding TPS. The S-band antenna (figure 67), Amecom M46325, is attached to a machined, aluminum antenna support with four #10 bolts. The antenna support (figure 68) is attached to the panel assembly with four #10 flush screws, and holds the antenna aperture flush with the outer skin surface. It is removed or replaced along with the antenna from the external side of the panel support assembly.

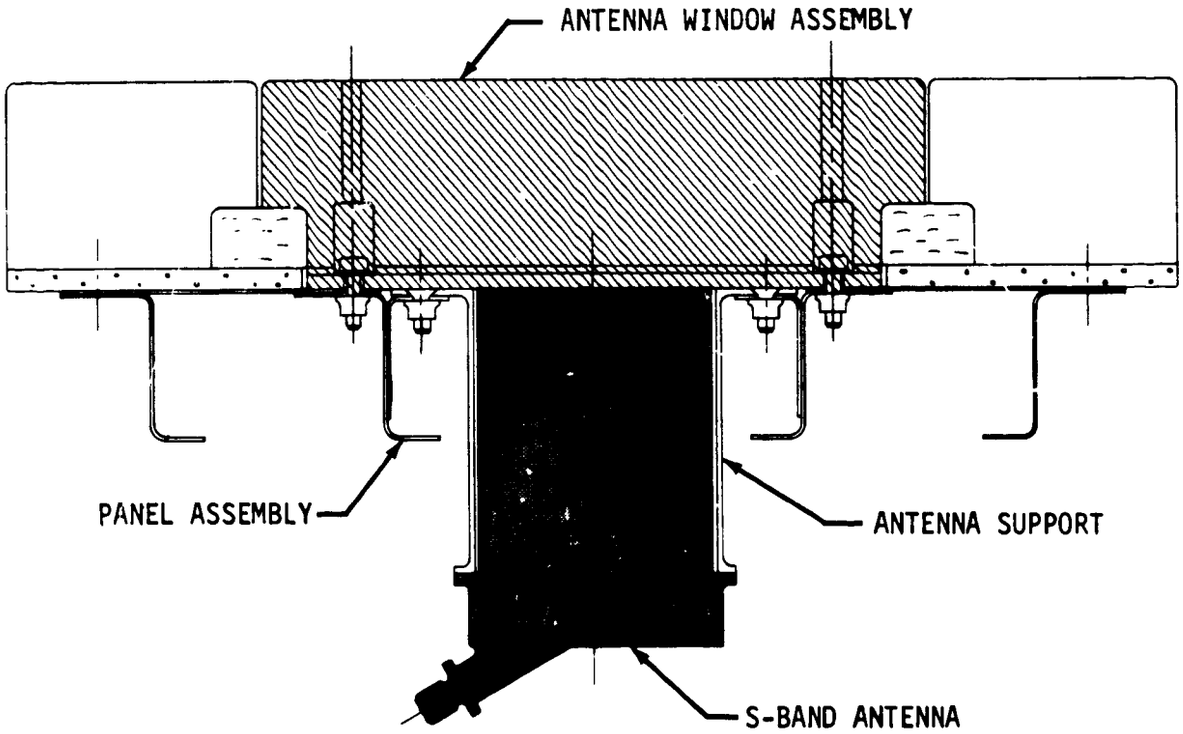

S-BAND ANTENNA SYSTEM FIGURE 66

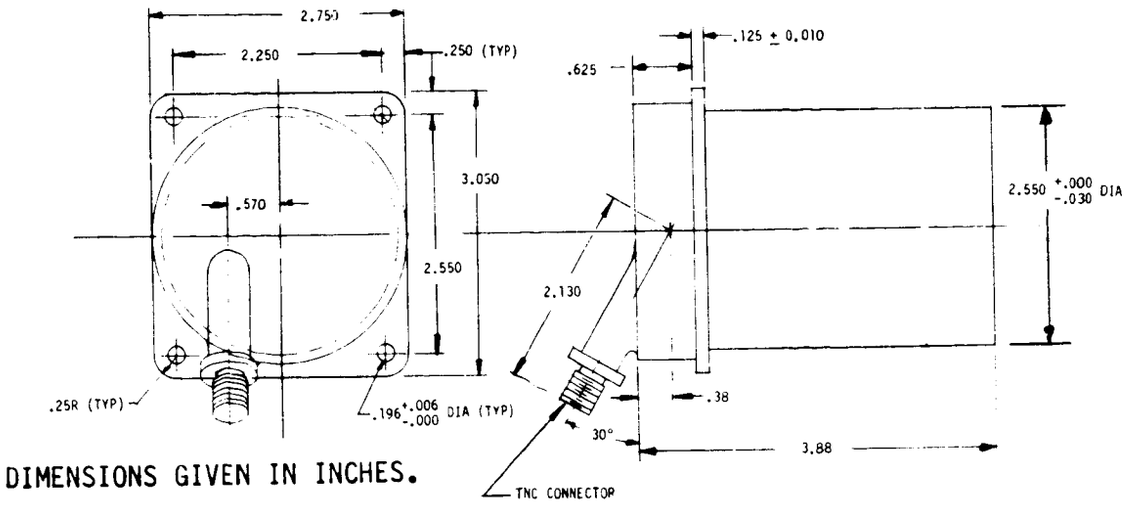

S-BAND ANTENNA

FIGURE 67

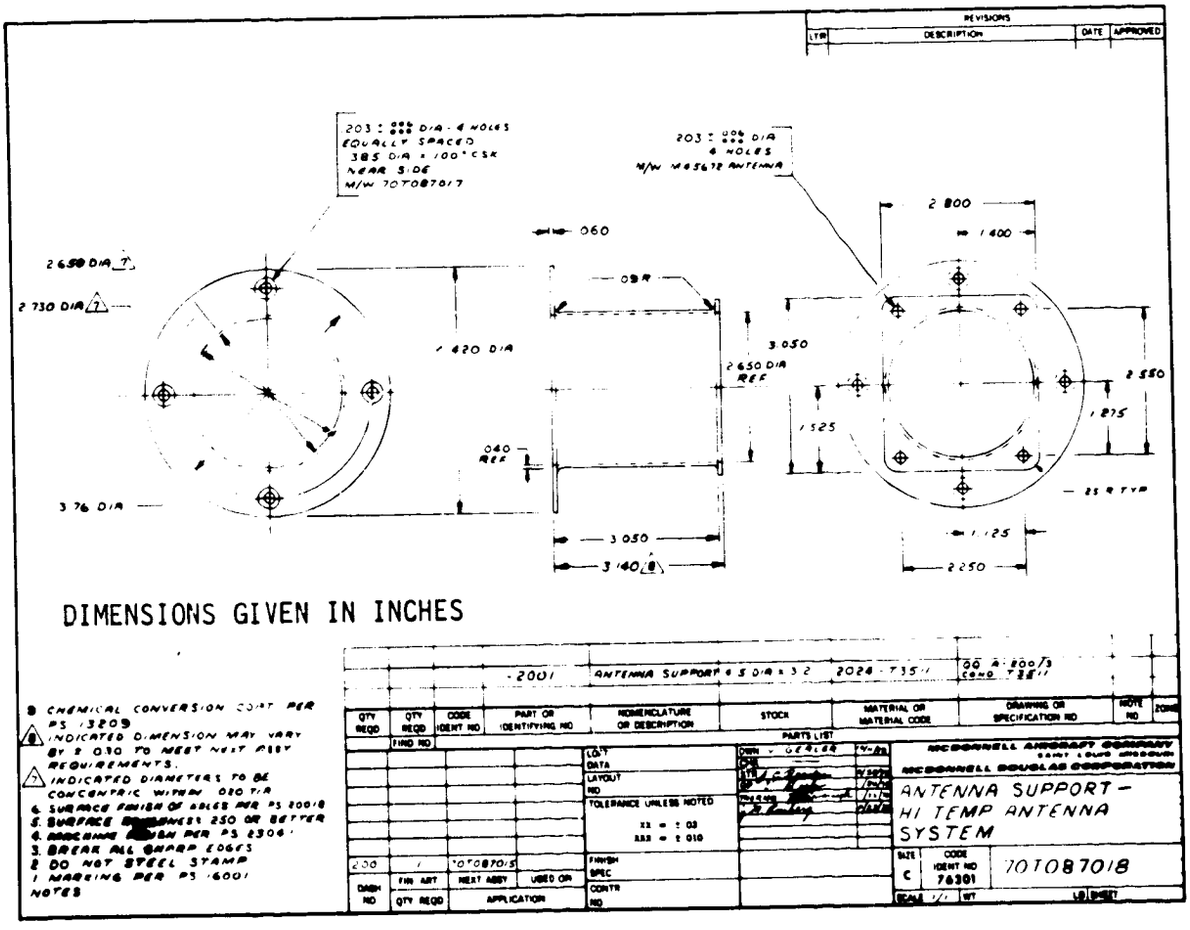

ANTENNA SUPPORT

FIGURE 68

The antenna window assembly, identified as -1003 in figure 69, consists of a 5.08 cm (2.00 in.) thick by 18.29 cm (7.20 in.) square tile of LI-1500 HRSI, a 0.203 cm (0.080 in.) thick pad of silicone sponge (RL-1973) and a 0.43 cm (0.17 in.) thick double-faced fiberglass-phenolic honeycomb panel, all bonded together with RTV-560 adhesive. The antenna window is attached to the panel support assembly with four #10 Allen head cap screw fasteners which are trapped in the window assembly. Access for turning the fasteners is provided for by 5.54 mm (0.218 in.) diameter holes extending through the LI-1500 window tile. The window is surrounded by four LI-1500 guard tiles which form the TPS around the antenna window. The joint design between window and guard tiles and between guard tiles is based on an overlap concept developed by Lockheed. The LI-1500 tile edges are under cut and overlap a nonrigid fibrous insulation filler strip (FI-600). The filler strip is compressed approximately 1.02 mm (0.040 in.). The gap width is nominally 1.27 mm (0.050 in.) and may vary from 0.76 mm (0.030 in.) minimum to 1.78 mm (0.070 in.) maximum.

Provisions were made for 2.45 cm (1.00 in.) diameter plugs in the window tile and one guard tile to permit indepth temperature measurements. Shallow grooves were machined in the outer surface of the window and guard tiles (see section B-B of figure 70) for surface thermocouples prior to application of the waterproof coating. This was done to minimize microcracking which may occur if a thin cut is made in the brittle surface coat to keep the thermocouple leads flush with its surface. The detail drawings defining the LI-1500 tiles, the FI-600 filler strips, and the silicone sponge pads are shown in figures 70, 71 and 72.

The panel assembly, identified as -1007 in figure 69, includes: (1) the TPS surrounding the antenna window; (2) the filler strips between the LI-1500 HRSI tiles; (3) the silicone sponge pads; and (4) the metallic support structure simulating the Orbiter structure. The panel support assembly (figure 73) consists of an aluminum skin-stringer structure with additional transverse stringers on the leading and trailing ends of the panel for stiffness. A 0.51 mm (0.020 in.) thick skin is spot welded to four 4.40 cm (1.73 in.) high stringers, 0.81 mm (0.032 in.) thick. The inboard side of the panel support structure is painted with a high emittance paint to obtain the proper internal heat radiation characteristics. A 6.35 mm (0.250 in.) thick silicone sponge strain isolation pad is bonded to the aluminum skin with RTV-560 adhesive around the antenna window area. Subsequently, the four guard tiles are bonded to the sponge pad with the filler strips in place to complete the TPS surrounding the antenna window. The guard tiles and the antenna window provide a 31.20 cm (12.68 in.) square surface area.

The complete test assembly (figure 74) shows the relationship of the S-band antenna system to the test container and cover assemblies and the channel nozzle.

Prototype unit design. - The prototype unit design is essentially the same as the breadboard unit except for the thermocouple arrangement. The plugs for indepth thermocouples and the grooves for surface thermocouples were eliminated. The thermocouple locations were revised to reduce the number of thermocouples and eliminate the thermocouple locations in the antenna window. The thermocouple locations and the LI-1500 tile configurations unique to the prototype unit are defined as the -1001 and -1005 assemblies in figure 69.

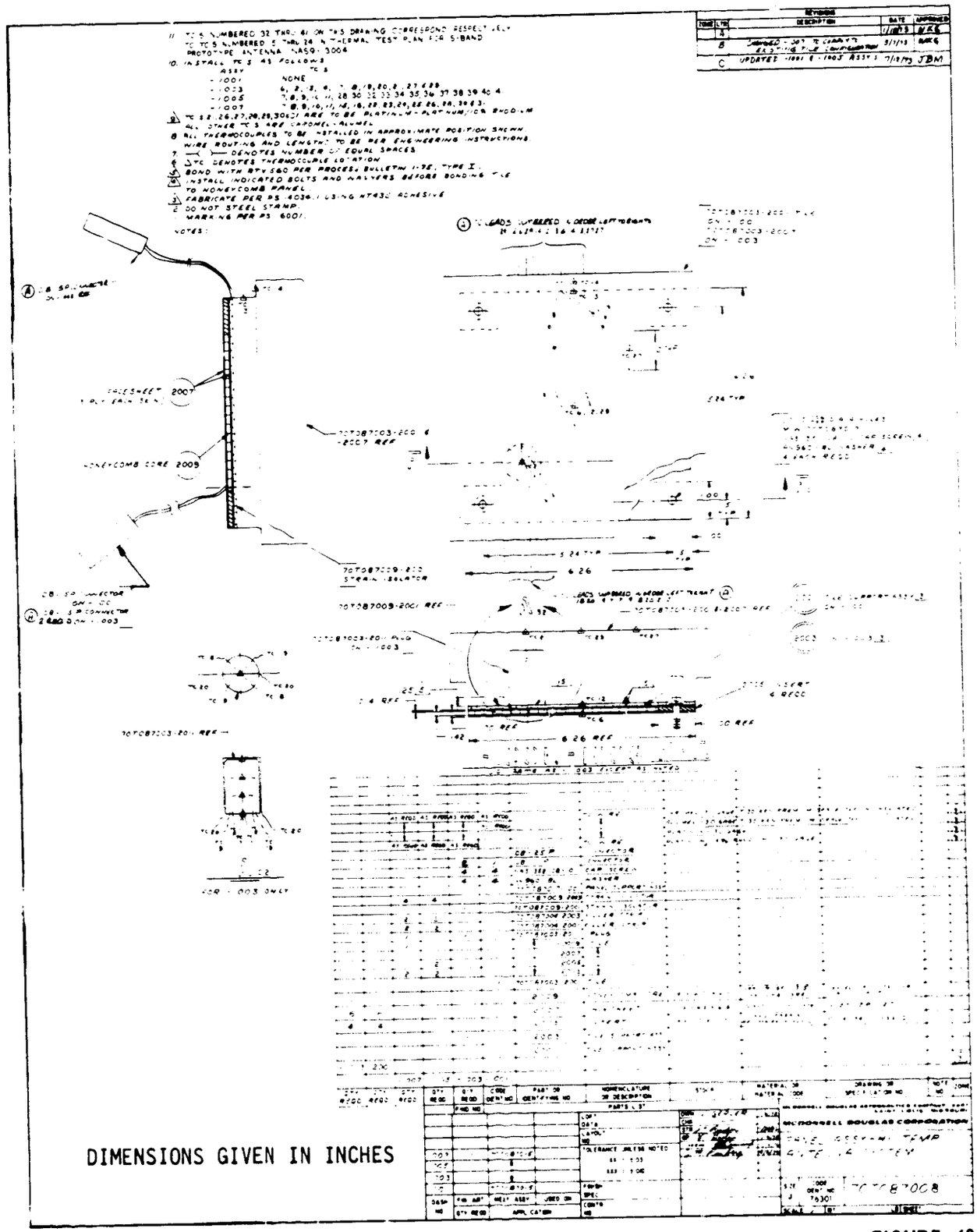

ANTENNA WINDOW AND PANEL ASSEMBLY

FIGURE 69

PAGE 7-36 INTENTIONALLY LEFT BLANK.

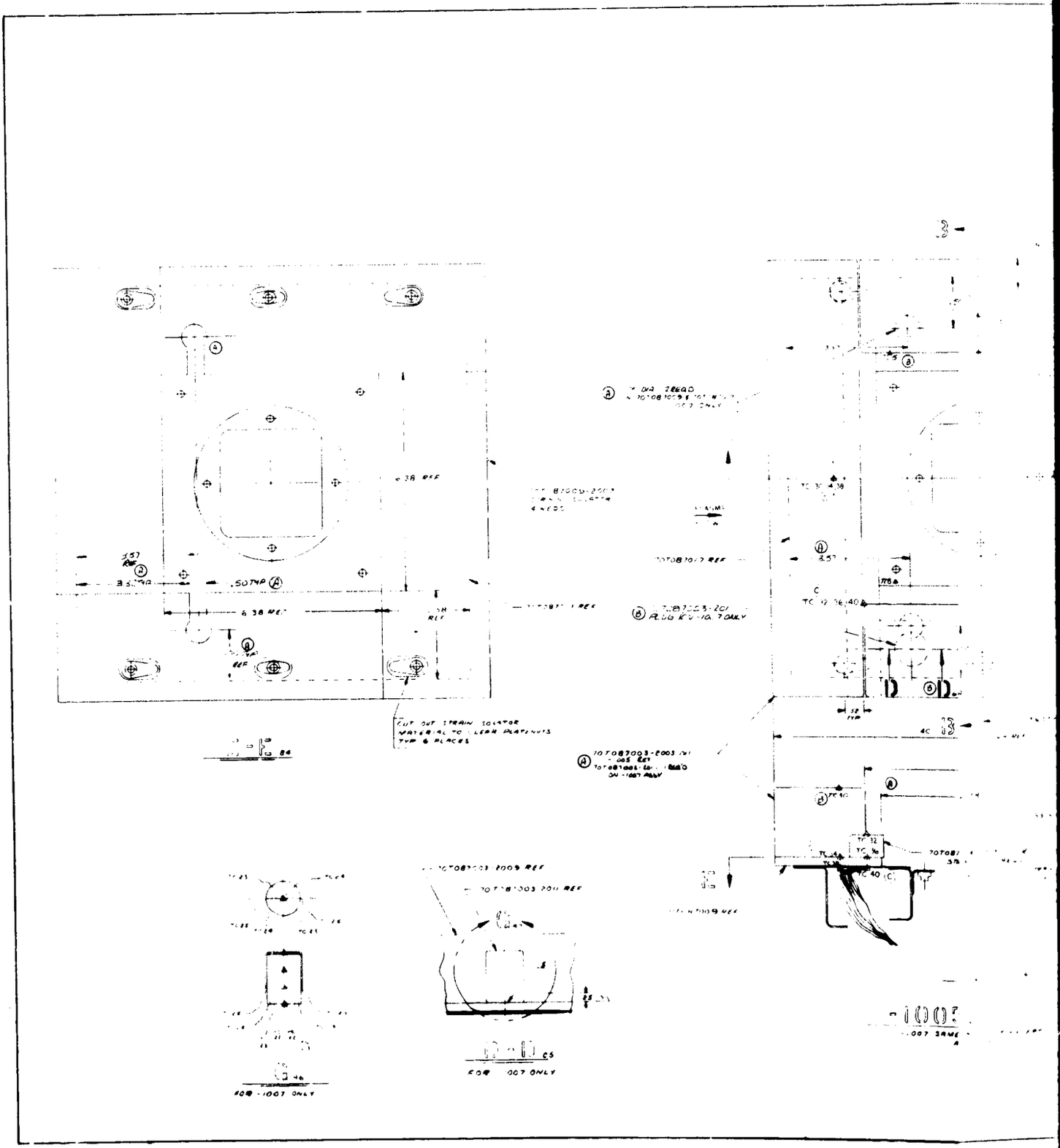

ANTENNA WINDOW AND PANEL ASSEMBLY **FIGURE 69 (Continued)**

PAGE 7-38 INTENTIONALLY LEFT BLANK.

PRECEDING PAGE BLANK NOT FILMED

FOLDOUT FRAME

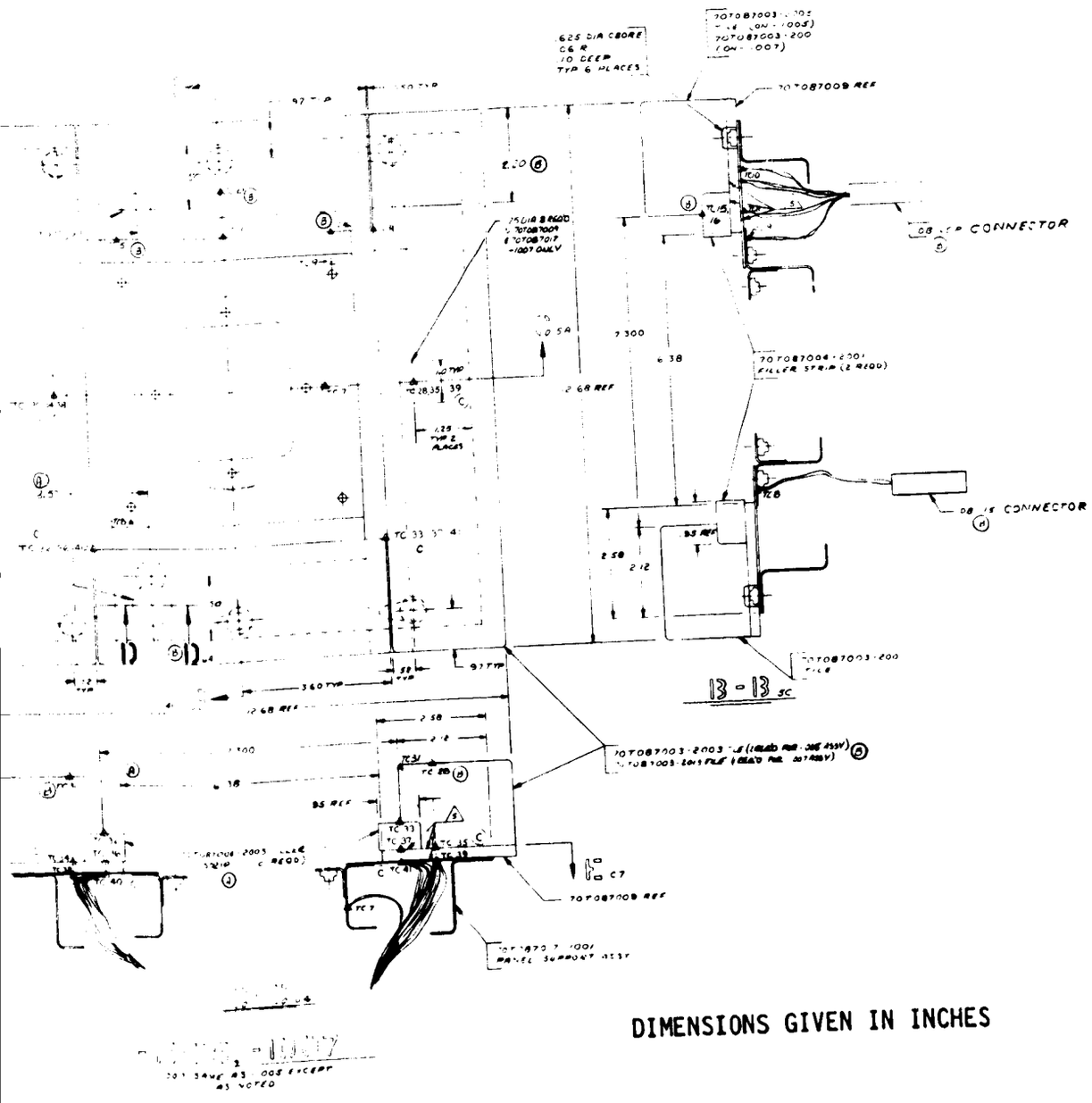

69 (Continued)

LEFT BLANK.

FOLDOUT FRAME

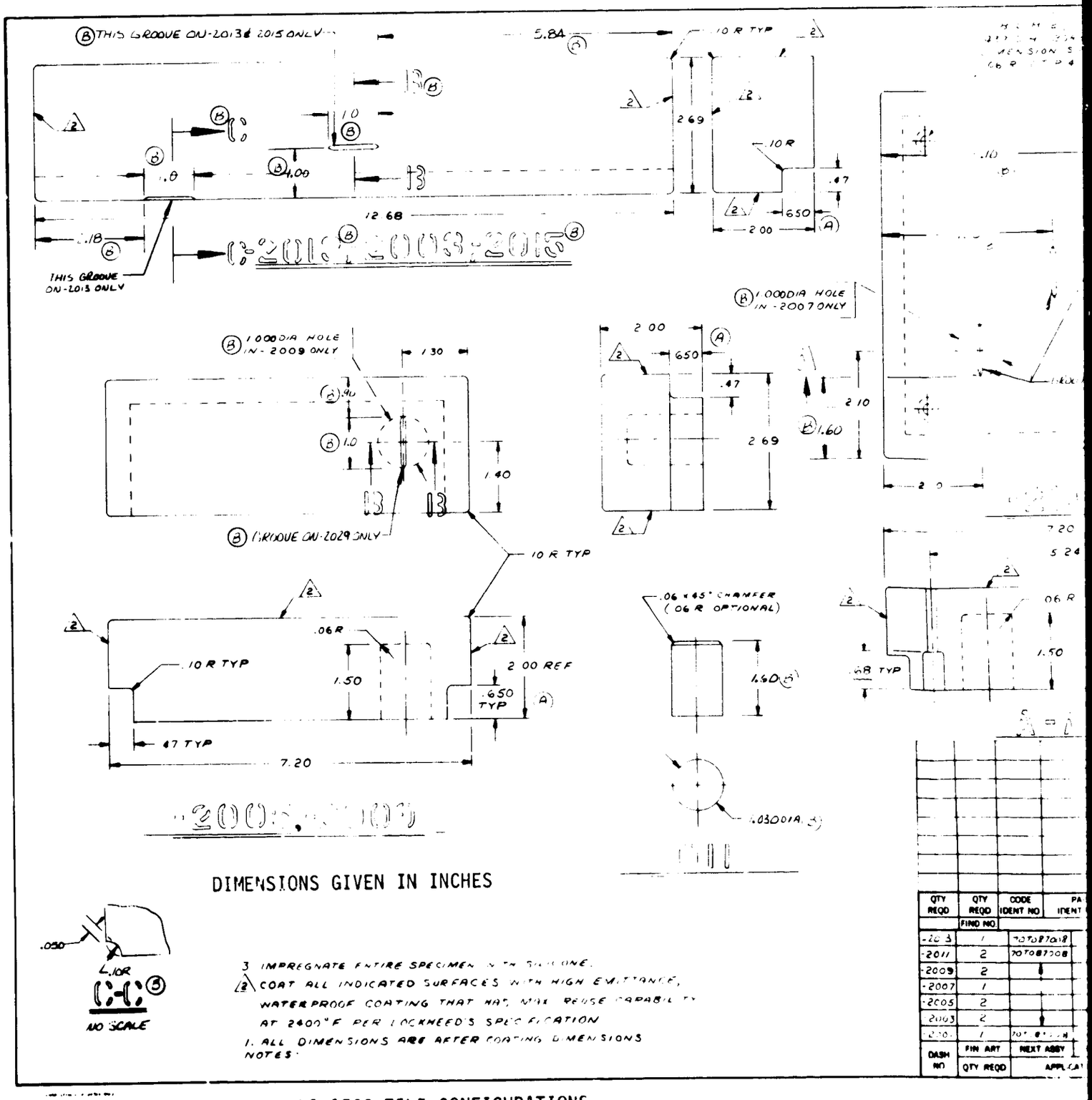

L1-1500 TILE CONFIGURATIONS

FIGURE 70

PRECEDING PAGE BLANK NOT FILMED

PAGE 7-40 INTENTIONALLY LEFT BLANK.

FOLDOUT FRAME

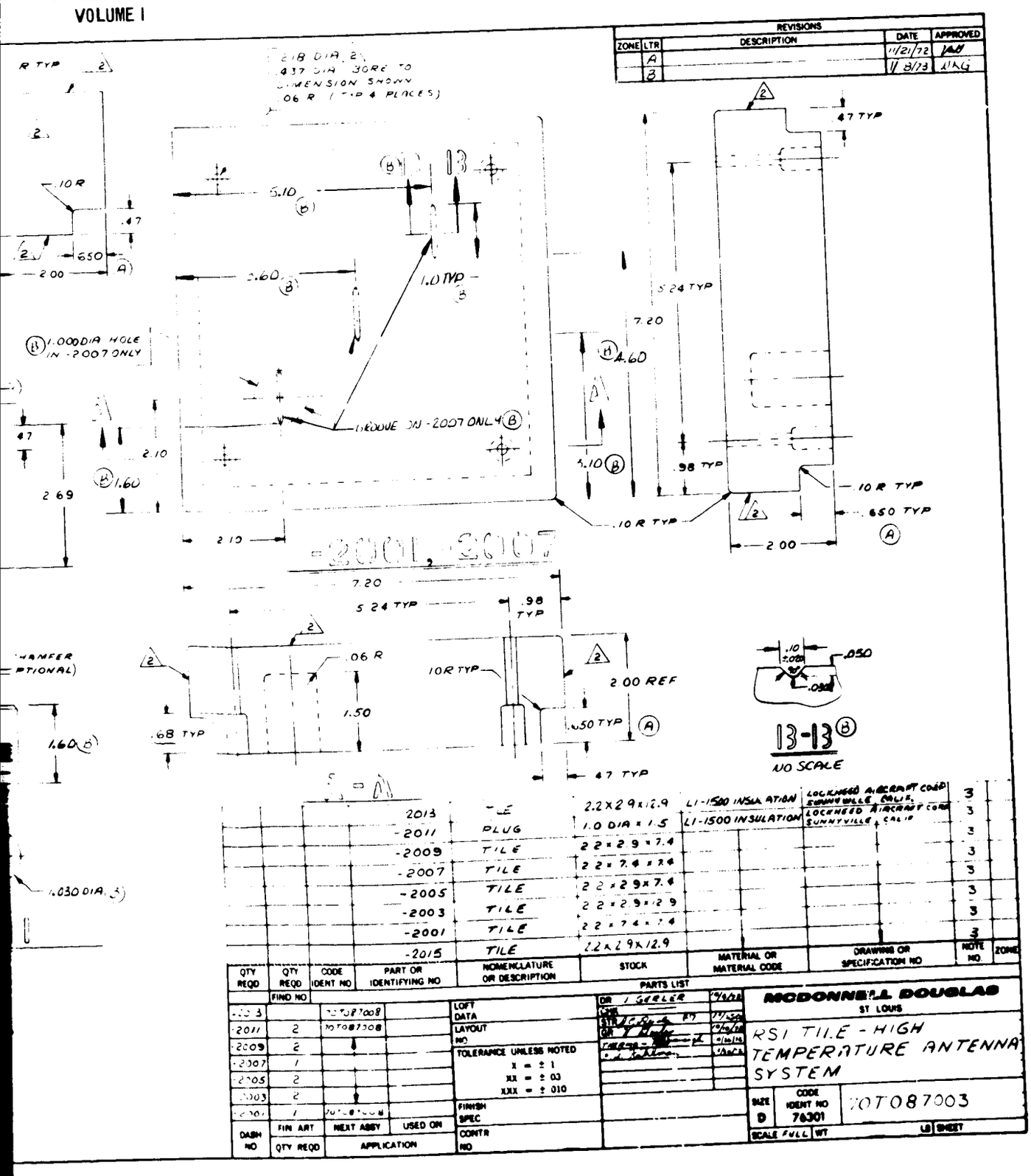

FIGURE 70

LLY LEFT BLANK.

FOLDOUT FRAME 2

AST

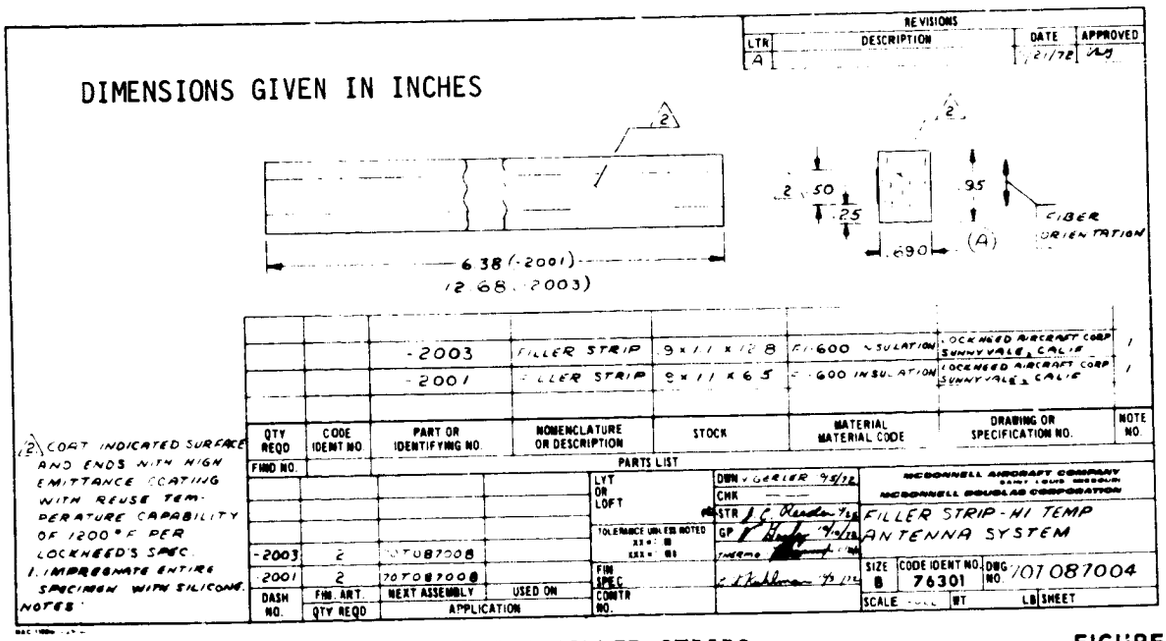

FI-600 FILLER STRIPS

FIGURE 71

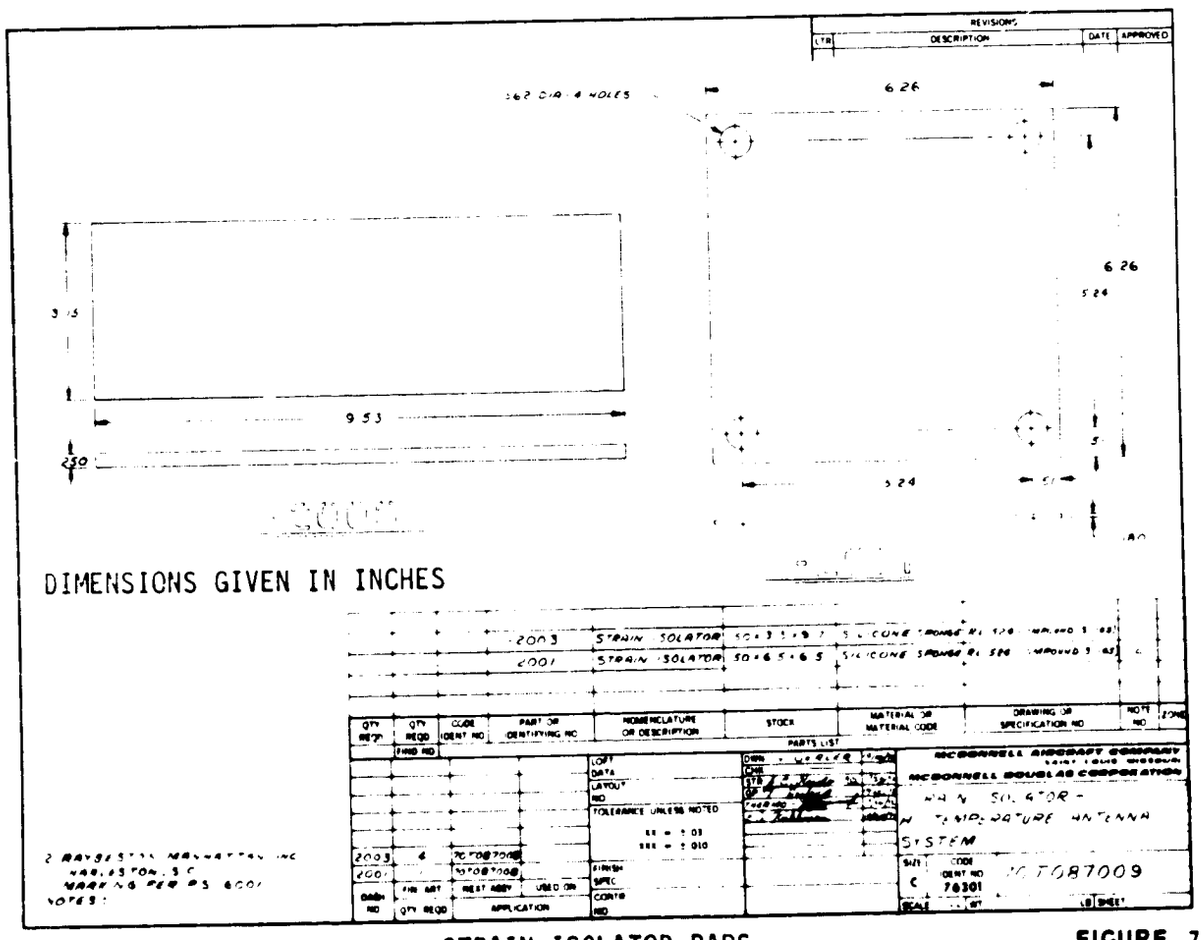

STRAIN ISOLATOR PADS

FIGURE 72

PAGE 7-42 INTENTIONALLY LEFT BLANK.

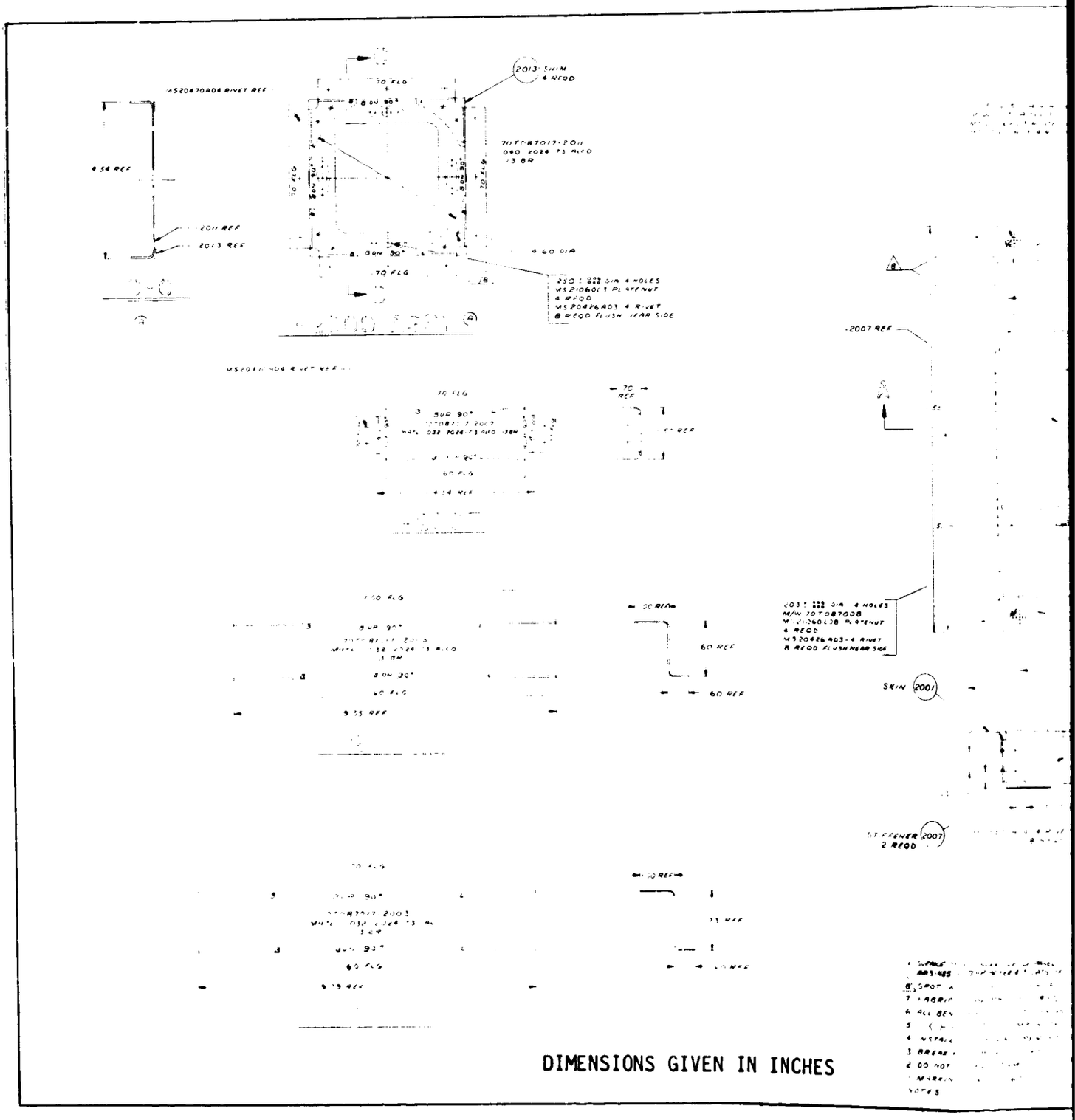

PANEL SUPPORT ASSEMBLY

FIGURE 73

PAGE 7-44 INTENTIONALLY LEFT BLANK.

FOLDOUT FRAME

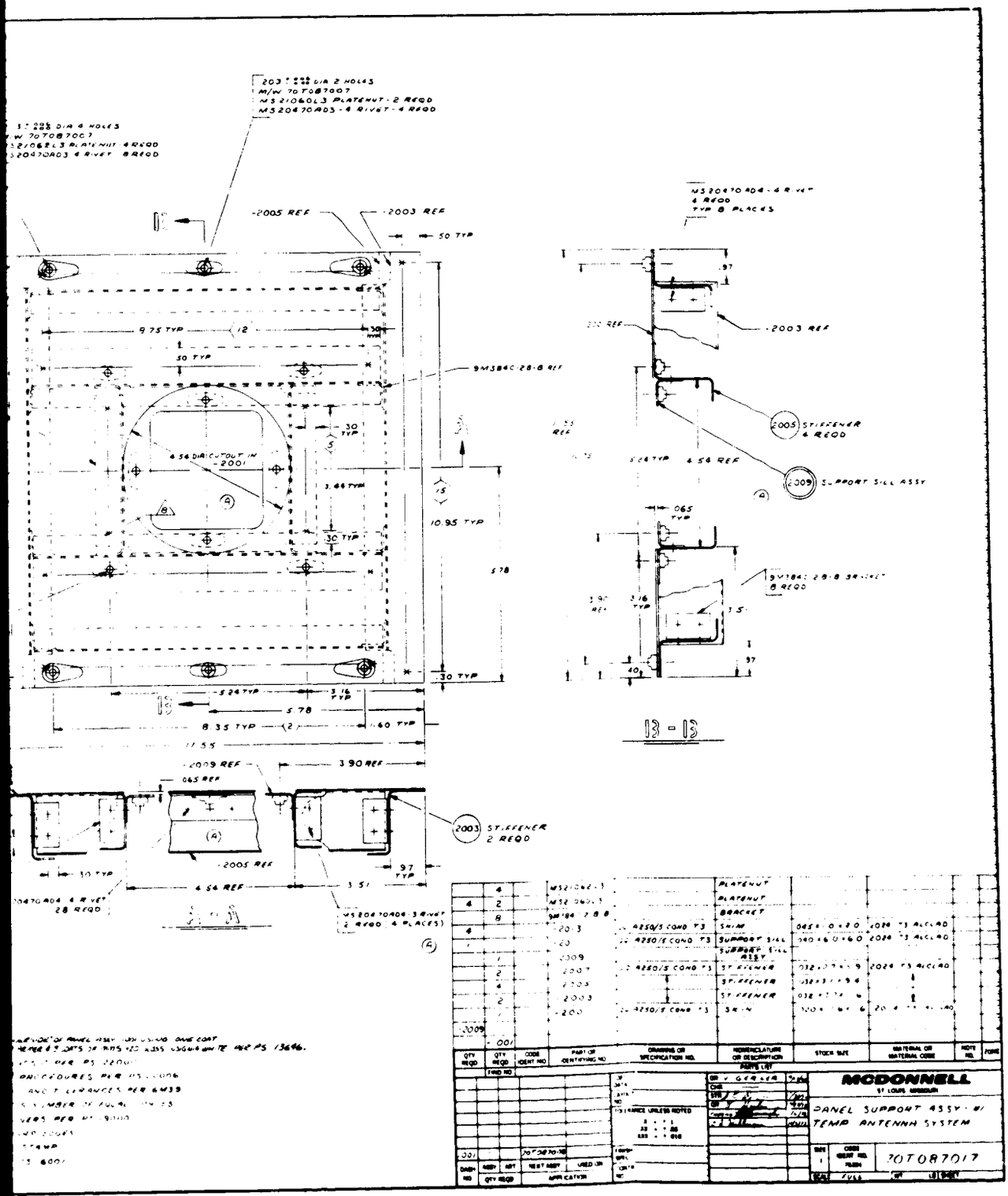

QTY REQD	QTY REQD	CODE IDENT NO	PART OR IDENTIFYING NO	DRAWING OR SPECIFICATION NO.	NOMENCLATURE OR DESCRIPTION	STOCK SIZE	MATERIAL OR MATERIAL CODE	NOTE NO.	ZONE
	FIND NO				PARTS LIST				
4			MS21042L3		PLATENUT				
4	2		MS21042L3		PLATENUT				
8			MS3184 2 8 8		BRACKET				
4			-203						
			-2001						
			-2009						
	2		-2007						
	4		-2003						
	2		-2003						
			-200						
-2009			-001						
				4250/5 COND T3	SHIM	.065 X 4.80 X 6.60	2024 T3 ALCLAD		
				4250/5 COND T3	SUPPORT SILL ASSY	.040 X 6.40 X 6.60	2024 T3 ALCLAD		
					SUPPORT SILL ASSY				
				4250/5 COND T3	ST. FITTING	.032 X 7.44 X 9	2024 T3 ALCLAD		
					ST. FITTING	.128 X 3.14 X 9.96			
					ST. FITTING	.032 X 7.44 X [illegible]			
				4250/5 COND T3	SHIM	.004 X 6.41 X 6	20 4 [illegible]		

DASH NO.	ASSY QTY REQD	ASY	NEXT ASSY	USED ON
-301			70T087016	

DIMENSIONS UNLESS NOTED	DR	GEORGE	DATE
.X ± .1	CHK		
.XX ± .05	STR		
.XXX ± .010	WT		
	PROJ		
	ENGR		

McDONNELL
ST LOUIS, MISSOURI

PANEL SUPPORT ASSY - W/ TEMP ANTENNA SYSTEM

SIZE	CODE IDENT NO.	70T087017
1	75082	

SCALE FULL | WT | SHEET

FOLDOUT FRAME

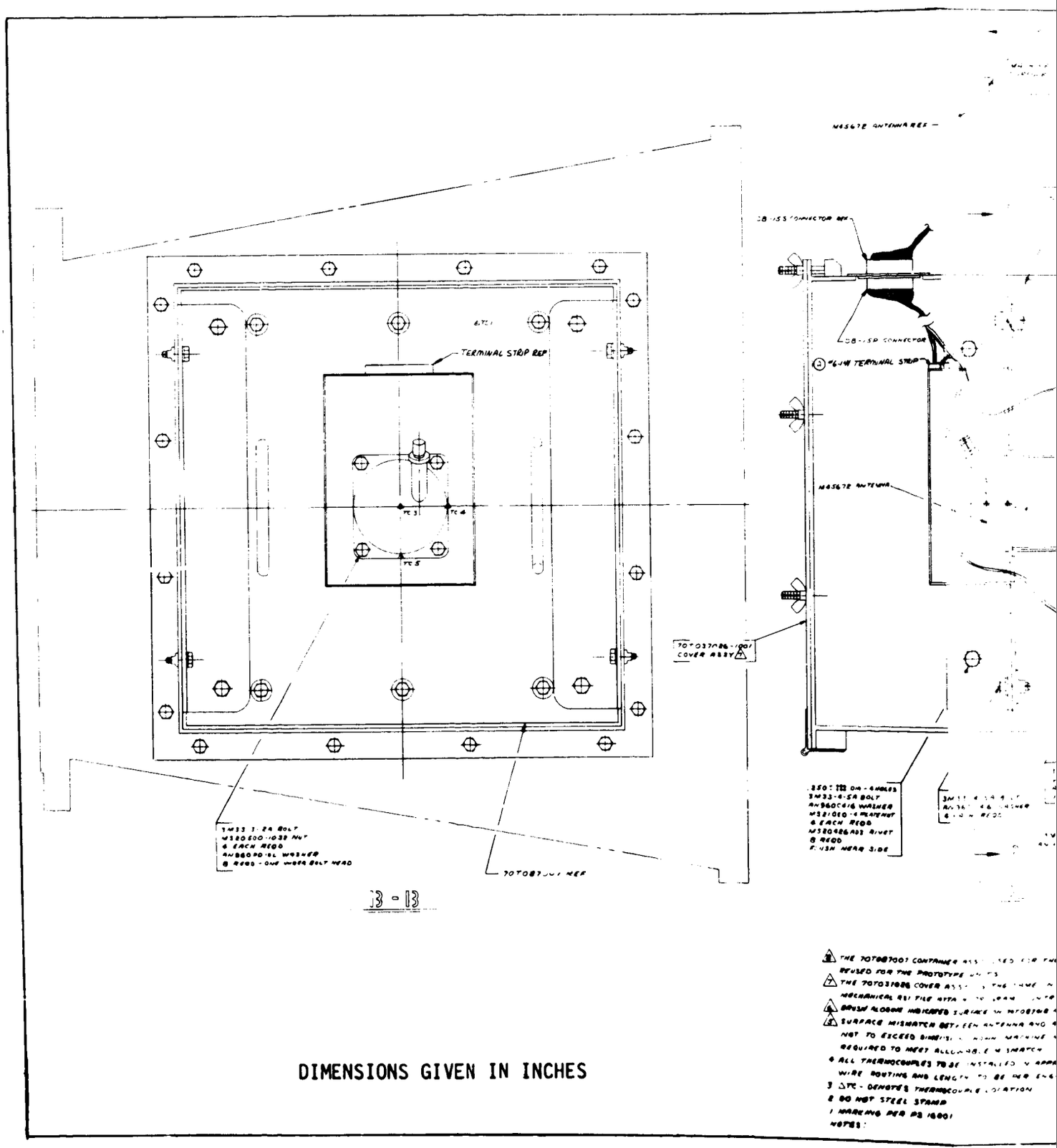

S-BAND ANTENNA TEST ASSEMBLY

FIGURE 74

PRECEDING PAGE BLANK NOT FILMED

PAGE 7-46 INTENTIONALLY LEFT BLANK.

FOLDOUT FRAME

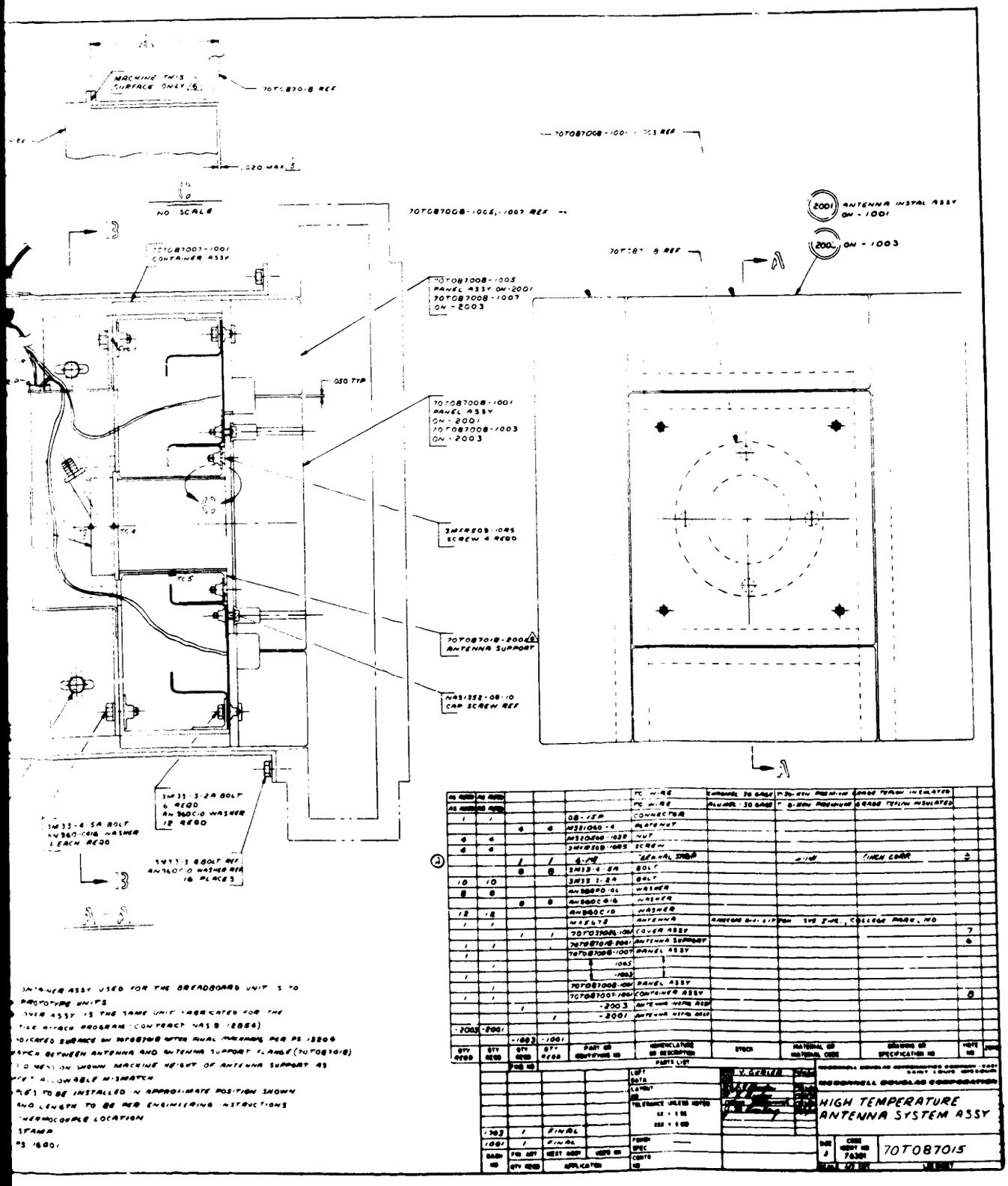

CONTAINER ASSY USED FOR THE BREADBOARD UNIT S TO PROTOTYPE UNITS
CONTAINER ASSY IS THE SAME UNIT FABRICATED FOR THE TILE ATTACH PROGRAM (CONTRACT NAS9-12854)
INDICATED SURFACE ON 70T08700B AFTER FINAL MACHINING PER PS 15206
MATCH BETWEEN ANTENNA AND ANTENNA SUPPORT FLANGE (70T08701B)
DIMENSION SHOWN MACHINE HEIGHT OF ANTENNA SUPPORT AS
"A" ALLOWABLE MISMATCH
PLUG TO BE INSTALLED IN APPROXIMATE POSITION SHOWN AND LENGTH TO BE PER ENGINEERING INSTRUCTIONS
THERMOCOUPLE LOCATION
STAMP
PS 16601

AS REQD	NO REQD								
					TC WIRE	CHROMEL 30 GAGE	TEFLON INSULATION	GRADE TEFLON INSULATED	
					TC WIRE	ALUMEL 30 GAGE	TEFLON INSULATION	GRADE TEFLON INSULATED	
1	1			08-15A	CONNECTOR				
4	4		4	4	MS21060-4	PLATENUT			
4	4			MS20060-1032	NUT				
4	4			3MF8508-1085	SCREW				
			1	1	4-14	THERMAL SWITCH	4-14	FIBER GLASS	2
			8	8	3M33-4-5A	BOLT			
10	10				3M33-3-2A	BOLT			
8	8				AN960PD-416	WASHER			
			8	8	AN960C416	WASHER			
12	12				AN960C10	WASHER			
1	1				NAS678	ANTENNA	ANTENNA DIV. GIANNINI SYS. 1140 E. WALNUT, COLLEGE PARK, MD		
1	1		1	1	70T037004-1001	COVER ASSY			7
1	1				70T08701B-2001	ANTENNA SUPPORT			6
1	1				70T08700B-1007	PANEL ASSY			
					-1005				
					-1003				
1	1				70T087008-1001	PANEL ASSY			
1	1				70T087007-1001	CONTAINER ASSY			8
			1		-2003	ANTENNA INSTAL ASSY			
				1	-2001	ANTENNA INSTAL ASSY			
-2003	-2001								
		-1003	-1001						
QTY REQD	QTY REQD	QTY REQD	QTY REQD	PART OR IDENTIFYING NO	NOMENCLATURE OR DESCRIPTION	STOCK	MATERIAL OR MATERIAL CODE	DRAWING OR SPECIFICATION NO	NOTE NO

PARTS LIST

-1003	1	FINAL							
-1001	1	FINAL							
DASH NO	FIG ITEM	NEXT ASSY	USED ON	APPLICATION	QTY REQD				

LAST DATA LAYOUT
TOLERANCE UNLESS NOTED
.XX ± 0.05
.XXX ± 0.010
FINISH
SPEC
CODE 1D

V SERIES

MCDONNELL DOUGLAS CORPORATION

HIGH TEMPERATURE ANTENNA SYSTEM ASSY

SIZE J | CODE IDENT NO 76301 | 70T087015

FOLDOUT FRAME

Test container assembly. - The test container assembly was designed as the interface link between the antenna test hardware and previously fabricated test support equipment. It was designed to be compatible with both channel nozzle and wedge mount test configurations as shown in figures 75 and 76. For the channel nozzle mount (figure 75), the container is placed within and attached to a water cooled cover assembly which is attached to the channel nozzle. The test container is supported by angle brackets with slotted holes which allow the outer surface of the antenna window and TPS to be mounted flush with the interior wall of the channel nozzle. For the wedge mount (figure 76), the container is positioned aft of a simulated leading edge and rests upon and is attached to the test mount support assembly.

The test container (figure 77) is a welded assembly fabricated from 3.18 mm (0.125 in.) thick, 321 stainless steel. The top of the container was held to 30.48 cm (12.00 in.) square, while its height was 7.98 cm (3.14 in.). Since the sides of the container would be exposed to the air flow in the wedge mount test arrangement, strips of ablator 9.9 mm (0.39 in.) thick were bonded to the container with DC 3145 adhesive. Two handles were attached to the bottom of the test container for safe handling during installation or removal.

Cover assembly. - The water cooled cover assembly (figure 78) supports the antenna test assembly in one wall of the channel nozzle. It remains attached to the channel nozzle during a test series. The hinged door provides quick access for installation and removal of the antenna test assembly. Four check valves in the walls and the hinged door eliminate any appreciable pressure differential between the interior of the cover assembly and the tunnel chamber. It was originally designed and fabricated by MDAC-E for use during the test phase of the "Development and Design Application of Rigidized Reusable Surface Insulation Thermal Protection Systems" study under NASA-JSC Contract NAS 9-12854, reference 7. In addition to supporting the test hardware, this cover assembly was designed to:

(a) Prevent leakage of the plasma stream through the cover assembly.

(b) Provide electrical interface (quick disconnects) for the thermocouples leads.

(c) Water cool the cover assembly to minimize heat transfer between the cover assembly and the test container assembly and to prevent abnormal heat buildup in the test hardware.

(d) Provide for air cooling the back side of the test hardware to reduce cooling time and subsequent down time between test runs.

Wedge mount assembly. - The wedge mount assembly (figure 76) holds the antenna test configuration in a free plasma stream near the exit nozzle. It is composed of leading edge and test mount assemblies which provide support for the test container assembly. The wedge mount assembly was furnished by MDAC-E for the "Supplementary Structural Test Program" study under NASA Contract NAS 8-26016 (ref. 8).

PRECEDING PAGE BLANK NOT FILMED

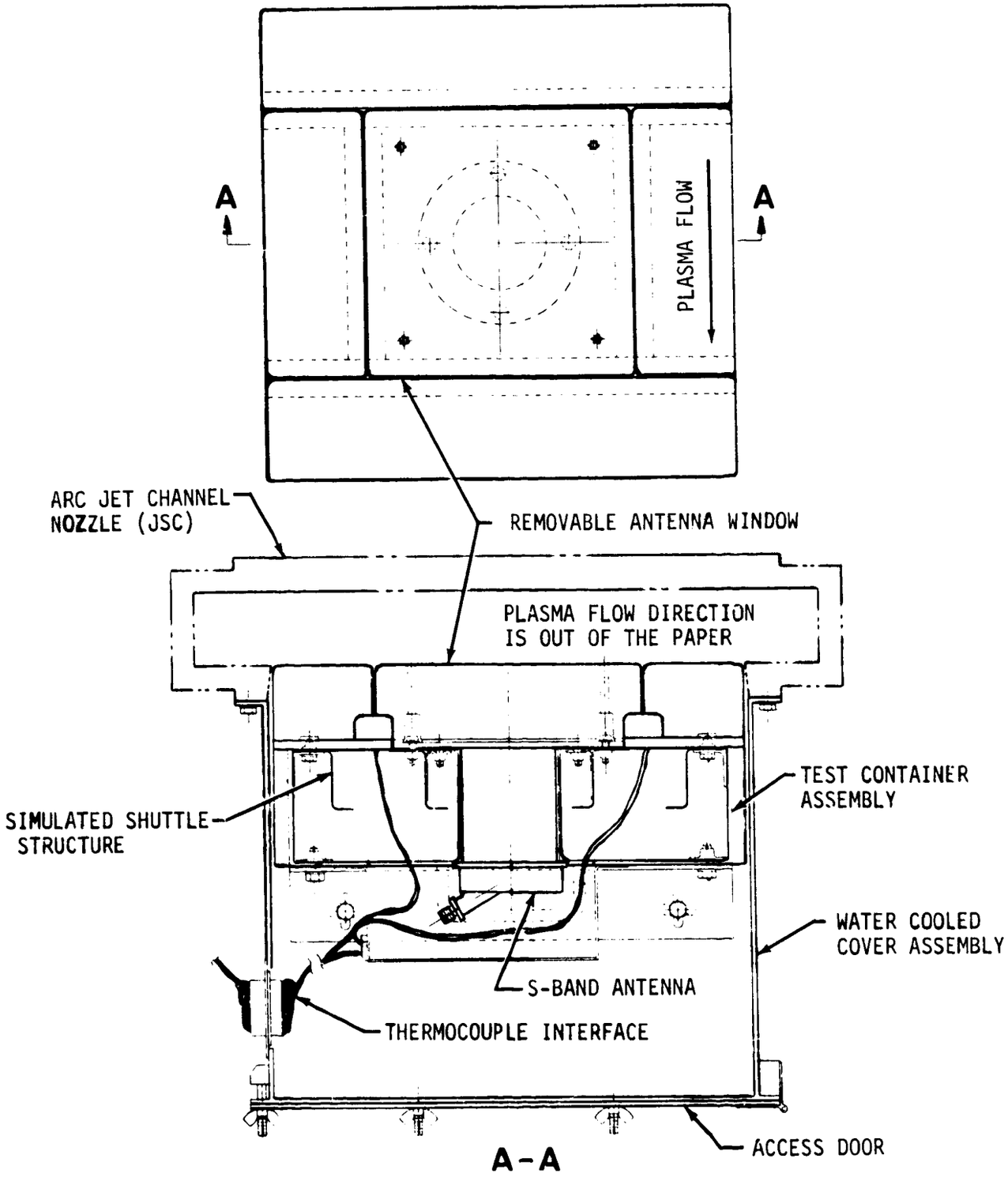

S-BAND ANTENNA SYSTEM/CHANNEL NOZZLE TEST CONFIGURATION

FIGURE 75

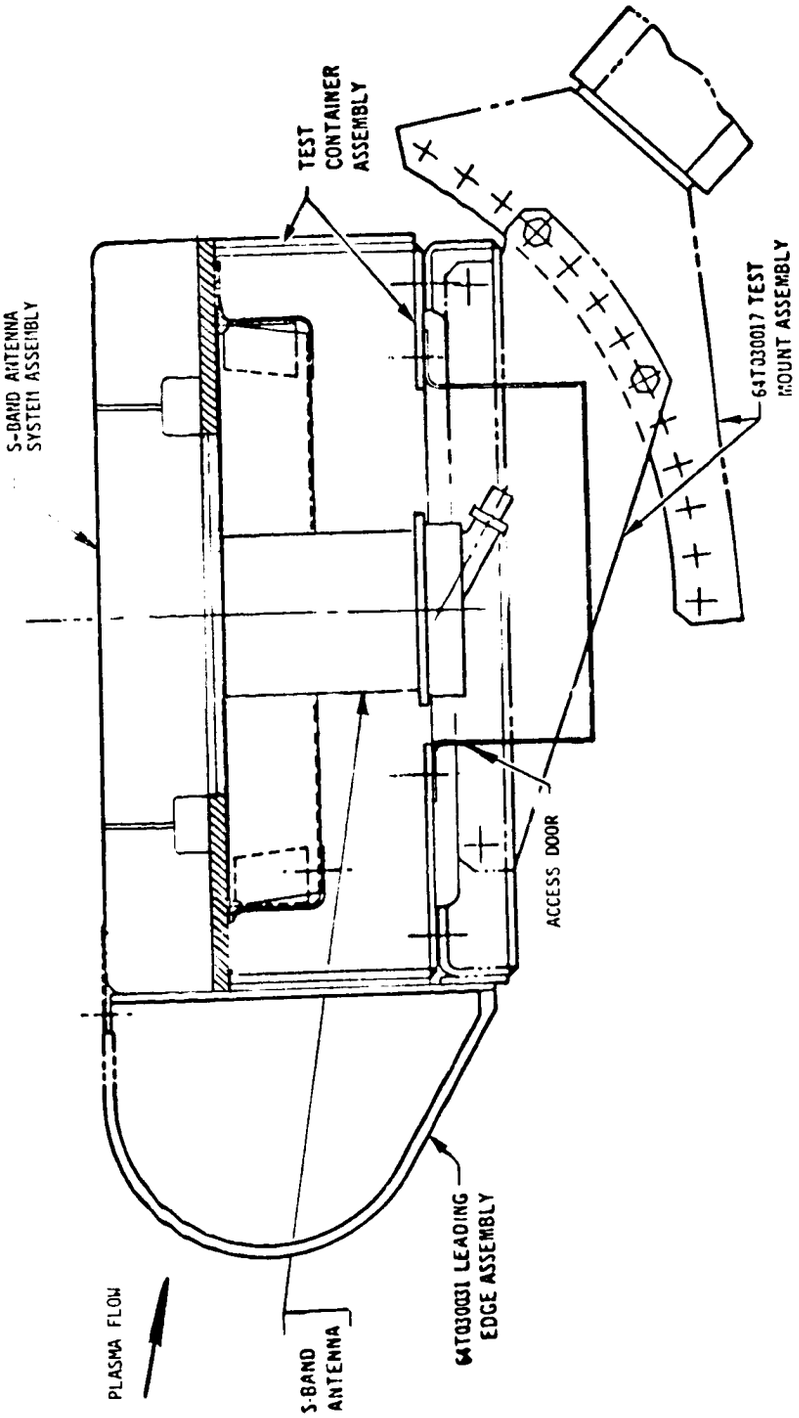

S-BAND ANTENNA SYSTEM/WEDGE MOUNT TEST CONFIGURATION

FIGURE 76

PAGE 7-50 INTENTIONALLY LEFT BLANK.

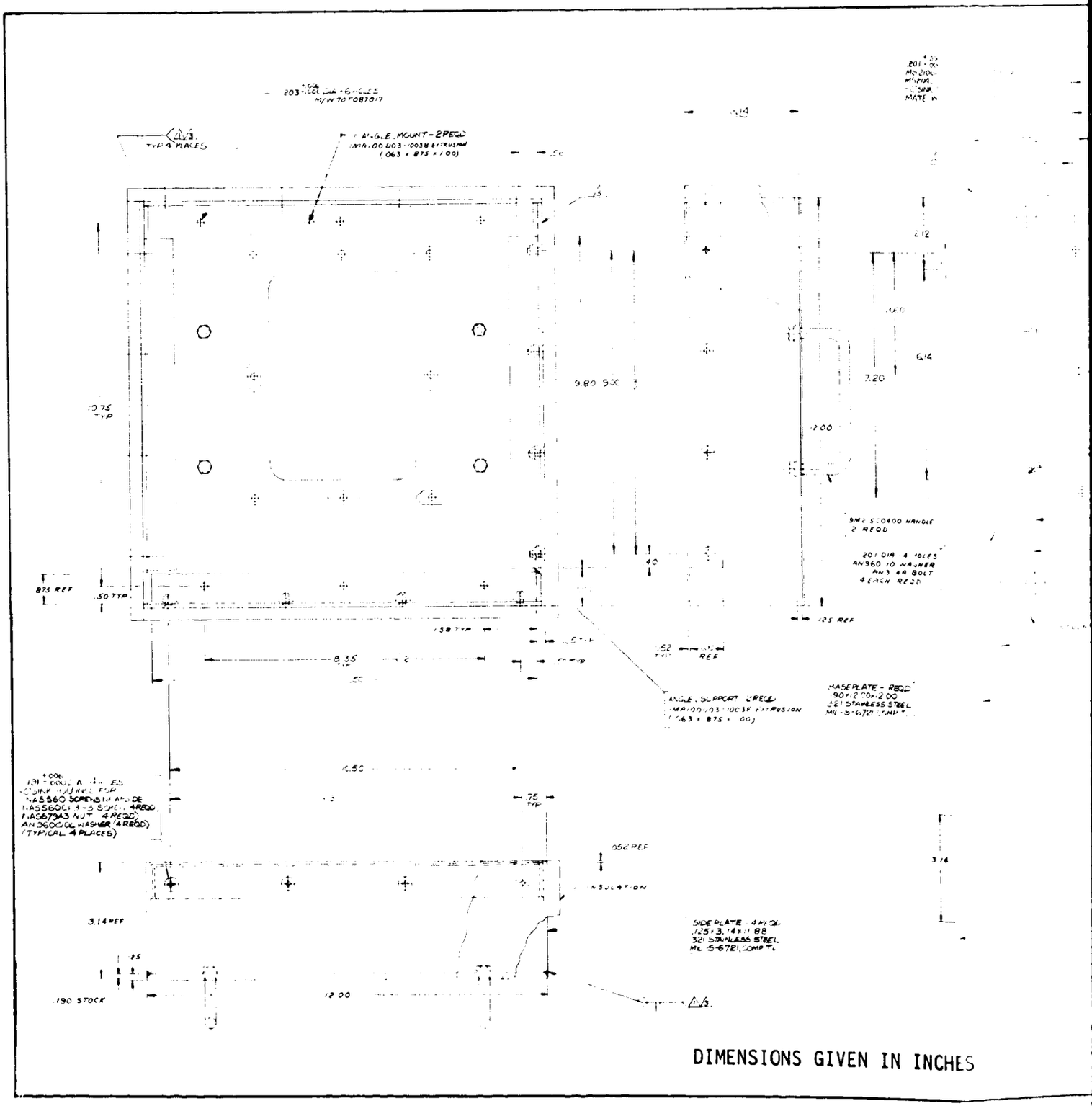

TEST CONTAINER ASSEMBLY

FIGURE 77

PRECEDING PAGE BLANK NOT FILMED

PAGE 7-52 INTENTIONALLY LEFT BLANK.

FOLDOUT FRAME

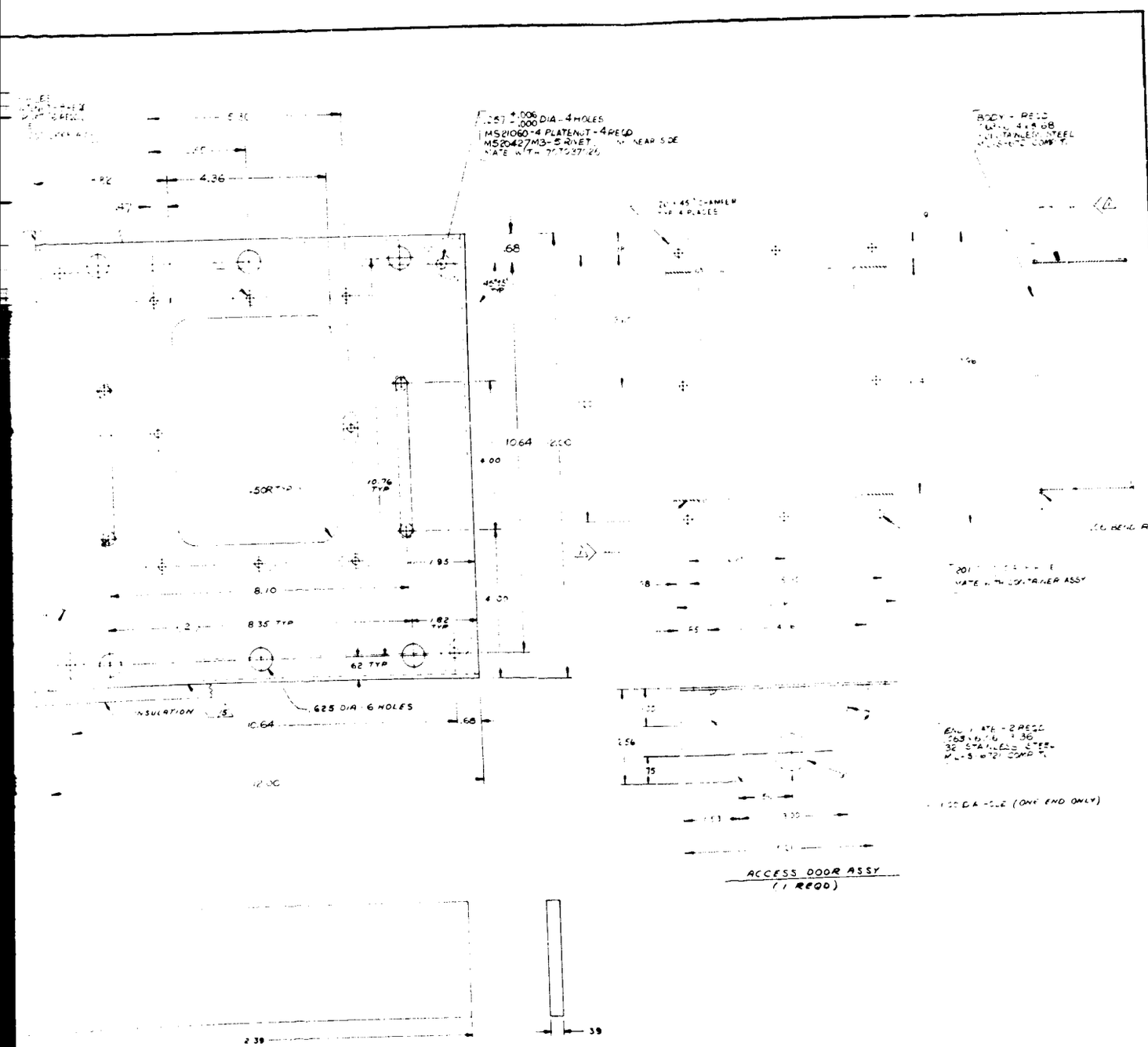

NOTES

1. SOVO INSULATION TO SIDES OF CONTAINER WITH DC 3/45 PER MS 11006
2. 4 UNIT NAS464P3A3 BOLTS ARE REQUIRED TO ATTACH ACCESS DOOR ASSY TO CONTAINER ASSY
3. FLUSH HELD WITH SIDES OF CONTAINER ASSY
4. REMOVE SHARP EDGES
5. WELD PER MS 22250

QTY REQD	QTY REQD	CODE IDENT NO	PART OR IDENTIFYING NO	NOMENCLATURE OR DESCRIPTION	STOCK	MATERIAL OR MATERIAL CODE	DRAWING OR SPECIFICATION NO	ITEM NO
FIND NO				PARTS LIST				

DASH NO	PER ASY QTY REQD	HEXT ASSY	USED ON APPLICATION

CONTAINER ASSY - HIGH TEMPERATURE ANTENNA -TEST INSTALLATION

SIZE	CODE IDENT NO	707087007
B	76381	

SCALE FULL WT

FOLDOUT FRAME

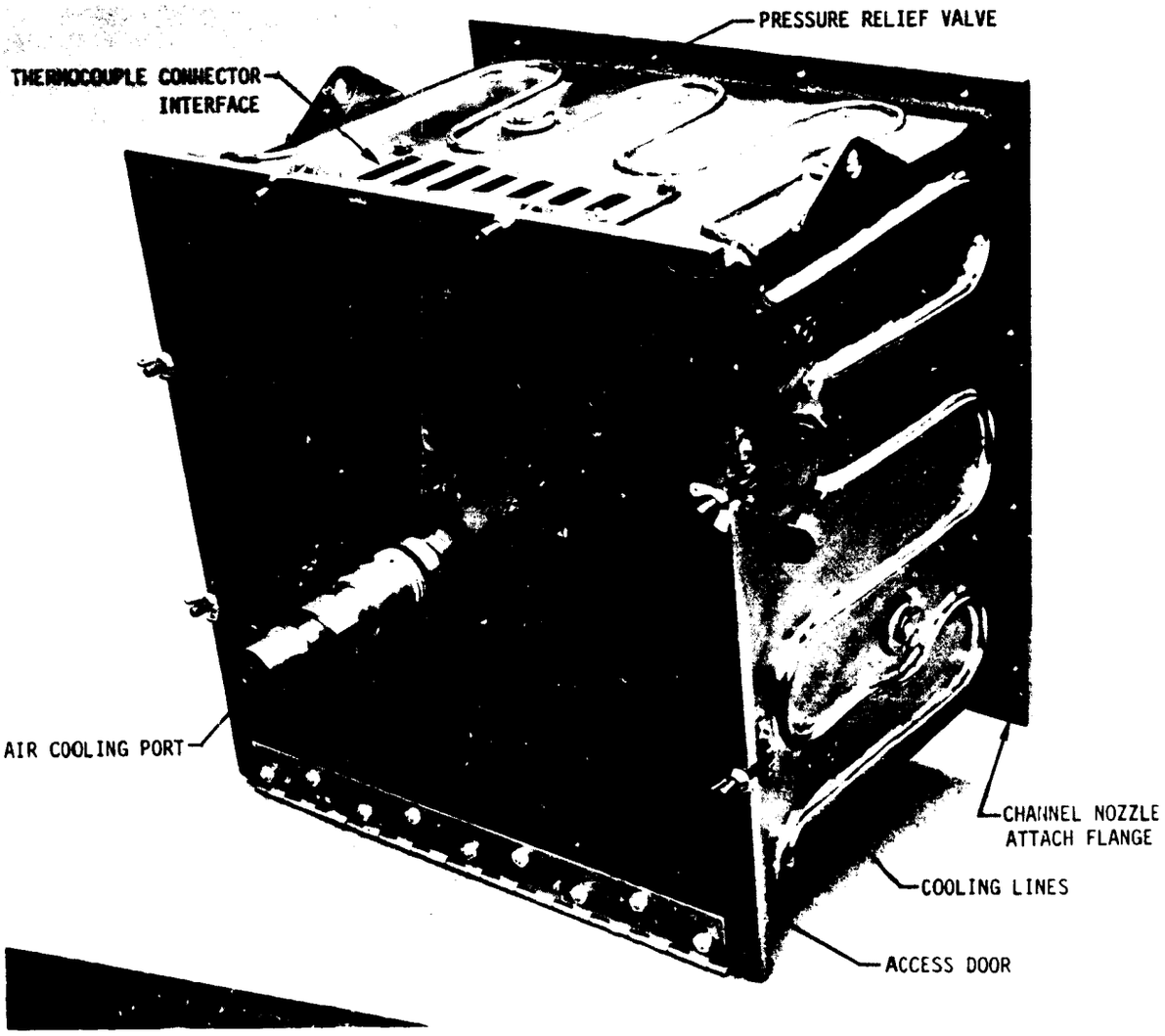

WATER COOLED COVER ASSEMBLY

FIGURE 78

Materials Evaluation

Materials evaluation for the S-band antenna system design was confined to the specific materials problems arising during design, fabrication, and testing.

S-band antenna. - The initial S-band antenna back cap design specified a nickel plate with a rhodium flash coat over a base metal of Kovar. However, neither the rhodium nor the nickel plating form a metal couple (ref. 9) within the 0.25 volt potential limit when mated with aluminum. This problem was solved by plating the Kovar with copper, and then a 60/40 tin-lead alloy. This alloy withstands 456 K (361°F) and the finish has a good appearance.

Thermocouple installation. - An attempt was made to eliminate or minimize microcracking caused by thin slots in the LI-1500 coating for surface thermocouples. Small grooves were added to the breadboard unit LI-1500 tiles before coating to permit location of the thermocouples just below the surface contour. The grooves were 1.3 mm (0.05 in.) deep and 2.54 cm (1.00 in.) long. Holes for the thermocouple leads were drilled in the surface coats at each end of the groove with a dental drill. It was necessary to burn away the silicone on the waterproof coating to obtain adequate adhesion between the surface and a high temperature adhesive. The surface thermocouples were held in place as near the surface as possible with AREMCO 505 cement. The grooves were completely filled with cement to provide a smooth surface contour. The curved cement surface was then coated with Lockheed's LI-0010 repair coating to obtain the proper surface emittance. A posttest examination of the breadboard unit did not show any loss of adhesion between the cement and the waterproof surface coating.

Strain isolator. - Problems were experienced in slicing the RL-524 silicone sponge rubber purchased for the breadboard and prototype S-band antenna systems. The finished sheets were uneven and rough in places and, therefore, were not considered satisfactory for use in the antenna systems. Subsequent discussions with the manufacturer (Raybestos Manhattan) indicated that development to alleviate the slicing problems had not proceeded due to lack of customer interest. Further, the technical literature indicates that the methyl-phenyl silicone elastomers are subject to stiffening when stored for a time below 200 K (-100°F). Although MDAC-E short term test results indicate RL-524 has superior cold temperature performance, the basis for originally selecting this material, additional tests would have to be performed to adequately show a long term superiority of the methyl-phenyl silicone formulation of RL-524 over that of RL-1973. Therefore, RL-1973, which is also the same sponge rubber used in Lockheed's TPS design, was substituted.

Bonding. - The procedure used for bonding the LI-1500 tiles to the silicone sponge pads or the silicone sponge pads to the fiberglass-phenolic honeycomb or aluminum skin is given in Appendix D. This procedure is a combination of both MDAC-E and Lockheed procedures. To ensure successful bonding during fabrication of the breadboard and prototype antennas, tests were performed to check out the bonding procedure. Three tensile tests were

conducted to evaluate the strength of the RTV-560 bond to both LI-1500 and aluminum. Each test specimen included two aluminum pull pads, one LI-1500 sample, two layers of silicone sponge, and four bondlines. Figure 79 shows a typical specimen after testing. The failure occurred in the LI-1500, the weakest material, and verified that the bonding procedure is satisfactory.

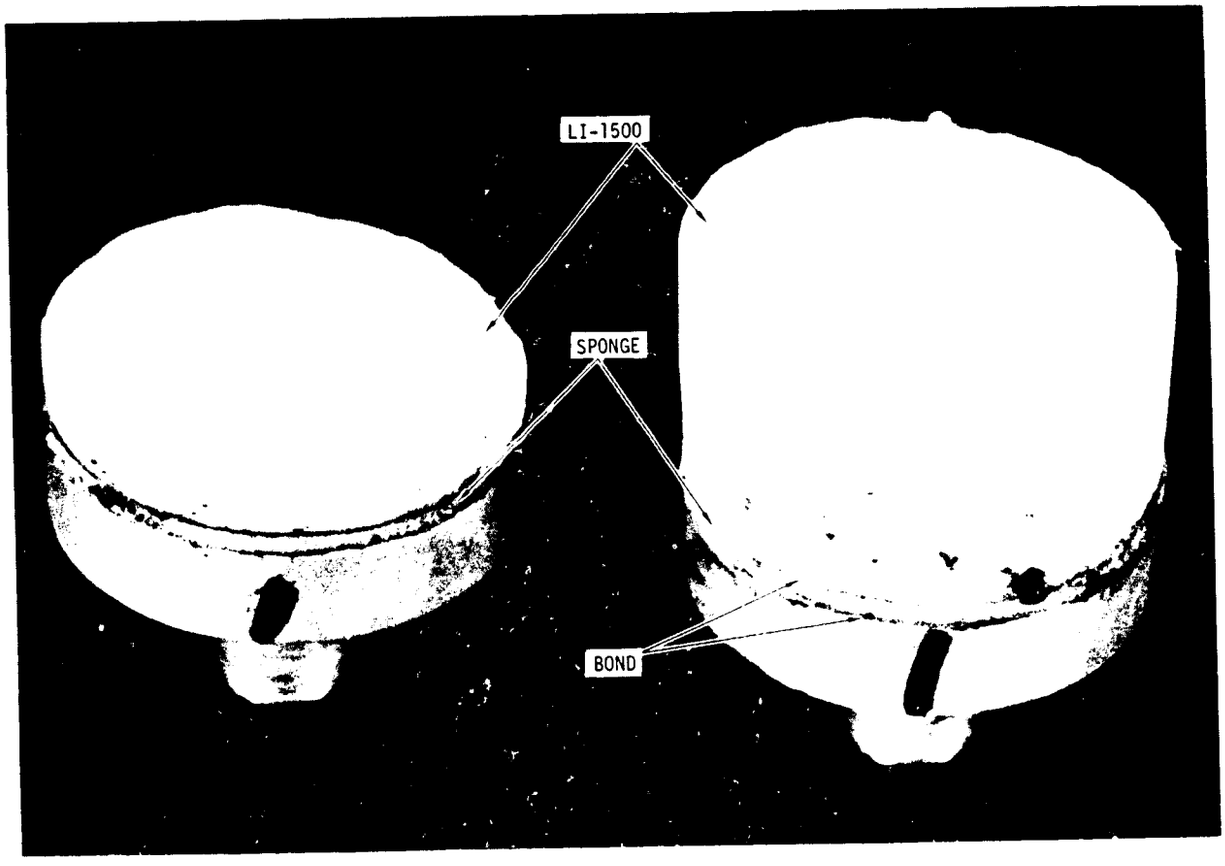

TYPICAL TPS PULL-TEST SPECIMEN

FIGURE 79

Thermal Analyses

Temperature distributions were calculated for the S-band antenna system. The data obtained was used for: (1) confirming antenna window materials selection, (2) determining antenna window thickness, (3) establishing antenna temperature requirements, and (4) providing data for thermal stress calculation.

Two approaches were considered. One approach was to demonstrate with conservative analysis that the design was adequate. As long as the measured test data did not exceed that predicted by conservative analysis, the design would be confirmed. The other approach was to demonstrate with a detailed analysis that an antenna system can be analytically modeled to accurately

predict the test results. Thus, the methods and assumptions used can be related to other antenna system installations in other locations, with confidence. The second approach was selected.

Two thermal modeling methods were also considered. One was a two-dimensional radial model in cylindrical coordinates; the other was a three-dimensional model in rectangular coordinates. The two-dimensional radial model which correctly simulated the thermal mass effect of the S-band antenna, yet had fewer nodes and lower computer costs per run, was selected for analyses.

S-band antenna system thermal model. - The S-band antenna system is shown in figure 32. Important thermal aspects include: (1) a square LI-1500 tile centered over the S-band antenna aperture; (2) double-lap strip joints between tiles; (3) FI-600 silica insulation strips under the joint gaps prevent boundary layer gas heating from reaching the bondline; (4) a high emittance coating covers the FI-600 strips in the region under the joint; and (5) fastener access holes through the tile with captive cap screws for antenna window assembly attachment and removal.

The thermal model for S-band antenna system including the cover assembly and test container assembly is shown in figure 80 and has 117 nodes and 213 connectors. The surface coating on the top and sides of the tile, the bondline adhesive, strain isolator pad, and honeycomb facesheets were included in the thermal model. Convective gap heating distributions for butt joints (ref. 7) were used.

Thermal response results. - Using the above thermal model and MDC's General Heat Transfer Program (HEATRAN Code), the following results were obtained. Maximum temperatures for the S-band antenna system for the Orbiter entry environment are shown in figure 81. Typical temperature histories associated with some of these maximum temperatures are shown in figure 82. As expected, maximum backface temperatures are between the one-dimensional results obtained for the S-band antenna backcap and the aluminum skin, given in figure 27 in the section on CONCEPT AND FEASIBILITY STUDIES under Thermal Studies. The aluminum structure under adjacent TPS, for a 5.08 cm (2.0 in.) LI-1500 insulation thickness, is about 62 K (111°F) cooler than the 422 K (300°F) maximum design temperature due to flow of heat to the antenna support and relatively massive test container assembly. In contrast, the maximum temperature of the S-band antenna backcap is somewhat higher than the one-dimensional results because of the heat conducted down the sheath-like cylindrical antenna support.

Maximum temperatures for the Orbiter entry heating environment and typical test local static pressure environment are shown in figure 83. The input gap heating in the tile joints was assumed to be more severe than expected on the fabricated test unit in this computation. However, the backface temperatures were 16.7 K (30°F) lower than those given in figure 81. The lower temperatures are due to lower test pressure and lower initial temperature (300 K (80°F)). The entry heated surfaces radiate to cold surroundings, and the back surfaces were assumed perfectly insulated for the two cases given in figures 81 and 83.

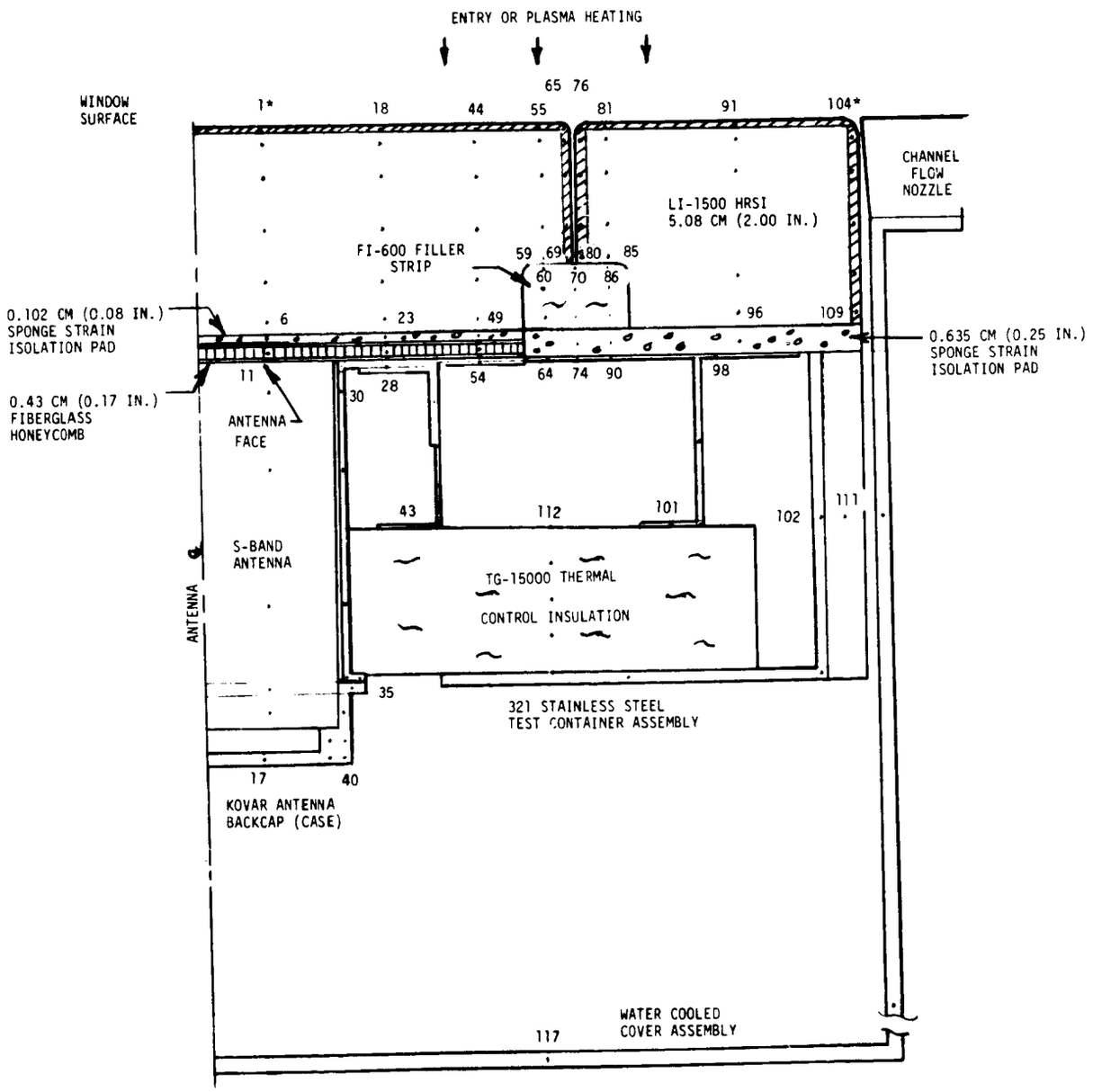

NOTES 1. *DESIGNATES NODE NUMBERS

S-BAND ANTENNA SYSTEM THERMAL MODEL

FIGURE 80

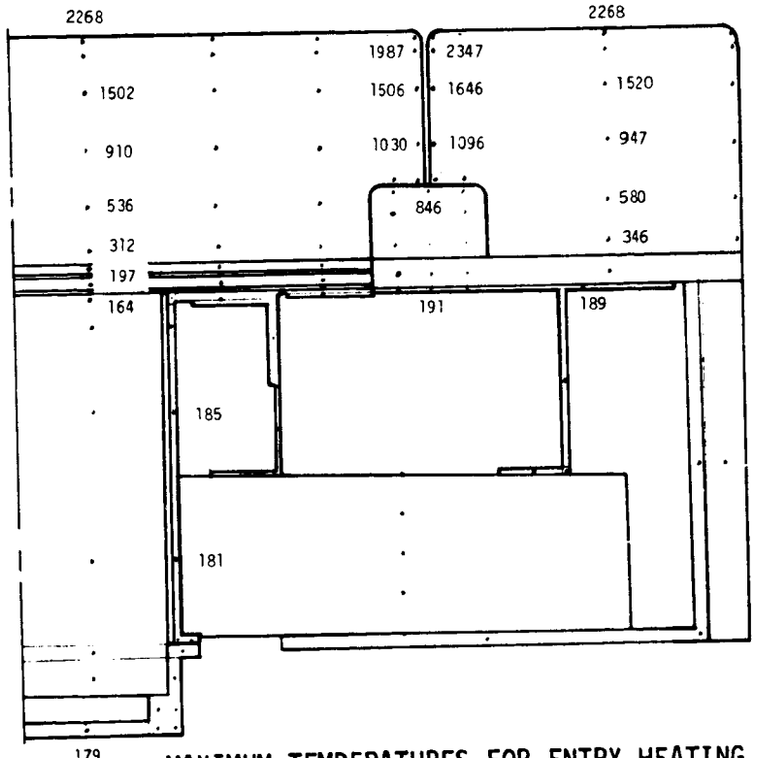

NOTES:
1. ALL TEMPERATURES IN °F (MAX. ANYTIME)
2. 100°F INITIAL TEMP.
3. NOMINAL 0.05 IN. GAP HEATING FOR BUTT JOINT.
4. ENTRY PRESSURE

MAXIMUM TEMPERATURES FOR ENTRY HEATING

FIGURE 81

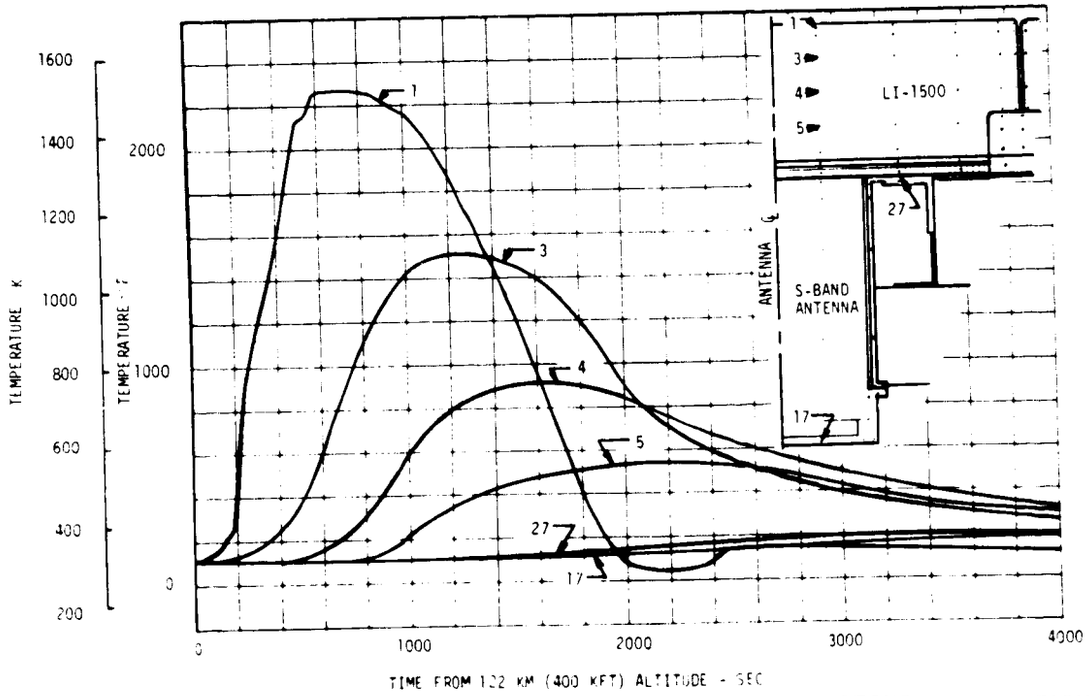

TEMPERATURE HISTORIES FOR ENTRY HEATING

FIGURE 82

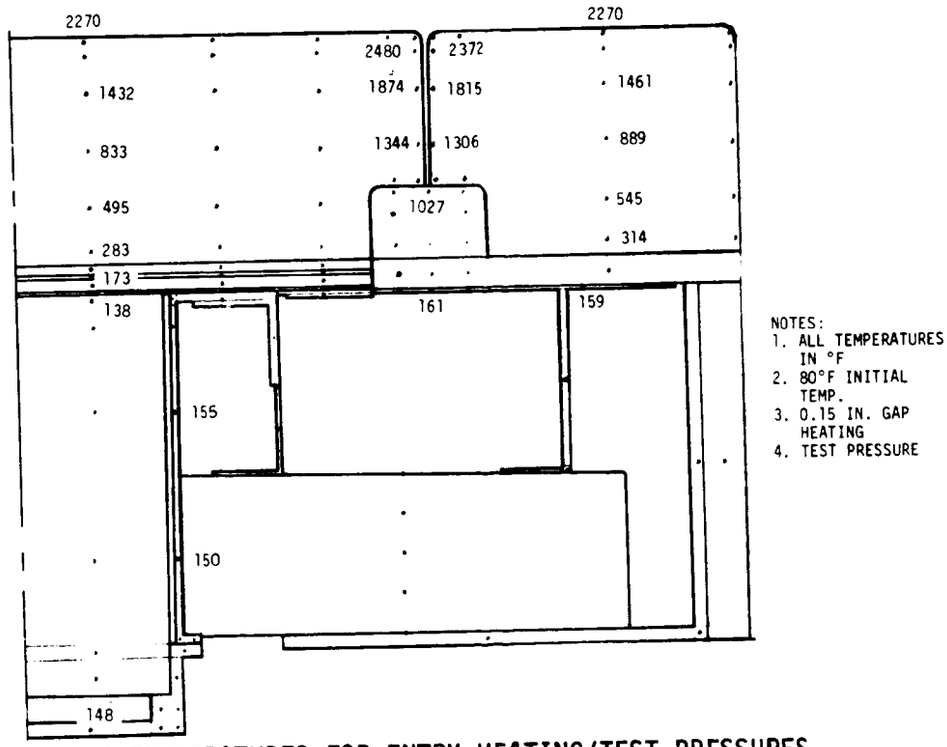

MAXIMUM TEMPERATURES FOR ENTRY HEATING/TEST PRESSURES

FIGURE 83

Maximum temperatures for typical breadboard and prototype test runs are shown in figures 84 and 85, respectively. Measured surface temperatures were used as input for these two cases; the cover assembly in back of the antenna model was assumed to radiate to 300 K (80°F) test chamber walls. The backface temperatures for the breadboard unit (figure 84) are 14 to 17 K (25 to 30°F) lower than predicted (figure 83) because of the lower test surface temperature and higher heat loss to the cover assembly. The higher backface temperatures for the prototype unit (figure 85) are comparable with predicted temperatures (figure 81) because of a longer heating time which compensated for the lower test pressures and surface temperatures. Therefore, the prototype testing is considered representative of entry flight.

Strength Analyses

The S-band antenna system was designed to withstand the loads given in the section on DESIGN CONSIDERATIONS AND CONSTRAINTS under Strength Requirements. Conventional analysis procedures were used. The results of the stringer analysis showed that the small increase in stringer spacing did not require an increase in stringer thickness. A thermal-stress analysis was not required for the antenna window because it is comparable in size to the C-band horn antenna system window (figure 36). The results for the C-band antenna window (ref. 1) show that the maximum stress due to thermal gradients is well within the allowables for the window materials.

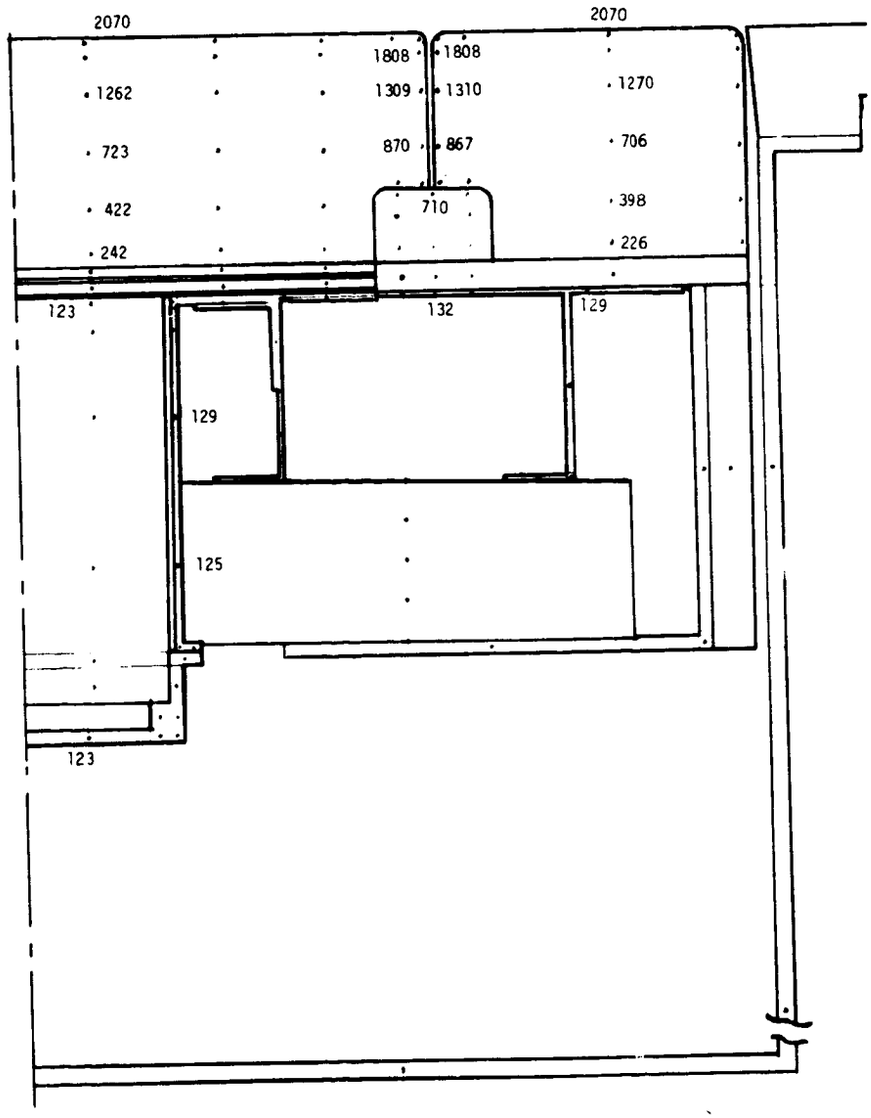

NOTES:
1. ALL TEMPERATURES IN °F
2. 80°F INITIAL TEMPERATURE
3. BREADBOARD TEST NO. 2 (.405) ENVIRONMENT

MAXIMUM TEMPERATURES FOR BREADBOARD UNIT

FIGURE 84

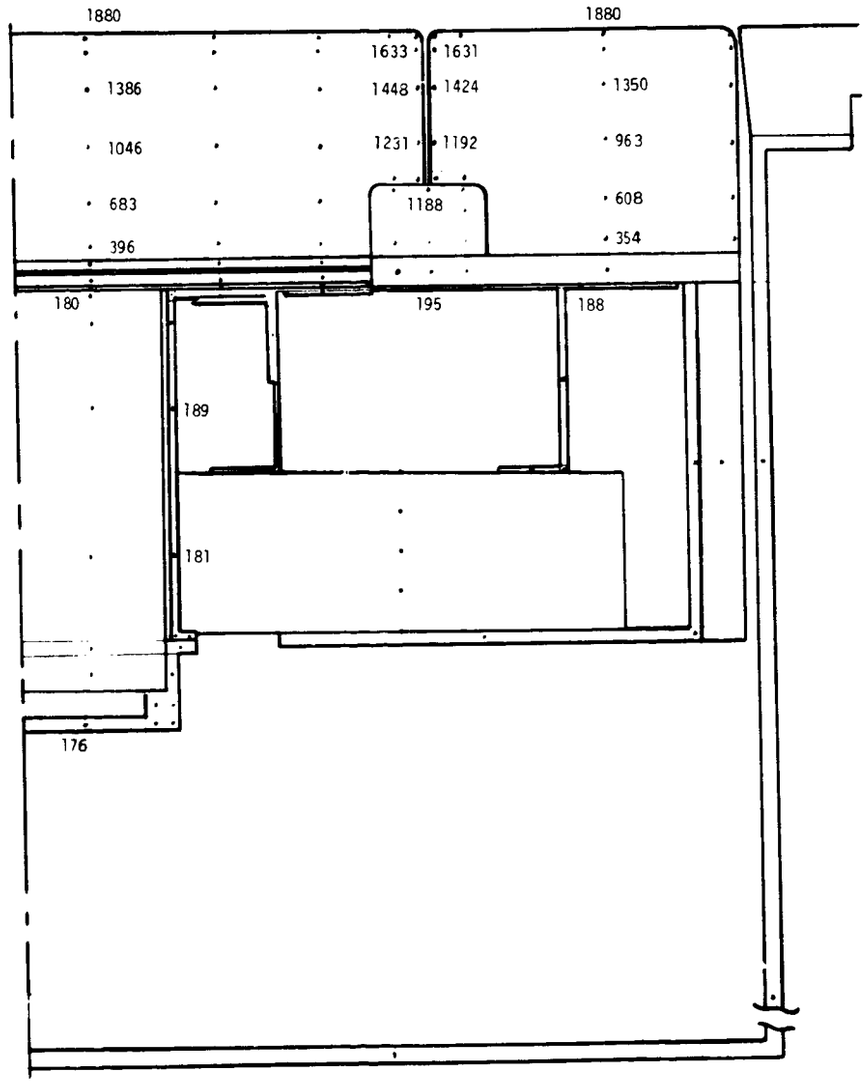

NOTES:
1. ALL TEMPERATURES IN °F
2. 80°F INITIAL TEMPERATURE
3. PROTOTYPE TEST NO. 10 (S451) ENVIRONMENT

MAXIMUM TEMPERATURES FOR PROTOTYPE UNIT

FIGURE 85

During early design studies, where the S-band antenna extended into the LI-1500 HRSI tile, a strength analysis was made to determine the limitations on penetration as a function of recess diameter. The assumptions used were:

(a) The allowable stress is equal to typical failing stress for LI-1500, 7.93×10^5 N/m^2 (115 psi).

(b) The LI-1500 tiles are large enough compared to the recess diameter so that the reduced thickness portion acts as a fixed edge plate.

(c) The ascent pressure, 7.31×10^4 N/m^2 (10.6 psi), is the most critical condition.

(d) The reduced thickness portion is not supported by direct contact with the antenna aperture.

The results (figure 86) show that the minimum thickness for the S-band antenna, which is 6.48 cm (2.55 in.) in diameter, is about 0.86 cm (0.34 in.). However, the stresses should be recalculated for a specific design configuration. The 0.86 cm (0.34 in.) thickness exceeds the LI-1500 thickness required for thermal protection of the S-band antenna as discussed in the section on CONCEPT AND FEASIBILITY STUDIES under Thermal Studies.

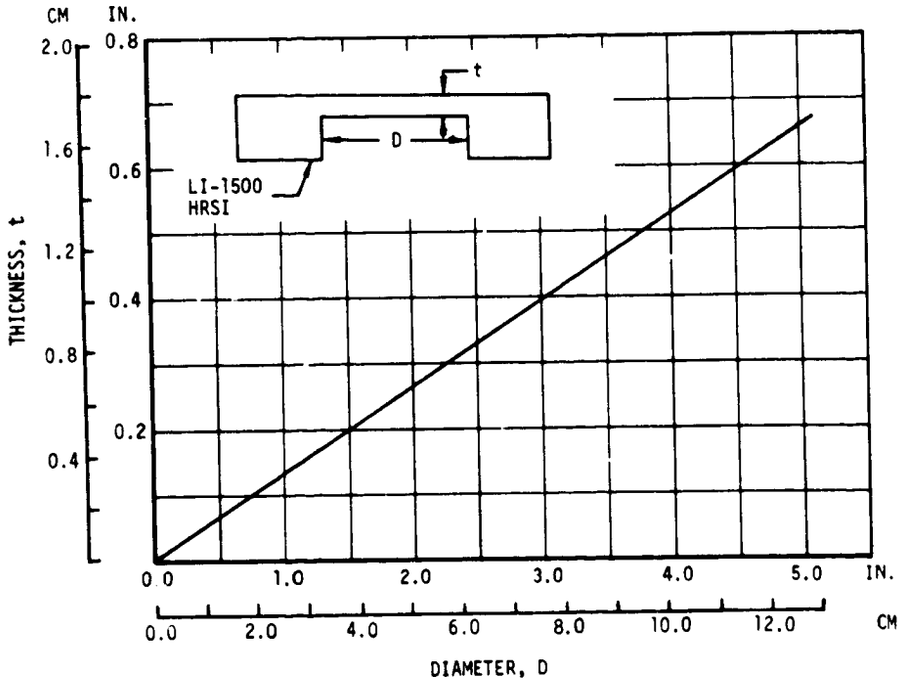

HRSI THICKNESS VERSUS RECESS DIAMETER

FIGURE 86

Quality Assurance

The Quality Assurance effort was directed primarily to the development of quality criteria, the review of technical documentation for incorporation of quality requirements and appropriate in-process inspection to ensure prototype hardware was fabricated and tested in accordance with engineering requirements.

Appropriate quality criteria was developed and coordinated with Design Engineering. The S-band antenna system drawings were reviewed by Quality Assurance to ensure the incorporation of quality criteria and that provisions for production process controls were included. The procurement and inspection of purchased items was accomplished in accordance with established procedures.

The LI-1500 tile was fabricated and controlled by Lockheed. The basic antenna was fabricated by Amecon in accordance with the improved Apollo S-band antenna specification M45672 developed under Contract NAS 9-8334, except for revision to the backcap mounting flange and finish revisions required to avoid a metal coupling problem. Purchased items were accepted based on supplier certification and visual inspection as to condition of the item on receipt. X-rays of each LI-1500 tile were furnished by Lockheed and were reviewed by Materials and Processes (M&P) engineering specialists to ensure that the material was free of significant voids and delaminations.

Documentation for the progressive fabrication and testing of the antenna components and assemblies, including the bonding and attachment of the LI-1500 material and the component and end item testing results, was initiated and is on file. Progressive in-house inspections were performed primarily by cognizant engineering personnel because of the experimental nature of this study. Fabrication operations were performed by personnel experienced in the fabrication of HCF materials in the Advanced Materials Fabrication facility due to the limited number of units and the complex process operations involved.

The bonding process procedures, Appendix D, were reviewed by the M&P engineering specialists and coordinated with Lockheed bonding procedures. The implementation of these bonding procedures on the initial breadboard unit was observed by the M&P engineering specialists and a representative from Lockheed. Material testing was performed and is discussed in the subsection on Materials Evaluation of this section.

The S-band antenna component testing is discussed and the measured electrical performance data is provided in the section on ELECTRICAL TESTING, under Component Testing. This performance data was used as a baseline for acceptance of the final hardware in conjunction with the engineering evaluation of radiation patterns and impedance measurements, physical examination and radiographic inspection. The final configuration and performance is considered to meet the overall objectives of this study.

Reliability

The objective of the reliability effort on the S-band antenna system was to review the design to uncover any design weakness and provide or recommend appropriate corrective action which may impact the reliability of the system. Figure 87 shows the components of the antenna system considered in the reliability analysis. The results of the reliability analysis (table XVI) indicate a reliable system providing that adequate controls are initiated to assure repeatability of parts and material characteristics and the system is used within the design environment. The tabulated results of table XVI define the parts or material, the most likely failure mode, possible causes that could initiate that failure mode, and reliability assurance status. The reliability assurance status is based on test results and is indicative of MDAC-E's confidence in the system reliability potential. There are no single failure points if this antenna system is properly installed and checked out.

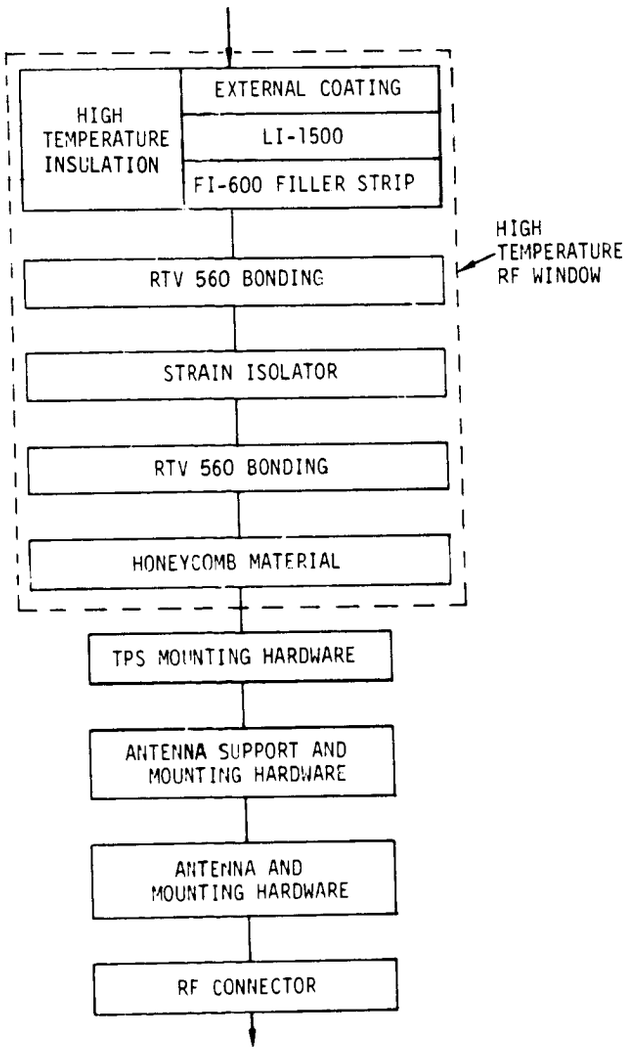

S-BAND ANTENNA SYSTEM BLOCK DIAGRAM FIGURE 87

TABLE XVI

QUANTITATIVE RELIABILITY EVALUATION

PART / MATERIAL	DESCRIPTION	FAILURE MODES	FAILURE MODE CAUSES	RELIABILITY ASSURANCE STATUS
HIGH TEMPERATURE INSULATION EXTERNAL COATING LI-1500 FI-600	COATING IS SILICA WITH SILICA CARBIDE. LI-1500 IS RIGIDIZED COMPACTED FIBROUS SILICA. FI-600 IS A RESILIENT FIBROUS SILICA. BOTH ARE IMPREGNATED WITH SILICONE.	BREAKAGE AND/OR SEPARATION OF EXTERNAL COAT FROM LI-1500. CHANGE IN RF TRANSMISSION CHARACTERISTICS. CHANGE IN THERMAL CHARACTERISTICS.	MISHANDLING DURING INSTALLATION AND FLUCTUATING PRESSURE IN TURBULENT BOUNDARY LAYERS (LAUNCH AND ENTRY). MOISTURE PENETRATION OF INSULATION. AGING DEGRADATION BY REUSE.	CAUTION IN HANDLING IS A MAJOR REQUIREMENT. SURFACE COATING CAN BE CHIPPED OR CRACKED. TEST SHOWS ADEQUATE WATERPROOFING WITH NO STRENGTH DEGRADATION AND NEGLIGIBLE CHANGE IN RF CHARACTERISTICS.
RTV-560	A METHYL-PHENYL RTV ADHESIVE. TEMPERATURE RANGE 144 to 561 K (-200°F TO 550°F).	LOSS OF ADHESIVE CHARACTERISTICS. CHANGE RF OR THERMAL CHARACTERISTICS.	REPEATED HIGH TEMPERATURE CYCLING AND/OR EXCEED DESIGN TEMPERATURE AND STRESS LIMITS.	TEST RESULTS SHOW ADEQUATE ADHESION STRENGTH AND NEGLIGIBLE CHANGE IN RF CHARACTERISTICS OVER TEMPERATURE RANGE.
STRAIN ISOLATOR RL-1973	A METHYL-PHENYL SILICONE MATERIAL WITH A SPONGE CONSISTENCY. TEMPERATURE RANGE 144 TO 477 K (-200°F TO 400°F)	POSSIBLE STIFFENING AND FRACTURE UNDER EXTREME COLD CONDITIONS AND STRESS.	ORBITAL COLD SOAK FOLLOWED BY ENTRY TEMPERATURE AND DYNAMIC STRESS.	NOT TESTED. RECOMMEND A SIMULATED TEST.
HONEYCOMB	FACE SHEETS AND CORE ARE A GLASS FABRIC REINFORCED PLASTIC WITH HEAT RESISTANT PHENOLIC RESIN. TEMPERATURE RANGE 116 TO 533°K (-250°F TO 500°F).	CHANGE IN RF CHARACTERISTICS. REDUCTION IN MECHANICAL STRENGTH.	REPEATED HIGH TEMPERATURE AND DYNAMIC STRESSING OF THE MATERIAL.	NEGLIGIBLE CHANGE IN STRENGTH AND RF CHARACTERISTICS ESTABLISHED BY TEST.
MOUNTING HARDWARE FOR THERMAL PROTECTION/RF WINDOW	ALLOY STEEL SOCKET HEAD CAP SCREW WITH A CARBON STEEL WASHER. SECURED BY SELF LOCKING 505 K (450°F) PLATENUT MOUNTED TO A STRUCTURE WITH ALUMINUM ALLOY RIVETS.	LOOSENING OF SCREWS OR FAILURE FROM FATIGUE DUE TO THERMAL AND DYNAMIC STRESS.	REPEATED DYNAMIC AND HIGH TEMPERATURE STRESS.	SELF LOCKING FEATURE MEETS REUSE REQUIREMENTS.
ANTENNA SUPPORT AND MOUNTING HARDWARE TO VEHICLE STRUCTURE	MACHINED ALUMINUM (2024-T3411) MOUNTED BY HEAT TREATED ALLOY STEEL SCREW. SECURED BY A 505 K (450°F) SELF LOCKING PLATENUT, MOUNTED TO STRUCTURE WITH ALUMINUM ALLOY RIVETS.	LOOSENING OF SCREWS OR FAILURE FROM FATIGUE DUE TO THERMAL AND DYNAMIC STRESS.	REPEATED DYNAMIC AND HIGH TEMPERATURE STRESS.	SELF LOCKING FEATURE MEETS REUSE REQUIREMENTS.
ANTENNA AND MOUNTING HARDWARE TO ANTENNA SUPPORT	IMPROVED APOLLO S-BAND ANTENNA CAPABLE OF REUSE AFTER SUBJECTED TO TEMPERATURES OF 450 K (350°F). TEMPERATURE LIMITED BY TEFLON IN CONNECTOR. ANTENNA SUPPORTED BY FOUR BOLTS WITH SELF LOCKING NUT. TWO FLAT TREATED ALUMINUM WASHERS PER BOLT-NUT COMBINATION.	LOOSENING OF SCREWS. FRACTURE OF ANTENNA.	REPEATED DYNAMIC STRESS. DYNAMIC SHOCK OR VIBRATION.	SELF LOCKING FEATURE MEETS PER SE REQUIREMENTS. ANTENNA PROVEN BY APOLLO APPLICATION.
RF CONNECTOR	TNC COAXIAL CONNECTOR WITH TEFLON INSERT.	SHORT OR OPEN.	LOSS OF TEFLON DIELECTRIC BY EXCEEDING TEMPERATURE LIMITS.	TEST ESTABLISHES THAT TEMPERATURE LIMITS WILL NOT BE EXCEEDED WITH RF WINDOW INTACT.

THIS PAGE INTENTIONALLY LEFT BLANK

TEST HARDWARE FABRICATION

The objective of the Test Hardware Fabrication task (Task 2) was to fabricate the S-band antenna system designed in Task 1.2 for electrical and thermal testing. This included fabrication of the various components, assembly of these components into the breadboard and prototype units and fabrication of auxiliary test fixtures.

Component Fabrication

The components of the breadboard and prototype units were fabricated by both subcontractors and the MDC Advanced Material Fabrication Facility.

S-band antenna. - The S-band antenna (figure 45) was manufactured by Amecom Division, Litton Systems, Inc. under subcontract to MDAC-E. It is basically an improved Apollo S-band antenna (Amecom Part No. M45672) with the backcap modified to include the mounting flange.

The Apollo S-band antenna is a cavity backed helix. The helix is imbedded in a cylinder of slip cast fused silica (Corning Code 794). The cylinder is coated with platinum except for the two ends. One end is fitted with a backcap which has electrical continuity with the platinum coating and contains the TNC input connector. The other end, the radiating aperture, is left open. The antenna may be tuned to optimize the axial ratio at a specified frequency within the nominal frequency range by adjusting the length of the helix.

The nominal finish of the backcap, a nickel plate with a rhodium flash coat, was changed to meet the Space Shuttle equipment metal couples requirement for a mounting interface of alodined aluminum. This was accomplished by first copper plating the Kovar backcap followed by a 60/40 tin-lead alloy electroplate per MIL-F-14072 finish M222.

Visual inspection and electrical testing were performed to show compliance with drawing and electrical performance requirements.

LI-1500 antenna window and guard tiles. - The LI-1500 antenna window, guard tiles and the FI-600 filler strips were fabricated by the Lockheed Missile and Space Company, Inc. (LMSC) under subcontract to MDAC-E. The tiles and filler strips were manufactured to the drawings shown in figures 70 and 71 respectively. The LI-1500 was first shaped to the drawing requirements and then coated on five sides with LI-0042 gray waterproof coating, which includes an emittance pigment. The coating was omitted from the four attachment holes in the antenna window tile. The waterproofing process was completed by impregnating the tiles with hydrolized silicone. The FI-600 filler strip was painted with an emittance coat on part of one side (figure 71) and impregnated with hydrolized silicone for waterproofing. X-rays of the finished parts were taken (figure 88) to detect any voids or delamination within the

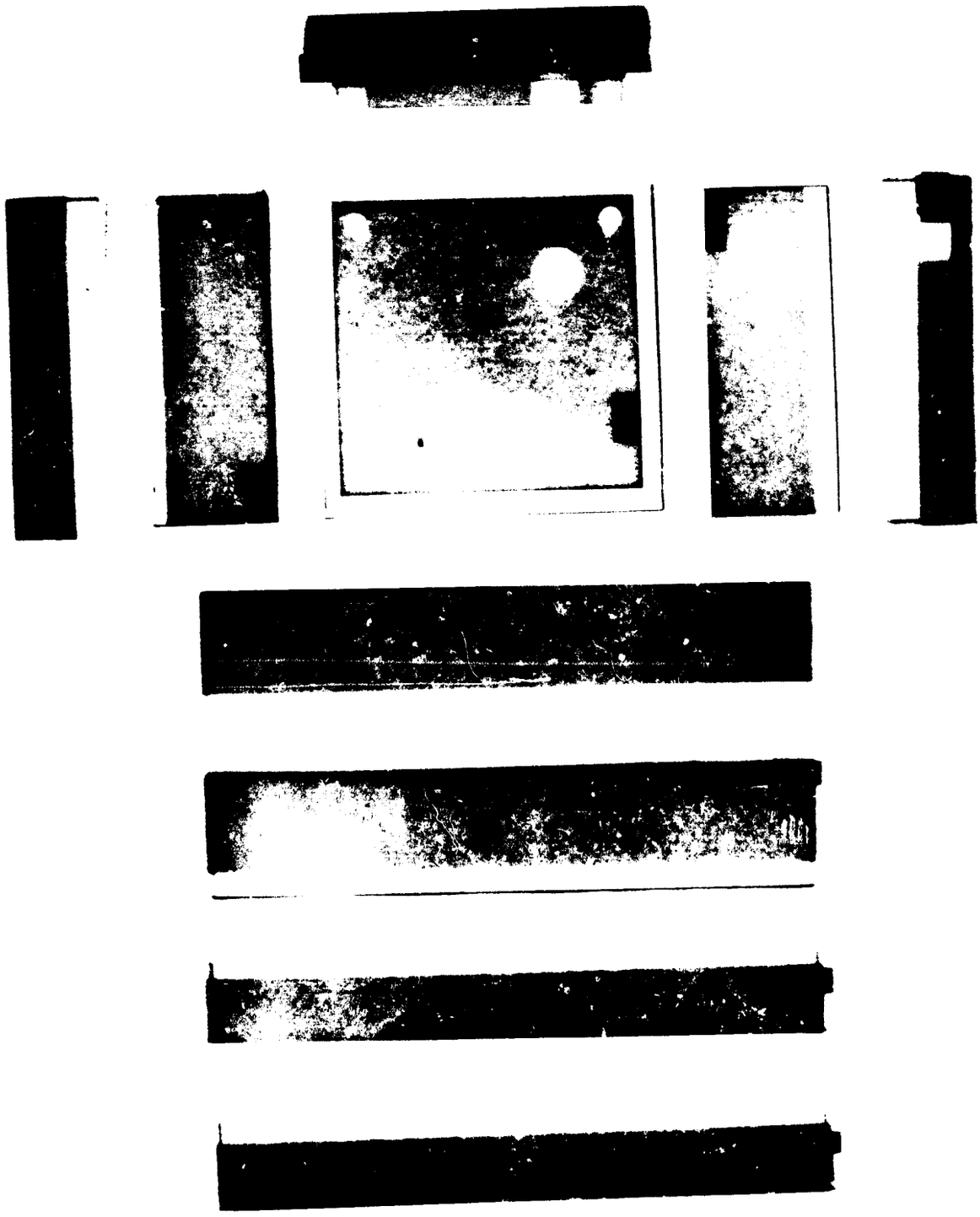

HRSI TILE X-RAYS

FIGURE 38

materials. The X-rays showed the finished parts to be satisfactory.

The results of a dimensional inspection of the finished tiles (figure 89) shows that during the firing of the waterproof coating, the tiles shrink more at the corners than at the center of the sides. Further, the shrinkage is greater where the top coated surface meets the sides than where the bottom uncoated surface meets the sides.

Silicone sponge. - RL-524 (type S-105) silicone sponge was purchased from Raybeston Manhattan in 1.27 cm (0.50 in.) thick sheets. It was sent to a local material processor (Crown Products) for slicing into 2.03 mm (0.080 in.) and 6.35 mm (0.250 in.) thick sheets. Problems were experienced in slicing, and the finished sheets were not satisfactory for use in the breadboard and prototype units. Subsequent study of the problem, as discussed in the preceding section on S-BAND ANTENNA SYSTEM DESIGN under Material Evaluation, lead to the decision to replace the RL-524 with RL-1973, the same silicone sponge used in Lockheeds TPS design. The RL-1973 sponge was sliced by Crown Products and cut into the required shapes (figure 72) by MDC.

Fiberglass-phenolic honeycomb panel. - The fiberglass-phenolic honeycomb panels (figure 69) were fabricated at MDC using standard vacuum bag techniques. The core, a hexagonal cell, honeycomb was manufactured by the Hexcel Company. The face sheets (fabricated at MDC) consisted of three layers of 1.02 mm (0.004 in.) thick fiberglass cloth impregnated with a phenolic binder. The warp direction was oriented at 30 and 60° to provide uniform strength properties in all directions. The facesheets were bonded to the core using HT-435 adhesive manufactured by the American Cynanamid Company.

Panel support assembly. - The components of panel support assembly (figure 73) were fabricated from sheet aluminum. The stringers and cross braces were riveted together and the skin spot welded to the stringers. The holes in a completed fiberglass honeycomb panel were used to locate the attachment holes to ensure a good fit. After completion of the panel support assembly, the inboard side was painted with a high emittance paint per MDC process specification (PS 13646).

Antenna support. - The antenna support (figure 68) was machined from aluminum bar stock. The finished part was alodined per MIL-C-5541 requirements. The part was made slightly long and machined to length after receiving the S-band antennas from Amecom to ensure proper mating of the aperture with the panel support assembly outboard skin surface. After trimming, the exposed surface was brush alodined per MIL-C-5541.

Breadboard Unit Assembly

The breadboard unit assembly includes: (1) installation of the thermocouples; (2) bonding the silicone sponge pads to the fiberglass honeycomb panel and the LI-1500 antenna window tile; (3) bonding the silicone sponge to the guard tiles and the panel support assembly around the antenna window; (4) installation of the antenna support in the panel assembly; and (5) instal-

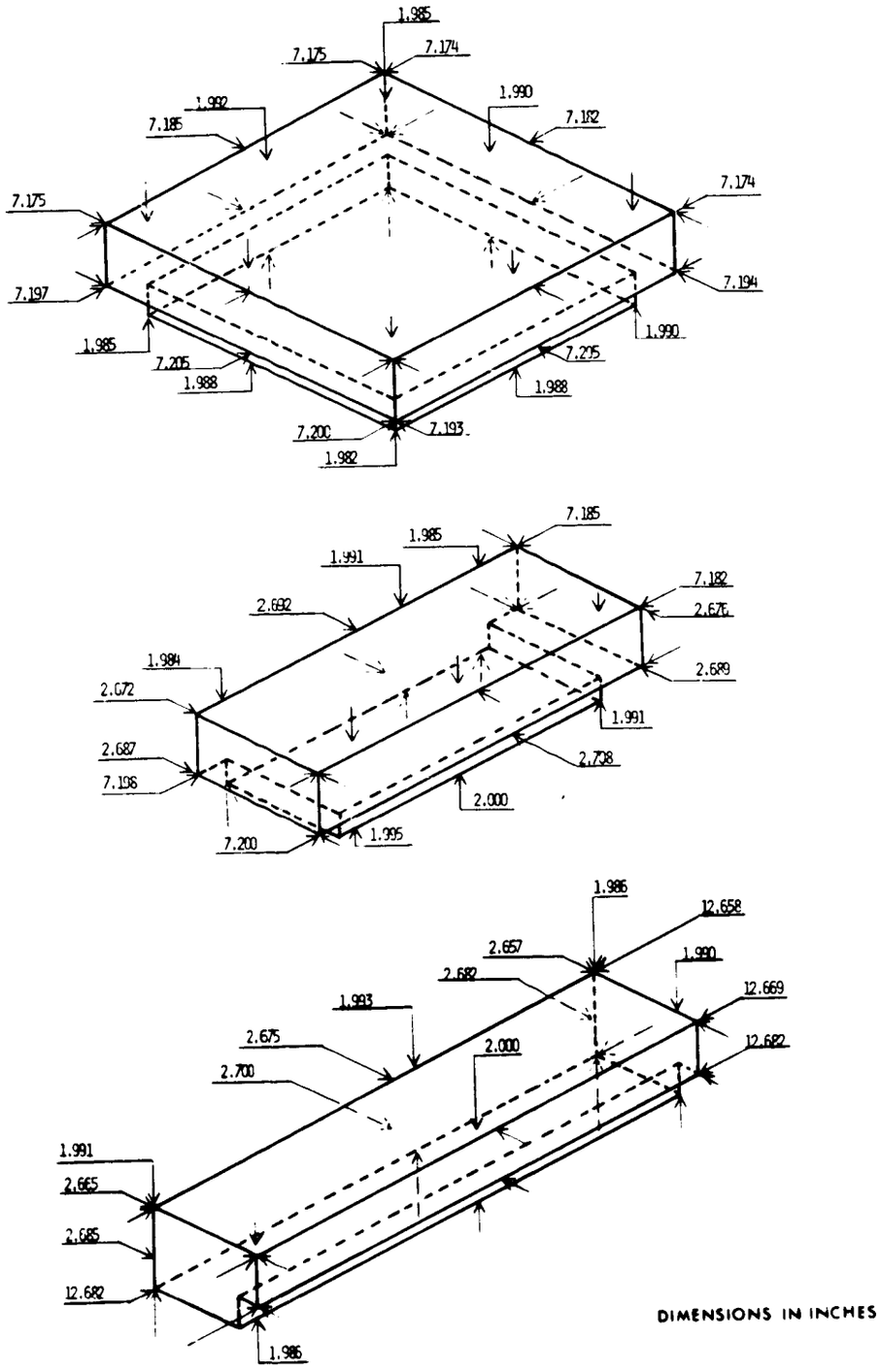

DIMENSIONS IN INCHES

TYPICAL HRSI TILE DIMENSIONS

FIGURE 89

lation of the antenna.

Thermocouple installation. - The thermocouples were installed in the antenna window and guard tiles prior to assembly. Small holes were drilled in each end of the grooves provided for the surface thermocouples in order to bring the thermocouple leads directly to the back side of the tile. The grooves were then filled with AREMCO 505 cement to hold the thermocouple in place to provide a smooth surface. To make the cement adhere to the LI-1500 waterproof coating, it was necessary to burn off the silicone resin in the local area. The indepth thermocouples were placed in the LI-1500 plugs and pressed into place.

Figure 90 shows the components of the antenna window before assembly with the thermocouples installed. Figure 91 shows the top and bottom surfaces of the antenna window and the surrounding guard tiles with the thermocouples installed. The cement covering the surface thermocouples was subsequently covered with Lockheed's LI-0010 emittance repair coating to obtain the proper surface emittance. Platinum-platinum-rhodium thermocouples were used for surface installation and Chromel-Alumel thermocouples were used for the indepth and bondline installations.

BREADBOARD UNIT ANTENNA WINDOW COMPONENTS

FIGURE 90

Antenna window assembly. - The components of the antenna window, consisting of the window tile, silicone sponge pad and fiberglass-phenolic honeycomb support panel, were bonded together with RTV-560 adhesive using the procedures and materials specified in Appendix D. A simple bonding fixture was used to hold the component parts in proper alignment. Bonding was accomplished in

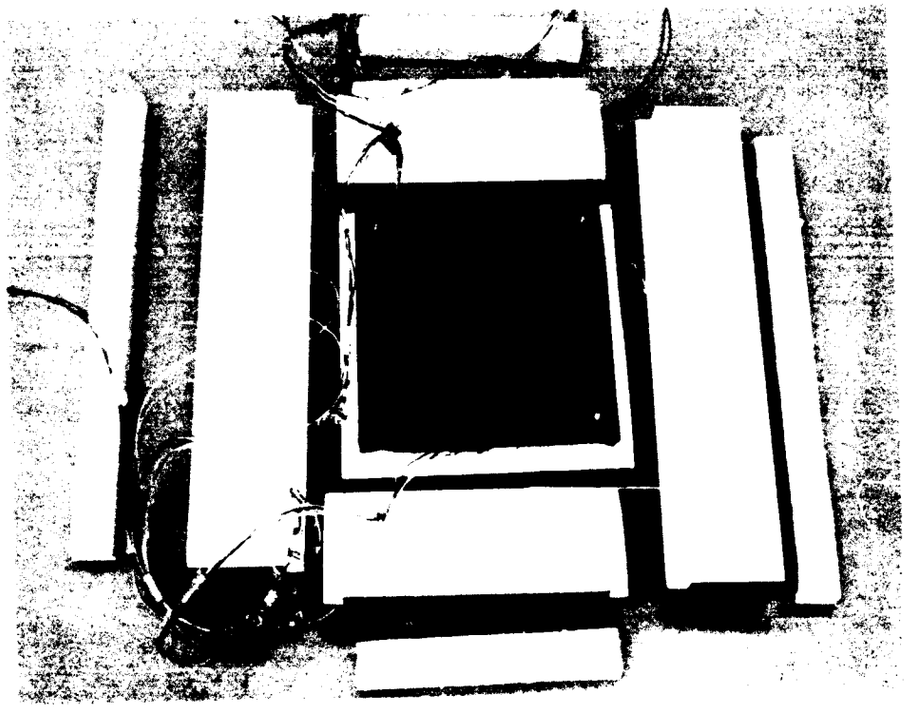

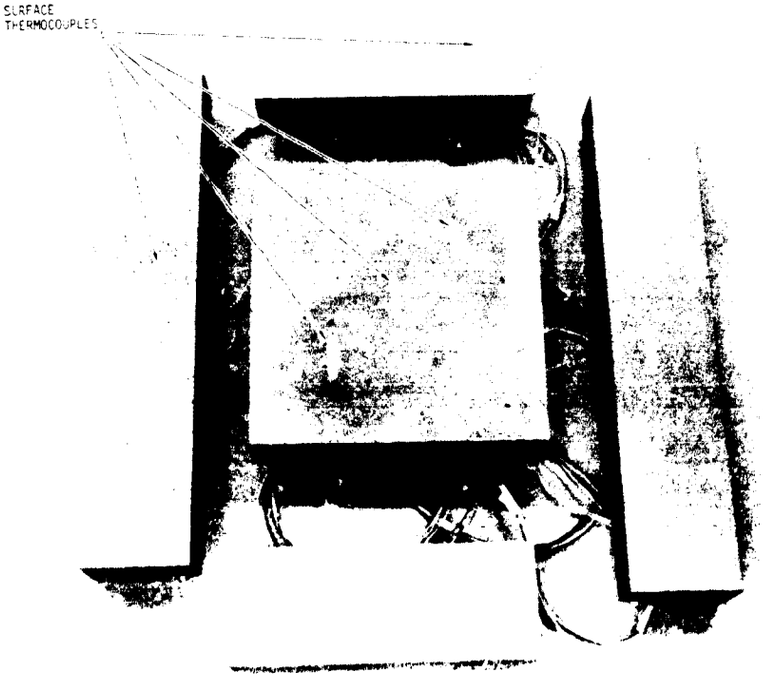

BREADBOARD UNIT ANTENNA WINDOW AND GUARD TILES

FIGURE 91

one operation using the following sequence of events:

(a) Clean and prime honeycomb panel.

(b) Clean silicone sponge pad.

(c) Apply adhesive to honeycomb panel.

(d) Apply adhesive to one side of the sponge.

(e) Position sponge pad on honeycomb panel with adhesive covered sides together.

(f) Apply adhesive to other side of sponge pad.

(g) Apply adhesive to LI-1500 antenna window tile.

(h) Install attachment washers and screws.

(i) Position window tile on adhesive covered sponge pad.

(j) Place thin silicone rubber pad on coated surface of window tile.

(k) Place weighted plate (6895 N/m^2 (1.0 psi)) on top of rubber pad.

(l) Place weight elbows around weighted plate to prevent lateral motion, which will result in misalignment between window tile, sponge pad, and honeycomb panel.

(m) Allow assembly to cure at ambient room temperature and humidity.

The curing time for the RTV-560 was sixteen hours due to the low local humidity. After curing, the excess adhesive was removed and the assembly inspected for compliance with applicable drawings.

Panel assembly. - The components of the panel assembly, consisting of the LI-1500 guard tiles, FI-600 filler strips, silicone sponge pads, and panel support assembly, were bonded together with RTV-560 adhesive in two operations using the procedures and specified materials in Appendix D. The completed antenna window assembly and rubber spacer strips were used as a tool to obtain the proper joint gap spacing around the window. A bonding fixture was used to hold the guard tiles in place around the antenna window during the bonding curing period. Figure 92 shows the panel assembly with the antenna window and joint gap spacers in the bonding fixture. The fixture sides, covered with Teflon tape, prevent any lateral motion of the guard tiles.

The first sequence of events was as follows:

(a) Clean and prime aluminum panel.

(b) Place and secure panel in bonding fixture.

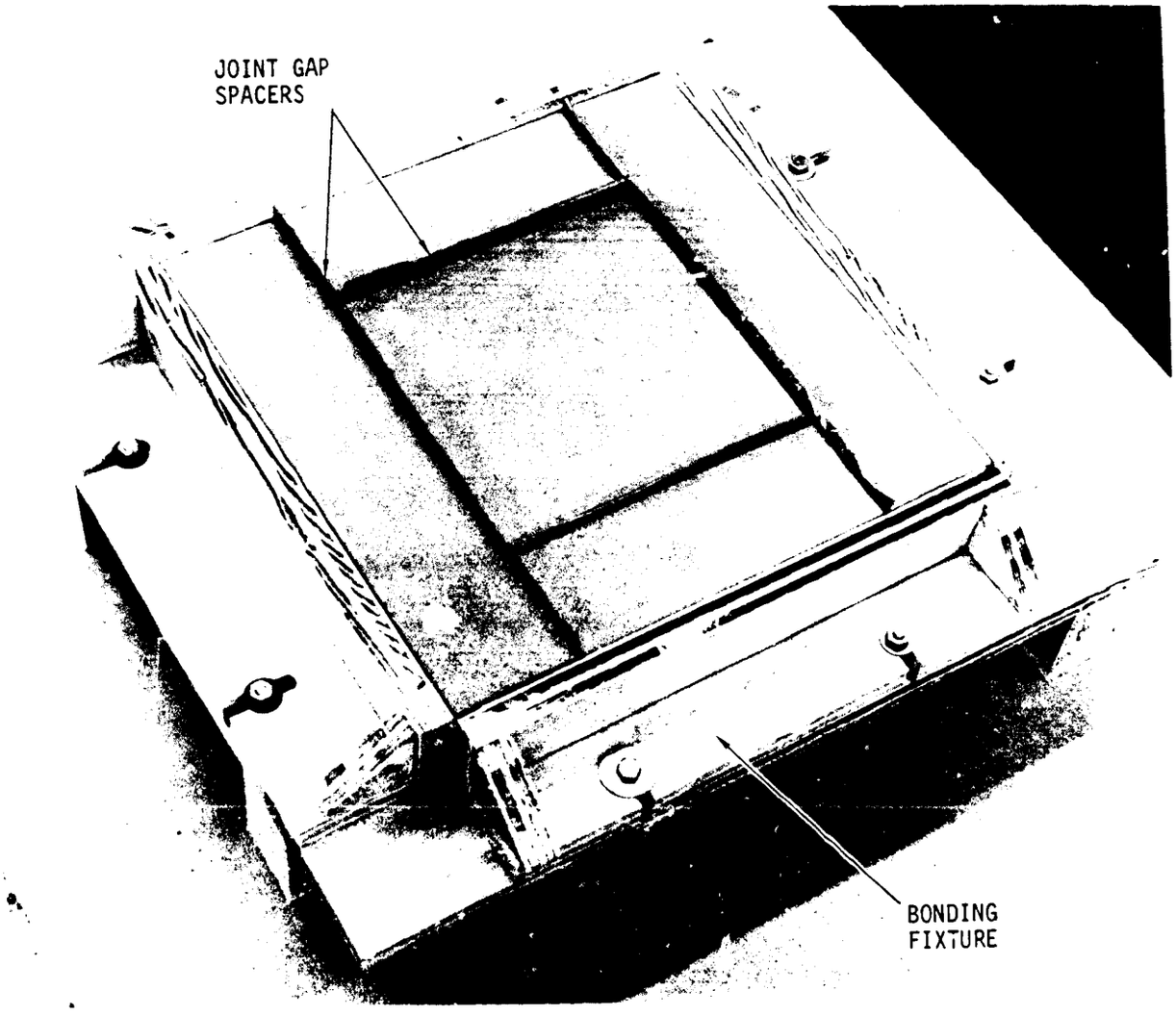

BREADBOARD PANEL ASSEMBLY IN BONDING FIXTURE

FIGURE 92

(c) Clean silicone sponge pads.

(d) Install antenna window assembly.

(e) Apply adhesive to aluminum panel.

(f) Apply adhesive to one side of sponge pad.

(g) Position sponge pad on aluminum panel around the antenna window with the adhesive covered side against the aluminum panel.

(h) Remove the antenna window.

(i) Place weighted plate (6895 N/m^2 (1.0 psi)) on sponge pad.

(j) Allow assembly to cure at ambient room temperature and humidity.

The second sequence of events was as follows:

(a) Install bondline thermocouples.

(b) Install antenna window assembly and FI-600 filler strips.

(c) Apply adhesive to sponge pad.

(d) Apply adhesive to LI-1500 guard tiles.

(e) Place guard tiles around antenna window.

(f) Insert silicone rubber spacers to control joint gap widths.

(g) Place thin silicone rubber pad on coated surface of antenna window and guard tiles.

(h) Place weighted plate (6895 N/m^2 (1.0 psi)) on top of rubber pad.

(i) Allow assembly to cure at ambient room temperature and humidity.

The curing time in both bonding operations was sixteen hours due to the low local humidity. After removal from the bonding fixture, the excess adhesive was trimmed away and the assembly inspected for compliance with applicable drawings.

Final assembly. - Following the bonding operations the antenna window was removed, the antenna support attached and the antenna window replaced. The thermocouples were than installed on the panel structure and antenna support and all the thermocouple leads attached to connectors. The completed assembly is shown in figure 93.

Prototype Unit Assembly

Two prototype units were assembled in the same manner as the breadboard unit with several minor exceptions. The exceptions were primarily in the method of surface thermocouple installation and procedure for assembling the antenna window.

In the prototype unit, all thermocouples were eliminated from the antenna window. Grooves were not provided in the guard tiles for surface thermocouples as was the case for the breadboard unit. Instead, narrow slits about 2.54 cm (1.00 in.) long were cut in the waterproof coating. After installing the thermocouples flush with the tile surface, the small voids around the thermocouple and its leads were filled with Lockheed's LI-0010 repair coating and

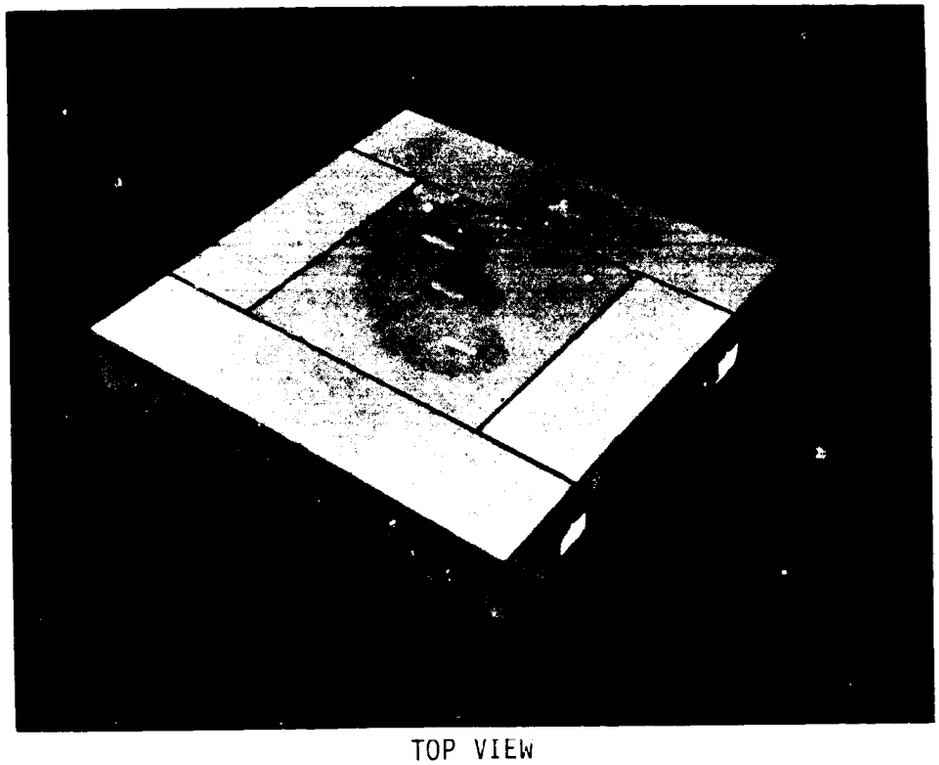

TOP VIEW

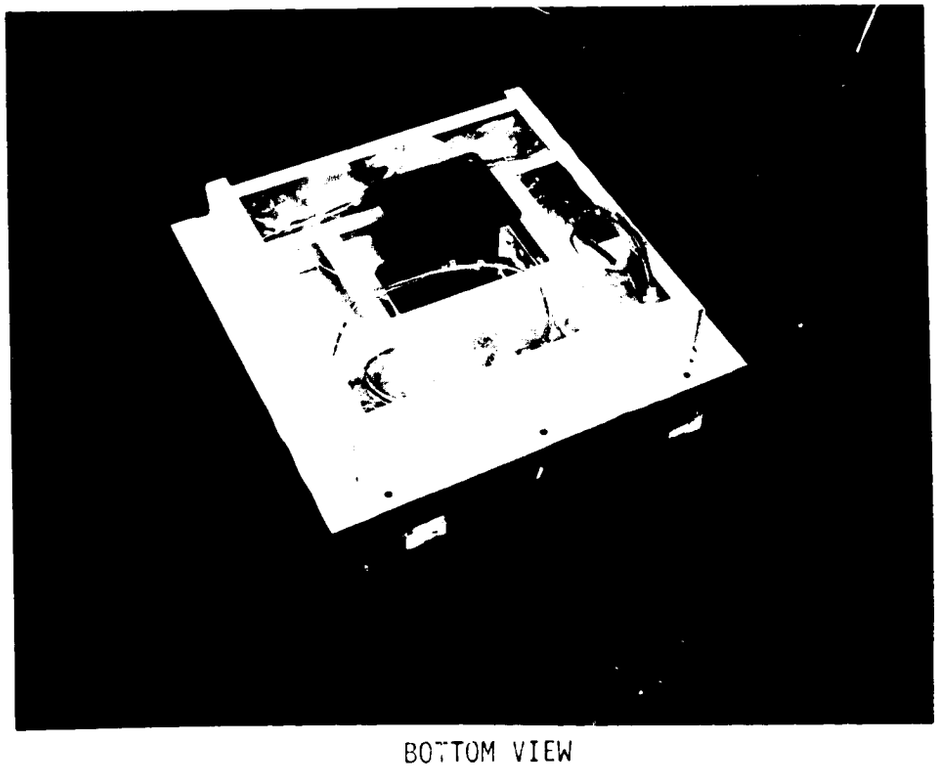

BOTTOM VIEW

BREADBOARD UNIT ASSEMBLY

FIGURE 93

permitting to cure at ambient room temperature.

The antenna window was assembled in two bonding operations rather than the one used for the breadboard unit. The silicone sponge pad was first bonded to the fiberglass support panel and cured. The antenna window tile was then bonded to the sponge pad. A bonding fixture was used to hold the components in position during the cure cycle.

The other steps in the assembly of the prototype unit were the same as the breadboard unit. However, after removal from the bonding fixture the joint gap width at the surface appeared to be larger than experienced with the breadboard unit. The increase in gap width is due to the pressure from the compressed FI-600 filler strips acting along one side of a long narrow tile. It is unlikely that such a condition would occur on an actual Orbiter installation since both sides of a tile would normally be subjected to the same force from filler strips. This could be compensated for by reducing the filler strip thickness. However, this must be done with caution. Too little pressure or a gap between the tile shoulder and the filler strips could allow hot gases to flow around the filler strips causing increased structural heating. Final assembly of the prototype was completed in the same manner as the breadboard unit. After thermocouple installation, all penetrations through the aluminum skin for thermocouple leads and antenna window attachment screws were sealed with either metallic tape or RTV-560 adhesive (figure 94). These holes were sealed, because there was evidence of heat flow through a large unsealed hole in the breadboard unit, which were used to pass the antenna window thermocouples leads through to the backside of the unit. Prototype Unit No. 1 is shown in figure 95.

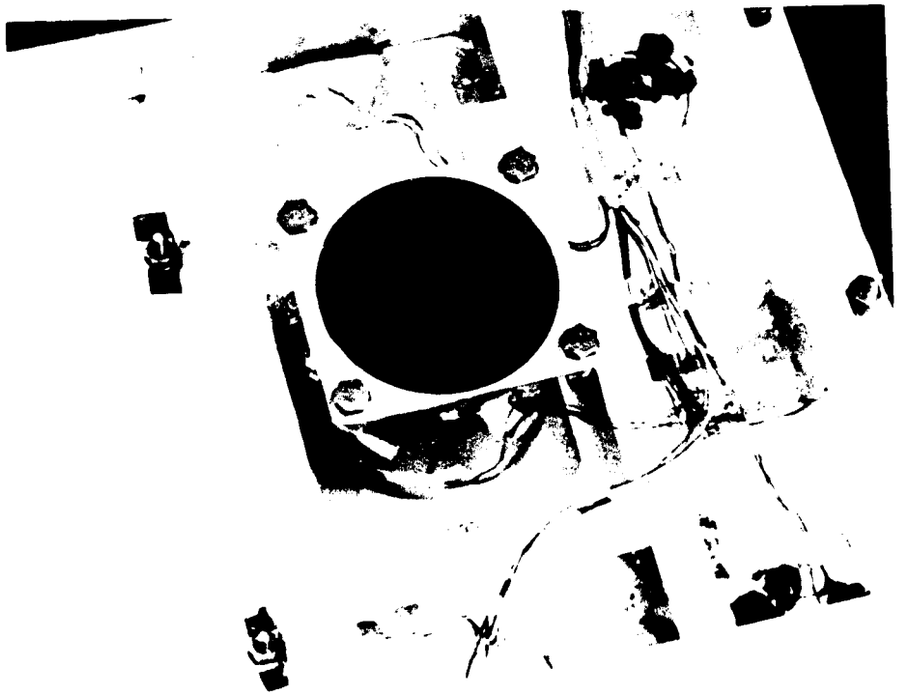

FIGURE 94

SKIN PENETRATION SEALS

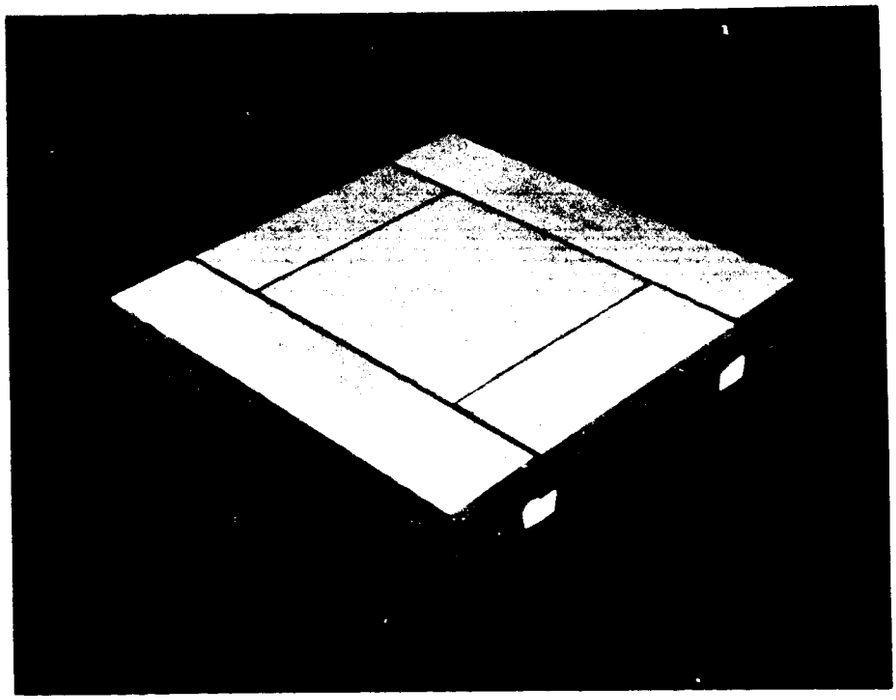

TOP VIEW

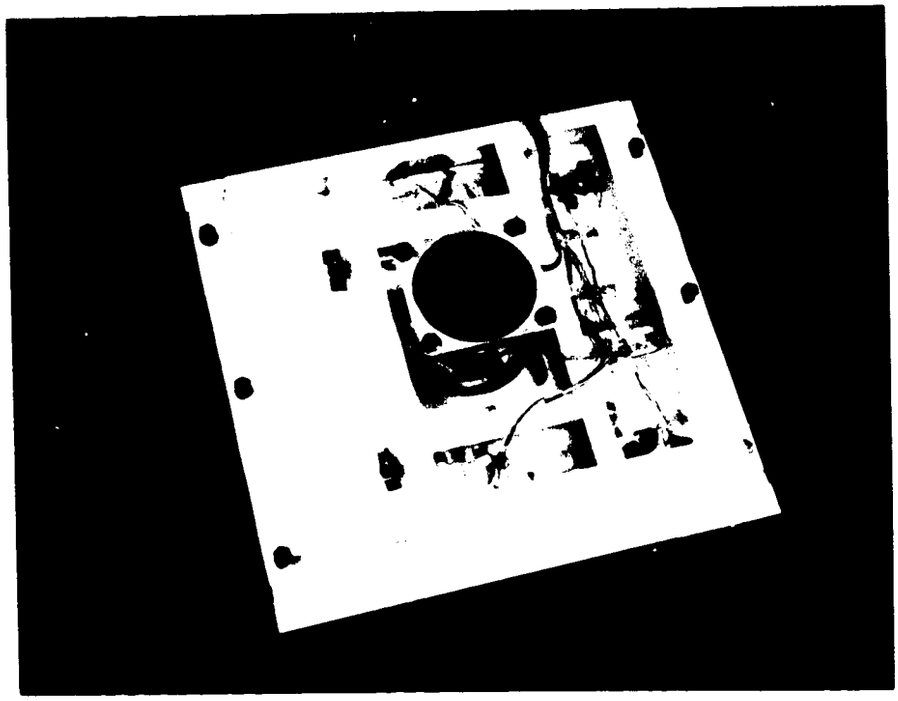

BOTTOM VIEW

PROTOTYPE UNIT NO. 1 ASSEMBLY

FIGURE 95

Test Fixture Fabrication

The test container assembly (figure 77) was fabricated in the MDC Laboratory Shop. Following the completion of welding, the surface mating with the breadboard and prototype units was machined to provide a flat surface. Sheets of ablator were then bonded to the sides of the test container.

The water cooled cover and the wedge mount assemblies were available from earlier programs as previously discussed.

THIS PAGE INTENTIONALLY LEFT BLANK

ELECTRICAL TESTING

The Electrical Testing task (Task 3) consists of component, breadboard unit, prototype unit and thermal test support testing. The objectives of this task was to verify compliance of component performance with design goals (Task 3.1), establish performance levels for the breadboard unit (Task 3.2) and prototype units (Task 3.3), and monitor the electrical performance, before and after the breadboard unit thermal tests and the prototype unit thermal reuse tests, to determine changes in performance attributable to the applied entry temperature environment (Task 3.4).

Component Testing

The S-band antennas were tested to verify compliance with component performance goals, Task 3.1, as defined in table XIV. Three antennas (S/N 101, 102 and 105) were tested. Radiation patterns were measured in both right (RHC) and left hand circular (LHC) polarization and rotating linear polarization. The axial ratio was derived from the rotating linear polarization patterns. A standard gain horn was used to obtain a 0 dB gain reference. The VSWR was derived from impedance measurement. The efficiency of only one antenna was measured.

Test configurations. - The radiation patterns and impedance measurements were made with the antenna aperture flush mounted in the center of an 86.4 cm (34.0 in.) square ground plane. A 5.1 cm (2.0 in.) wide border of Emerson & Cuming Inc. AN-75 absorber was placed around the ground plane edge to reduce pattern scalloping due to edge radiation effects. The antenna feed was pointed toward $\phi = 270°$ relative to the coordinate system (figure 19). The pattern orientation is $\phi = 0°$ on pattern right for the X-plane patterns and $\phi = 90°$ on pattern right for the Y-plane patterns.

Test techniques. - The test techniques used for the component tests are essentially the same as those described in the section on S-BAND ANTENNA SYSTEM DESIGN, under Electrical Design. The RF fields used for measuring the RHC and LHC patterns were probed to establish a circularity of less than 0.5 dB for RHC polarization and 1.0 dB for LHC polarization.

Test results. - Typical results of radiation pattern measurements for the S-band antennas are shown in figure 96, using antenna S/N 101. The patterns for S/N 102 and 105 antennas are given in Appendix E. The patterns shown in figure 96 have good symmetry except at 2.1 GHz where the pattern appears to be tilted about 20°. The axial ratio distribution is also unsymmetrical. Since these conditions occur in both planes, the reasons for the dissymetry is not apparent.

The axial ratios are higher than expected and higher than measured by Amecom. Attempts to obtain patterns with lower axial ratios by duplicating Amecom's test conditions at MDAC-E failed. Therefore, an S-band antenna

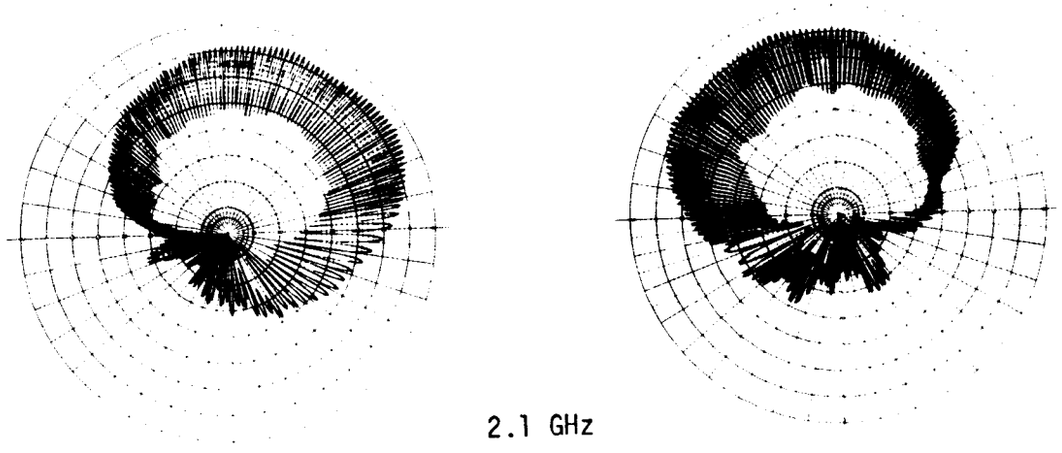

2.1 GHz

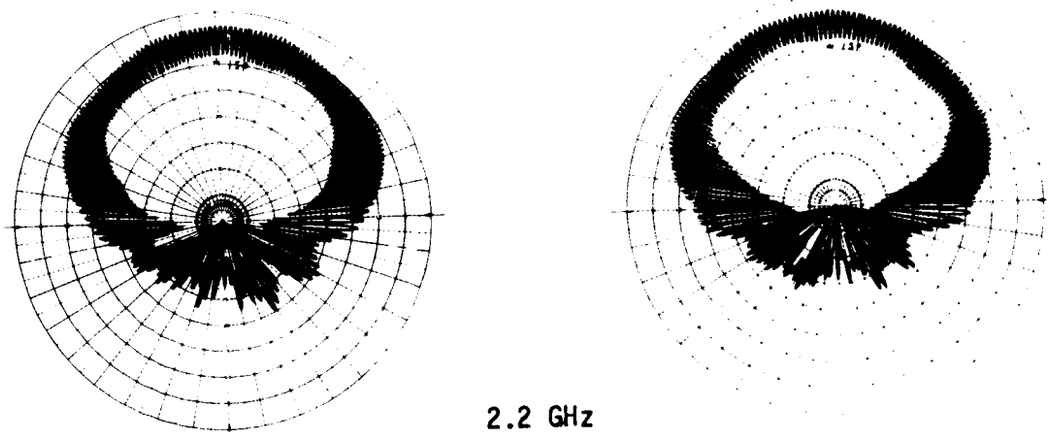

2.2 GHz

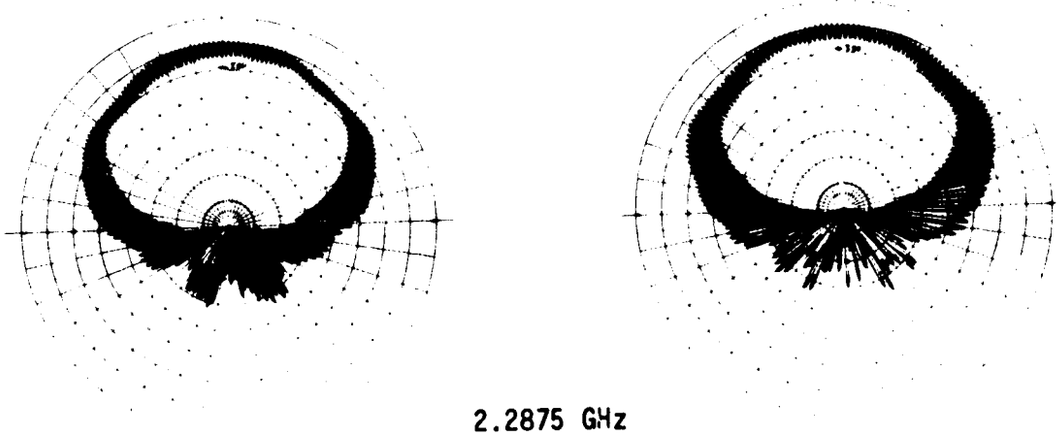

2.2875 GHz

Y-PLANE

X-PLANE

RADIATION PATTERNS - ANTENNA S/N 101

FIGURE 96

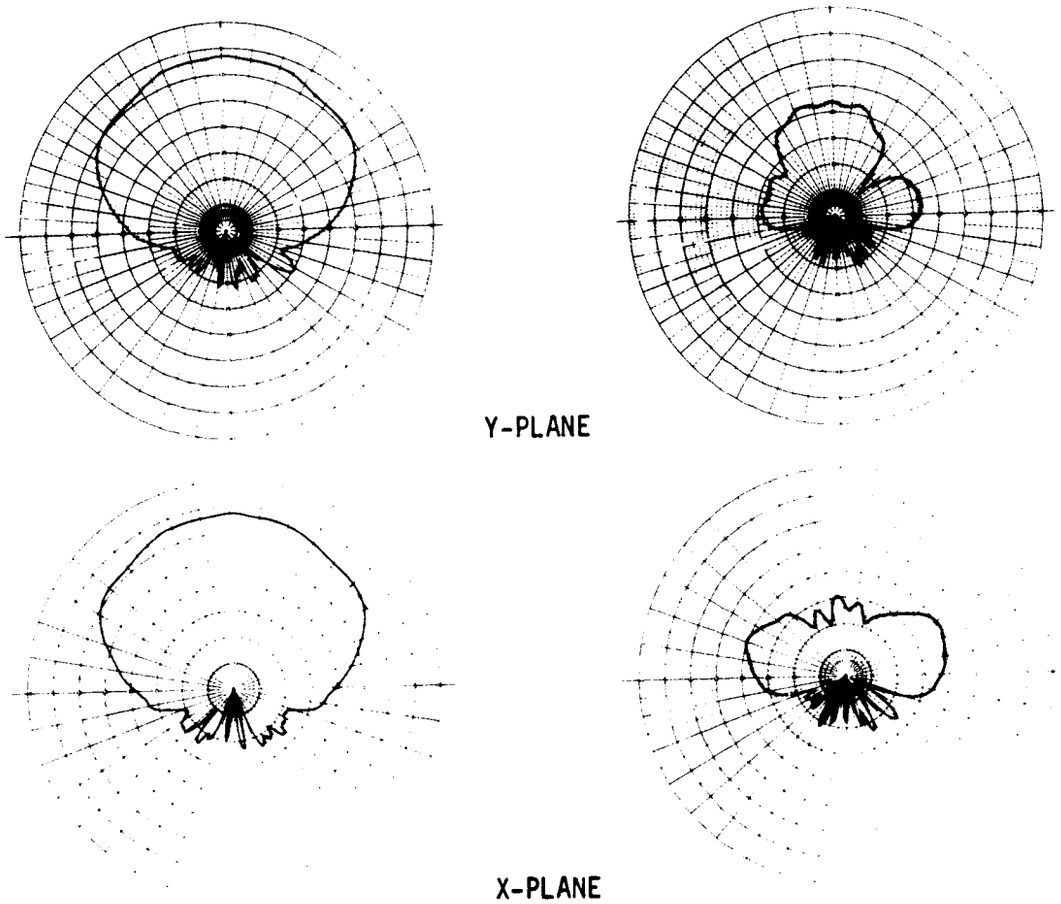

RADIATION PATTERNS - ANTENNA S/N 101

FIGURE 96 (Continued)

(S/N 101) was returned to Amecom for test. Their test results (figure 97) with the antenna aperture sealed to the ground plane with copper tape show that the axial ratio is about the same as that measured by MDAC-E. With the antenna not sealed to the ground plane (Amecom's standard test setup) and the antenna attached to the ground plane with long bolts, the axial ratio decreases 1 to 1.5 dB over the 120° beamwidth as shown in figure 97. Sealing the antenna to the ground plane is a close simulation of the mounting technique used in the S-band antenna system design. The antenna pattern orientation used by Amecom is 180° from that used at MDAC-E. This should be considered when comparing the patterns in figure 97 with those in figure 96. These results show that the axial ratio is sensitive to the mounting configuration, and that considerable care in the test setup is required to obtain repeatable results.

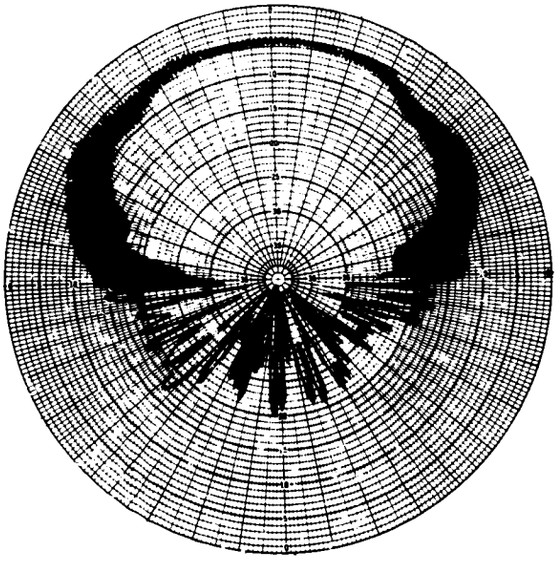

STANDARD AMECOM TEST MOUNTING

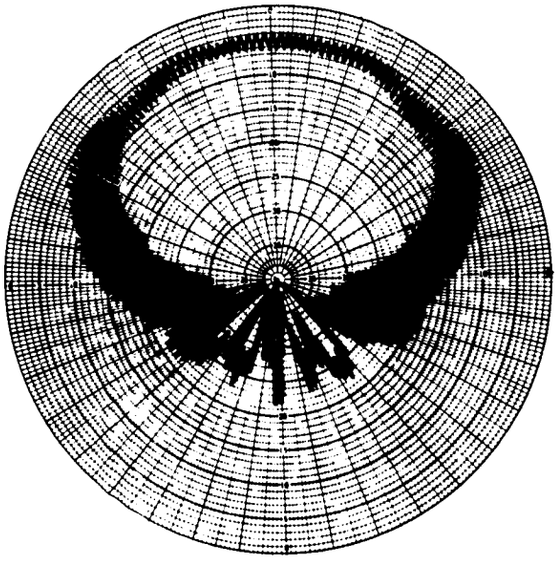

ANTENNA SEALED TO GROUND PLANE WITH COPPER TAPE

EFFECT OF MOUNTING CONFIGURATION ON AXIAL RATIO

FIGURE 97

The results of impedance measurements are shown in figures 98, 99 and 100, for S-band antennas S/N 101, 102 and 105, respectively. The VSWR's are less than 1.5:1 for S/N 101, 1.5:1 for S/N 102, and 1.9:1 for S/N 105. The VSWR for S/N 105 is less than 1.5:1 above 2.15 GHz. The VSWR data supplied by Amecom using a reflectometer measurement technique shows the VSWR is less than 1.5:1 in all cases and generally about 1.25 to 1.35:1. The Amecom measurements were performed without the antenna mounted in a ground plane.

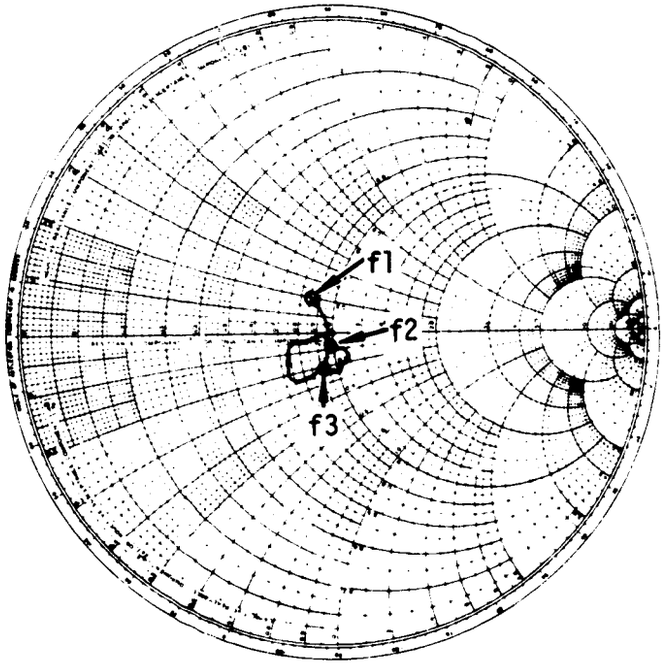

Z_o = 50 OHMS
f1 = 2.1 GHz
f2 = 2.2 GHz
f3 = 2.3 GHz

IMPEDANCE - ANTENNA S/N 101

FIGURE 98

The S-band antenna efficiency was determined from measurements of directivity and antenna gain. Total directivity was obtained using the pattern integration method (ref. 10). Total gain was measured by comparison to a standard gain horn. Using these values and the relationship that gain is equal to the product of directivity and efficiency (i.e., gain = (efficiency) x (directivity)) the efficiency was found to be 91%. This is over 10% greater than the design goal. For high efficiency antennas such as this, considerable care is required to avoid measured efficiencies greater than 100%.

Breadboard Unit Testing

The breadboard S-band antenna system electrical tests were performed to verify electrical performance and establish a standard for comparing with thermal test data. However, the thermocouple wires used to instrument the

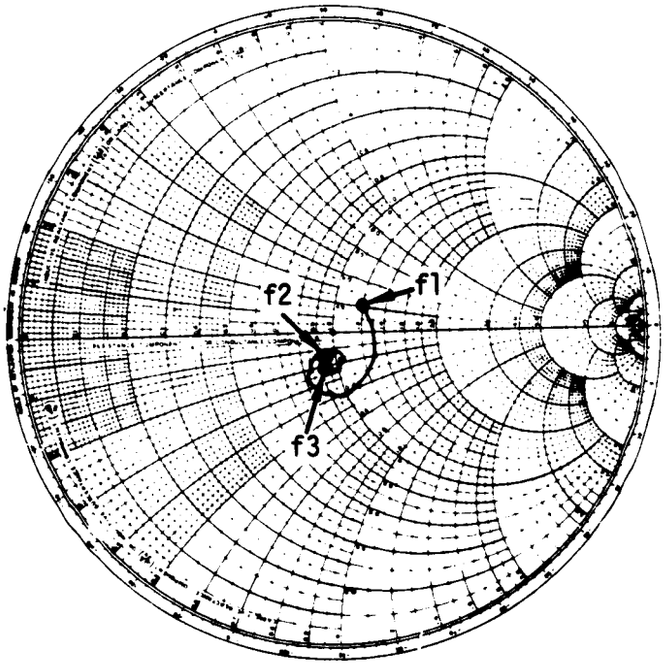

Z_o = 50 OHMS
f1 = 2.1 GHz
f2 = 2.2 GHz
f3 = 2.3 GHz

IMPEDANCE - ANTENNA S/N 102

FIGURE 99

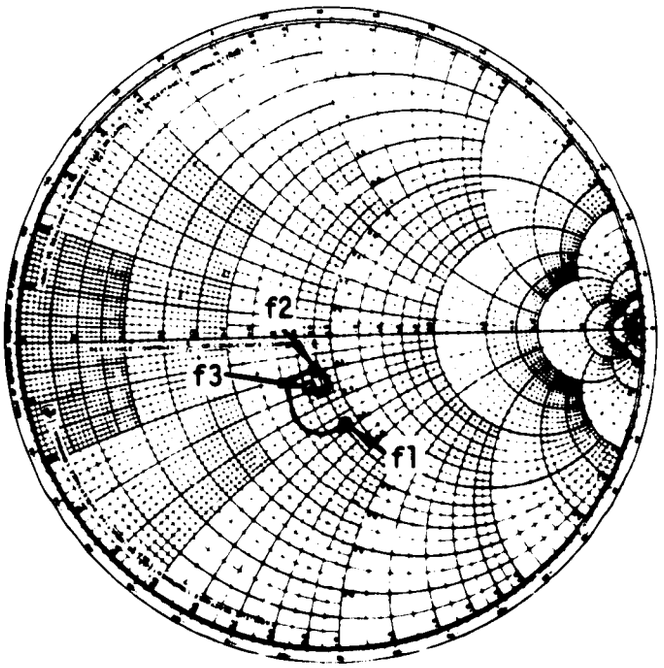

Z_o = 50 OHMS
f1 = 2.1 GHz
f2 = 2.2 GHz
f3 = 2.3 GHz

IMPEDANCE - ANTENNA S/N 105

FIGURE 100

breadboard unit resulted in a gain reduction and degraded radiation patterns. The impedance of the antenna system was affected by the thermocouple leads to a much lesser degree.

Test configuration. - The breadboard S-band antenna system was installed in the test container assembly (figure 77). The antenna system and the test container assembly were installed in the center of an 86.4 cm (34.0 in.) square ground plane. The antenna aperture and surrounding structural skin were positioned flush with the ground plane surface, leaving the TPS extending above the ground plane. A border of AN-75 absorber was placed around the ground plane edges to reduce edge effects. Front and back views of a typical test installation are shown in figure 101. The orientation of the antenna in the coordinate system was identical to that used for the component tests.

Test techniques. - The test techniques used for the breadboard unit radiation patterns are the same as those used for the component tests. A photo of the test setup used for the impedance measurements is shown in figure 102.

Test results. - The results of radiation pattern measurements for the breadboard unit are shown in figure 103. A comparison of these patterns with the patterns from the component tests (figure 96) shows lower gain, pattern distortion, higher LHC polarization levels, and higher axial ratios. The degraded performance is attributed to the thermocouple wires (figures 90 and 91) required for temperature measurements during the breadboard unit thermal tests. Since thermocouple installation was necessary during fabrication, electrical measurements on a "clean" breadboard unit were not possible.

The results of breadboard unit impedance tests are shown in figure 104. The impedance is shifted to the right on the Smith Chart plot. The impedance shift increases the maximum VSWR to about 1.8:1, somewhat higher than the 1.3:1 measured for the antenna system mockup tests (figure 64).

Prototype Unit Testing

The prototype S-band system electrical tests were performed to verify electrical performance and establish reference parameters prior to the thermal reuse tests. A revision of the number and placement of the thermocouples significantly improved the electrical performance. The test configuration and technique used for the prototype unit tests were the same as used for the breadboard unit tests.

Test results. - The results of radiation pattern measurements for the Prototype Unit No. 1 are shown in figure 105. A comparison of these patterns with those of the antenna system mockup (figure 63) show that the prototype unit patterns are essentially equivalent. The circular gain at $\phi = 0°$ is about 1 dB lower and the axial ratio about 1.5 dB higher than that obtained for the antenna system mockup patterns (figure 63). The LHC polarization patterns have increased magnitudes, due to the thermocouple wires, which are accompanied

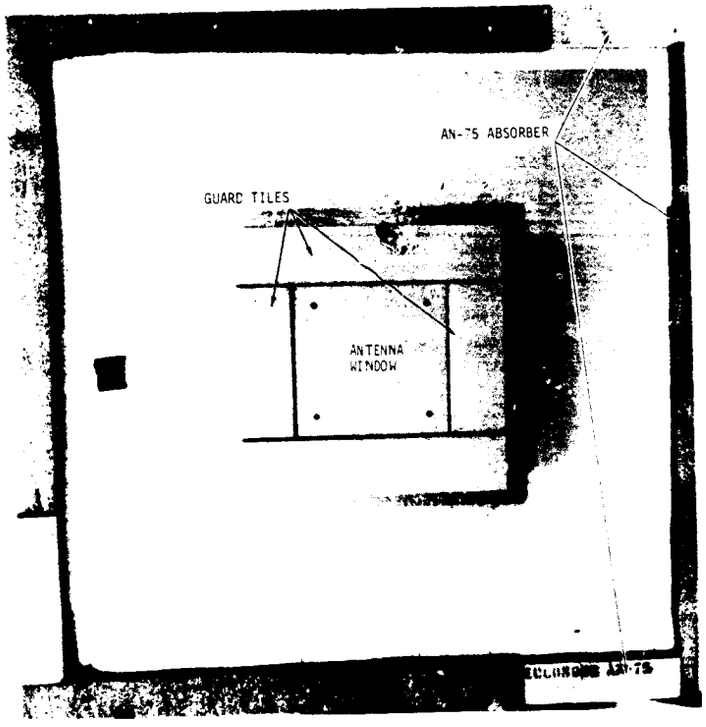

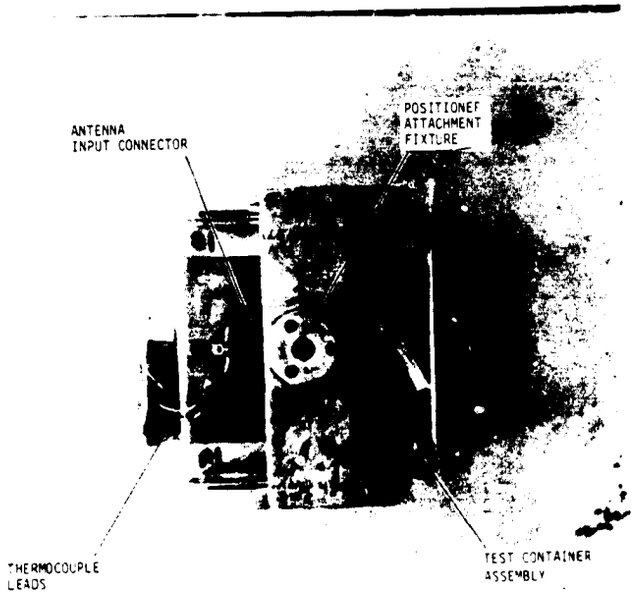

S-BAND ANTENNA SYSTEM TEST CONFIGURATION

FIGURE 101

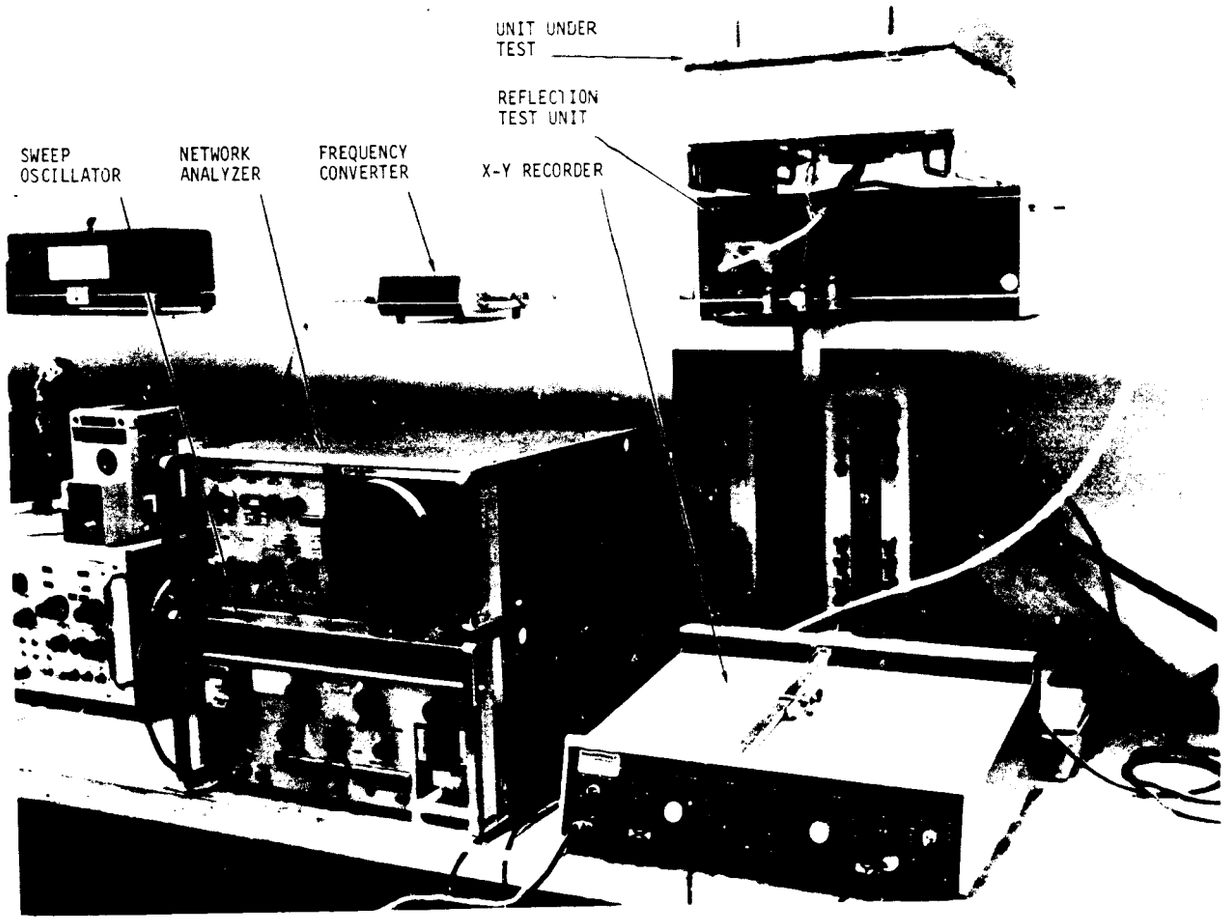

SWEPT FREQUENCY IMPEDANCE MEASUREMENT TEST SET-UP

FIGURE 102

by the increase in axial ratio. Radiation patterns for Prototype Unit No. 2 are given in Appendix F.

The results of the prototype unit impedance test are shown in figure 106. The impedance is shifted slightly at the low frequency end of the band but the VSWR is still less than 1.35:1, as obtained in antenna system mockup tests.

Thermal Test Support

Thermal Test Support (Task 3.4) electrical tests were performed before and after the thermal test of the breadboard and prototype S-band antenna system to detect changes in electrical performance resulting from exposure to

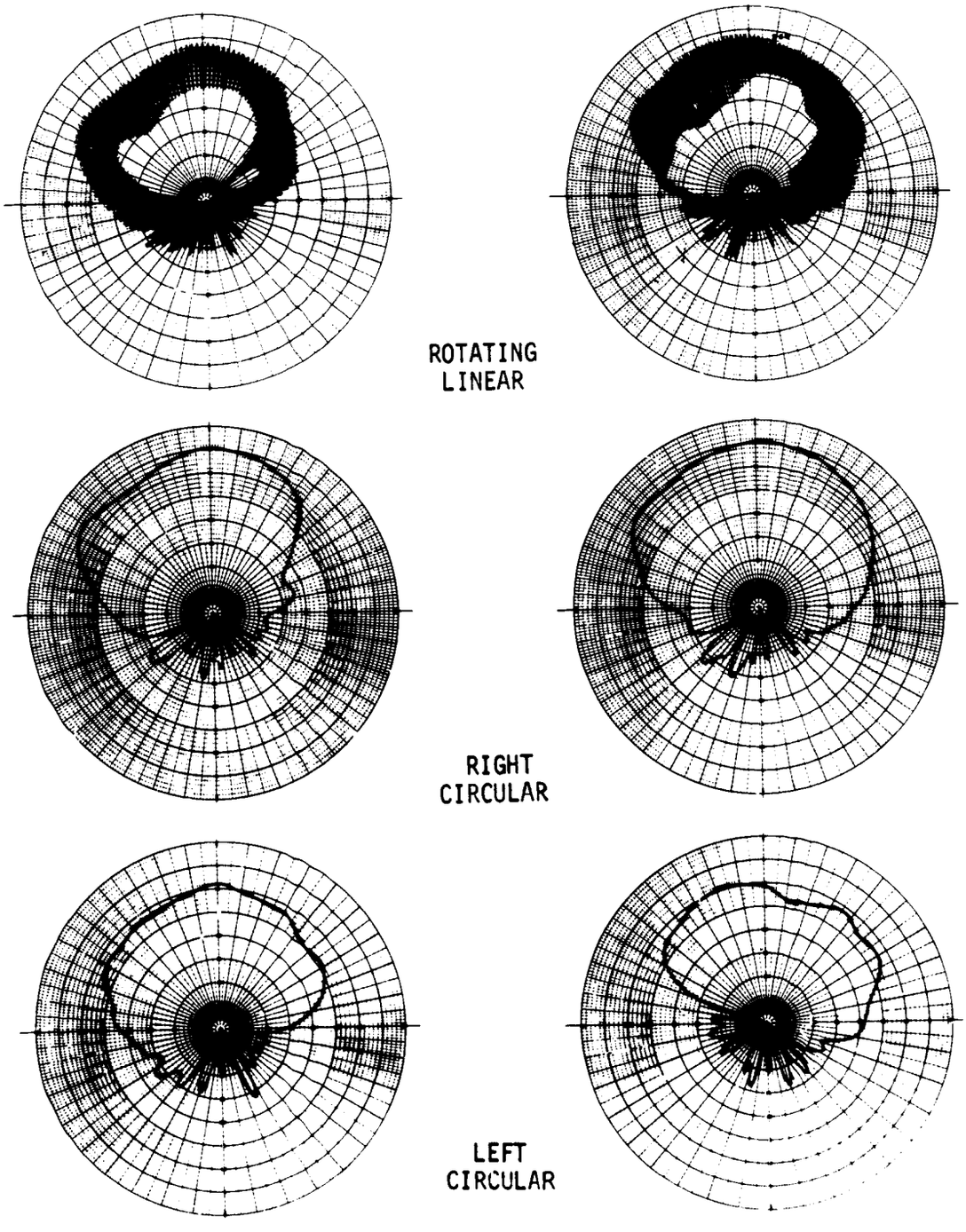

BREADBOARD UNIT RADIATION PATTERNS

FIGURE 103

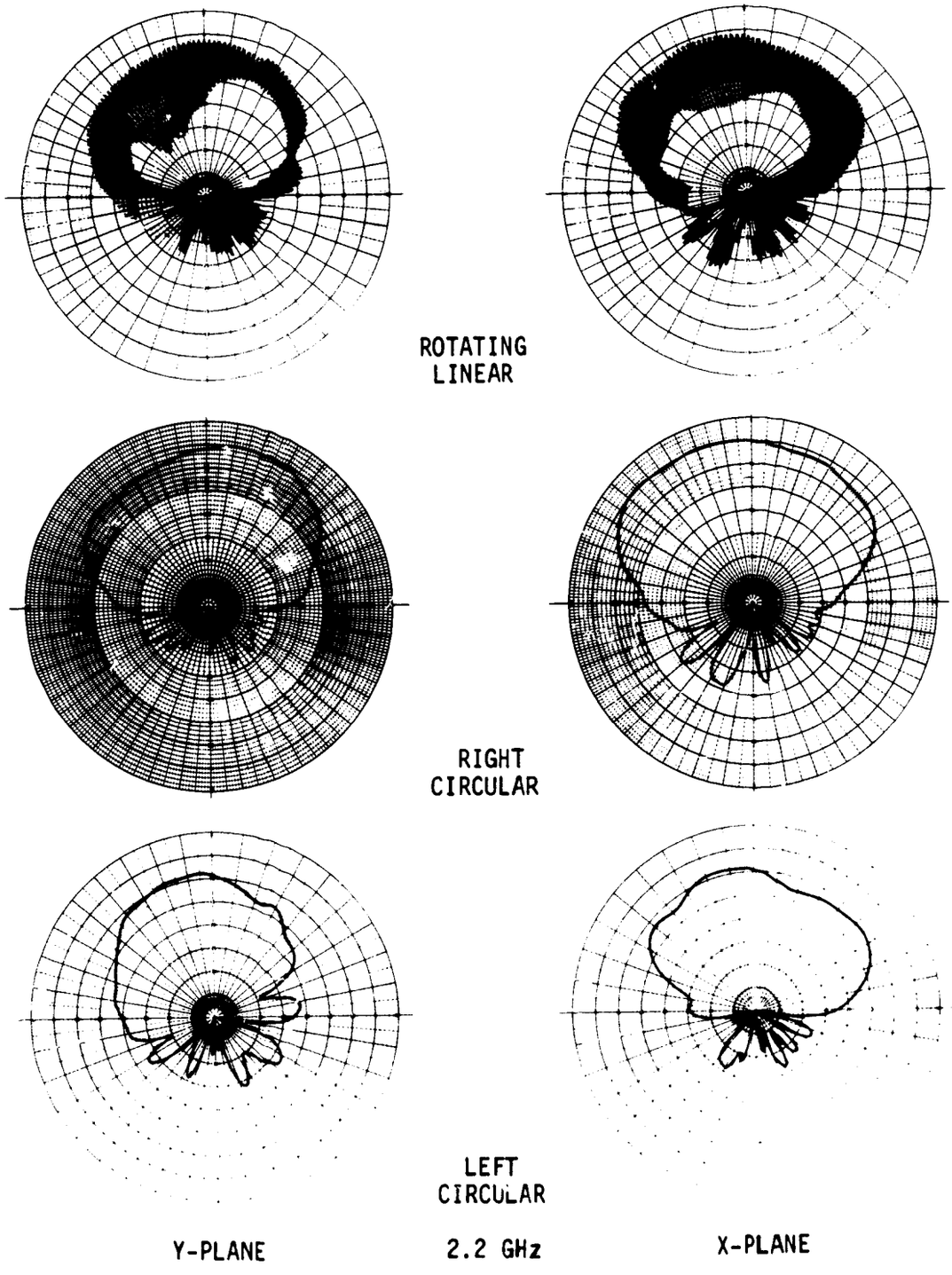

BREADBOARD UNIT RADIATION PATTERNS

FIGURE 103 (Continued)

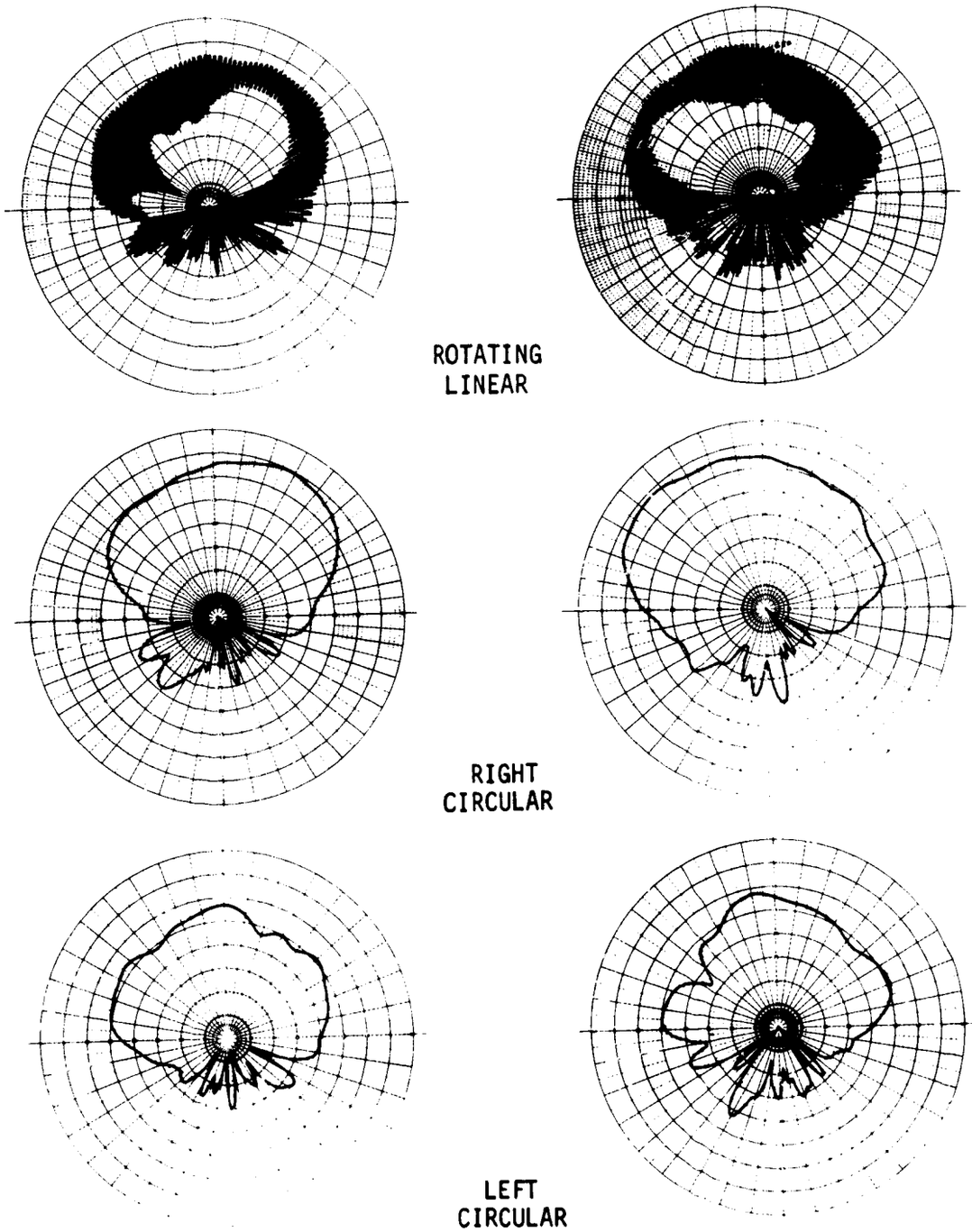

BREADBOARD UNIT RADIATION PATTERNS

FIGURE 103 (Continued)

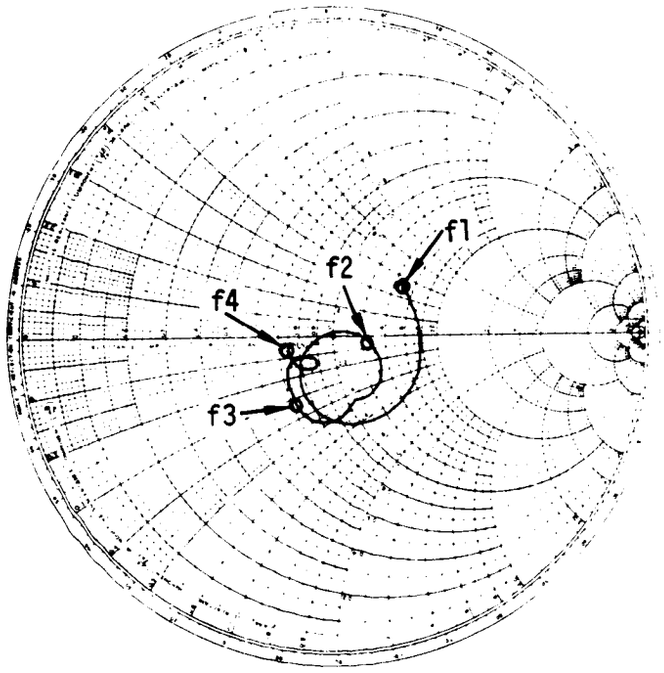

Z_o = 50 OHMS
f1 = 2.0 GHz
f2 = 2.1 GHz
f3 = 2.2 GHz
f4 = 2.3 GHz

BREADBOARD UNIT IMPEDANCE

FIGURE 104

entry temperatures. The tests consisted of radiation pattern, axial ratio and impedance measurements. The tests were performed at both NASA-JSC and MDAC-E.

Test configuration. - For the tests at NASA-JSC, the S-band antenna system, mounted in the test container assembly, was installed on a rotator unit as shown in figure 107. A Scientific Atlanta SGH-1.7 standard gain horn was mounted to the rear of the test unit. The test unit and the transmitting antennas were placed inside a small anechoic chamber with a transmission distance of 9.1 m (30 ft). For the test at MDAC-E, the test configuration used for the breadboard and prototype unit postthermal tests were the same as used for the breadboard unit tests.

The impedance measurements were made with the antenna system and test container assembly placed above the measurement equipment as shown in figure 102. The same test configuration was used at both NASA-JSC and MDAC-E.

Test techniques. - Standard radiation pattern and impedance measuring techniques were used for the thermal support. For the test at NASA-JSC a standard gain horn was used to set and record a reference level at 15 dB on the polar pattern paper. The test unit patterns were then taken with the same equipment settings. To obtain better pattern resolution, the receiver attenuation was decreased 18 to 20 dB and the patterns were retaken. Only X-plane patterns (RHC and LHC polarization) were measured. The axial ratio was measured only at $\theta = 0°$. For the tests at MDAC-E, the test technique used for the breadboard and prototype unit postthermal tests were the same as used for the breadboard unit tests.

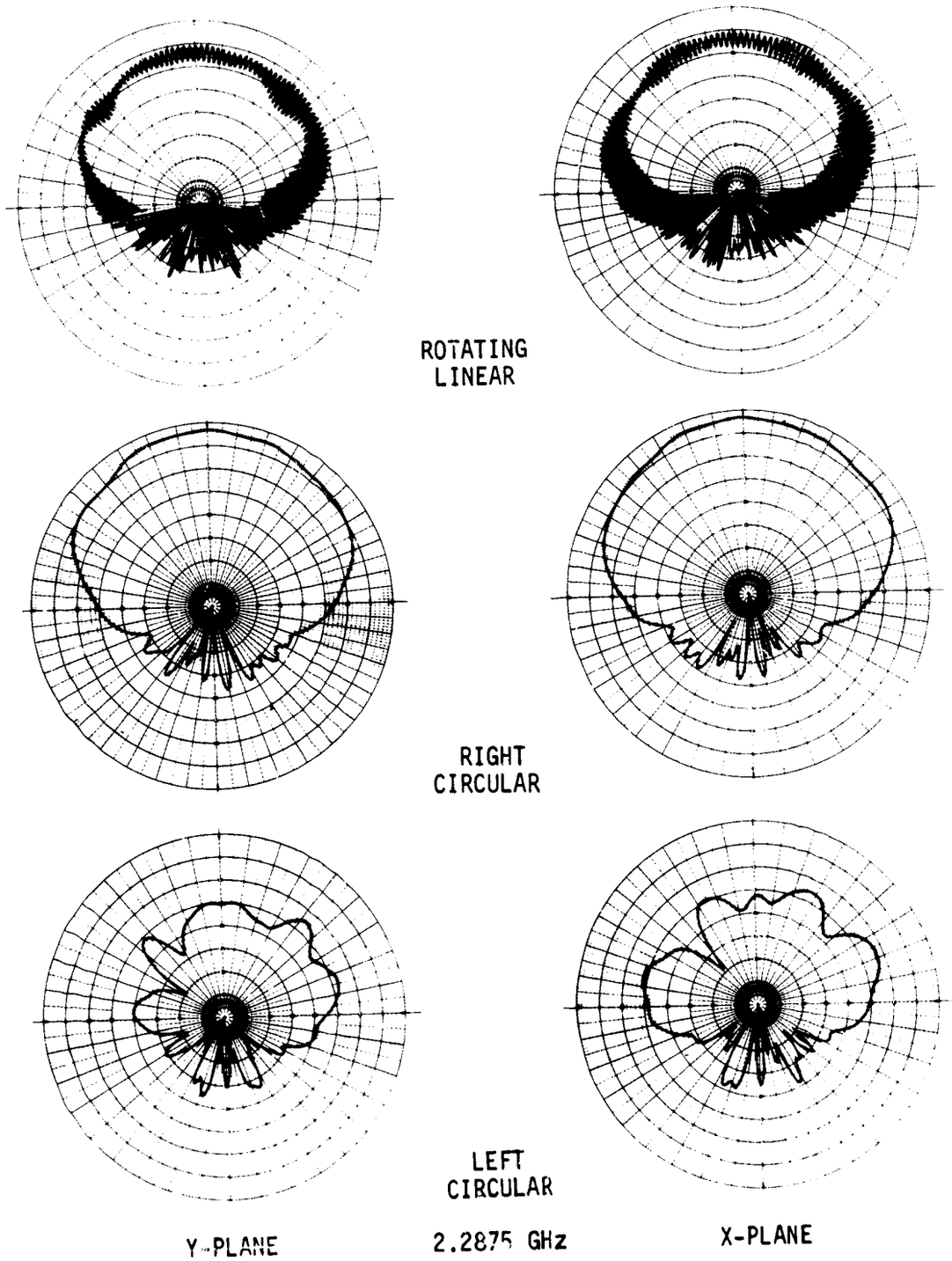

PROTOTYPE UNIT NO. 1 RADIATION PATTERNS

FIGURE 105

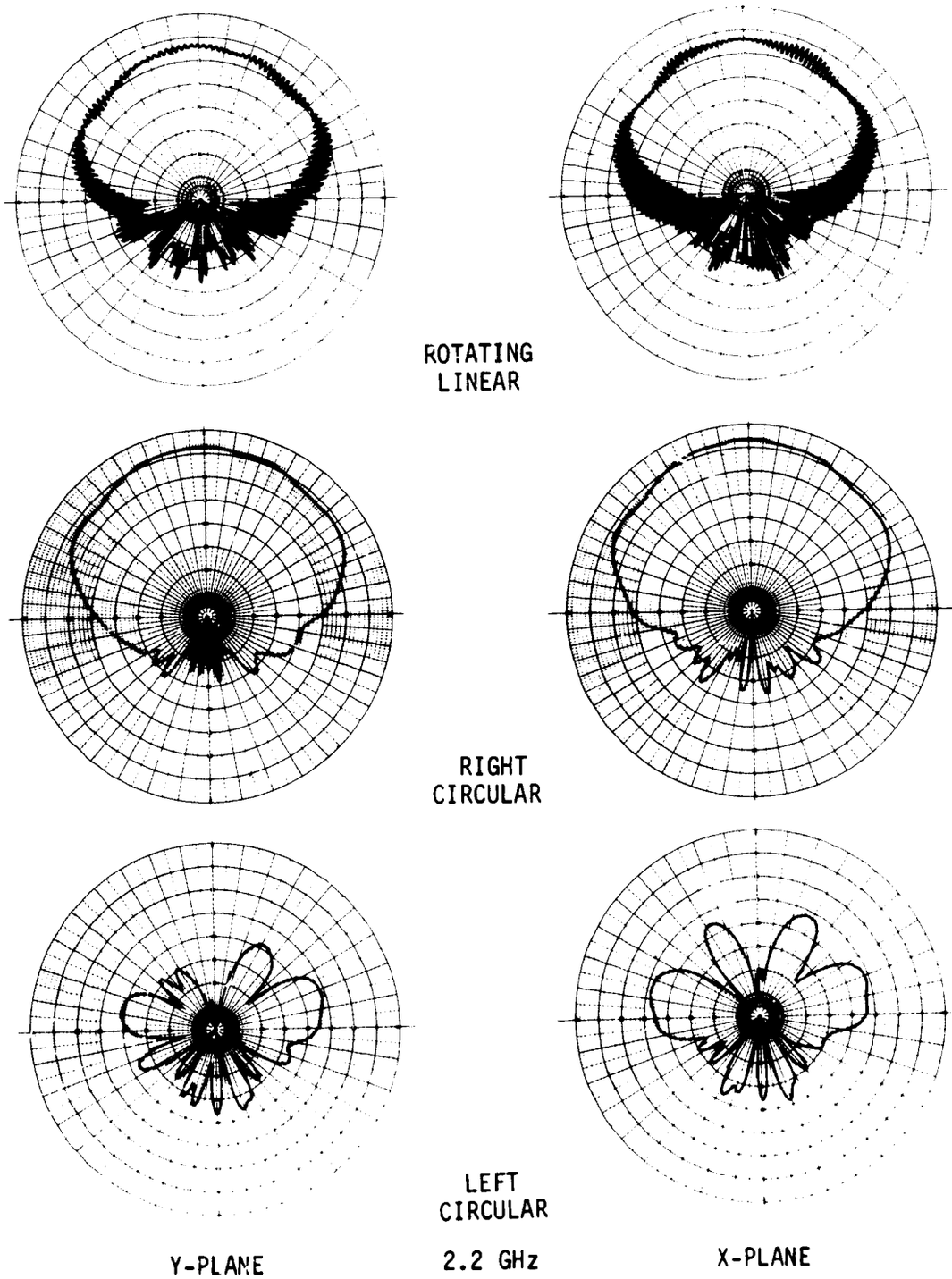

PROTOTYPE UNIT NO. 1 RADIATION PATTERNS

FIGURE 105 (Continued)

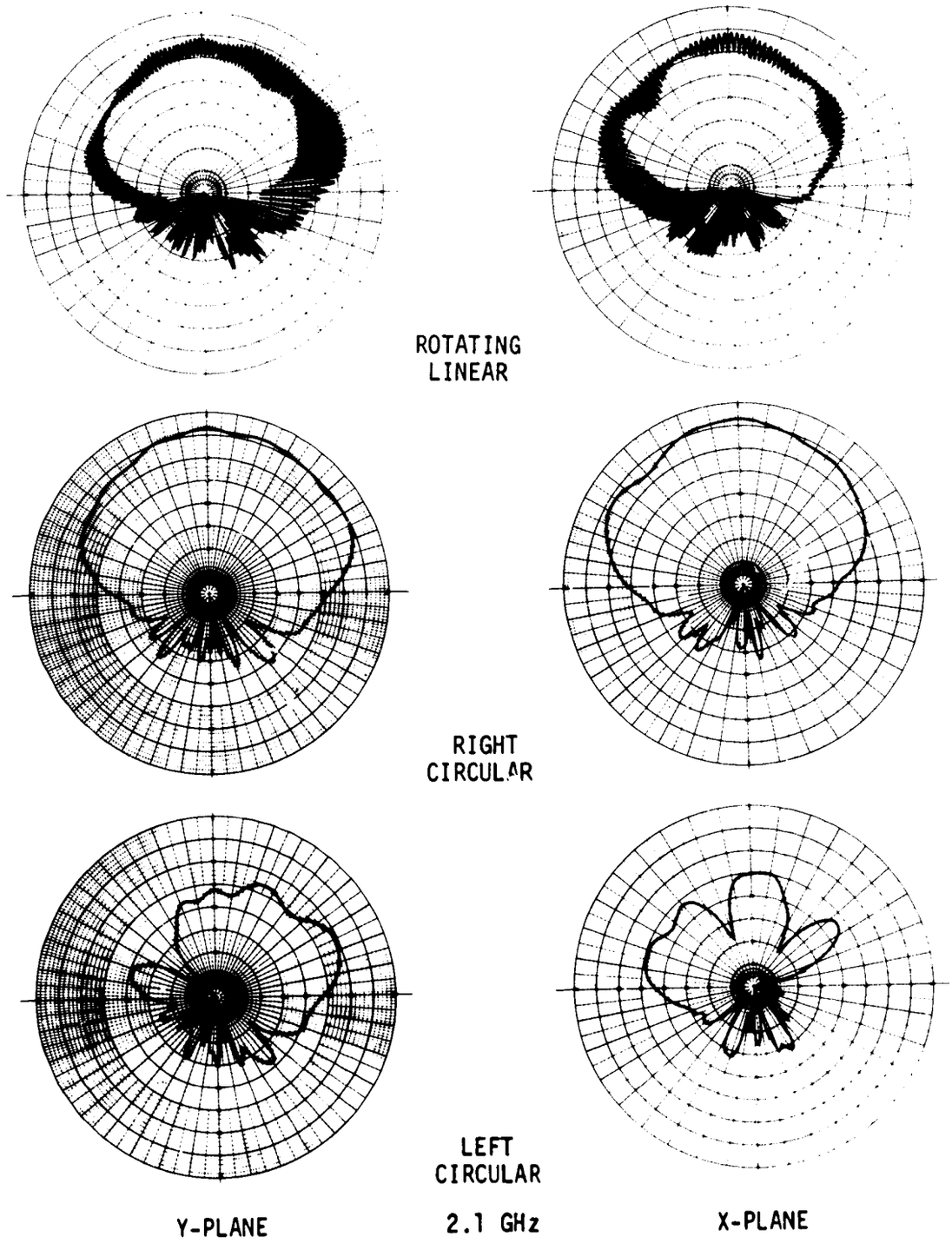

PROTOTYPE UNIT NO. 1 RADIATION PATTERNS

FIGURE 105 (Continued)

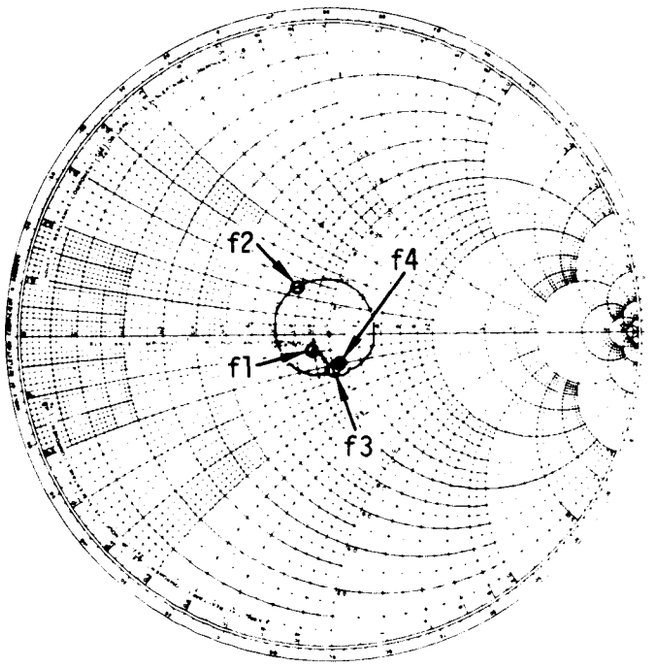

Z_o = 50 OHMS
f1 = 2.0 GHz
f2 = 2.1 GHz
f3 = 2.2 GHz
f4 = 2.3 GHz

PROTOTYPE UNIT NO. 1 IMPEDANCE

FIGURE 106

Test results - breadboard unit. - The results of the radiation pattern measurements taken before and after the thermal tests are shown in figure 108. Comparison of the pre and postthermal patterns show magnitude variations of 1.0 to 5.0 dB, but that basic pattern characteristics are unchanged. The maximum change occurred at 2.1 GHz over a sector of $\theta = \pm 50°$. At 2.2875 GHz, the maximum change was only about 1.0 dB over a smaller sector.

The results of the axial ratio measurements are shown in table XVII. The axial ratio decreased 15.2 dB at 2.1 GHz and 2.4 and 3.7 dB at 2.2 and 2.2875 GHz respectively. Subsequent testing reported in the section on EVALUATION shows that the placement of the thermocouple wire bundle behind the test article is sufficient to cause the changes discussed above. Therefore, these data should not be taken too seriously in arriving at conclusions regarding antenna performance.

The results of impedance measurements are shown in figure 109. There is only a slight change in the postthermal impedance, and no significant change in VSWR.

Postthermal electrical performance tests were conducted at MDAC-E following the thermal test at NASA-JSC. These tests were performed using the same test configuration and techniques used for the breadboard electrical tests. The results of postthermal radiation pattern measurements are shown in figure 110. The changes in pattern magnitude are smaller than those obtained

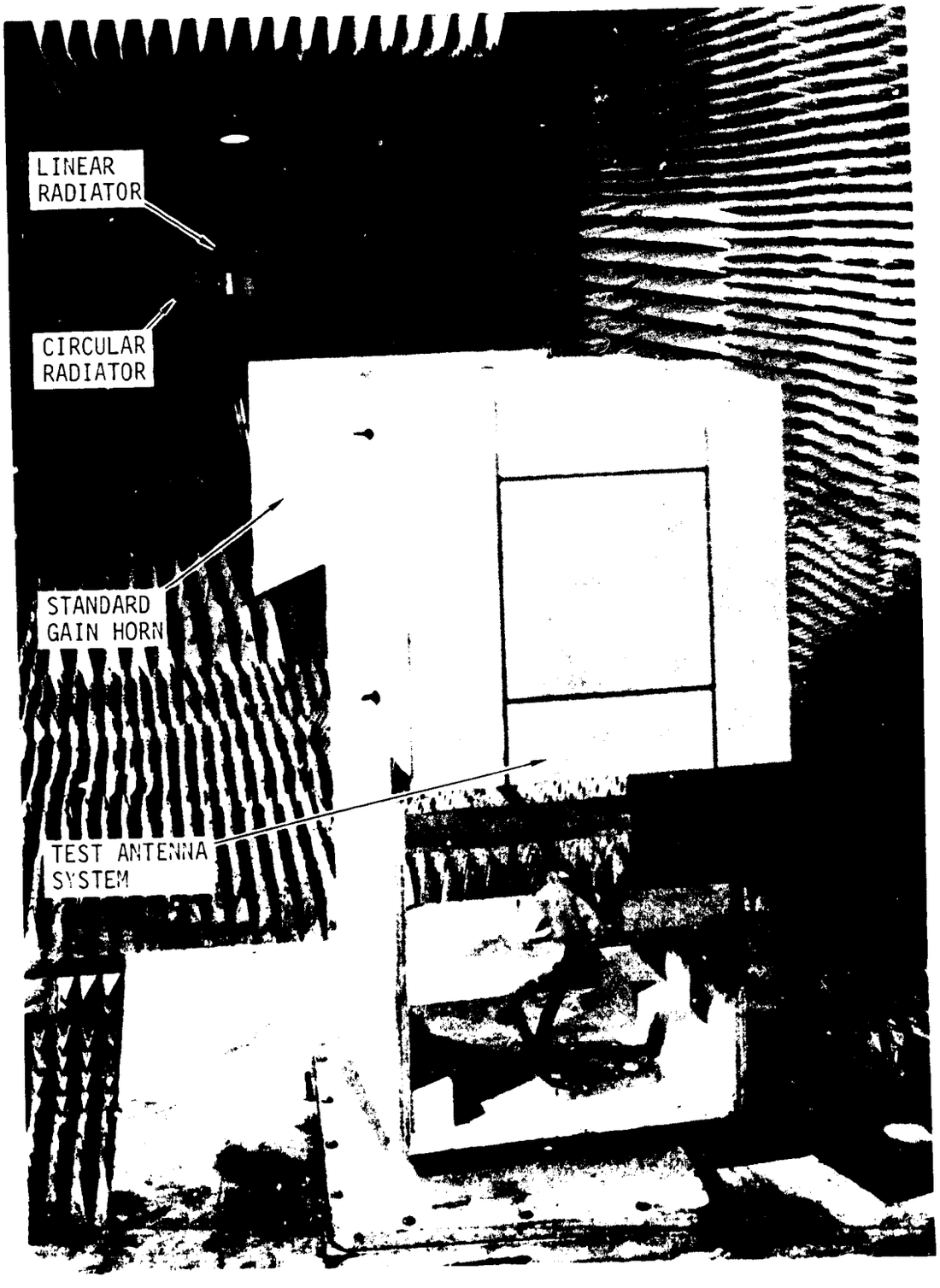

RADIATION PATTERN TEST CONFIGURATION AT NASA-JSC

FIGURE 107

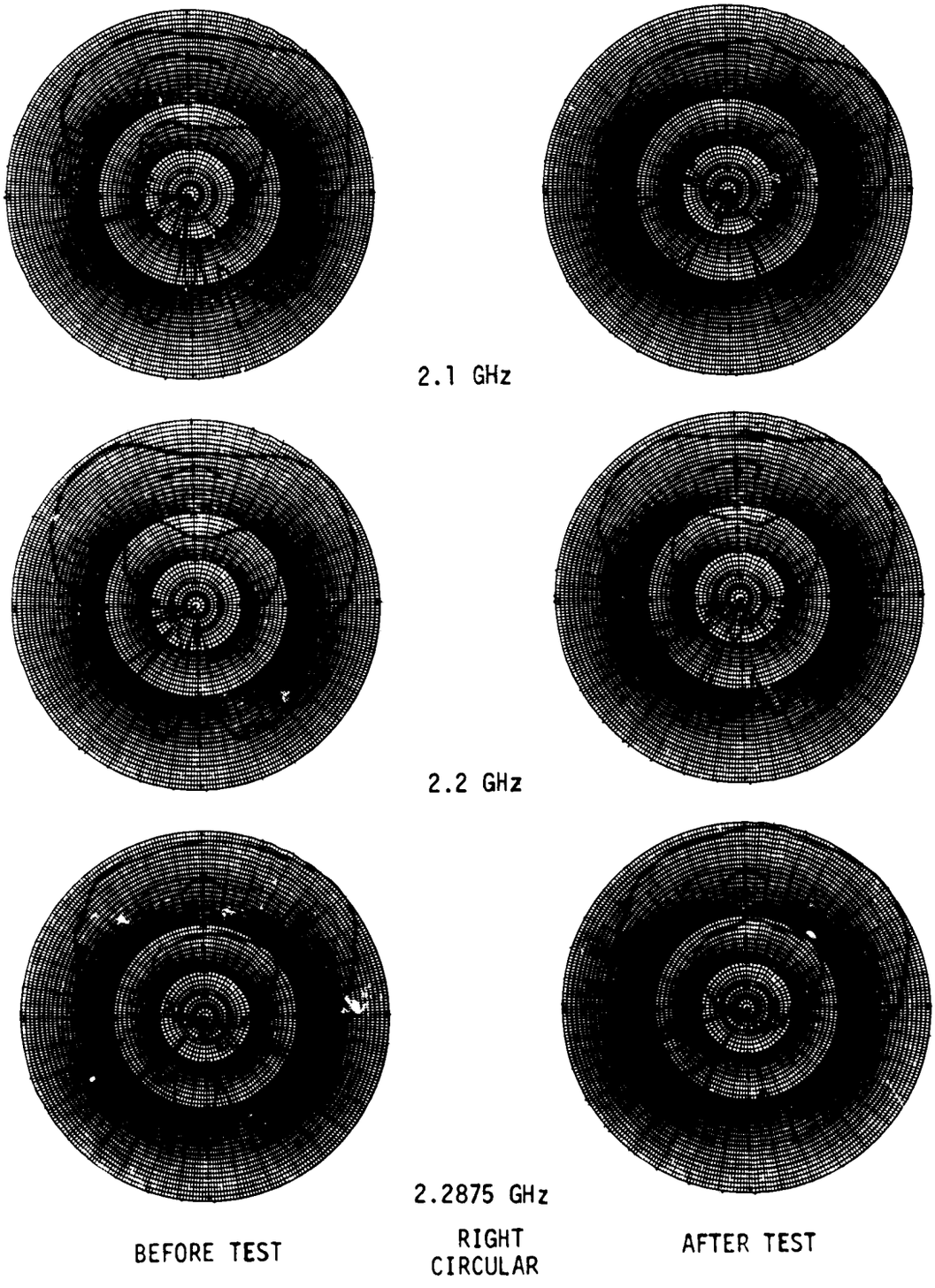

BREADBOARD UNIT RADIATION PATTERNS - EFFECTS OF HIGH TEMPERATURE

FIGURE 108

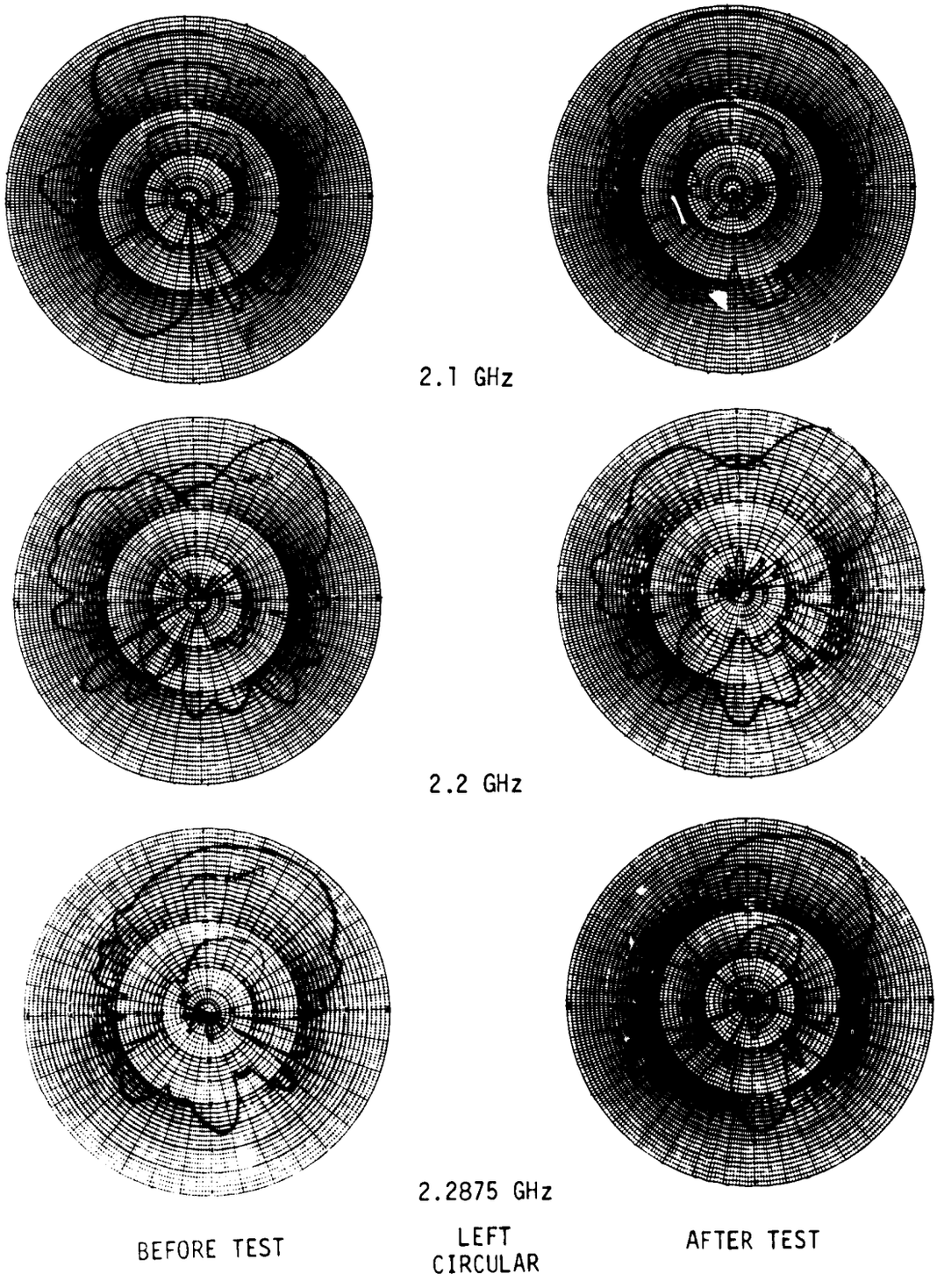

BREADBOARD UNIT RADIATION PATTERNS - EFFECTS OF HIGH TEMPERATURE

FIGURE 108 (Continued)

TABLE XVII

BREADBOARD UNIT AXIAL RATIOS - EFFECTS OF HIGH TEMPERATURE

AXIAL RATIO (dB) AT θ=0°			
FREQ (GHz)	2.1	2.2	2.2875
PRETEST	25.0	12.6	14.2
POSTTEST	9.5	10.0	11.4
ANTENNA ONLY	12.5	3.2	1.0

in the tests at NASA-JSC. However, there was a general increase in both the axial ratios and linear gain. The results of postthermal impedance measurements are shown in figure 111. Comparing these results with those obtained in the breadboard unit test, shows more change in the impedance plot than that observed in the results obtained immediately following the thermal tests (figure 109).

Test results - prototype unit. - The results of radiation pattern measurements taken before and after the first, fifth, and tenth thermal cycles is shown in figure 112. The results after the second cycle are not shown because the difference between the first and second results were insignificant. The most significant change in gain (RHC polarization) occurred after the first cycle where the circular gain decreased about 1.0 dB at 2.1 GHz and increased about 0.5 dB at 2.2875 GHz. The change in circular gain at 2.2 GHz was somewhere between these values. The results of the axial ratio measurements are shown in table XVIII. The axial ratio tends to increase at 2.1 GHz and decrease at 2.2875 GHz. The changes in LHC polarization levels are consistent with the changes in axial ratio.

The results of the impedance measurements (figure 113) show an insignificant change in the character of the impedance plot. The results of measurements after the first, second and fifth thermal cycles were omitted because they were essentially identical to the impedance measured before the first thermal test.

Postthermal electrical performance tests were also conducted at MDAC-E following the completion of thermal test at NASA-JSC. These tests were performed using the same test configuration and technique used for the prototype electrical tests. The results of the postthermal radiation pattern measurements are shown in figure 114. Compared to the prethermal patterns (figure 105) the change is very small. Small differences, less than 1.0 dB, can be found at discrete points. The LHC polarization patterns, however, show some increase in level after the thermal tests. However, the LHC polarization

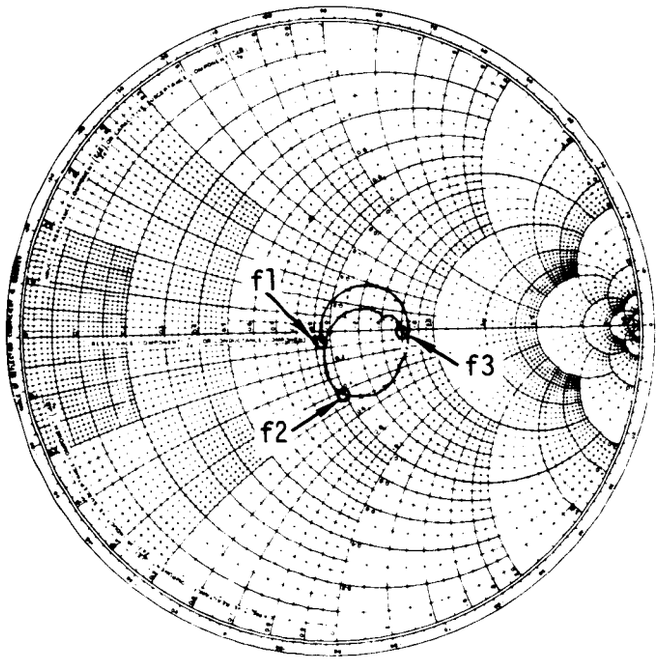

BEFORE TEST

Z_o = 50 OHMS
f1 = 2.1 GHz
f2 = 2.2 GHz
f3 = 2.3 GHz

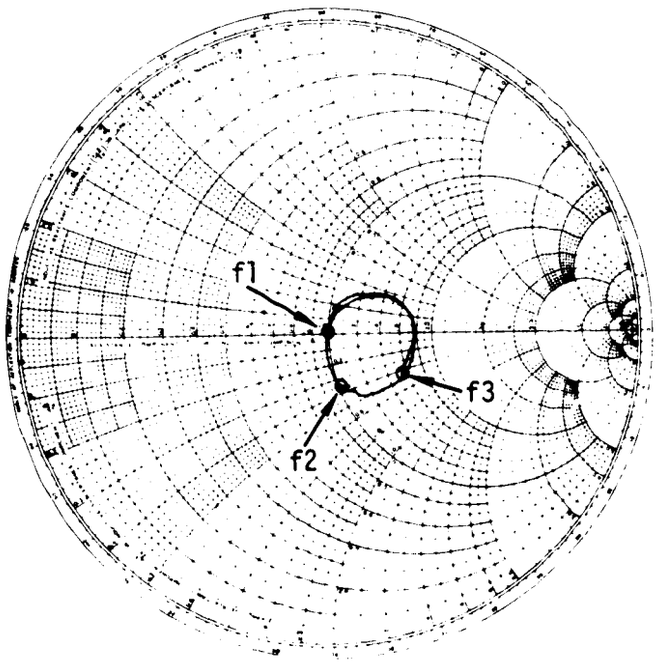

AFTER TEST

BREADBOARD UNIT IMPEDANCE - EFFECTS OF HIGH TEMPERATURES

FIGURE 109

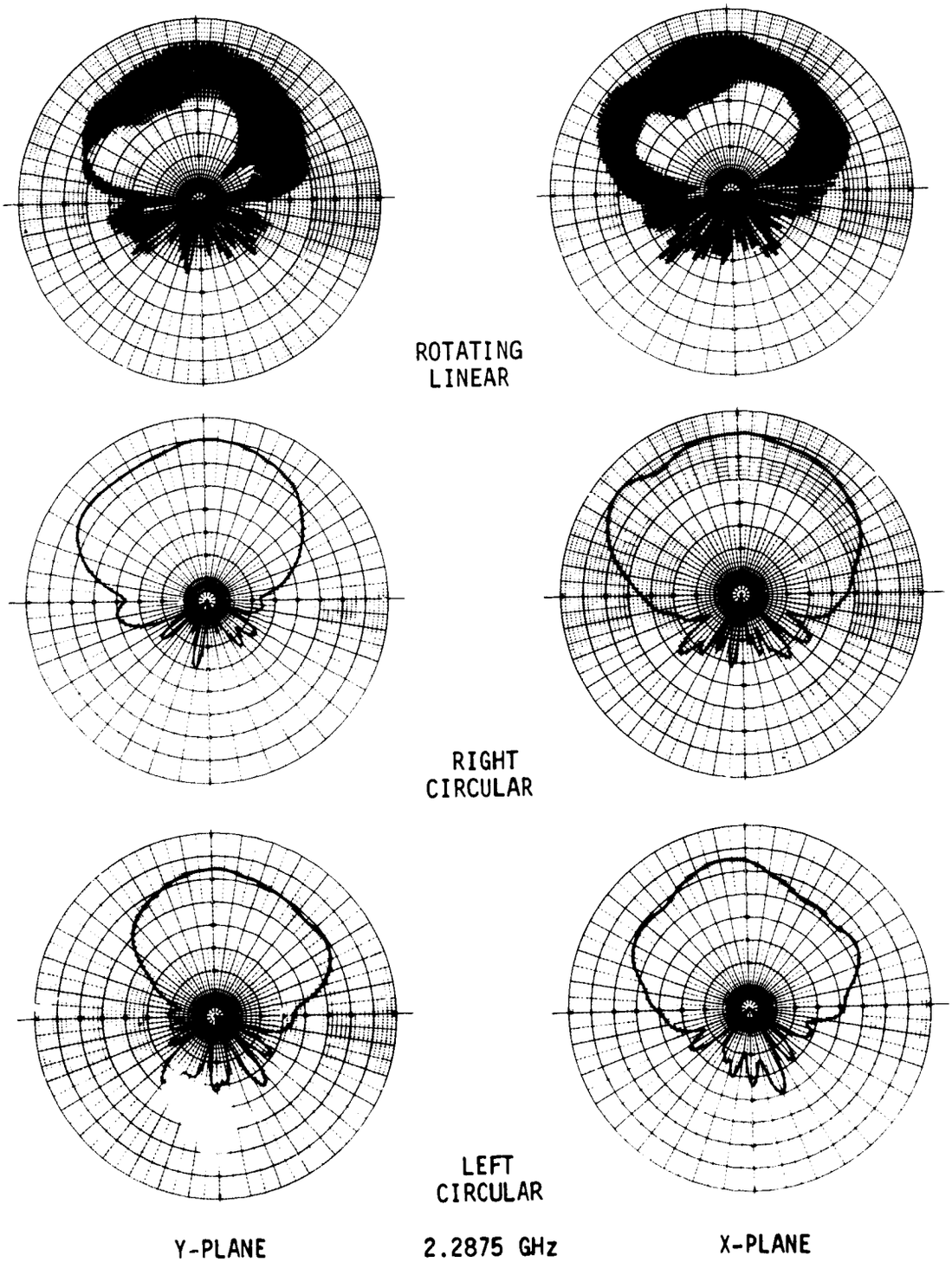

BREADBOARD UNIT RADIATION PATTERNS - POST THERMAL TEST

FIGURE 110

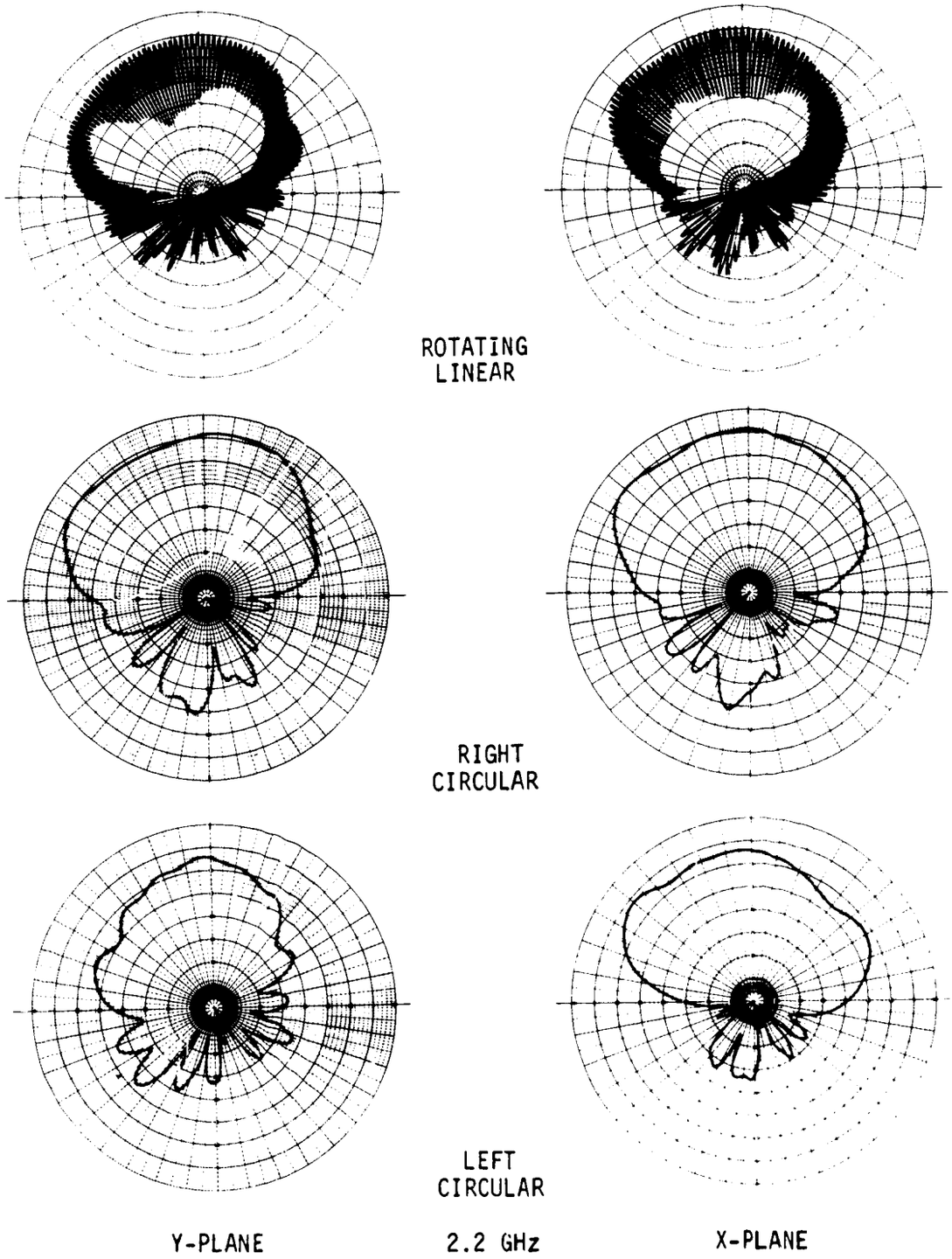

BREADBOARD UNIT RADIATION PATTERNS - POSTTHERMAL TEST

FIGURE 110 (Continued)

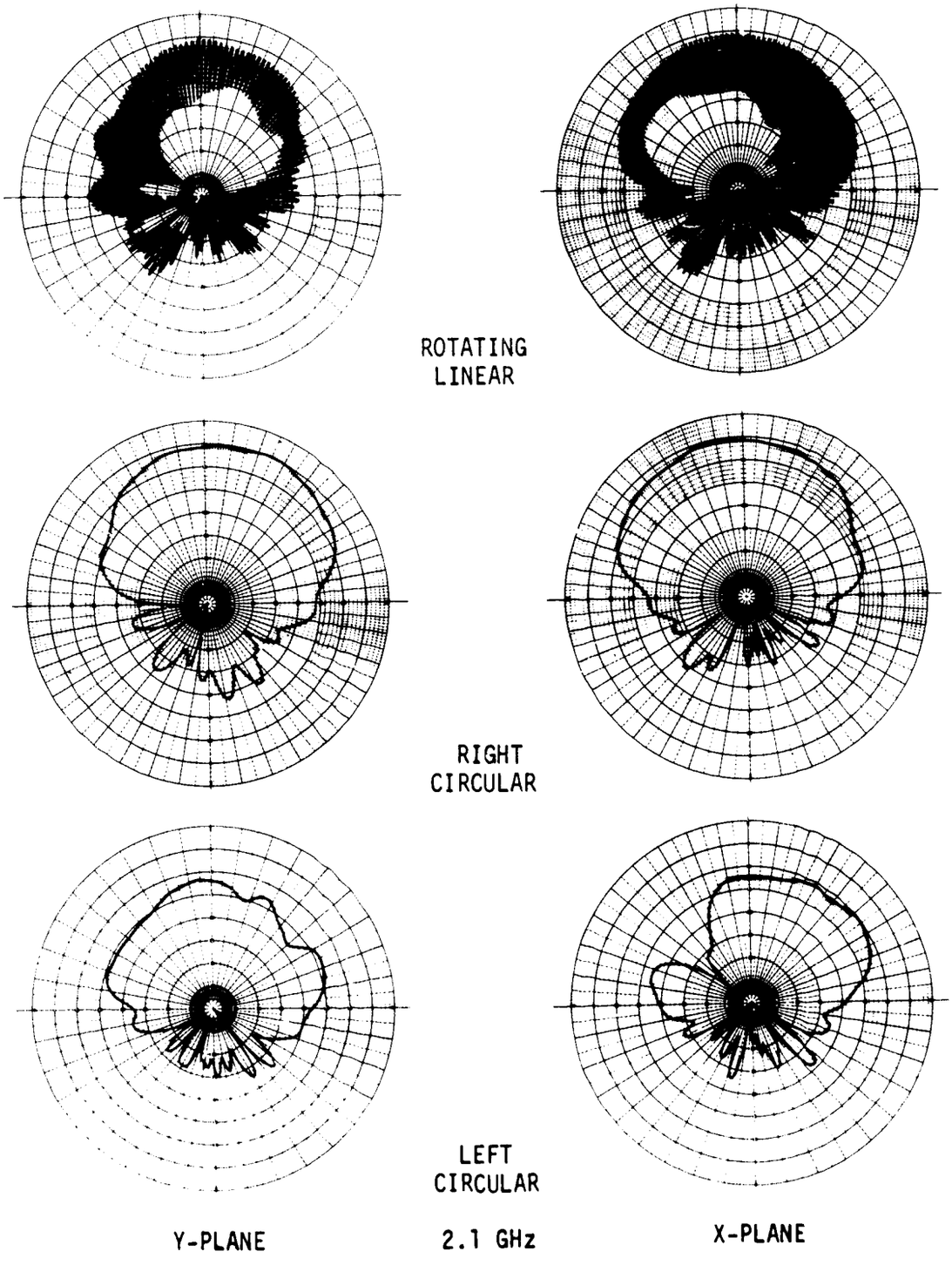

BREADBOARD UNIT RADIATION PATTERNS - POSTTHERMAL TEST

FIGURE 110 (Continued)

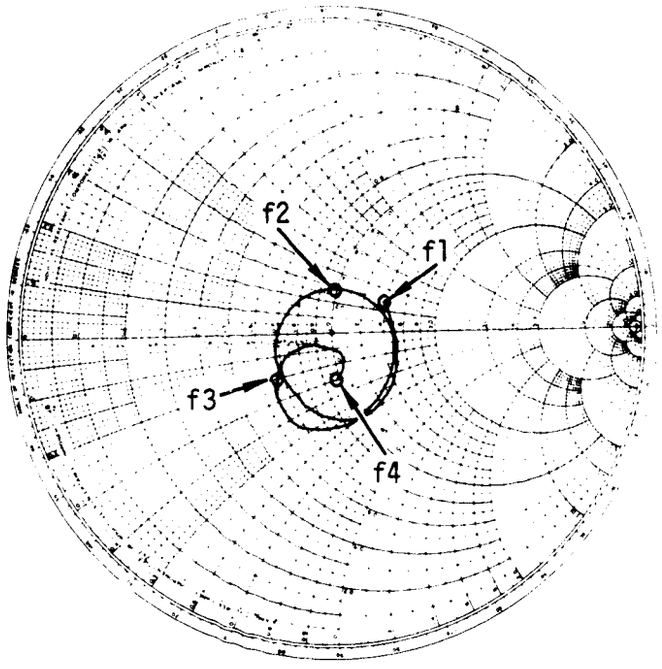

Z_o = 50 OHMS
f1 = 2.0 GHz
f2 = 2.1 GHz
f3 = 2.2 GHz
f4 = 2.3 GHz

BREADBOARD UNIT IMPEDANCE - POSTTHERMAL TEST

FIGURE 111

patterns are about 10 dB and 15 dB below the RHC polarization pattern peaks at 2.1 and 2.2875 GHz respectively. Comparison of the rotating linear polarization patterns shows small changes in the axial ratio.

The results of the impedance measurements are shown in figure 115. The shift in the position of the point for 2.1 GHz (f2) is partially due to repeatability limitations of the swept frequency generator. In the region between f1 and f3, the impedance changes very rapidly as a function of frequency. Therefore, a minor error in setting f2 could result in a significant change in the f2 marker position on the Smith Chart plot.

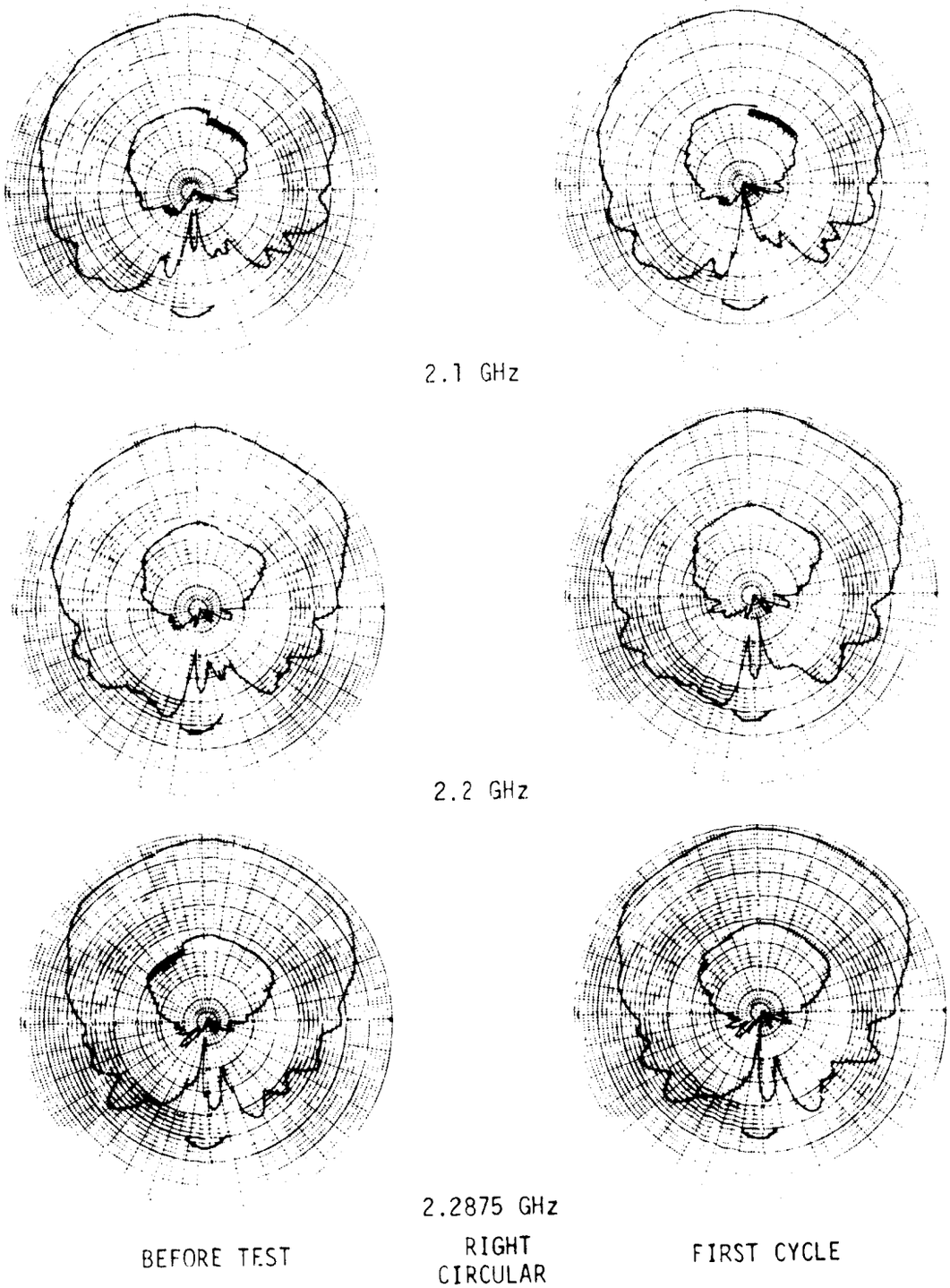

PROTOTYPE UNIT NO 1 RADIATION PATTERNS - EFFECTS OF HIGH TEMPERATURE CYCLING

FIGURE 112

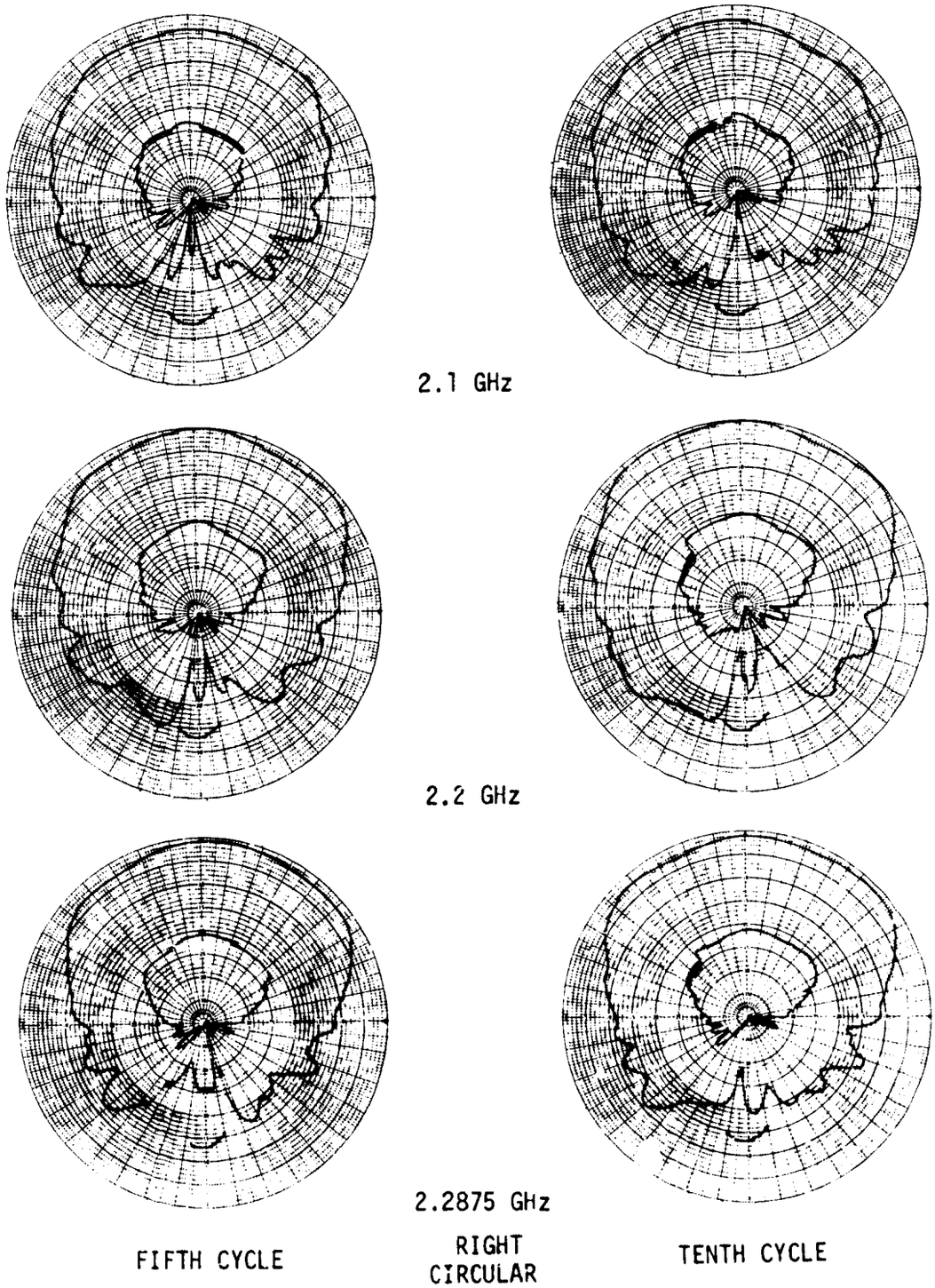

PROTOTYPE UNIT NO. 1 RADIATION PATTERNS - EFFECTS OF HIGH TEMPERATURE CYCLING

FIGURE 112 (Continued)

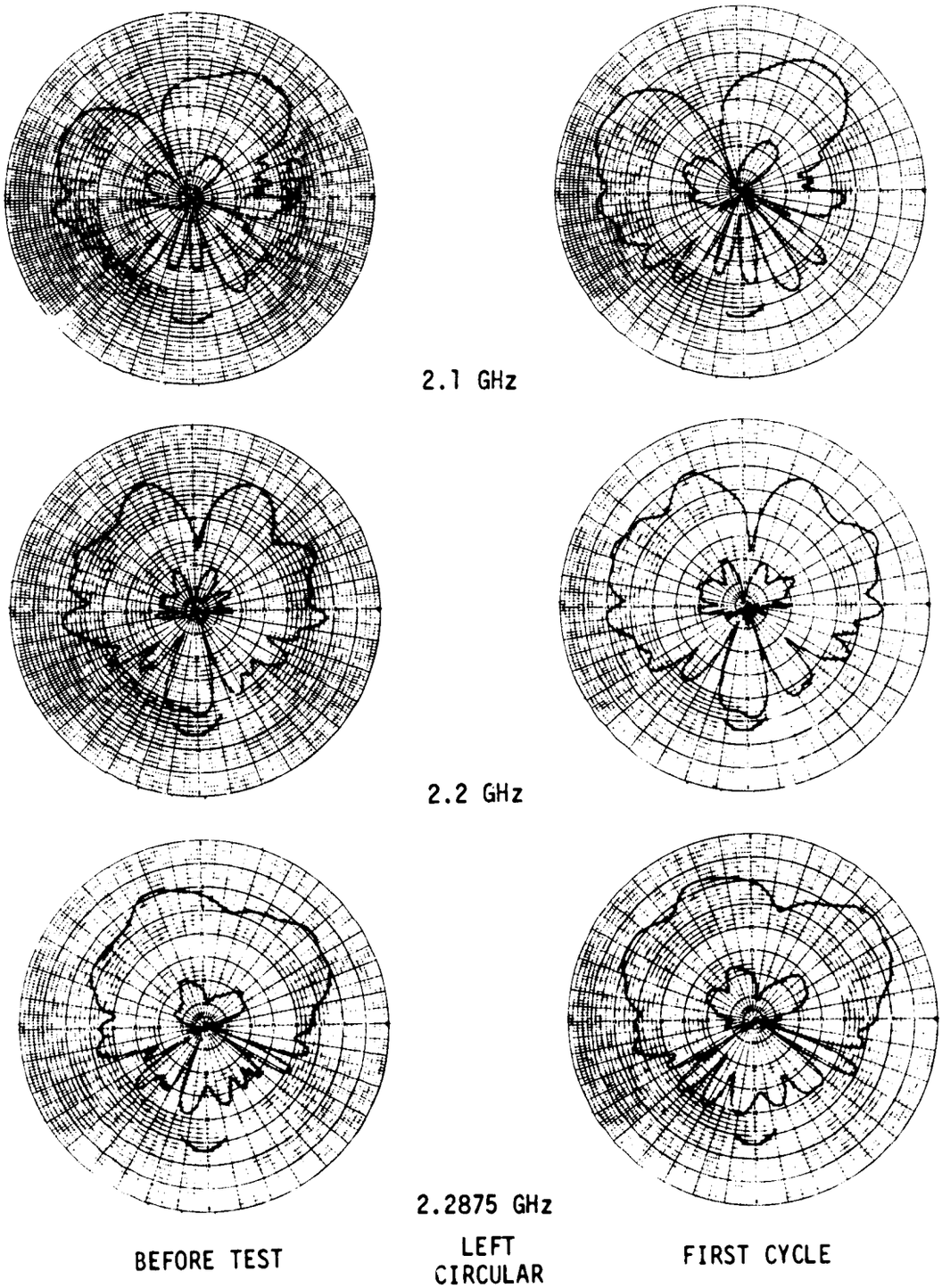

PROTOTYPE UNIT NO. 1 RADIATION PATTERNS - EFFECTS OF HIGH TEMPERATURE CYCLING

FIGURE 112 (Continued)

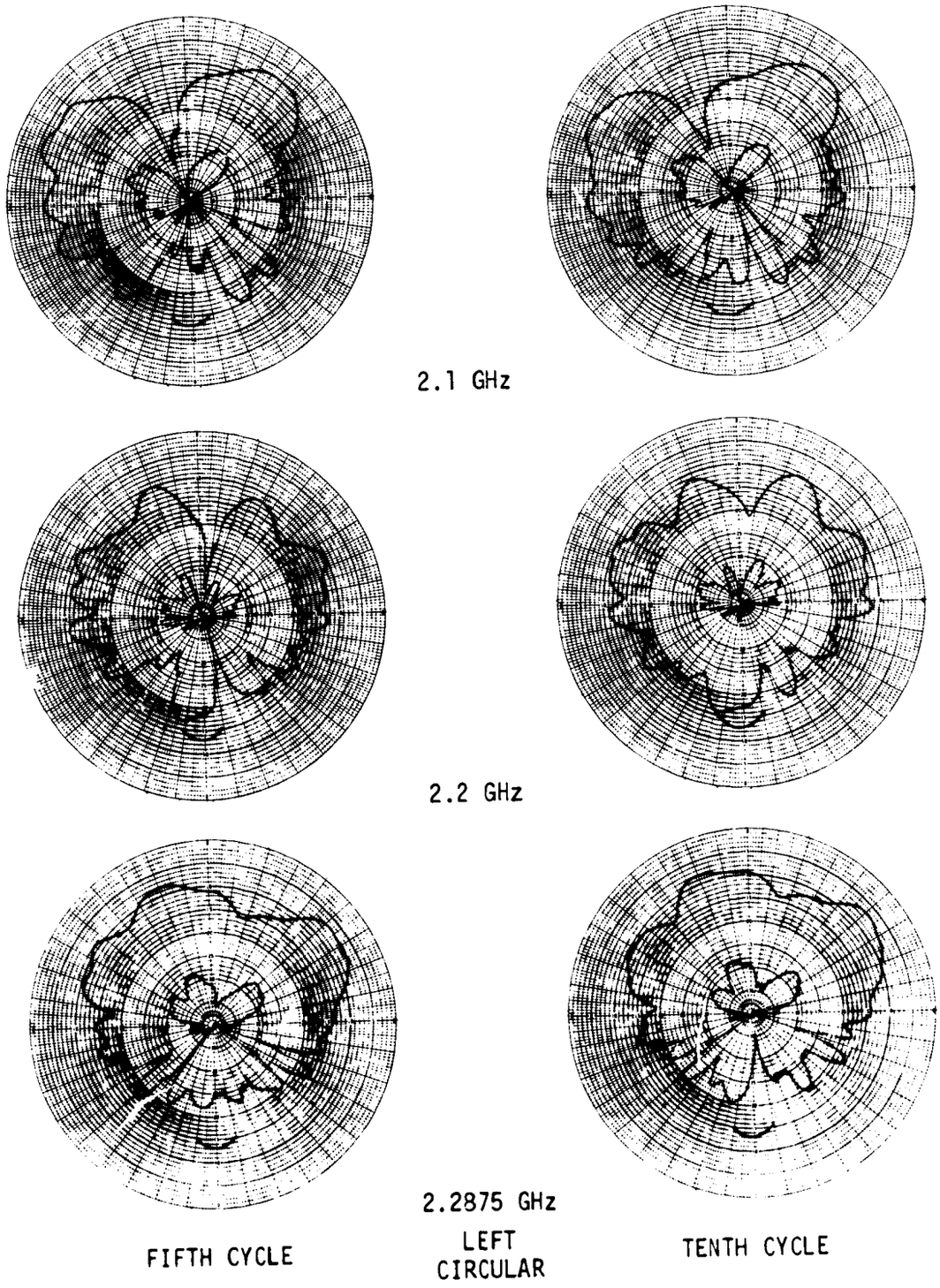

PROTOTYPE UNIT NO. 1 RADIATION PATTERNS - EFFECTS OF HIGH TEMPERATURE CYCLING

FIGURE 112 (Continued)

TABLE XVIII

PROTOTYPE UNIT NO. 1 AXIAL RATIOS - EFFECTS OF HIGH TEMPERATURE CYCLING

FREQUENCY GHz	THERMAL CYCLE				
	PRE.	FIRST	SECOND	FIFTH	TENTH
2.1	10.1 dB	12.6 dB	13.5 dB	12.2 dB	11.1 dB
2.2	6.8 dB	6.0 dB	5.9 dB	5.7 dB	4.2 dB
2.2875	4.0 dB	3.9 dB	3.7 dB	3.0 dB	3.0 dB

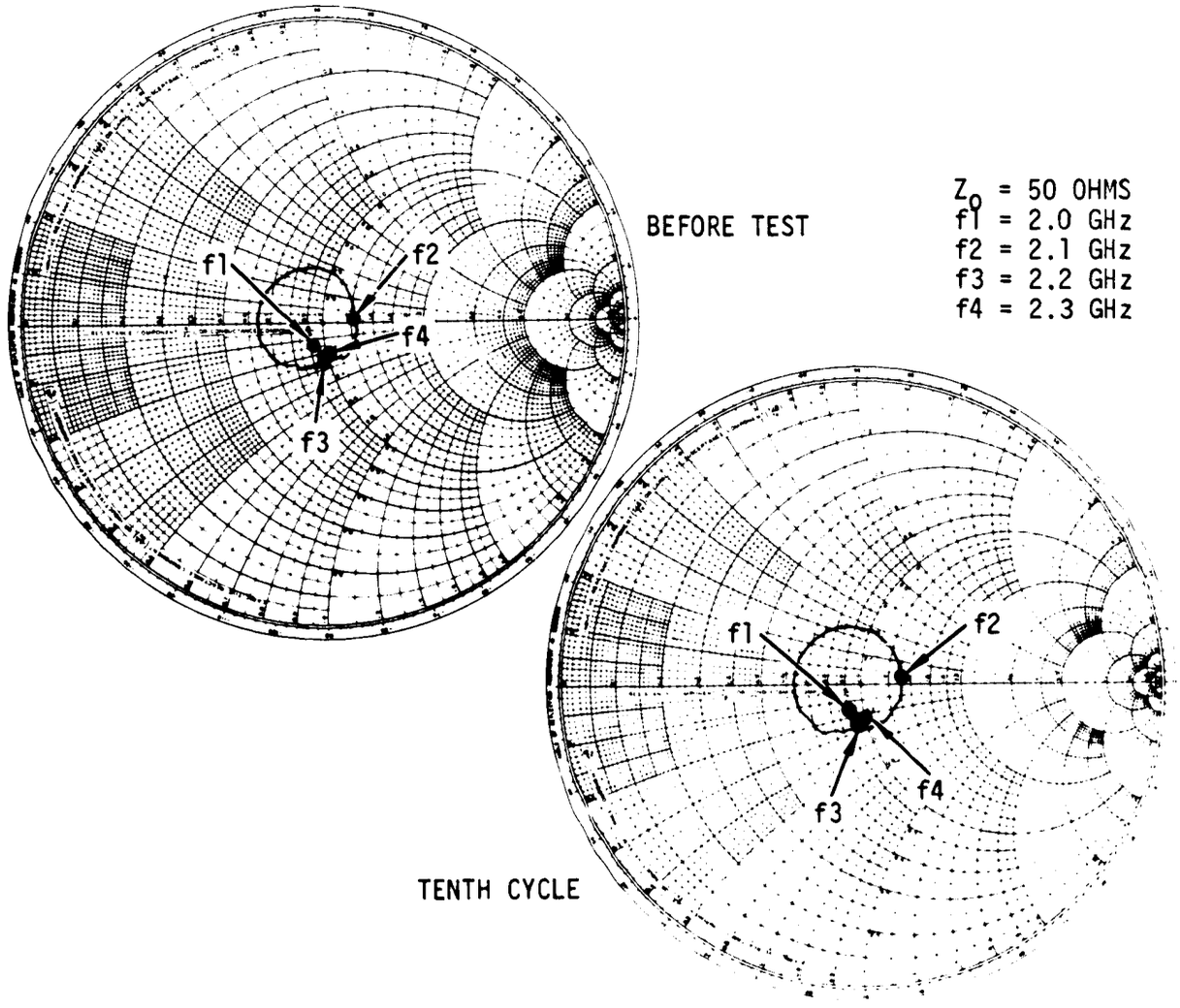

PROTOTYPE UNIT NO. 1 IMPEDANCE - EFFECTS OF HIGH TEMPERATURE CYCLING

FIGURE 113

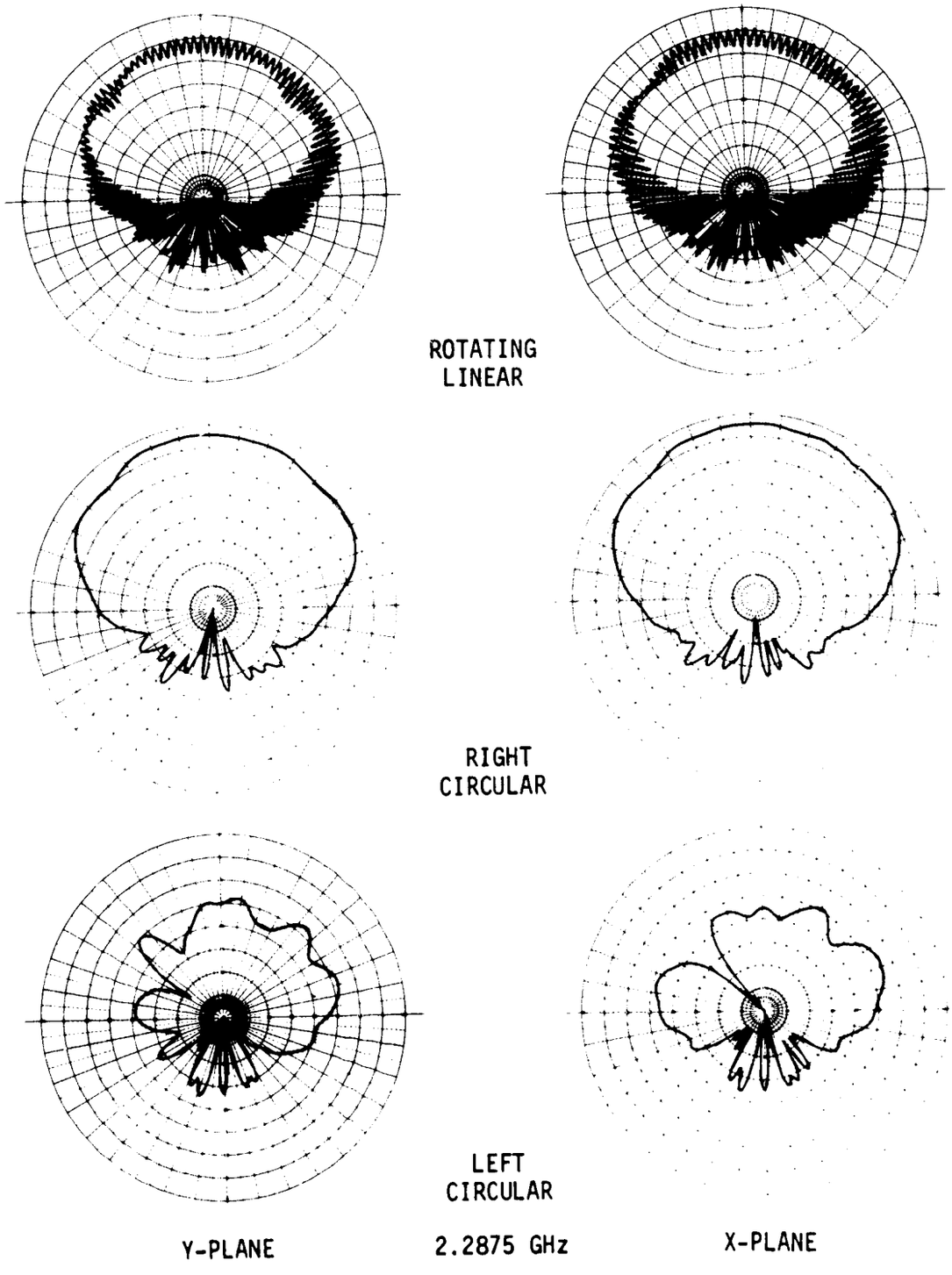

PROTOTYPE UNIT NO. 1 RADIATION PATTERNS - POSTTHERMAL REUSE TEST

FIGURE 114

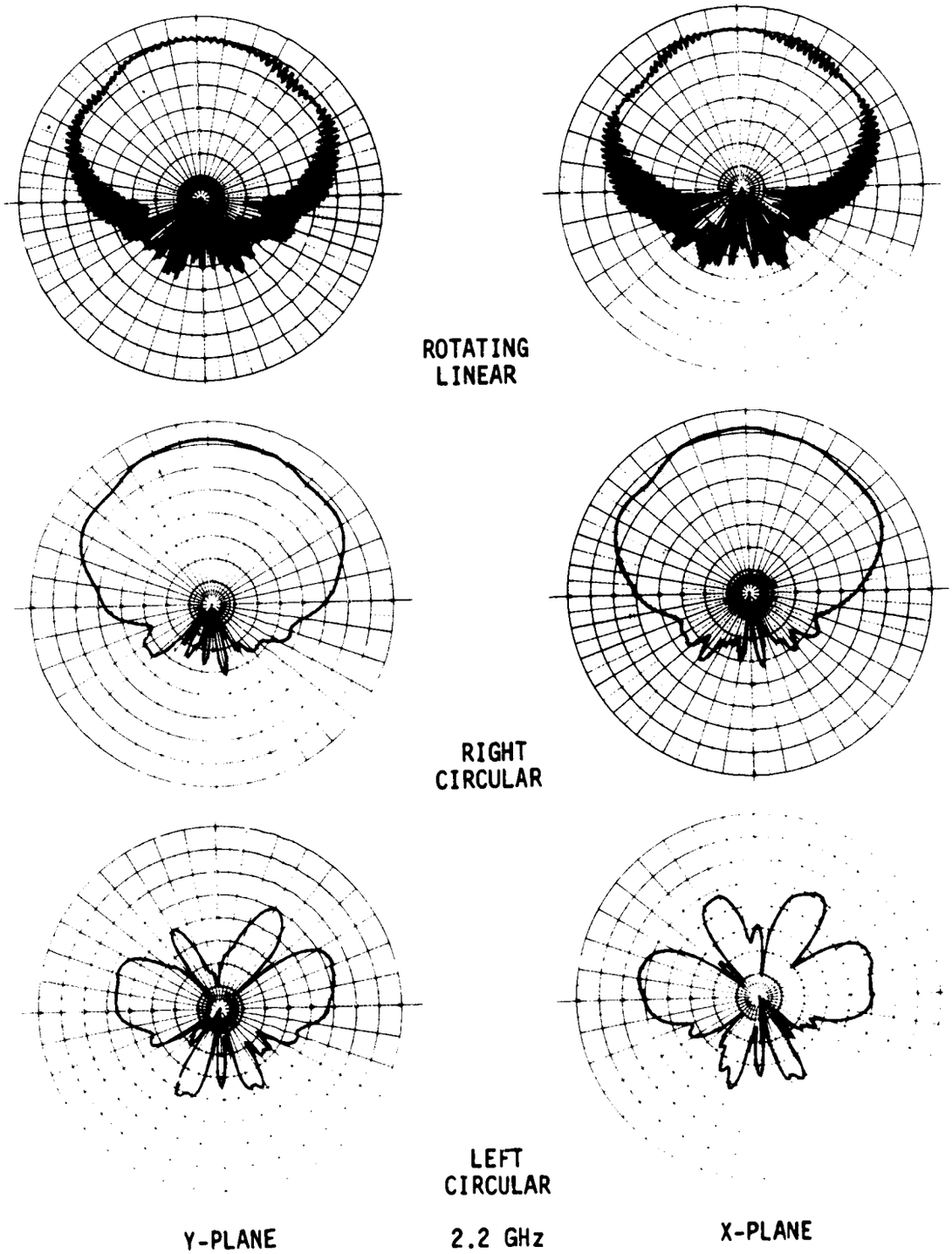

PROTOTYPE UNIT NO. 1 RADIATION PATTERNS - POST THERMAL REUSE TEST

FIGURE 114 (Continued)

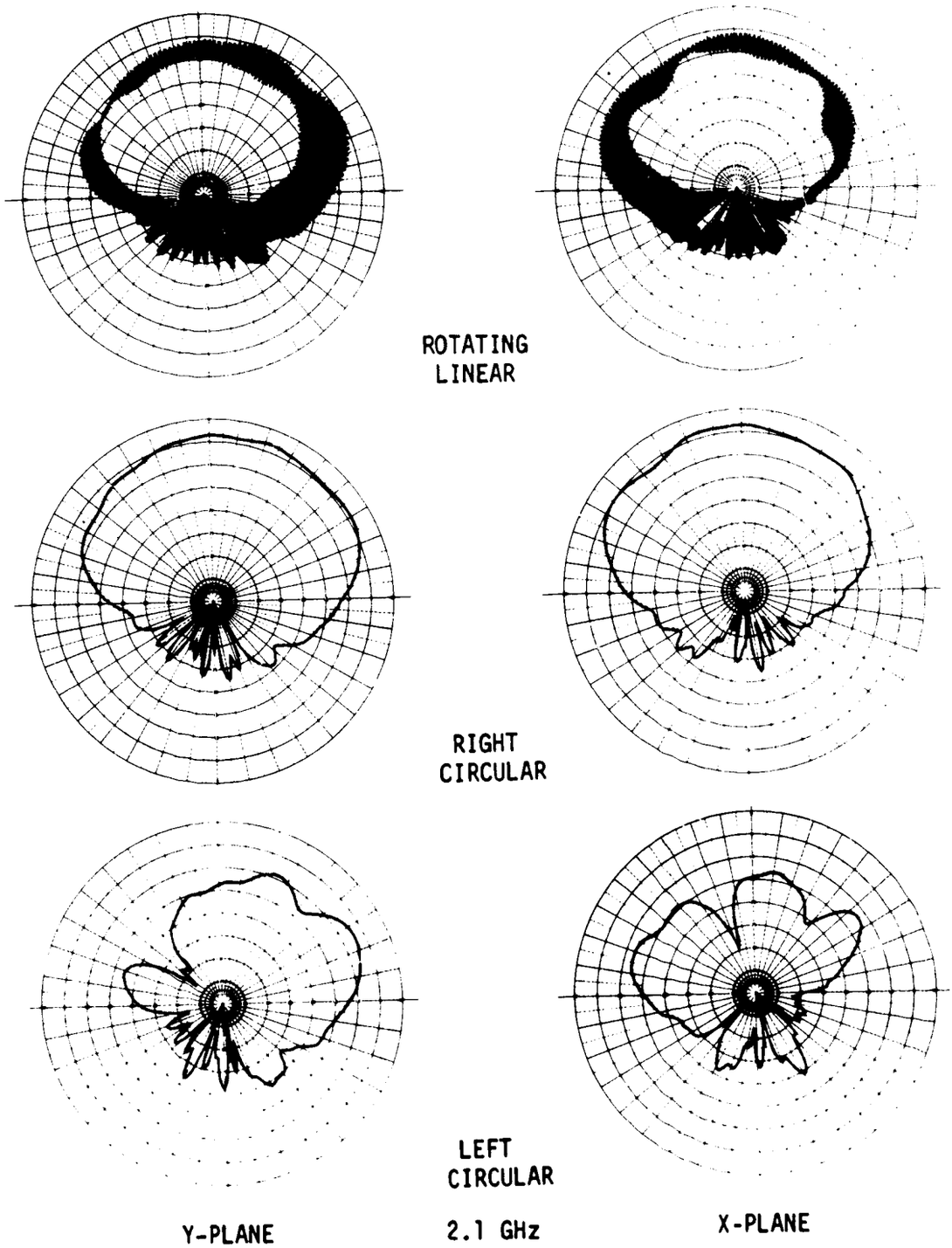

PROTOTYPE UNIT NO. 1 RADIATION PATTERNS - POSTTHERMAL REUSE TEST

FIGURE 114 (Continued)

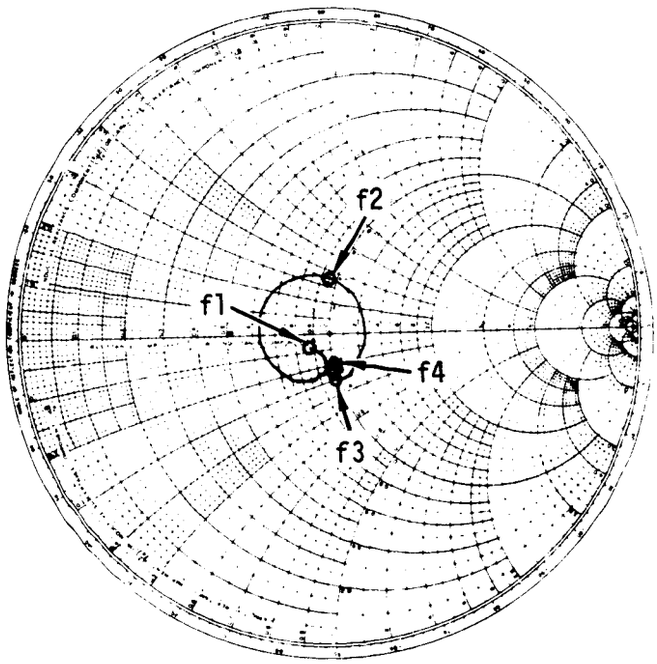

Z_o = 50 OHMS
f1 = 2.0 GHz
f2 = 2.1 GHz
f3 = 2.2 GHz
f4 = 2.3 GHz

PROTOTYPE UNIT NO. 1 IMPEDANCE - POSTTHERMAL REUSE TEST

FIGURE 115

THIS PAGE INTENTIONALLY LEFT BLANK

THERMAL TESTING

The Thermal Testing task (Task 4) consists of design temperature verification and reuse tests. The objective of this task was to validate the design approach and reuse capabilities of the S-band antenna system designed in the S-BAND ANTENNA SYSTEM DESIGN task (Task 1.2). Thermal performance was verified by exposure to a simulated entry environment with appropriate instrumentation and auxiliary physical tests. These tests were accompanied by electrical tests described in the previous section on ELECTRICAL TESTING.

The thermal testing was performed in two phases: one with a breadboard S-band antenna system and the other with a prototype S-band antenna system. The breadboard unit thermal tests were used to validate the design approach, verify temperature predictions, and contribute to the final design of the prototype unit. The prototype unit thermal tests, consisting of ten simulated high temperature entries, were used to determine the reuse capability of the prototype unit.

Facility Description

All thermal tests were conducted in the NASA-JSC 10 megawatt Atmospheric Reentry Materials and Structures Evaluation Facility (ARMSEF). ARMSEF is an arc heated continuous flow tunnel. Oxygen and nitrogen at high pressure is mixed and heated by a direct current arc. The resulting two gas (air) plasma is then expanded through a flow nozzle to the vacuum chamber. After passing through the nozzle and over the test model surface, the air plasma is cooled and pumped out of the tunnel by a four stage steam ejector vacuum pumping system supplied by a 454 g/sec (36 000 lb/hr) steam boiler. The tunnel chamber will accommodate several arc heater and nozzle configurations.

The ARMSEF capabilities that are ideally suited for the antenna system tests include: (1) large model size permitting full scale antenna and adjacent TPS hardware; (2) demonstrated capability to provide convective heating and flow shear environment for testing Orbiter thermal protection materials; (3) capability to determine influence of joint gap size and surface discontinuities with adjacent TPS; and (4) capability to sustain entry heating environments for long time periods.

The arc tunnel configuration selected for the antenna tests consists of a five megawatt multirange arc heater and a supersonic channel flow nozzle as shown in figure 11b. The calibration plate has been removed to show the antenna system test unit in place. The channel flow nozzle expands from throat dimensions of 2.54 x 5.08 cm (1.00 x 2.00 in.) to accommodate a 32.2 x 32.2 cm (12.7 x 12.7 in.) test sample surface area. Two walls are 5.08 cm (2.00 in.) apart and are parallel; the other two walls have a total divergence angle of 20°. An opening on each parallel side wall is provided; one for the test model and the other for a calibration plate. The walls are made of chromium copper alloy 182 and are water cooled. The reflection off a mirror on top of the

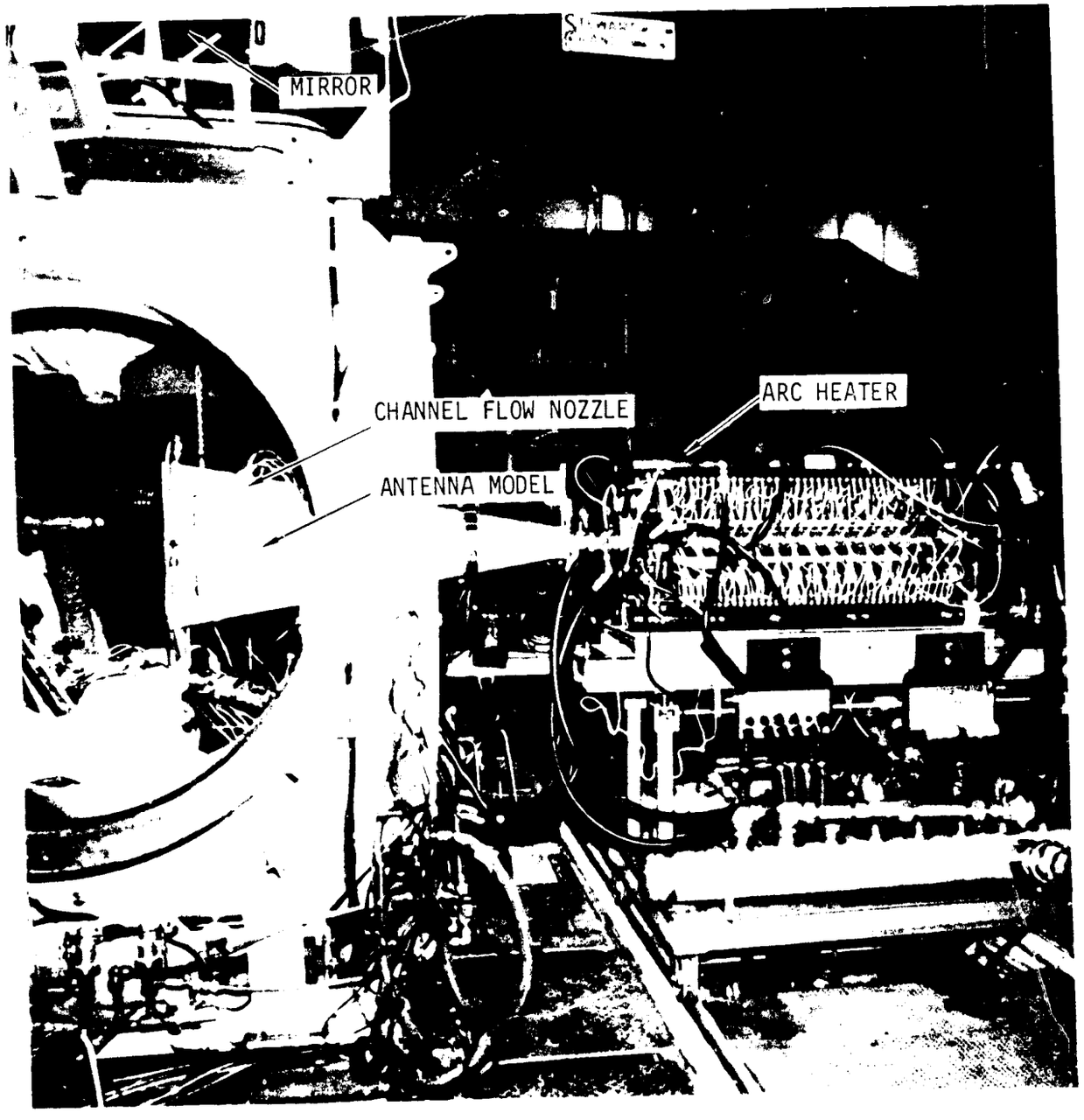

NASA-JSC 10 MEGAWATT ARMSEF ARC TUNNEL

FIGURE 116

test chamber (figure 116) and TV cameras were used to monitor the uniformity of plasma flow from the channel flow nozzle exit. The model surface could not be viewed during testing because of the poor view angle through the narrow nozzle exit to the model.

Test Installation

The channel nozzle test configuration (figure 75) was used for both the breadboard and prototype unit thermal tests. The water cooled cover assembly is mounted to the side of the channel flow nozzle and normally remains in place through a test series. The hinged door on the backside of the cover assembly provides quick access for both installation and removal of the test model. The test model consists of a breadboard or prototype test unit installed in the test container assembly. The test container assembly: (1) provides a mounting fixture; (2) provides thermal isolation; and (3) facilitates handling. The test model, mounting brackets and cover assembly are shown in figure 117. The test model is positioned in the cover assembly so the surface of the test model is flush with the inner wall of the channel flow nozzle. The final installation into the channel nozzle is shown in figures 118, 119, and 120. Fiberfrax fibrous insulation was packed between the edges of the test unit surface and channel wall opening to prevent leakage of the hot plasma to the back of the test model.

TG-15000 insulation (figure 120) was placed behind the aluminum skin stringer structure to simulate the internal Orbiter thermal control insulation.

Series D Cannon copper connectors (figure 120) were used to interface the test unit thermocouple leads with a cable which was connected to the facility thermocouple reference junction box. This permitted the test article to be removed from the cover assembly without disturbing the facility test model instrumentation setup. The copper connectors were considered adequate because of the constant temperature environment immediately around the connectors.

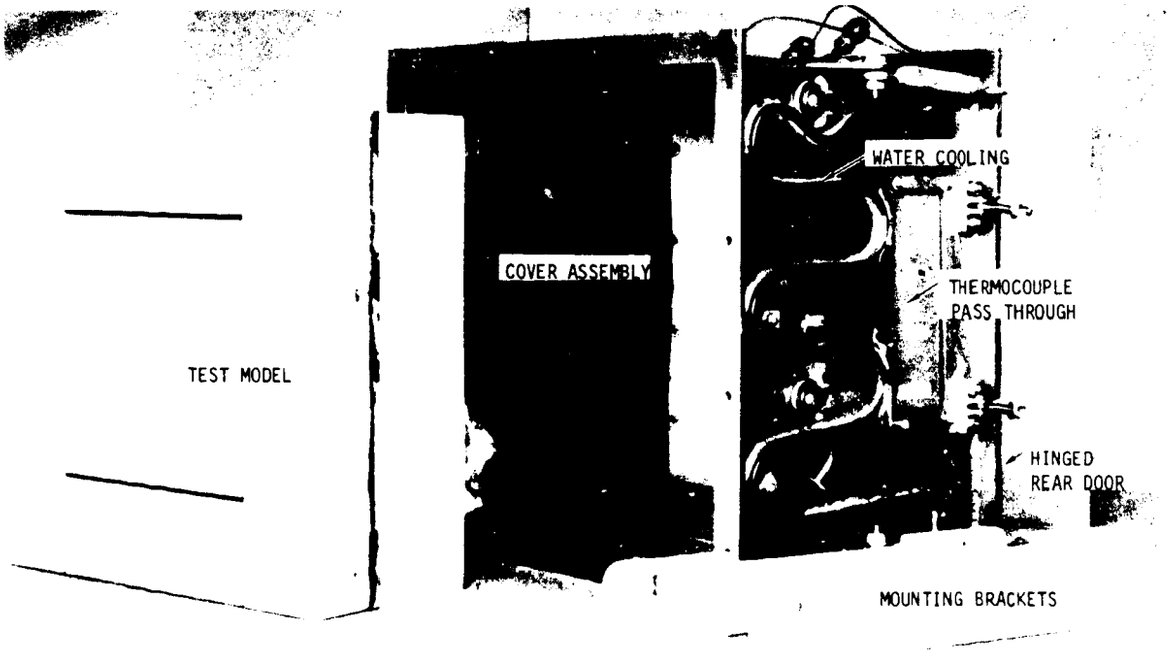

TEST COMPONENTS

FIGURE 117

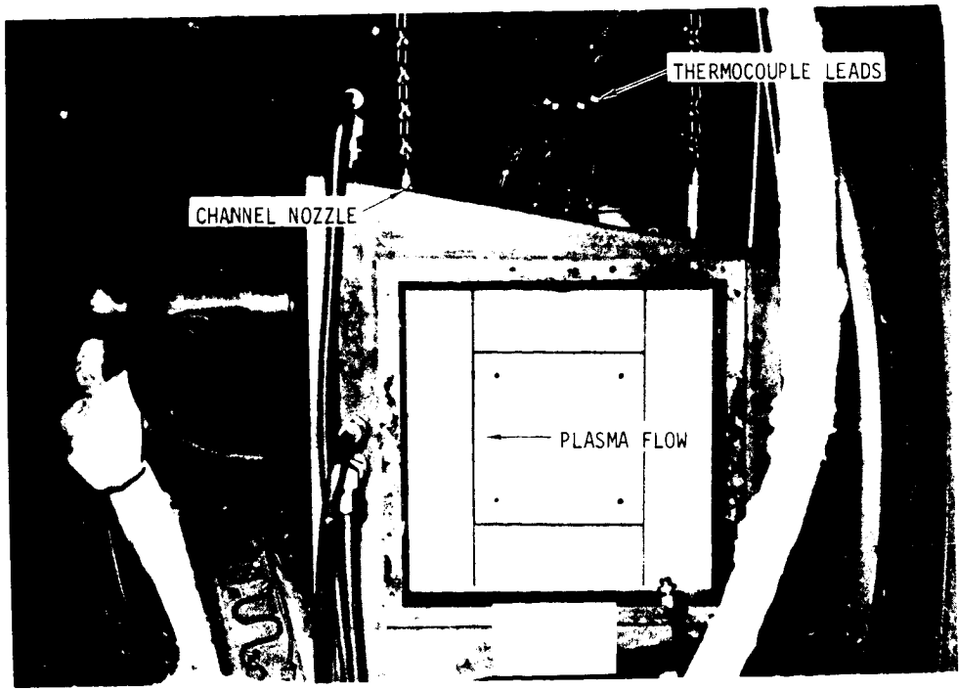

TEST INSTALLATION - SIDE VIEW THROUGH CALIBRATION PORT

FIGURE 118

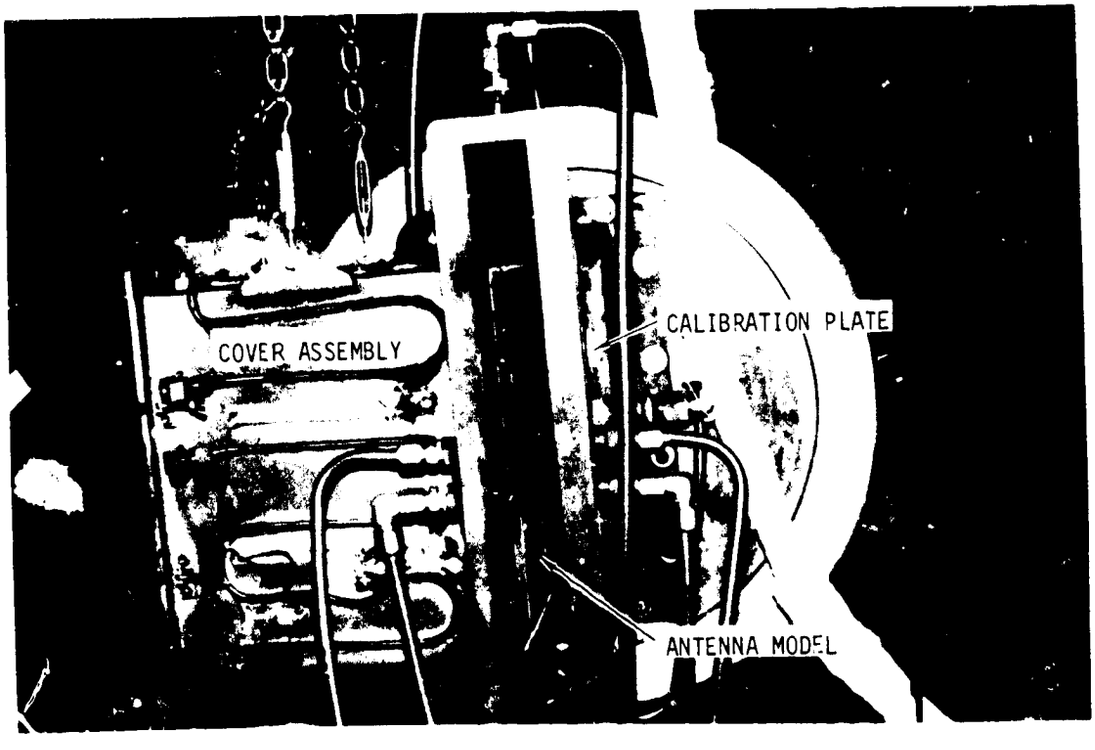

TEST INSTALLATION - END VIEW

FIGURE 119

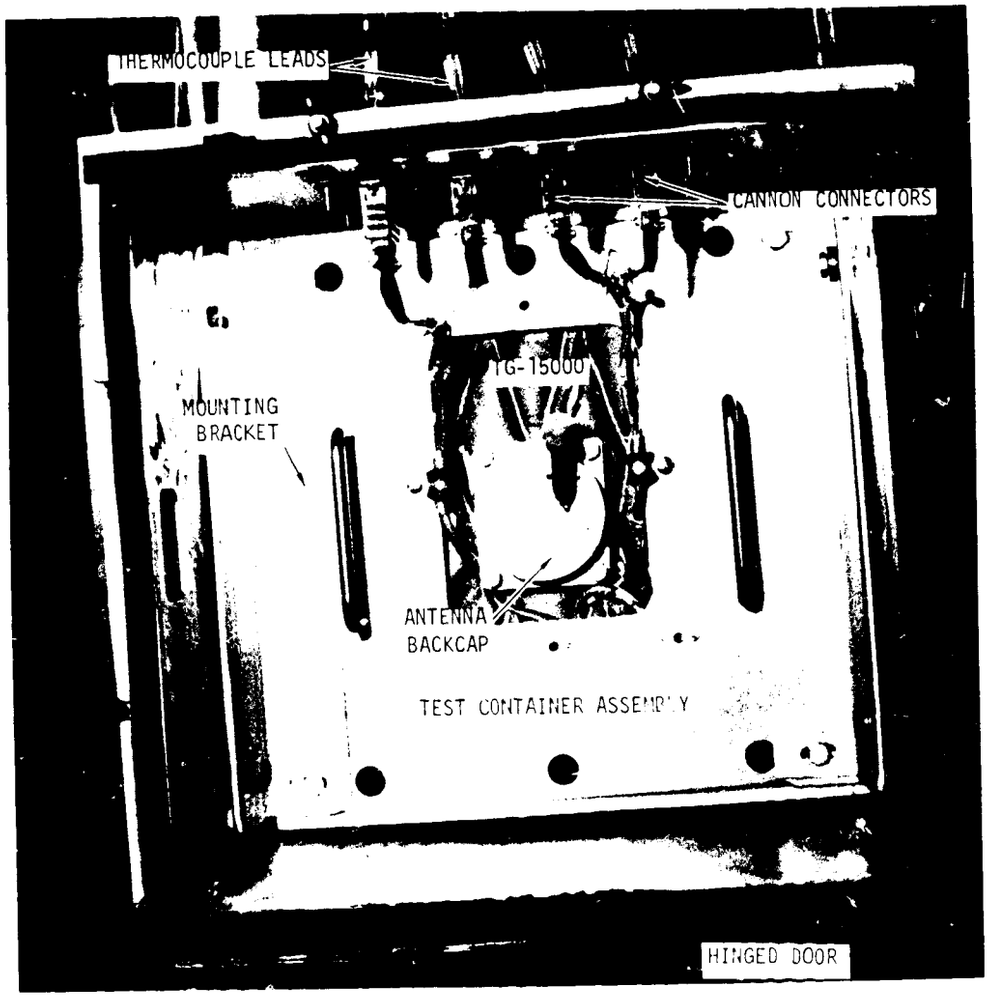

TEST INSTALLATION - BACK VIEW

FIGURE 120

Test Environment

The test environment was based on a design entry trajectory for the Space Shuttle Orbiter. Selection of this entry trajectory and associated thermal environment is duscussed in the section on DESIGN CONSIDERATIONS AND CONSTRAINTS under Thermal Requirements. Since the heating calculated by the MDAC-E MINIVER aerodynamic heating program is insignificant before 200 seconds flight entry time, the "arc on" condition and start of test time was considered to correspond to 200 seconds flight entry time. The surface temperature, hot wall convective heating rate, and enthalpy environment experienced by the antenna window surface for the selected trajectory are shown in figure 121. The local static surface pressure and the aerodynamic flow parameters (i.e., Mach number and boundary layer displacement thickness are shown in figures 122

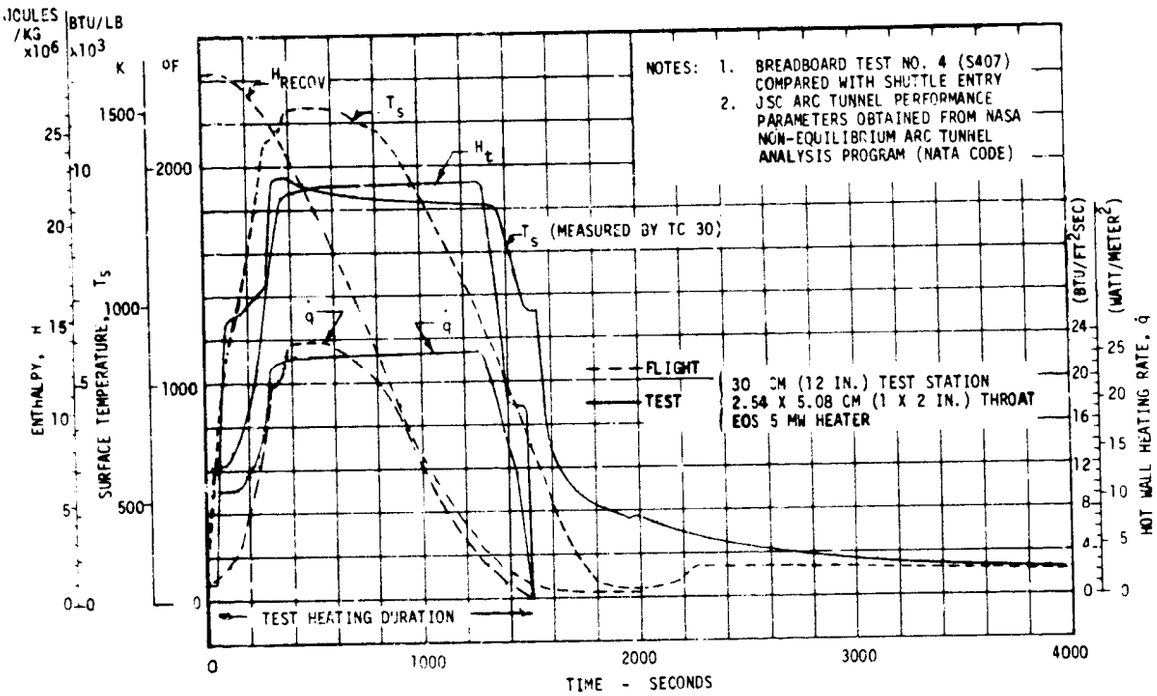

ENTRY AND TEST HEATING CONDITIONS

FIGURE 121

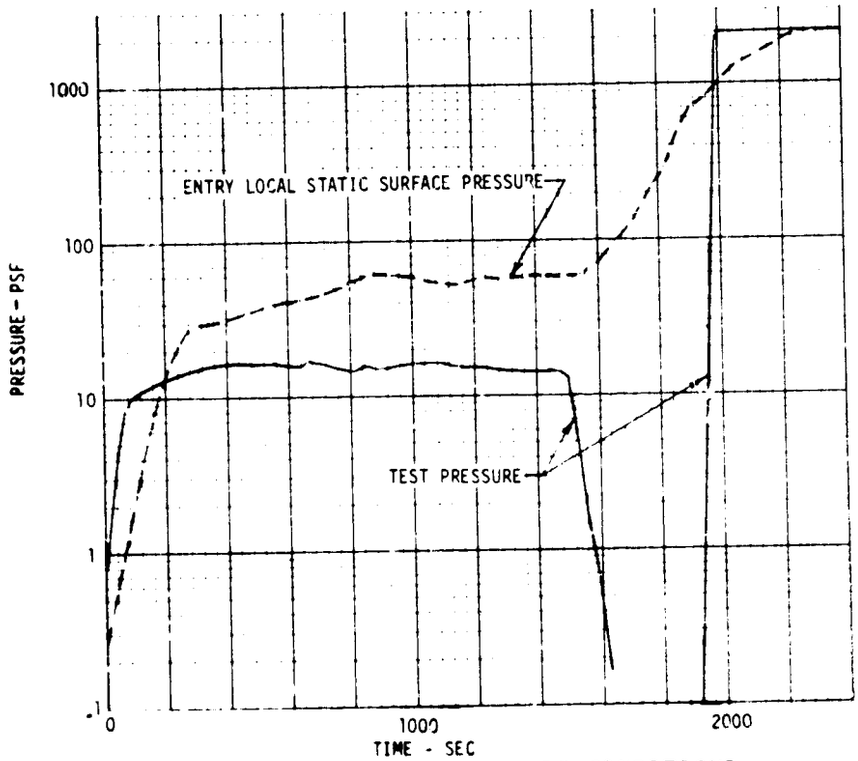

ENTRY AND TEST PRESSURE CONDITIONS

FIGURE 122

and 123 respectively). The breadboard unit test conditions are superimposed on figures 121, 122 and 123 for comparison with entry conditions.

The test environment for the prototype tests was similar to that used for the breadboard tests except the arc heater run times were extended to bring maximum bondline temperatures closer to 422 K (300°F).

Test environment control. - Programmed arc heater operation was used for the entry heating simulation. A Data Trak control curve was constructed from calibration test points obtained prior to the breadboard unit test runs. Data Trak curves for the breadboard and prototype tests are shown in figures 124 and 125.

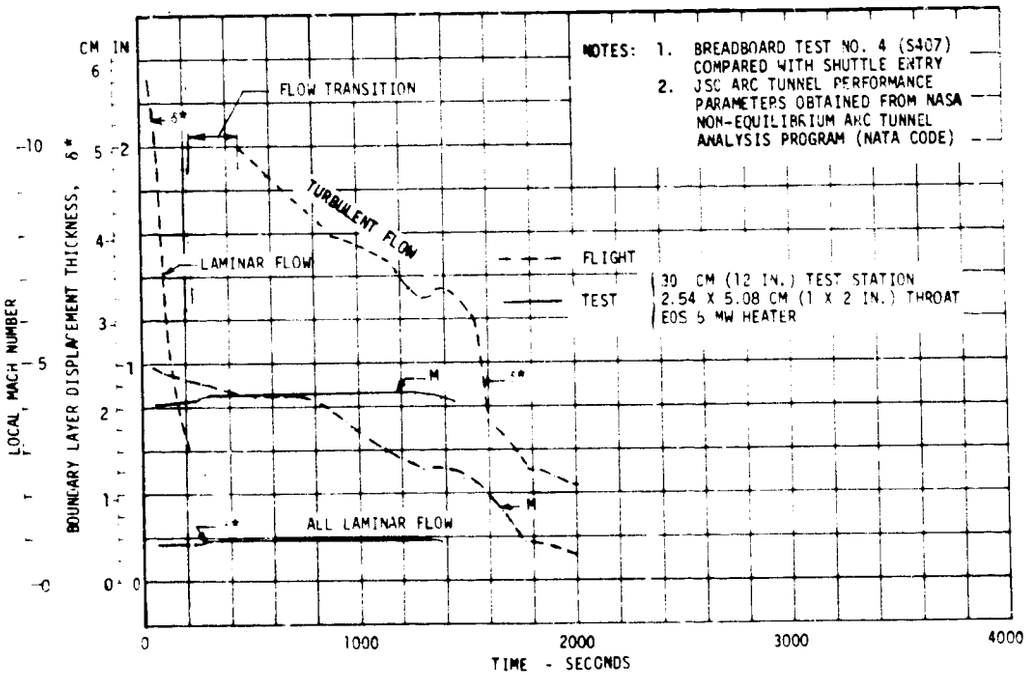

ENTRY AND TEST FLOW PARAMETERS

FIGURE 123

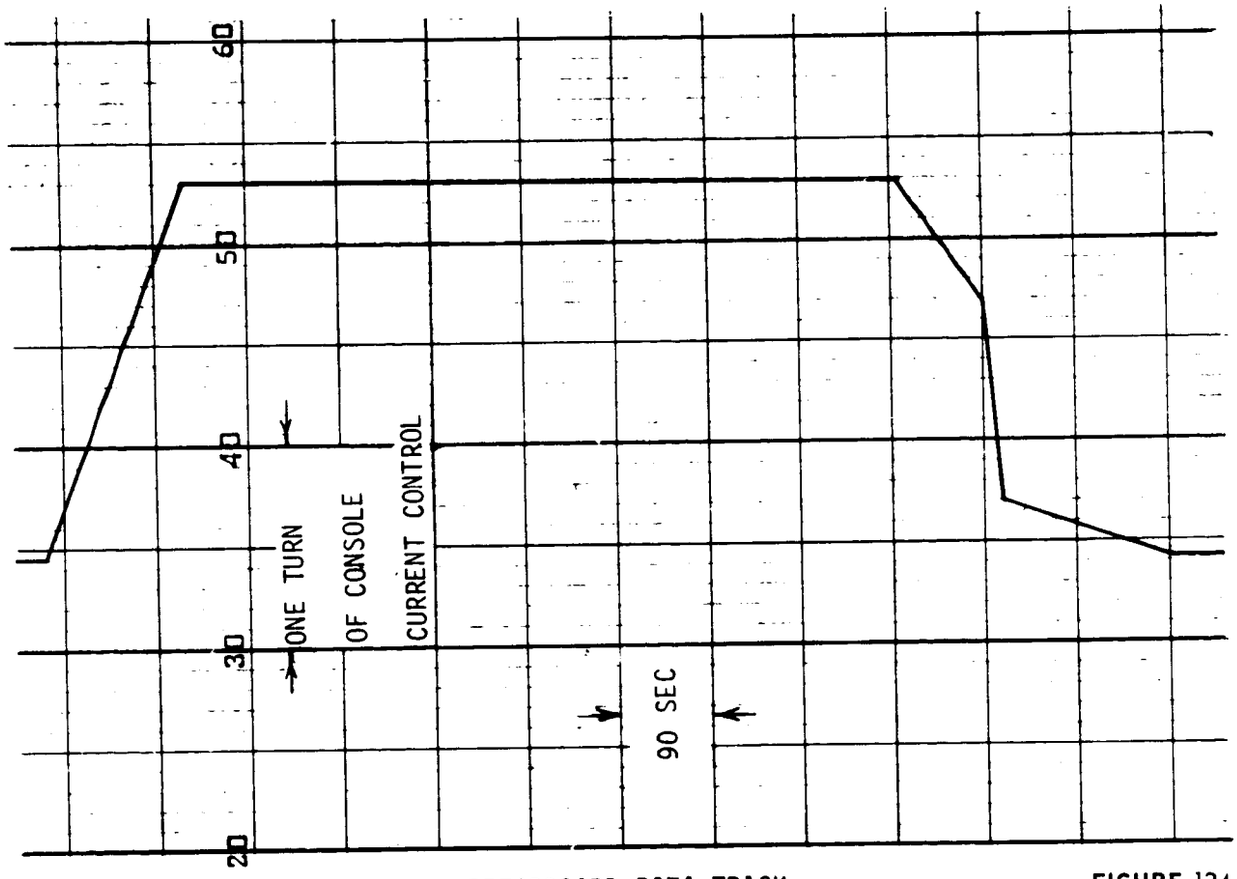

BREADBOARD DATA TRACK

FIGURE 124

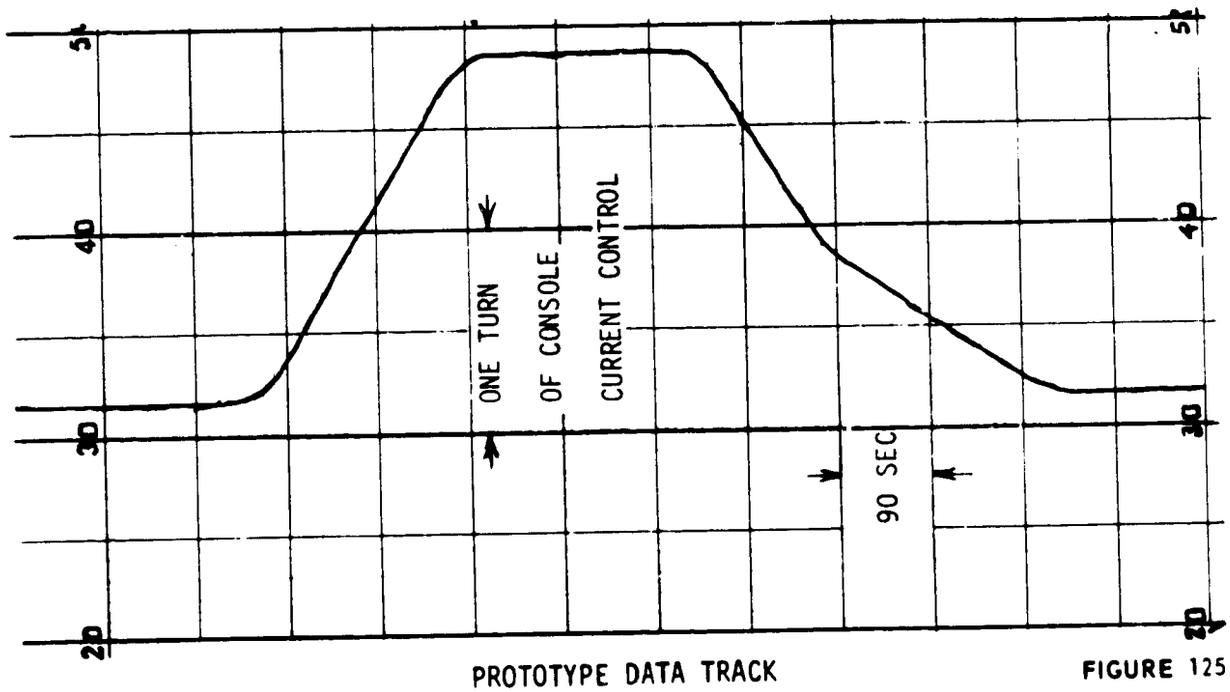

PROTOTYPE DATA TRACK

FIGURE 125

Breadboard Unit Testing

The breadboard unit tests were conducted on 28 March 1973. Four test cycles were run, starting with low heating and increasing to higher heating. The breadboard unit used for test is shown in figure 93. The test plan for the breadboard unit testing is given in Appendix G.

Instrumentation. - Thirty thermocouples were used to record breadboard unit temperature distributions. Thermocouple locations shown in figure 126 were based on the thermocouple layout shown in figure 69. Thermocouples were located on the surface of the HRSI, indepth in the HRSI, on the backside aluminum skin adjacent to window attachment holes, on the bondline and in back of the honeycomb support panel over the antenna, on the antenna backcap, and on the bottom and downstream-end of a tile joint gap parallel to plasma flow direction. Plan and side view X-rays of the breadboard unit (figures 127 and 128) show the thermocouple installation. Platinum - 10% rhodium (+)/platinum (-) thermocouples (ISA type S, 30 gage wire) were used for the surface temperature measurements. Chromel (+)/Alumel (-) thermocouples (ISA type K, 30 gage wire) were used for the indepth, bondline and backside temperature measurements. The thermocouple installation is discussed in the section on TEST HARDWARE FABRICATION.

A calibration plate mounted on the opposite side of the nozzle from the test model was used during each test to measure the nozzle heating and pressure environment. The calibration plate contained 13 heat calorimeters, one of which was a 2.54 cm (1 in.) water cooled model, and 3 pressure transducers.

Test results. - The first test cycle of the breadboard unit was conducted with a 1200 K (1700°F) peak surface temperature intended to check out instrumentation with the test unit. The Data Trak (figure 124) was followed until surface thermocouples indicated 1200 K (1700°F), and then the arc heater was switched to manual control, holding at peak temperature for 640 seconds. The arc heater was then allowed to follow the Data Trak down slope. The arc heater operated longer than intended at the bottom of the Data Trak curve. The total heating time was 1696 seconds. Posttest inspection of the breadboard unit, seen through the end of the channel flow nozzle, did not show any adverse effect. The strip chart responses from the thermocouples, one calorimeter and two local static pressure transducers were visually monitored and indicated satisfactory results.

A short term temperature peak, coincident with tunnel repressurization, occurred during the first breadboard test for thermocouples (TC's) 13, 14, 15 and 16. These thermocouples were located on or near an FI-600 filler strip at the bottom of a tile joint gap parallel to plasma flow. The measured temperature response is shown in figures 129 and 130. On top of the filler strip, TC's 15 and 16 reached long term maximum temperatures of 644 K (700°F) and 714 K (825°F) respectively; TC 16 was downstream from TC 15. Short term temperature peaks of 722 K (840°F) and 833 K (1040°F) were recorded by TC 15 and 16 respectively. Similar results occurred for TC's 13 and 14 on the window tile adjacent to the sides and top of the filler strip.

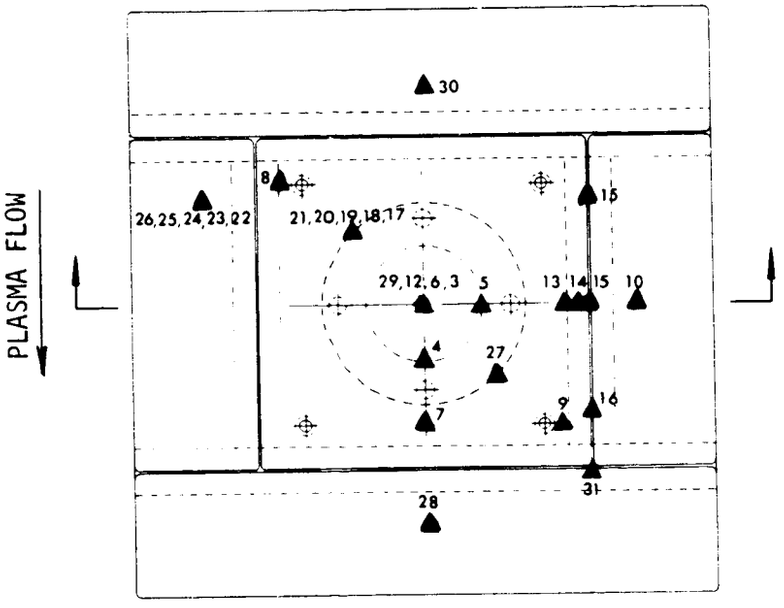

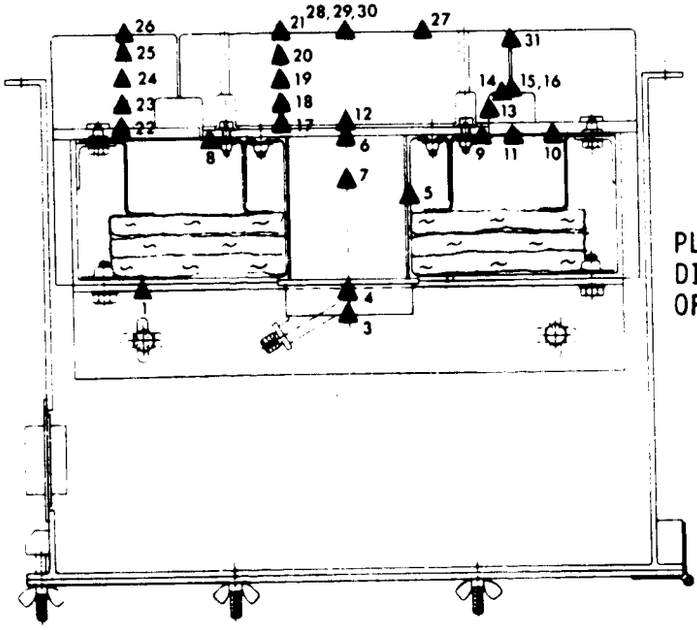

PLASMA FLOW
DIRECTION IS OUT
OF THE PAPER

BREADBOARD THERMOCOUPLE LOCATIONS

FIGURE 126

PLASMA FLOW →

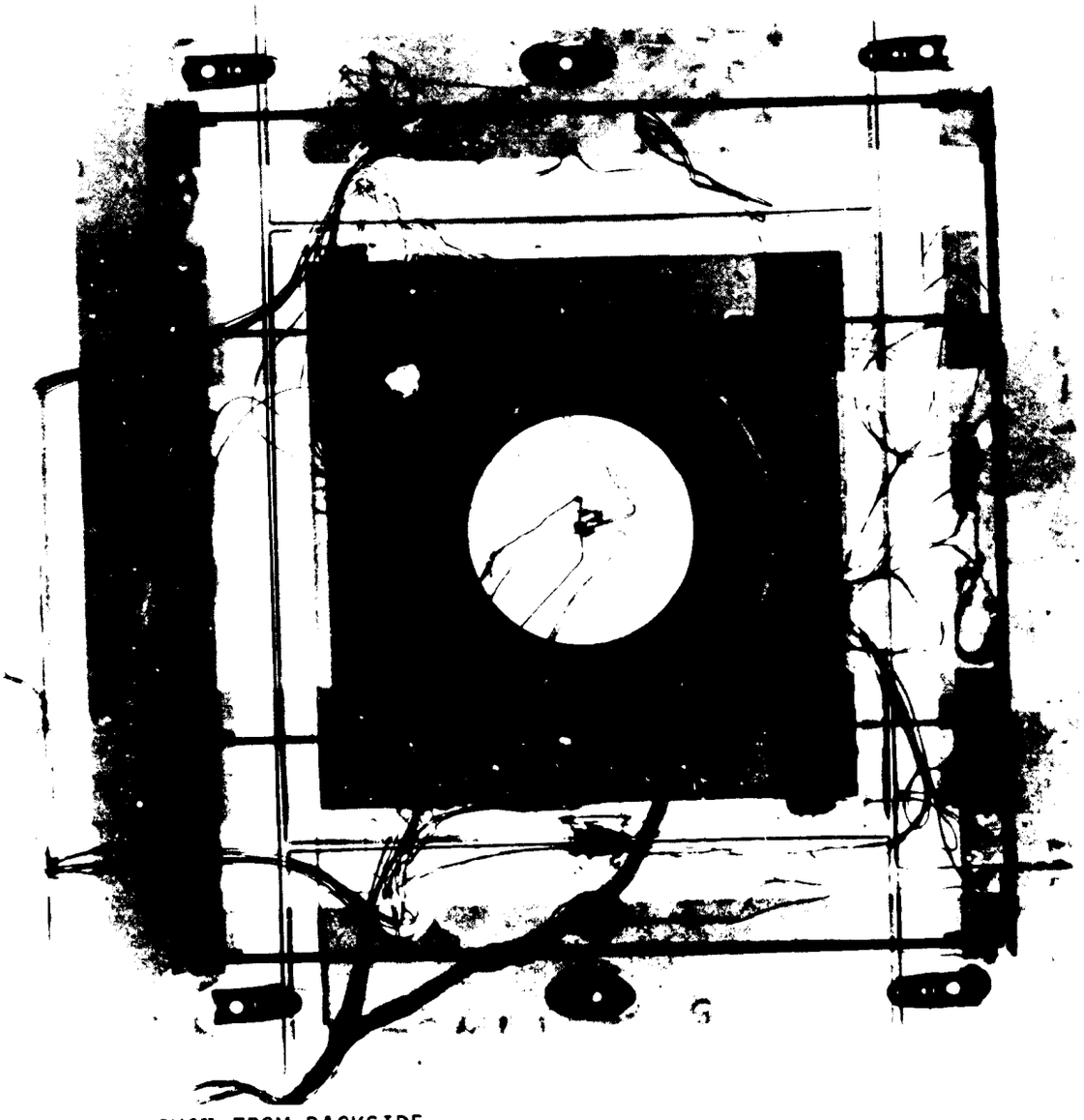

SHOT FROM BACKSIDE

BREADBOARD PLAN VIEW X-RAY

FIGURE 127

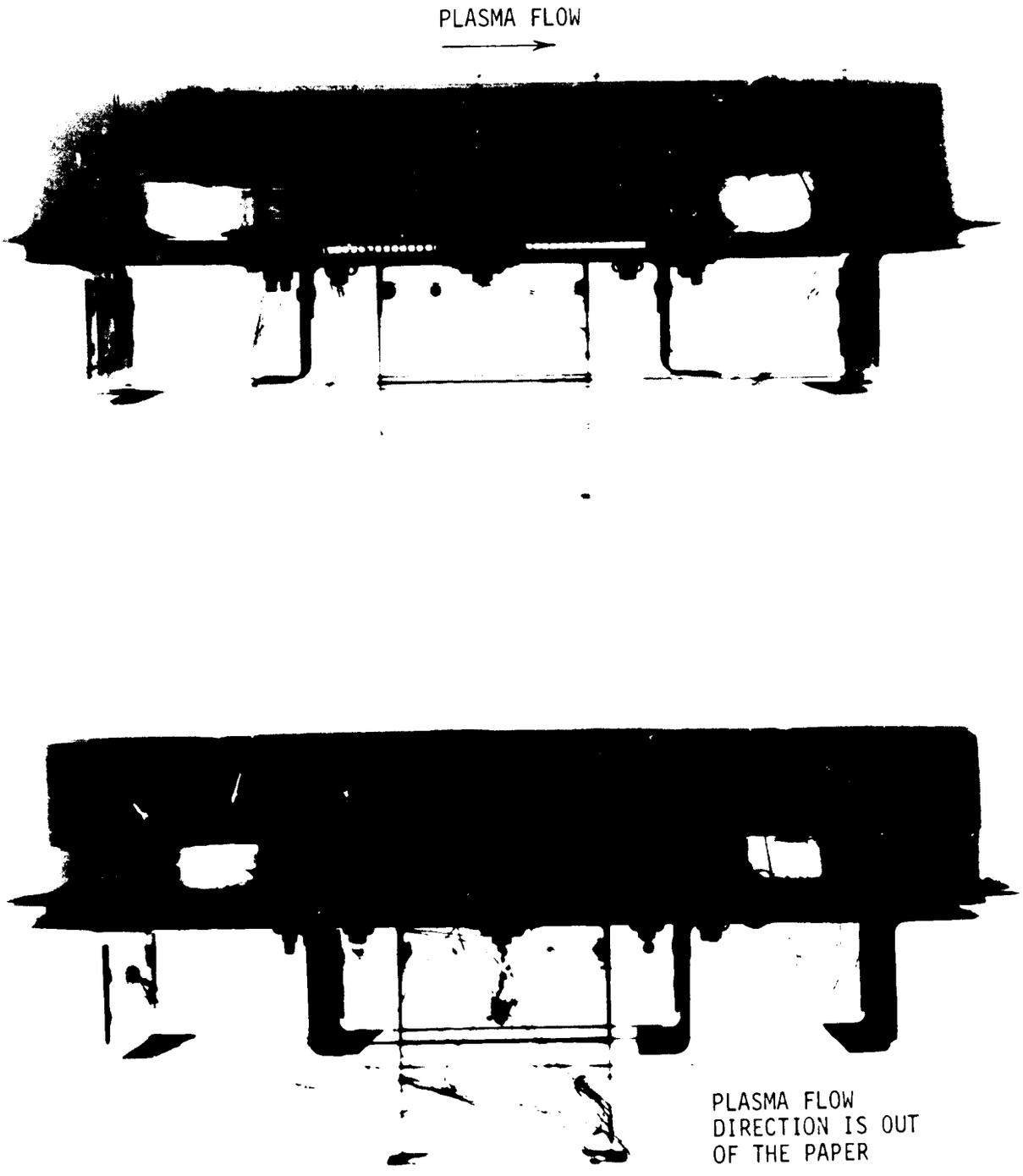

BREADBOARD SIDE VIEW X-RAYS

FIGURE 128

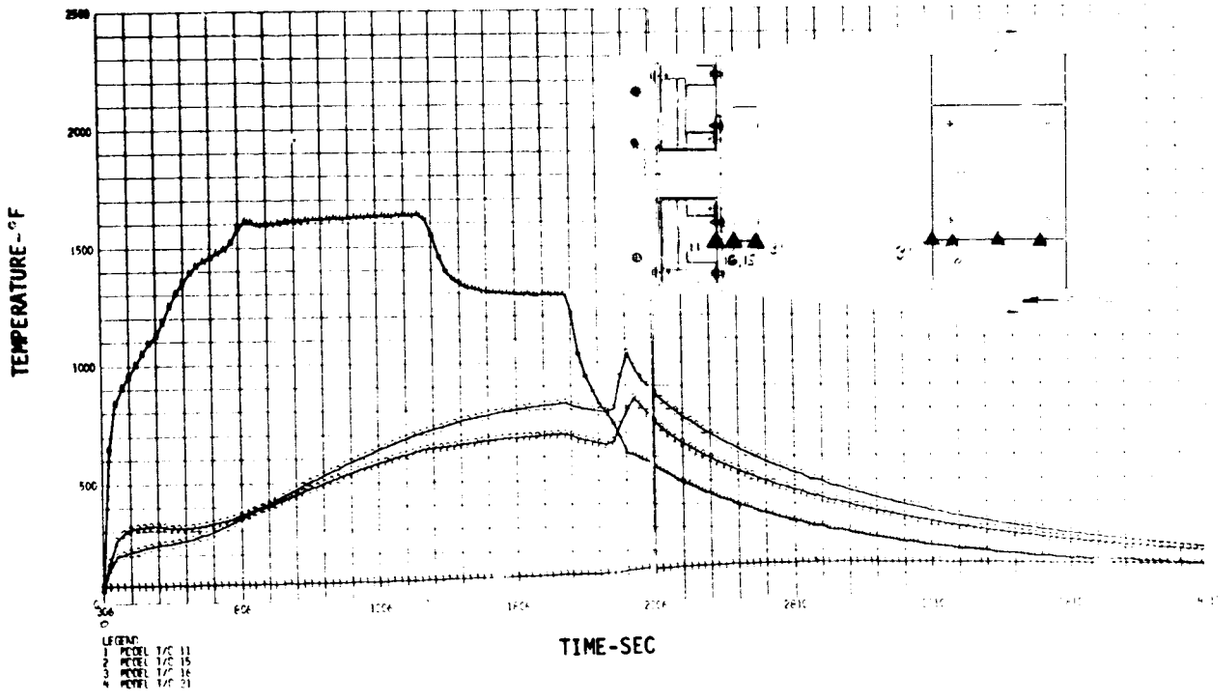

GAP (DOWNSTREAM END), FILLER STRIP AND SKIN (TEST B-1) FIGURE 129

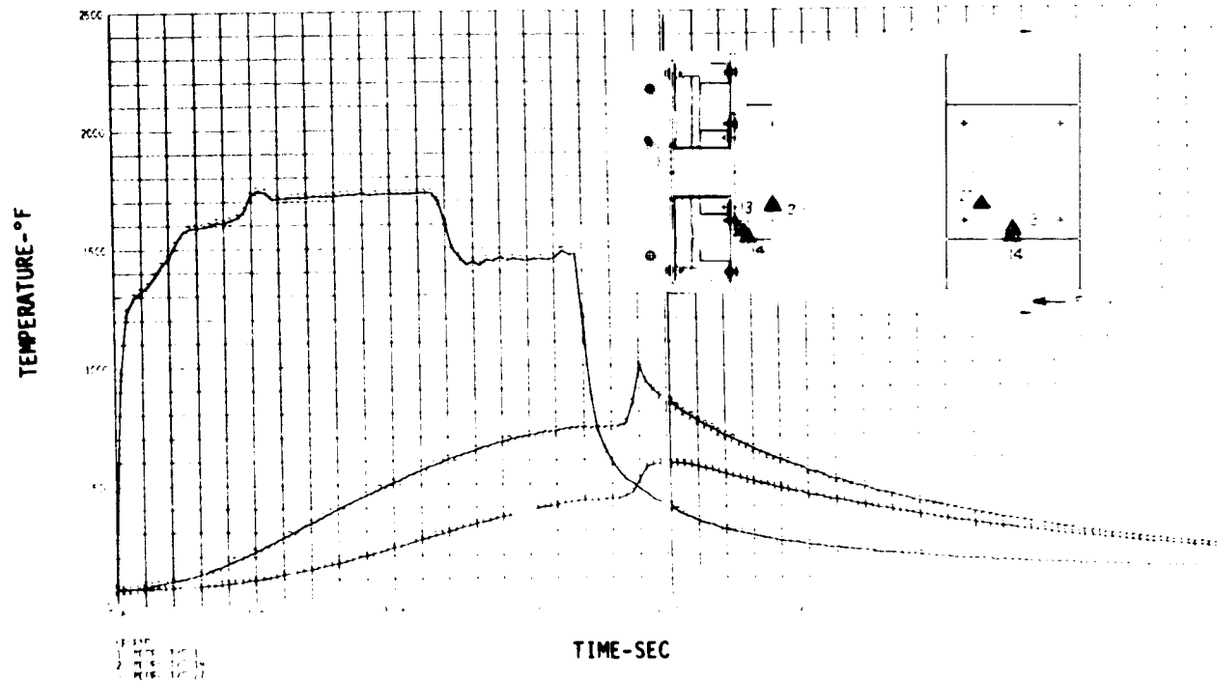

ANTENNA WINDOW JOINT (TEST B-1) FIGURE 130

The second breadboard test was run with the Data Trak as constructed during the calibration tests. The measured control parameters are shown in figure 131. The heating time for this test was 1215 seconds. The surface temperatures reached their peak values after 300 seconds heating time as shown in figure 132. These were the highest surface temperatures obtained during both breadboard and prototype tests. Since the facility was being operated at the limit of its capability, the surface temperatures for the third run could not be raised to the 1517 K (2270°F) temperature predicted for the Orbiter (figure 121). Therefore, it was decided to subject the breadboard unit to the same total heat predicted for the Orbiter in order to obtain expected backside temperatures.

The extension time at the test peak temperature to obtain the approximate total heat predicted for the Orbiter entry was estimated using two approaches. The first approach,based on Mezines' method (ref. 11), yielded a test extension time of 86 seconds. The second approach, based on obtaining an integrated area equal to the integrated area of the Orbiter entry heating curve using Simpson's Rule, yielded an extension time of 250 seconds. Since the extension time from the two methods did not agree, both were used. The heating time for the third and fourth breadboard tests were 1391 and 1504 seconds, respectively, compared to 1215 seconds for the second run.

The measured data from the third test run is shown in a set of sixteen plot frames (figures 133 through 148). Eleven of these show temperature histories selected to present the temperature distribution in various regions. For example, the temperature distribution through the antenna window (figure 134) and on the antenna window surface (figure 136) are given. Pressure distributions are shown in figures 144 and 145. Heating rate is shown in figures 146, 147 and 148. These data are also typical of the other breadboard test runs.

Examination of the test data from the third and fourth test runs did not show the desired increase in backside temperature for either of the test extension times given above.

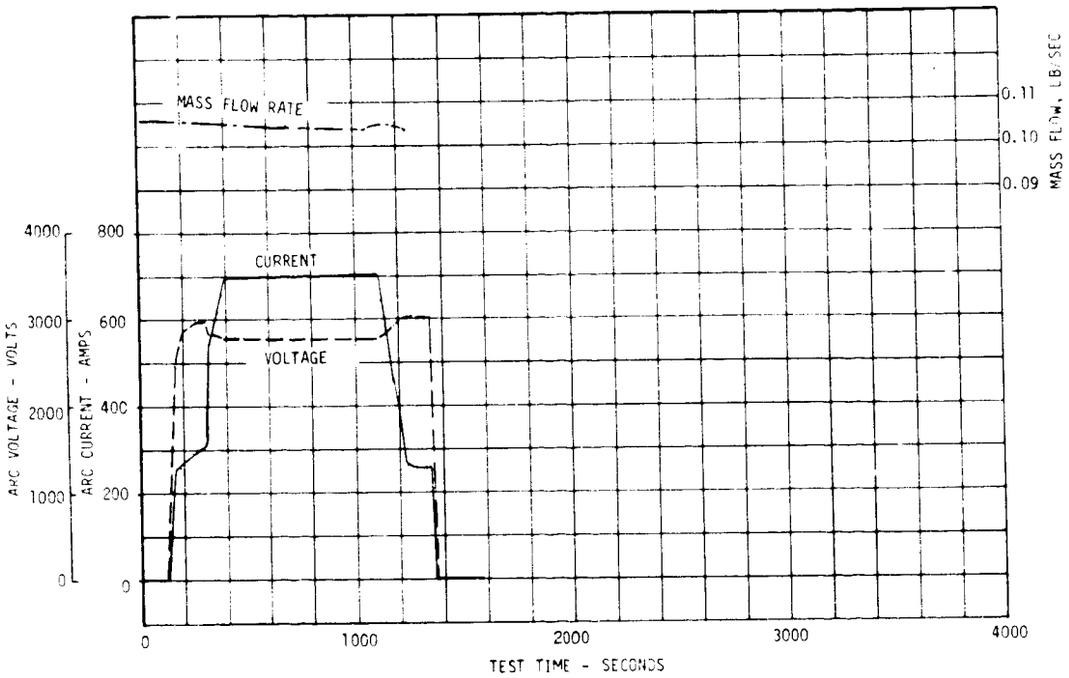

BREADBOARD TEST CONTROL PARAMETERS

FIGURE 131

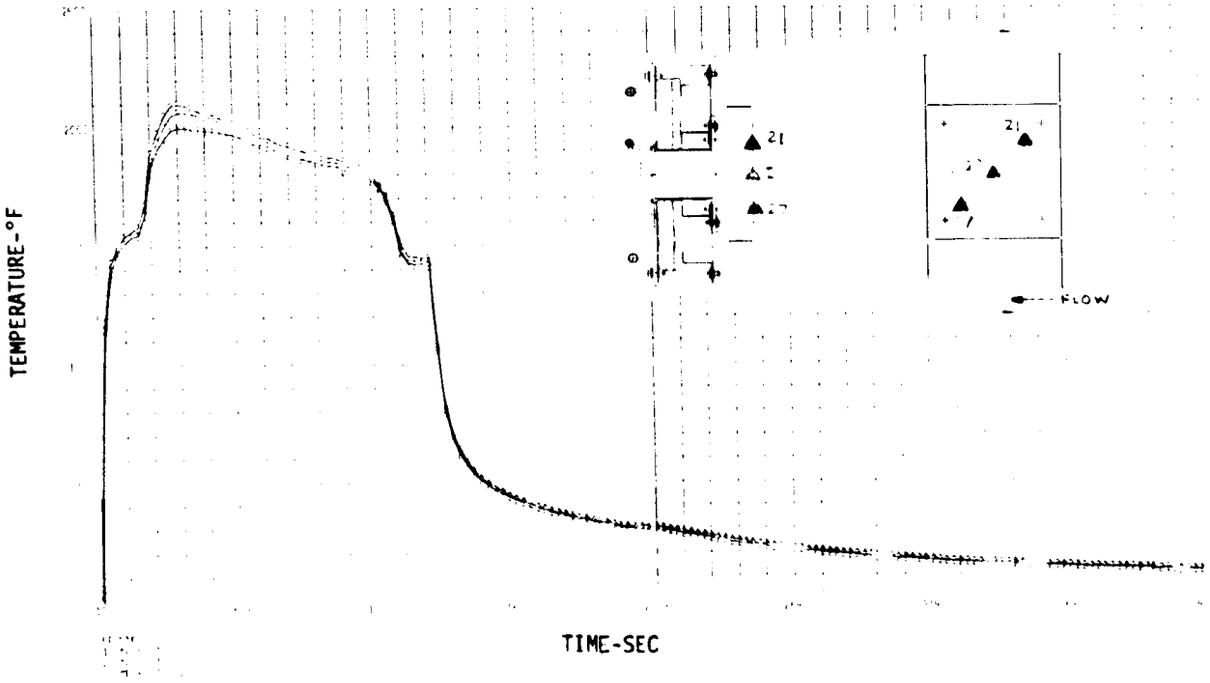

ANTENNA WINDOW SURFACE (TEST B-2)

FIGURE 132

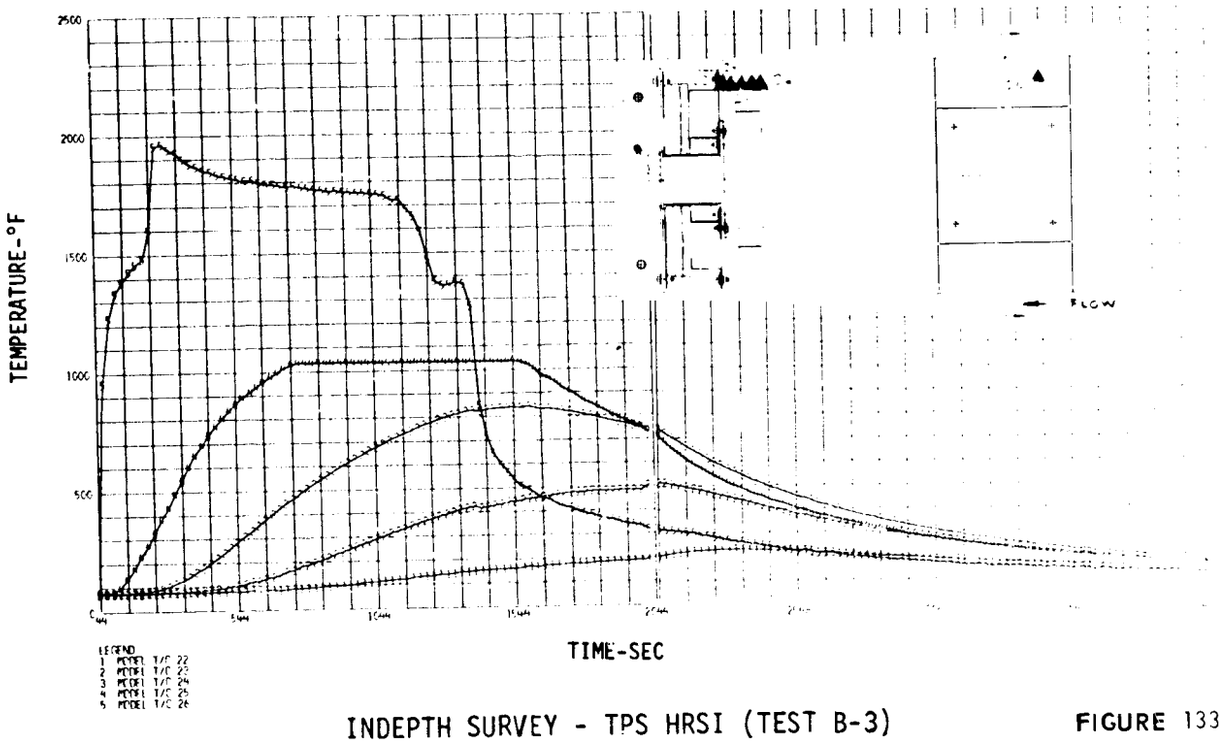

INDEPTH SURVEY - TPS HRSI (TEST B-3) FIGURE 133

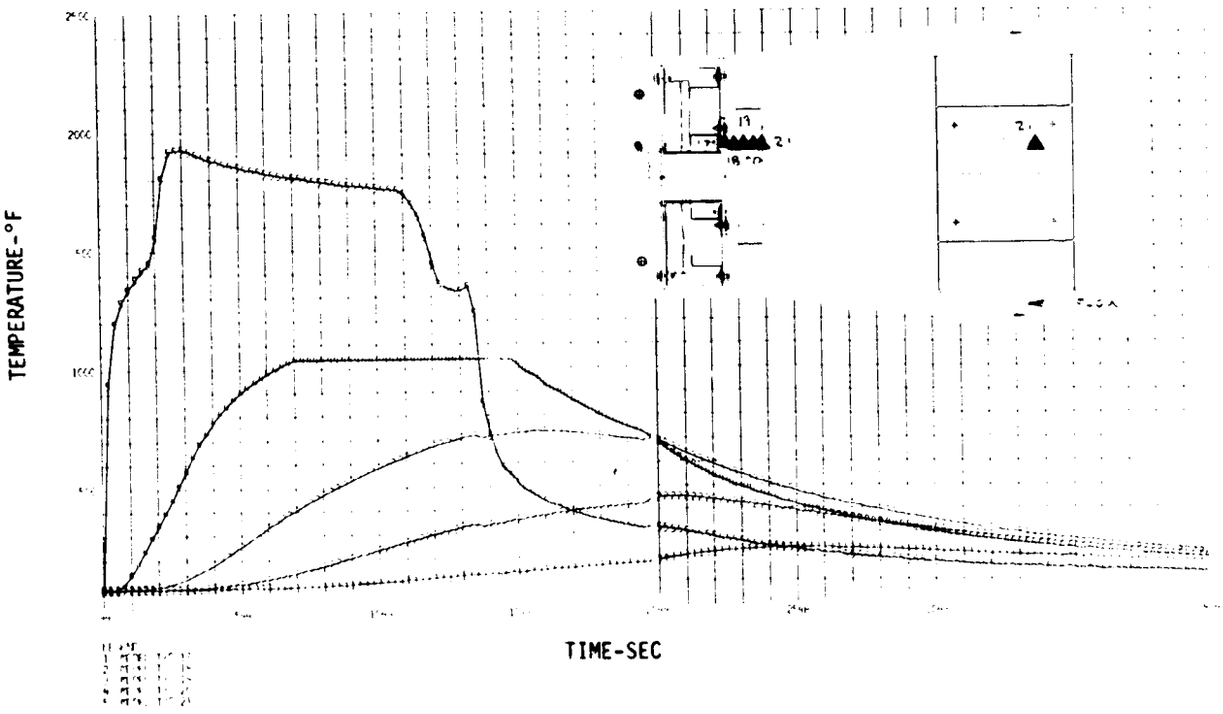

INDEPTH SURVEY - ANTENNA WINDOW HRSI (TEST B-3) FIGURE 134

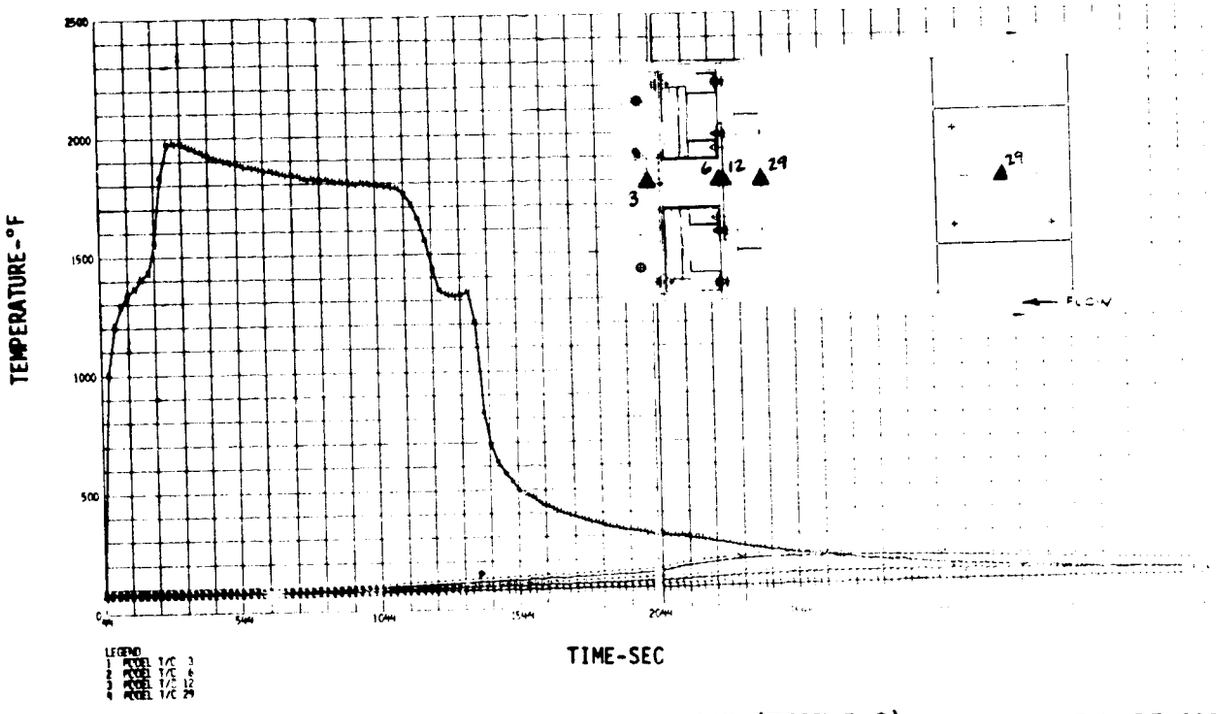

ANTENNA WINDOW AND BACKCAP (TEST B-3)

FIGURE 135

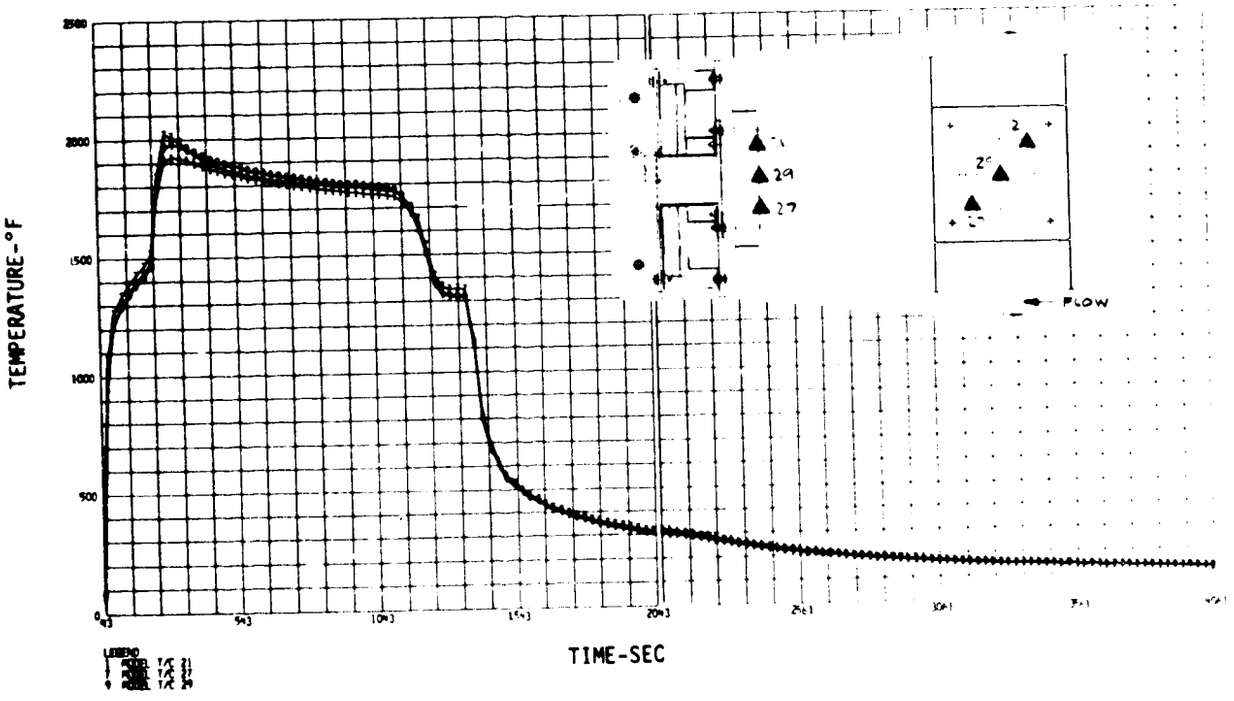

ANTENNA WINDOW SURFACE (TEST B-3)

FIGURE 136

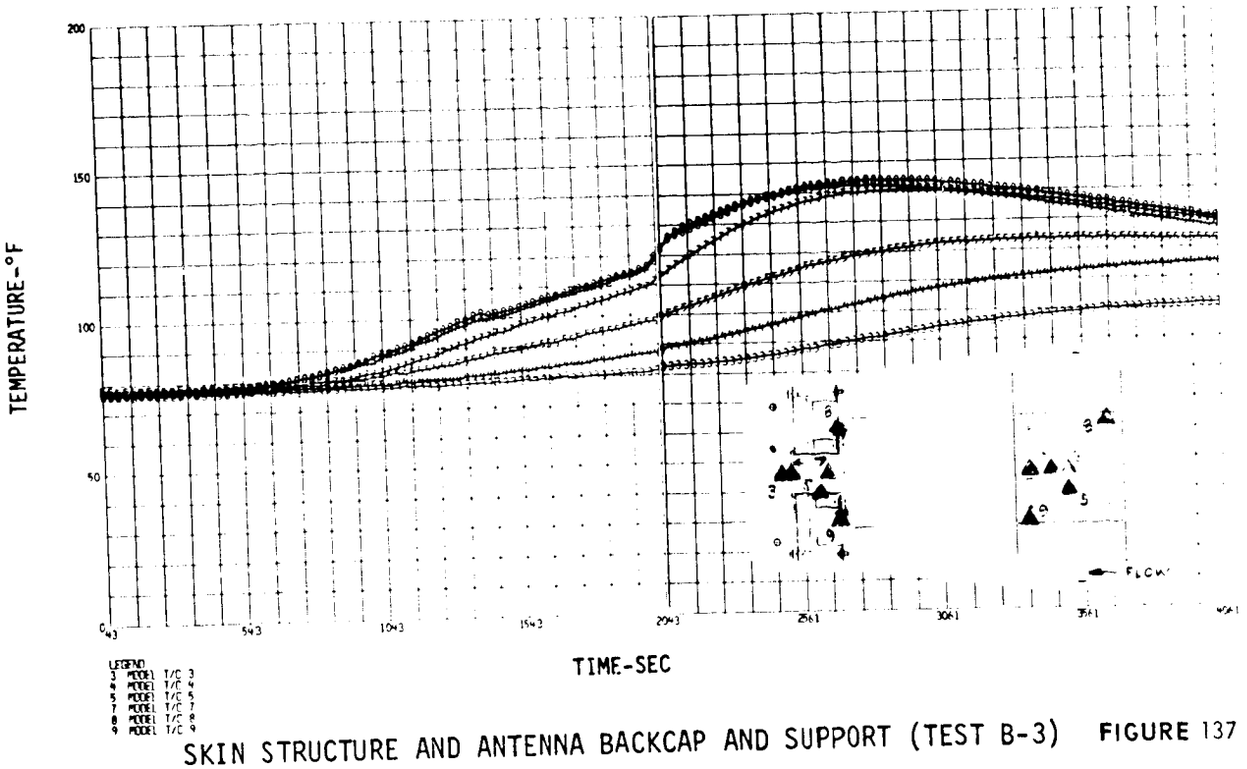

SKIN STRUCTURE AND ANTENNA BACKCAP AND SUPPORT (TEST B-3) FIGURE 137

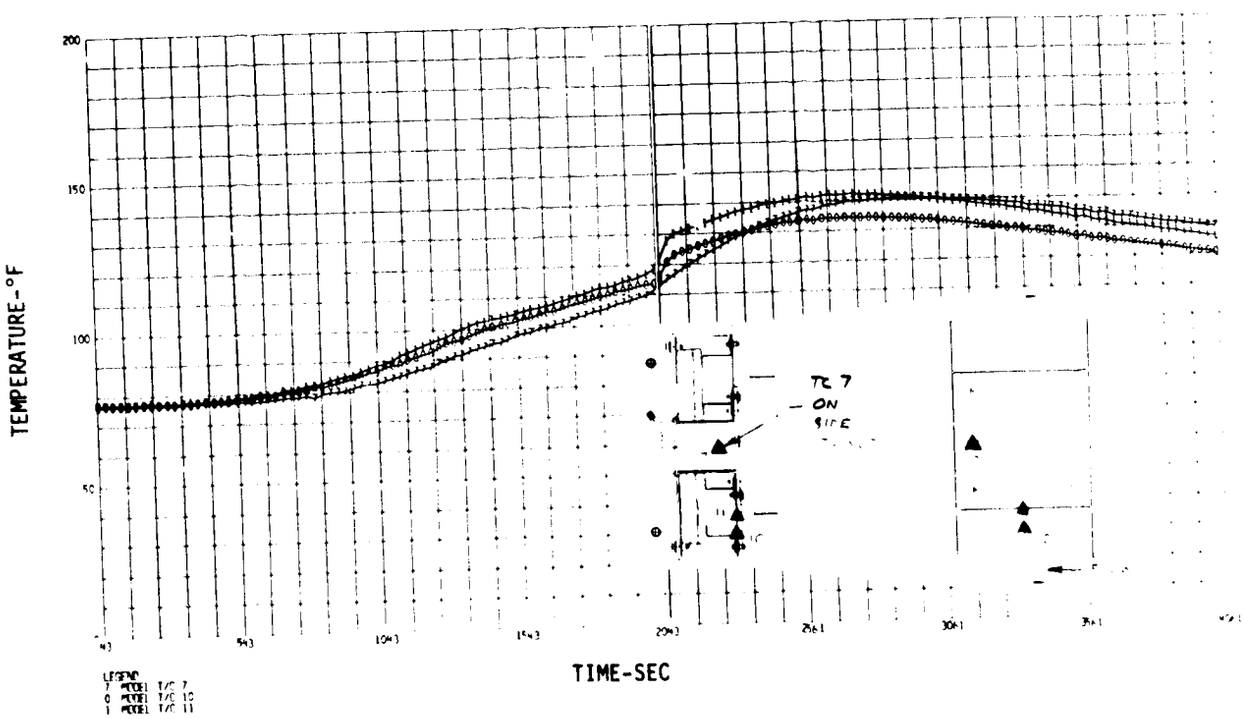

SKIN STRUCTURE (TEST B-3) FIGURE 138

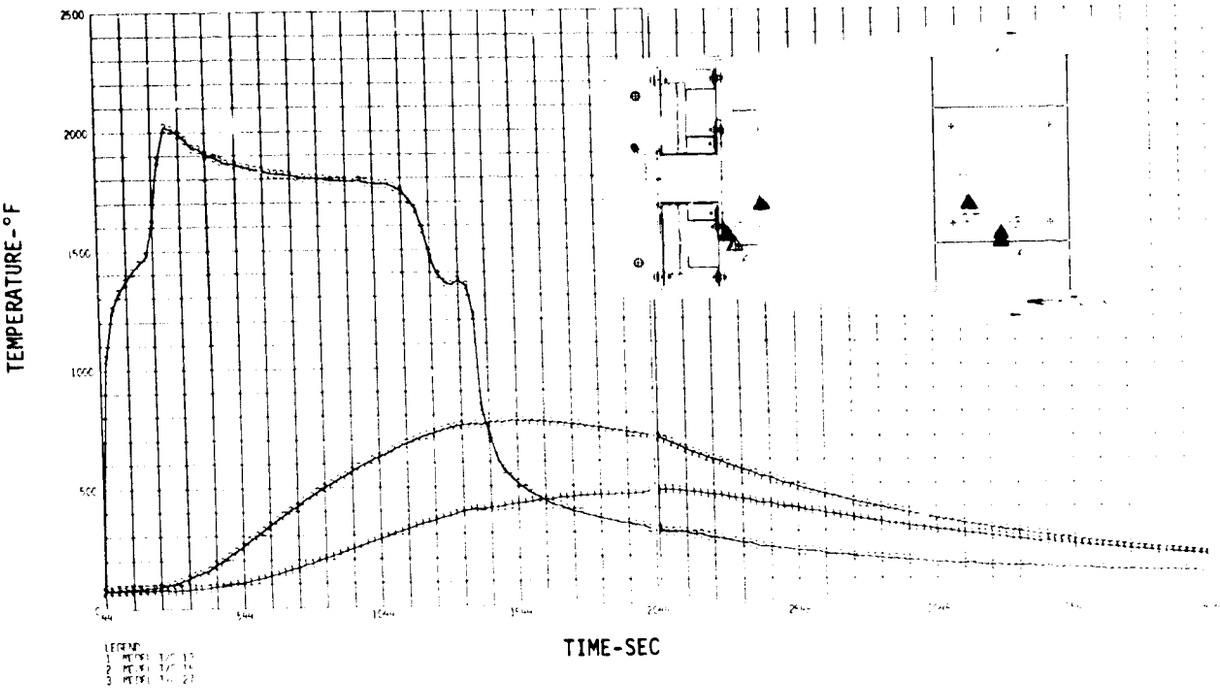

ANTENNA WINDOW JOINT (TEST B-3) FIGURE 139

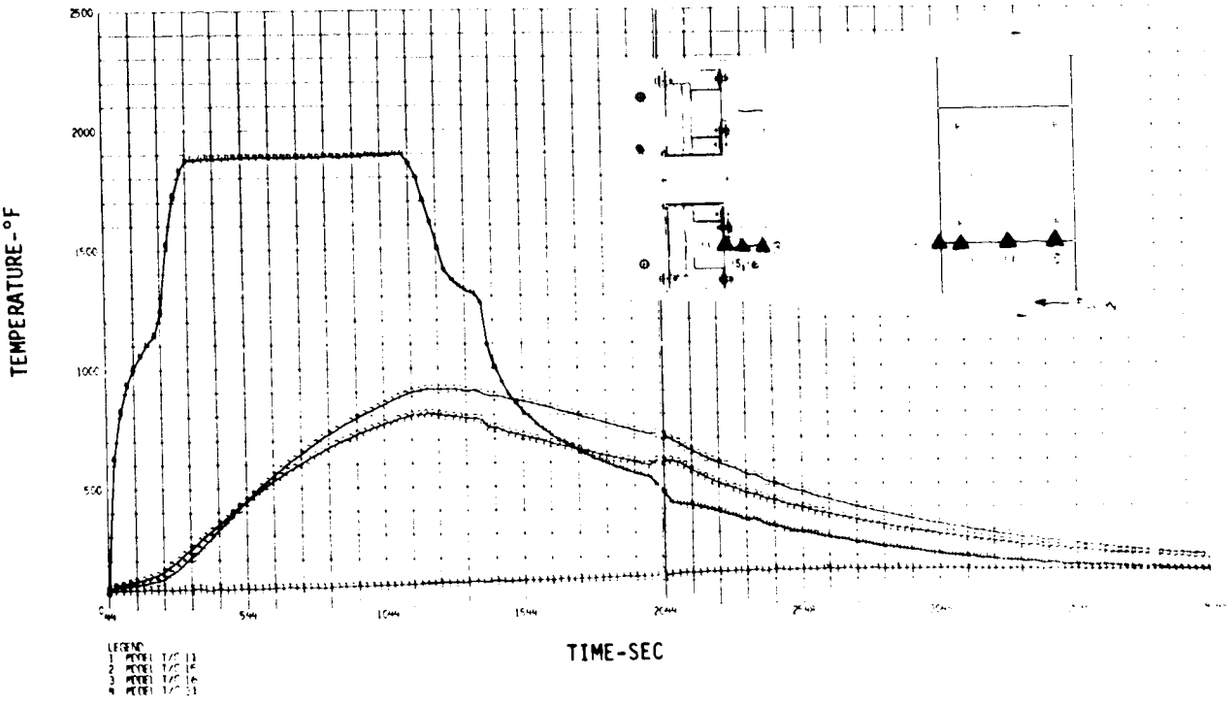

GAP (DOWNSTREAM END), FILLER STRIP AND SKIN (TEST B-3) FIGURE 140

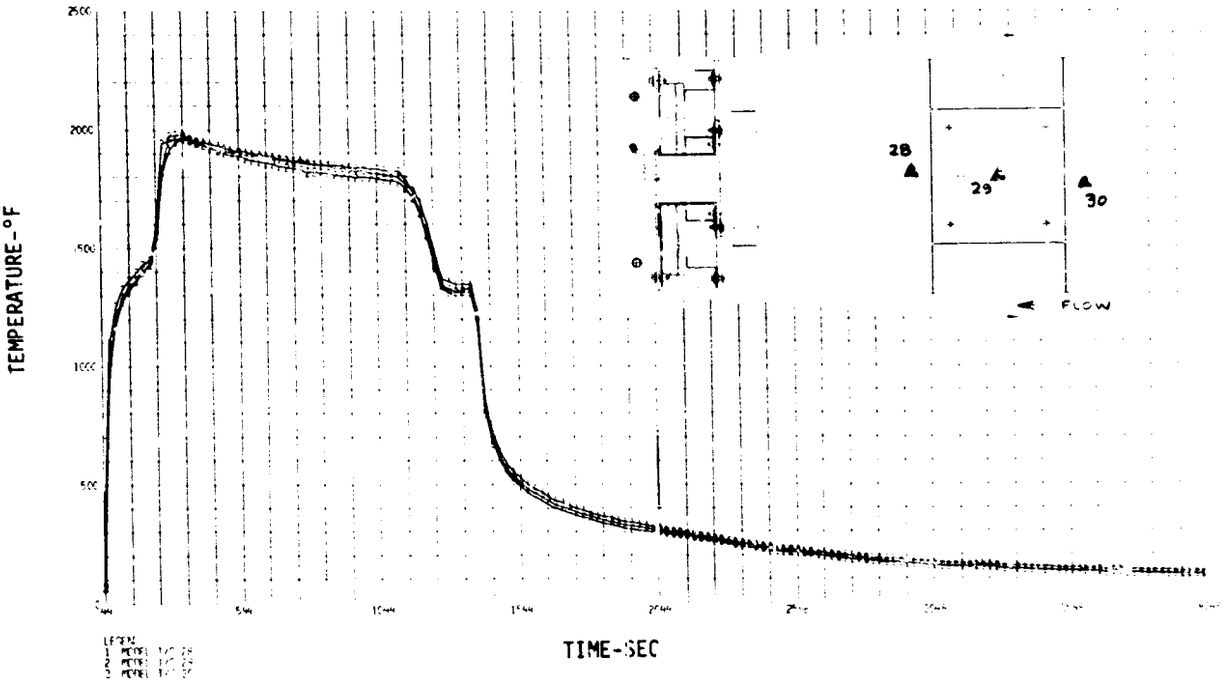

ANTENNA TEST UNIT SURFACE - AXIAL (TEST B-3) FIGURE 141

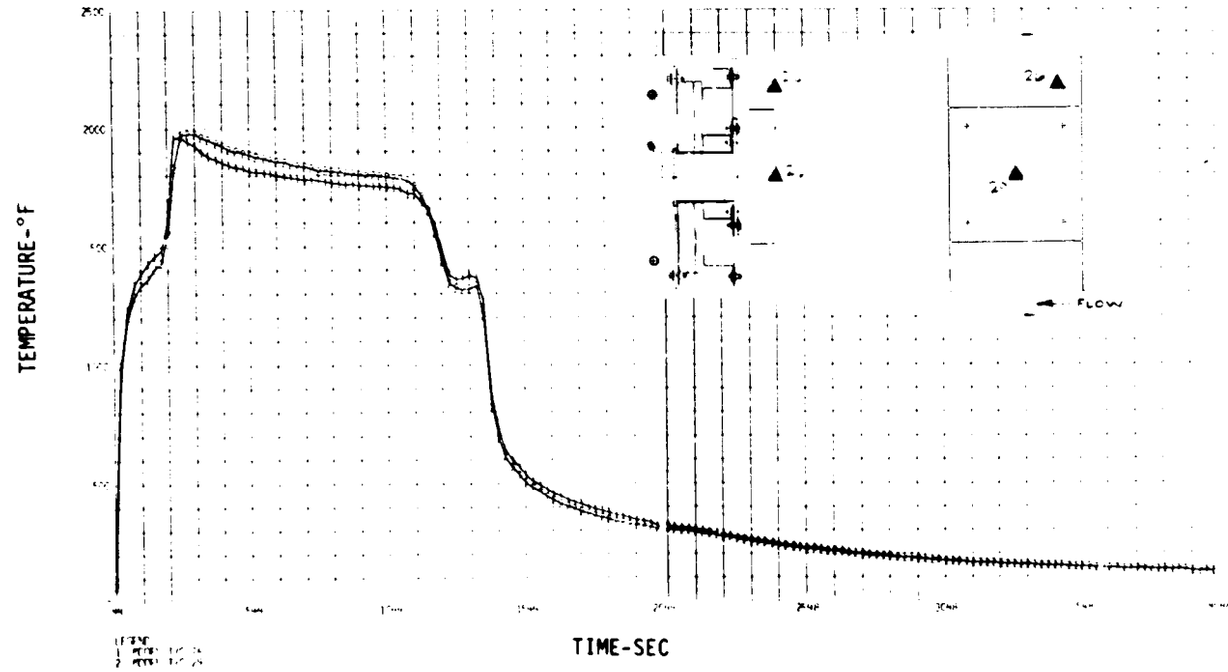

ANTENNA TEST UNIT SURFACE - TRANSVERSE (TEST B-3) FIGURE 142

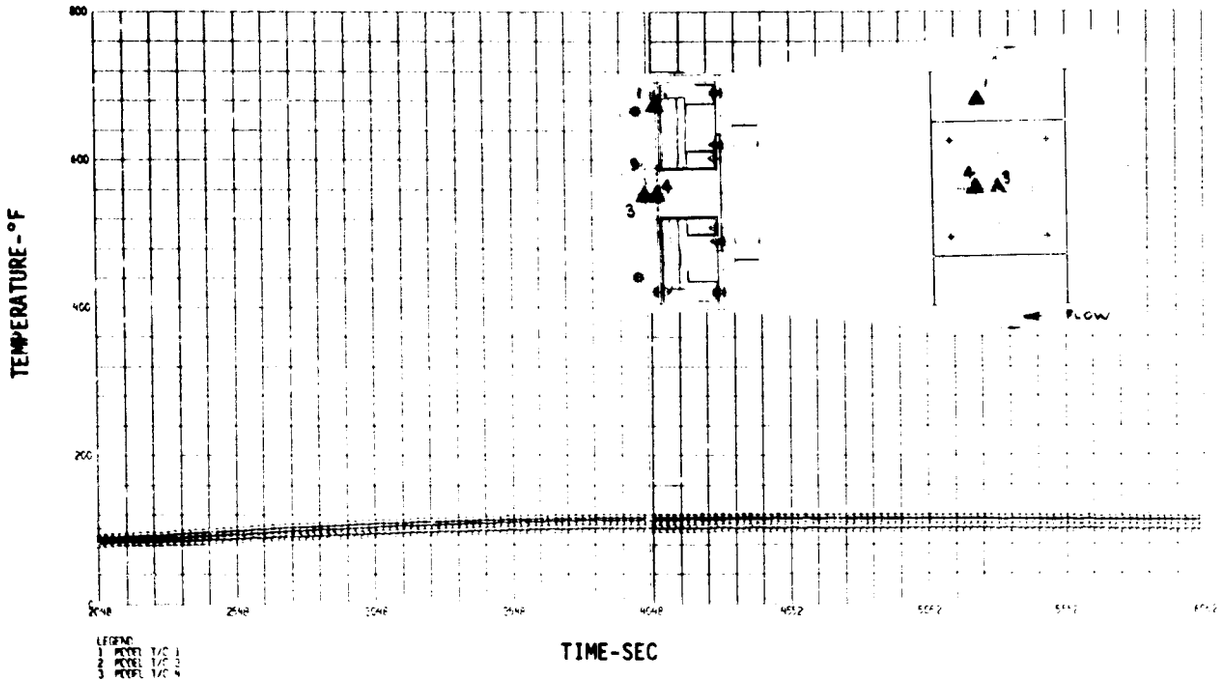

ANTENNA BACKCAP AND TEST CONTAINER ASSEMBLY (TEST B-3)

FIGURE 143

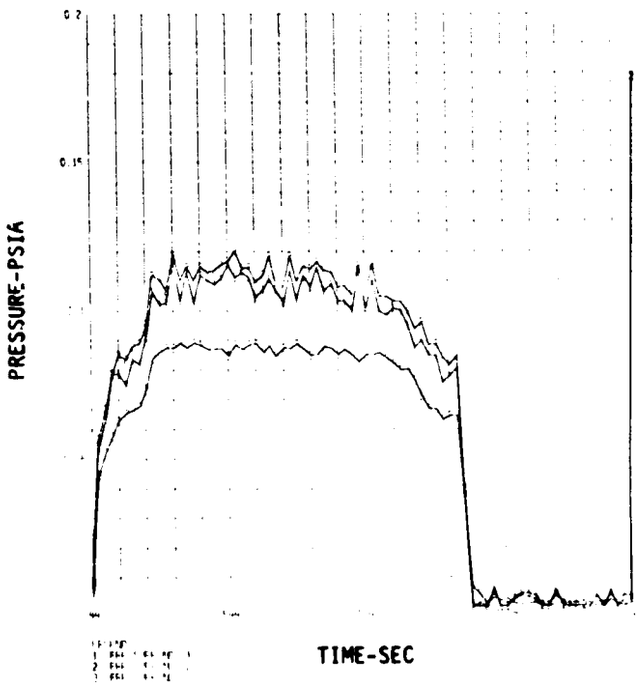

LOCAL STATIC SURFACE PRESSURES - CALIBRATION PLATE (TEST B-3)

FIGURE 144

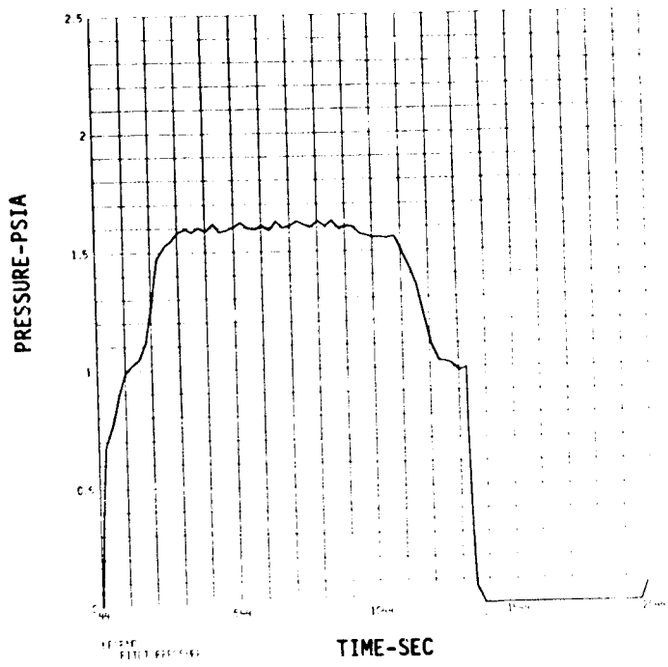

PILOT PRESSURE - NOZZLE EXIT (TEST B-3)

FIGURE 145

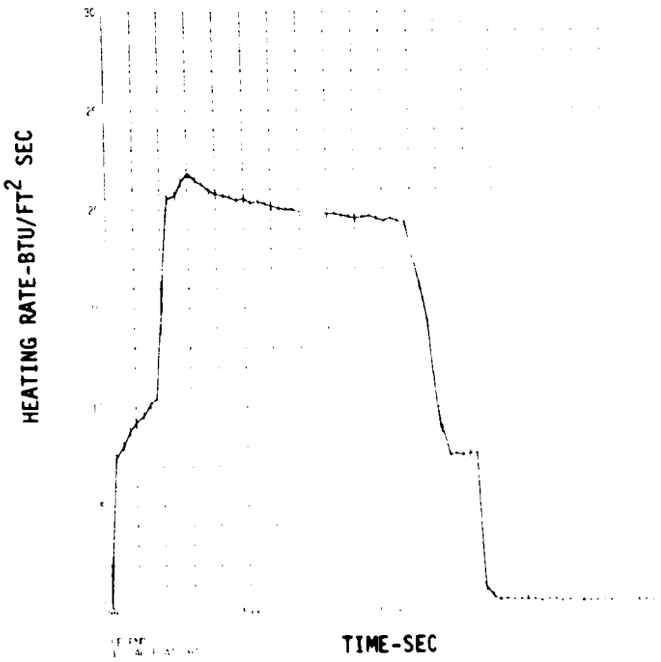

HEATING RATE - CALIBRATION PLATE WATER COOLED CALORIMETER (TEST B-3)

FIGURE 146

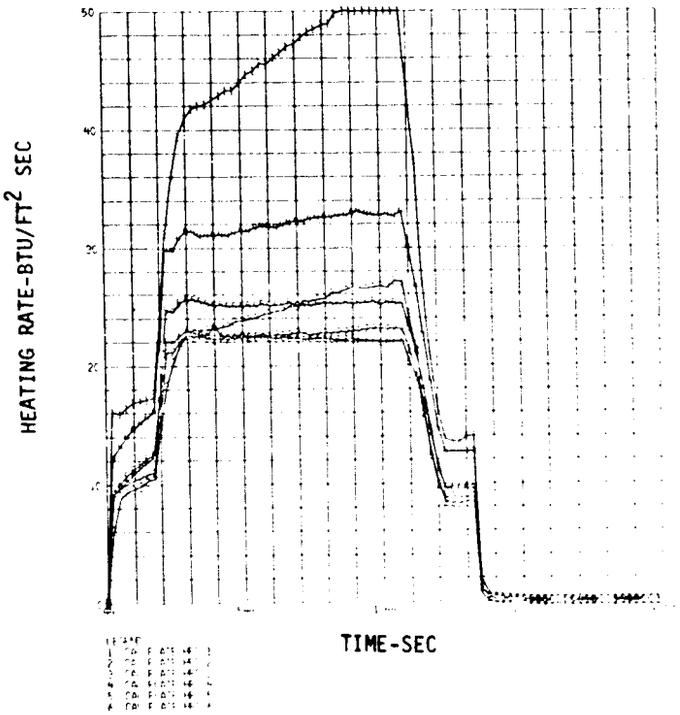

HEATING RATES - CALIBRATION PLATE HRS 1 THRU 6 (TEST B-3)

FIGURE 147

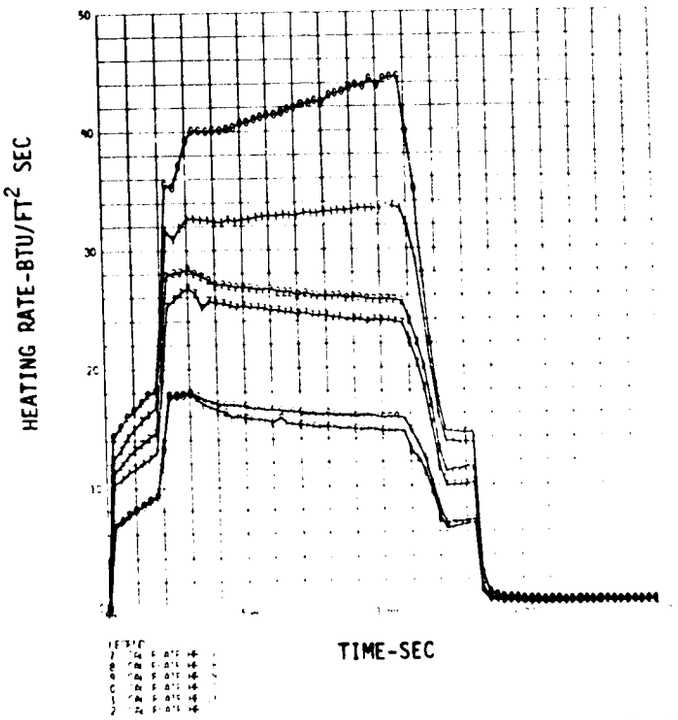

HEATING RATES - CALIBRATION PLATE HRS 7 THRU 12 (TEST B-3)

FIGURE 148

Prototype Unit Tests

The prototype unit was subjected to ten thermal cycles during the period 24 to 31 May 1973. The prototype unit used for the thermal tests is shown in figure 95. The test plan for the prototype unit tests is given in Appendix H. The joint gap space at the surface between the antenna window and one of the transverse (i.e. to plasma flow) guard tiles was greater than 1.778 mm (0.070 in.) as discussed in the section on TEST HARDWARE FABRICATION. The gaps were reduced as much as possible by increasing the Fibrefrax insulation thickness between the edges of the guard tiles and the opening in the channel nozzle wall.

The calibration test indicated the peak attainable surface temperature for the prototype test series was about 1311 K (1900°F). Therefore, to obtain the desired backside heating, an increased heating time was required. Since the extended test times calculated for the breadboard unit did not produce the estimated backside temperature levels, a third approach was used. The breadboard unit bondline thermal response rise slope was extrapolated to roughly estimate the increased heating time required to obtain a bondline temperature of at least 422 K (300°F). This required a test time of approximately 2352 seconds, 848 seconds longer than the fourth breadboard test run. The increase run times were implemented by stopping the Data Trak 180 seconds after reaching peak current and controlling the test manually. The Data Trak was then restarted after a predetermined pause to complete the test run.

TG-15000 insulation was placed behind the antenna, which protruded from the test container assembly, to prevent heat loss to the cooled cover assembly (figure 149). The prototype unit was removed from the thermal test installation to perform electrical tests after the first, second, fifth, and tenth thermal test cycles. After removal, wet film acetaldehyde NDE tests were performed to detect cracks in the LI-1500 coating. The model was then transported to the NASA-JSC Anechoic Chamber Test Facility for electrical tests. After the electrical tests were completed, emittance and water absorption tests were performed. The water absorption test was performed after electrical testing to ensure that absorped moisture would not affect electrical test results.

Instrumentation. - The thermocouples located in the breadboard antenna window and indepth in the LI-1500 around the window were eliminated in the prototype unit to obtain improved electrical performance. Twenty-one thermocouples (figure 150) were used to record temperature distributions. Only two surface thermocouples were used; one each in the leading and trailing guard tiles. Two were located on top of the FI-600 filler strip at the leading and trailing ends of a parallel gap. Four were placed in LI-1500/SPONGE bondline directly under the above four thermocouples. The remaining thermocouples were located on the backside structure. A plan view X-ray of the prototype unit (figure 151) shows the thermocouple installations. Platinum - 10% rhodium (+)/platinum (-) thermocouples (ISA type S, 30 gage wire) were used for the surface temperature measurements. Chromel (+)/Alumel (-) thermocouples (ISA type K, 30 gage wire) were used for the bondline and backside temperature

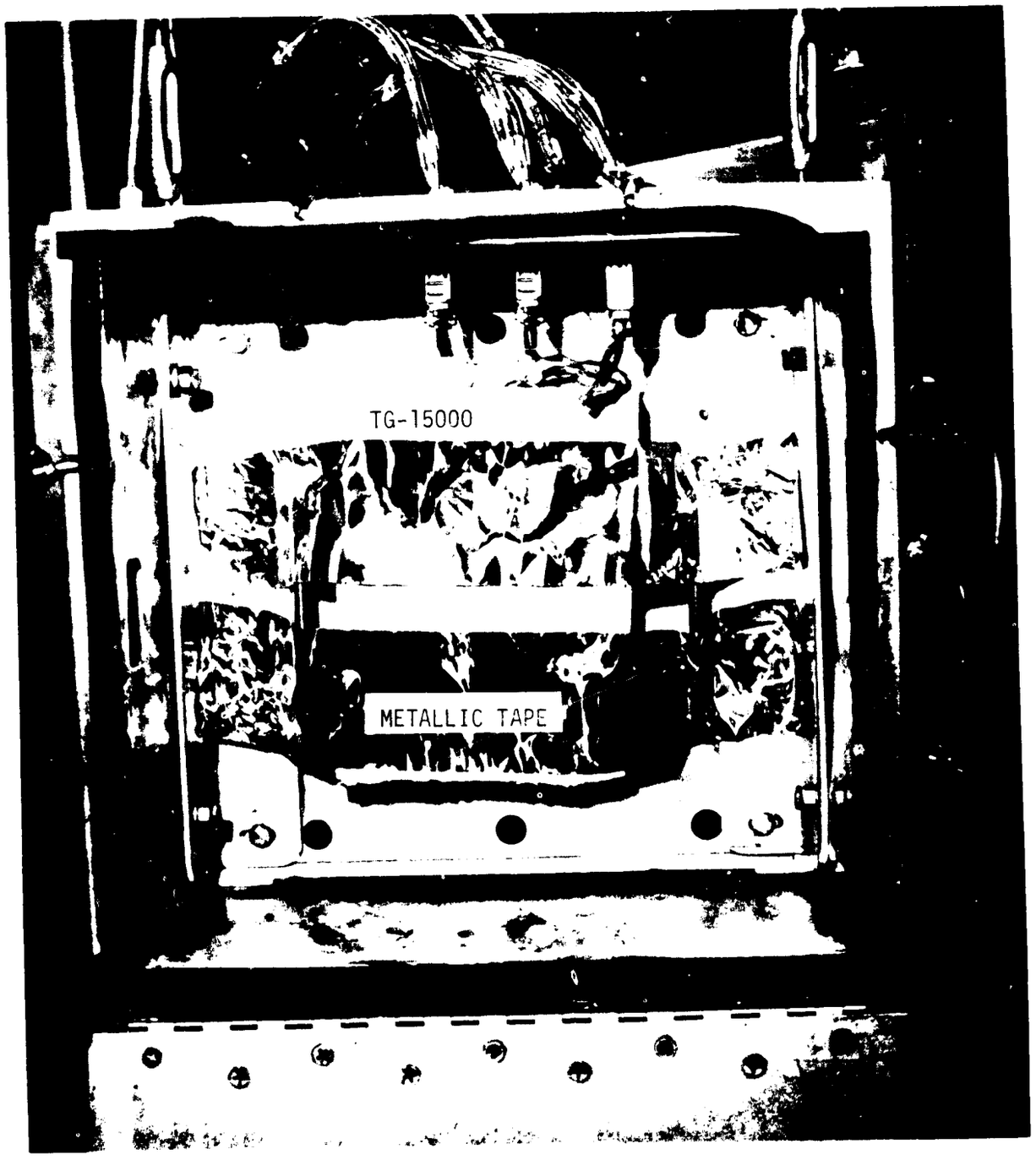

PROTOTYPE INSTALLATION - BACK VIEW

FIGURE 149

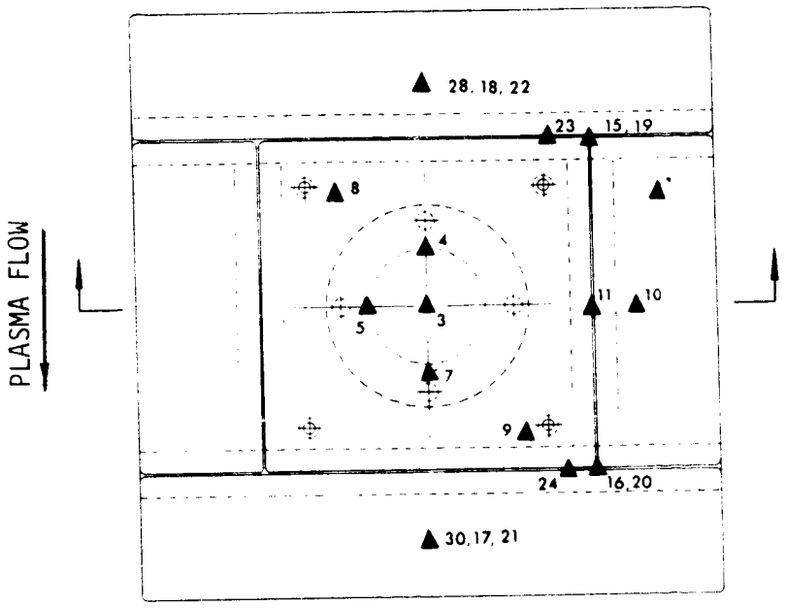

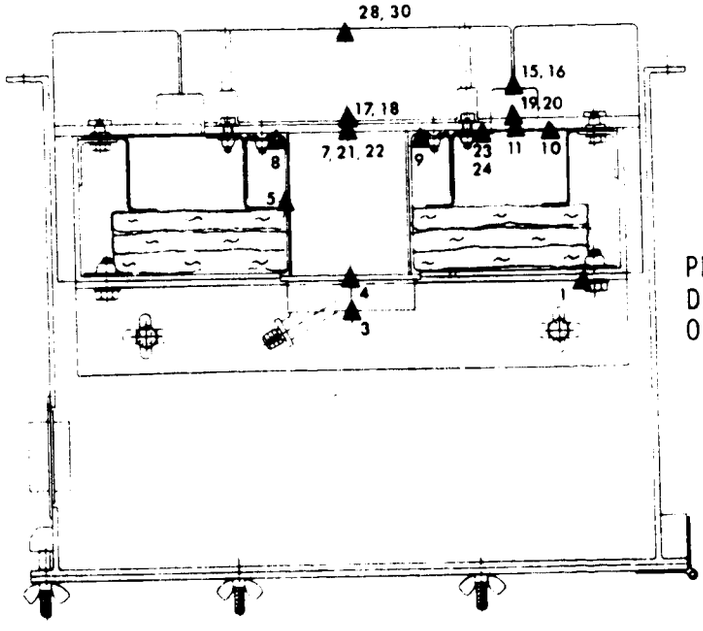

PLASMA FLOW
DIRECTION IS OUT
OF THE PAPER

PROTOTYPE THERMOCOUPLE LOCATIONS

FIGURE 150

PLASMA FLOW →

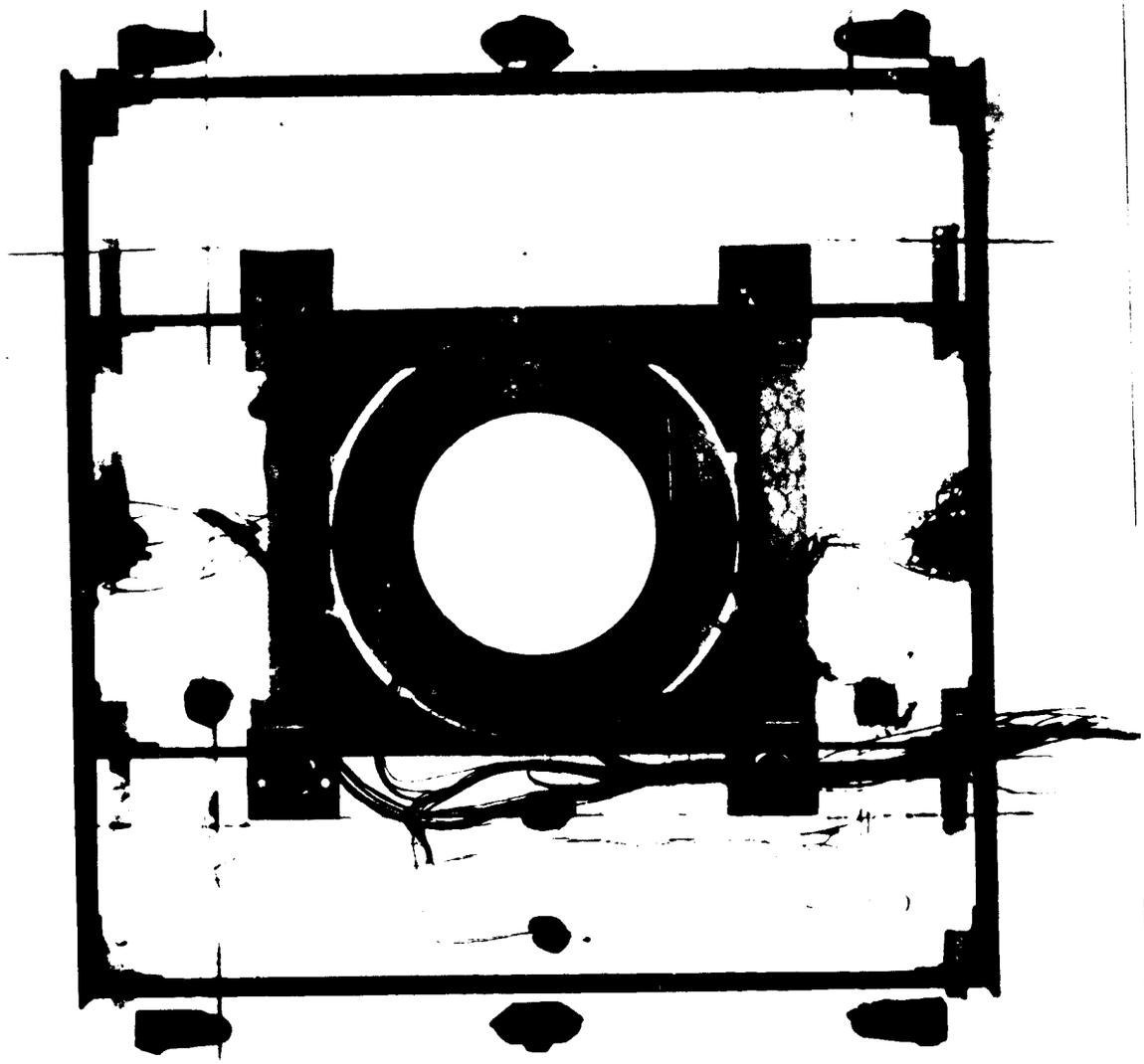

SHOT FROM BACK SIDE

PROTOTYPE PLAN VIEW X-RAY

FIGURE 151

measurements. The thermocouple installation is discussed in the section on TEST HARDWARE FABRICATION.

The calibration plate (figure 152) on the opposite side of the nozzle from the test model, contained 14 calorimeters, one of which was a 2.54 cm (1.00 in.) water cooled model, and 6 pressure transducers. A new set of calorimeters were used for the prototype tests.

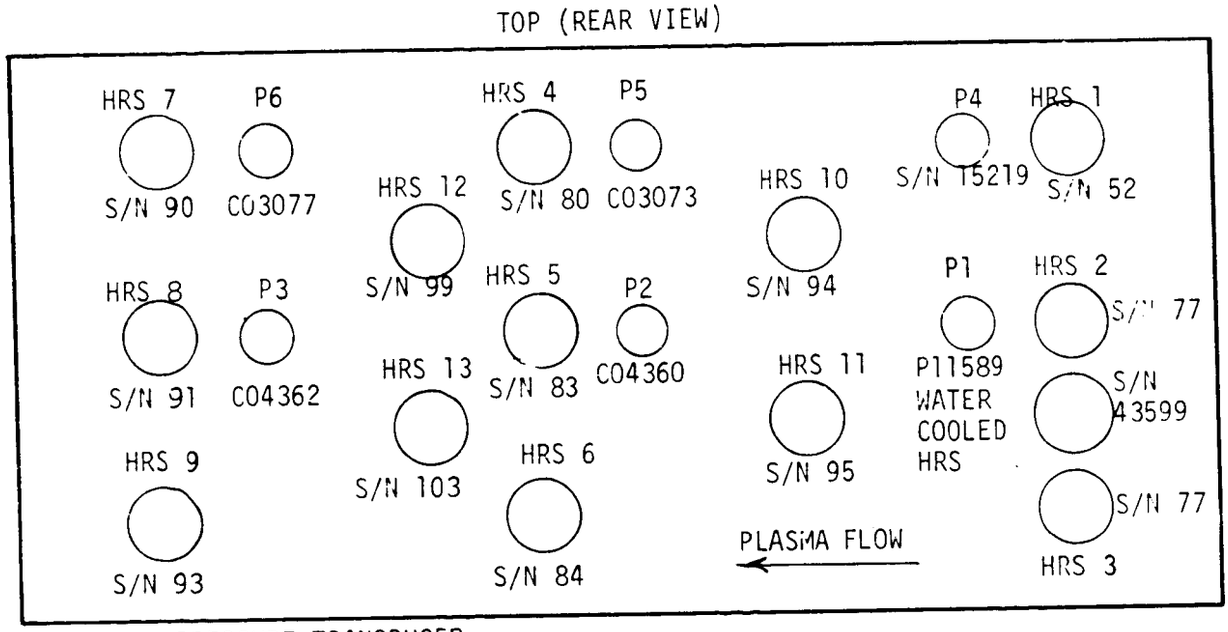

CALIBRATION PLATE MAP

FIGURE 152

Test results. - The peak surface temperature achieved on the first test of the prototype unit was about 1258 K (1805°F). The difference in temperature measured by the two surface thermocouples was 44 K (80°F). The arc heater run time was 2352 seconds. The maximum bondline temperatures for bondline TC 17 monitored on the strip chart recorders was 402 K (265°F).

A short term temperature peak coincident with repressurization was measured by TC 15 on top of the FI-600 filler strip during the first test, as shown in figure 153. This result was similar to the first breadboard test. However, a temperature peak did not occur for TC 16, which was similarly located, as shown in figure 154.

Based on the results of the first prototype test, the run time for the second test was extended 614 seconds for an arc heater run time of 2966 seconds. The maximum bondline temperature measured by TC 17 increased 23 K (41°F) to 425 K(306°F). However, the aluminum-skin temperatures measured by TC's 10 and 11 decreased about 3.3 K (6°F).

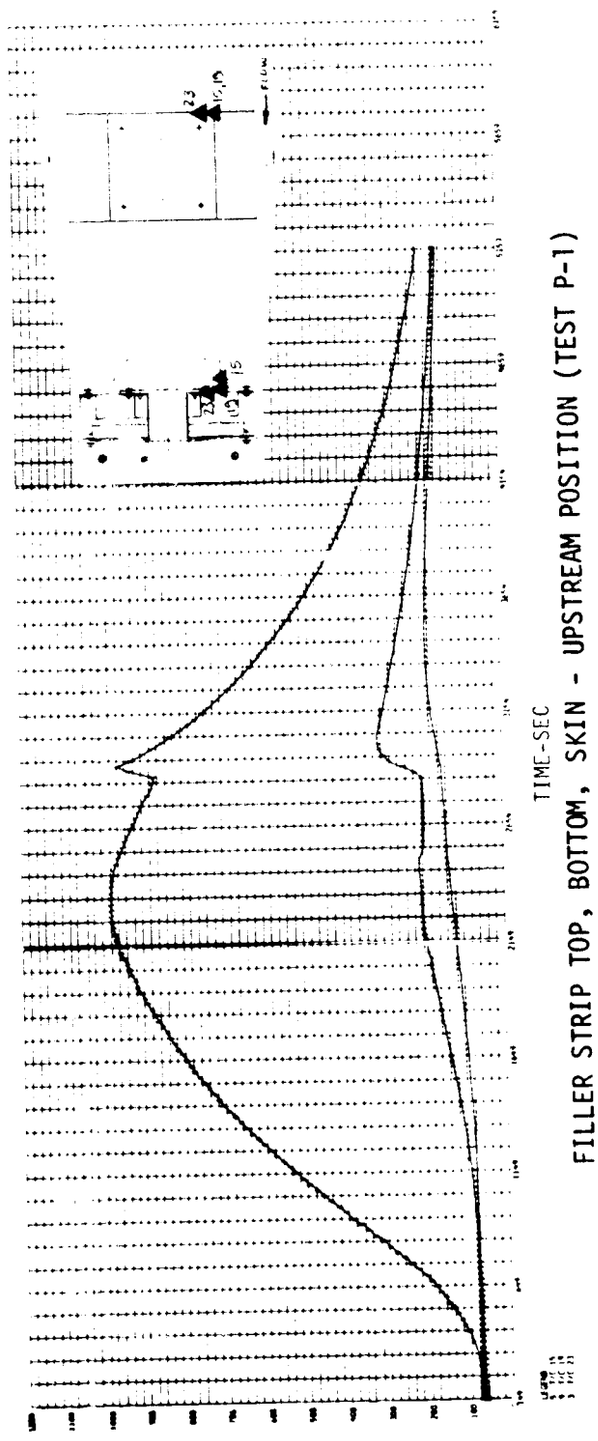

FILLER STRIP TOP, BOTTOM, SKIN - UPSTREAM POSITION (TEST P-1)

FIGURE 153

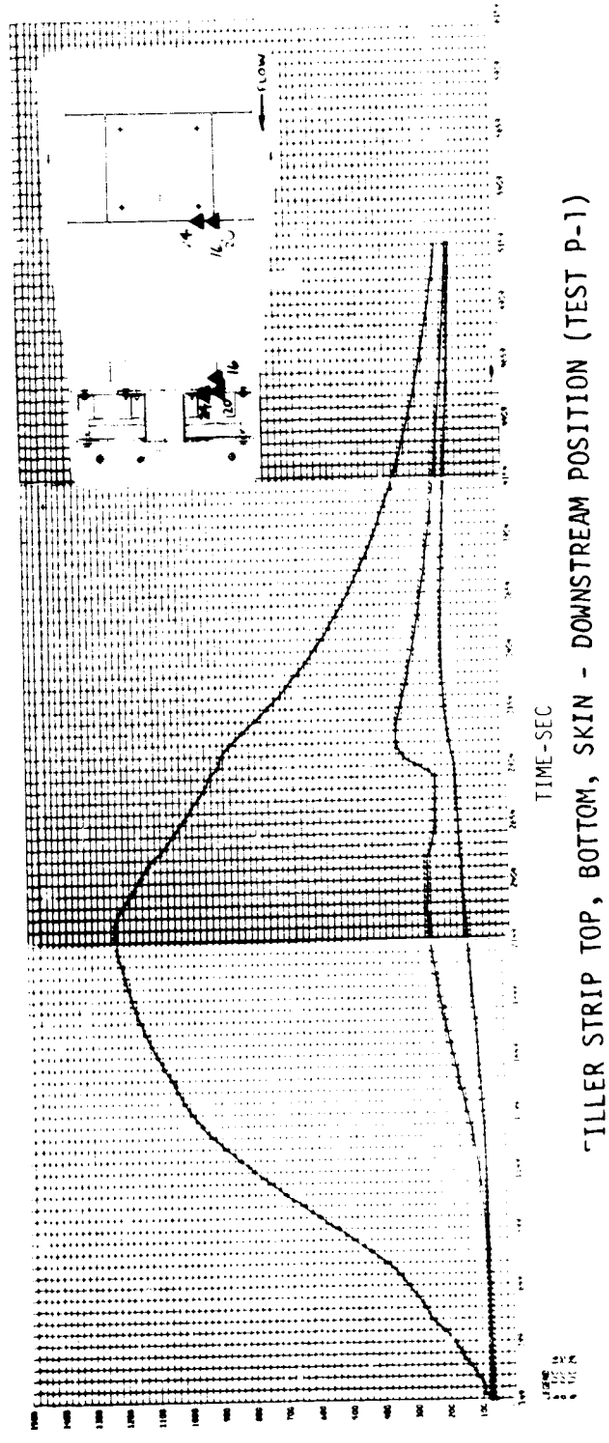

FILLER STRIP TOP, BOTTOM, SKIN - DOWNSTREAM POSITION (TEST P-1)

FIGURE 154

On the third test, the bondline and aluminum skin thermocouples were monitored and the test was to be terminated when the bondline temperatures were within about 28 K (50°F) of the desired maximum. The arc heater run time for the third test was 3927 seconds. Further time extension was deemed to have diminishing returns, and tests four through ten were run with the same test time as the third test run.

On the fourth test, the thermal response for TC 20 located under a filler strip was as shown in figure 155. The shape of the short term temperature spike is analogous to the first test exothermic reaction of silicone resin.

The measured control parameters for the tenth test run are shown in figure 156. The data from the tenth test run is shown in a set of three plot frames (figures 157 through 169). Nine show temperature histories selected to present the temperature distribution in various regions. Heating rate is shown in figures 166 through 169. These curves show uniform heating over the calibration plate for the water cooled calorimeter and thirteen heat rate sensors (HRS), where similar data for the breadboard test did not. This may be due to a new set of calorimeters and a flat black, high emittance, paint added to the calibration plate prior to these tests.

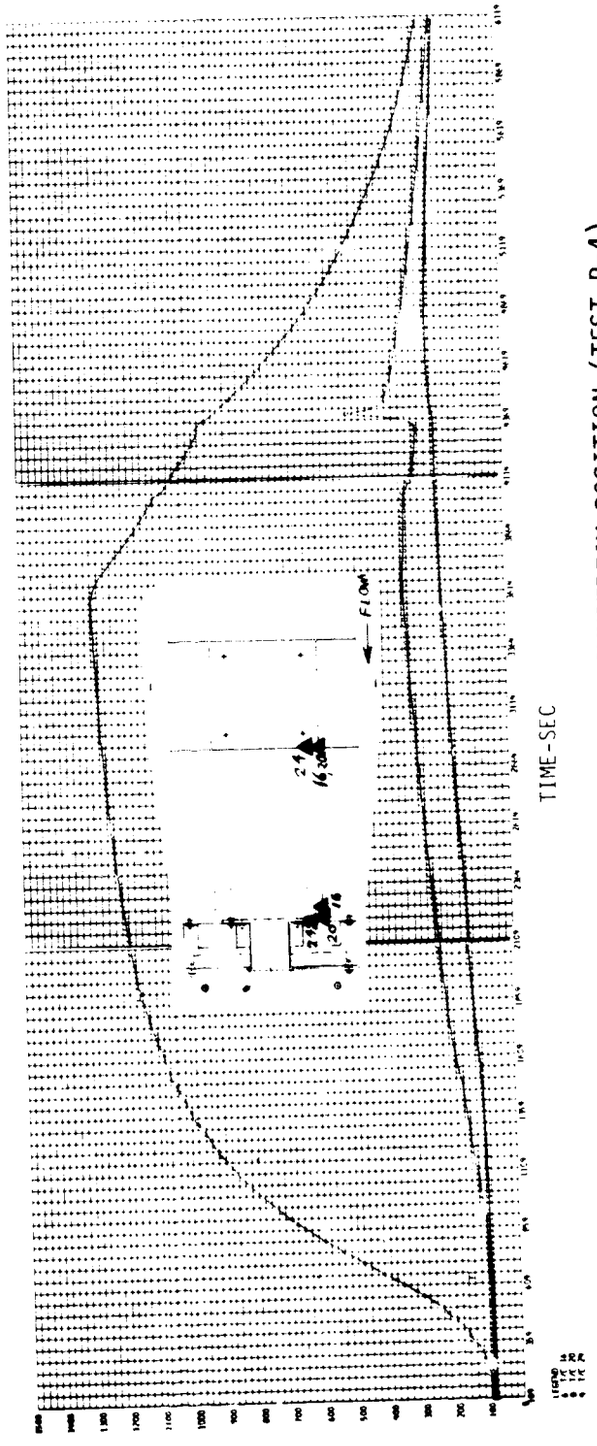

FILLER STRIP TOP, BOTTOM, SKIN - DOWNSTREAM POSITION (TEST P-4)

FIGURE 155

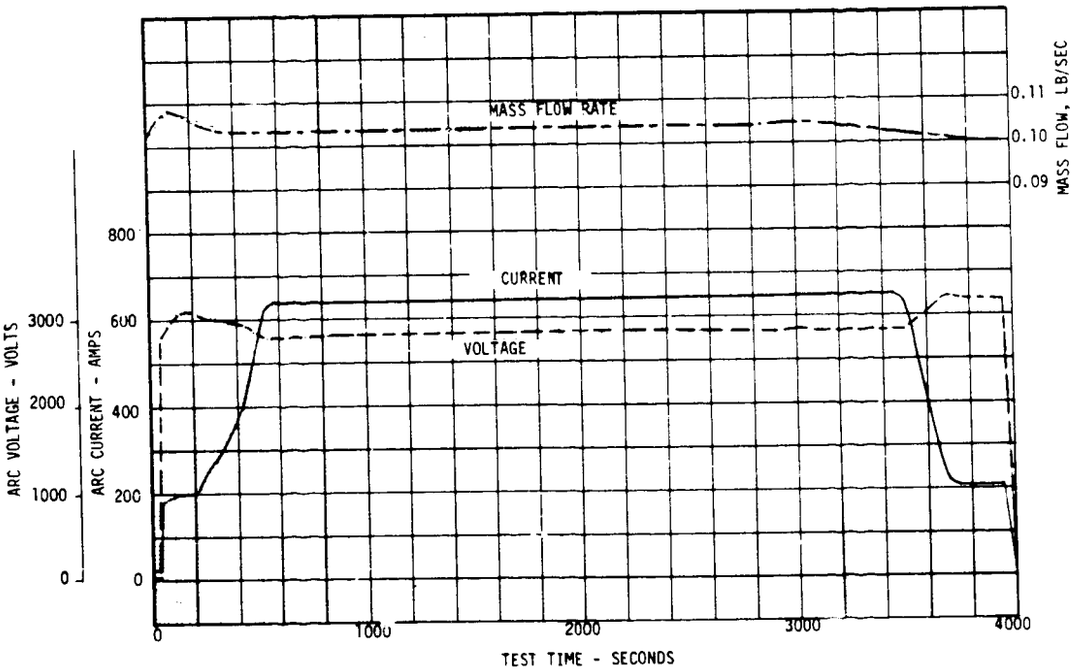

PROTOTYPE TEST CONTROL PARAMETERS

FIGURE 156

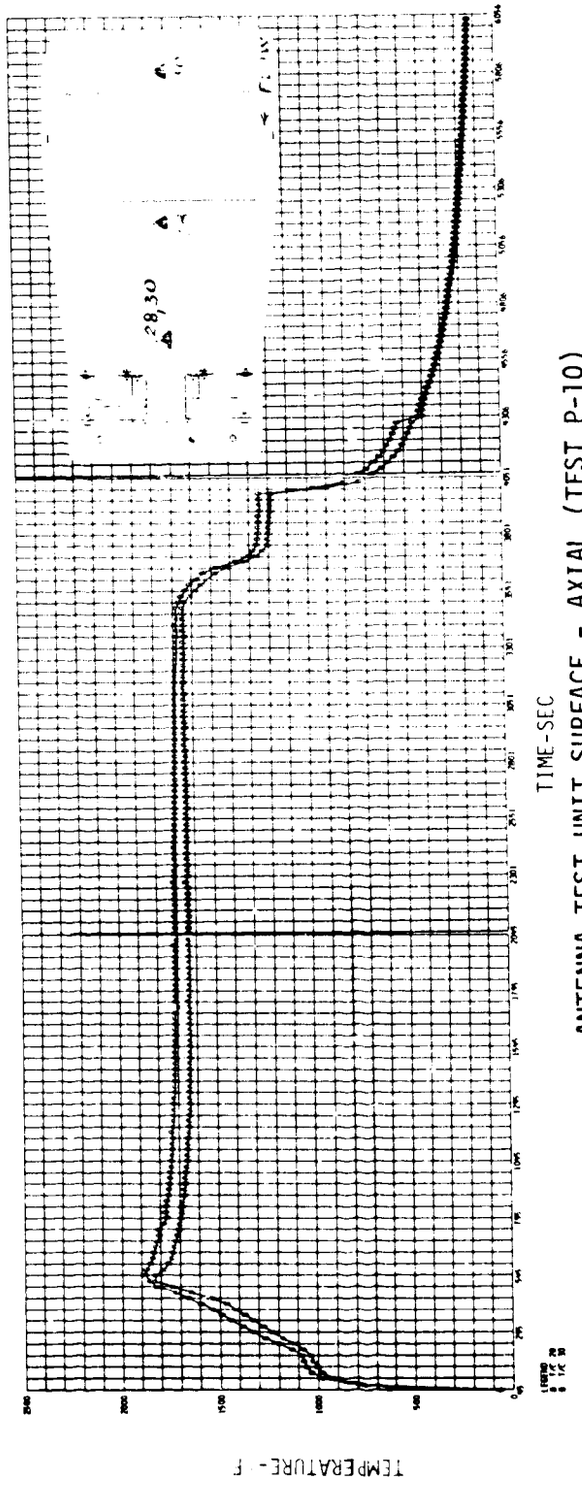

ANTENNA TEST UNIT SURFACE - AXIAL (TEST P-10)

FIGURE 157

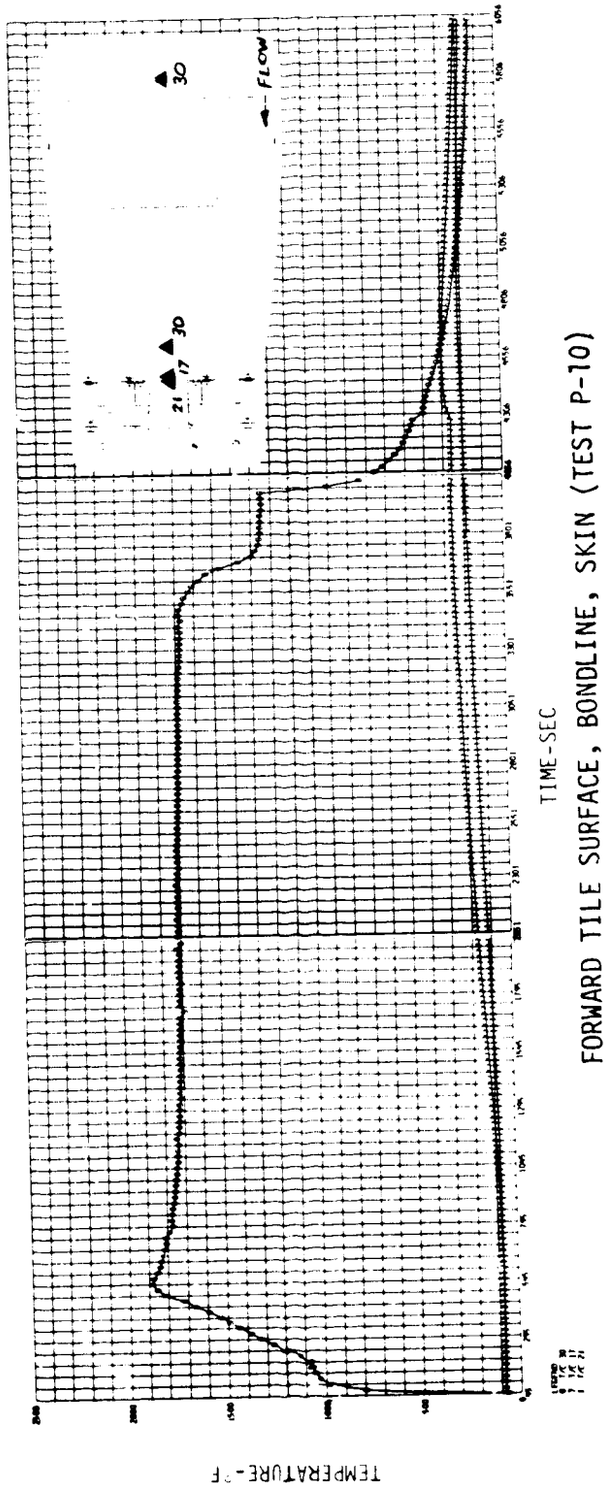

FORWARD TILE SURFACE, BONDLINE, SKIN (TEST P-10)

FIGURE 158

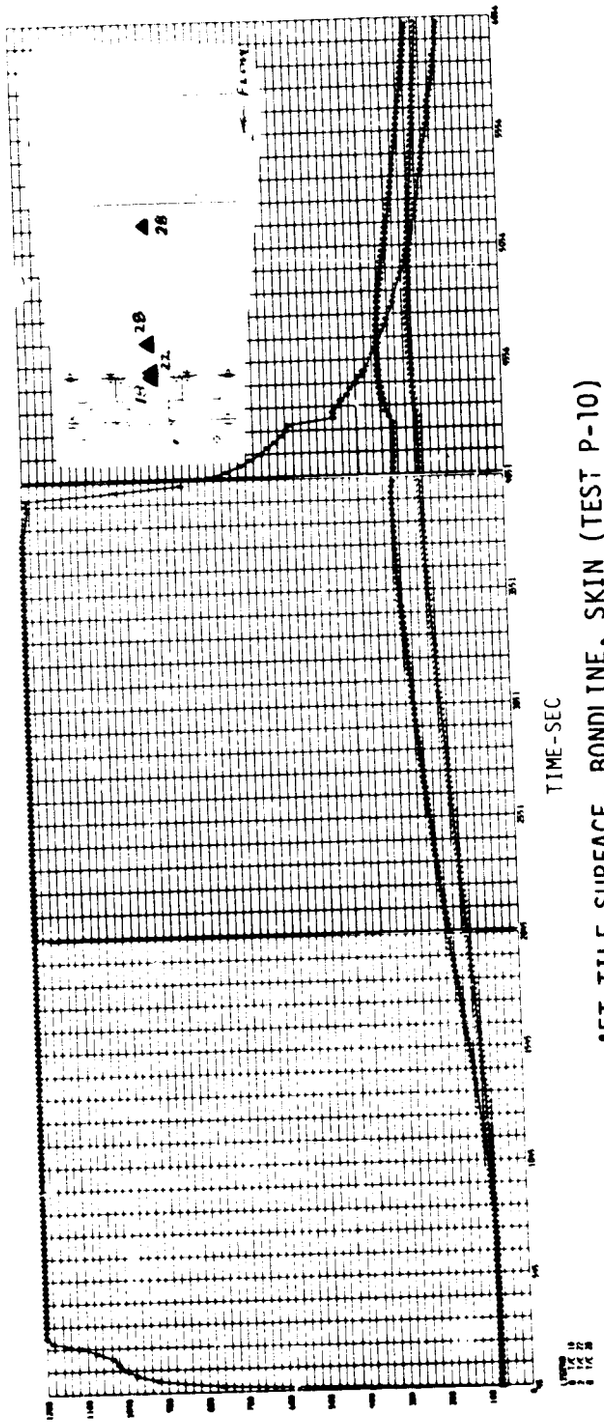

AFT TILE SURFACE, BONDLINE, SKIN (TEST P-10)

FIGURE 159

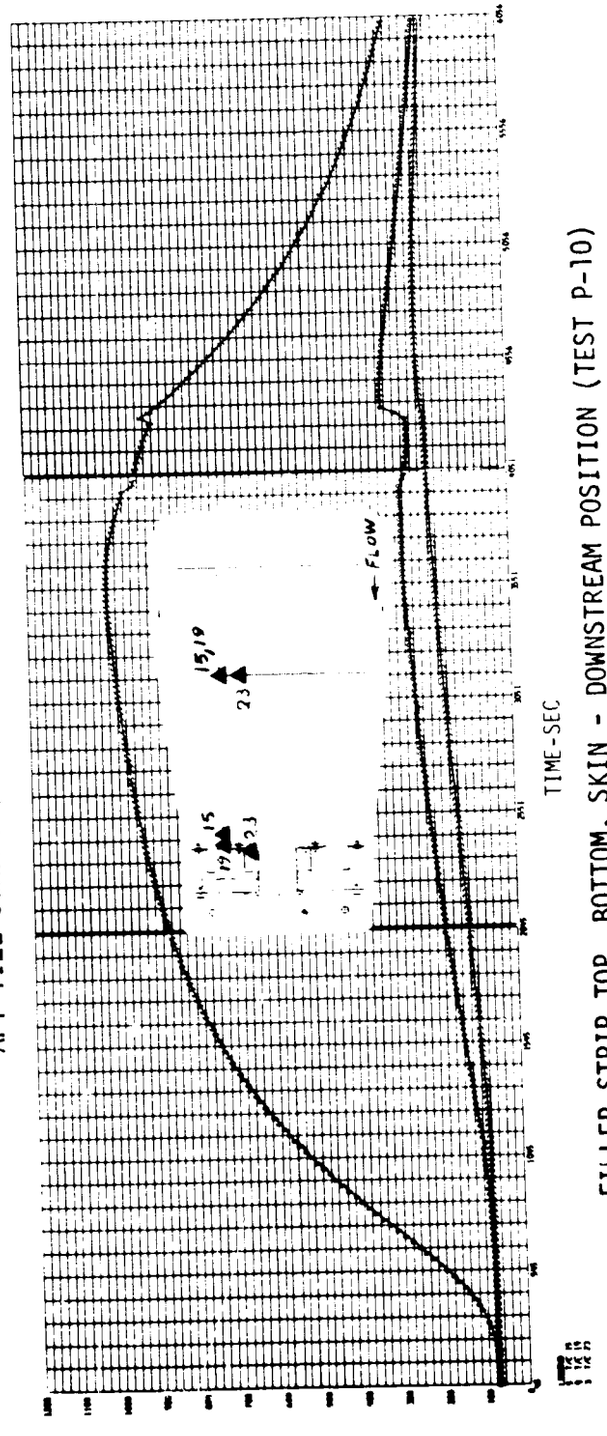

FILLER STRIP TOP, BOTTOM, SKIN - DOWNSTREAM POSITION (TEST P-10)

FIGURE 160

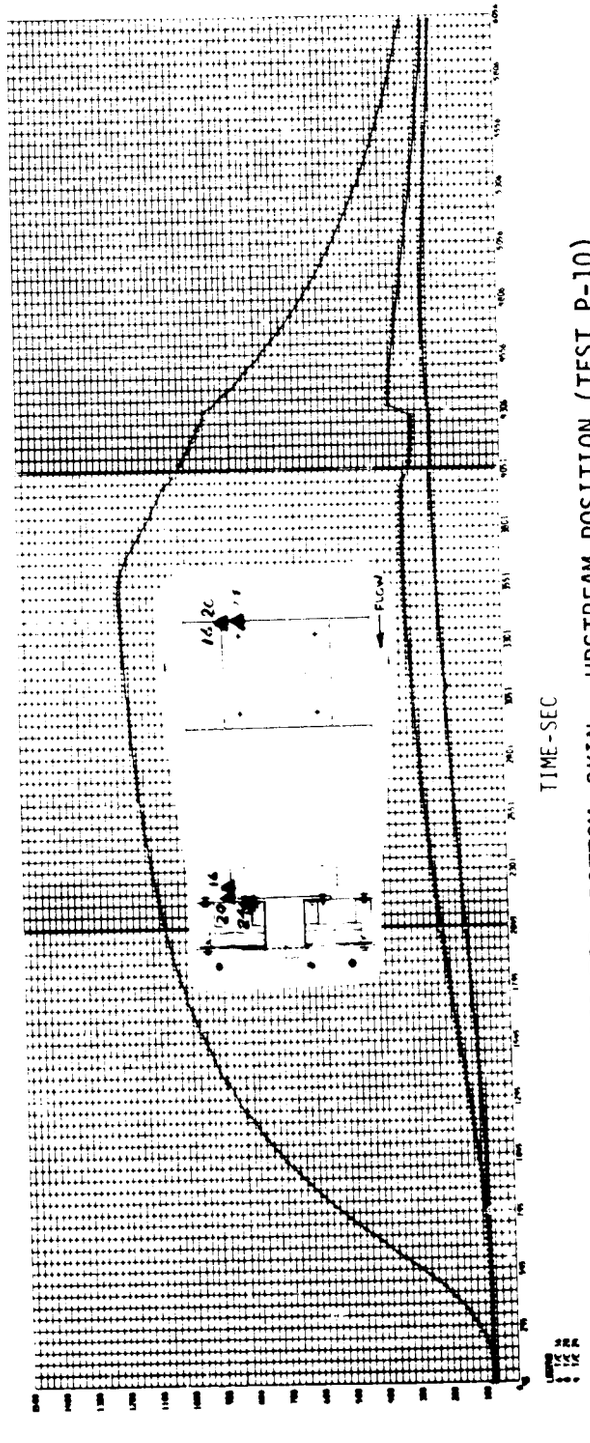

FILLER STRIP TOP, BOTTOM, SKIN - UPSTREAM POSITION (TEST P-10)

FIGURE 161

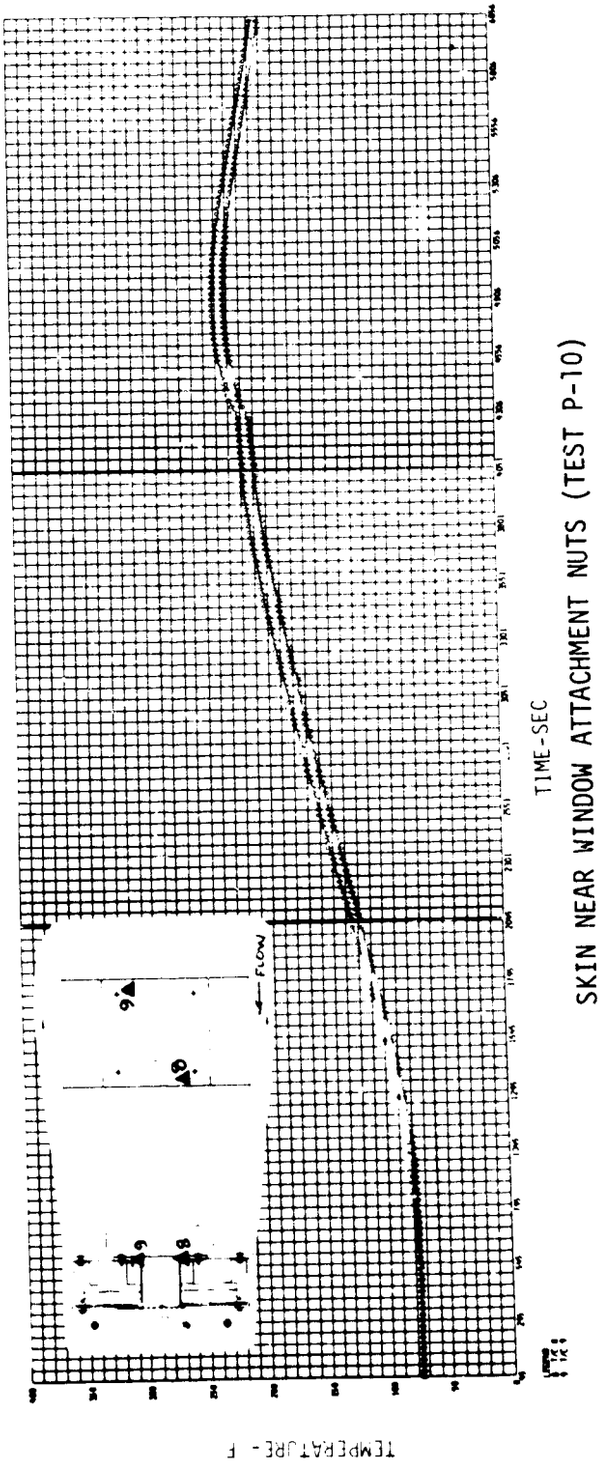

SKIN NEAR WINDOW ATTACHMENT NUTS (TEST P-10)

FIGURE 162

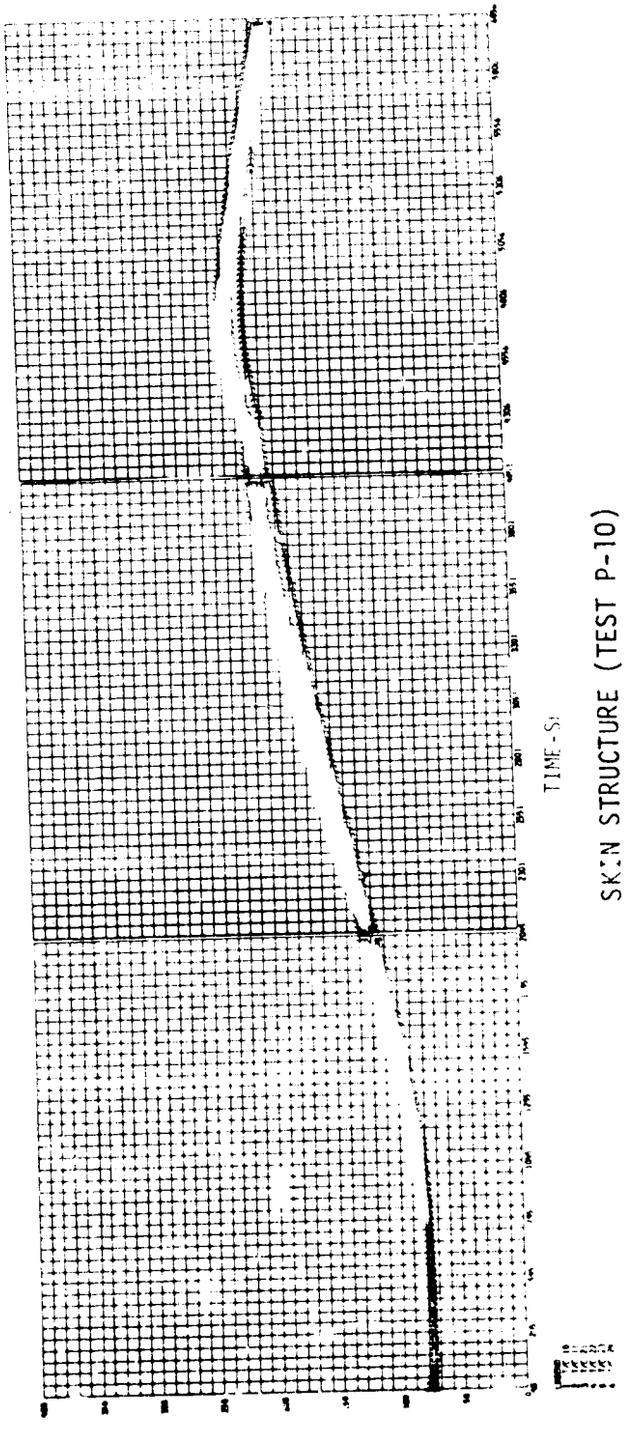

SKIN STRUCTURE (TEST P-10)

FIGURE 163

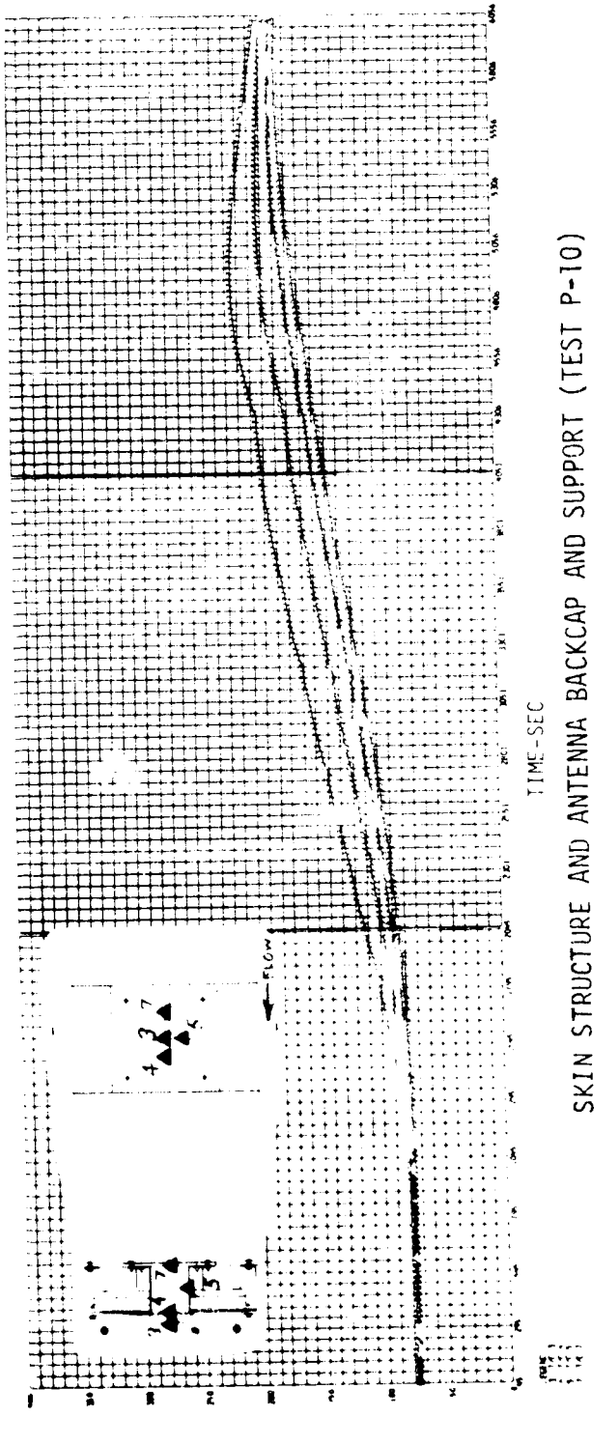

SKIN STRUCTURE AND ANTENNA BACKCAP AND SUPPORT (TEST P-10)

FIGURE 164

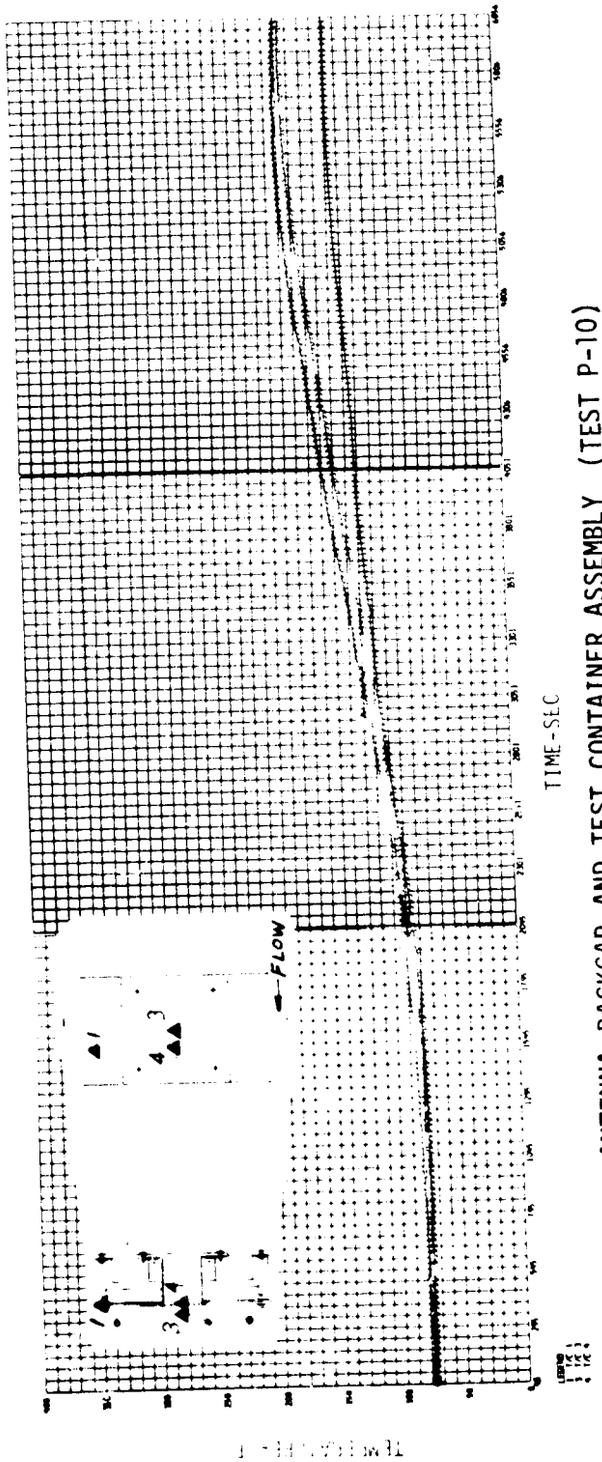

ANTENNA BACKCAP AND TEST CONTAINER ASSEMBLY (TEST P-10)

FIGURE 165

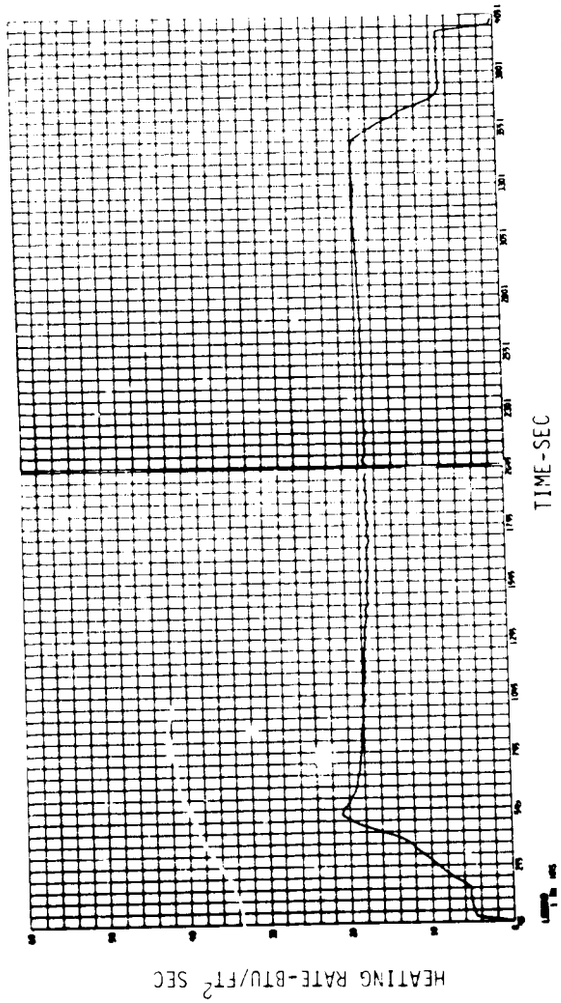

HEATING RATE - CALIBRATION PLATE WATER COOLED CALORIMETER (TEST P-10)

FIGURE 166

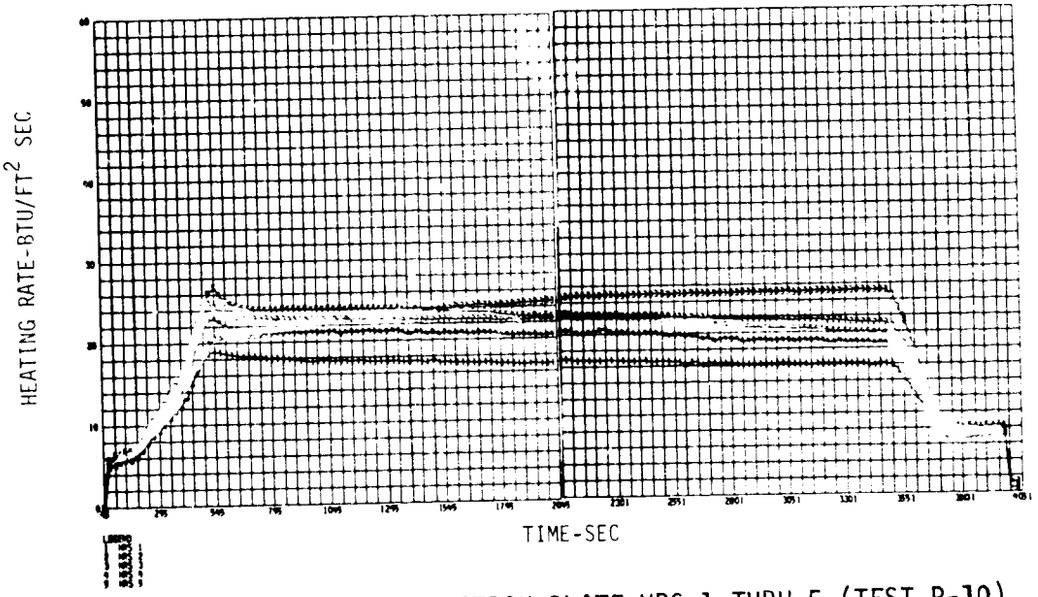

HEATING RATES - CALIBRATION PLATE HRS 1 THRU 5 (TEST P-10)

FIGURE 167

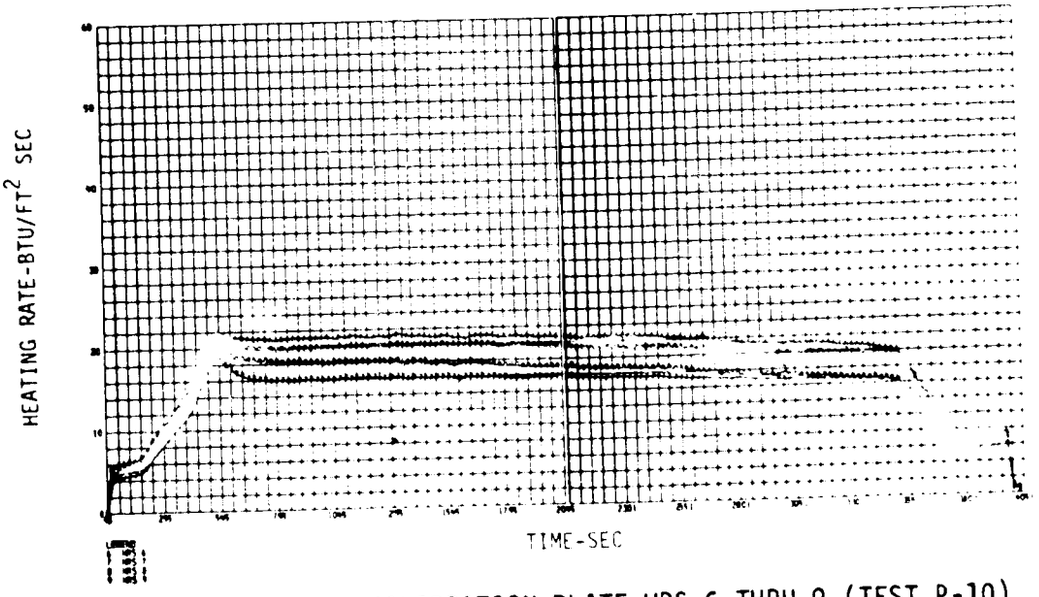

HEATING RATES - CALIBRATION PLATE HRS 6 THRU 9 (TEST P-10)

FIGURE 168

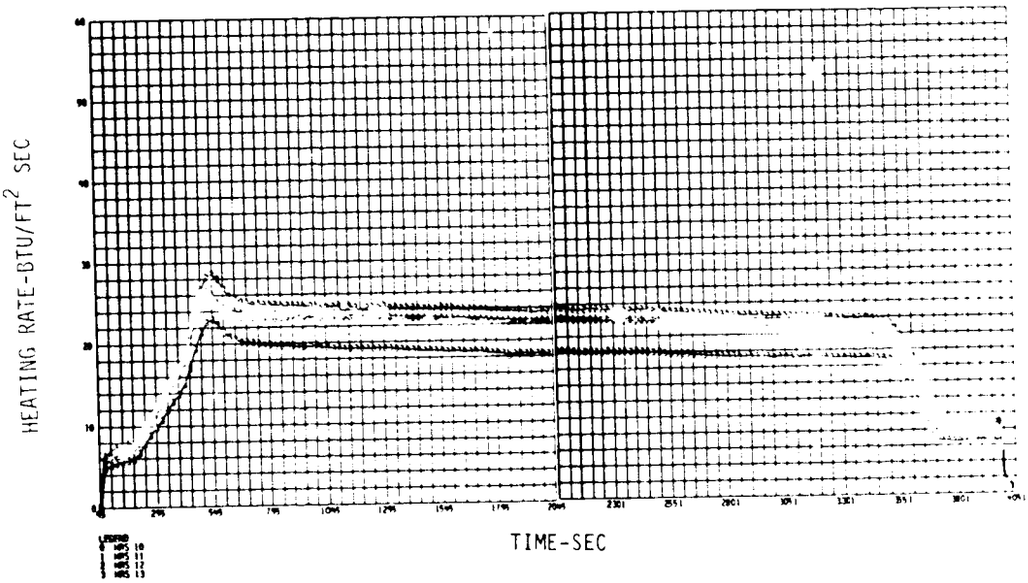

HEATING RATES - CALIBRATION PLATE HRS 10 THRU 13 (TEST P-10)

FIGURE 169

THIS PAGE INTENTIONALLY LEFT BLANK

EVALUATION

The Evaluation task (Task 5) determines: (1) compliance with electrical performance goals; (2) validity of the design approach; (3) reuse capability based on thermal and electrical performance and physical examination; and (4) agreement between predicted and measured temperatures.

The results show good electrical and thermal performance, and no physical changes or failures limiting reuse capability.

Electrical Test Data Evaluation

This section gives an evaluation of the electrical test results described in the section on ELECTRICAL TESTING. Comparisons are made to show changes resulting from the Orbiter entry environment.

Component test. - The component test results were analyzed to evaluate the S-band antenna performance and compliance with design goals. In general the axial ratios were somewhat higher than expected at the beam edges ($\theta = \pm 60$) at the design frequency (2.2875 GHz). However, the circular gain at the beam edges is greater than 0 dB over most of the frequency band. The VSWR is well within the 1.5:1 goal except at the very low end of the band where VSWR is slightly greater.

The axial ratios for each of the S-band antennas tested are given in table XIX. At low frequencies the axial ratios are generally greater than the 4 dB goal. This was expected, since the antennas are tuned for the lowest axial ratio at 2.2875 GHz. The axial ratios at the beam edges, however, are affected by the ground plane edge effects to some degree as shown by comparison of figures 59 and 61 in the section on S-BAND ANTENNA SYSTEM DESIGN. Therefore, the axial ratios at the beam edges of the patterns at 2.2875 GHz, for example, can be expected to vary to some degree as the ground plane size varies. The average axial ratio around the beam center is more indicative of the true axial ratio of the antenna. At angles greater than $\theta = 60°$, the axial ratio can always be expected to increase, since the ground plane begins to affect the parallel component of the RF field.

The circular gain for each of the S-band antennas is given in table XX. The gain is generally higher than the 0 dB goal over the 120° beamwidth. The LHC polarization gain levels range from 7 to 17 dB below the peak RHC gain. The higher LHC levels occur at the lower frequencies as shown by the patterns in figure 96 in the section on ELECTRICAL TESTING.

Table XXI gives the design performance parameters and the corresponding measured results for each of the S-band antennas. This data shows reasonable compliance with the design goals except for the axial ratio at the lower frequencies. The impact of the higher axial ratios is an increase in

TABLE XIX

COMPONENT TEST AXIAL RATIOS

	AXIAL RATIO (dB)						
ANTENNA S/N	101			102	105		
FREQ (GHz)	2.1	2.2	2.2875	2.2875	2.1	2.2	2.2875
θ=0°	11.8	5.0	2.2	1.6	6.2	3.6	2.0
θ=±60° ①	16.5	9.9	8.0	6.8	15.4	8.6	8.0

① MAXIMUM AXIAL RATIO ON X OR Y PLANE

TABLE XX

COMPONENT TEST CIRCULAR GAINS

	CIRCULAR GAIN (dB)						
ANTENNA S/N	101			102	105		
FREQ (GHz)	2.1	2.2	2.2875	2.2875	2.1	2.2	2.2875
θ=0°	2.0	5.8	7.0	6.2	5.6	5.8	6.8
θ=±60° ①	-10.0	2.8	2.3	1.0	-0.7	1.9	1.0

①MAXIMUM GAIN ON X OR Y PLANE

TABLE XXI

DESIGN GOAL AND MEASURED ANTENNA PARAMETERS

PARAMETER	DESIGN	MEASURED					
		ANTENNA S/N 101			ANTENNA S/N 105		
		2.1 GHz	2.2 GHz	2.2875 GHz	2.1	2.2 GHz	2.2875 GHz
BEAMWIDTH	120° (0 dB Gain)	-81°,+19°	·120°	·120°	+55°,-75°	·120°	120
VSWR	·1.5:1	1.35:1	1.07:1	1.28:1	1.8:1 ①	1.26:1	1.44:1

① · 1.5:1 ABOVE 2.15 GHz

transmission loss due to polarization loss. A 6 dB increase in axial ratio above the 4 dB nominal value results in an increase of about 1 dB in transmission loss.

Breadboard tests. - The breadboard test results were analyzed to evaluate the S-band antenna system performance relative to design goals. The presence of the thermocouple wires, particularly in the antenna window area, precluded using the test results as a model to show compliance with design goals. However, the test results of the S-band antenna system mockup essentially show compliance with the design goals. The model used for this test contained the essential features of the final S-band antenna system except for minor differences. ECCOFOAM dielectric material was used in place of the LI-1500 HRSI and a simpler joint design was used around the antenna window. Therefore, the prethermal breadboard unit tests were considered primarily as standard for comparison with postthermal test data.

Table XXII shows a comparison of the prethermal and postthermal axial ratio and linear gain data (figures 103 and 110) from the Breadboard Unit Test at MDAC-E. The changes in these parameters are not as great as measured during the thermal support tests (figure 108) and appear somewhat random in character.

TABLE XXII

BREADBOARD UNIT AXIAL RATIOS AND PEAK LINEAR GAINS

	AXIAL RATIO (dB)								
FREQ (GHz)	2.1			2.2			2.2875		
ϕ(DEGREES)	0°	+60°	-60°	0°	+60°	-60°	0°	+60°	-60°
PRETHERMAL	11.2	19.0	3.5	13.6	15.8	12.0	9.5	17.2	10.8
POSTTHERMAL	12.5	19.0	6.0	20.0	13.0	19.0	12.6	18.5	9.7
Δ CHANGE	+1.3	0.0	+2.5	+6.4	-1.2	+7.0	+3.1	+13.	-1.1
	PEAK LINEAR GAIN (dB)								
PRETHERMAL	1.9	-2.1	0.5	3.7	-0.4	1.8	3.9	-1.7	0.0
POSTTHERMAL	4.6	-0.5	-0.4	4.9	-4.5	3.4	4.9	-0.8	3.8
Δ CHANGE	+2.7	+1.6	-0.7	+1.2	-4.1	+1.6	+1.0	+0.9	+3.8

Since the changes observed in the radiation pattern were greater than expected, somewhat random in character and, therefore, not establishing a clear trend, additional tests and analyses were performed. The primary items considered for investigation were: (1) thermocouple lead wire bundle position;

(2) thermocouple position change inside HRSI; and (3) copper deposition on the surface of the antenna window.

Radiation pattern measurements were made to assess the effects of the thermocouple lead wire bundle position. Figure 170 shows the typical effects of two different wire bundle positions, one with the wire bundles coiled and the other with the wire bundles held straight behind the test unit. There are changes in both pattern shape and axial ratio. The smaller changes in radiation pattern shape compared to those observed in tests at NASA-JSC (figure 108), are due in part to the larger ground plane used in the tests at MDAC-E.

Changes in thermocouple position were evaluated by comparing an X-ray of the breadboard unit taken after the thermal test with one taken before. No changes were detected.

An atomic absorption test was performed to determine if copper from the arc tunnel electrodes was deposited on the breadboard unit surface. Surface coating samples of equal areas were taken from the side and top of the forward TPS tile. The side sample was not subjected to the plasma stream and, therefore, served as a control sample. The results showed 0.06×10^{-6} gm/cm^2 (8.6×10^{-10} lb/in.^{2}) of copper on the top sample and less than 0.03×10^{-6} gm/cm^2 (4.4×10^{-10} lb/in.^{2}) on the side sample. The sensitivity of the atomic absorption test instrument is 0.03×10^{-6} gm/cm^2 (4.4×10^{-10} lb/in.^{2}). Therefore, it is possible that no copper is present on the side sample. If the copper was considered to be evenly distributed, which is unlikely, the equivalent thickness would be about 0.0055 micron. The skin thickness for copper is 1.4 microns at 2.2 GHz. Further, a significant part of the copper is probably in an oxide form. Therefore, it does not appear that the copper deposit is sufficient to cause any significant effect on the S-band antenna performance.

From these results it was concluded that the changes in radiation patterns of the breadboard thermal tests could be attributed primarily to changes in the position of the thermocouple leads from test run to test run.

The changes in the impedance measurement results (figure 109) are minor. It appears that the S-band antenna impedance is not affected by the surrounding environment as much as the radiation patterns. Since the changes in impedance were small and there was no increase in VSWR, specific tests were not conducted to evaluate the effects of the wire bundle. However, since the changes in results of the radiation pattern measurements can be attributed to changes in wire bundle position, it appears reasonable to also attribute the changes in impedance to wire bundle position changes.

The above evaluation of the breadboard unit electrical test data leads to the conclusion that the entry environment did not cause a significant change in the S-band antenna system performance. Therefore, no electrical design changes were made in the prototype S-band antenna systems. However, changes in the number and position of the thermocouples were made in order to obtain adequate electrical performance for comparison with the electrical design goals.

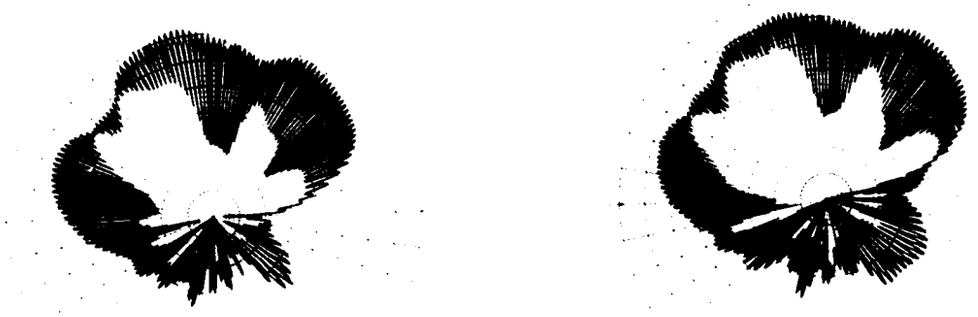

2.1 GHz

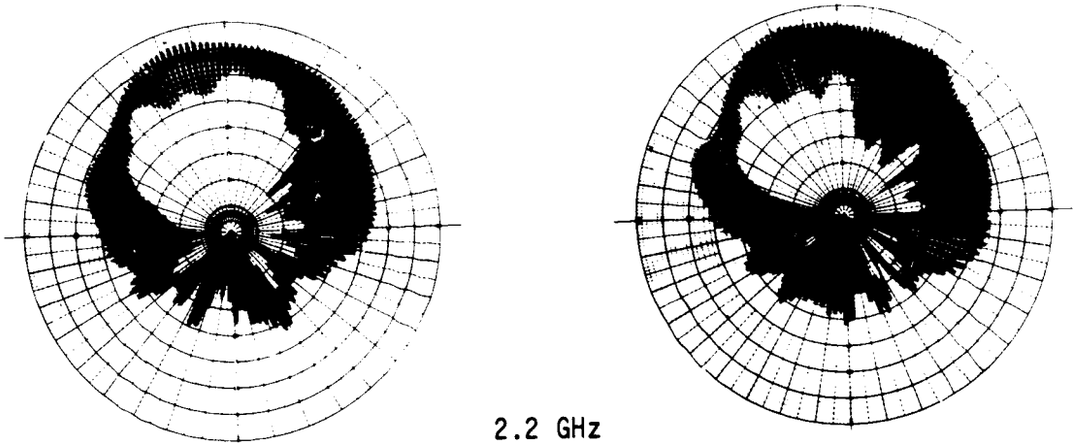

2.2 GHz

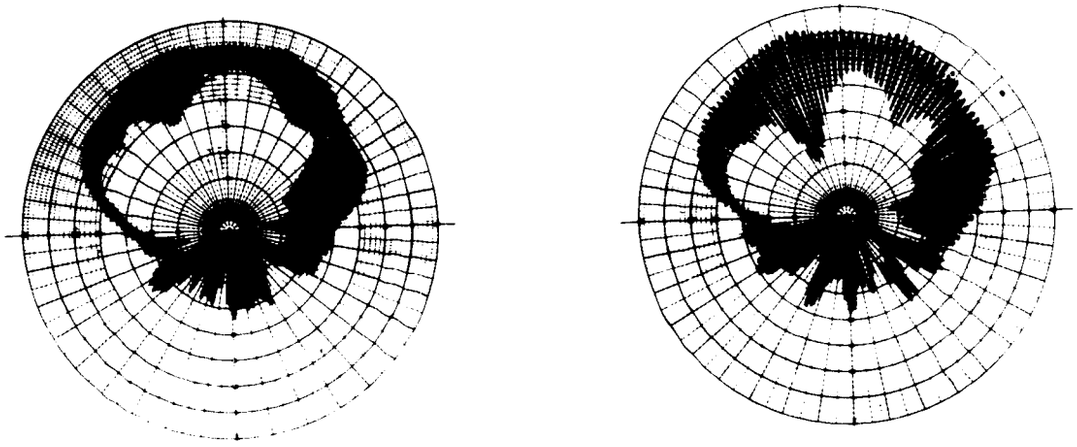

LEADS COILED 2.2875 GHz LEADS STRAIGHT

TYP CAL EFFECTS OF THERMOCOUPLE LEAD ROUTING
ON BREADBOARD UNIT RADIATION PATTERNS

FIGURE 170

Prototype tests. - The prototype test results were analyzed to evaluate the S-band antenna system performance relative to the design goals and to establish reference parameters for evaluation of the thermal reuse test results.

The results of the prototype electrical tests and the design goals are shown in table XXIII. The desired VSWR of 1.5:1 is exceeded only slightly (1.6:1) at the low end of the frequency range. The axial ratio exceeds the design goal by 3 dB near the beam edges and 1 dB at about $\theta = 45°$ at 2.2875 GHz. The axial ratio is within the design goal at 2.2 GHz and increases to as much as 10 dB on the beam edge at 2.1 GHz. The lower axial ratio at 2.2 GHz was unexpected since the results of the electrical design and component tests show the axial ratio was usually slightly higher at 2.2 GHz than at 2.2875 GHz. This reversal may be due in part to the thermocouples which extend into the TPS above the ground plane. The thermocouples form loops above the ground plane and could be excited sufficiently to result in small changes in axial ratio.

TABLE XXIII

DESIGN GOAL AND MEASURED PROTOTYPE UNIT PERFORMANCE PARAMETERS

PARAMETER	VALUE	
	DESIGN	MEASURED
OPERATING FREQUENCY	2.1 - 2.3 GHz	2.1 - 2.3 GHz
BEAMWIDTH	>120° (≥0.0 dB GAIN)	>120° (≥0.0 dB GAIN)
AXIAL RATIO	<4 dB OVER ±60°	<7 dB OVER ±60°
VSWR	<1.5:1	<1.6:1

Alternatively, the change in axial ratio may be due to differences in characteristics between the simulated and actual antenna window materials. However, the latter notion seems remote since the dielectric constant and loss tangent of the simulated and actual materials are low and small changes in them should not be significant. For example, the transmission loss change with a small change in loss tangent, dielectric constant, or an increase in bondline thickness is less than 0.15 dB as shown by figure 65 in the section on S-BAND ANTENNA SYSTEM DESIGN, under Electrical Design.

The results of the radiation pattern measurements (figure 112) in support of the thermal reuse tests at NASA-JSC are compared in figure 171. The RHC polarization patterns measured for reference prior to the first thermal cycles are compared with the patterns taken after each thermal cycle, or group of cycles, at 2.1 and 2.2875 GHz. The greatest changes occurred after the first thermal cycle. This is attributed to burn-off of the silicone resin in the

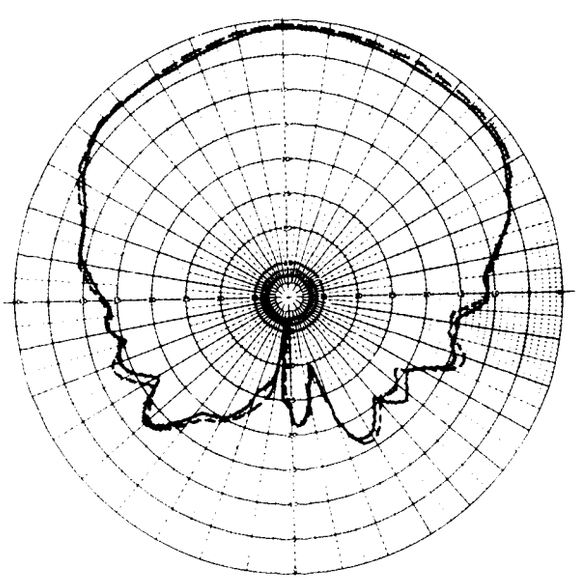

FIRST CYCLE

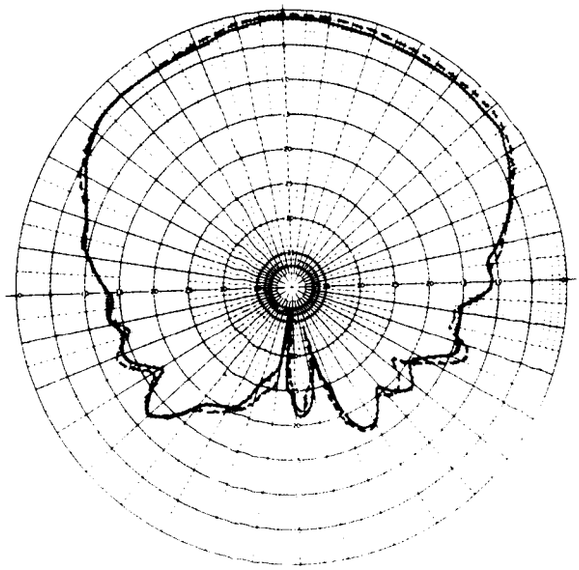

SECOND CYCLE

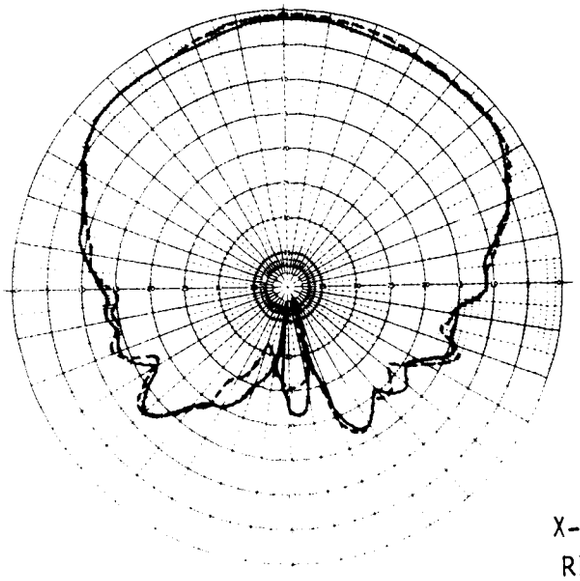

FIFTH CYCLE

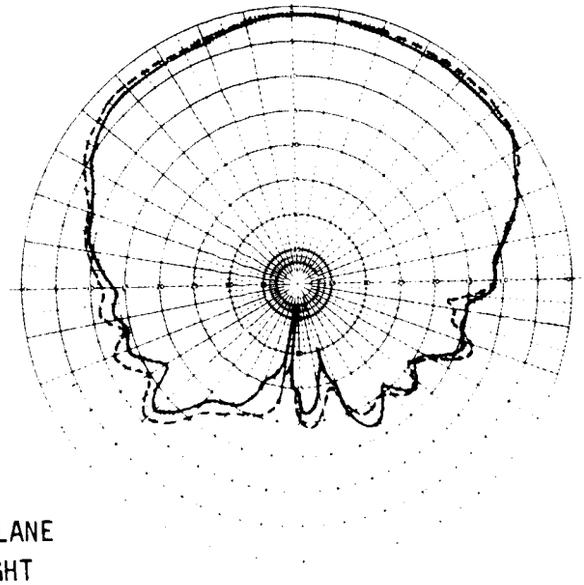

TENTH CYCLE

X-PLANE
RIGHT
CIRCULAR
2.2875 GHz

——- REFERENCE PATTERN BEFORE THERMAL TEST
– – – PATTERN AFTER THERMAL TEST CYCLE NOTED

EFFECT OF HIGH TEMPERATURE ON RADIATION PATTERNS - PROTOTYPE UNIT

FIGURE 171

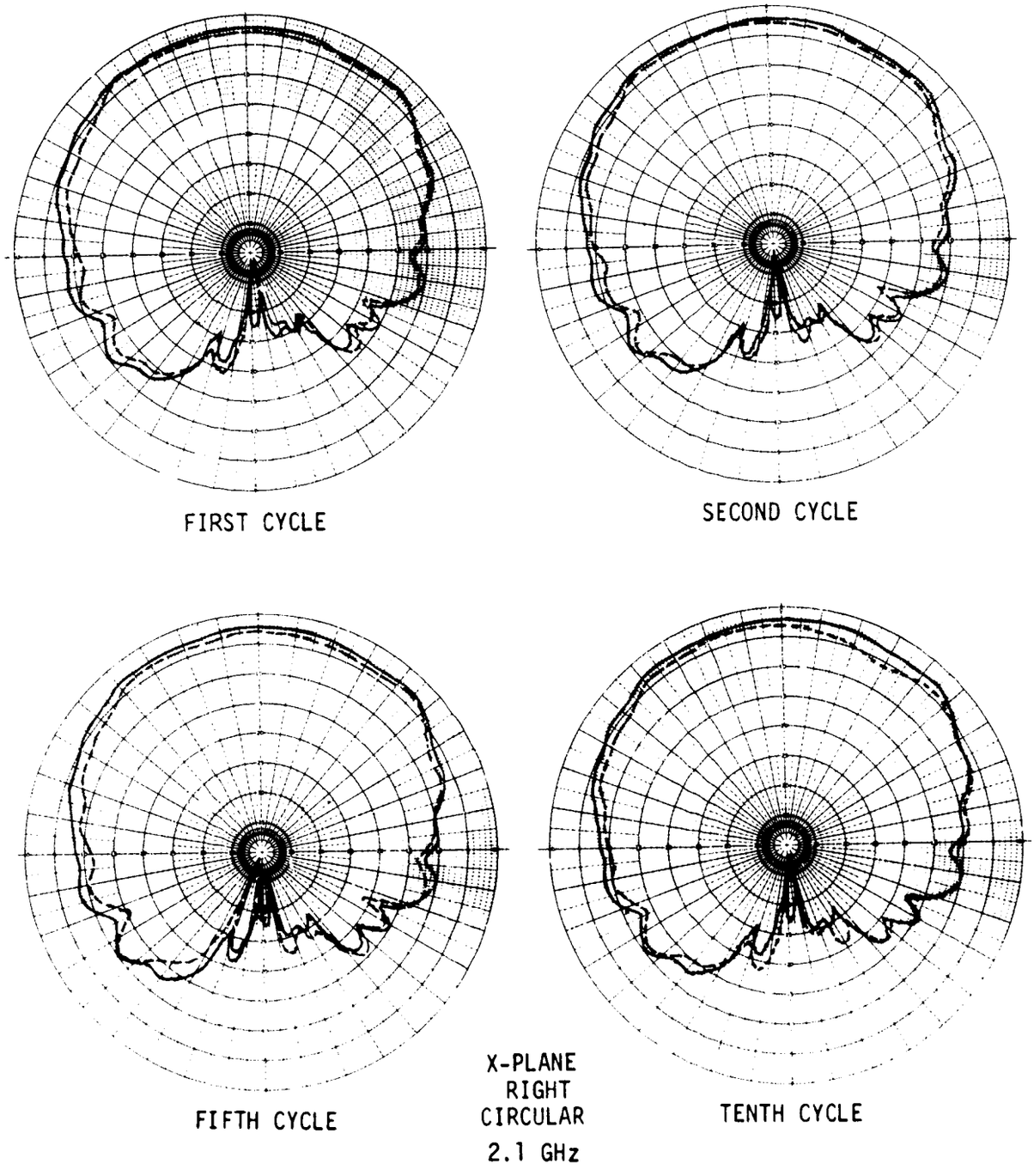

EFFECT OF HIGH TEMPERATURE ON RADIATION PATTERNS - PROTOTYPE UNIT

FIGURE 171 (Continued)

LI-1500 which occurs during the first thermal cycle. Burn-off occurs in the outer half of the LI-1500 where the temperature exceeds approximately 811 K (1000°). Subsequent test results did not reveal an accumulative trend in system performance which would support another conclusion. The radiation pattern comparisons shown in figure 171 also show a decrease in gain at 2.1 GHz and a contrasting increase in gain at 2.2875 GHz. The magnitude of change is relatively small in both cases, averaging about 1.0 dB at the low frequency and 0.5 dB at the high frequency.

The LHC polarization patterns (figure 112) also show minor changes after the first thermal cycle. Small changes in the backlobe levels and nulls were also observed, but the retention of general pattern characteristics was excellent. After the first thermal cycle, the observed changes in the radiation patterns are insignificant, since the accuracy of the measuring equipment is of the order of $\pm$0.25 dB. The 3 dB change observed in the RHC pattern at 2.1 GHz measured after the tenth thermal cycle may be due in part to small changes in the test setup, since the equipment was used for other tests between the fifth and tenth cycles.

A comparison of the peak linear gain and axial ratio of the prethermal and postthermal prototype radiation pattern measurements, figures 105 and 114, respectively, is given in table XXIV. The changes are, in general, smaller than observed in the test performed at NASA-JSC as described above. The decrease in gain at 2.1 GHz and an increase in gain at 2.2875 GHz was also observed. The change in axial ratio is opposite that measured at NASA-JSC where the axial ratio increased at 2.1 GHz and decreased at 2.2 and 2.2875 GHz. However, the changes in both gain and axial ratio are not sufficient to cause any significant change in the S-band antenna system performance.

TABLE XXIV
PROTOTYPE UNIT NO. 1 GAIN AND AXIAL RATIO COMPARISONS

	PEAK LINEAR GAIN (dB)					
FREQ (GHz)	2.1			2.2875		
θ(DEGREES)	0°	+60°	-60°	0°	+60°	-60°
PRETHERMAL	2.2	-2.6	0.0	2.5	1.4	-0.5
POSTTHERMAL	1.9	-2.0	0.5	3.2	2.2	0.1
Δ CHANGE	-0.3	+0.6	+0.5	+0.7	+0.8	+0.6
	AXIAL RATIO (dB)					
PRETHERMAL	4.0	5.1	4.5	3.0	7.0	4.0
POSTTHERMAL	3.1	6.9	5.2	3.5	6.6	3.5
Δ CHANGE	-0.9	+1.8	+0.7	+0.5	-0.4	-0.5

The results of the impedance measurements (figure 113) show that the change in impedance after ten thermal cycles is insignificant. This result parallels the result of the breadboard thermal test which showed a very minor difference in impedance after exposure to entry temperature.

Comparison of the Prototype Unit No. 1 prethermal and postthermal test impedance measurements, figures 106 and 115, respectively, shows a small transformation in the impedance plot after ten thermal test cycles. The result is a slight increase in VSWR below 2.11 GHz and a slight decrease in VSWR at frequencies above 2.11 GHz. The change, however, is insignificant and the results generally agree with those obtained during the tests at NASA-JSC. The evaluation of the prototype unit electrical test data leads to the conclusion that the thermal environment will not significantly affect the antenna window characteristics and/or the performance of the S-band antenna system. This conclusion is also supported by test results obtained by Bassett and Bomar (ref. 5), where the dielectric constant and loss tangent was measured, using transmission techniques, during ten cycles with simulated Orbiter entry temperature conditions. The changes in radiation pattern and impedance measured before, between and after completion of thermal tests were very small and could be caused by the local environment as much as by the effects of the thermal environment. The most significant effect detected appears to result from the burnoff of the silicone resin impregnation. Therefore, the design approach used for the S-band antenna system and presented as a concept applicable to other Space Shuttle Orbiter antenna systems, is considered valid. Further, no significant changes are required for implementation. However, the manner in which a particular installation is implemented is flexible, so long as the essential electrical configuration is maintained.

Thermal Test Data Evaluation

The evaluation of the thermal test data was conducted to detect any indication of progressive deterioration in thermal performance with reuse and to show the adequacy of the thermal model used to predict thermal performance. The scope of the evaluation precluded generation of design data concerning heating distributions in joints, etc.

Test heating time. - Measured surface temperature histories for the prototype and breadboard antenna units are compared with the study baseline shuttle entry temperature environment in figure 172. The initial rise slopes are comparable. Note that the prototype and breadboard temperature histories had a more pronounced peak than the domed shuttle entry curve. After reaching the peak temperature, the prototype and breadboard surface temperatures drifted downward 110 K (200°F), although the arc heater parameters were constant. If the shuttle entry curve was transformed 200 seconds to the left, the breadboard and shuttle entry curves would match very well. Note that significantly longer heating times were used for prototype unit testing. The corresponding LI-1500 bondline temperatures are shown in figure 173 for comparison. In this figure, the time scales were lengthened to 5000 seconds to show the bondline response data. The bondline temperatures peaked closer

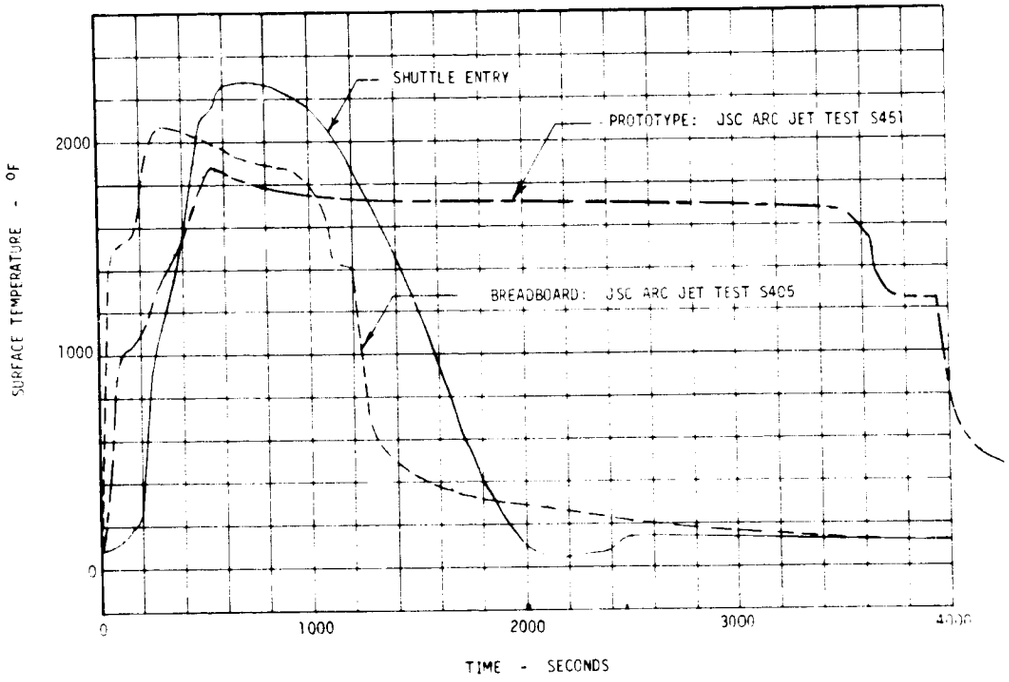

TEST AND ENTRY SURFACE TEMPERATURES

FIGURE 172

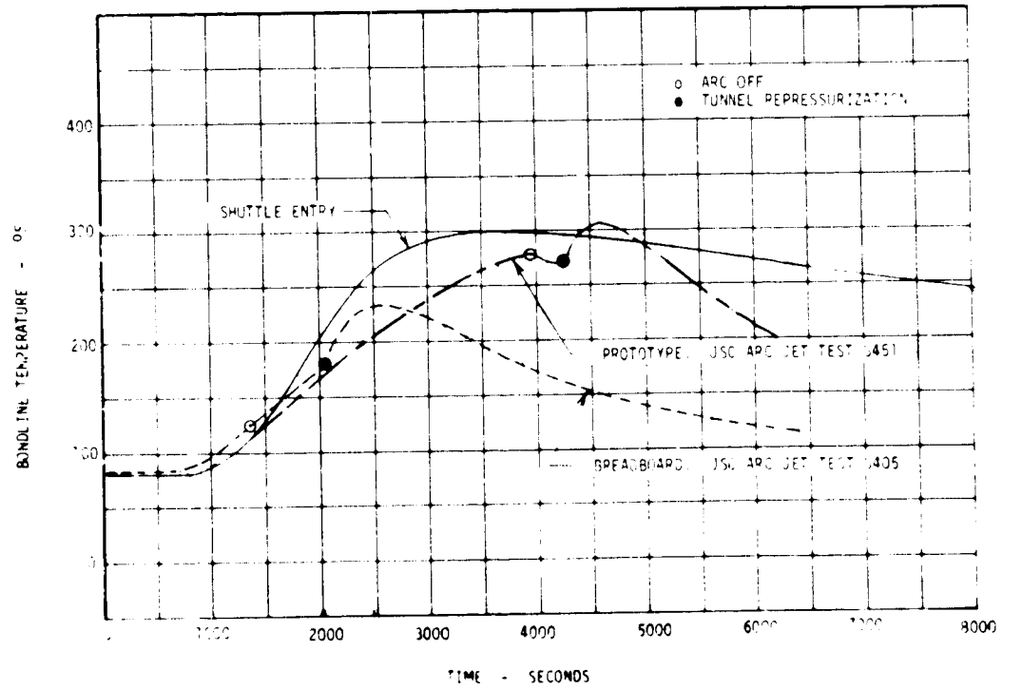

TEST AND ENTRY HRSI BONDLINE TEMPERATURES

FIGURE 173

to 422 K (300°F) for the prototype tests. The total heating exposure time for the prototype unit was 36 720 sec (10.2 hrs) compared with 5760 sec (1.6 hrs) for the breadboard unit, totaling all the test cycles.

Thermal performance. - The thermal test results were basically repeatable for the same facility test conditions. There was no progressive deterioration in thermal performance. The test approach for the breadboard unit was that of increasing severity with peak surface temperatures increasing from 1200 K (1700°F), then 1367 K (2000°F) and finally 1533 K (2300°F). However, the peak temperature achieved was only 1422 K (2100°F). For the prototype thermal tests the peak temperature achieved was only 1311 K (1900°F). The test approach for subsequent testing, therefore, was to lengthen heating time to produce expected temperatures at the bondline.

Maximum temperatures measured by selected thermocouples on the breadboard and prototype antenna system models for each thermal cycle are shown in figure 174. Arc heater "on times" for each test cycle are also indicated. The crossover in prototype unit surface temperatures between the fifth and sixth test cycle is due to a 180° rotation of the test model to minimize potential disturbance to plasma flow by an HRSI tile chipped during electrical tests. The higher temperatures on one of the two thermocouples on the top of the filler strip are attributed to a larger local gap width. Gap width appears to be more significant than gap running length or variation in surface heating distribution. For example, TC 15 located at the bottom of a nominal width gap intersection, 1.143 mm (0.045 in.) transverse gap and 0.762 mm (0.030 in.) parallel gap, on the prototype unit showed no sensitivity to channel surface heating distributions, whether it was located at the upstream or downstream end of the gap parallel to the plasma stream (i.e., before and after the 180° rotation). Temperatures indicated by TC 16, which, coincidently, was at the bottom of a 2.794 mm (0.110 in.) gap for both the breadboard and prototype unit, were about 56-139 K (100-250°F) higher than TC 15. The temperatures measured by TC 16 were about 83 K (150°F) higher on the downstream end than at the upstream end.

Thermal conductivity. - The maximum bondline temperature rise versus test cycle number for both the breadboard and prototype unit tests are shown in figure 175. The average initial bondline temperatures are also indicated as well as arc heater run duration for each test cycle. The lower temperatures measured by TC 12 of the breadboard unit demonstrate the effect of the proximity to the large thermal mass of the S-band antenna. In general, the temperature at the interface between the filler strip and sponge pad was higher than at the bondline between the LI-1500 tile and sponge pad. The results are within the data scatter expected, except the fourth cycle prototype response for TC 20 located under a filler strip. No trend of increasing or decreasing thermal conductivity relative to number of test cycles was indicated by the test data.

Thermal conductivity verification: Enough temperature response data was available during the first 300 seconds of heating time to get thermal conductivity checks using a NASA-JSC computer program. A comparison of the thermal conductivity results with LMSC thermal conductivity design data (ref. 12) is

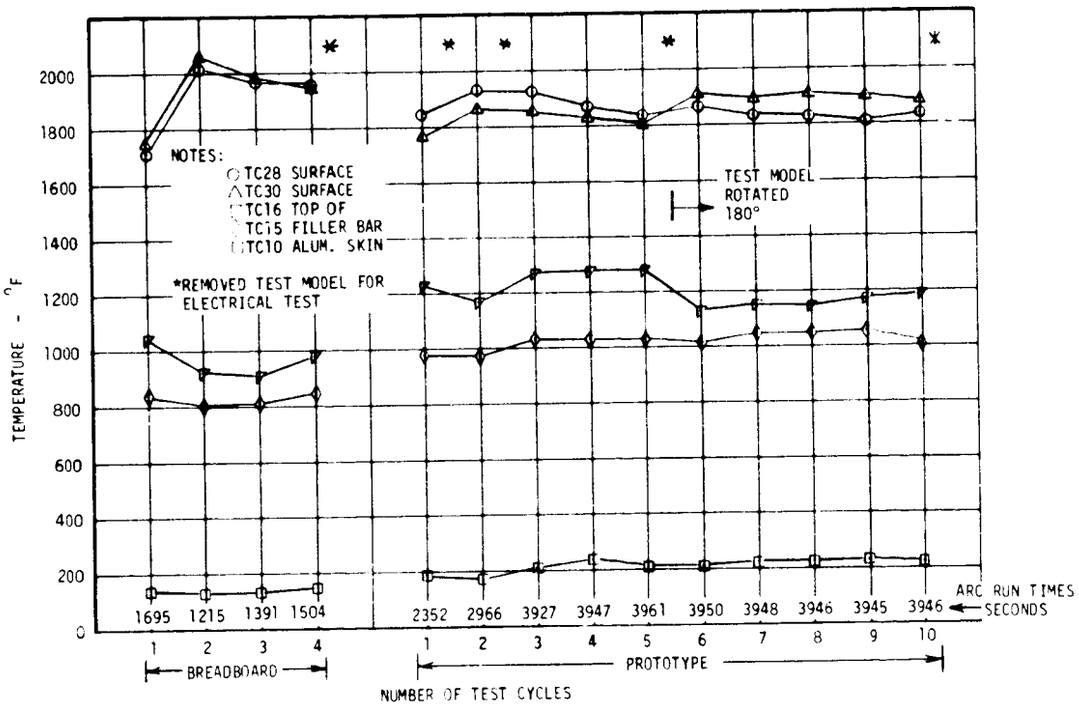

MAXIMUM MEASURED TEMPERATURES OF S-BAND ANTENNA SYSTEM TEST MODELS

FIGURE 174

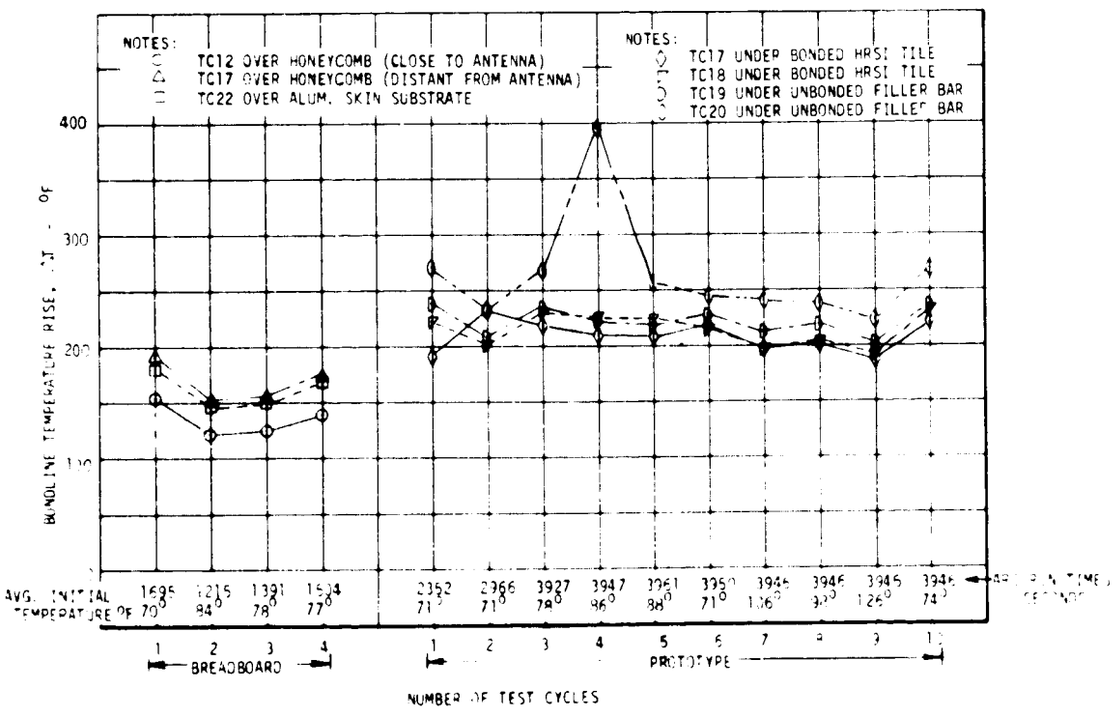

EFFECT OF REPEATED THERMAL CYCLES ON BONDLINE TEMPERATURE RISE

FIGURE 175

shown in figure 176. The local static surface pressure varied from zero to the maximums shown in figure 176 during the 300 second period.

Channel flow nozzle heating. - Outer surface thermocouples indicated a fairly uniform maximum temperature response on the breadboard unit. The average of the peak measured temperatures and the temperature range between the highest and lowest of six surface thermocouple readings are given in table XXV. With exception of the first test, TC 27 read the highest surface temperature; instead of being flush, this installation formed a slight hump in the surface.

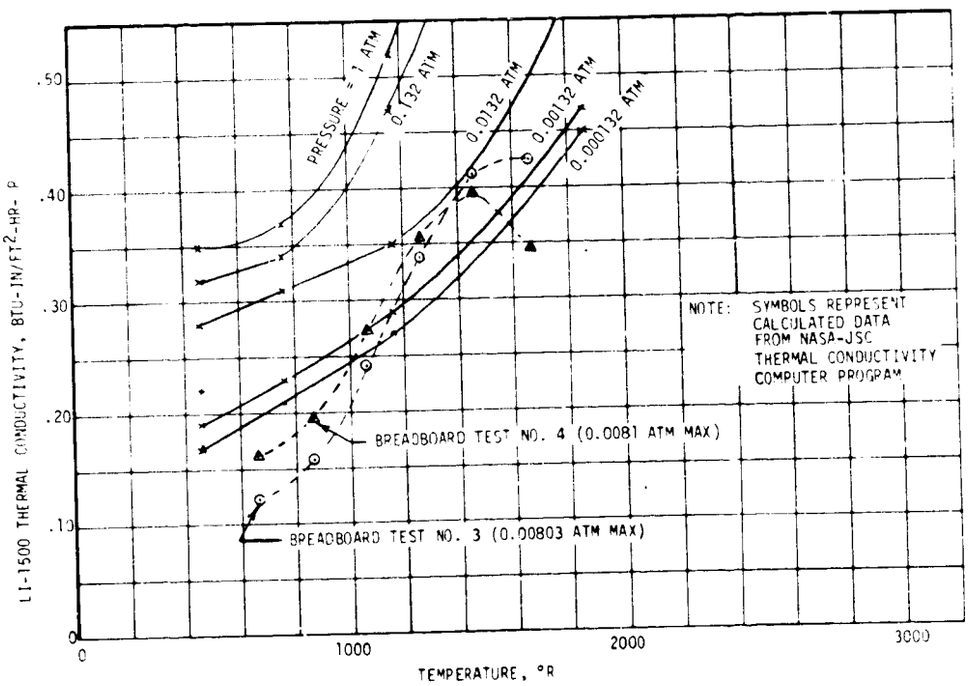

LI-1500 THERMAL CONDUCTIVITY VERIFICATION

FIGURE 176

TABLE XXV

AVERAGE PEAK SURFACE TEMPERATURES

TEST NO.	JSC NO.	PEAK TEMPERATURE K (°F)	TEMPERATURE RANGE K (F°)
1	S-404	1223 (1741)	39 (70)
2	S-405	1397 (2055)	56 (100)
3	S-406	1352 (1974)	53 (95)
4	S-407	1349 (1968)	53 (95)

Attachment hole heating. - Holes through the LI-1500 antenna window tile permit outside access to the window attachment screws. The maximum skin temperature near the attachment holes was about 6 K (10°F) higher than in other areas of the b ckside aluminum skin structure. Thus, attachment hole heating was essentially no more severe than conduction heat transfer through the LI-1500.

Bondline thermal response. - The prototype bondline temperatures decreased after the arc heater was turned off and increased again when the tunnel was repressurized to make a curve with a double peak as shown in figures 173 and 177. This contrasts with the breadboard unit tests where the temperatures continued to rise. The double peak response was typical of all the prototype unit bondline thermocouples as well as those at the interface between the lower density flexible filler strip and sponge pad. The peak temperature following tunnel repressurization is attributed to a sharp increase in thermal conductivity due to an almost instantaneous change to atmospheric pressure.

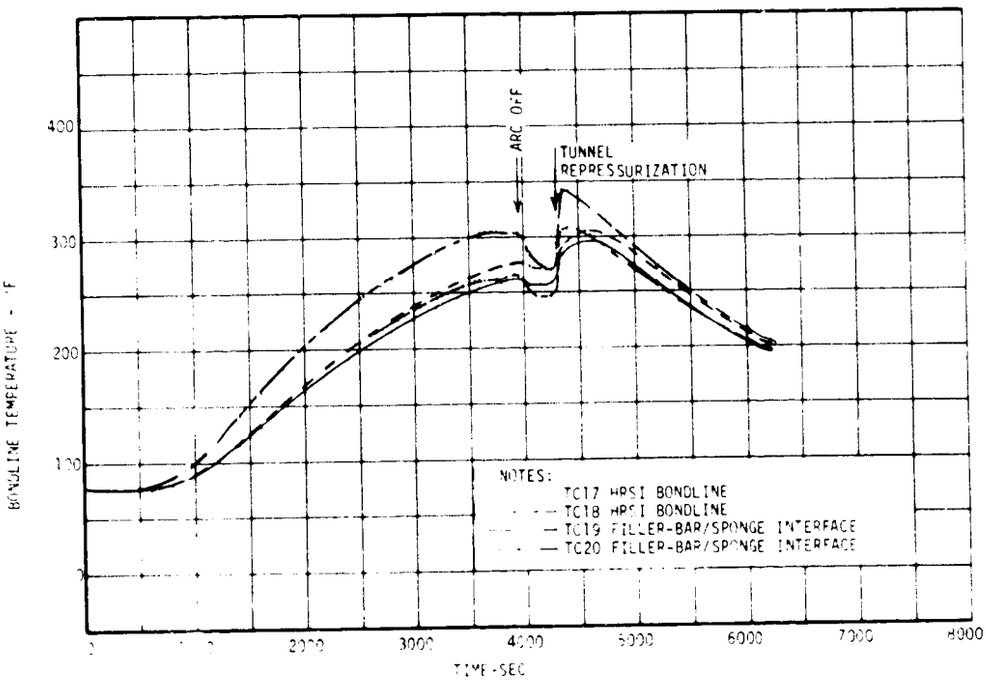

DOUBLE PEAK TEMPERATURE RESPONSE - PROTOTYPE (TEST P-10)

FIGURE 177

Silicon resin exothermic reaction. - A short term temperature peak (figure 178) was measured by TC 15 on the filler strip coincident with tunnel repressurization during the first thermal test of both the breadboard and prototype units. These sharp temperature rises are attributed to an exothermic reaction associated with the silicone resin, which apparently consumes the volatile constituents of the resin. The reasons for this conclusion are:
(1) the short term temperature peaks did not occur on succeeding tests;
(2) they occurred on the initial test of both the breadboard unit and prototype

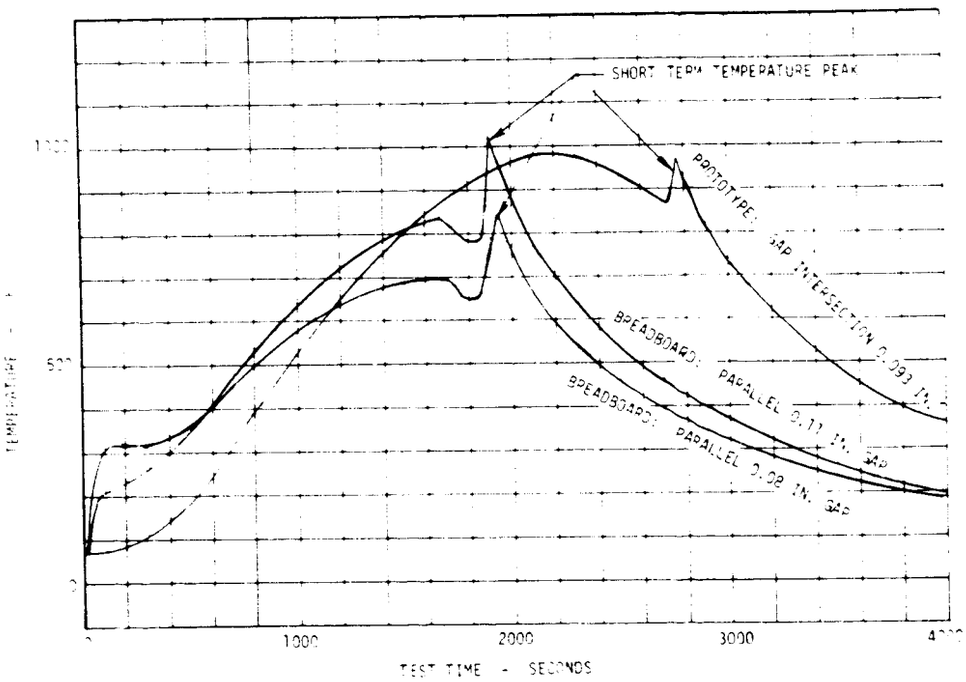

FI-600 FILLER STRIP SURFACE TEMPERATURE BEHAVIOR ON FIRST TEST

FIGURE 178

unit; (3) they coincided with the opening of the tunnel chamber to an ambient pressure environment and thus to a higher partial pressure of oxygen; (4) the temperatures prior to the short term peaks were near the ignition temperature of silicone resin; and (5) the filler strip was scorched and the tile coating on the gap sides was darkened.

Comparison of calculated and measured data. - Measured surface temperature and pressure histories were used as the boundary condition for the thermal model described in the section on S-BAND ANTENNA SYSTEM DESIGN. A comparison of predicted and measured histories through the LI-1500 antenna window for Breadboard Test Cycle No. 2 is shown in figure 179. The corresponding maximum temperature distribution through the antenna window is shown in figure 180. Predicted and measured data for the antenna backcap and antenna support for the same breadboard test is shown in figure 181. A similar comparison for Prototype Test Cycle No. 10 with longer heating time is shown in figure 182.

Physical Examination

Both the breadboard and prototype units were subjected to a number of auxiliary tests to determine performance characteristics as well as reuse capability in conjunction with electrical and thermal tests. These auxiliary tests included: (1) visual inspection; (2) coating crack detection; (3) water absorption; and (4) emittance. Some were conducted before and after breadboard thermal testing, and some before and after the first, second, fifth and tenth

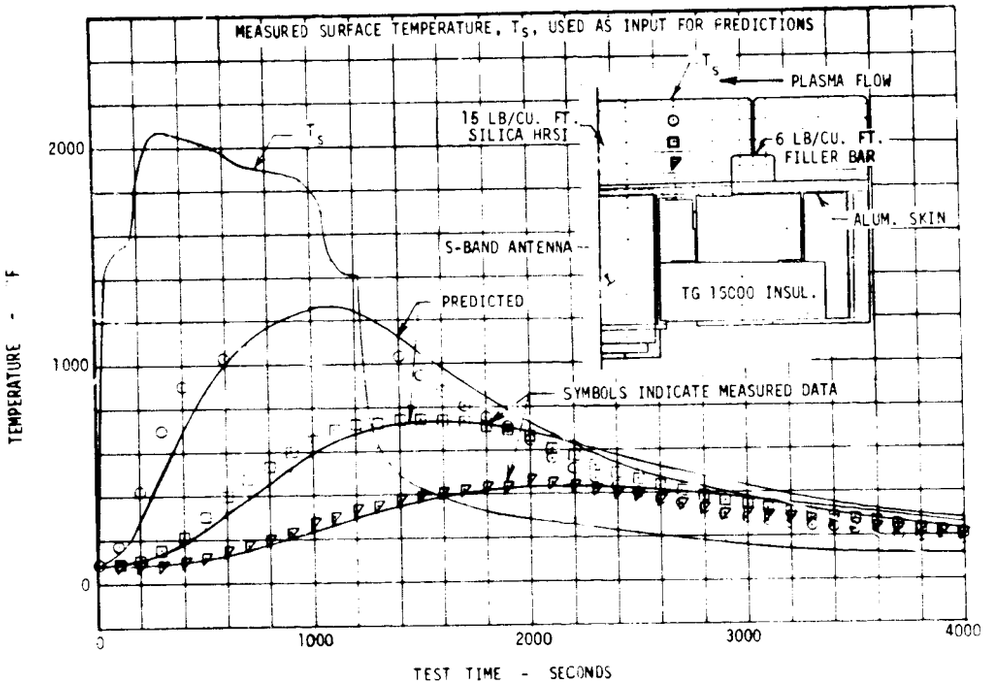

CORRELATION OF HRSI ANTENNA WINDOW TEMPERATURES (TEST B-2)

FIGURE 179

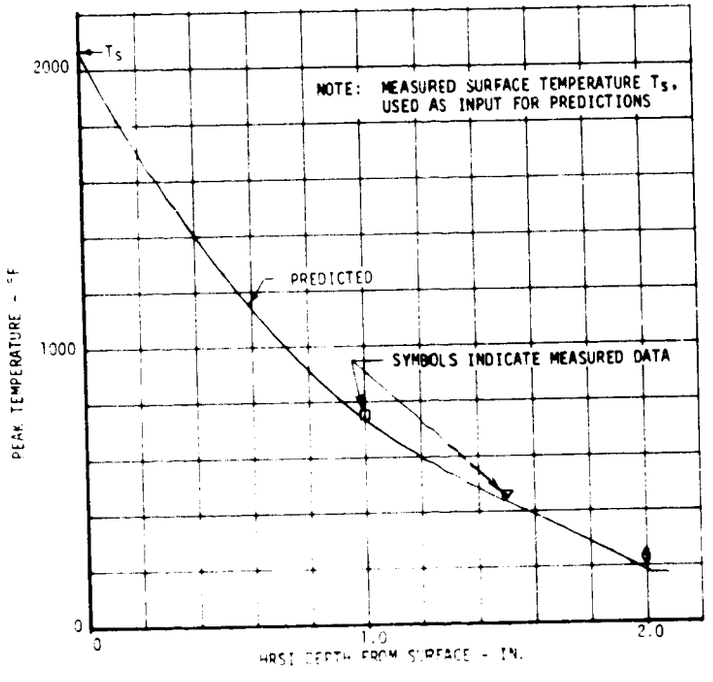

PEAK TEMPERATURE DISTRIBUTION OF HRSI OVER HONEYCOMB PANEL (TEST B-2)

FIGURE 180

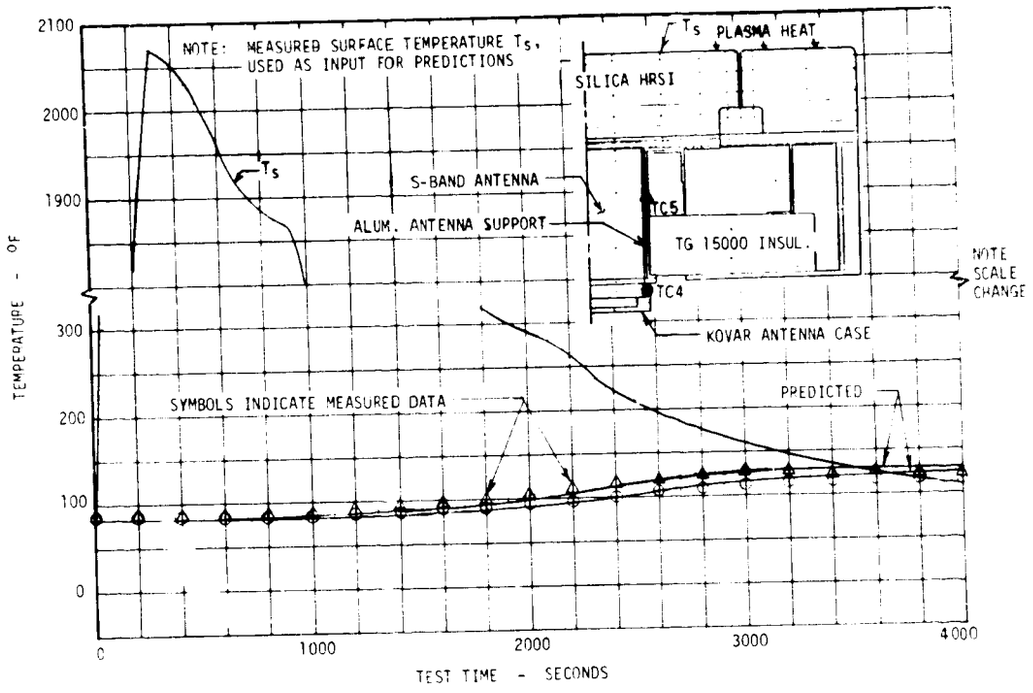

BREADBOARD TEMPERATURE CORRELATION (TEST B-2)

FIGURE 181

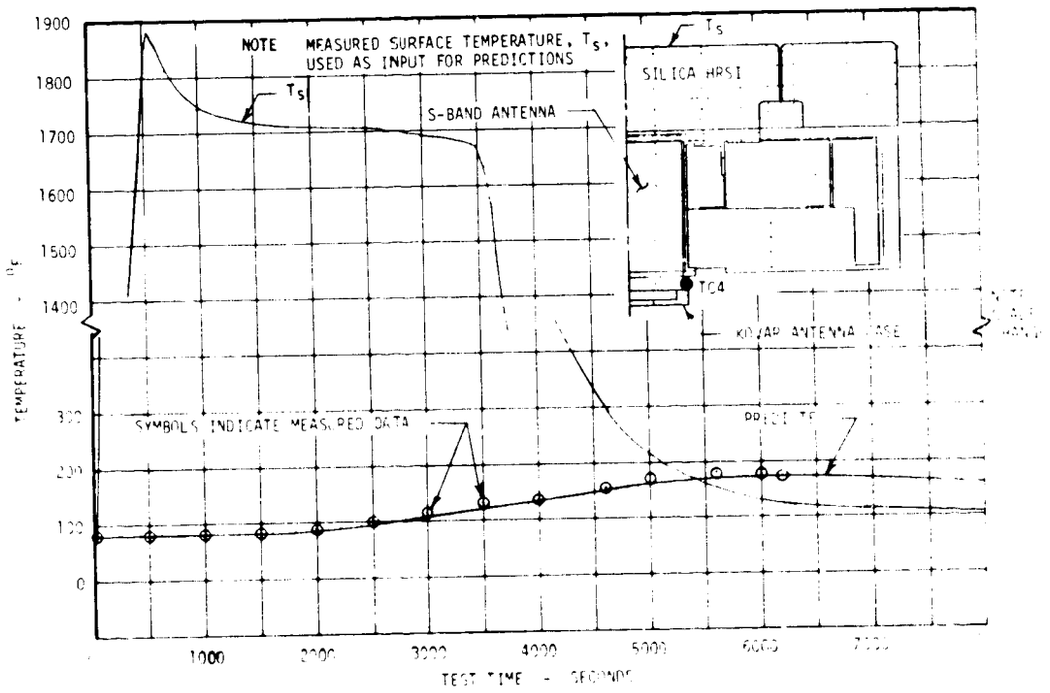

PROTOTYPE TEMPERATURE CORRELATION (TEST P-10)

FIGURE 182

thermal test cycles of the prototype thermal tests. Other tests were conducted only once or as needed.

Visual inspection. - No obvious physical changes or failures in antenna assembly materials occurred due to thermal testing. However, some handling damage, scorching and surface streaks happened to the test model coating surface or filler strips.

Surface coating: The appearance of the surface coating of the breadboard unit after four thermal cycles is shown in figure 183. The coating generally remained a bluish-grey color. Harmless streak discolorations, about 7.62 cm (3.00 in.) long in the downstream direction from the attachment holes, were noted. These streaks are believed due to silicone resin volatiles, which cooked out during the first cycle. The repair coating over the surface thermocouples had a flaky appearance, but it appeared to be excess coating since the underneath surface was still adequately coated after the final thermal cycle. The long narrow upstream guard tile had a small chip removed from the coating during arc tunnel installation. The damaged area was coated with repair coating and did not cause any apparent problem.

The appearance of the surface coating of the prototype unit after 10 thermal cycles is shown in figure 184. The most noticeable feature is the chip damaged area which occurred during electrical testing after the fifth thermal cycle. A thin 5.08 cm (2.00 in.) diameter chip was knocked from the surface of the upstream guard tile during removal from the electrical test fixture. Before succeeding thermal testing, a repair coating was painted on the damaged area. It was also rotated 180° in the test fixture to place the chipped, damaged area in a downstream position and minimize potential disturbance to plasma flow over the antenna window. The repair coating survived the next five thermal cycles, as can be seen in figure 184. No adverse effects from the chipped area or new surface streaks from the attachment holes were noted. Some minor speckling (figure 184) attributed to copper deposition from the arc tunnel electrodes appeared after the fifth cycle. The spots appeared to be a shiny metallic copper color at first, but rapidly oxidized. The tips of tiny protrusions in the natural texture of the surface coating appeared slightly whitened or abraided after the fifth cycle. After completion of thermal testing, the surface coating seemed more brittle and the surface texture felt slightly dryer and rougher than before testing.

Antenna window: The antenna window was detached from the breadboard unit as shown in figure 185. The inboard edge of the downstream corner of the window tile was scorched. The side of the tile was darkened near the scorching. There was also evidence of soot deposit near a thermocouple lead cutout. The teflon insulation on some of the thermocouple leads was slightly melted indicating local temperatures of about 433 K (500°F). The increased temperature at the thermocouple insulation is attributed to the silicone resin exothermic reaction.

The uncoated antenna window attachment holes, originally all white, were totally black after the initial thermal cycle. After additional thermal cycles, a 7.62 mm (0.30 in.) wide white band appeared at 2.54 mm

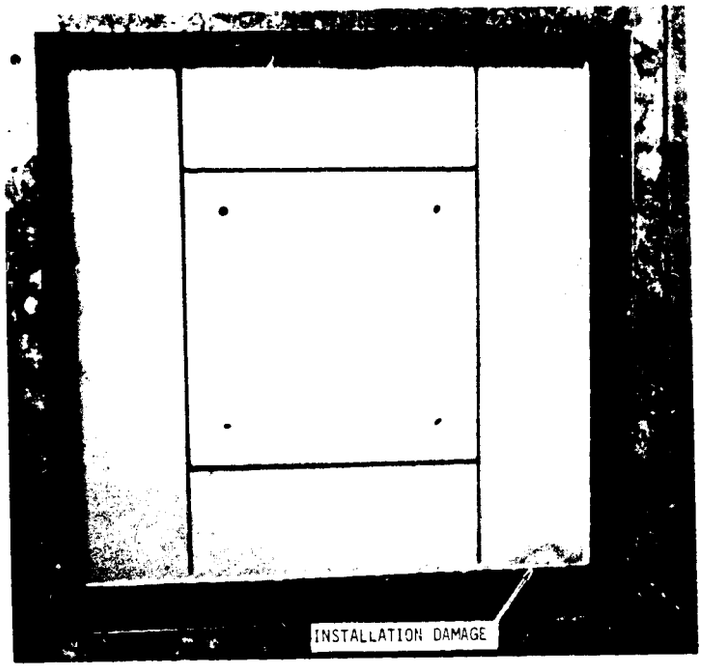

PRETEST

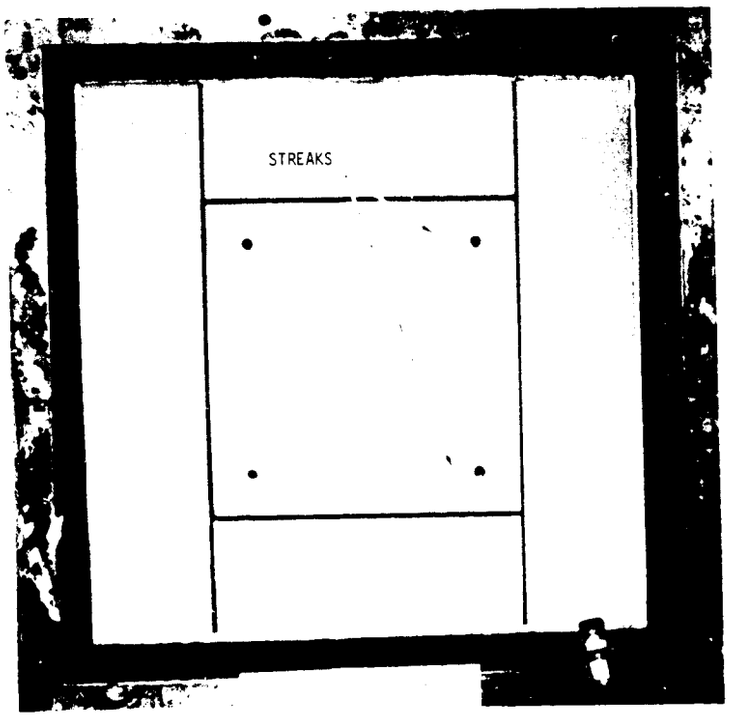

POSTTEST

BREADBOARD UNIT SURFACE

FIGURE 183

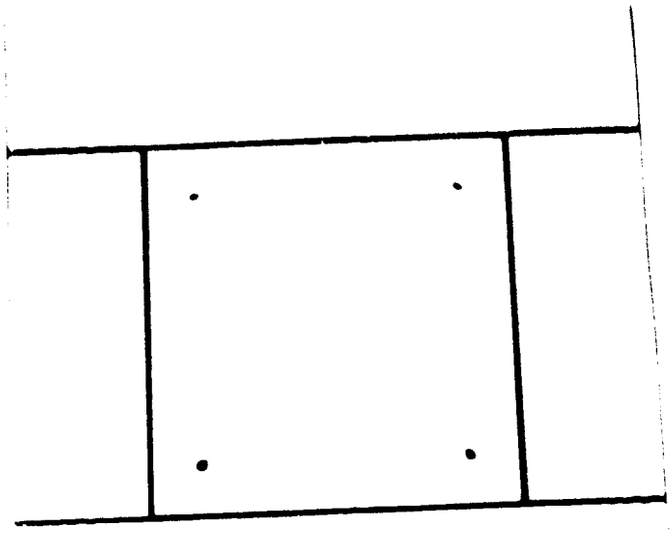

PRETEST

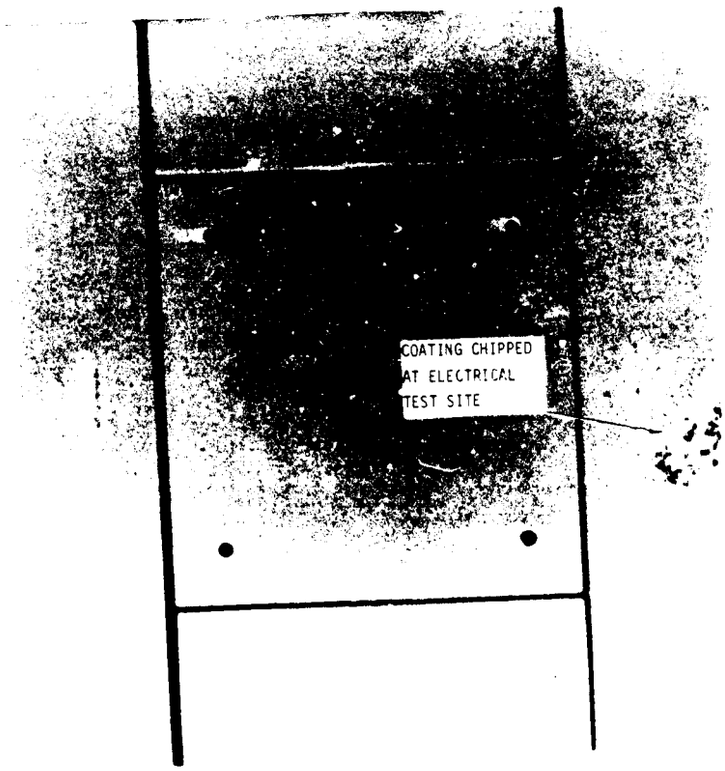

POSTTEST
PROTOTYPE UNIT SURFACE

FIGURE 184

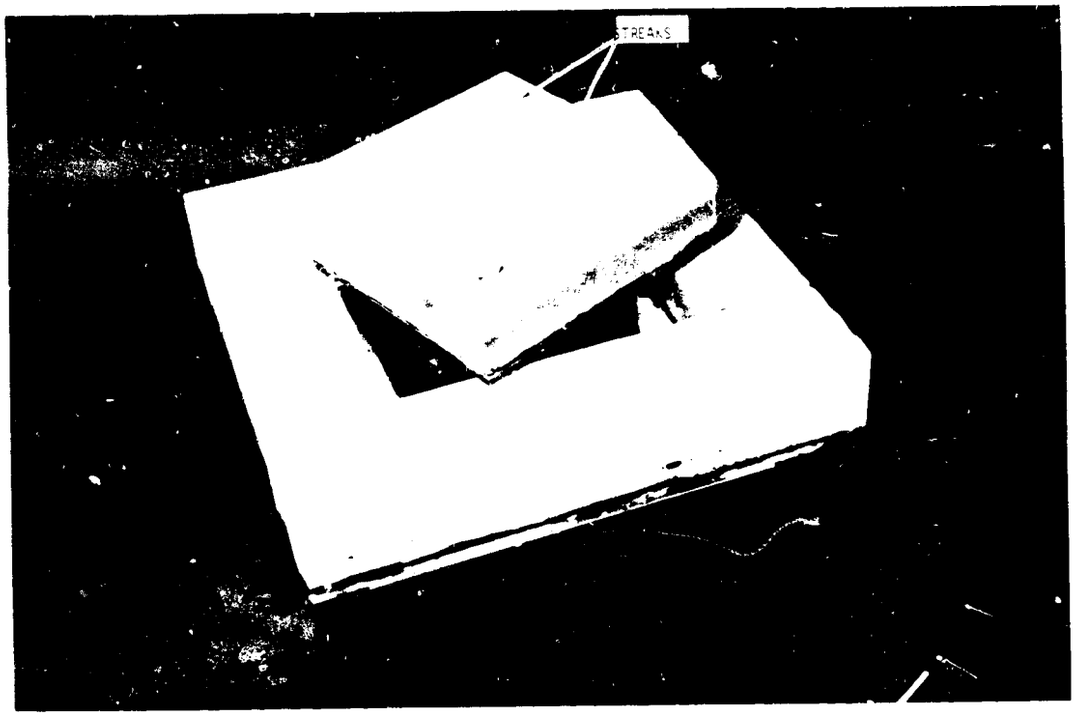

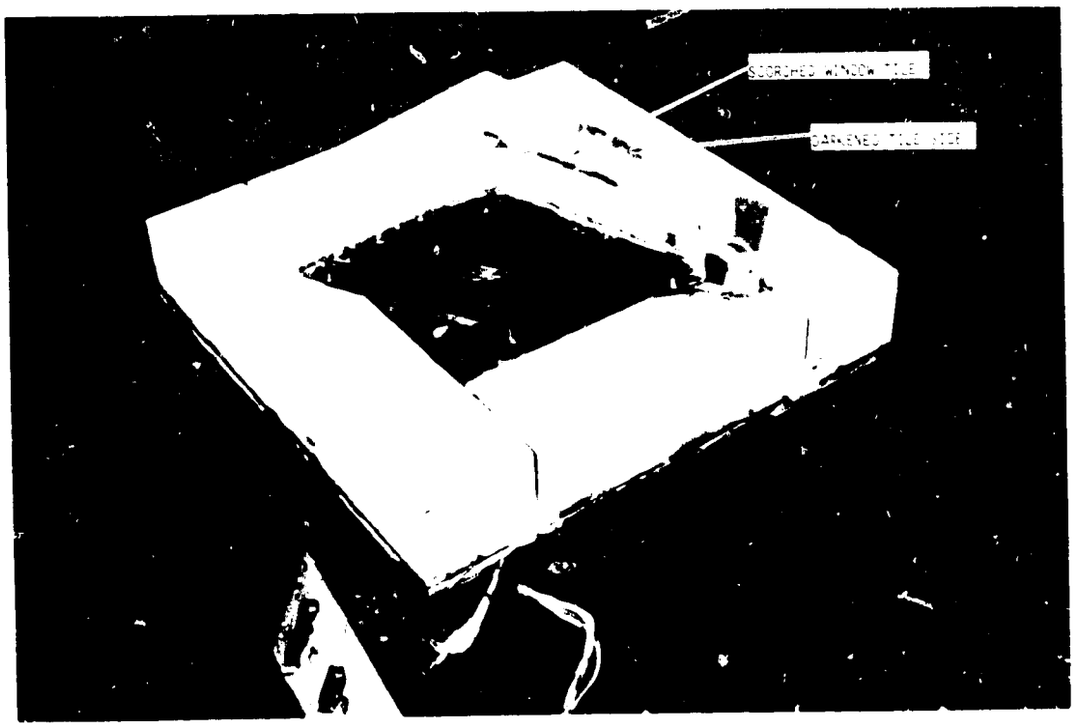

HIGH TEMPERATURE EFFECT ON ANTENNA WINDOW - BREADBOARD UNIT

FIGURE 185

(0.10 in.) depth below the surface. The dark soot deposit appeared to have been burned away by the high surface temperatures. A closeup of an attachment hole is shown in figure 186.

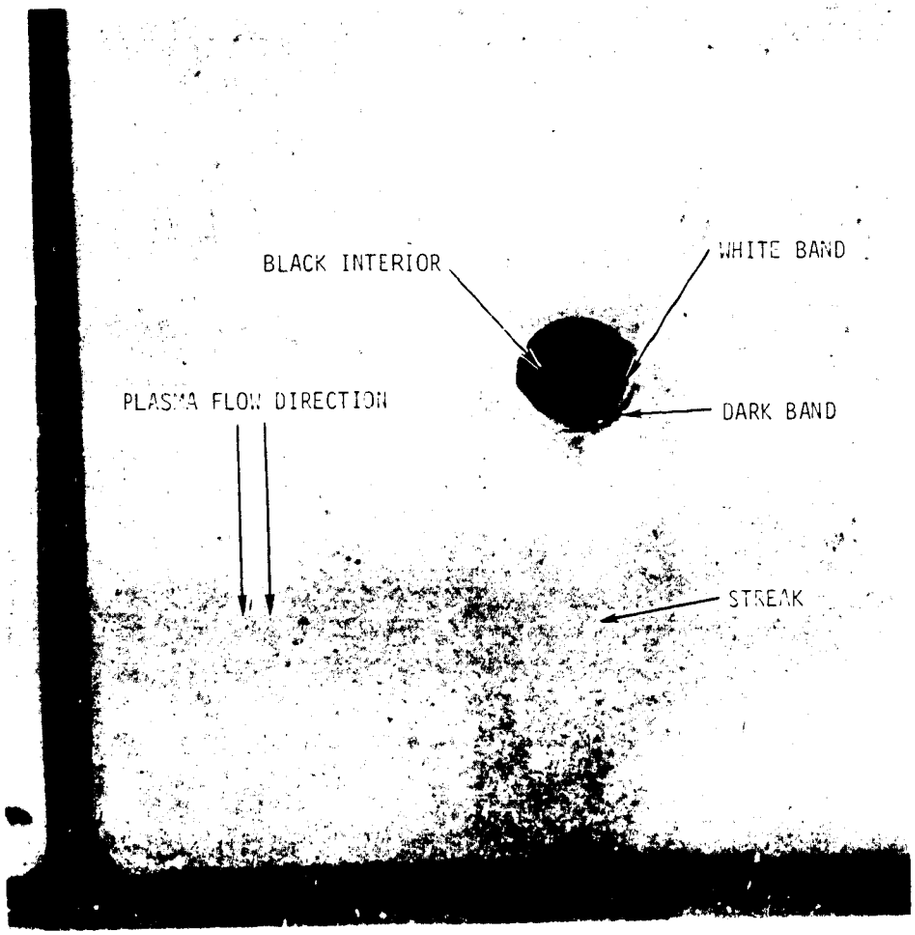

PLASMA FLOW EFFECT ON ATTACHMENT HOLE

FIGURE 186

Tile joints: The gaps between the LI-1500 tiles on the breadboard unit were measured with a feeler gauge prior to channel flow nozzle installation. The results of these measurements are shown in figure 187. The antenna window LI-1500 tile was slightly larger in the middle than at the corner, and slightly larger at the bottom than at the top surface as discussed in the section on TEST HARDWARE FABRICATION. The largest gap between tiles was 2.79 mm (0.11 in.) in a gap parallel to plasma flow at one downstream corner of the

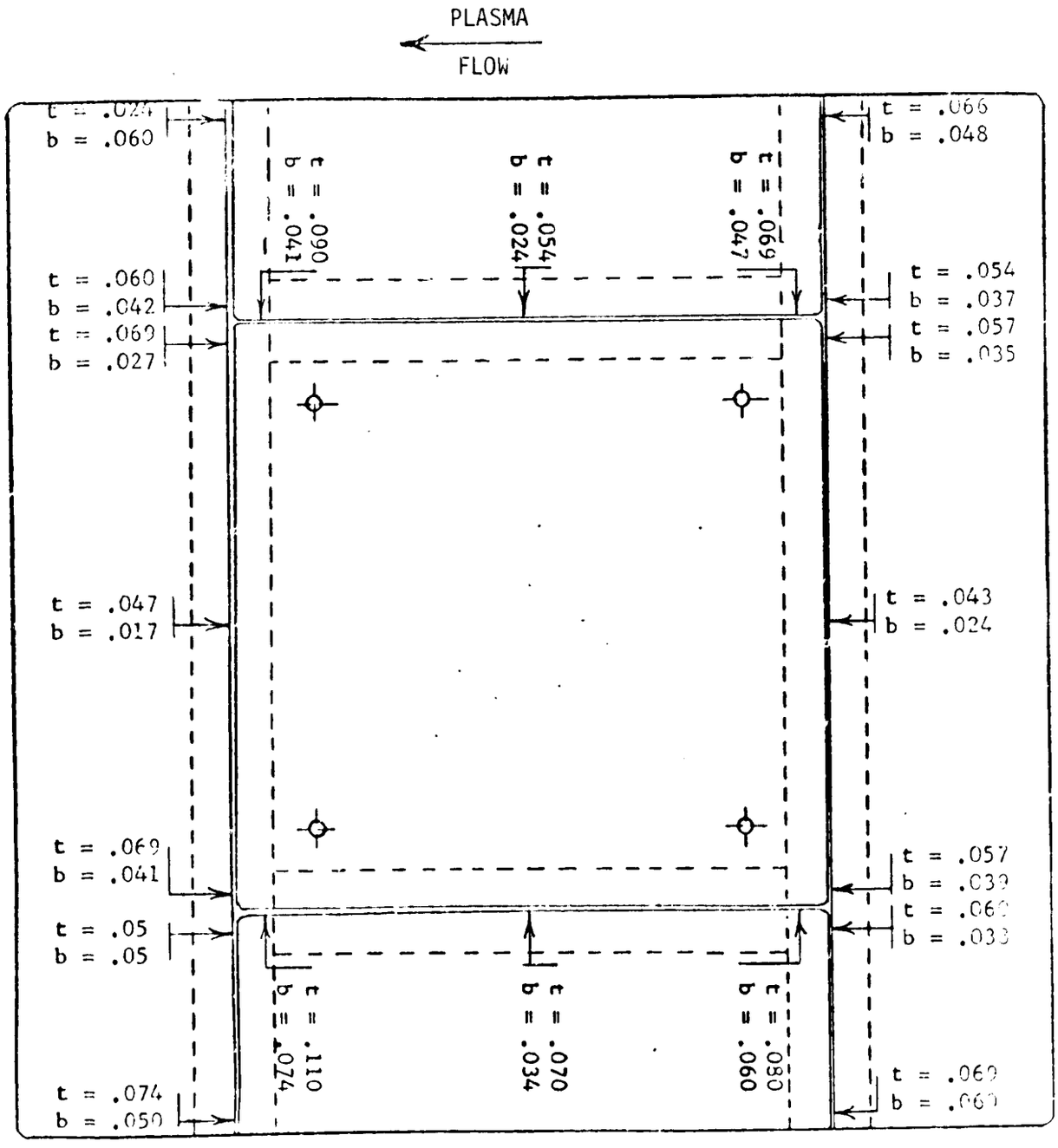

t : TOP OF GAP
b : BOTTOM OF GAP

GAP MEASUREMENT RESULTS FOR BREADBOARD UNIT

FIGURE 187

antenna window. This is the same corner where scorching of the bottom edge was noted above (figure 185). The scorching of the filler strip at this corner is shown in figure 188. The smallest gap was 0.432 mm (0.017 in.) on the bottom of the downstream transverse gap. The largest aft facing step in a transverse gap was 0.64 mm (0.25 in.) and the largest forward facing step due to surface mismatch between tiles was 0.51 mm (0.020 in.). A 1.04 mm (0.041 in.) gap between the tile lap and top of the FI-600 filler strip was noted; the top of the filler strip was locally scorched due to plasma flow down the gap and under the tile lap. A closeup of this area is shown in figure 189. After the tests, the antenna window was removed for visual inspections before gap measurements were made. However, no significant changes in gap dimensions were noticed during visual inspection.

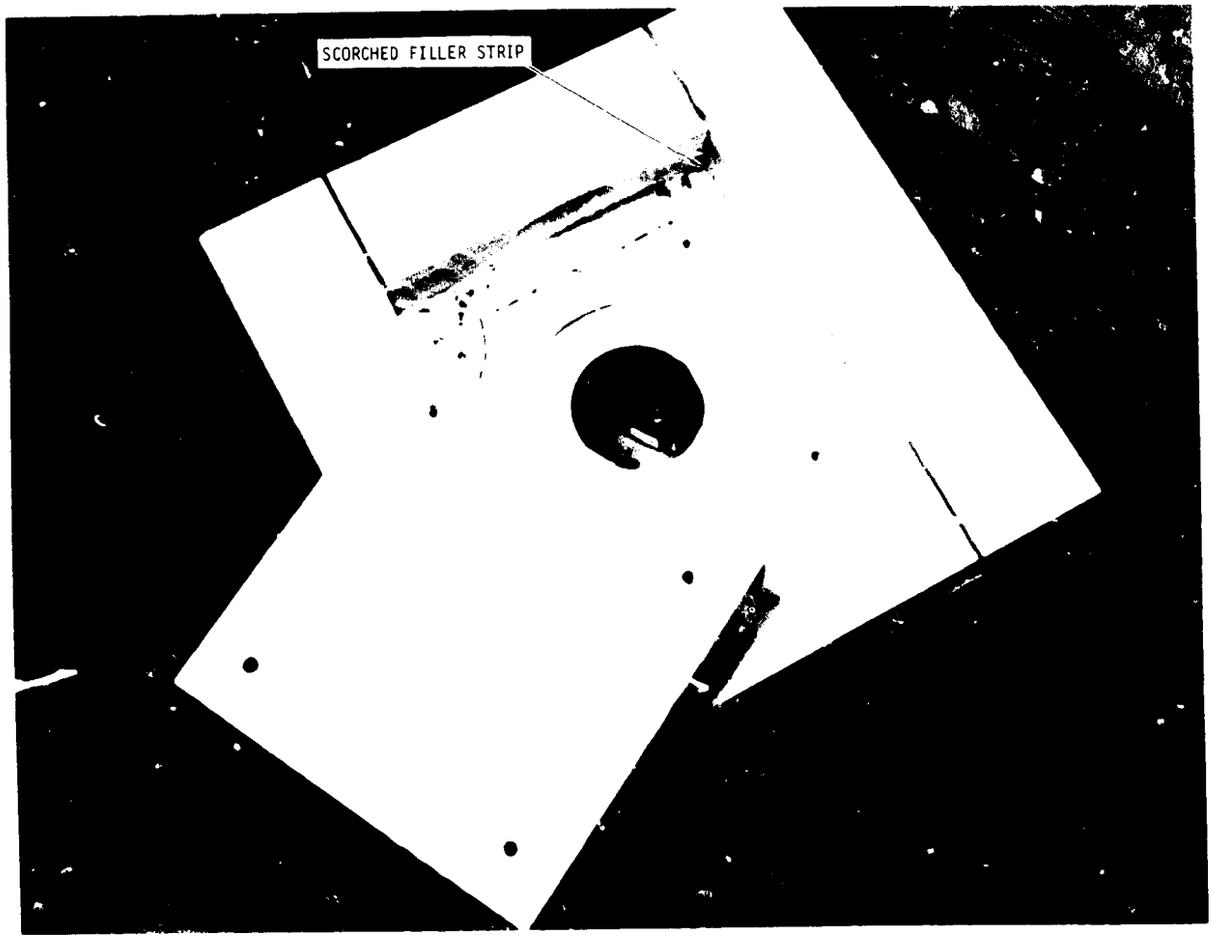

HIGH TEMPERATURE EFFECTS ON FILLER STRIP - BREADBOARD UNIT FIGURE 188

The prototype unit exhibited a yellowish flow-pattern deposit on the side of the guard tiles near the FI-600 filler strips. The top exposed surface of the filler strips was unchanged for gap widths less than 2.281 mm (0.090 in.); slight scorching was observed under one long transverse gap ranging from 2.36 mm (0.093 in.) to 2.79 mm (0.110 in.). Thinner gaps experience less heating.

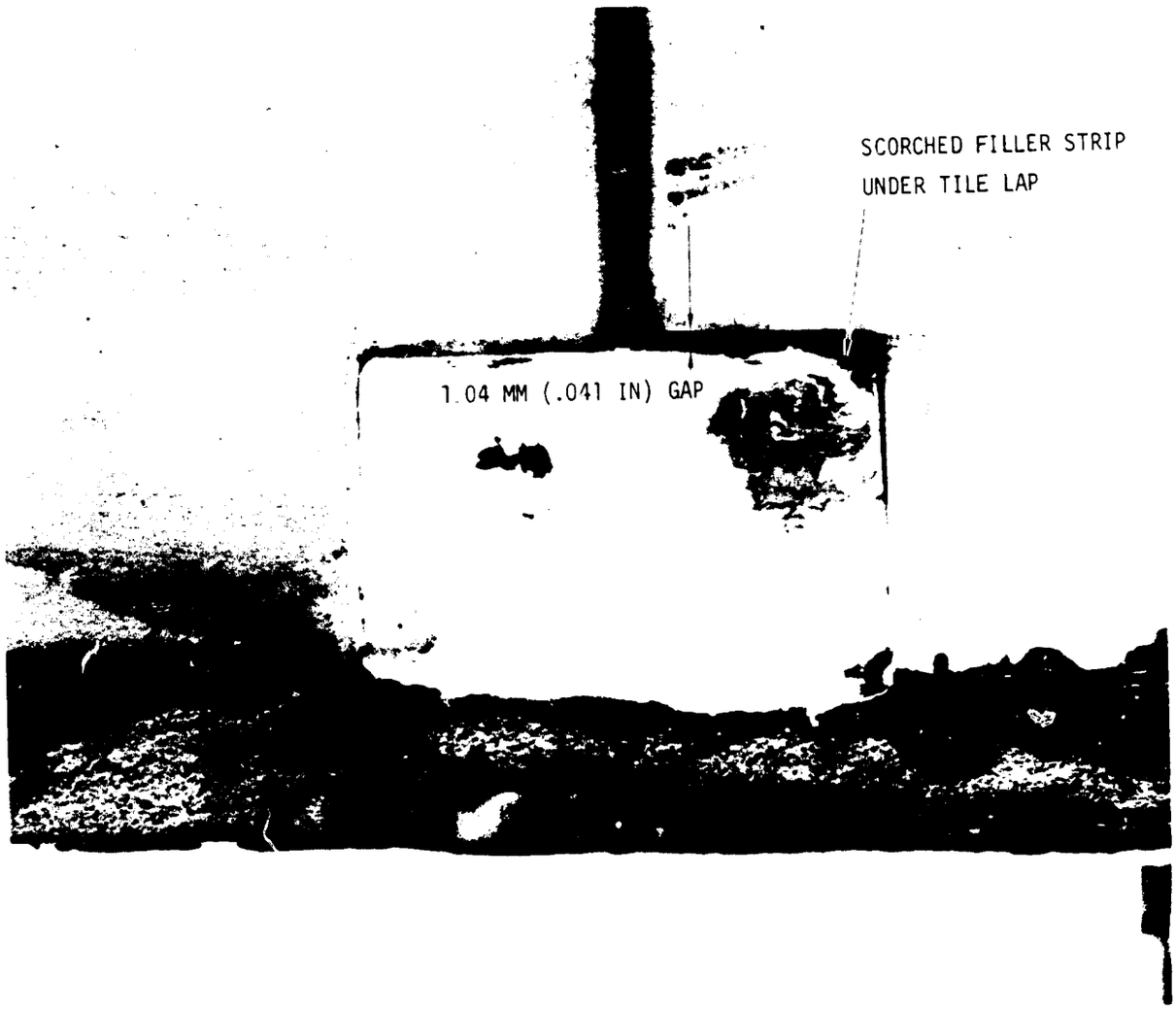

FILLER STRIP CLOSEUP - GUARD TILE

FIGURE 189

The outer edges of the sponge pad under the filler strips appeared somewhat lighter in color and felt slightly stiffer and dryer to the touch after the tests of the prototype unit.

Coating cracks. - Wet film acetaldehyde NDE tests for coating cracks were performed before and after the thermal tests. No coating cracks were found before the thermal tests; some pin holes and porosity were found. Several fine, hairline microcracks, which were mostly invisible to the naked eye, were detected after the thermal tests.

The coating crack pattern detected on the breadboard unit after the tests is shown in figure 190. These microcracks are believed to be caused by stress concentration due to the small holes drilled in the surface for the thermocouple leads; or the differential expansion of the AREMCO 505 cement that was

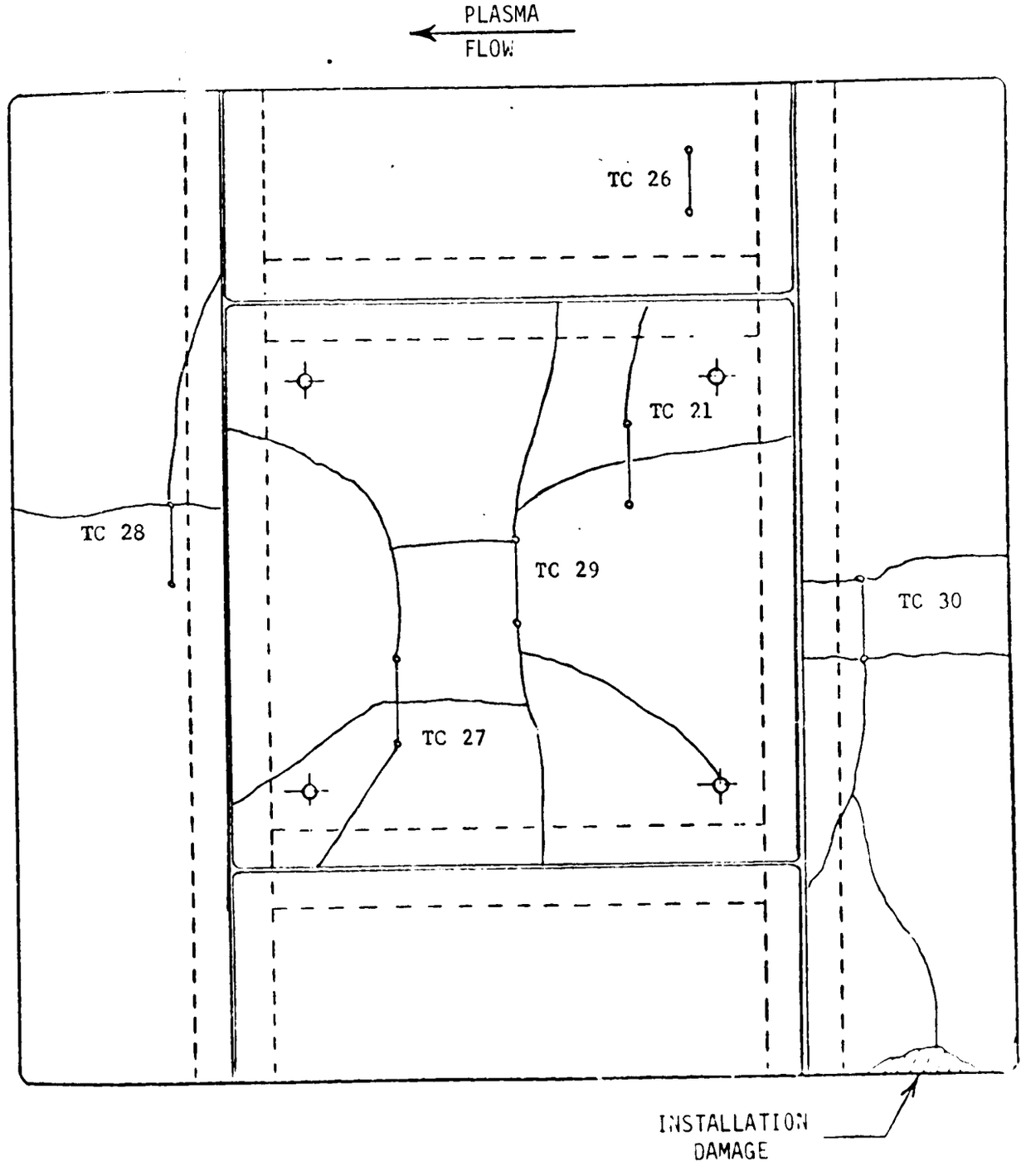

COATING CRACK PATTERN ON BREADBOARD UNIT

FIGURE 19

used to hold the surface thermocouples in place, which may have penetrated the thermocouple lead holes. Only one crack (figure 190) goes to an attachment hole in the antenna window. However, this crack appears to emanate from TC 29. Although cracks pass near the other three attachment holes, none pass through them.

Wet film acetaldehyde NDE tests on the LI-1500 coating were performed each time the prototype unit was removed for electrical testing. Pin holes, but no microcracks, were found in the coating before thermal testing. The sequence of coating crack patterns after each thermal cycle (figure 191) shows the cracks lengthen with each cycle. No microcracks were detected on the center antenna window tile until after the tenth thermal cycle, when a 1.27 cm (0.50 in.) microcrack appeared at the edge of the tile. No microcracks were detected around or through the window attachment holes. Microcracks occurred at one surface thermocouple installation on the guard tiles after the first thermal cycle. One microcrack appeared on each of the other guard tiles later during the test series and progressively lengthened with each subsequent thermal cycle.

Water absorption. - The prototype unit was checked for moisture resistance integrity by water bead testing (absorption). The surface coating on LI-1500 remained resistant to water absorption except at surface thermocouple installation, at pin holes and microcracks, and at the 5.08 cm (2.0 in.) diameter chip-damaged area. The LI-0010 repair coating was not water resistant. Although the surface coating was initially nonwetting to water, after thermal cycling, water tended to wet rather than bead on the coating surface. On the sides of the guard tiles, unexposed to direct plasma heating, water tended to wet the upper half nearest the heated surface and bead on the lower half.

Surface emittance. - Surface coating emittance at room temperature was measured on the prototype unit by a reflectometer after the second thermal test cycle. It remained constant at 0.845 through the ten thermal cycles.

PLASMA FLOW

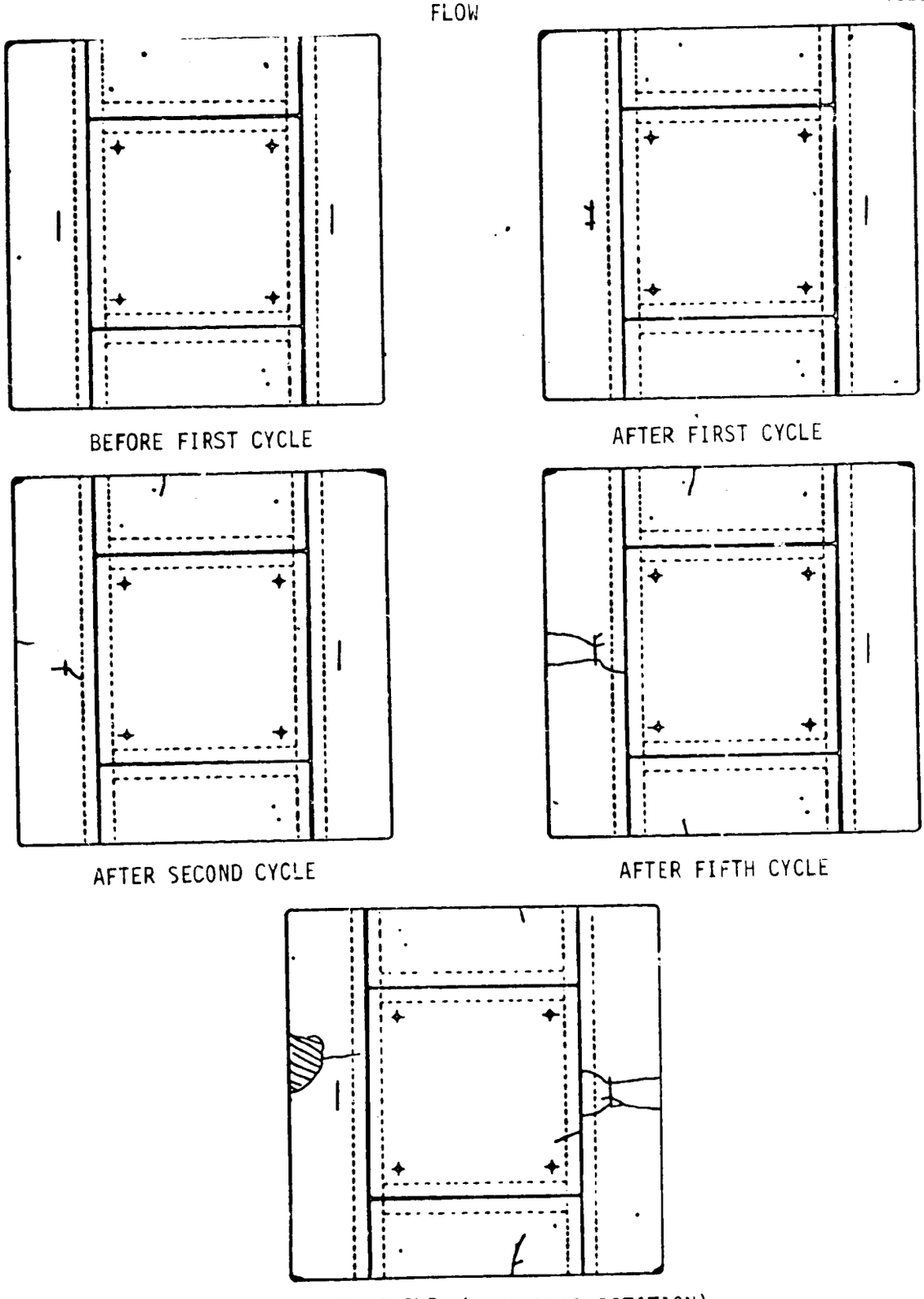

BEFORE FIRST CYCLE

AFTER FIRST CYCLE

AFTER SECOND CYCLE

AFTER FIFTH CYCLE

AFTER TENTH CYCLE (NOTE 180° ROTATION)
COATING CRACK PATTERN SEQUENCE ON PROTOTYPE UNIT

FIGURE 191

THIS PAGE INTENTIONALLY LEFT BLANK

REFERENCES

1. Kuhlman, E. A.: Space Shuttle High Temperature Antenna Design and Integration. NASA CR-2294 (to be published).

2. Munson, R. T.: Microstrip Phase Array Antennas. Abstracts of the Twenty-second Annual Symposium of USAF. Antenna Research and Development Program, October 1972.

3. Howell, J. Q.: Microstrip Antenna. 1972 G-AP International Symposium Digest, December 1972.

4. Jasik, H.: Antenna Engineering Handbook, McGraw-Hill Book Company, (New York) 1961, pp 32-5.

5. Bassett, H. L. and Bomar, S. H., Jr.: Complex Permittivity Measurements During High Temperature Recycling of Space Shuttle Antenna Window and Dielectric Heat Shield Materials. NASA CR-2302 (to be published).

6. Gilreath, [illegible]. and Castellow, S. L., Jr.: High Temperature Dielectric Properties of Candidate Space Shuttle Thermal Protection Systems and Antenna Window Materials. NASA TDN-xxxx (to be published).

7. Rusert, E. L.: Development and Design Application of Rigidized Reusable Surface Insulation (RSI) Thermal Protection System (TPS). (NAS 9-12854) McDonnell Douglas Astronautics Company - East, Final Report MDC E0725 (NASA MSC-07010), 31 December 1972.

8. Anon: Supplementary Structural Test Program - Large TPS Panels. (NAS 8-26016) McDonnell Douglas Astronautics Company - East, Final Report MDC E0562, 30 March 1972.

9. Anon: Metals and Metal Couples - Restriction on Use. NASA-JSC Design and Procedural Standard No. 63, 6 March 1970.

10. Fulmer, H. R. and Moseley, R. E.: Determination of Antenna Directivity by the Pattern Integration Method. The Essay, No. 2, Scientific - Atlanta, Inc., August 1960.

11. Mezines, S. A.: A Rapid Technique For Estimating Ablative Heat Shield Weights From Plasma Jet Test Data. Thermal Design Principles of Spacecraft and Entry Bodies, Volume 21 of Progress in Astronautics and Aeronautics series, Academic Press (New York) 1969, pp 203-223.

12. Buttram, R. P.: Midterm Summary Report For Space Shuttle Thermal Protection System Development (NAS 9-12083), Lockheed Missiles and Space Company, Report LMSC-A997045, 12 November 1971, Table 4.1-6, pp 4-17.

13. Collins, R. E.: Field Theory of Guided Waves, McGraw-Hill Book Company, (New York) 1960, pp. 87-94.

14. Bein, G. P.: Plane Wave Transmission and Reflection Coefficients for Lossy Inhomogeneous Plasma. IEEE Transactions on Antennas and Propagation, July 1966.

15. Anon: Reference Data for Radio Engineers, Fifth ed., Howard W. Sams and Company (New York), 1969, Chap. 24.

APPENDIX A

MATERIAL DESIGN PROPERTIES

The material properties given in tables XXVI through XXIX were used in analyses performed on this program.

TABLE XXVI
LI-1500 THERMAL PROPERTIES

DENSITY: 15.0 LB/FT^3

THERMAL CONDUCTIVITY (BTU/HR FT ^{0}R)

TEMPERATURE (^{0}R)	PRESSURE (LB/FT^2)				
	2.785	27.85	278.5	2116.	9000.
460	0.0142	0.0234	0.0267	0.0292	0.0292
760	0.0175	0.0258	0.0283	0.0308	0.0308
1160	0.0225	0.0292	0.0392	0.0433	0.0433
1860	0.0375	0.0500	0.0750	0.0834	0.0834
2460	0.0558	0.0850	0.1167	0.1300	0.0130
2960	0.0766	0.1125	0.1565	0.1740	0.1740
3460	0.1050	0.1470	0.2000	0.2220	0.2220

EMITTANCE:

TEMPERATURE (^{0}R)	EMITTANCE
532	0.9

SPECIFIC HEAT

TEMPERATURE (^{0}R)	SPECIFIC HEAT (BTU/LB ^{0}R)
360	0.0716
540	0.1510
720	0.1980
900	0.2340
1000	0.2630
1260	0.2800
1440	0.2870
1800	0.2940
2160	0.3060
2520	0.3160
2960	0.3200

TABLE XXVII
FI-500 THERMAL PROPERTIES

DENSITY: 6.00 LB/FT^3

THERMAL CONDUCTIVITY (BTU/HR FT ^{0}R)

TEMPERATURE (^{0}R)	PRESSURE (LB/FT^2)			
	0.278	27.8	2116.	9000.
200	0.00045	0.00245	0.0059	0.0059
400	0.0017	0.0068	0.0138	0.0138
600	0.00375	0.0112	0.0228	0.0228
980	0.00916	0.025	0.04	0.04
1460	0.0208	0.0408	0.069	0.0691
1960	0.035	0.0692	0.097	0.0967

EMITTANCE:

TEMPERATURE (^{0}R)	EMITTANCE
532	0.9

SPECIFIC HEAT:

TEMPERATURE (^{0}R)	SPECIFIC HEAT (BTU/LB ^{0}R)
360	0.0716
540	0.1510
720	0.1980
900	0.2340
1000	0.2630
1260	0.2800
1440	0.2870
1800	0.2940
2160	0.3060
2520	0.3160
2960	0.3200

TABLE XXVIII

RL-524 TYPE S-105 THERMAL PROPERTIES

DENSITY:	20.0 LB/FT^3
THERMAL CONDUCTIVITY:	0.12 BTU/HR FT ^{0}R
SPECIFIC HEAT:	0.32 BTU/LB ^{0}R

TABLE XXIX

MECHANICAL PROPERTIES

MATERIAL	TEMPERATURE °F	MODULUS OF ELASTICITY IN TENSION IN PLANE PSI	MODULUS OF ELASTICITY IN TENSION CROSS PLANE PSI	ν POISSON'S RATIO	SHEAR MODULUS PSI	COEFFICIENT OF THERMAL EXPANSION IN PLANE IN/IN/°F	COEFFICIENT OF THERMAL EXPANSION CROSS PLANE IN IN °F	ULTIMATE TENSILE STRESS IN PLANE PSI	ULTIMATE TENSILE STRESS CROSS PLANE PSI
LI-1500 RSI [f]	70	10^5	10^4	0.1 [d]	6600	3×10^{-7}	[e]	115	15
	2500	10^5	10^4	0.1	6600	3×10^{-7}		166	15
PHENOLIC FIBER-GLASS CLASS D SHEET [g] MIL-H-17 PAGE 4-100	70	3.2×10^6		0.2	0.835×10^6 [a]	4.5×10^{-6}	16×10^{-6}	40 000	
	150	3.14×10^6		0.2	0.82×10^6	4.5×10^{-6}	16×10^{-6}	37 750	
	200	3.04×10^6		0.2	0.792×10^6	4.5×10^{-6}	16×10^{-6}	36 360	
	300	2.7×10^6		0.2	0.703×10^6	4.5×10^{-6}	16×10^{-6}	33 700	
	400	2.3×10^6		0.2	0.60×10^6	4.5×10^{-6}	16×10^{-6}	30 000	
PHENOLIC [c] [h] FIBERGLASS HONEY-COMB AVERAGE OF L&W PROPERTIES	70	10 000 [b]		0.01	10 700 [a]				
	150	10 000		0.01	10 450				
	200	10 000		0.01	10 100				
	300	10 000		0.01	9 000				
	400	10 000		0.01	7 700				
S-105 SPONGE STRAIN ISOLATOR	70	60		0.01	30	2.35×10^{-4}		100	
	400	60		0.01	30	2.35×10^{-4}		100	

NOTES

a. VARIATION WITH TEMPERATURE DETERMINED BY MULTIPLYING ROOM TEMPERATURE VALUE BY THE RATIO OF THE [illegible] FIBER-GLASS SHEET AT TEMPERATURE TO E AT ROOM TEMPERATURE

b. ARBITRARY VALUE

c. WHEN FIBERGLASS HONEYCOMB PROPERTIES ARE NOT SHOWN FIBERGLASS SHEET PROPERTIES WERE ENTERED IN THE COMPUTER PROGRAMS AS HONEYCOMB PROPERTIES

d. ESTIMATED BY CONSIDERING DATA FOR MDC RSI

e. WHERE CROSS-PLANE DATA IS NOT SHOWN IN-PLANE DATA WAS ENTERED IN THE COMPUTER PROGRAMS AS CROSS-PLANE DATA

f. "EVALUATION OF NONMETALLIC THERMAL PROTECTION MATERIALS FOR THE MANNED SPACE SHUTTLE" VOLUME V BATTELLE MEMORIAL INSTITUTE, DATED JUNE 1 1972

g. MIL HDBK 17A "PLASTICS FOR AEROSPACE VEHICLES PART I REINFORCED PRACTICE" DATED JANUARY 1971

h. BROCHURE D "HONEYCOMB SANDWICH DESIGN DATA AND TEST METHODS" HEXCEL PRODUCTS INC.

APPENDIX B

EQUATIONS FOR CALCULATING POWER TRANSMISSION LOSS
THROUGH
MULTIPLE LAYERS OF LOSSY DIELECTRIC

Plane wave transmission loss through N layers of a lossy dielectric may be calculated using several approaches (refs. 13 and 14). The equations used for the results given in the section on CONCEPT AND FEASIBILITY STUDIES, under "Antenna window transmission loss", are given below.

(1) MODEL

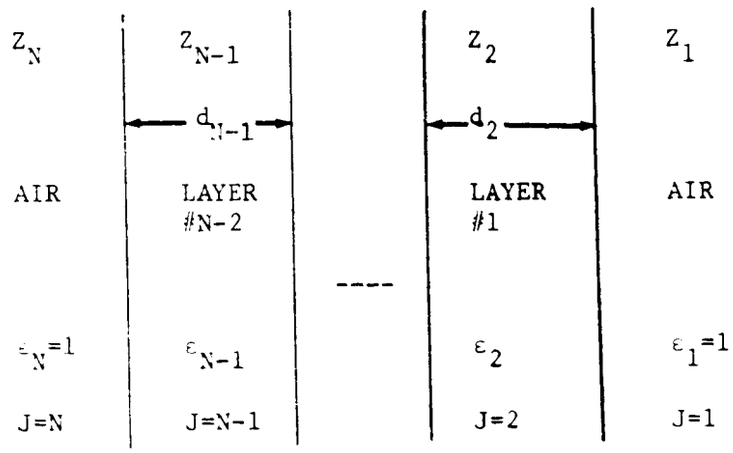

(2) SNELL's LAW

$$\theta_J = \arcsin \left[\sqrt{\varepsilon_1/\varepsilon_J'} \, (\sin \theta_1) \right]$$

where

θ_J = angle of propagation in dielectric sheet number J

θ_1 = angle of incidence

ε_1 = relative dielectric constant of air

ε_J' = relative dielectric constant of sheet number J

(3) WAVE IMPEDANCE

$$Z_J = \left(\frac{\mu_o}{\varepsilon_o}\right)^{1/2} \frac{1}{\sqrt{\varepsilon_J \cos \theta_J}} \quad \text{(for perpendicular polarization)}$$

$$Z_J = \left(\frac{\mu_o}{\varepsilon_o}\right)^{1/2} \frac{\cos \theta_J}{\sqrt{\varepsilon_J}} \quad \text{(for parallel polarization)}$$

where

Z_J = characteristic impedance of dielectric sheet number J.

μ_o = permeability of free space

ε_o = permittivity of free space

ε_J = complex dielectric constant ($\varepsilon_J = \varepsilon'_J (1 - j\tan \delta)$)

(4) PROPAGATION CONSTANT IN MEDIA

$$\gamma = \alpha + j\beta = j\omega\sqrt{\mu_o \varepsilon_o \varepsilon_J}$$

where

α = attenuation constant

β = phase constant

ω = angular frequency

(5) IMPEDANCE TRANSFORMATION

$$ZI_{J+1} = Z_J \frac{ZI_J \cosh \gamma d_J + Z_J \sinh \gamma d_J}{Z_J \cosh \gamma d_J + ZI_J \sinh \gamma d_J}$$

where

ZI_J = the equivalent impedance at the right boundary of dielectric sheet number J, which represents the load impedance for that sheet,

d_J = thickness of dielectric sheet number J.

Note that

$$ZI_2 = Z_1 = \frac{1}{\cos \theta_1}$$

(6) POWER TRANSMISSION COEFFICIENT

$$T = \left| \frac{E_{TRANSMITTED}}{E_{INCIDENT}} \right|^2 = \left| \frac{E_1}{E_{J=N}} \right|^2$$

where

N = TOTAL NUMBER of dielectric sheets (including air sheets)

E_1, E_J = voltage at left surface of dielectric sheet number J

At the left air-dielectric interface

$$\frac{E_N}{E_{N-1}} = \frac{1}{1 + \rho_N}$$

where

$$\rho_N = \frac{ZI_N - Z_N}{ZI_N + Z_N}$$ (Note: $Z_N = Z_1$ since sheet N is also air.)

However,

$$\frac{E_{N-1}}{E_{N-2}} = \frac{1}{ZI_{N-1}} [ZI_{N-1} \cosh \gamma_{N-1} d_{N-1} + Z_{N-1} \sinh \gamma_{N-1} d_{N-1}],$$

and

$$\frac{E_2}{E_1} = \frac{1}{ZI_2}(ZI_2 \cosh \gamma_2 d_2 + Z_2 \sinh \gamma_2 d_2),$$

therefore,

$$\frac{E_N}{E_1} = \frac{E_N}{E_{N-1}} \quad \frac{E_{N-1}}{E_{N-2}} \quad - - - - \quad \frac{E_2}{E_1}$$

and

$$\frac{E_{INCIDENT}}{E_{TRANSMITTED}} = \frac{1}{1+\rho_N} \quad \frac{E_{N-1}}{E_{N-2}} \quad - - - - \quad \frac{E_2}{E_1}$$

APPENDIX C

RELATIONSHIP OF CIRCULAR AND LINEAR GAIN

The relationship between peak linear and circular gain can be derived from the propagation relationship for elliptically polarized waves. The relative power received by an elliptically polarized receiving antenna as it is rotated in a plane normal to the direction of propagation of an elliptically polarized wave (ref. 15) is given by:

$$P_R = K\left[\frac{(1\pm r_1 r_2)^2 + (r_1 \pm r_2)^2 + (1-r_1^2)(1-r_2^2)\cos 2\theta}{(1+r_1^2)(1+r_2^2)}\right] \tag{1}$$

where

K = constant

r_1 = axial ratio of elliptically polarized wave $(0 \leq r_1 \leq 1)$

r_2 = axial ratio of elliptically polarized antenna $(0 \leq r_2 \leq 1)$

θ = angle between the direction of maximum amplitude in the incident wave and the direction of maximum amplitude of the elliptically polarized antenna

The + sign is used if both the receiving and transmitting antenna have elliptical polarization of the same sense.

For a linearly polarized transmitted wave, $r_1 = 0$, and an elliptically polarized receiving antenna, equation (1) becomes:

$$P_R = K\left[\frac{1+r_2^2 + (1-r_2^2)\cos 2\theta}{(1+r_2^2)}\right] \tag{2}$$

The peak occurs when $\cos 2\theta = 1$ and:

$$P_R' = K\left[\frac{2}{1+r_2^2}\right] \tag{3}$$

Assuming a circularly polarized transmitted wave, $r_1 = 1$, equation (1) becomes:

$$P_R = K \left[\frac{(1+r_2)^2}{1+r_2^2} \right] \tag{4}$$

The constant K can be expressed as a function of gain, power and distance as follows:

$$K = \frac{1}{2} P_T G_T G_R \left(\frac{\lambda}{4\pi R} \right)^2 \tag{5}$$

where

P_T = transmitted power

G_T = transmitting antenna gain

G_R = receiving antenna gain

λ = wavelength

R = distance

Assuming equal power densities for the linear and circular transmitted fields the relationship of circular power to peak linear power received by the antenna is:

$$P_R = P_R' \frac{1}{2} (1+r_2)^2 \tag{6}$$

Therefore the circular gain of an antenna can be determined from rotating linear patterns, which are referenced to linear isotropic power levels, and the relationship of equation (6). A plot of equation (6) is shown in figure 50. To obtain the circular gain it is necessary to add the gain factor (figure 50) which is a function of axial ratio (A.R.), to peak linear gain at the particular angle, where A.R. = $1/r_2$. For example: (1) if the A.R. is zero (0) dB the circular gain is 3 dB greater than indicated directly by the pattern; (2) if the A.R. is 2 dB, 2.05 dB is added to the peak linear gain shown on the respective patterns; and (3) if the A.R. is very large (> 40 dB, -3 dB is added to peak linear gain. The large A.R. indicates a linear antenna and therefore polarization loss of 3 dB when transmitting to or receiving from a circularly polarized antenna.

APPENDIX D

BONDING LIGHTWEIGHT THERMAL INSULATION

1.0 SCOPE

The bonding procedures currently utilized for bonding lightweight thermal insulation to silicone sponge and silicone sponge to metallic and fiberglass-phenolic substrates are presented.

2.0 MATERIALS AND EQUIPMENT REQUIREMENTS

2.0.1 End Item Identifiable Materials. -

(1) Silicone Sponge, Raybestos-Manhattan RL-1973

(2) Silicone Compound, General Electric RTV-560

(3) Primer for RTV Silicone, Dow Corning DC 1200

(4) Dibutyl Tin Dilaurate DC 1200

2.0.2 Process Consumables. -

(1) TT-1-735 Isopropyl Alcohol

2.0.3 Material Control. - All material used for bonding lightweight thermal insulation to substrate shall conform to requirements established by specification.

2.0.4 Equipment. - Equipment shall be cleaned thoroughly immediately following any period of bonding application, and shall be kept clean for the next bonding application.

2.0.5 Facilities. - The bonding area and its immediate surroundings shall be provided with housekeeping provisions to minimize dust, dirt, lint, and other air-borne contaminants.

2.0.6 End Item Requirements. -

(1) The end-item shall be inspected to engineering drawing requirements.

(2) All the component parts, weight, density, dimension and the final assembly weight are to be documented.

3.0 PROCEDURES

3.0.1 Preparation of Aluminum Substrates. -

(1) Wet sand with 320 grit wet or dry sandpaper.

(2) Scrub with Ajax and Scotchbrite pads until all the oxide film is removed.

(3) Rinse with deionized water.

(4) Check for water break free surface. If a water bead surface is not obtained, repeat above cleaning procedure until it is obtained.

(5) Blow off with heated dry nitrogen

3.0.2 Priming of Aluminum Substrate. -

(1) Apply primer to the cleaned, dry metal surface. Pour a quantity of primer into a clean suitable container. Immediately apply Dow Corning 1200 primer to the metal surface with a wadded-up Kimwipe. A thin film will give best results. Correct thickness should give only a pink tinge to the substrate.

(2) Follow MDC primer hydrolyzation schedule per PB 1-75, Rev. A. (The primer should air dry for a minimum of 60 minutes before bonding. Low humidity will necessitate longer times for drying the primer).

3.0.3 Preparation of Fiberglass-Phenolic Substrate For Bonding. -

(A) Scuff sand bond surface of phenolic substrate with 120 grit sand paper.

(B) Wipe dust from substrate with clean cheesecloth and isopropyl alcohol until there is no discoloration on cheesecloth.

(C) Allow to air dry for a minimum of 30 minutes or until there is no longer a solvent smell.

3.0.4 Priming of Fiberglass-Phenolic Substrate. - Prime fiberglass-phenolic substrate using same procedure as priming aluminum substrate.

3.0.5 Preparation of the Sponge (RL-1973 Silicone Sponge)

(1) Record nominal thickness and weight and average density of the sponge.

(2) Cut the sponge to dimensions according to engineering drawing.

(3) Scrub the sponge with cheesecloth dampened with isopropyl alcohol to remove dirt and contamination. Change clothes frequently so that dirt is removed and not transferred.

(4) After cleaning cloth shows no contamination, air dry sponge until free of solvent. (Forced air may blow holes through the sponge, since RL-1973 is easily torn.)

3.0.6 Preparation of Lightweight Thermal Insulation Interface. -

(1) Record the dimensions, weight and density of the insulation.

(2) Check for surface defects. Defects may be cause for rejection.

(3) Remove all dust particles with clean shop air (25 psi).

3.0.7 Bonding of Insulation Sponge to Substrate. -

(1) Thoroughly mix the required amount of adhesive (GE RTV-560) with 0.5% of dibutyl tin dilaurate catalyst. Weigh, using a precision laboratory balance.

(2) Apply a thin layer (0.005 in thick) on both the substrate and to one surface of the sponge.

(3) Mate surfaces and cure at room temperature for sixteen hours under approximately 1.0 psi pressure.

3.0.8 Bonding of Insulation Tiles to Sponge. -

(1) Thoroughly mix the required amount of adhesive (GE RTV-560) with 0.5% of dibutyl tin dilaurate catalyst. Weigh, using a precision laboratory balance.

(2) Apply a thin layer (0.005 in thick) on both the insulation tile and to one surface of the sponge.

(3) Mate surfaces and cure at room temperature for sixteen hours under approximately 1.0 psi pressure.

(4) Trim-off excess cured adhesive.

THIS PAGE INTENTIONALLY LEFT BLANK

APPENDIX E

RADIATION PATTERNS FOR ANTENNAS S/N 102 AND 105

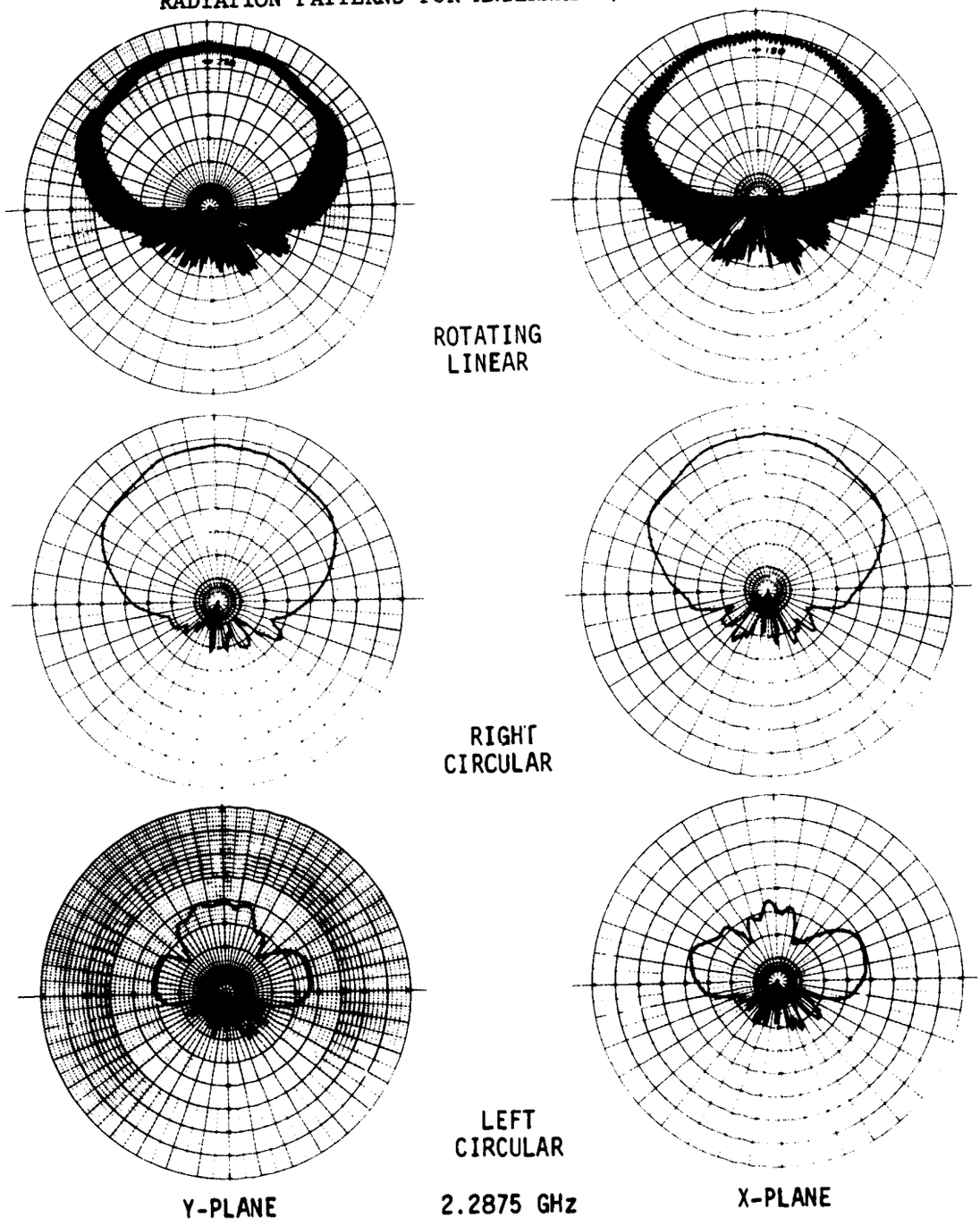

RADIATION PATTERNS - ANTENNA S/N 102

FIGURE 192

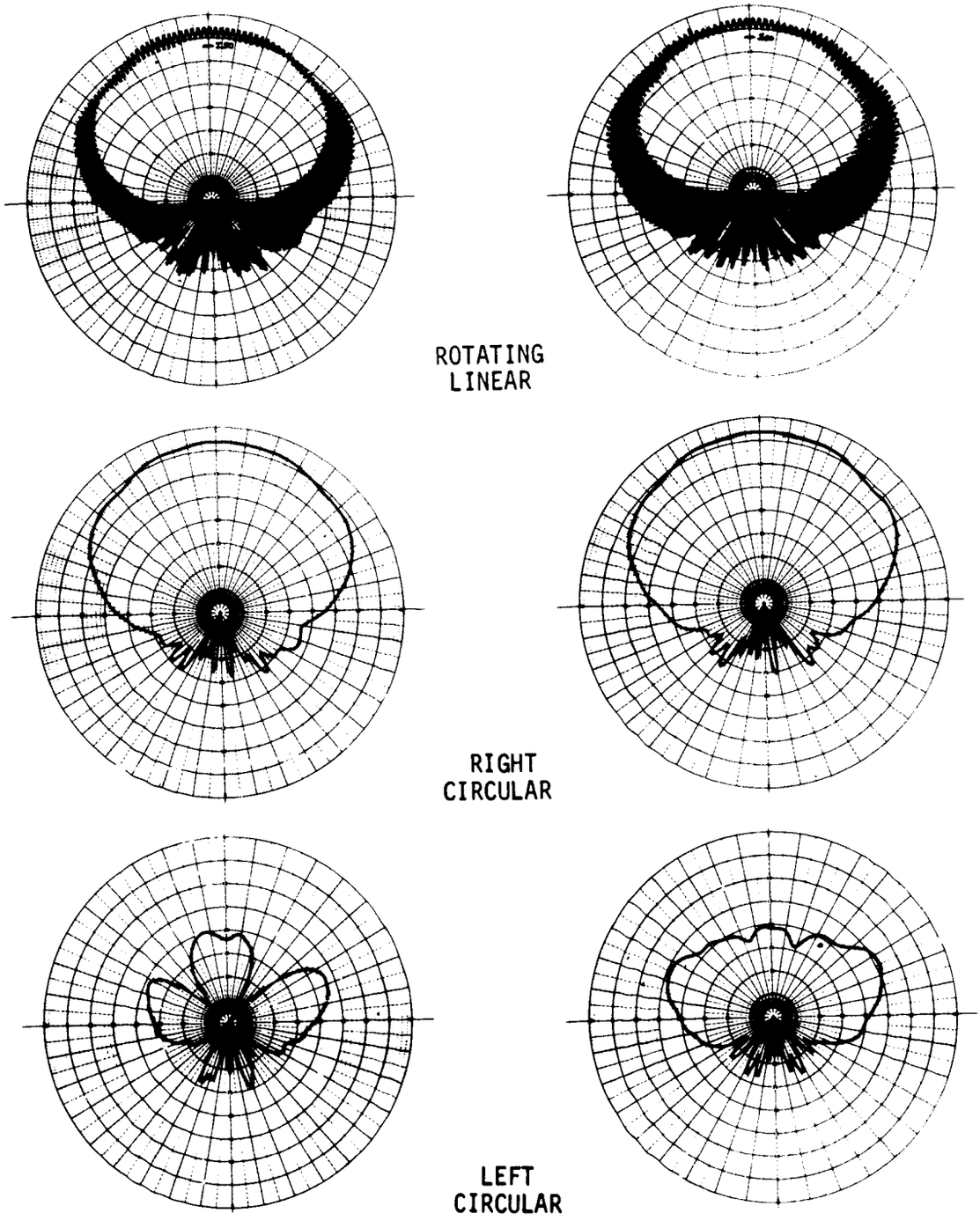

RADIATION PATTERNS - ANTENNA S/N 105

FIGURE 193

APPENDIX F

TEST DATA FOR PROTOTYPE UNIT NO. 2

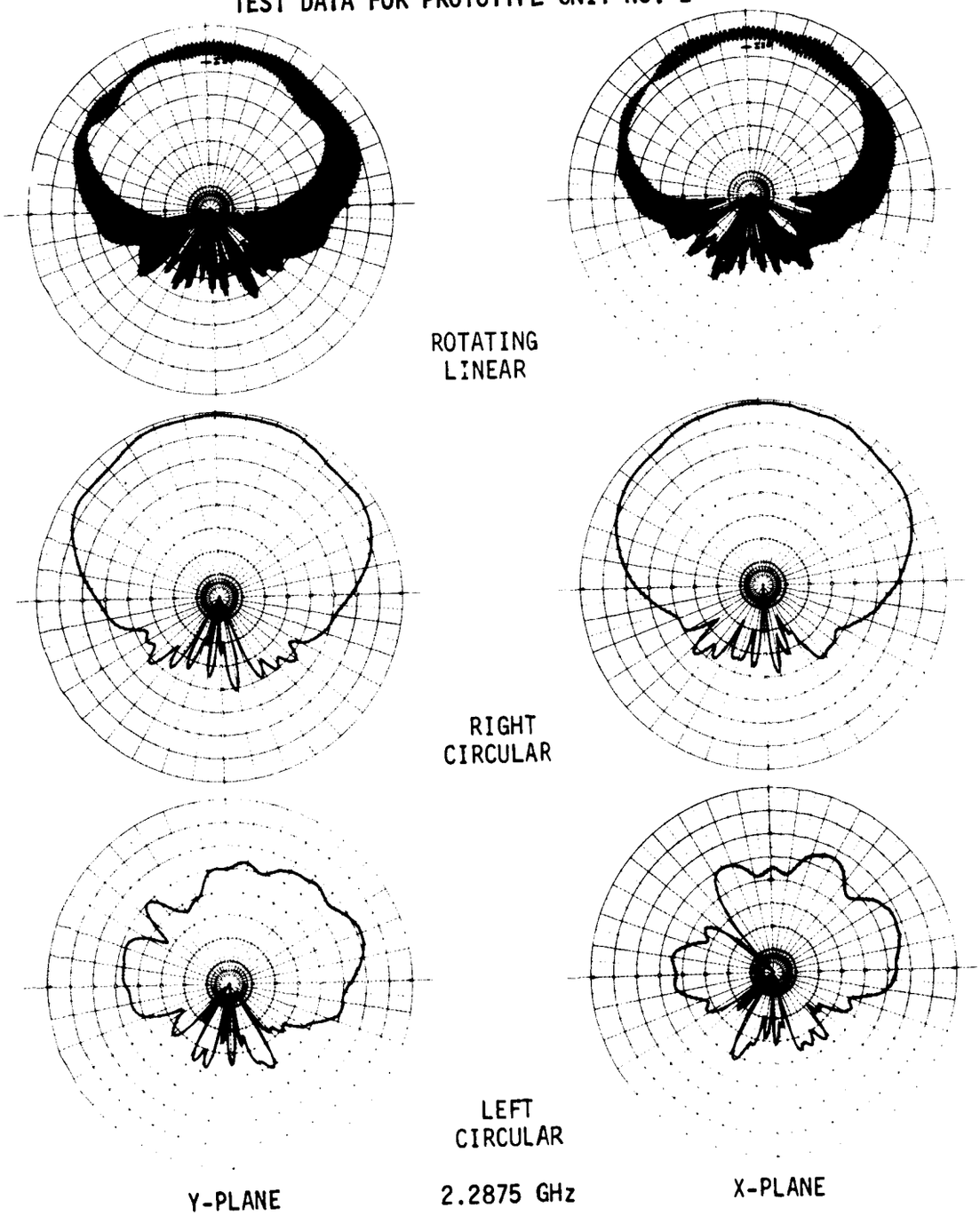

RADIATION PATTERNS - PROTOTYPE UNIT NO. 2

FIGURE 194

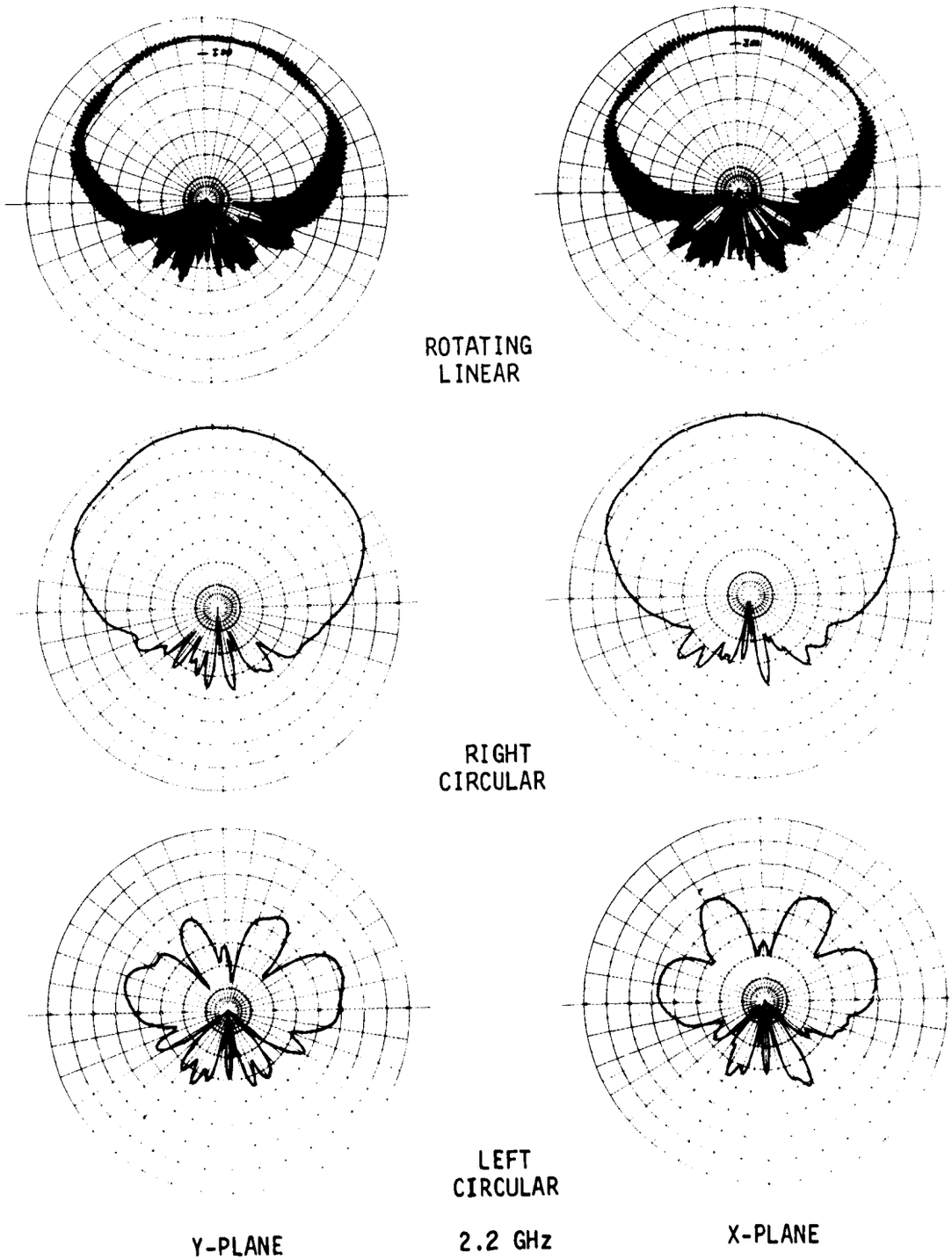

RADIATION PATTERNS - PROTOTYPE UNIT NO. 2

FIGURE 194 (Continued)

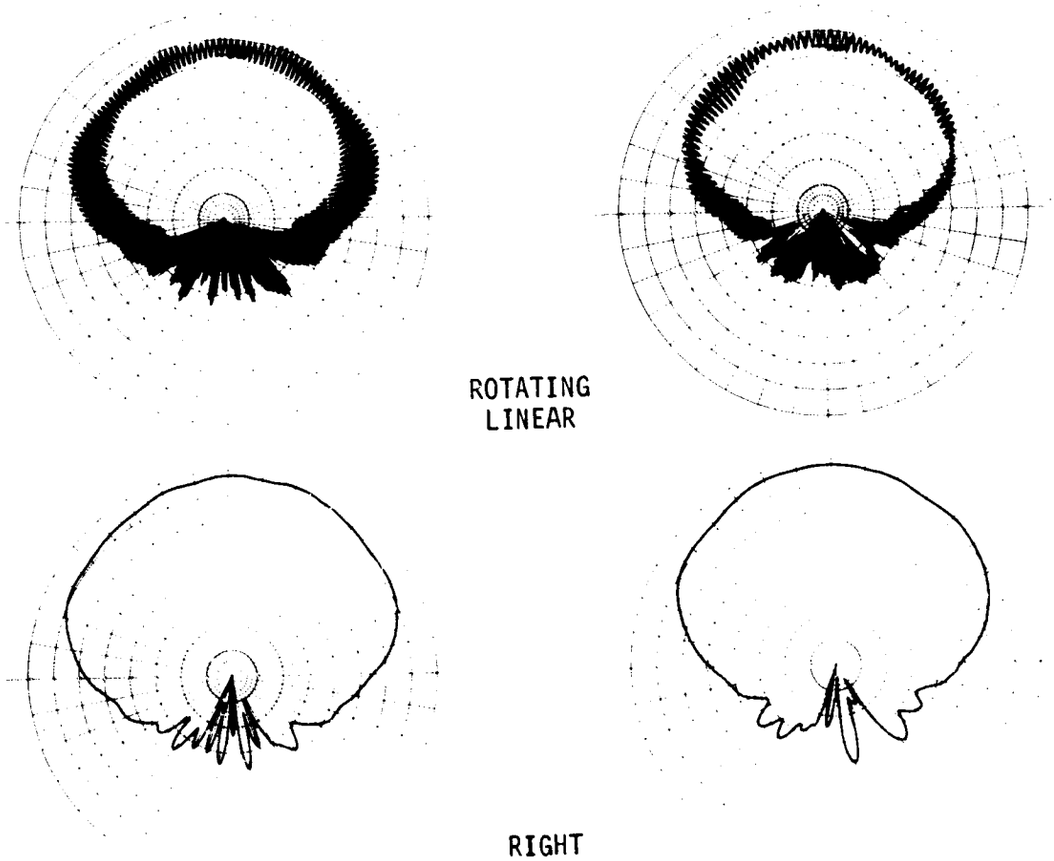

RADIATION PATTERNS - PROTOTYPE UNIT NO. 2

FIGURE 194 (Continued)

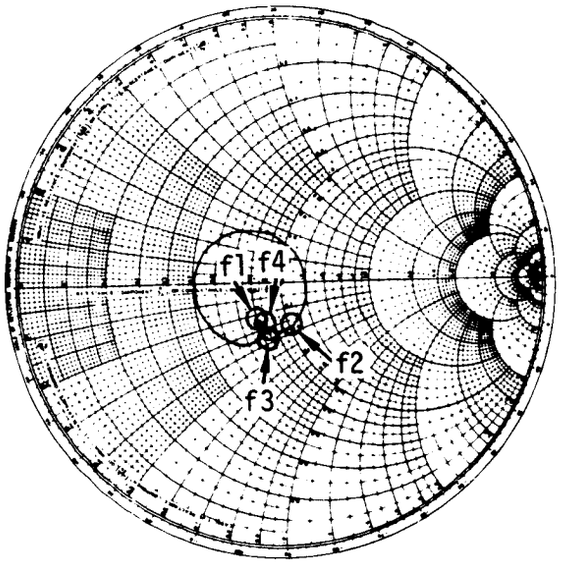

Z_0 = 50 OHMS
f1 = 2.0 GHz
f2 = 2.1 GHz
f3 = 2.2 GHz
f4 = 2.3 GHz

IMPEDANCE - PROTOTYPE UNIT NO. 2

FIGURE 195

APPENDIX G

BREADBOARD UNIT THERMAL TEST PLAN

NAS9-13004

NATIONAL AERONAUTICS AND SPACE ADMINISTRATION

LYNDON B. JOHNSON SPACE CENTER

HOUSTON, TEXAS

Prepared by:

Bill Kavanaugh
Senior Engineer, Thermodynamics

Concurrence by:

Gilbert R. Gaumer
Senior Project Engineer, Thermodynamics

Approved by:

E. A. (Al) Kuhlman
Study Manager

MCDONNELL DOUGLAS ASTRONAUTICS COMPANY • EAST
Saint Louis, Missouri 63166

PLAN FOR MSC 10MW CHANNEL NOZZLE TESTING

OF S-BAND BREADBOARD ANTENNA

1.0 Introduction: We intend to thermally test a breadboard S-band antenna system in the NASA-MSC 10MW Arc Tunnel Facility in early March, 1973. We will conduct electrical tests before and after each thermal test cycle. The purpose of the tests is to validate our design approach and contribute to the final design of a prototype antenna system. The prototype antenna system will then be reuse tested in the NASA-MSC 10MW Arc Tunnel Facility in May, 1973.

Design techniques and materials most common to all shuttle antenna requirements will be incorporated into our breadboard S-band antenna system design. Our objective is to determine the functional predictability and suitability of this S-band system design such that the results are extendable to other types of flush mounted antenna systems. In this manner, early assessment of basic design concepts applicable to Shuttle Orbiter Antennas will be accomplished.

This plan provides the test requirements and planning associated with breadboard S-band antenna system tests. These tests will use the channel nozzle in the NASA-MSC 10MW Arc Tunnel because the channel mount produces more uniform heating than the wedge mount. This plan is submitted under Contract NAS9-13004.

2. Objectives: Test objectives were established for the breadboard tests of the S-band antenna system. The breadboard thermal tests shall provide temperature data resulting from prescribed thermal inputs to:

(1) Confirm analytically predicted temperature distributions;
(2) Verify stresses (strain compatibility) resulting from thermal input;
(3) Verify required antenna window thickness;
(4) Confirm design of test specimen holder for subsequent prototype reuse tests.

The electrical test objective is to determine if changes have occurred in electrical performance due to simulated entry heating.

By demonstrating that the antenna system can be adequately characterized analytically, methods and assumptions used can be related to similar antenna designs with more confidence, and less testing.

The definition of the S-band breadboard test article, test holder assembly and test planning are guided by the stated test objectives.

3.0 Material and Equipment Supplied: One S-band breadboard test article including instrumentation and a test specimen holder assembly, as shown in Dwg. 70T087015, will be supplied by MDAC (see Figure 1). The test article consists an S-band antenna integrated into skin structure and TPS. The antenna window consists of a 18.3 cm (7.20 in) square LI-1500 tile bonded with 0.203 cm (0.080 in) thick silicone sponge to a 0.43 cm (0.17 in) thick honeycomb panel. This tile is surrounded on each side by four other LI-1500 guard tiles. The tiles are arranged to present a 32.2 cm (12.68 in) square specimen surface. The four LI-1500 guard tiles are bonded with a 0.635 cm (0.25 in) silicone sponge to aluminum skin-stringer structure. The joint design between tiles is a double-lap concept with FI-600 insulation filler strips. An AMECOM M 45672 S-band antenna is mounted in back of the honeycomb panel.

Two tile locations are instrumented (see Figure 2) from surface to bondline (see MDAC Drawing 70T087008). Other thermocouples are located on the LI-1500 surface, on tile joints, on the structure and antenna. A total of thirty-one thermocouples are used.

An existing adapter-cover assembly, MDAC Drawing 70T037026, will mate the test container assembly to the MSC channel nozzle. The adapter incorporates brazed cooling lines, airtight sealing from the atmosphere with relief valves to prevent occurrance of damaging pressure differentials and a fitting to provide auxiliary air cooling if needed. This adapter cover is the same unit as fabricated for evaluation for convective heating in RSI gaps and joints (Contract NAS 9-12854).

FIGURE 1 S-BAND ANTENNA SYSTEM TEST CONFIGURATION

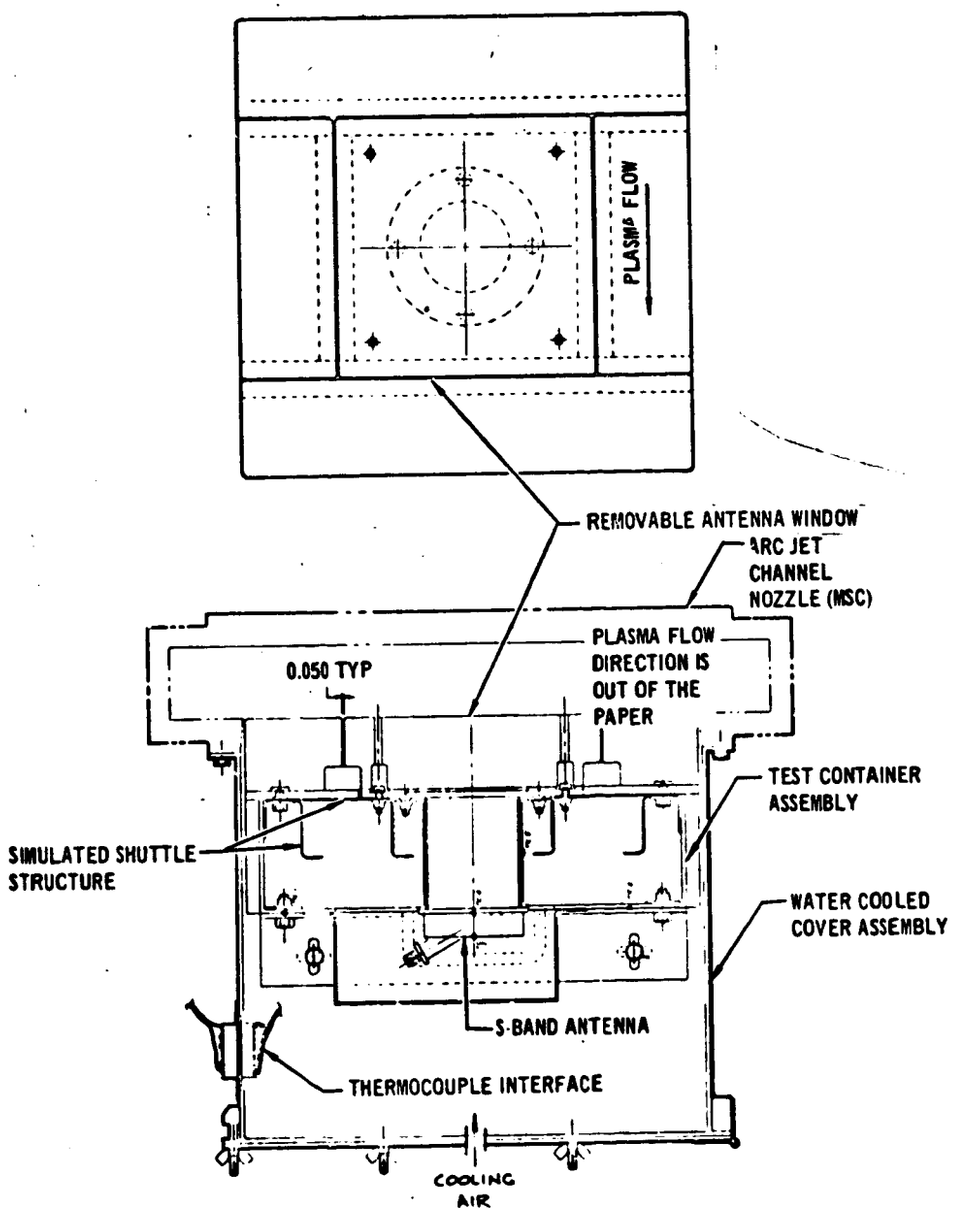

NOTE: SEE PROGRESS REPORT NO. 4, 1 NOV 72 FOR DETAIL CALLOUTS ON S-BAND ANTENNA SYSTEM

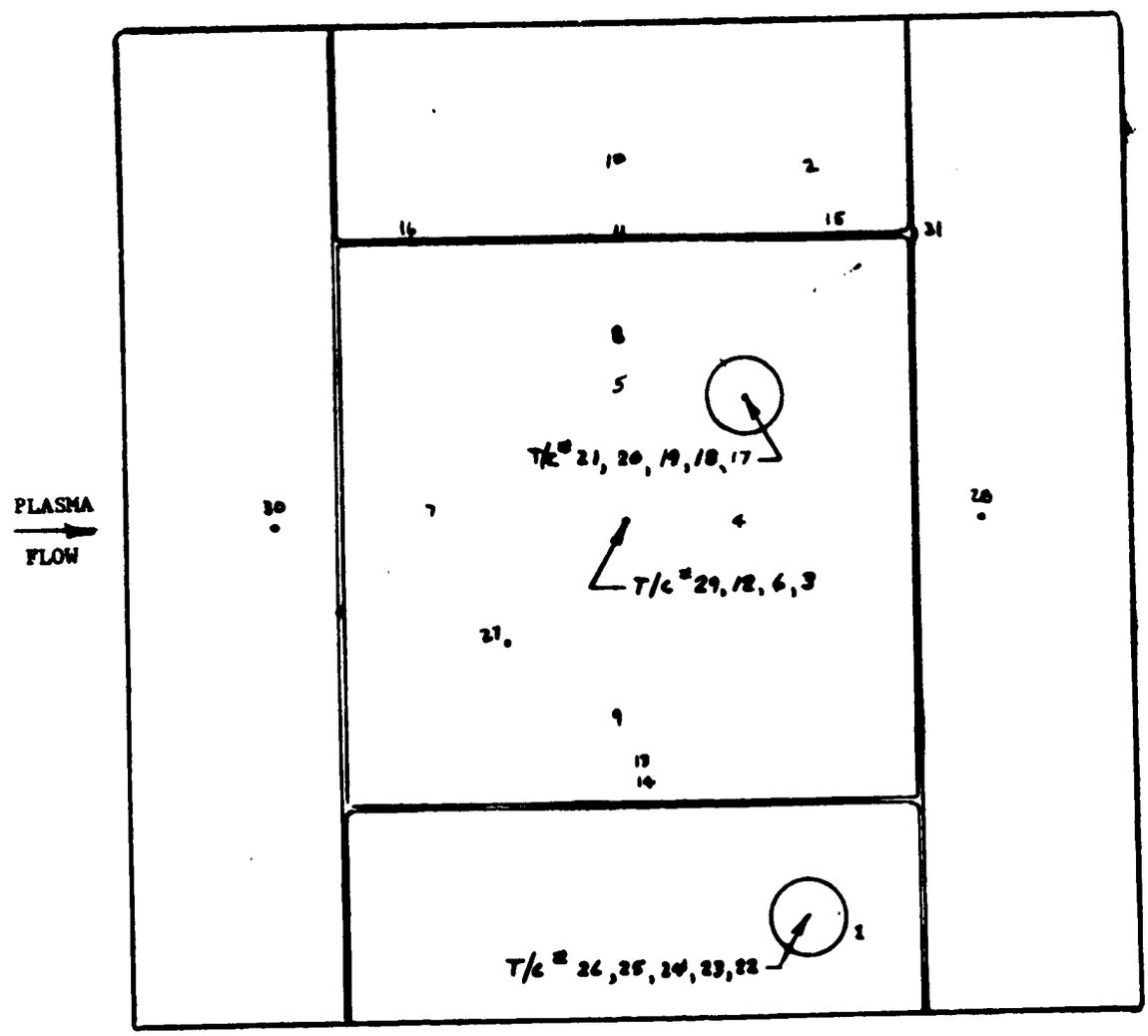
PLASMA
FLOW
T/C # 21, 20, 19, 18, 17
T/C # 29, 12, 6, 3
T/C # 26, 25, 24, 23, 22

For the electrical tests, a mounting framework constructed of 2 x 4 inch board lumber will be supplied by MDAC. Laboratory space for the framework will be required during the breadboard test series.

4.0 Test Schedule: Three successful thermal tests of the S-band antenna system will be required for design temperature verification. Heating will be applied to the breadboard unit to determine the thermal response for verifying the thermal analytical model. Before and after each thermal cycle, electrical tests will be conducted with test unit removed from the thermal test set-up.

The thermal tests will be of increasing severity. Thus, minimum risk runs are implemented first to avoid damage to the S-band antenna. The test environment simulated for the first run (Figure 3) will be above minimum arc heater operating conditions and will be the specified entry surface temperature history of our Program Plan truncated at a constant peak temperature of 1200°K (1700°F). This will provide thermal analysis correlation at less than total heat load. The test environment simulated for the second run (Figure 4) will be the specified temperature history truncated at a constant peak temperature level of 1366°K (2000°F). The third test run environment (Figure 5) will be the full specified temperature history. These tests will ensure that the antenna will not be overheated during the initial full exposure of the reuse tests scheduled in May, 1973.

5.0 Calibration: The tunnel must be calibrated for the minimum operating condition and at several points on the heating-time curve.

The tunnel operating parameters can thus be determined which will produce various average heating rates to give the required temperature versus time curve. In this way the required tunnel operating conditions versus time can be generated. Heating rate distribution over the calibration plate should be recorded for each average heating rate.

We suggest using argon plasma heat up, then air plasma during peak heating, and argon plasma cool down to achieve required test temperature history, total heat load and heat soak-back characteristics on the test article.

FIGURE 3 TEST ENVIRONMENT FOR RUN NO. 1

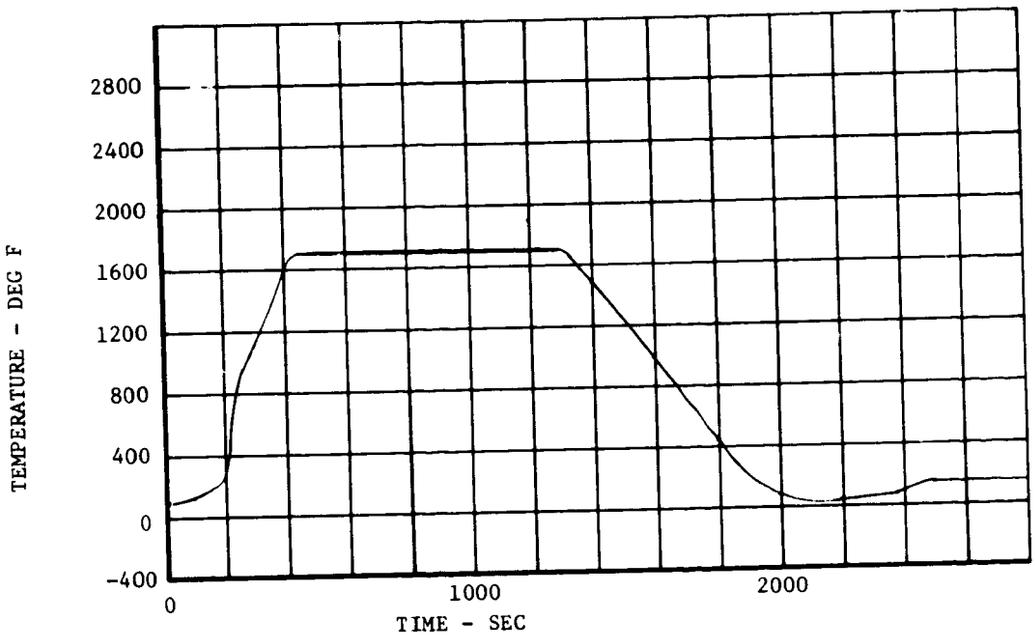

FIGURE 4 TEST ENVIRONMENT FOR RUN NO. 2

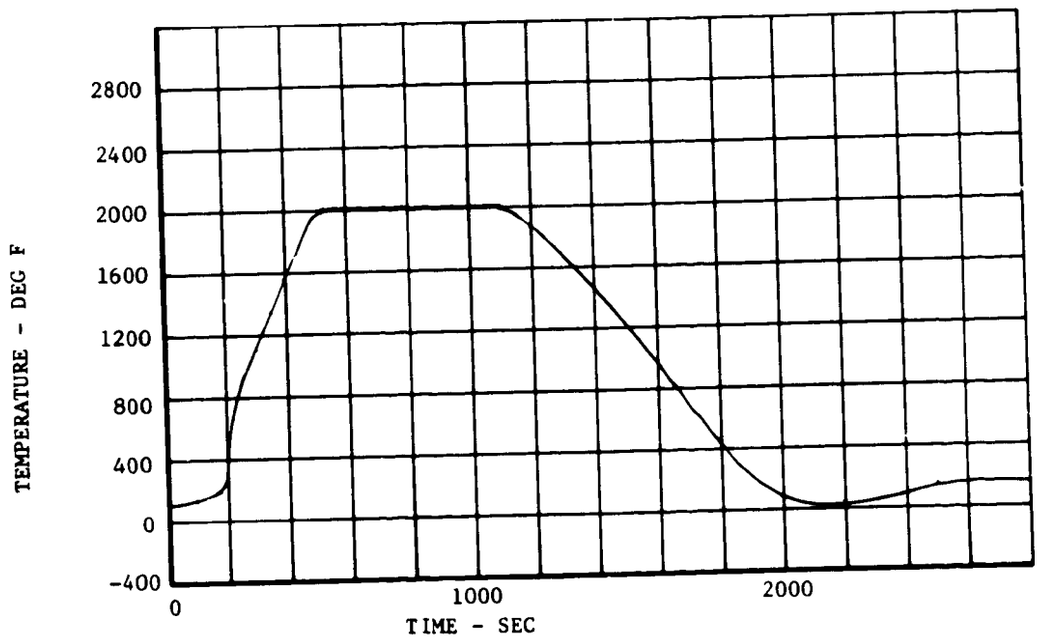

FIGURE 3 TEST ENVIRONMENT

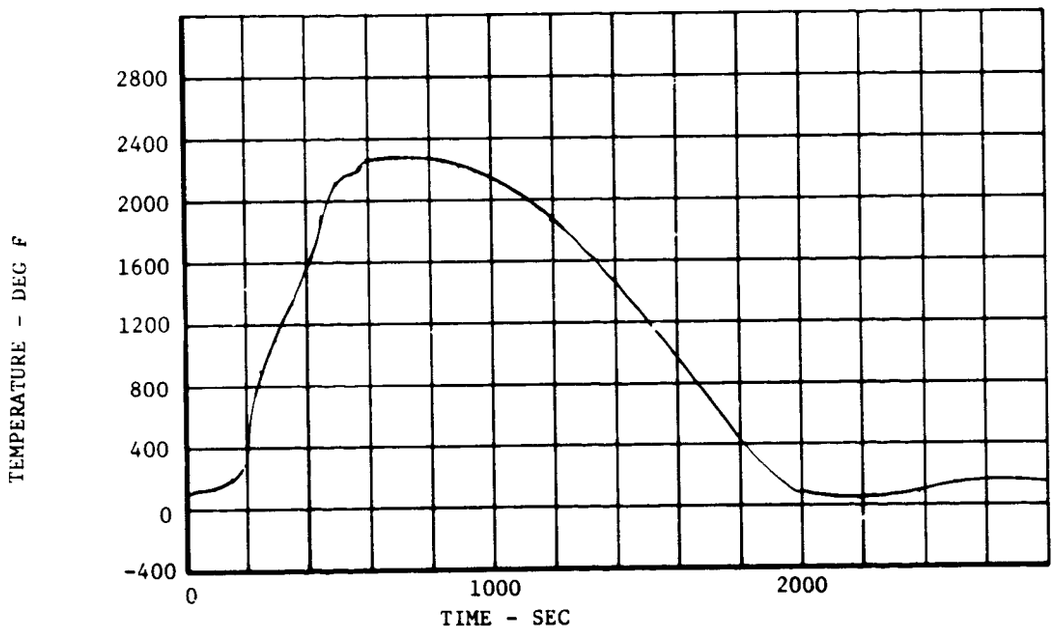

6.0 Test Procedure: The adapter cover assembly should be installed and remain installed in the tunnel wall, with an airtight seal between mating surfaces. The hinged rear wall of the adapter allows access to the test container assembly.

Before each thermal cycle, the VSWR and gain relative to a standard gain reference horn will be measured with and without window to establish the fitness of the breadboard test unit.

Then, the test unit will be placed into the adapter-cover assembly by tightening the four fasteners and connecting three DB-15P and one DB-25P thermocouple connectors. The test container backplate will be adjusted until the specimen surfaces are flush with the inside surface of the channel nozzle. To seal the adapter from ambient pressure, a thin layer of silicone adhesive (DC 3145) may be used between the hinged rear door and its mating flange. Auxiliary air cooling shall be connected.

After the thermal test cycle, the breadboard test unit will be removed from the adapter-cover for: (1) visual inspection and evaluation, and (2) measurement of the VSWR and relative gain (or transmission) under conditions identical (as near as is practical) to the pre-thermal cycle. We will use a second standard gain horn antenna to establish the proper reference level before each transmission test.

7.0 Data Required: Calibration data tunnel operating parameters and test data are to be tabulated and plotted. Stream average enthalpy, heating rate, pressure, and temperature data shall be included as normally processed through the NASA MSC generalized data processing program. Provision for 31 thermocouple responses shall be provided. The temperature plot scale for RSI surface and in-depth T/C's shall be 0 to 1700°K (-460 to 2600°F) and time scale shall extend 6000 seconds (1.67 hrs). The temperature plot scale for antenna backface T/C's shall be 0 to 700°K (-460 to 800°F) and time scale shall extend 10,000 seconds (2.8 hrs). The selected plot groupings for data presentation, along with plot scale requirements, are shown in Table I.

TABLE 1

Data Reduction Grouping
of Thermocouple Response for
S-Band Breadboard Antenna Test

OBJECTIVE	THERMOCOUPLE	PLOT SCALE (°K)	RUN TIME (sec)
1) Indepth survey of antenna window RSI	TC26,TC25,TC24,TC23,TC22	0 - 1700 (-460 - 2600°F)	6,000
2) Indepth survey of TPS RSI	TC21,TC20,TC19,TC18,TC17	0 - 1700 (-460 - 2600°F)	6,000
3) Antenna window aperture	TC29,TC12,TC6,TC3	0 - 1700 (-460 - 2600°F)	10,000
4) Uniformity of antenna window surface temperatures	TC21,TC29,TC27	0 - 1700 (-460 - 2600°F)	6,000
5) Orbiter skin stringers,antenna support sheath,and antenna case	TC9,TC8,TC5,TC4,TC3	0 - 700 (-460 - 800°F)	10,000
6) Orbiter skin structure gradient	TC10,TC11,TC8	0 - 700 (-460 - 800°F)	10,000
7) Antenna window lap-joint gradient	TC13,TC14,TC27	0 - 1700 (-460 - 2600°F)	6,000
8) Antenna window joint gap bottom heating of FI-600 filler strip and skin	TC16,TC15,TC11, T31	0 - 1700 (-460 - 2600°F)	10,000
9) Uniformity of test specimen surface temperatures along centerline	TC28,TC29,TC30	0 - 1700 (-460 - 2600°F)	6,000
10) Uniformity of test specimen surface temperature - diagonal across	TC26,TC29	0 - 1700 (-460 - 2600°F)	6,000
11) Test container - skin structure - antenna	TC1,TC2,TC4,TC3	0 - 700 (-460 - 800°F)	10,000

In addition, thermocouple (etc) responses are to be also recorded on MDAC furnished magnetic tape for direct processing in MDAC computers. The tape will be BCD tape, 7X8A8 for the tile and 10E13.3 for each time step through the test.

8.0 Photographic Services Required: A low-speed color motion picture film (with timing) of the test specimen during the thermal cycle is desired.

Still photographs of the arrangement of the electrical test setup, closeup and distant (showing arrangement in facility) are required.

Still photographs of the channel mount showing breadboard S-band antenna system installation, close-up and distant (showing arrangement in facility) are required.

Pre-and post-test photographs of the breadboard antenna system test specimen are required.

9.0 Test Equipment Cabling: We intend to use the 15-foot extension wire bundle cable used for contract NAS9-12854 which we understand has a 32 thermocouple capability (8 platinum-rhodium and 24 chromel-alumel) with 4 cannon connectors and with tagged bare-lead ends for attachment to NASA test panel.

THIS PAGE INTENTIONALLY LEFT BLANK

APPENDIX H

PROTOTYPE UNIT THERMAL TEST PLAN

NAS9-13004

NATIONAL AERONAUTICS AND SPACE ADMINISTRATION

LYNDON B. JOHNSON SPACE CENTER

HOUSTON, TEXAS

Prepared by:

Bill Kavanaugh
Senior Engineer, Thermodynamics

Concurrence by:

Gilbert R. Gaumer
Senior Project Engineer, Thermodynamics

Approved by:

E. A. (Al) Kuhlman
Study Manager

MCDONNELL DOUGLAS ASTRONAUTICS COMPANY • EAST
Saint Louis, Missouri 63166

THERMAL TEST PLAN

FOR S-BAND PROTOTYPE ANTENNA

1.0 Introduction: McDonnell Douglas Astronautics Company intends to thermally reuse-test a prototype S-band antenna system in the NASA-JSC 10MW Arc Tunnel Facility in May, 1973. The prototype model consists of an S-band antenna integrated into aluminum skin structure and LI-1500 silica reusable surface insulation (RSI) TPS. We will also conduct electrical tests at the NASA-JSC Anechoic Chamber Test Facility before and after the first, second, fifth and tenth thermal test cycles.

This plan provides the test requirements and planning for the prototype model reuse tests. A channel flow nozzle will be used because it produces more uniform heating than a conical nozzle. This plan is submitted under Contract NAS 9-13004.

2.0 Test Objective: The definition, assembly and test planning of the prototype model was guided by the purpose of demonstrating reuse capability of the antenna TPS structural interfaces.

3.0 Material and Equipment Supplied: One S-band prototype model including instrumentation and a test container assembly, as shown in Dwg 70T087015 will be supplied by MDAC (see Figure 1). The test article consists of an S-band antenna integrated into skin structure and TPS. The antenna window consists of a 18.3 cm (7.20 in) square LI-1500 tile bonded with 0.203 cm (0.080 in) thick RMRL 1973 silicone sponge; the window tile and sponge is bonded to a 0.43 cm (0.17 in) thick honeycomb panel. This tile is surrounded on each side by four other LI-1500 guard tiles. The tiles are arranged to present a 32.2 cm (12.68 in) square specimen surface. The four LI-1500 guard tiles are bonded with a 0.635 cm (0.25 in) silicone sponge to aluminum skin-stringer structure. The joint design between tiles is a double-lap concept with FI-600 insulation filler stripes. An AMECOM M46325 S-band antenna is mounted behind the honeycomb panel; its aperture is flush with the aluminum skin.

FIGURE 1 S-BAND ANTENNA SYSTEM TEST CONFIGURATION

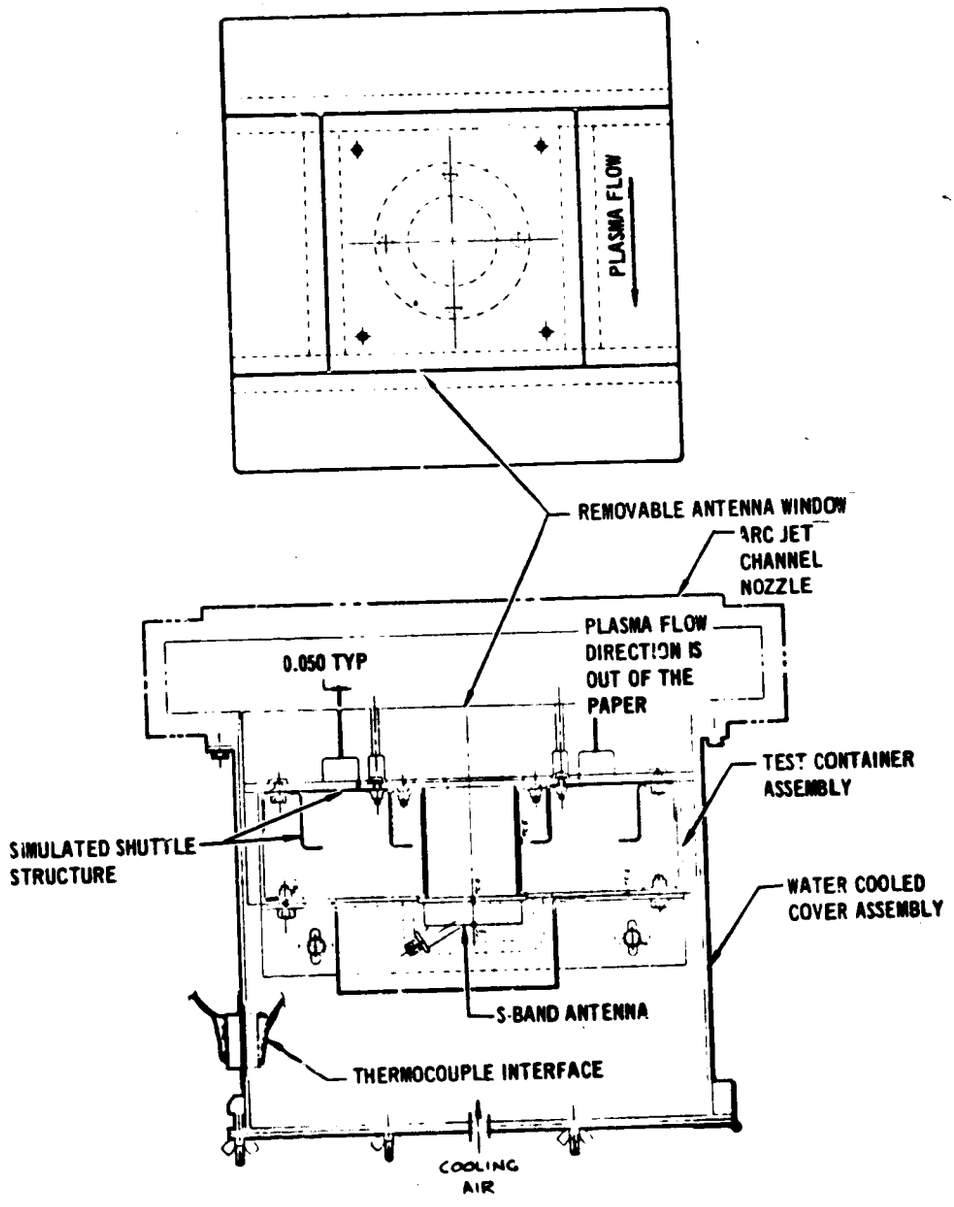

NOTE: SEE PROGRESS REPORT NO. 4, 1 NOV 72 FOR DETAIL CALLOUTS ON S BAND ANTENNA SYSTEM

MCDONNELL DOUGLAS ASTRONAUTICS COMPANY - EAST
Saint Louis, Missouri 63166

An existing water-cooled cover-assembly, MDAC Drawing 70T037026, will mate the test container to JSC channel flow nozzle. The cover-assembly has brazed cooling lines, airtight sealing (with relief valves) from the atmosphere, and a fitting to provide auxiliary air cooling, if needed. This cover assembly is the same unit as fabricated for evaluation of convective heating in RSI gaps and joints (Contract NAS 9-12854).

The breadboard model, previously tested in March 1973, will be furnished for arc tunnel calibration and "Data Trak" checkout runs. The AMECOM S-band antenna unit will be removed from the breadboard model assembly.

We intend to use the 15-foot extension wire bundle cables used for Contract NAS 9-12854 with tagged bare-lead ends for attachment to the reference junction box.

4.0 Instrumentation - Twenty-one thermocouples (see Figure 2) will be used to record temperature distributions in the prototype antenna model. One surface thermocouple will be located on each of the forward and aft large LI-1500 guard tiles. Other thermocouple locations are selected to provide minimum interference to antenna performance; no thermocouples are located in depth in the LI-1500 RSI or in the antenna window. Two thermocouples are located on the FI-600 filler strip at the bottom of tile joint gaps at upstream and downstream corners of the antenna window. Four thermocouples are located in the bondline. The remaining thermocouples are located on the backside skin structure and antenna. The instrumentation consists of:

2 Type S - Platinum/10% Rhodium (+) vs Platinum (-)

19 Type K - Chromel (+) Alumel (-)

Calibration plate calorimeters, thermocouples, and pressure sensors, as well as prototype antenna model thermocouples, will be recorded continuously during heating and cooldown of all thermal tests.

FIGURE 2 TYPICAL THERMOCOUPLE INSTALLATION SCHEMATIC

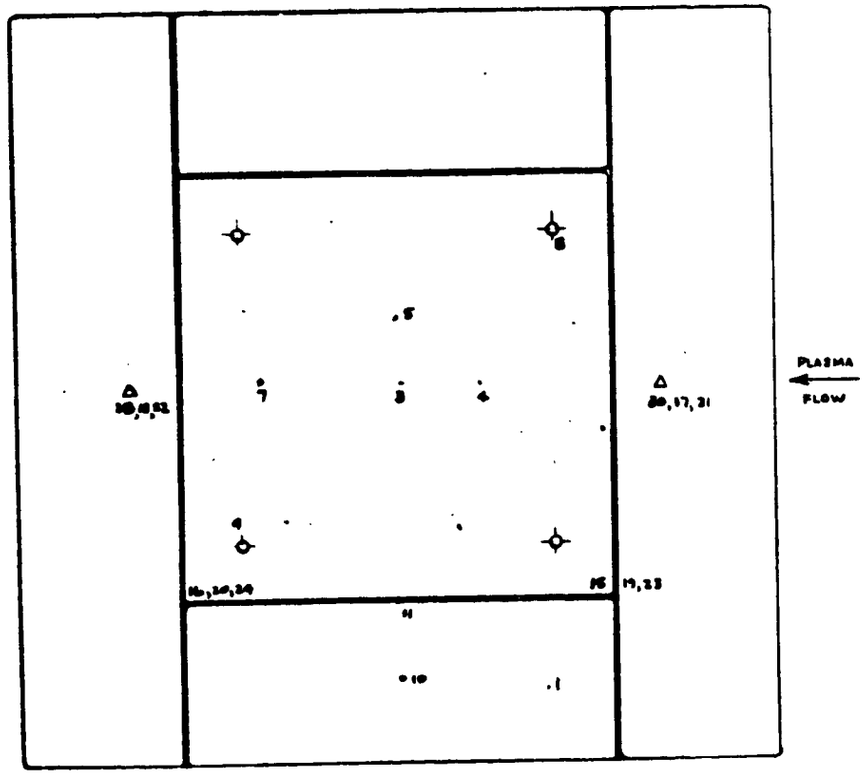

CHANGE SUMMARY:

DELETED 3, 6, 12 → 27, 29, 31

ADDED NEW 15 → 24 TO BE DEMONSTRATED ON SEAMING STRIPING WITH TC 32.

WAS 31 TC'S - TC'S

NOW 31.

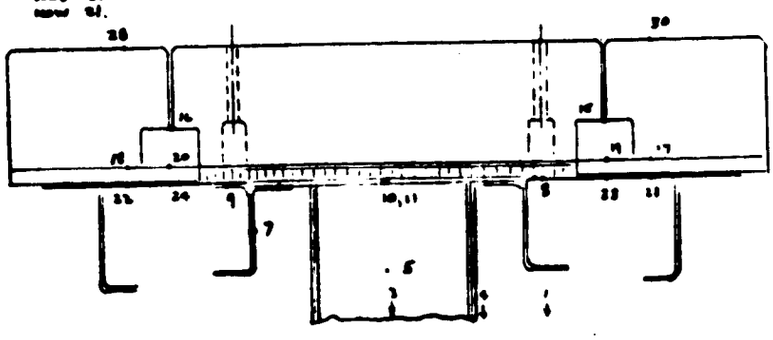

3.0 Calibration: The tunnel must be calibrated for the minumum operation condition and at several points on the heating-time curve.

The tunnel operating parameters can thus be determined which will produce various average heating rates to give the required temperature versus time curve. In this way, the required tunnel operating conditions versus time can be generated. Heating rate distribution over the calibration plate should be recorded for each average heating rate.

Programmed arc-heater operation will be used for the entry heating simulation. A "Data Trak" control curve will be constructed from test points obtained from the calibration runs prior to the prototype test runs.

Surface temperature histories measured on the breadboard antenna will be used for the calibration and "Data Trak" checkout runs. Indepth thermocouple data will be recorded, as well. A secondary benefit of these runs will be to obtain design temperature verification for a case representative of a lower thermal mass antenna configuration.

6.0 Test Environment: The test environment will be based on the Shuttle entry temperature history shown in Figure 4 page 3-6 of the Program Plan. The "arc on" condition will correspond to 200 seconds entry time; insignificant heating occurs before them. The surface temperature, hot wall convective heating rate and local static surface pressure, in terms of test time from "arc on", are summarized in Figure 3.

7.0 Test Procedure: The water-cooled cover-assembly should be installed and remain installed in the wall of the channel flow nozzle. An airtight seal shall be maintained between mating surfaces. The hinged rear wall of the adapter allows access to the test container assembly. Before the thermal tests the following electrical tests will be performed:

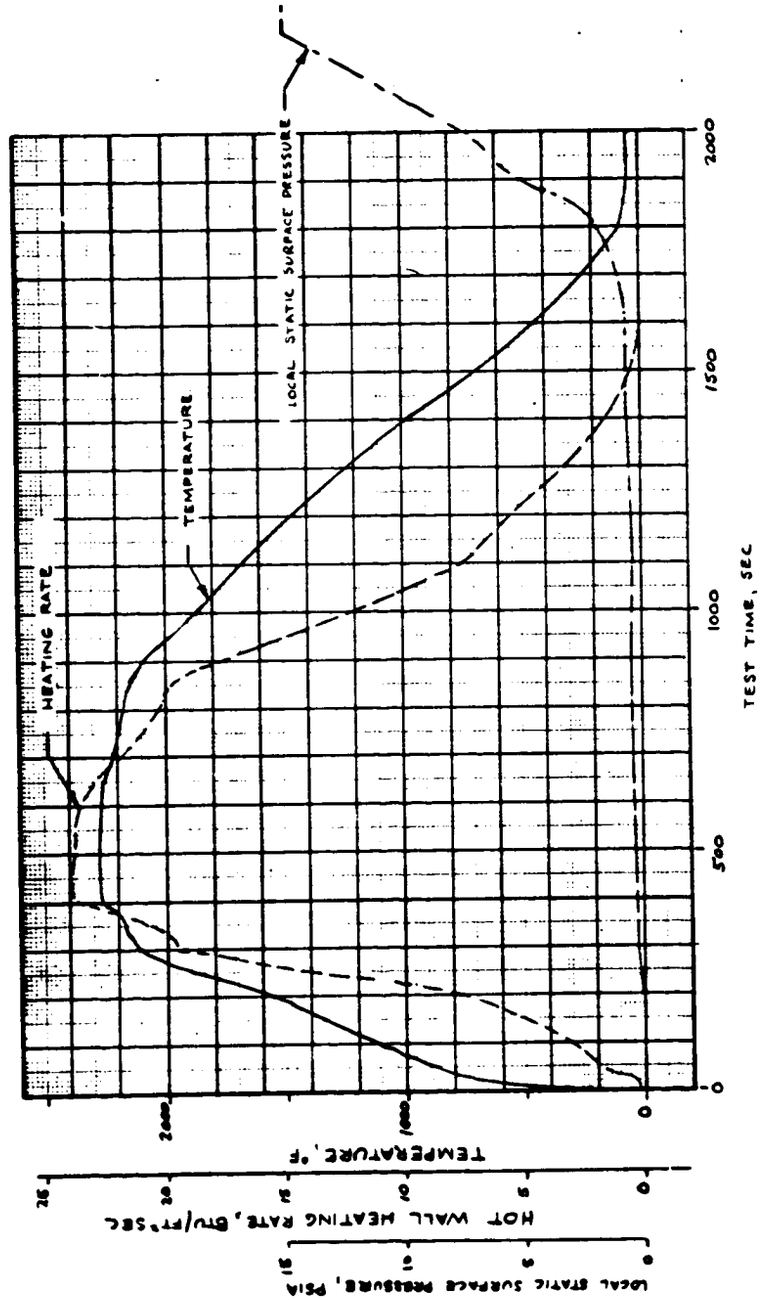

FIGURE 3 TEST ENVIRONMENT

1) Swept frequency impedance from 2.0 to 2.3 GHz plotted on Smith Charts (Hewlett Packard 9280-0137).

2) Right and left hand circular radiation taken at 2.1 and 2.2875GHz. Pattern levels to be referenced to Scientific Atlanta SGH-1.7, or equivalent standard gain horn. Patterns to be recorded on 40 db polar graph paper.

3) On axis, $\theta = 0°$, axial ratio taken at 2.1, 2.2 and 2.2875 GHz. A Scientific Atlanta SGH-1.7, or equivalent, standard gain horn will be used as the radiating antenna.

In addition, acetaldehyde NDT tests for LI-1500 surface coating cracks and pre-test photographs will be made.

The prototype antenna model will then be placed in the cover-assembly. Thin sheet-metal guards will be provided to protect RSI tiles during installation; the test unit shall be gently nudged into place on a 0.2 inch-thick skid sheet, clearing the bevel in nozzle walls. The two long guard tile joints shall be transverse to plasma flow direction; the two surface thermocouples shall line up with flow axis. The model surface shall be flush ($\pm$ .02 in) with inside surface. The four fasteners will then be tightened and the thermocouple plugs, connected. Fibrous insulation shall be packed in the gaps between nozzel wall port and test specimen sides to: (1) prevent plasma flow and (2) close-up gaps between window and guard tiles to 0.070 inch or less. The extension wire bundle shall be installed at the thermocouple reference junction compensator box. The relationship between extension wire bundle bare lead end and prototype thermocouple number is given, as follows:

Extension Wire Bundle Lead Number	Prototype Thermocouple Plug	Prototype Thermocouple Number
1	A	1
4	A	3
5	A	4
6	A	5
7	A	15
8	A	16

Extension Wire Bundle Lead Number (Cont'd)	Prototype Plug	Thermocouple Number
9	A	19
10	A	10
11	A	11
12	A	20
13	B	7
14	B	28
16	B	18
17	B	9
18	B	22
19	B	24
20	C	8
21	C	30
23	C	17
25	C	21
26	C	23

Thermocouple continuity shall be checked. Pretest photographs of tile surface, tile-joint gap measurement and an emittance check on the tile coating shall be made. Auxiliary air cooling lines shall be connected.

A layer of TG-15000 insulation shall be placed on inside of adapter hinged rear door. To seal the adapter from ambient pressure, a thin layer of silicone adhesive (DC 3145) may be used between the hinged rear door and its mating flange.

The prototype antenna model will then be exposed to plasma heating to achieve a maximum 2270°F model surface temperature with programmed arc heater operation. All thermocouple data shall be recorded during the test and after the test until the maximum backface temperatures are recorded. Then, auxiliary air cooling will be turned on until all thermocouples indicate a temperature of less than 100°F.

After the first, second, fifth and tenth cycle, the prototype model will have a photograph and emittance check through the calibration port and then will be removed from the adapter-cover for: (1) visual inspection, NDT evaluation, and water bead testing (absorption) and (2) electrical test under conditions identical (as near as is practical) to the pre-thermal cycle. The same pre-thermal tests will be performed.

In the event we detect progressive changes after the first or second thermal cycle, we will increase the frequency of removal and testing to better assess the

rate of deterioration.

7.0 Data Required: Calibration data tunnel operating parameters and test data are to be tabulated and plotted. Plasma sonic throat average enthalpy, heating rate, pressure, and temperature data shall be included as normally processed through the NASA/JSC generalized data processing program. Provision for 21 thermocouple responses shall be provided. The temperature plot scale for RSI surface shall be 0 to 2500°F and time scale shall extend 6000 seconds (1.67 hrs) in plot frames of 2000 sec each. The temperature plot scale for antenna backface T/C's shall be 0 to 200°F and time scale shall extend 6000 seconds. The selected plot groupings for data presentation, along with plot scale requirements, are shown in Table 1.

In addition, thermocouple (etc) responses are to be also recorded on MDAC furnished magnetic tape for direct processing in MDAC computers. The tape will be BCD tape, 7X8A8 for the tile and 10E13.3 for each time step through the test.

8.0 Photographic Services Required: Still photographs of the arrangement of the electrical test setup, closeup and distant (showing arrangement in facility) are required.

Still photographs of the channel mount showing prototype S-band antenna system installation, close-up and distant (showing arrangement in facility) are required.

Pre- and post-test photographs of the prototype antenna system test specimen are required.

TABLE 1

DATA REDUCTION PLOT GROUPING OF THERMOCOUPLE RESPONSE FOR

S-BAND PROTOTYPE ANTENNA TEST

OBJECTIVE	THERMOCOUPLE	PLOT SCALE	TIME *
1) Surface Temperature	TC 30, TC 28	0 - 2500°F	2000.
2) Forward Surface Temperature, Bondline, Aluminum Skin	TC 30, TC 17, TC 21	0 - 2500°F	6000.
3) Aft Surface Temperature, Bondline, Aluminum Skin	TC 28, TC 18, TC 22	0 - 2500°F	6000.
4) Upstream Corner Gap, Filler Strip Base, Aluminum Skin	TC 15, TC 19, TC 23	0 - 1200°F	6000.
5) Downstream Corner Gap, Filler Strip Base, Aluminum Skin	TC 16, TC 20, TC 24	0 - 1200°F	6000.
6) Window Attachment Hole Base	TC 8, TC 9	0 - 200°F	6000.
7) Skin Gradients	TC 10, TC 11, TC 21, TC 22, TC 23, TC 24	0 - 200°F	6000.
8) Antenna Support, Antenna Case, Skin Stringer	TC 3, TC 4, TC 5, TC 7	0 - 200°F	6000.
9) Antenna Case, Test Container Assembly	TC 1, TC 4, TC 3	0 - 200°F	6000.

* THREE PLOT FRAMES OF 2000 SEC EACH

END

DATE

FILMED

JAN 25 1974